Syntheses and applications of small molecule inhibitors of miRNAs miR-21 and miR-122

by

Méryl Thomas

Bachelor of sciences, ESCPE Lyon, 2009

Master degree, ESCPE Lyon, 2012

Submitted to the Graduate Faculty of the

Dietrich School of Arts and Sciences in partial fulfillment

of the requirements for the degree of

Doctor of Philosophy

University of Pittsburgh

2015

UNIVERSITY OF PITTSBURGH

Dietrich School of Arts and Sciences

This thesis was presented

by

Méryl Thomas

It was defended on

July 24th, 2015

and approved by

Dr. Andrew W. Duncan, Assistant Professor, Department of Pathology

Dr. Seth Horne, Associate Professor, Department of Chemistry

Dr. Kabirul Islam, Assistant Professor, Department of Chemistry

Committee Chair: Dr. Alexander Deiters, Professor, Department of Chemistry

Syntheses and applications of small molecule inhibitors of miRNA miR-21 and miR-122

Méryl Thomas, PhD

University of Pittsburgh, 2015

MicroRNAs (miRNAs) are regulatory RNA molecules of 22 nucleotides that (in part) control up to 60% of all genes in humans. They act by binding to the 3' untranslated regions of target messenger RNAs, leading either to translational repression or mRNA degradation. In addition to being involved in the regulation of several fundamental cellular processes, the misregulation of miRNAs has been linked to a wide range of diseases including cancer. Particularly, miR-21 is significantly upregulated in nearly all types of human cancers, and its overexpression is often associated with poor prognosis. The downregulation of miR-122 is found in more than 70% of hepatocellular carcinoma cases and miR-122 is a required factor for the replication of the HCV virus. The modulation of miRNA function is commonly achieved using oligonucleotide agents. However, compared to oligonucleotides, small molecules have several advantages, such as fast activity, systemic delivery, and excellent cell permeability. Taking advantage of luciferase-based reporters, two separate high-throughput screens of >300,000 compounds each, were conducted to discover new small molecule inhibitors of miR-21 or miR-122. Several hit compounds were re-synthesized, their ability to inhibit miR-21 was validated, and the most promising compounds were investigated by SAR studies, which revealed two additional, structurally diverse classes of miR-21 inhibitors. Similarly, extensive SAR studies of previously discovered miR-122 inhibitors were performed in order to better understand the molecular requirements for the miR-122 inhibitory activity. The hit compounds identified in the HTS were analyzed through secondary assays that led to the identification of two new promising miR-122 inhibitors. Furthermore, the

knowledge gained during the SAR studies was further used to synthesize several small molecule miR-21/miR-122 inhibitors as probes to explore their mechanisms of action. MicroRNAs represent promising, novel drug targets, and small molecule miRNA inhibitors provide tools to study the molecular mechanisms of miRNA biogenesis and have the potential to be new therapeutic agents for the treatment of cancers and viral infections.

TABLE OF CONTENTS

LIST OF TABLES

LIST OF FIGURES

LIST OF SCHEMES

PREFACE

Acknowledgments.

I would like to thank my advisor Dr. Alexander Deiters for his guidance, his support, and for giving me the opportunity to work in his lab and conduct exciting research projects. He has been a great mentor throughout the years, and his high expectations pushed me to become a better scientist.

I would also like to thank the members of my committee, Dr. Andrew W. Duncan, Dr. Seth Horne, and Dr. Kabirul Islam for their review of my work.

I would like to acknowledge the past and present Deiters lab members: Jeane, Kalyn, James, Alex, Rajendra, Yan, Andrew, Jessica, Qingyang, Colleen, Laura, Matt, Ji, Jihe, Yuta, Nick, Subhas, Kim, Luis, Rohan, Xinyu, and Nathan for always being willing to share their time and knowledge, for their valuable suggestions, their encouragements, and for making all the time spent in lab so much more fun and enjoyable! A special thanks to the girls Jeane, Colleen, Jessica, Kalyn, Yan, Qingyang, Kim, and Laura for their friendship and always being there in the bad and the good times! I would also like to give a special thanks to Kalyn, Alex, James, and Subhas who helped in setting us a new lab in Pittsburgh and made the transition more bearable by their presence.

I would like to extend my appreciation to the faculty and staff of the Department of Chemistry at the University of Pittsburgh. Especially to Dr. Steve Weber, Christie Hay, Jay Auses, Mary Beth Conroy, Darlene Lanz, LaShawn Youngblood, Josh Jones, Albert-John Krall, and Lori Neu who have been providing excellent help with all the non-scientific issues associated with the daily life in grad school and for facilitating the transition to the lab to

Pittsburgh. I would also like to thank the faculty, the staff, and my friends back in the Department of Chemistry at North Carolina State University.

I am very grateful for the many collaborators that have contributed to my research, including Kate Hartland and all the members of the Broad Institute's Probe Development Center, Dr. Glenn Randall from the University of Chicago, Dr. Nathan Yates from the Biomedical Mass Spectrometry Center at the University of Pittsburgh, and Nedyalka Dicheva at the UNC Michael Hooker Proteomics Center.

I would like to thank all my friends, who despite the distance, have always been a great support and have made the effort to stay in touch. I am also very grateful to my boyfriend Sergey, for all his support, his encouragements, and being part of my life.

And last but not least, I would like to thank my family. Je remercie mes parents Philippe et Marie et mon petit frère Antoine qui ont été un soutien essentiel pendant toutes ces années. Malgrè la distance, les difficultés, et parfois les doutes ils ont toujours supporté mes choix, ils m'ont toujours poussé à avancer et donné les moyens de réaliser mes rêves. Je leur suis infiniment reconnaissante et je les aime plus que tout!

1.0 INTRODUCTION TO MICRORNAS

It was recently discovered that 80% of the human genome is transcribed mostly generating a vast amount of non-coding RNA transcripts, as only about 2% is being subsequently translated.[1] Non-coding RNAs used to be considered as non-functional "junk" until recent studies revealed their importance in the regulation of many biological processes, creating a significant interest in non-coding RNA biology. MicroRNAs (miRNAs) are single stranded endogenous RNA molecules of 21-25 nucleotides and constitute the most established class of non-coding RNAs.[1] Over 2,500 human miRNAs have been registered in miRbase[2] and they represent one of the most abundant classes of gene regulatory molecules as they are estimated to control up to 60% of genes in humans.[3] Lee, Feinbaum, and Ambros discovered the first miRNA, *lin-4*, in 1993.[4] They found that instead of coding for a protein, the gene *lin-4*, which is responsible for the larval development of *Caenorhabditis elegans* (*C. elegans*), produces a pair of small RNAs that have antisense complementarity to several sites in the 3′ untranslated region (3′-UTR) of lin-14 messenger RNA (mRNA). It was later demonstrated that the regulation of *lin-14* by *lin-4* resides in the complementarity of this small RNA for the 3′-UTR of the lin-14 mRNA and that the binding of the small RNA significantly reduces the amount of LIN-14 protein.[4] A second miRNA, *let-7*, which is also responsible for the developmental timing of *C. elegans*, was discovered seven years later. Similar to *lin-4*, *let-7* encodes a small 21-nucleotide RNA which shows complementarity to multiple regions of the 3′-UTRs of the heterochronic

genes *lin-14*, *lin-28*, *lin-41*, *lin-42*, and *daf-12*.[5] More importantly, the discovery that miRNAs are generally conserved in evolution, *let-7* was detected in human, *Drosophila*, and several other animals,[6] highlighted the importance of miRNAs as a new class of gene regulatory molecules and spurred research efforts to understand their biogenesis, mechanism of regulation, and function.[7]

1.1 MIRNA BIOGENESIS AND FUNCTION

miRNA genes are transcribed by RNA polymerase II into transcripts ranging from hundreds to thousands of nucleotides in length, called primary miRNAs (pri-miRNAs).[2] In most cases, precursor miRNAs (pre-miRNAs), hairpin intermediates of 70-100 nucleotides, are obtained after processing of the pri-miRNAs in the nucleus by the RNase III enzyme Drosha and DGCR8 (DiGeorge syndrome critical region gene 8). However, some pre-miRNAs have also been found to be generated by mRNA splicing via an alternative pathway, bypassing Drosha processing.[2] Pre-miRNAs are then exported to the cytoplasm by the nuclear export protein Exportin 5 (Figure 1.1). In the cytoplasm another RNase III enzyme, Dicer, aided by the proteins dsRBD and TAR RNA binding protein (TRBP) cleaves the pre-miRNA to release the miRNA double-stranded RNA duplex.[8] After unwinding of the duplex the mature miRNA strand, which is selected based on its relatively unstable 5' terminus, is loaded into the RNA-induced silencing complex (RISC), and the passenger strand is degraded.[9] RISC along with the Argonaute protein, facilitate binding of the miRNA to its single stranded target mRNA (Figure 1.1).

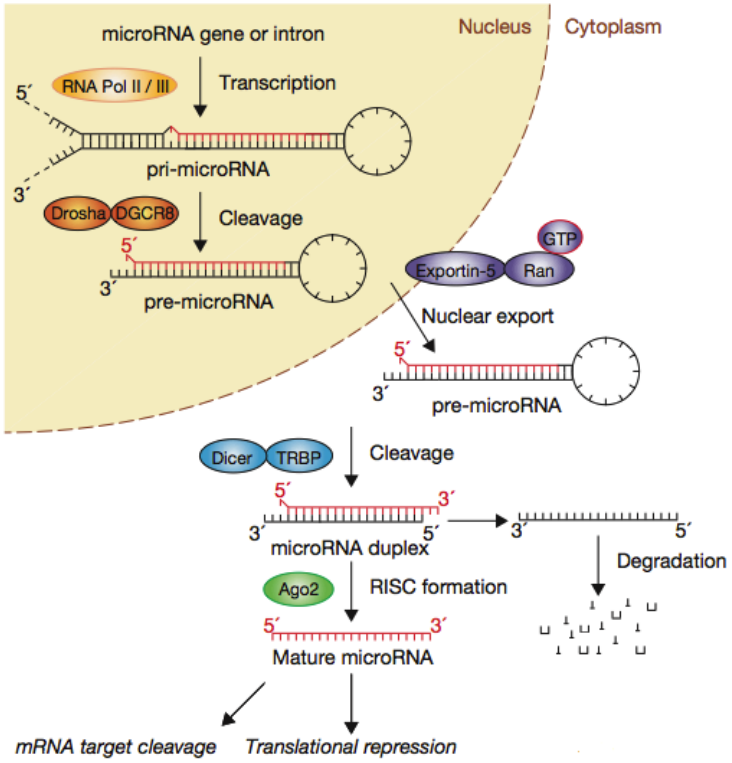

Figure 1.1: The canonical pathway of miRNA processing.
The endogenous miRNA gene is transcribed into a mature microRNA which is then loaded into RISC and matched with its target mRNA to lead to translational repression or mRNA cleavage. Adapted by permission from Macmillan Publishers Ltd: *Nat. Cell Biology*, **2009**, *11*, 3, 228, copyright (2009).

In general, miRNAs regulate gene expression in a sequence-specific fashion by binding to specific regions in the 3'-UTR of target mRNAs. The nucleotides 2-8 located at the 5′-end of the miRNA, called the seed region, is particularly important in mediating the binding of the miRNA to its target mRNA.[10] Recent studies showed that miRNAs can bind to mRNA within their 5′-UTR or their open reading frame, and can interact with promoter regions at the DNA level too.[11] More surprisingly, it was recently discovered that miRNAs can also upregulate protein translation; either by recruiting protein complexes to AU-rich elements of target mRNA, by directly interacting with proteins blocking the translation of the target genes, or by enhancing ribosome biogenesis which stimulates global protein synthesis.[11] These additional miRNA-

regulatory mechanisms have only been observed in a few instances, thus it is not clear whether they represent a new general phenomenon or are only exceptions.[11]

The outcome of miRNA/mRNA interaction is dictated by the degree of base-pairing complementarity between the miRNA and its target mRNA.[2] miRNA binding can induce mRNA degradation when perfect complementarity is observed; this is mostly found in plants. Most commonly in humans, miRNA and its target mRNA bind with imperfect complementarity, leading to the inhibition of translation or inducing the destabilization or de-adenylation of the mRNA.[8, 12] Translational repression can occur through blocking of the initiation of translation, or by sequestering the mRNA in P-bodies away from translational machinery.[13] As there is no need for perfect sequence matching between the miRNA nucleotide sequence and the 3′-UTR target site of the mRNA, a single miRNA can interact with numerous mRNAs, and thus can regulate hundreds of different genes with different strengths,[9] adding an additional layer of complexity. Though the origin of miRNAs remains poorly understood, one hypothesis is that expansion of the miRNA repertoire may be associated with evolution in complex organisms and major body-plan innovations. Indeed, the temporal and spatial expression of distinct sets of tissue-specific miRNAs is critical for the regulation of tissue development and differentiation.[14] Additionally, miRNAs are thought to play essential roles in regulatory networks, conferring them robustness and "fine-tunability", and reducing the developmental noise in these networks by regulating the amounts of proteins resulting from an imprecise number of transcripts.[15]

1.2 MIRNAS AS POTENTIAL DRUG TARGETS

miRNAs are involved in many cellular pathways, notably in fundamental cell processes, such as development, differentiation, proliferation, survival, and death.[16] The misregulation of microRNAs has been linked to a wide range of diseases including viral infections, cardiovascular diseases, and various cancers.[2] miRNAs can be universally expressed throughout an organism or their expression can be limited to a specific developmental stage, a specific tissue, a specific cell type or their expression can follow a disease-specific pattern.[17]

The first evidence of miRNAs involvement in cancer derived from a study of the chromosome 13q14 frequently deleted in chronic lymphocitic leukemia (CLL). The loss of chromosome 13q14 occurs in 69% of CLLs as well as other cancers, such as myelomas and prostate cancer. This region was instinctively expected to contain a tumor suppressor gene but instead this study revealed that it contains the two miRNA genes miR-15a and miR-16-1.[18] It was later established that a downregulation of miR-15a and miR-16-1 induces an increased expression of the anti-apoptotic gene BCL2.[19] Subsequent experiments performed in mice, that developed CLL after being engineered to lack the miR-15/16 cluster, demonstrated that the deregulation of these miRNAs alone can be responsible for cells becoming neoplastic.[20] In a follow-up study it was discovered that many miRNA genes are located in fragile loci or loci prone to amplification in human cancers.[21] Upon cancer development the amplification of a chromosomal region encompassing for an oncogenic miRNA results in the increased expression of this miRNA, and ultimately in the silencing of the targeted tumor suppressor genes. Such miRNAs are commonly named ‘oncomirs’.[8] On the contrary, tumor suppressor miRNAs, which target oncogenes, are often located in regions prone to deletion or mutation. Such events result in

the downregulation of the miRNA and consequently to an increased expression of the target oncogenes.[8]

To maintain homeostasis in cells, miRNAs are organized in precise networks. Similarly, the development and proliferation of cancers are governed by specific networks of miRNAs. For example, 64 aberrantly expressed miRNAs are involved in lung cancer.[22] Studies of 540 patient samples including lung, breast, stomach, prostate, colon, and pancreatic tumors showed a strong correlation between aberrant expression of certain miRNAs and the type of cancer studied.[23] In addition, it was demonstrated through genome-wide profiling that it is possible to distinguish between normal healthy cells, and cancerous cells by investigating the miRNA expression signatures, since a specific pattern in miRNA misregulation and the type of cancer has been observed in several cases.[22] miRNA expression signatures not only allow for the differentiation of healthy and cancerous cells, but can also predict with high accuracy the type of cancer presented as well as the primary origin of the malignant tissue.[8, 19, 23] This observation is highly significant and highlights the potential of using miRNAs for diagnostic purposes.[24]

In addition, it was recently established that circulating miRNAs represent novel, predictable, and non-invasive biomarkers.[25] Quantitative real-time PCR (qRT-PCR) measurements of eight miRNAs expressed in the liver of twenty patients chronically infected with the hepatitis B virus (HBV) and fifteen healthy individuals showed that levels of miR-122 were significantly higher in HBV infected subjects than in the control group. A high plasma concentration of miR-122 coincided specifically with viral-, alcohol-, and chemical-induced liver diseases.[26] Although very appealing, the clinical use of circulating miRNAs as diagnostic and prognostic tools remains a great challenge as there is currently limited overlap between the findings of similar studies of the same disease.[27]

Supported by the initial demonstration of specific miRNAs playing key roles in carcinogenesis, several groups investigated the mechanistic involvement of miRNAs in cancer (**Error! Reference source not found.**).[11] For example, it was reported that miR-17 and miR-21 are consistently upregulated in colon, lung, stomach, prostate, and pancreatic tumors; while miR-155 is upregulated in breast, lung, and colon cancers.[16] In addition to well-known functions of miRNAs as oncogenes or tumor suppressors, it was recently demonstrated that some miRNAs can promote metastasis by regulating cell invasion and migration. An example of these would be miR-10a, whose overexpression in non-metastatic breast cancer cells initiated invasion and metastasis.[28]

The concept of generating potential therapies for human diseases by specifically regulating miRNA activity is rapidly gaining attention. Particularly in the development of cancer therapeutics, where targeting specific miRNAs that regulate entire gene networks rather than targeting a single gene or protein may be highly beneficial.[11] Indeed only a subset of miRNAs is misregulated in cancer, compared to a large number of genes and proteins involved in malignancies.[8] It was reported that 192 miRNAs are deregulated in cancer cells and among them 168 are overexpressed.[29] Over 60% of mRNAs possess at least one conserved miRNA-binding site. In addition, bioinformatics predictions and subsequent experimental confirmations revealed that the 3′-UTRs of single genes can also be targeted through non-conserved binding sites, suggesting that most protein-coding genes may be under the control (at least partial) of miRNAs.[16]

Thus, miRNAs have potential as new, highly promising drug targets, since the specific control of misregulated miRNAs offers the possibility of reversing disease phenotypes. Furthermore, since miRNAs are capable of specifically controlling multiple genes, therapies

targeting one single misregulated miRNA offer the great possibility of regulating entire gene networks.[30]

ncRNA	Type (genomic location)	Cancer involvement	Mechanism of action (target genes)
miR-10b	miRNA (chromosome 2)	Breast cancer	Promotes breast cancer metastasis (*HOXD10*)
miR-15a–miR-16-1	miRNA cluster (chromosome 13)	Downregulated in chronic lymphocytic leukaemia, diffuse large B cell lymphoma, multiple myeloma as well as prostate and pancreatic cancers	Induces apoptosis in leukaemia cells and regulates the cell cycle (*BCL2*, *CCND1*, *CDK6*, *DMTF1*, *MCL1*, *VEGF* and *TP53*)
miR-17–miR-92	miRNA cluster (chromosome 13)	Overexpression in lung and colon cancer, lymphoma, multiple myeloma and medulloblastoma	Increases tumour growth and tumour vascularization (*BIM*, *CDKN1A*, *E2F1*, *E2F2*, *E2F3*, *HIF1A*, *PTEN* and *TGFBR2*)
miR-21	miRNA (chromosome 17)	Overexpression in glioblastoma, breast, lung, prostate, colon, stomach, oesophageal and cervical cancers as well as diffuse large B cell lymphoma	Promotes invasion and metastasis in colorectal cancers; knockdown induces apoptosis in glioblastoma cells (*BCL2*, *SERPINB5*, *PDCD4*, *PTEN*, *TPM1* and *RECK*)
miR-22	miRNA (chromosome 17)	Breast cancer	Regulates breast cancer stemness and metastasis (*TET*)
miR-31	miRNA (chromosome 9)	Breast cancer	Inhibits breast cancer metastasis (*RHOA*)
miR-34a, miR-34b, miR-34c	miRNA family (chromosomes 1 and 11)	Downregulated in pancreatic cancer, Burkitt's lymphoma without *MYC* translocation, $CD44^+$ prostate cancer and human primary breast tumours with lymph node metastases	Transcriptionally activated by p53; miR-34a inhibits prostate cancer stemness and metastasis; miR-34a, miR-34b and miR-34c suppress breast cancer cell invasion and metastasis (*BCL2*, *CCND1*, *CCNE2*, *CDK4*, *MYC*, *MYCN*, *MET*, *HMGA2*, *SIRT1*, *CD44* and *FRA1*)
miR-155	miRNA (chromosome 21)	Overexpression in paediatric Burkitt's lymphoma, Hodgkin's lymphoma, diffuse large B cell lymphoma as well as in breast, lung, colon and pancreatic cancers	Pre-B cell proliferation and lymphoblastic leukaemia or high-grade lymphoma in miR-155 transgenic mice (*AID* and *TP53INP1*)
miR-335	miRNA (chromosome 7)	Breast cancers	Inhibits breast cancer metastasis (*SOX4* and *TNC*)
miR-373, miR-520c	miRNA (chromosome 19)	Breast cancer	Promote migration and invasion of breast cancer cells *in vitro* and *in vivo* (*CD44*)
let-7 family	miRNA family (multiple locations)	Suppressor: downregulated in lung, breast, gastric, ovarian, prostate and colon cancers as well as in chronic lymphocytic leukaemia	Suppressor: represses cell proliferation and growth (*CCND1*, *CDK6*, *HOXA9*, *MYC*, *RAS* and *TLR4*)
		Oncogenic: overexpressed in acute myeloid leukaemia	Oncogenic: let-7a represses *NF2* and decreases chemotherapy-induced apoptosis *in vitro* (*CASP3*)

Table 1.1: Selected miRNAs misregulated in different cancers.
Reprinted by permission from Macmillan Publishers Ltd: *Nat. Rev. Drug Discov*. **2013**, 12, 847. copyright (2013).

1.3 ENDOGENOUS REGULATION OF MIRNAS

Since miRNAs play critical regulatory functions in almost all biological processes and are deregulated in many human disorders, Nature has evolved many means to tightly regulate each and every step of miRNA biogenesis.[31]

Transcription of miRNA genes delivers the pri-miRNAs, which similarly as mRNAs, bear a 5′ 7-methylguanylate cap and have a poly-A tail at their 3′ end.[9] It was shown that miRNA gene promoters share many characteristics with protein-coding gene promoters, including the frequencies of CpG islands, a TATA box, and DNA-binding factors, suggesting that miRNA genes are also subjected to epigenetic regulation.[32] For example the transcription factor c-Myc regulates approximately 15% of all human genes along with some miRNA genes, such as the miR-17-miR-92 cluster. c-Myc controls important genes associated with cell growth and apoptosis and is frequently overexpressed in cancer. Consistently the miR-17-miR-92 is often upregulated in a broad range of cancers.[11] One major hallmark in carcinogenesis lies in epigenetic alterations such as changes in DNA methylation status and chromatin modifications.[33] It is then not surprising that the promoters of several miRNAs have been found to be hypermethylated in multiple cancers. For example, promoter hypermethylation of miR-127 is responsible for aberrantly low levels of miR-127 in bladder cancer.[32] miRNA genes are also regulated by histone modifications. For instance, it was demonstrated that high HDACs expression in CLL causes epigenetic silencing of miR-15a, miR-16, and miR-29b. Treatment with SAHA (an FDA approved HDACs inhibitor) restored the expression of miR-15a, miR-16, and miR-29b and triggered apoptosis.[34]

The processing step of pri-miRs to pre-miRs is carried out by a large complex known as ‘Microprocessor’ composed of Drosha, its binding partner DGCR8, and other cofactors.[32] Multiple mechanisms exist to control the expression level, the activity, and specificity of Drosha. The homeostatic maintenance of the Microprocessor is controlled by a feedback loop involving Drosha and DGCR8. Drosha can specifically cleave a hairpin in the second exon of DGCR8 mRNA, resulting in the destabilization of DGCR8; whereas DGCR8 stabilizes Drosha through

protein-protein interactions.[35] Additionally, the activity, the nuclear localization, and stability of the Microprocessor are tightly regulated by post-translational modifications.[9] The phosphorylation of Drosha at Ser300 or Ser302 by the glycogen synthase kinase 3β (GSK3β) is ensuring its nuclear localization.[36] An unidentified protein can acetylate Drosha which protects it from degradation.[9] DGCR8 is also subjected to modifications, for example HDAC1 was found to deacetylate critical lysine residues in the RNA-binding domains of DGCR8, increasing the affinity of DGCR8 to pri-miR transcripts and causing an increased miRNA processing.[37] Phosphorylation of DGCR8 by the protein kinase ERK promotes its stability.[38] The DEAD-Box RNA helicases p68 and p72 have been reported to associate with DGCR8 and promote the processing of a subset of miRNAs.[32] The maturation of certain miRNAs can also be induced upon interaction of p68 with different proteins such as the signal transducers SMADs, the tumor suppressor protein p53, and the estrogen receptor α.[32] The interaction of two specific SMAD signal transducers with p68 within the Microprocessor was shown to promote a rapid increase in the expression of mature miR-21.[39] Furthermore, the terminal loops of pri-miRNAs are enriched with *cis*-elements that promote the binding of regulatory proteins. For example, Drosha-processing of pri-miR-18a and pri-let-7 is stimulated by the heterogeneous nuclear ribonucleoprotein A1 (HNRNPA1) and KSRP binding to the terminal loops, respectively.[9] LIN28 can specifically bind to the terminal loops of pri-let-7 and pre-let-7, preventing both Drosha- and Dicer-mediated processing.[40] Interestingly, let-7 in turn inhibits LIN28. Few miRNAs are similarly regulated via negative feedback loop mechanisms.

The Dicer mediated-processing of the pre-miRs is also tightly regulated, particularly via the interaction of Dicer and various RNA-binding proteins. For example, Dicer association with TRBP and protein kinase R-activating protein promotes its stability and processing activity.[41]

The homeostatic regulation of Dicer activity is thought to be controlled by a negative feedback loop involving Dicer and the miRNA let-7, as several let-7 binding sites are contained within Dicer mRNA.[42] The stability of the Dicer processing complex is also influenced by diverse signaling pathways. For example, the phosphorylation of TRBP by the mitogen activated protein kinase (MAPK) Erk stabilizes the Dicer-TRBP processing complex, which results in an increased production of growth-promoting miRNAs, such as miR-17, miR-20a, and miR-92a, as well as in the downregulation of the let-7a tumor-suppressor miRNA.[43]

Similarly to Drosha and Dicer, AGO proteins are subject to numerous modifications.[9] For instance, AGO2 phosphorylation at Tyr529 reduces its small RNA binding properties.[44] The maturation and turnover of miRNAs can be affected by alterations in the structure or sequence of the RNA.[9] miRNA biogenesis or target specificity can be altered by single nucleotide polymorphisms. For example, the single substitution of a C to T nucleotide in the pri-miR-16 negatively affects Drosha processing and results in low expression of miR-16.[45] The association of the miRNA-AGO complex to target mRNA not only negatively regulates gene expression, as discussed above, but can also affect the stability of the miRNA itself. When bound to an RNA target, miRNAs are prone to degradation via the addition of adenosine or uracil to the miRNA ('tailing') followed by the 'trimming' or 3′ to 5′-exonucleolytic degradation of the miRNAs.[46] All miRNAs may be susceptible to target RNA-mediated tailing and trimming, but the probability of miRNAs to be degraded via this pathway increases as the complementarity between miRNA and mRNA becomes greater. Highly complementary RNAs have a slower dissociation rate, which facilitates the modification and degradation of miRNAs.[46] For example, the protein LIN-28 has been shown to recruit some terminal uridylyl transferases promoting 3′ uridylation of pre-let-7 and resulting in the degradation of pre-let-7.[47] In the contrary, mass

spectrometry analyses of miR-122 isolated from human hepatocytes and mouse livers, revealed that the 3′ adenylation of miR-122 mediated by the poly (A) polymerase GLD-2 promotes the selective stabilization of miR-122 in the liver.[48] These observations suggest that the consequences of miRNA tailing might be context-dependent and the causes for these differences remain to be elucidated. Other modifications affecting the miRNA sequences have been identified, such as RNA editing and RNA methylation. Adenosine deaminases (ADARs) promote the conversion of adenosine to inosine within the stem region of some pri-miRs, making them poor substrate for Drosha.[9] Drosha and Dicer-mediated processing of miRNAs leave them with a 5′ monophosphate group. The efficient miRNA processing and the stability of the RISC complex are critically driven by the specific interaction of the negatively charged monophosphate at the 5′-end of miRNAs and positively charged pockets in Dicer and AGO2 proteins.[49] It was recently found that the enzyme BCDIN3D can *O*-methylate the 5′ monophosphate group of pre-miR-145, therefore annihilating the negative charge of the transcript and diminishing Dicer-mediated processing.[49] Upon loading into RISC, miRNAs are highly stable since AGO proteins protect both ends. Although miRNA turnover has been investigated in various systems and several nucleases have been proposed to degrade miRNAs, a lot of questions remain unanswered about their selectivity and whether there is a conserved machinery regulating miRNA decay.[9]

All considering, it is evident that Nature has evolved many regulatory mechanisms to tightly control the expression levels of specific miRNAs, and a more precise understanding of these mechanisms will provide exciting opportunities for the development of tools to manipulate the miRNA machinery for therapeutic applications.[50]

1.4 MODULATING MIRNA FUNCTION WITH OLIGONUCLEOTIDES

With the realization of the potential therapeutic significance of miRNAs, substantial efforts have been made to build tools to better understand the mechanisms of action of miRNAs and to enable the control of miRNA function. Based on the finding that several miRNAs are overexpressed in cancer,[19] strategies have been developed in order to inhibit these specific miRNAs. The most commonly employed method is the specific inhibition of miRNA by anti-miRNA oligonucleotides (AMOs).[51] AMOs are synthetic, chemically modified oligonucleotides that possess the exact complementary sequence of the miRNA of interest.[52] They act as competitive inhibitors as they can bind to the mature miRNA guide strand thereby blocking the interaction between the miRNA and its target mRNA. Unlike antisense oligonucleotides, which have been used to repress mRNA expression for over thirty years, unmodified DNA oligonucleotides were not efficient in silencing miRNAs, presumably due to rapid endogenous degradation by exo- and endonucleases.[52] The use of oligonucleotides to repress miRNA function is straightforward in the design of the probes, but can display disadvantages such as limited reagent stability, poor cellular uptake, and low hybridization affinity.[52] These limitations have partially been overcome by installing different chemical modifications on the oligonucleotides (Figure 1.2).[53]

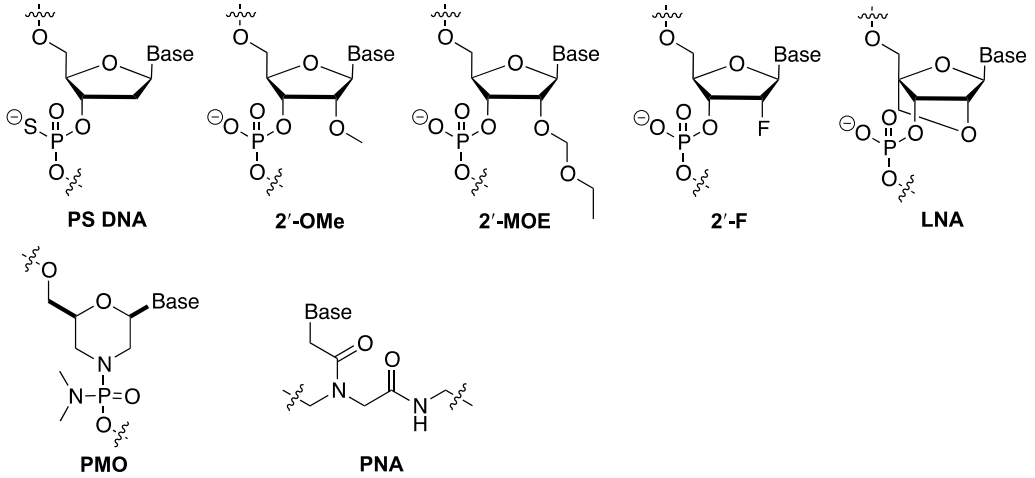

Figure 1.2: Common chemical modifications of AMOs
Include a phosphorothioate linkage (PS DNA), a 2′ methoxy group (2′-OMe), a 2′ methoxyethyl group (2′-MOE), a 2′ fluoro atom (2′-F), a methylene bridge connecting the 2′-O and 4′-C of the ribose ring (LNA), and also replacement of the ribose-backbone with morpholinos (PMO) and peptide nucleic acids (PNA). Base is either a purine motif (adenine or guanine) or a pyrimidine motif (cytosine, uracil, thymine).

The first reports of successful miRNA inhibition using AMO technology appeared in 2004, and employed 2′-*O*-methyl (2′-OMe) AMOs (Figure 1.2).[54] The introduction of 2′- *O*-methyl groups in the ribose ring induces a North conformation in the sugar, similar to RNA, thus 2′-OMe AMOs exhibit an increased binding affinity for RNA targets, as well as an increased nuclease stability.[52] Other substitutions, such as 2′-*O*-methoxyethyl (2′- MOE), and 2′-fluorine (2′-F), similarly resulted in an increased binding affinity and nuclease resistance.[55] These analogs demonstrated more effective miR-21 inhibition than 2′-OMe AMOs (Figure 1.2). Another modification applied to improve oligonucleotide stability consists of replacing a non-bridging oxygen in the phosphate backbone by a sulfur atom, thus preventing nucleases from cleaving the phosphate bonds in between nucleotides (Figure 1.2).[56] Although, the phosphorothioate (PS) motif can be introduced throughout the sequence of the AMO, since the introduction of a sulfur atom in the phosphate backbone decreases the hybridization affinity, phosphodiester and PS linkages have been used in mixed compositions.[56]

Krutzfeldt *et al.* developed a new class of AMOs, called antagomirs. Antagomirs are similar to AMOs but combine complete 2′-OMe modification with PS backbones, and are conjugated at their 3′-end with a cholesterol moiety.[57] Conjugation with a cholesterol motif facilitates AMO delivery into cells (see Chapter 5 for a more in-depth discussion). MicroRNA miR-122 levels were significantly reduced in mice treated with an antagomir bearing six PS modifications; this was the first example of the successful utilization of the AMO technology *in vivo*.[57] Similar rules were established regarding the potency and the specificity of antagomirs. For example they need to consist of >19-nucleotides in length and are sensitive to single base-pair mismatched at certain positions.[57]

AMOs were also generated through addition of a methylene bridge connecting the 2′-*O* and 4′-*C* of the ribose ring, and are known as locked nucleic acids (LNAs) (Figure 1.2). This additional bond locks the sugars of the nucleosides into a North conformation, favorably pre-organizing them for Watson-Crick interactions with target miRNAs.[58] Among all the 2′ modifications developed so far, the introduction of LNA motifs results in the highest increase in binding affinity, adding 1.5-6 °C stabilization per nucleotide.[56] In some cases, it can be beneficial to combine multiple modifications into an AMO. For instance, Fabani *et al.* constructed a miR-122 LNA/2′-OMe mixmer which displayed better potency in miR-122 inhibition than a 2′-OMe AMO.[59] The fate of the miRNAs upon inhibition with an AMO has been unclear and largely debated in the literature.[60] A recent study revealed that the binding of the AMO to the miRNA prevents the miRNA to be properly recovered during the RNA isolation step using common guanidinium-thiocyanate-phenol-choloroform RNA extraction protocols, and could possibly explain the discrepancies observed in different publications. Using an improved RNA isolation method, the authors demonstrated that high affinity-AMOs such as LNA, LNA/OMe mixmers,

and PNA anti-miRs act by sequestering the miRNA, whereas 2′-OMe AMOs seem to promote the degradation of the targeted miRNA.[60]

Taken together, these modifications enable fine-tuning the properties of the AMOs and can dramatically affect the binding affinity to their miRNA targets. Increased binding affinity allowed for shorter oligonucleotides, when the truncations are performed in the 5′-end of the AMO, in order to not disrupt the critical interactions with the seed region of the miRNA (bases 2-8 from the 5′-end).[56] An unconjugated, fully PS modified, 16-mer alternating between two-DNA and one-LNA units resulted in substantial miR-122 knockdown in mice.[61] "Tiny LNAs" correspond to the shortest AMOs that have been successfully used to either repress an entire family of miRNAs (miR-221/222) or an individual miRNA (miR-21).[62] Tiny LNAs are 8-mer, fully LNA and PS modified AMOs that target the seed region of the desired miRNA with a high level of specificity and no undesired off-target effects.

Another class of miRNA inhibitors, miRNA sponges, consists of RNA transcripts containing multiple binding sites for a specific miRNA and can be transiently or stably expressed in cells. The targeted miRNA is sequestered by the multiple binding sites present in the decoys, effectively outcompeting endogenous mRNA targets.[63] Modified oligonucleotides, so called miR-masks, compete with endogenous miRNAs in the binding of the target mRNAs, thereby hiding the miRNA binding site and inhibiting miRNA repression.[64] Unlike AMOs, which prevent miRNA:mRNA interaction by creating AMO:miRNA complex, miR-masks induce gene-specific repression via oligo:mRNA binding, leaving intact the function of the miRNA towards other gene targets.[64]

Likewise, methods have emerged to increase the levels of specific miRNAs. These include the use of miRNA overexpression vectors[65] and miRNA mimics.[66] MicroRNA mimics are small, double-stranded, chemically modified oligonucleotides that function the same way as an endogenously expressed miRNA and are expected to silence the same target genes.

Although chemical modifications allowed for improvements in the stability, the specificity, and the affinity of the oligonucleotides, resulting in a specific, efficient, and long-lasting regulation of miRNA function, this regulation approach still suffers from several limitations (Table 1.2). The main consideration for the development of miRNA therapeutics is to be able to achieve specific delivery of the oligonucleotides (AMOs or miRNA mimics) at a concentration high enough to induce the desired biological effect.[16] Introduction of phosphorothioate linkages, cholesterol conjugation, and 2′-*O*-alkyl groups resulted in an enhanced lipophilicity and greater cell membrane permeability. However, the intestinal absorption of AMOs remains limited, and even though they are broadly distributed, they have a tendency to accumulate in the liver and in the kidneys.[67] In addition, oligonucleotides are rapidly cleared from the bloodstream but are stable in cells, where they have a slow clearance rate and half-lives of several weeks. Since AMOs rapidly disappear from plasma, the nature and the duration of their pharmacological effects are challenging to evaluate.[67] Another obstacle in developing oligonucleotide-based drugs stems from the size and the negative charge of the oligonucleotides. Since these oligos have molecular weights of 2-6 kDa and low intestinal membrane permeability, they are more conveniently formulated as an intravenous injection than as an orally available drug to ensure their bioavailability.

An additional strategy aimed at enhancing the biodistribution and the cellular uptake of oligonucleotides consist of replacing their highly negatively charged backbone with a neutral

backbone. To this end, peptide nucleic acid (PNA) and phosphorodiamidate morpholino oligomers provide effective miRNA inhibitors (Figure 1.2).[59, 68] In addition, high thermal stability of the PNA:target complex is observed. A PNA analog targeting mature miR-122 coupled with four lysine residues, induced miR-122 knockdown after being efficiently taken up by Huh7 cells without requiring any transfection reagent.[59] Morpholino oligonucleotides designed to target the Drosha and Dicer cleavage sites of pre-miR-205 were successfully used to silence miR-205 in zebrafish.[69] Another method aimed at interfering with the processing of precursor miRNAs consists of using DNAzymes.[70] These 30-mer oligonucleotides contain a DNA catalytic domain and two LNA-modified regions that are complementary to the pre-miRNA of interest. Exposure to DNAzymes targeting the precursors of hsa-miR-372 and hsa-miR-373 – at high concentrations – resulted in the specific cleavage of these miRNAs, thus inhibiting their silencing function.

	Advantages	Disadvantages	Modifications	Improvements
Anti-miRNA oligonucleotides	easy design/optimization based on miRNA sequences specific and efficient miRNA inhibitors long-lasting effect	delivery poor cellular-uptake off-target effects toxicity limited stability low hybridization affinity possible stimulation of immune-responses limited biodistribution PC/PK properties difficult to study	phosphorothioate	increased resistance to nuclease degradation and cellular uptake
			2′-*O*-alkyl	increased stability, affinity toward RNA targets, and cellular uptake
			LNA	highly enhanced hybridization affinity lower doses required low toxicity
			cholesterol conjugation	good bioavailability facilitate delivery
miR-masks	gene-specific effects no off-target effects	delivery limited scope (one target)	-	-
miRNA sponges	suitable to silence an individual or an entire family of miRNAs	delivery off-target effects	-	-
PNAs/PMOs	neutral backbone resistant to degradation high stability of the probe-target duplex	delivery	addition of 4-K residues (PNAs)	good cellular-uptake
miRNA mimics	easy design/optimization based on miRNA sequences	global up-regulation off-target effects delivery	same as for AMOs	same as for AMOs
Specific small molecules	good bioavailability fast and reversible effect specific inhibitors/activators systemic delivery good drug-like profile easy delivery regulation possible at different steps of miRNA processing	difficult to identify extensive SAR often required for optimization	-	-

Table 1.2: Limitations and advantages of miRNA regulatory tools.
Adapted with permission from Macmillan Publishers Ltd: *Nat. Rev.* 2010, *9*, 775. Copyright (2010).

1.4.1 Clinical Development of miRNA Therapeutics

Oligonucleotide chemistry and delivery technologies have greatly advanced within the last decade, allowing for the development of highly promising anti-miRNA targeted drugs. The concept of generating potential therapies for human diseases by specifically regulating miRNA activity is rapidly gaining attention and several pharmaceutical companies are actively developing some anti-miR agents for a variety of indications. There is a high number of such anti-miR therapeutics currently in preclinical studies and some examples are shown in Table 1.3.[2]

Santaris Pharma has developed Miravirsen, a new fully PS modified 15-mer comprised of seven DNA and eight LNA nucleotides specific to miR-122, and its successful preclinical studies are paving the way for the application of miRNA-targeted therapies.[71] miR-122 is essential for the replication of the hepatitis C virus (HCV), so specific inhibition of miR-122 by Miravirsen could provide a potential new treatment for HCV.[71] Phase I clinical studies demonstrated that Miravirsen was well tolerated and was not associated with any toxicity issues. Results of the Phase II studies were very promising as four out of the nine patients who received the drug for 4 weeks exhibited a complete reduction in HCV levels.[72] Another candidate, RG-101, is being pursued by Regulus Therapeutics to specifically inhibit miR-122. To improve the biological properties of their anti-miR-122 oligonucleotide, they conjugated the oligonucleotide with *N*-acetylgalactosamine (GalNAc) a highly efficient ligand for the asialoglycoprotein receptor. This receptor is highly expressed on hepatocytes and facilitates liver accumulation as well as the cellular uptake of the GalNAc-conjugated-oligonucleotides via endocytosis.[73] RG-101 has just entered into Phase II clinical studies after an encouraging Phase I completed recently, as no

toxicity or adverse effects were observed, and treatment with a single subcutaneous dose of RG-101 elicited a significant and sustained reduction of viral load in all HCV treated patients.

Using the same strategy, Regulus Therapeutics is developing, RG-125, a GalNAc-conjugated anti-miR targeting miR-103/107 for the treatment of non-alcoholic steatohepatitis in patients with type 2 diabetes. miR-103 and miR-107 directly target a critical regulator of the insulin receptor, the voltage-gated calcium channel Cav1. The silencing of miR-103 and miR-107 has been shown to improve glucose homeostasis and insulin sensitivity.[2] The new insulin sensitizer, RG-125, is expected to enter Phase I studies by the end of 2015. This company is also developing some anti-miR targeted drugs to inhibit miR-21, miR-221, and miR-10b as new anticancer therapies, in particular to treat hepatocellular carcinoma (HCC) and glioblastoma.

Mirna Therapeutics is tackling liver cancer using the opposite approach, which consists of delivering a miRNA mimic of miR-34, MRX34, to reinstate the normal regulation of this miRNA and its target genes.[2] miR-34 is frequently lost or downregulated in a variety of cancers and is estimated to regulate at least 24 known oncogenes involved in proliferation, anti-apoptosis, metastasis, and chemoresistance.[74] MRX34 is delivered by a new liposome-based technology, which enhances the uptake of the mimic into tumor cells and accumulation in the liver. Administration of the miR-34 mimic in mice models induced a reduction in tumor growth and increased overall survival. MRX34 represents the first miRNA mimic to enter clinical trials and is currently being tested in Phase I in patients with primary liver cancers or metastatic cancers with liver involvement.[2]

MicroRNA	Oligonucleotide format	Indications	Companies	Developmental stage
miR-122	LNA-modified antisense inhibitor	HCV infection	Santaris Pharma	Phase II
miR-122	GalNAc-conjugated antisense inhibitor	HCV infection	Regulus Therapeutics	Phase I
miR-34	miRNA mimic replacement	Liver cancer or metastasized cancer involving liver	miRNA Therapeutics	Phase I
Let-7	miRNA mimic replacement	Cancer (details undisclosed)	miRNA Therapeutics	Preclinical
miR-21	2′-F and 2′-MOE bicyclic sugar modified antisense inhibitor	Cancer, fibrosis	Regulus Therapeutics	Preclinical
miR-208	Antisense inhibitor	Heart failure, cardiometabolic disease	miRagen/Servier	Preclinical
miR-195 (miR-15 family)	Antisense inhibitor	Post-myocardial infarction remodelling	miRagen/Servier	Preclinical
miR-221	Antisense inhibitor	Hepatocellular carcinoma	Regulus Therapeutics	Preclinical
miR-103/105	Antisense inhibitor	Insulin resistance	Regulus Therapeutics	Preclinical
miR-10b	Antisense inhibitor	Glioblastoma	Regulus Therapeutics	Preclinical

Table 1.3: Selected examples of miRNA-targeted therapies under development**.**
Adapted with permission from Macmillan Publishers Ltd: *Nat. Rev. Drug Discov*. **2014**, 13, 622. Copyright (2014).

1.5 MODULATING MIRNA FUNCTION WITH SMALL MOLECULES

Although the recent advances in oligonucleotide-based miRNA therapeutics are very exciting and promising, several challenges still remain to be tackled, particularly due to their less than ideal pharmacodynamic and pharmacokinetic properties.[3] Small molecules capable of specifically modifying the activity of miRNAs provide excellent new alternative therapeutic approaches, as they possess several advantages over oligonucleotides (Table 1.2). For example, they are typically cell permeable, enabling systemic delivery, they induce fast and reversible regulation, and their biological effect is directly linked to their concentration, facilitating a dose-dependent modulation of biological activity.[75] Small molecules generally have a molecular weight <800 Da and can be modified with functional groups that provide good solubility, good

bioavailability, and good pharmacokinetic properties.[29] However, it is important to note that specific small molecule regulators of miRNA activity are challenging to discover. Their discovery often requires the screening of large size libraries to identify a hit compound, followed by several confirmatory assays and extensive structure-activity relationship (SAR) studies to optimize their activities and properties. In contrast the binding affinity and the specificity of AMOs are inherent to their sequence and backbone modifications are more readily introduced than the SAR investigations of small molecules. While nucleic acid-based inhibitors typically interact with mature miRNAs, small molecules have the potential to control miRNA function on multiple levels of the miRNA pathway, including pre-transcription, transcription, and post-transcription.[3] Small molecules are easier to deliver into humans and animals than oligonucleotides, they are cheaper to manufacture, resistant to nucleases and typically exhibit lower toxicity. Therefore small molecules possess a better drug-like profile and are more amenable for drug discovery than oligonucleotides.

Recently, several small molecules that can modulate miRNA activity, either in a general or specific fashion have been discovered (Figure 1.3 and Figure 1.5).

1.5.1 Small Molecule General Modulators of the siRNA and miRNA Pathways

Although RNA molecules have had a long reputation of being "undruggable" because of their highly negatively charged surfaces, their flexibility, and the paucity of information regarding the interaction of RNA/small molecules, as well as the lack of structural information (X-ray or NMR), the discovery of ligands that can successfully bind with ribosome RNAs or viral transactivation response RNAs, have encouraged efforts involving the design of small molecules to directly target miRNAs.[29] The secondary structure of miRNAs, especially the stem-

loops found in pre-miRNAs and the bulges found in mature miRNAs, represent attractive target sites for small molecule ligands. A screen of different classes of small molecules, including approved drugs, antibacterial agents, anticancer therapeutics, and DNA/RNA intercalating agents, against pre-miR-155 and Dicer-catalyzed miRNA maturation, revealed that some aminoglycoside antibiotics and some anticancer agents can bind to the precursor pre-miR-155 with good affinity.[76] This study represented a proof-of-principle for the promising concept of directly targeting miRNAs. However, the aminoglycosides framycetin and kanamycin B, which exhibited the strongest binding to pre-miR-155 lacked specificity and were ineffective in repressing miRNA maturation.[76] A small series of aminoalkoxy-substituted thioxanthones was synthesized and the binding of the derivatives to RNA bulges and loops was subsequently investigated using pre-miR-29a as a model. Although it was demonstrated that the thioxanthone analog **1** is able to bind the pre-miR-29a proximal to a processing site, thereby preventing Dicer processing, the selectivity of **1** was not addressed.[77] Given pre-miRNAs display a high degree of structural similarity, it can be envisioned that targeting pre-miRNAs with small molecules might result in a lack of selectivity. A series of multimodal ligands composed of two RNA binding motifs, an artificial nucleobase and the aminoglycoside neomycin, was designed to target the oncogenic pre-miR-372 and pre-miR-373.[78] The best analog (**2**) was found to efficiently inhibit Dicer processing of pre-miR-372 and -373 with an IC_{50} of 2.4 μM, and more importantly it was shown to inhibit the cell growth of AGS gastric cancer cells, which express high levels of miR-372 and -373. Following qRT-PCR experiments highlighted a lack of specificity for **2** since at least three other miRNAs (miR-17-5p, miR-21, and miR-200b) were downregulated upon treatment with the ligand **2**.[78] A set of 1,990 compounds from the NCI Diversity Set was screened in a computational screening approach based on the 3D structure of the Dicer binding

site on the pre-miR-21.[79] Out of the 5 hit compounds, having the highest docking scores, the carbonitrile AC1MMYR2 (**3**) was found to reduce the levels of miR-21 by 50% after 6 h treatment at a dose of 30 μM. This inhibitor blocked miR-21 maturation in 4 cancer cell lines and induced a decrease in tumor growth, invasiveness, and metastasis by upregulating known tumor-suppressor genes targeted by miR-21. Unfortunately **3** did not appear to be specific for miR-21, as 5 randomly tested miRNAs (out of 11) were also downregulated after 24 h treatment.[79]

The fluoroquinolone antibacterial agent enoxacin (**4**), which acts an RNA interference (RNAi) enhancer, was identified via a screen of 2,000 FDA-approved drugs in a cell-based assay monitoring RNAi activity. The majority of the miRNAs altered by enoxacin exhibited decreased levels of pri- and pre-miRNAs, and inversely they displayed up to 2-fold increased levels of mature miRNAs. It was shown that the presence of **4** improved the binding affinity of the trans-activation-responsive region RNA-binding protein (TRBP) for pre-miRNAs, thereby promoting the processing and loading of miRNAs into the RISC.[80] Similarly, a general activator of miRNA function (**5**) was identified after screening of eight products obtained from the photoreaction of naphthalene-1,4-dione and acetylenes in cellular assays using a luciferase reporter under the control of several mature miRNAs.[81] The exact mode of action for the anthracene derivative **5** has not been fully elucidated, but preliminary results suggest that it generally up-regulates mature miRNA levels by promoting the maturation of miRNAs.

An *in vitro* assay measuring the interaction between miR-21 and the Argonaute 2 (Ago2) protein was used to screen 1,280 compounds from the LOPAC collection and 1,040 compounds from the National Institute of Neurological Disorders and Stroke. The Argonaute proteins constitute the catalytic components of the RISC assembly and are therefore indispensable to the

loading of miRNAs into RISC.[82] The inhibitors suramin (**6**), aurintricarboxylic acid (**7**), and oxidopamine (**8**) were identified, however only **7** was effective in repressing the loading of small RNAs to Ago2 in a cell-based assay (Figure 1.3). The triphenylene compound **7** does not disturb the catalytic activity of Ago2 but rather prevents its binding with small RNAs in a non sequence-specific fashion.[83] A new inhibitor of Ago2 (**9**) was recently identified via an *in silico* HTS based on the crystallographic structure of Ago2 bound to miR-20a. The inhibitor **9** was found to efficiently bind to Ago2, and to impair Ago2 loading of miRNA, non-specifically.[84] Two additional suppressors of miRNA function, poly-L-lysine (**10**) and tripaflavine (**11**), were discovered from a library of 530 compounds by screening for the inhibition of the RNAi pathway using a firefly luciferase reporter system and a simultaneously expressed shRNA targeting the firefly gene in HEK293T cells. Since shRNAs and miRNAs follow a similar processing pathway in cells, **10** and **11** were tested for their ability to inhibit miRNA function. Each compound exhibits a different inhibitory mechanism, as **10** interferes with the association of pre-miRNAs and Dicer, and **11** prevents the formation of Ago2/RNA (siRNAs or miRNAs) complexes.[85] Additional inhibitors (**12**, **13**) of the siRNA pathway were discovered via screening of a small library of ATP analogs in HeLa cells co-transfected with a plasmid harboring the red- and green-fluorescent proteins and an siRNA targeting EGFP.[86] These two RNAi inhibitors (**12**, **13**) were found to affect an early ATP-dependent step of the RNAi pathway, specifically they prevent the unwinding of the siRNA.[86]

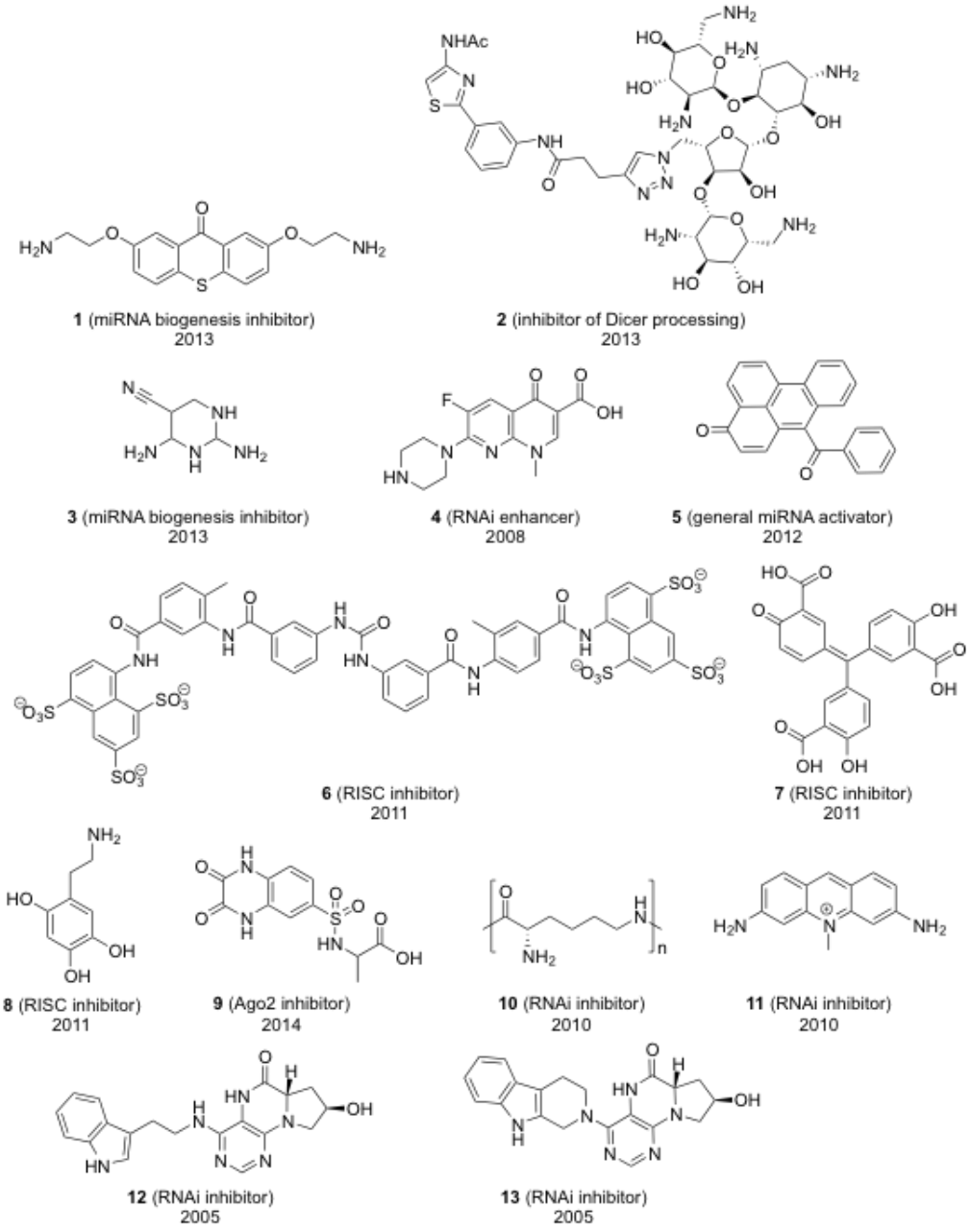

Figure 1.3: Reported small molecule general modifiers of the miRNA or siRNA pathway.
The year of their discovery is indicated.

Overall, these small molecules constitute good tools to investigate miRNA biogenesis in a general fashion; however, they are not suitable for studying the effects and regulation of individual miRNAs.

1.5.2 Regulation of miRNA Function with Approved Drugs

Since it was established that the deregulation of miRNA function is closely associated with many disease-states, the opposite approach consisting in evaluating the effects on miRNA expression after treatment revealed that some of the beneficial effects provided by some approved drugs, were due in part to the drugs' ability to modify the expression levels of a few miRNAs. The reference drug against colorectal malignancies, 5-fluorouracil (5-FU, **14**), was shown to significantly alter the expression levels of 22 miRNAs (over 153 were tested) in colon carcinoma cell lines, and most of those are known to target genes involved in cell proliferation and carcinogenesis.[87] Although the combination treatment of 5-FU and oxaliplatin (**15**) is widely used against colorectal cancer, notably in patients who present metastasis, the molecular mechanisms for the anti-tumor effects remained unknown.[88] It was demonstrated that some miRNAs were significantly up- or downregulated upon co-treatment of 5-FU and oxaliplatin in colon cancer cells. Out of the 15 downregulated miRNAs, the 6 miRNAs (miR-191, miR-93, miR-92a, miR-222, miR-197, miR-1826) most strongly affected by the drugs are overexpressed in various cancers. The pharmacodynamic mechanisms of these anticancer agents could in part be due to their influence on miRNA gene expression.[88] A recent study aimed at investigating the miRNA expression profile following treatment with the chemotherapeutic agent doxorubicin (**16**), showed that miRNA expression was altered differently depending on the breast cancer cell subtypes luminal-A or triple negative. Upon exposure to doxorubicin thirteen miRNAs were found to be generally modified in all subtypes tested, whereas the expression levels of twenty-five miRNAs were specifically modified in the triple negative cells and sixty-nine only changed in the luminal-A cell line. As previously observed, cancer-associated miRNAs were the most strongly perturbed by treatment with doxorubicin.[89]

Similarly, some natural products currently used in therapies or in the diet have been found to possess anticancer properties due to their involvement in the regulation of multiple signaling pathways. Since a hallmark of miRNAs is the targeting of multiple genes, miRNAs were hypothesized to be key intermediates in the regulation of the broad range of gene networks targeted by natural agents.[90] A natural product derived from turmeric, curcumin (**17**), exhibits potent anticancer properties in cell culture as it was shown to inhibit cell proliferation, angiogenesis, migration, and to promote apoptosis in a wide range of cancers. Some insights into the pharmacodynamic mechanisms of curcumin revealed that it causes the upregulation of several tumor suppressor miRNAs, for example miR-181b, miR-15a, miR-16, miR-203, miR-22, and/or the downregulation of diverse oncomiRs, such as miR-21.[90] The isoflavone derivative genistein (**18**) exhibits antioxidant and anticancer activities and causes cell cycle arrest, apoptosis and inhibits angiogenesis and metastasis in various cancers. In a similar fashion as curcumin, genistein exerts its anticancer properties via the upregulation of three tumor suppressor miRNAs, including miR-34a, and the inhibition of at least seven miRNAs whose overexpression is strongly associated with cancer phenotypes, such as miR-221 and -222.[90] A few additional examples encompass the phytoalexin resveratrol (**19**), the major polyphenol component of green tea epigallocatechin-3-gallate (**20**), the vegetable glucosinolates indole-3-carbinol (**21**) and 3,3'-diindolylmethane (**22**), which all up- or downregulate several miRNAs to counteract with the deregulation of principal pathways involved in the development of cancer (Figure 1.4).[90] Based on these observations, there has been a rising interest in studying naturally occurring substances as new lead compounds to treat human diseases.[91] A recent study reported that a combination of plant-derived polyphenols could limit fatty liver diseases by slightly upregulating miR-103 and miR-107 expression levels and downregulating miR-122.[92] The fungal metabolite diaporine A

(**23**) was identified in a recent screen of endophyte-derived products, and was found to efficiently inhibit the viability, the proliferation, and the colony formation of non-small cell lung cancer cells. Further analysis into the mode of action of diaporine A revealed that its anticancer effects rely in part on the regulation of the mTor signaling pathway via the upregulation of miR-99a, in a non-highly specific fashion since at least four other miRNAs were also found upregulated, albeit less strongly than miR-99a.[91]

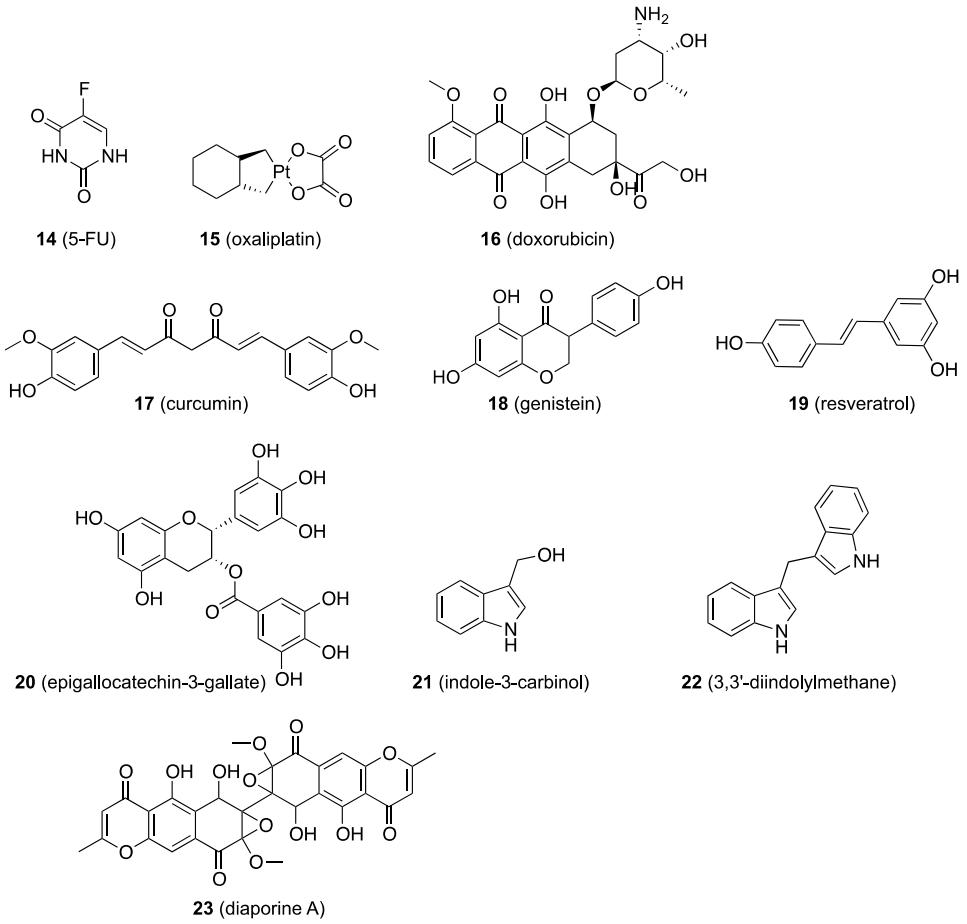

Figure 1.4: Structures of selected approved drugs (14, 15, and 16) and natural products (17-23) known to exert anticancer properties via the regulation of miRNA expression.

1.5.3 Specific Small Molecule Modifiers of miRNA Function

In 2008 the first small molecule inhibitor of a specific miRNA, the oncogenic miR-21, was discovered by the Deiters and Huang labs.[93] A primary screen of the LOPAC collection and additional custom synthesized compounds against a luciferase sensor of miR-21 expression in HeLa cells revealed a diazobenzene hit compound, which was further structurally modified to discover the potent inhibitor **24**. Its selectivity for miR-21 inhibition was confirmed in a counter screen with a miR-30a reporter and by qRT-PCR. A combinatorial library composed of 14,024 peptoid analogs were screened for ligands able to bind to the apical loop of pri-miR-21. The hit compound **25** was shown to specifically interfere with the proper processing of the pri-miR-21, at a high concentration (150 μM).[94] Based on the known interactions of aminoglycosides with stem-loops and bulges in RNA molecules, fifteen aminoglycosides were tested as potential inhibitors of pre-miR-21.[95] Here, MCF-7 cells transfected with a construct expressing firefly luciferase under control of mature miR-21 revealed that streptomycin (**26**) is able to inhibit miR-21 function by directly interacting with its precursor pre-miR-21, thereby preventing processing by Dicer. The expression levels of nine oncomiRs were measured following exposure to streptomycin, as eight miRNAs were unaffected streptomycin was reported to be mostly a miR-21 inhibitor.[95] Although quite appealing, the idea of designing ligands to directly bind with specific miRNAs appears highly challenging as numerous miRNAs have similar stem-loop hairpin structures. As the understanding of the rules for RNA-small molecules binding expands, it might become conceivable to predict and fine-tune the selectivity of the ligands to specifically target one desired miRNA.

Some computational-based methods have recently been implemented which allow for a "bottom-up" or rationale design of small molecules targeting RNA. One such strategy, named

Informa, analyzes the targetable motifs present in the RNA transcripts of interest and generates a list with corresponding molecules previously shown to bind to those motifs.[96] The Informa screening platform was used to identify small molecules interfering with the Dicer processing of a subset of pre-miRNAs. To assess the validity of these newly predicted lead compounds, three small molecule/pre-miRNA pairs were further investigated. Very interestingly, the compound **27** efficiently blocked the maturation of its target pre-miR-96 as it reduced the expression level of miR-96 by 90%, and was found to be more selective towards miR-96 than an LNA oligonucleotide targeting the miR-96's seed region.[96] Following a similar approach, wherein a library of aminoglycoside analogs was screened against an RNA library containing discrete secondary structural elements to identify favored small molecule/RNA internal loops interactions, the specific miR-10b inhibitor **28** was discovered. Since it was recognized that one of the internal loop motif presents in the library corresponds to the Drosha processing site of pri-miR-10b, the associated binding partner, guanidinylated neomycin (**28**), was tested for miR-10b inhibition. As expected, **28** was found to inhibit the biogenesis of the metastasis-associated miR-10b.[97]

A dual luciferase-based reporter system for miR-122 in Huh7 cells was used to identify the two specific inhibitors **29** and **30**, and the specific activator **31** from a screen of 1,364 compounds (NCI Diversity Set II).[98] MicroRNA-122 was targeted because of its involvement in several liver disorders, including Hepatitis C virus infection and hepatocellular carcinoma (the potential therapeutic of these compounds will be discussed in chapter 3). A similar screening approach was employed to identify a small molecule specific activator of miR-34a. The plant chalcone derivative, rubone (**32**), was found to specifically upregulate miR-34a in a p53-dependent pathway and to potently inhibit tumor growth in HCC cell lines, even more efficiently

than the reference anti-HCC drug sorafenib.[99] Aza-flavanone compounds display a broad spectrum of biological activities, and it was discovered that they can act as specific inhibitors of miR-4644 and its fly homologue miR-14. Aza-flavanones that showed cytotoxicity against MCF7 cells were tested in a cell-based assay against the anti-apoptotic miR-14 (Drosophila)/miR-4644 (human). The aza-flavanone analogs **33** and **34** were identified as highly effective small molecule inhibitors of miR-4644, promoting cell death in breast tumors.[100] The small molecule miR-1 inhibitor **35** was recently discovered after screening of 10 products derived from the [2+2] photocycloaddition of diverse aryl acetylenes with 2-methoxy-1,4-naphthalenequinone. The selectivity of **35** was assessed by qRT-PCR and using a subset of reporter constructs having the luciferase gene under the control of different miRNAs. The quinoline derivative efficiently and selectively inhibits miR-1, whose dysregulation has been reported in coronary artery diseases.[101]

A new class of specific miR-122 inhibitor has been reported that combines an Ago2 active site binder with a small PNA targeting a short specific sequence within the seed region of miR-122.[102] 627,000 compounds were screened *in silico* to find privileged scaffolds that can interact with Ago2 binding site. A small series of Ago2 binders were synthesized and further derivatized with a PNA tetramer specific for miR-122. Two mixed-inhibitors, including **36**, were found to inhibit the Ago2 RNA cleavage activity with an IC_{50} of 100 nM. Although these mixed inhibitors provide a quick and interesting approach to the inhibition of virtually any miRNA - the general Ago2 binder can be coupled to any short PNA sequence of interest - these inhibitors have a high molecular weight (<1500 Da) and might suffer from delivery issues similar to AMOs. Further insights into the activity in cell-based assays and the selectivity of these mixed inhibitors are needed to fully evaluate this new inhibition strategy.

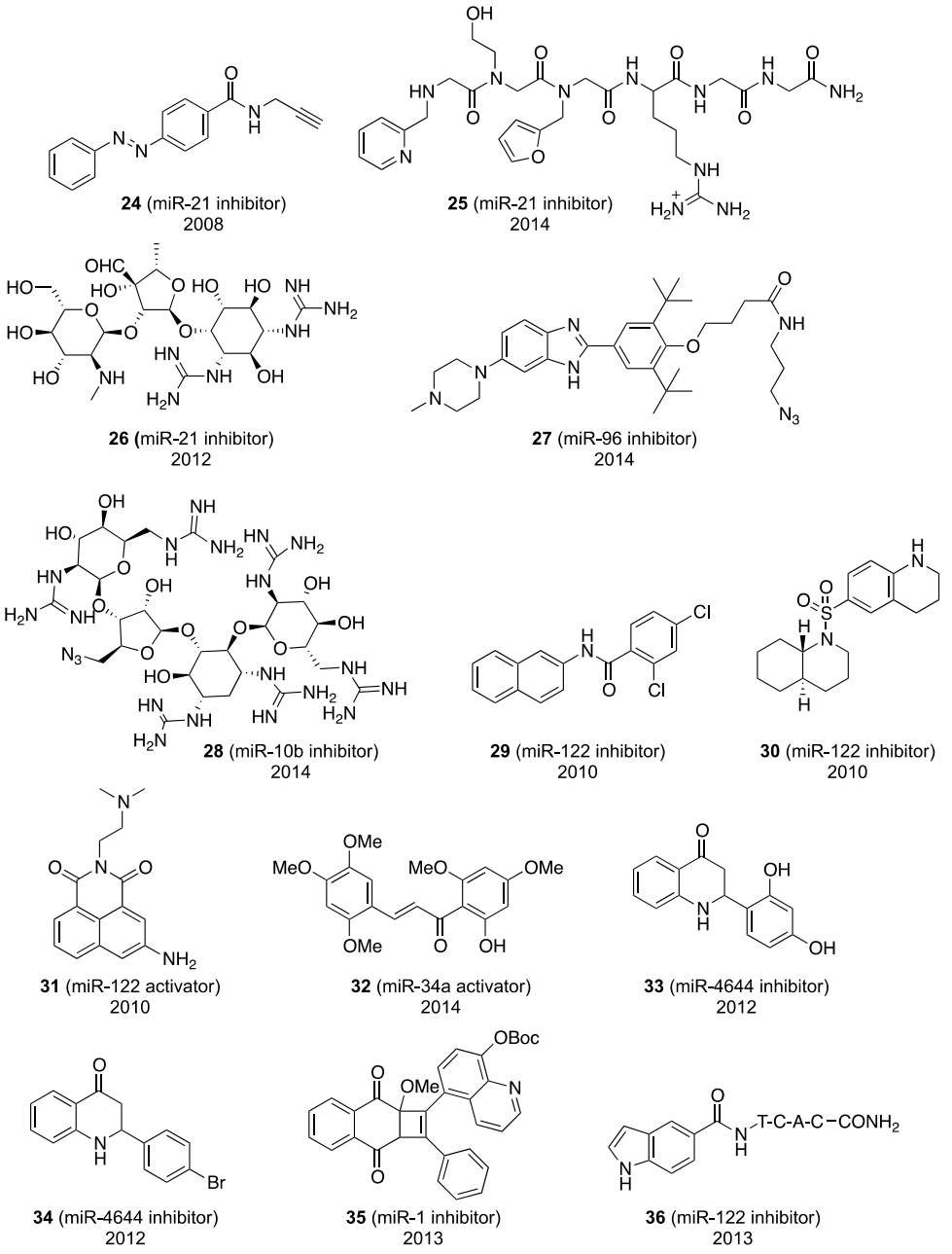

Figure 1.5: Reported small molecule specific modifiers of the miRNA function.
Specific miRNA inhibitors include (**14-20**, **23-26**) and specific miRNA activators include (**21** and **22**). The year of their discovery is indicated.

The research presented here attempts to expand on the existing tools to specifically regulate the activity of miR-21 and miR-122. The precise regulation of specific miRNAs is highly sought after as a mechanistic tool to study miRNA biogenesis and function as well as new

therapeutic avenues. Extensive investigations of the previously discovered miR-21 and miR-122 inhibitors (Figure 1.5) were conducted through high-throughput screening, hit validation, and structure-activity relationship studies. Also discussed here is the development of chemical probes and assays to study the mechanism of action of the presented small molecule miR-21 and miR-122 inhibitors. The discovery of specific miRNA/small molecule pairs provides a novel way to study miRNA biogenesis as well as to investigate the development of different diseases, such as cancer, and offers new therapeutic approaches to specifically target different stages of the disease for a better treatment efficacy.

2.0 SYNTHESIS OF SMALL MOLECULE INHIBITORS OF MIR-21

2.1 INTRODUCTION TO MIR-21

miR-21 is derived from a gene located on chromosome 17q23.2, and though the miR-21 coding gene overlaps with the TMEM49 protein coding gene, miR-21 contains its own dedicated promoter.[103] miR-21 is arguably the most studied miRNA due to its implication in many human disorders, such as cardiovascular and pulmonary diseases, and more notably in cancers.[103] miR-21 is significantly up-regulated in nearly all types of human cancer; for instance, miR-21 overexpression has been established in breast, colon, lung, pancreas, prostate, stomach, and leukaemic cancers.[104] These observations spurred investigations into miR-21 regulation and the development of chemical tools as specific miR-21 inhibitors. The genes targeted by miR-21 are similarly involved at various stages in the development of human carcinomas. The principal target of miR-21, programmed cell death 4 (PDCD4), is a potent tumor suppressor. As a result of miR-21 ectopic expression, PDCD4 is downregulated in various cancers and loss of PDCD4 expression in lung and colorectal cancers is often associated with a poor patient prognosis.[105] Other miR-21 targets include the reversion inducing cysteine-rich protein with kazal motifs (RECK), a membrane protein whose inactivation seems to promote invasion and metastasis of various cancers,[106] tropomyosin 1 (TPM1), whose expression potentially slows down cell growth and invasiveness of breast carcinomas, and the protein Sprouty2 (SPRY2) whose downregulation

affects cellular outgrowths, branching, and migration.[107] Another notable miR-21 target is the well-known tumor suppressor phosphatase and tensin (PTEN) homologue.[108] It was demonstrated that direct repression of PDCD4 by miR-21 promotes chemoresistance to the chemotherapeutic agent docetaxel. Treatment of docetaxel-resistant cells PC3R with a 2′-OMe-modified AMO to selectively inhibit miR-21 restored both PDCD4 expression and sensitivity to docetaxel.[109] The first *in vivo* demonstration of the importance of miR-21 in cancers was established by the Slack group.[110] They developed a mouse model based on Cre and Tet-off technologies where miR-21 expression can be easily turned on/off by doxycycline induction/withdrawal. Expression of miR-21 was normal in mice fed with doxycycline, whereas in mice fed with standard food (without the drug) miR-21 was highly overexpressed. Mice taken off doxycycline showed a tenfold increase in miR-21 expression levels, which is comparable with the miR-21 overexpression commonly observed in several human malignancies. Three months after doxycycline withdrawal, serious signs of lymphoma started to appear, whereas mice continually fed the drug were healthy. These results suggested that miR-21 up-regulation is necessary for the initiation of the cancer phenotype.[110] After the mice showed unambiguous signs of lymphoma, they were fed doxycycline; miR-21 expression levels were returned to normal within a week and, importantly, full tumor regression was observed in all mice. Taken together, this data demonstrated that overexpression of miR-21 not only largely increases the risks of initiation of tumors but is also necessary for the maintenance of malignancies.[110] Small molecule regulators of miR-21 activity represent unique and novel tools to investigate the molecular mechanisms of chemoresistance and provide fundamentally new therapeutic agents for the treatment of cancer.

2.2 PREVIOUS WORK: DEVELOPMENT OF A REPORTER ASSAY FOR MIR-21 FUNCTION AND ITS APPLICATION TO THE DISCOVERY OF THE FIRST SMALL MOLECULE INHIBITORS OF MIR-21

The first small molecule inhibitor of miRNA, miR-21, was identified by the Deiters lab in collaboration with Dr. Qihong Huang at the Wistar Institute.[93] They developed a lentiviral reporter assay to identify small molecules that specifically modulate miR-21 activity. Since mature miRNAs bind to the 3′-UTR of their target mRNAs to negatively affect gene expression, plasmids containing a luciferase gene with a miRNA target sequence located in the 3′-UTR can be used as sensors. A reduction in the luminescence signal indicates the presence of the miRNA, whereas restoration of the signal indicates any interference with the function of the miRNA of interest, for example its inhibition with a small molecule. A lentiviral reporter construct for miR-21 (Luc-miR-21) was created by introducing the complementary sequence of mature miR-21 downstream of the firefly luciferase reporter gene (Figure 2.1). A similar lentiviral construct containing the target sequence for miR-30a was also constructed as a selectivity control.

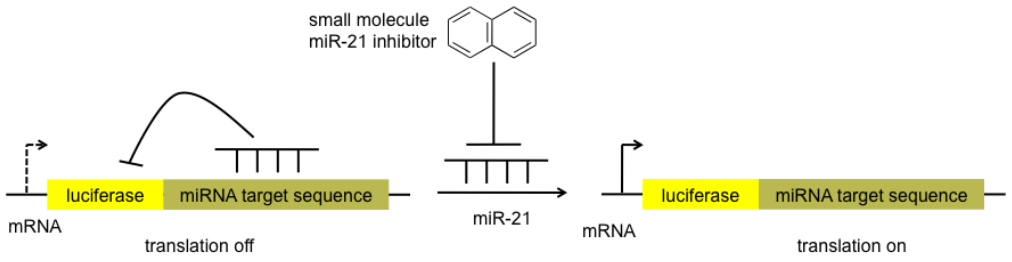

Figure 2.1: Assay for small molecules interfering with miR-21 function.
A miR-21 target site was introduced in the 3′-UTR of a firefly luciferase gene. The presence of mature miR-21 in cells transfected with the reporter construct leads to a decrease in luciferase expression. The presence of a small molecule that inhibits miR-21 prevents the interaction of miR-21 with its target site, leading to an increase in luciferase signal.

The reporter construct was transfected into the human cervical cancer HeLa cell line, selected based on its high expression levels of miR-21 but relatively low levels of miR-30a.[111] A

90% decrease in the luciferase signal was observed when the cells were transfected with the Luc-miR-21 reporter compared to the control luciferase-linker construct that does not possess any known miRNA target sequence, indicating the ability of the sensor to detect endogenous miR-21.[93] When the cells were transfected with the Luc-miR-30a construct, only a slight decrease in the luciferase signal was observed due the low level of endogenous miR-30a. These results demonstrated the feasibility to use the reporter system to accurately and selectively detect endogenous miRNAs, as the reporter is sensitive enough to distinguish between different miRNAs. A pilot screen of 1,000 small molecules (Library of Pharmacologically Active Compounds and in-house set of compounds) was then performed in HeLa cells stably transfected with the Luc-miR-21 reporter assay. This primary screen revealed the initial hit compound **37**, which produced a 251% increase in the luciferase signal, in comparison with DMSO (dimethyl sulfoxide) treated cells that did not have any effect on the signal intensity. This hit compound was then submitted to structural modifications and additional screening rounds that led to the identification of the structurally similar diazobenzene **24**. Compound **24** is the most potent miR-21 inhibitor discovered so far. At a concentration of 10 μM, it induces a 485% increase in luciferase signal in the miR-21 assay.[93] Chemical modifications were performed on compounds **24** and **37** to understand which functional groups are responsible for their high activity in the miR-21 assay and to further improve their activity (Figure 2.2).

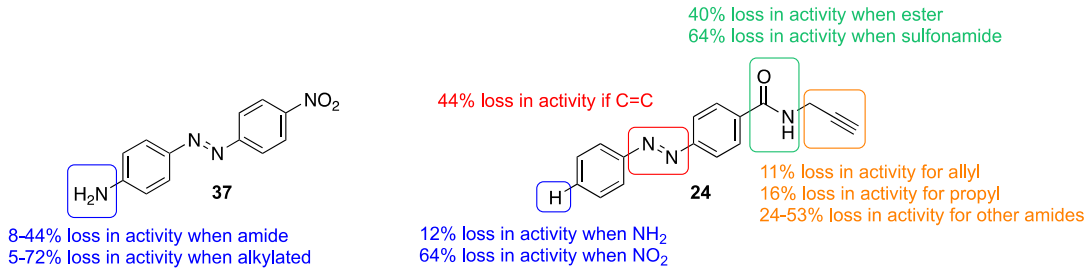

Figure 2.2: Preliminary structure-activity relationship data for compounds 37 (left) and 24 (right).
Adapted from *Angew. Chem. Int. Ed.* **2008**, *47*, 7482.

Dose-response studies for compound **24** were carried out at concentrations ranging from 0-10 μM and revealed a dose-dependent response, as well as an EC_{50} value of 2 μM for **24**.[93] To assess the specificity of the inhibitor, HeLa cells stably transfected with either the luciferase linker construct or with the Luc-miR-30a reporter were treated with **24** at 10 μM for 48 h. The diazobenzene inhibitor had no effect on the luciferase signal of the linker construct (without any known miRNA target site), nor did it affect the signal intensity of the Luc-miR-30a reporter. These results confirmed that **24** is not a general inhibitor of the miRNA pathway and displays some selectivity for miR-21. qRT-PCR experiments were performed to measure the intracellular level of miRNAs. In accordance to what was observed in the luciferase reporter assay, treatment of HeLa cells with **24** at 10 μM did not affect the expression of miR-30a, nor miR-93, as the levels of mature endogenous miR-30a and miR-93 were not diminished. In comparison, treatment with **24** led to a reduction of 78% in miR-21 expression in HeLa cells relative to DMSO treatment. Likewise, qRT-PCR measurement of the intracellular levels of pri-miR-21 after treatment with compound **24** revealed an 87% reduction in pri-miR-21 levels in HeLa cells. These results suggested that the diazobenzene **24** might inhibit transcription of the miR-21 gene into pri-miR-21, rather than the downstream maturation processes.[93]

2.2.1 Structure Activity Relationship Studies of the Previously Discovered miR-21 Inhibitor 24

The previously discovered miR-21 inhibitor represents the first example of specific regulation of miRNA with small molecules, but even though **24** is quite active and selective towards miR-21 downregulation, this compound suffers from poor solubility in water and presents a metabolically susceptible diazo-bond, thus preventing its application in animal studies.

Indeed, azo linkages are rapidly reduced and metabolized by azo-reductase enzymes. Actually, the introduction of an azo bond into an active compound is a well-established prodrug strategy, particularly in agents used to treat localized diseases of the colon.[112] These azo derivatives pass unaffected through the intestine where they are poorly absorbed, which allows them to be site-specifically released in the colon where there is a high level of azo-reductases secreted by colonic bacteria.[113] For that reason it seemed desirable to replace the azo-bond of **24** with a more stable motif. The preliminary SAR study revealed that an alkene bond instead of the nitrogen double bond negatively affected the activity, so it was decided to introduce an amide linkage instead (Figure 2.3). The exact analog of **24** substituted with an amide bond in place of the diazo-bond (**38**) displayed a 20% reduced activity in comparison with **24** (Figure 2.3). Modification of the propargyl group with a bulkier benzyl group (**39**) further reduced the activity. Since the inhibitor possesses an alkyne bond, which can be used in a click reaction to modify the compound with various tags, for example with a fluorophore, the benzophenone **40** was designed to assess its potential application in target identification experiments (as will be discussed later). The benzophenone group is a good photoprobe and is commonly used to map small molecule/protein interactions.[114] Unfortunately modification in the *para* position of the amide bond was not tolerated as **40** and **41** exhibited a 40% reduction in activity compared to **24**.

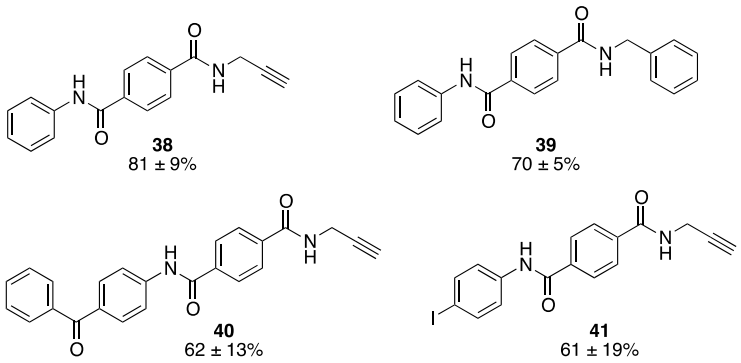

Figure 2.3: Analogs of **24** designed to replace the azo-bond with an amide group.
The numbers represent the activity relative to **24** within the same luciferase assay. Experiments were performed in triplicate and the standard deviations of three independent assays were calculated. Cell-based assays were performed by Colleen Connelly.

The amide derivatives **38** and **39** were synthesized in 3 steps (Scheme 2.1), starting with the amide coupling of terephthalic acid monomethyl ester chloride (**42**) and aniline, followed by hydrolysis of the methyl ester **43** with KOH (potassium hydroxide). The carboxylic acid **44** was obtained in 97% yield and subsequently treated with the corresponding amines and the amide coupling reagents EDCI (1-ethyl-3-(3- dimethylaminopropyl) carbodiimide) and HOBt (hydroxybenzotriazole). The analogs **40** and **41** were also obtained in 3 steps under similar conditions (Scheme 2.1). The acyl chloride **42** was coupled with propargyl amine to deliver the methyl ester **45**, which was then hydrolyzed with KOH. The acid **46** was stirred in DMF (dimethylformamide) in the presence of HATU (2-(1*H*-7-azabenzotriazol-1-yl)-1,1,3,3-tetramethyl uranium hexafluorophosphate), DIPEA (diisopropylethylamine), and the corresponding anilines to afford the compounds **40** and **41**. Although pretty disappointing yields were observed in the last coupling steps, the conditions were not optimized as it was decided not to pursue this series of analogs further based on their low activity in the miR-21 luciferase assay (Figure 2.3).

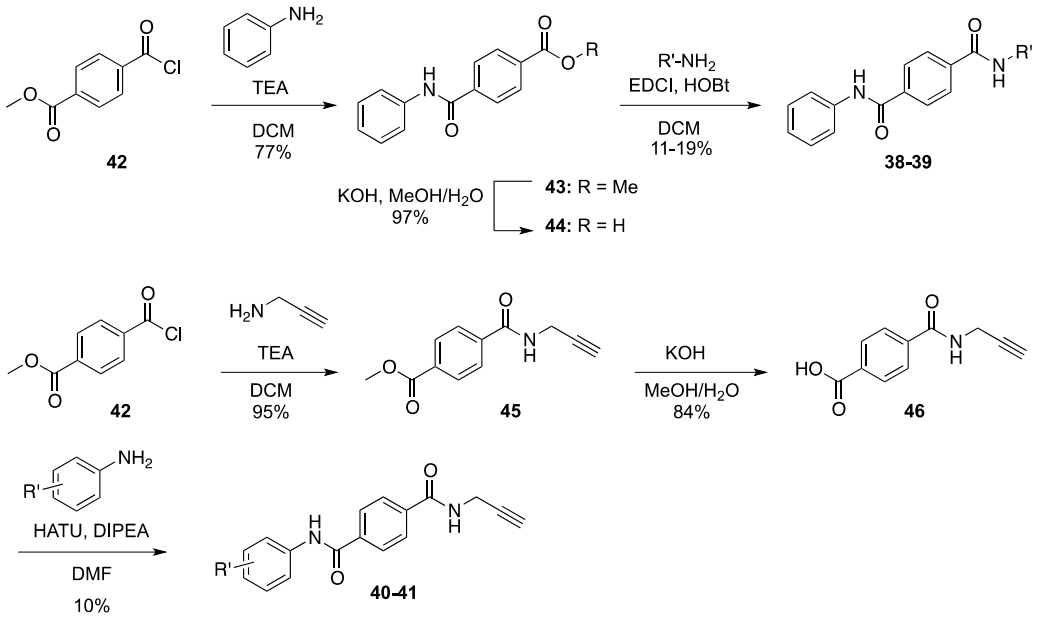

Scheme 2.1: Synthesis scheme of the amide analogs (**38**-**41**) of the previously discovered miR-21 inhibitor.

2.3 DISCOVERY OF SMALL MOLECULE MIR-21 INHIBITORS THROUGH HIGH-THROUGHPUT SCREENING

In order to identify additional small molecule miR-21 inhibitors, a high-throughput screen of 333,519 compounds was performed by the National Institute of Health (NIH) Chemical Genomic Center using the luciferase assay for miR-21 (pubchem AID 2289). The 3,282 small molecules identified in the primary screen were subsequently tested in a cell-based assay expressing the miR-30a reporter construct to evaluate their selectivity. The derivatives found active in both the miR-21 and miR-30a assays were disregarded as they were not considered selective for miR-21, but rather may be general miRNA modulators or non-specifically target firefly luciferase. The remaining compounds were re-tested in the miR-21 assay in dose-response experiments, and only the small molecules exhibiting satisfactory EC_{50} values were selected to deliver about 60 additional hit miR-21 inhibitors. These hits were then tested by qRT-PCR and

ranked according to their ability to downregulate miR-21 expression levels. The most promising compounds from the HTS included the ether-amides, *N*-acylhydrazones, oxadiazoles, and aryl-amides (Figure 2.4); therefore, several of these compounds were re-synthesized to further assess their activity and selectivity for miR-21 inhibition.

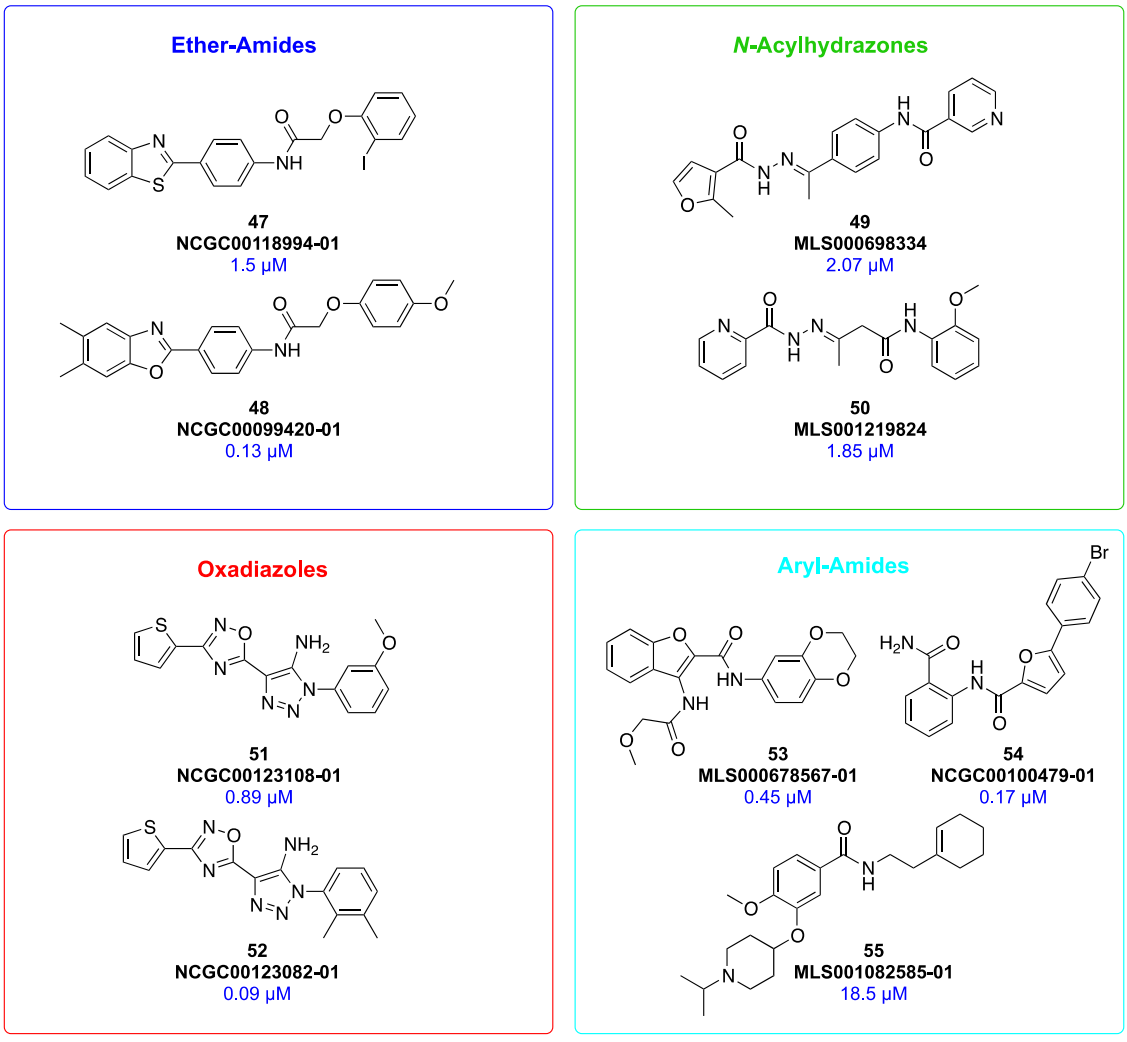

Figure 2.4: Structure of potential new miR-21 inhibitors identified from the HTS.
The EC_{50} values determined in the HTS are indicated in blue.

2.3.1 Validation of Potential Ether-amide miR-21 Inhibitors

The investigation started with the validation of the ether-amide hit compound **47** (Figure 2.5), which was re-synthesized, characterized, and tested in the miR-21 luciferase assay. First, a route was envisioned to access the 2-(2-iodophenoxy)acetic acid intermediate **58** in only one step (Scheme 2.2). 2-Iodophenol was treated with 2-bromoacetic acid and NaOH (sodium hydroxide) in H_2O and heated to reflux for 24 h. The expected carboxylic acid **58** was obtained once in 38% yield, but efforts to reproduce and increase the yield were unsuccessful. A different route was then opted to synthesize 2-(2-iodophenoxy)acetyl chloride (**59**), which was one step longer but high yielding and reproducible and was therefore more amenable for large scale syntheses of various analogs (Scheme 2.2). A mixture of 2-iodophenol (**56**) and *tert*-butylbromoacetate was stirred at 65 °C for 2 h in acetone in the presence of Cs_2CO_3 (cesium carbonate),[115] the *tert*-butyl **57** was subsequently deprotected by addition of TFA (trifluoroacetic acid) (Scheme 2.2). The deprotected carboxylic acid **58** was converted into the acyl chloride **59** with oxalyl chloride. Then, 2-aminothiophenol (**60**) and 4-nitrobenzoyl chloride (**61**) were heated to reflux in pyridine to yield the nitrobenzothiazole intermediate **62**.[116] The nitro group was reduced with $SnCl_2$ (tin chloride) in refluxing EtOH (ethanol).[116] Finally, 4-(benzothiazol-2-yl)aniline (**63**) and 2-(2-iodophenoxy)acetyl chloride (**59**) were coupled to give compound **47** as a yellow solid in 50% yield (Scheme 2.2).

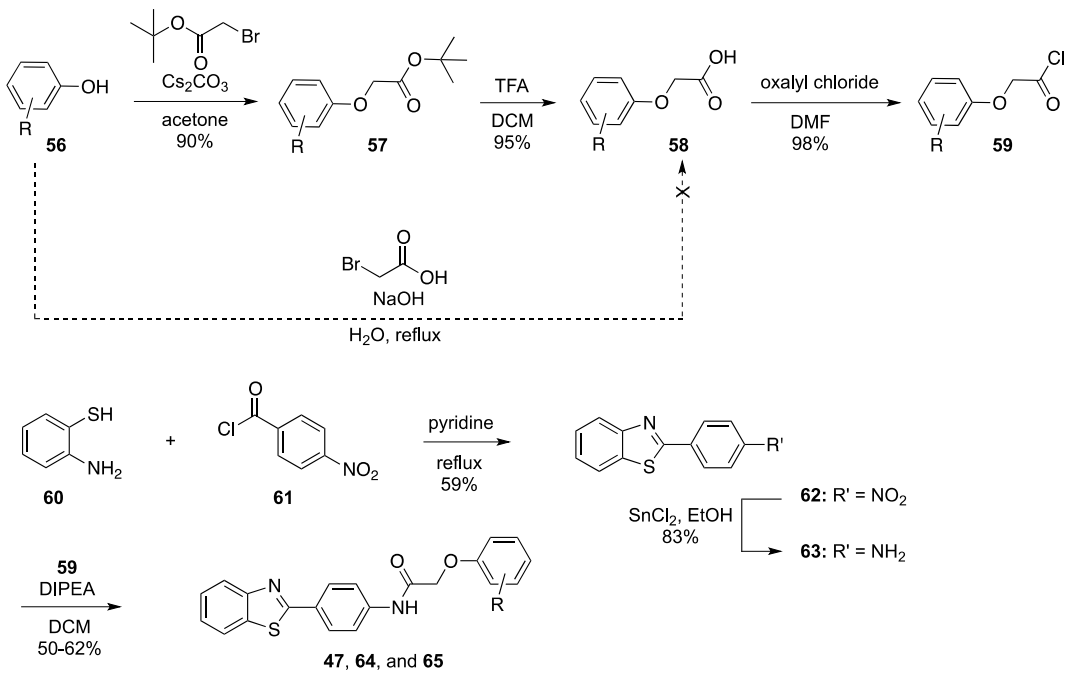

Scheme 2.2: Synthetic route to benzothiazole derivatives.
R = 2-Iodo for compound **47**, R = 4-OMe for **64**, and R = H for **65**.

Starting with the commercially available 4-methoxyphenol and phenol, the previous route was used to synthesize the analogs **64** and **65** (Scheme 2.2). Following the synthesis these three small molecules were tested in the miR-21 luciferase assay in Hela cells by Colleen Connelly (Figure 2.5). The HeLa-miR21-Luc cells were exposed to the small molecules at 10 μM in triplicate for 48 h and then assayed using a Bright Glo Luciferase Assay Kit (Promega). The luminescence data was normalized to a 1% DMSO control, and the previously identified miR-21 inhibitor **24** was used as a positive control. Unfortunately the ether-amide **47**, which was active in the HTS, showed a very low activity compared to the positive control **24** (Figure 2.5). A few structural modifications were made on **47** as a preliminary SAR investigation. Since the second ether-amide (**48**) identified as a hit in the HTS has a methoxy substituted in the *para* position (Figure 2.4), **64** was synthesized with a *para*-methoxy instead of an *ortho*-iodo group. This substitution did not affect the activity since **47** and **64** induced a similar increase in the luciferase

signal (Figure 2.5). Absence of any ring substituent seemed to be beneficial since **65** was about 10% more active than the parent compound **47**.

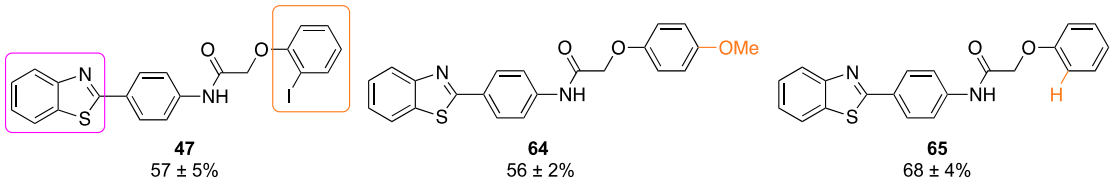

Figure 2.5: Preliminary SAR investigation of the ether-amide hit compound **47.**
The analogs were synthesized and tested in the miR-21 luciferase assay. The activities are relative to **24** within the same luciferase assay. Experiments were performed in triplicate and the standard deviations of the three independent assays were calculated. Cell-based assays were performed by Colleen Connelly.

Since the activity of the re-synthesized hit **47** was 43% less than that of compound **24**, it was decided to not investigate in more details the effects of different substitutions on the phenyl ring (shown in orange in Figure 2.5). Instead, benzoxazole analogs were synthesized (Figure 2.6). The 4-(benzoxazol-2-yl)aniline intermediate **69** was assembled according to a procedure developed by Laura Gardner. 2-Aminophenol (**66**) and 4-nitrobenzoyl chloride (**61**) were stirred in THF in the presence of TEA (triethylamine).[117] The resulting amide **67** was condensed in refluxing xylene in presence of PTSA (*para*-toluenesulfonic acid) to yield the 4-nitrobenzoxazole precursor **68**.[118] The nitro group was quantitatively reduced to the amine upon reduction with tin chloride in refluxing EtOH (Scheme 2.3).[116] Compound **69** was finally coupled with the three different acetyl chlorides (Scheme 2.3) to yield the final derivatives **70**-**72** (Figure 2.6).

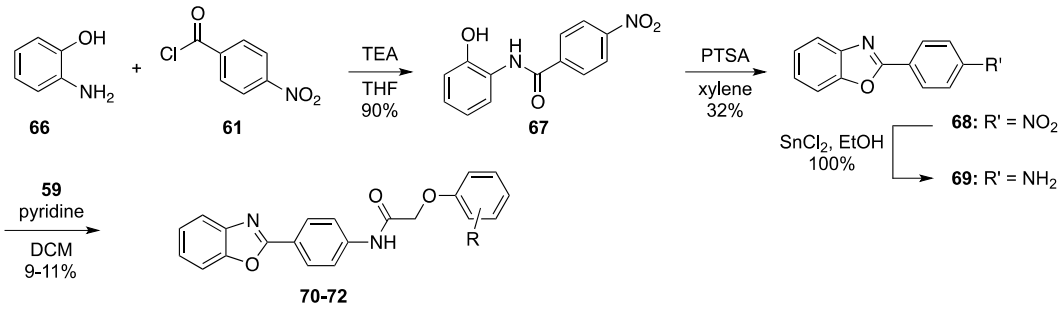

Scheme 2.3: Synthetic route to the benzoxazole derivatives **70-72.**
R = 2-I (**70**), R = 4-OMe (**71**), and R = H (**72**).

The benzoxazole analogs were tested in the previously described miR-21 assay by Colleen Connelly (Figure 2.1).[93] Replacement of the sulfur atom with an oxygen did not dramatically modify the potency of these additional miR-21 inhibitors. Both compounds **70** and **72** showed an activity equivalent to that of their respective benzothiazole analogs **47** and **65**. As previously observed, removal of the iodine functionality led to a slightly more active molecule **72** compared to its parent compound **70**. Unlike the *o*-iodo and *p*-methoxy derivatives, the benzoxazole **71** was 20% less active than its counterpart benzothiazole **64** (Figure 2.5 and Figure 2.6). Since all of the small molecules synthesized in this series were less active than the previously developed miR-21 inhibitor **24**, it was decided not to study the hit compounds ether-amides **47** and **48** more thoroughly, but instead to investigate another class of compounds.

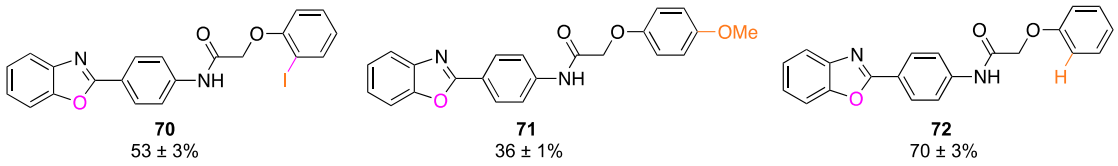

Figure 2.6: Investigation of the benzoxazole derivatives 70-72 for miR-21 inhibition.
The analogs were synthesized and tested in the miR-21 luciferase assay. The numbers represent the activity relative to **24** within the same luciferase assay. Experiments were performed in triplicate and the standard deviations of the three independent assays were calculated. Cell-based assays were performed by Colleen Connelly.

2.3.2 Validation of Potential *N*-Acylhydrazone miR-21 Inhibitors

Next, the hit *N*-acylhydrazones **49** and **50** were re-synthesized to verify their activity in the miR-21 assay. The commercially available ethyl picolinate (**73**) was heated to reflux in hydrazine hydrate to yield the corresponding hydrazide **74**.[119] The hydrazide was then refluxed in a mixture of EtOH/MeOH (1:1) in the presence of *o*-acetoacetaniside (**75**) to give the final compound **50** as an off-white solid in 81% yield (Scheme 2.4).[120]

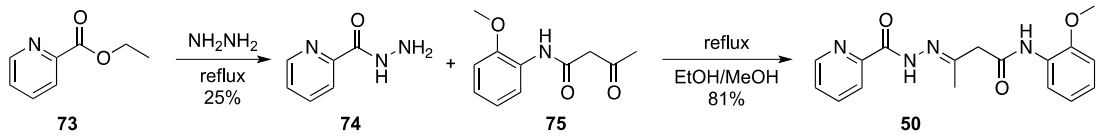

Scheme 2.4: Synthetic route to the *N*-Acylhydrazone hit compound **50.**

The same conditions were unsuccessful in delivering hit compound **49**. Specifically, the final product was not recovered when the hydrazide intermediate **83** and the *N*-(4-acetylphenyl)nicotinamide (**81)** were refluxed in a 1:1 mixture of EtOH/MeOH. In order to determine better conditions, a few test reactions were run with the commercially available 2-furoic acid hydrazide (**77**) and 4-methylacetophenone (**76**). First, these reagents were heated to reflux in MeOH and one drop of glacial acetic acid was added to catalyze the reaction.[121] The expected hydrazone **78** was obtained in 52% yield (Scheme 2.5). Another test reaction was performed, where the furoic hydrazide **77** and **66** were heated to reflux in EtOH.[122] The expected product was obtained in 70% yield. These conditions were then applied to the synthesis of **49** and the other analogs **84**-**93** (Scheme 2.5). Methyl-2-methyl-3-furancarboxylate was heated to reflux in MeOH in presence of hydrazine to form the hydrazide intermediate **82**,[123] which was subsequently heated to reflux in EtOH in the presence of *N*-(4-acetylphenyl)nicotinamide (**81**).

The amide **81** resulted from the coupling of 4-aminoacetophenone (**80**) and 3-nicotinoyl chloride (**79**). The hydrazone **49** was finally obtained in 62% yield as a yellow solid (Scheme 2.5).

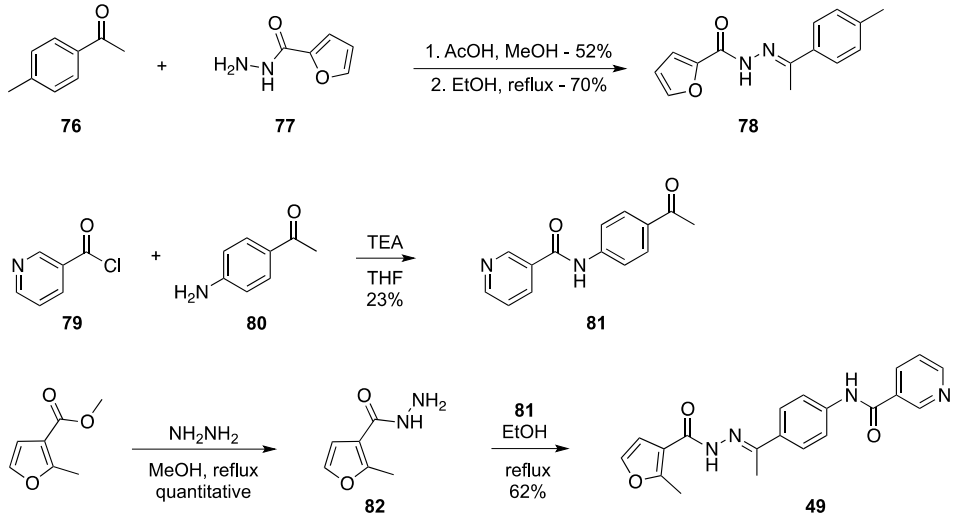

Scheme 2.5: Synthetic route to the hit compound **49** and other *N*-Acylhydrazone analogs.

.

Compounds **49** and **50** were then tested in the miR-21 luciferase assay by Colleen Connelly to measure their efficiency as miR-21 inhibitors (Figure 2.7). Unfortunately, both compounds showed activities that were about 50% lower than the reference inhibitor **24**. The structurally similar compound **78**, which was obtained during the test reactions, was also tested in the miR-21 assay (Figure 2.7). Interestingly, this analog was quite potent as it displayed an activity of 95% relative to **24**.

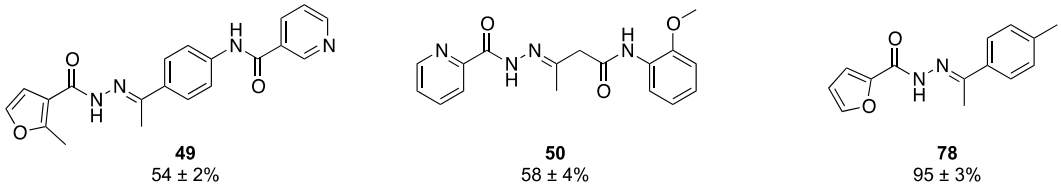

Figure 2.7: Activities of the *N*-acylhydrazones **49** and **50** identified from the NIH HTS as potential miR-21 inhibitors and the test compound **78.**
The numbers represent the activity relative to **24** within the same luciferase assay. Experiments were performed in triplicate and the standard deviations of the three independent assays were calculated. Cell-based assays were performed by Colleen Connelly.

Encouraged by the high activity of compound **78**, it was decided to make some structural modifications on **78** for preliminary SAR studies (Figure 2.8). First the importance of the two methyl groups, on the benzene ring (shown in blue in Figure 2.8) and on the hydrazone linkage (shown in red in Figure 2.9), was evaluated. Removal of both methyl groups was well tolerated as the analog **84** exhibited the same activity as the parent compound **78**. The *p*-phenyl group was modified with various functional groups, such as pyridine (**84**), *o*-acetoacetaniside (**85**), butyl (**86**), *p*-diphenyl (**87**), and naphthalene (**88**) (Figure 2.8). Replacement of the *p*-phenyl group with a pyridine, a butyl, and a bulky *p*-diphenyl functionality led to a significant loss in activity. However, introduction of the *o*-acetoacetaniside group (**85**), similar to the hit compound **50**, maintained the activity; as did the introduction of the naphthalene motif (**88**). The furan group was then substituted with 2-methyl furan (**89**) as in hit compound **49**, which slightly improved the activity. Replacement of the furan motif with a benzene ring had no effect on the activity since **83** and **90** displayed a similar potency. Introduction of an additional aromatic ring was beneficial as the benzofuran analog **91** exhibited a 22% increase in activity, compared to **83**. Lastly, substitution of the acylhydrazone motif with a more stable amide bond led to a more potent inhibitor **92**, which was 16% more active than the reference inhibitor **24** (Figure 2.8).

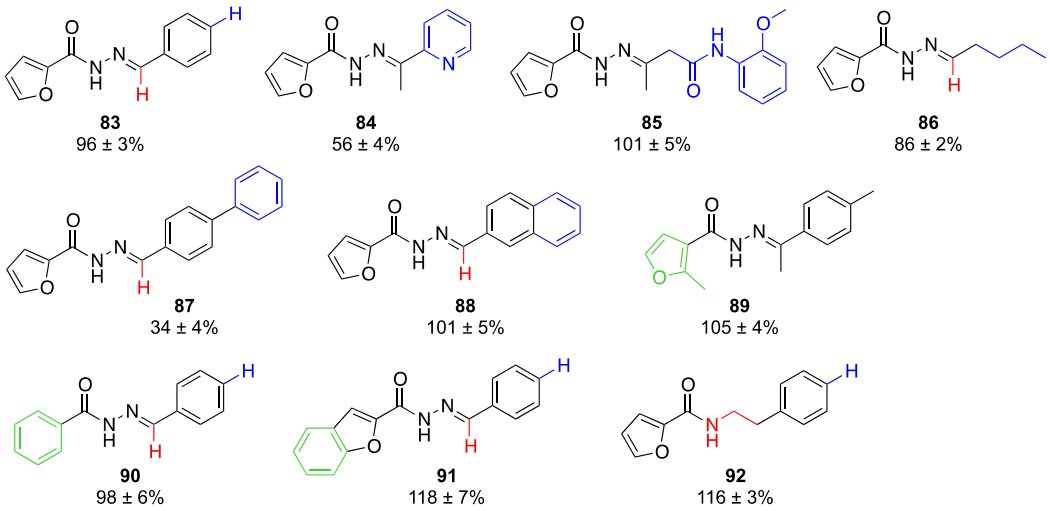

Figure 2.8: Preliminary SAR investigation of the *N*-acylhydrazone inhibitor **78.**
The numbers represent the activity relative to **24** within the same luciferase assay. Experiments were performed in triplicate and the standard deviations of the three independent assays were calculated. Cell-based assays were performed by Colleen Connelly.

To investigate each inhibitor's selectivity for miR-21, inhibitors **49**, **50**, and **83-92** were tested at 10 μM in the miR-122 luciferase assay (Figure 2.9). This construct is similar to the miR-21 reporter, except the reporter assay for miR-122 was further improved by inserting the miR-122 binding site downstream of the *Renilla* luciferase gene of the plasmid psiCHECK-2. This plasmid also contains the firefly luciferase gene, which serves as an internal control. Huh7-psiCHECK-miR122 cells, which stably express the miR-122 reporter,[124] were exposed to each inhibitor at 10 μM (0.1% final DMSO concentration) for 48 h. The cells were then assayed with a Dual Luciferase Kit (Promega), which allows to simultaneously measure the luminescence signals of both *Renilla* and firefly luciferases. The *Renilla* luciferase readings were normalized to the firefly luciferase readings to give relative luciferase units (RLUs). In that case, an increase in the *Renilla* signal would indicate that the compounds show some degree of miR-122 inhibition, whereas an increase in the firefly signal would suggest a non-miRNA specific effect on the reporter.

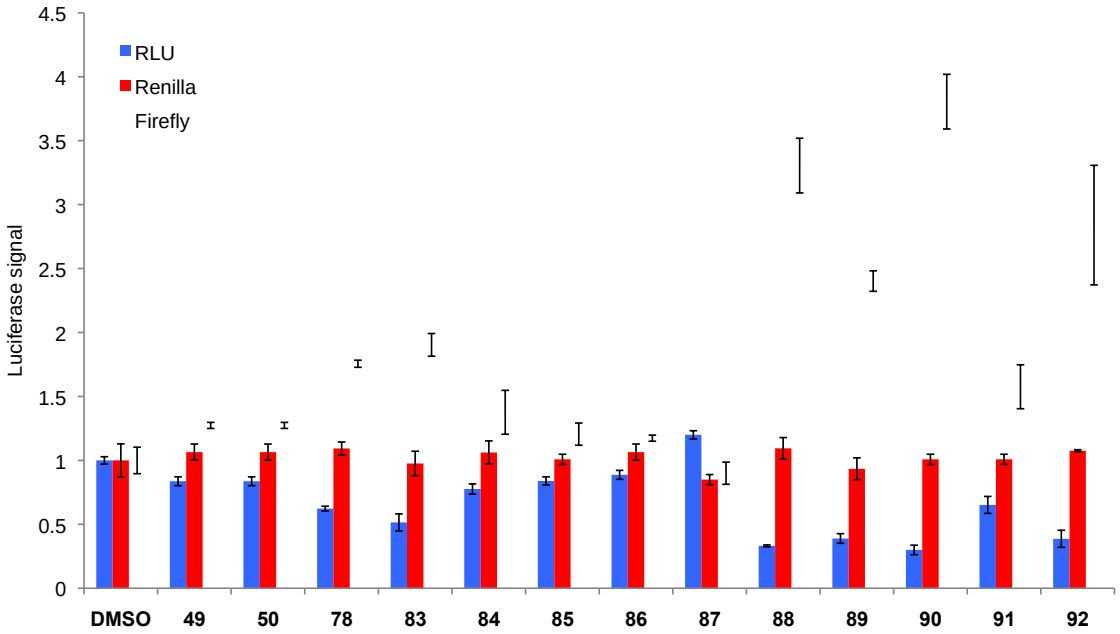

Figure 2.9: Evaluation of the selectivity of the *N*-acylhydrazone inhibitors in the miR-122 assay.
Dual Luciferase Assay of Huh7-psiCHECK-miR-122 cells treated with the hit compounds **49** and **50** and the analogs **83**-**92** at 10 μM. The luciferase signal was normalized to a DMSO control. Experiments were performed in triplicate and the standard deviations of the three independent assays were calculated.

None of the inhibitor showed any effect on the *Renilla* luciferase (Figure 2.9), implying that these compounds might be selective towards miR-21 inhibition. A few analogs, **83**, and **88**-**92**, induced a large increase in the firefly luminescence (Figure 2.9), which indicates that the high activity previously observed in the miR-21 assay for these compounds (Figure 2.8) might be due to a non-specific stabilization of the firefly enzyme, rather than true miR-21 downregulation. It has recently been reported that the firefly luciferase enzyme is sensitive to ligand-based stabilization by small molecule inhibitors, which leads to protein stabilization and accumulation.[125] In a cell-based assay, treatment with an inhibitor can lead to an increase in luciferase signal, whereas *in vitro* evaluation of the direct interaction between the enzyme and these same inhibitors causes a significant decrease in luciferase signal. Certain chemotypes of small molecules were presented as apparent inhibitors of the enzyme and can lead to false positive hits in screening events relying on firefly luciferase-based assays.[126] One of the

identified FLuc inhibitors, the compound **93**, was synthesized by Laura Gardner to provide a positive control (Figure 2.10A). In order to further test the effect of the *N*-acylhydrazone inhibitors on firefly luciferase, an *in vitro* luciferase (FLuc) assay was performed (Figure 2.10B). The positive control **93** displayed a 90% FLuc inhibition. The analogs **78**, **83**, **84**, **87**-**90**, and **92** showed a non-specific modulation of the firefly enzyme as they exhibited 30-65% FLuc inhibition. These data indicate that these analogs might inhibit the firefly luciferase rather than miR-21.

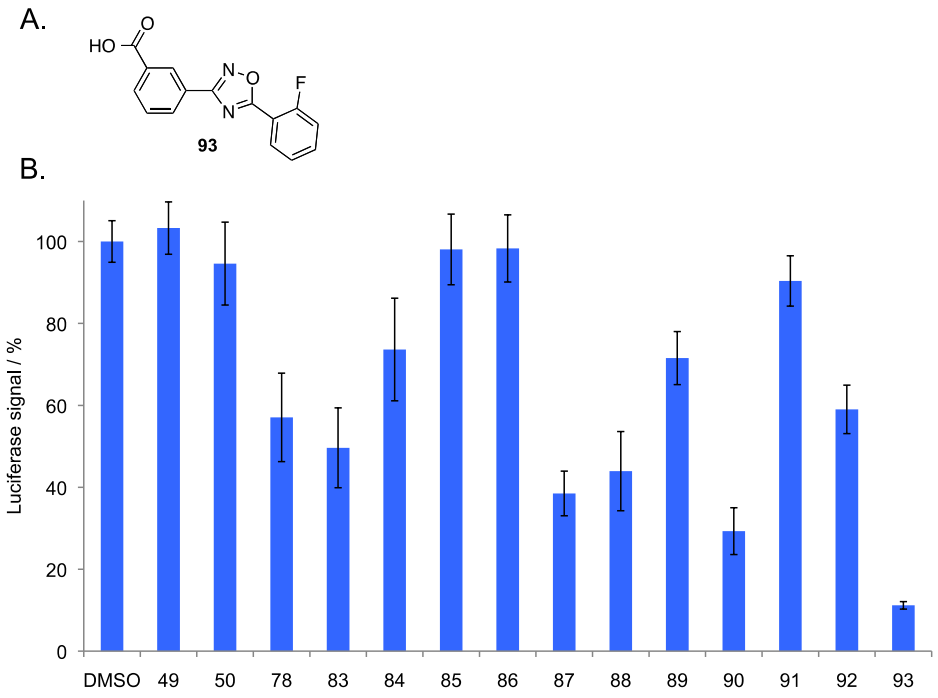

Figure 2.10: Specifity study of the *N*-acylhydrazone inhibitors.
A. Structure of the reported FLuc inhibitor. **B**. *In vitro* FLuc assay of the miR-21 inhibitors **49**, **50**, **78** and **83**-**92**. The luciferase signal was normalized to a 1% DMSO control. The error bars indicate the standard deviations determined from three independent measurements.

Based on this data, additional experiments were performed by Colleen Connelly to investigate the selectivity of the *N*-acylhydrazone derivatives (Figure 2.11). HeLa cells containing the luciferase reporter constructs for miR-21 or miR-30a were exposed for 48 h to 10 μM of each of the small molecules **78**, **89**, **83**, and **84** (Figure 2.11A). The four analogs tested

displayed the same level of activity in both the miR-21 and the miR-30a assays, which was expected since both of these reporters are based on the firefly luciferase enzyme. In addition, the levels of mature miR-21, miR-20a, miR-24, and miR-27b in HeLa cells treated with the inhibitors **78** and **83** at 10 μM were measured by qRT-PCR. Both **78** and **83** induced a reduction in the expression levels of the three miRNAs tested (Figure 2.11B). Although the compounds did not interfere with the expression of miR-122, as determined in the luciferase assay (Figure 2.9), the levels of mature miR-122 could not be measured in HeLa cells by qRT-PCR because of the very low endogenous levels of miR-122 in that cell line. Taken together, all these data suggest that the *N*-acylhydrazone analogs do not inhibit miR-21 selectively, as at least four other miRNAs are being similarly reduced upon treatment with these inhibitors (Figure 2.11).

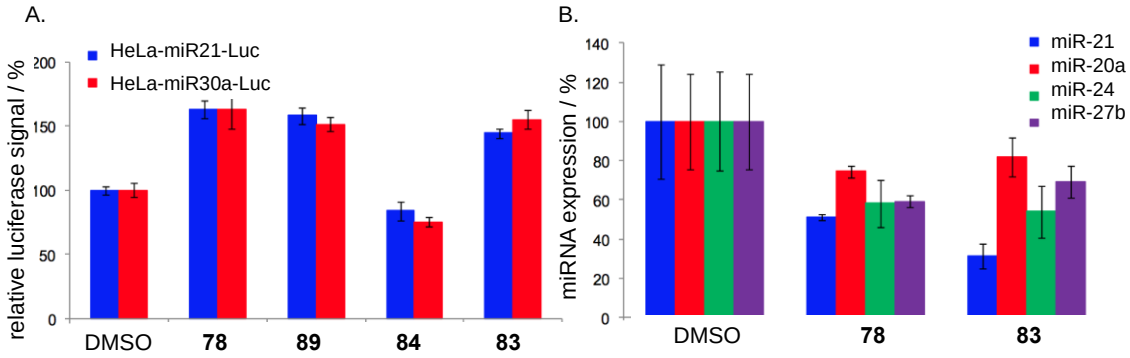

Figure 2.11: Assessment of the selectivity of the *N*-acylhydrazone inhibitors.
A. Bright Glo Luciferase Assays of HeLa-miR21-Luc and HeLa-miR30A-Luc cells treated with the hydrazones at 10 μM. The luciferase signal was normalized to a DMSO control. **B.** qRT-PCR measurements of mature miR-21, miR-20a, miR-24, and miR-27b levels in HeLa cells treated with the hydrazones **78** and **83** (10 μM). The expression of each miRNA for small molecule treated cells was normalized to a DMSO control (100% expression) and RNU19 expression. The error bars indicate the standard deviation determined from three independent measurements. Cell-based assays were performed by Colleen Connelly.

2.3.3 Validation of Potential Ether-amide miR-21 Inhibitors

Next, the two oxadiazole hit compounds **51** and **52** identified from the HTS were validated through synthesis and SAR investigation (Figure 2.4). The oxadiazole derivatives were

synthesized in four steps following a procedure established by Laura Gardner. The commercially available anilines were converted to the corresponding arylazides (**95**) by treatment sequentially with excess of concentrated H_2SO_4 (sulfuric acid), $NaNO_2$ (sodium nitrite) and NaN_3 (sodium azide) in water at 0 °C; the mixture was slowly allowed to warm up to rt and stirred overnight.[127] 2-Thiophenecarbonitrile (**96**) was dissolved in a mixture of 15% EtOH in H_2O and a solution of Na_2CO_3 (sodium carbonate) and $H_2NOH{\bullet}HCl$ (hydroxylamine hydrochloride) in H_2O was added.[128] The hydroxamide **97** was then heated to reflux in dioxane in the presence of **98**.[129] The oxadiazole precursor **99** was stirred overnight with the arylazide **95** in presence of NaOMe (sodium methylate) in MeOH at 60 °C to deliver the final compounds (Scheme 2.6).[130]

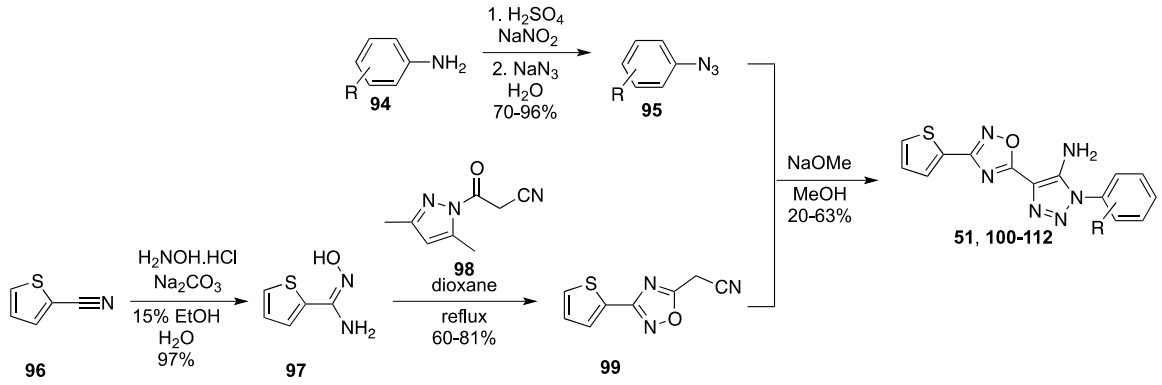

Scheme 2.6: Synthesis scheme for oxadiazole hit compound **51** and analogs.
Definitions **51:** R = 3-OMe, **100:** R = 3,5-OMe, **101**: R = H, **102**: R = 3-Et, **103**: R = 3-NMe_2, **104**: R = 3-iPr, **105**: R = 3-CF_3, **106**: R = 3-OCF_3 **107**: R = 3-F, **108**: R = 6-OMe, **109**: R = 4-OMe, **110**: R = C_4H_4, **111:** R = 3-C_6H_5, **112**: R = 3-OH.

The two re-synthesized hit compounds were tested in the miR-21 luciferase assay by Colleen Connelly (Figure 2.12). Gratifyingly, **52** displayed the same level of miR-21 inhibition as the reference miR-21 inhibitor **24**, and **51** showed a 40% increase in activity compared to **24** (Figure 2.12), and an improved EC_{50} value of 0.15 μM. Encouraged by these results, diverse chemical modifications were performed on these structures to better understand the molecular requirements for the activity of the miR-21 inhibitors **51** and **52**.

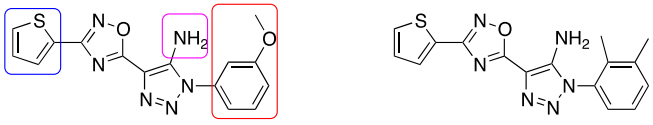

Figure 2.12: Activities of the oxadiazole hit compounds **51** and **52** identified in the HTS.
The numbers represent the activity relative to 24 within the same luciferase assay. Experiments were performed in triplicate and the standard deviations of the three independent assays were calculated. Compound **52** was synthesized by Laura Gardner and cell-based assays were performed by Colleen Connelly.

The main oxadiazole-triazole core of compounds **51** and **52** was kept constant. Several analogs were designed that contained structural modifications either on the phenyl ring (shown in red in Figure 2.13), on the thiophene motif (shown in blue in Figure 2.14) or in place of the amino group (shown in magenta in Figure 2.15). This SAR investigation was aimed at understanding which functionalities on the molecule are necessary for its miR-21 inhibitory activity as well as to identify compounds with increased potency. First, the importance of the methoxy group in the *meta* position of the phenyl ring was investigated (Figure 2.13). All of these analogs were synthesized according to the procedure previously described (Scheme 2.6). As the parent compound **51** is *meta* substituted with a methoxy group, compound **100** was synthesized with two methoxy groups in the *meta* positions to see if it would further enhance the activity, but the introduction of a second methoxy group led to a 20% loss in activity (Figure 2.13). The oxadiazole **101** was designed to reveal the importance of having a substituent on the phenyl ring, and see if a smaller analog would fit better in the putative binding pocket of the target protein, resulting in a more potent inhibitor. The absence of any substituent dramatically affected the activity since **101** only showed 32% residual activity (Figure 2.13). In order to understand the necessity of having a hydrogen-bond acceptor in the *meta* position, **102**, **103**, and **104** were synthesized. Replacement of the methoxy group with an ethyl substituent (**102**) or a more basic dimethylamino functionality (**103**) slightly improved the activity. Substitution of the

dimethylamino group with an isopropyl functionality (**104**) abolished the formation of any putative hydrogen-bond, and led to a 13% loss of activity (Figure 2.13). A deactivating group was then installed in the *meta* position (**105**) which yielded a 39% reduction in the activity. To understand whether the beneficial effect of the *meta* substituent was due to a steric or an electronic effect, analogs **106** and **107** were synthesized. Replacement of the *meta* methyl group with the more electron-withdrawing group trifluoromethyl (**106**) caused a 28% reduction in the activity. However, the activity was maintained when the small highly electronegative fluoro motif was introduced (**107**). These results and the data collected from compounds **102**, **103**, and **104** suggested that a subtle balance needs to be established between the size and the electronegativity of the functionalities introduced in the *meta* position in order to maintain the activity of the miR-21 inhibitors (Figure 2.13). The methoxy group was then installed in the *ortho* or *para* positions. Substitution in *ortho* (**108**) dramatically reduced the activity, whereas *para* substitution (**109**) led to a 16% increase in activity (Figure 2.13). Modification of the aromatic ring with the bulkier naphtalene (**110**) motif yielded a 16% decrease in activity, however, the *m*-diphenyl (**111**) group was well tolerated. The methoxy group was then removed to give compound **112**, which now contains a potential hydrogen-bond donor group in the *meta* position (Figure 2.13). The introduction of a hydroxy group (**112**) caused a 23% loss of activity.

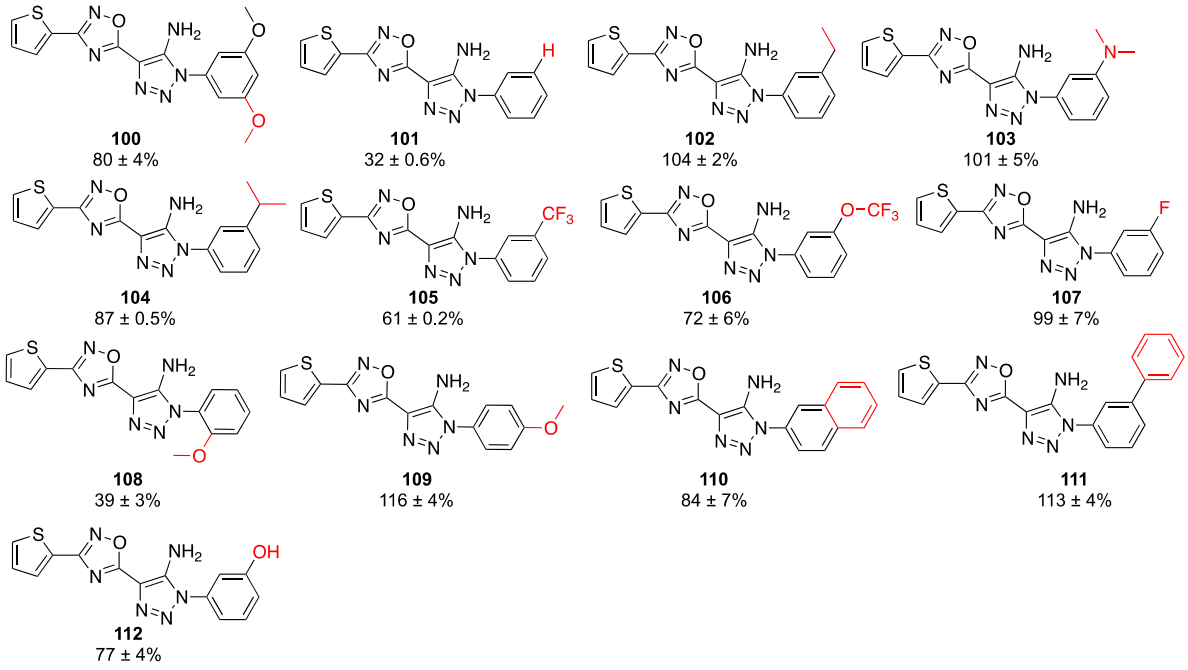

Figure 2.13: Structure-activity relationship studies of the miR-21 inhibitor **51** through modification of the phenyl ring (variations to the original structure are shown in red).
The numbers represent the activity relative to **51** within the same miR-21 luciferase assay. Experiments were performed in triplicate and the standard deviations of the three independent assays were calculated. Cell-based assays were performed by Colleen Connelly.

The conditions used to synthesize the previous analogs were unsuccessful in delivering the hydroxy derivative **112**. When *o*-azidophenol was heated in the presence of the nitrile-oxadiazole intermediate **99** and sodium methylate, the expected product could not be isolated. Indeed, the other analogs were isolated by filtration after addition of water to the reaction mixture, which caused the products to precipitate out of solution. The introduction of the hydroxy group might have enhanced the water solubility of **112**, which made it difficult to recover it under these conditions. The product **112** was successfully obtained in 78% yield after deprotection of the methoxy group of compound **51** with three equivalents of BBr_3 (boron tribromide) (Scheme 2.7).[131]

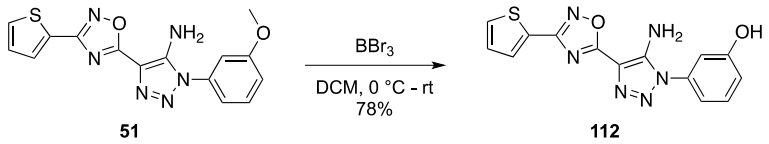

Scheme 2.7: Synthesis of the alcohol derivative **112.**

Next, the importance of the amino group (shown in magenta in Figure 2.14) was assessed. Analog **115** was synthesized as a direct derivative of the lead compound **51**, where the amino group was removed from the triazole moiety. In a first attempt to introduce the triazole ring via the well-known "click-reaction",[132] 1-azido-3-methoxybenzene (**95**) and propiolic acid were treated with $CuSO_4 \bullet 5H_2O$ (copper sulfate pentahydrated) and sodium ascorbate in a mixture of THF/H_2O (1:1).[133] Although some product **114** was obtained using these conditions, it was contaminated with some impurities that could not be eliminated through additional acid/base extraction or column chromatography. Instead, the arylazide **95** was treated with propargylic alcohol, $CuSO_4 \bullet 5H_2O$ and sodium ascorbate to afford the alcohol **113**, which was easier to purify than the acid **114** since it was less polar. The alcohol derivative **113** was oxidized with Jones' reagent to give the carboxylic acid intermediate **114** in 60-71% yield depending on the ring substituent.[134] The precursor **114** was heated at 120 °C overnight in acetonitrile, in presence of hydroxythiophene-2-carboximidamide (**97**) and EDCI to deliver the final product (Scheme 2.8). Although this last reaction was pretty low yielding, only 20-30% products were obtained due to some loss of material on the column, no optimization was performed as the analogs synthesized displayed a rather low activity (Figure 2.14).

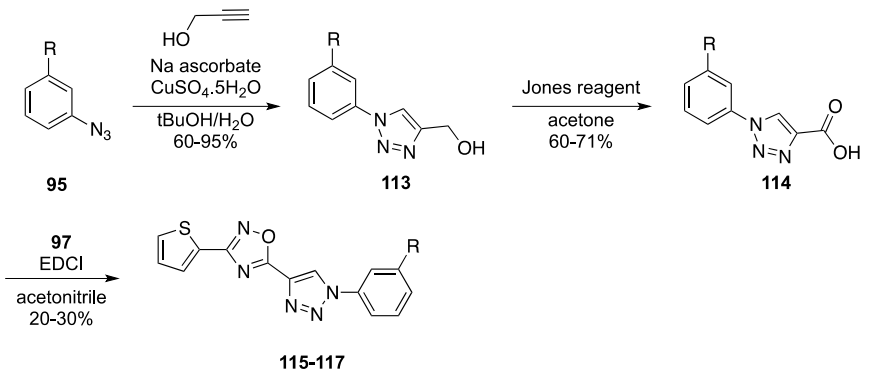

Scheme 2.8: Synthetic route to oxadiazole analogs **115-117.**
Definitions **115**: R = 3-OMe, **116**: R = H, and **117**: R = 3-F.

Removal of the free amino group on the triazole ring generally led to a loss of activity (Figure 2.14). The analog **115** displayed a 13% reduced activity in comparison with the parent compound **51**. Similarly, **117** was approximately 10% less active than its direct amino-counterpart **107**. As expected, the analog **116** without any substituent on the phenyl ring exhibited a reduced activity in comparison to **115**. However, unlike **115** and **117**, the activity of **116** was about 30% higher than its direct amino-derivative **101** (Figure 2.14). Overall, comparing the hit compound **51** and the triazole **115** it seems that the amino group has a slightly positive effect on the miR-21 inhibitory activity.

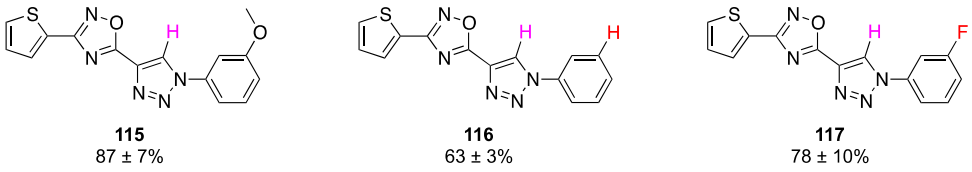

115
87 ± 7%

116
63 ± 3%

117
78 ± 10%

Figure 2.14: Structure-activity studies of the miR-21 inhibitor **51** through removal of the amino group (variations to the original structure are shown in magenta and red).
The numbers represent the activity relative to **51** within the same luciferase assay. Experiments were performed in triplicate and the standard deviations of the three independent assays were calculated. Cell-based assays were performed by Colleen Connelly.

Next, acylation of the primary amine in **51** was attempted, through reaction with acetic anhydride and DIPEA in DCM; however even after several days the TLC showed only unreacted

starting material. In an attempt to optimize the reaction conditions, different small-scale test reactions were performed: with/without DMAP (4-dimethylaminopyridine), with different equivalents of base and anhydride, or heating to reflux for 48 h.[135] As none of these conditions delivered the acetylated product, **51** was treated with the more reactive acetyl chloride (AcOCl). These reagents were stirred under reflux in DCM in presence of TEA and catalytic amount of DMAP but no reaction was observed even after a few days.

Lastly, the replacement of the thiophene ring with different heterocycles was investigated (Figure 2.15). Compound **118** was synthesized by Colleen Connelly according to the procedure previously described (Scheme 2.6) and possesses a furan ring in place of the thiophene. The activity of the furan derivative **118** was improved by 20% in comparison with the hit compound **51** (Figure 2.15). The analogs **119**, **120**, and **121** were also synthesized with the conditions previously discussed (Scheme 2.6). Replacement of the thiophene ring with a slightly larger benzene ring (**119**) was tolerated, as this modification only caused a 2% loss of potency. Substitution with the more basic pyridine ring (**120**) led to a slight increase in the activity. To verify whether the introduction of a pyridine ring would consistently lead to a more potent inhibitor, compound **121** was synthesized with a *m*-fluoro group instead of the *m*-methoxy (shown in red in Figure 2.15) since it was previously observed that this modification is well tolerated (Figure 2.13). Substitution of the thiophene with a pyridine ring did not improve the activity as expected, since **107** and **121** were equipotent. The compound **122** was designed to investigate whether an aromatic ring was necessary to maintain the activity or if an aliphatic group would be tolerated (Figure 2.15). Reaction of 1-cyanoacetyl-3,5-dimethylpyrazole (**98**) and hydroxypentanimidamide in dioxane failed to deliver the product, therefore the alkane derivative **122** was synthesized without the amino group using the conditions described in

Scheme 2.8. Introduction of the butyl group in place of the thiophene motif did not significantly affect the activity as **115** and **122** showed similar potency. The same conditions were used to synthesize the analog **124**. Substitution with the sterically more demanding benzothiophene functionality (**123**) slightly improved the activity (Figure 2.15) relative to the triazole anolog **115**.

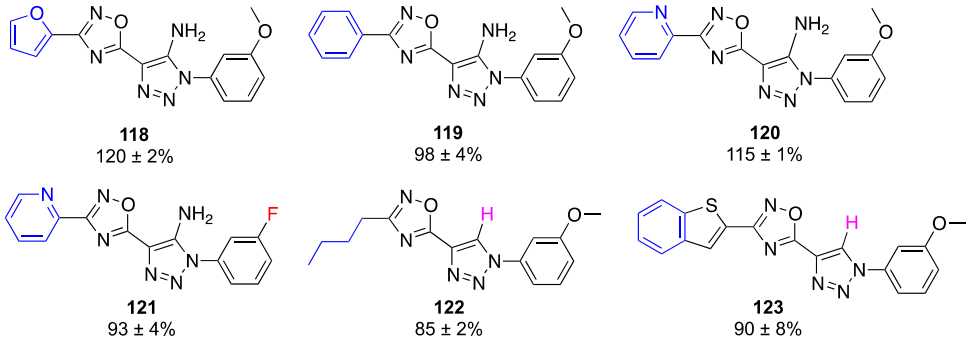

Figure 2.15: Structure-activity relationship investigation of the miR-21 inhibitor **51** through modifications of the thiophene motif (variations to the original structure are shown in color).
The numbers represent the activity relative to **51** within the same luciferase assay. Experiments were performed in triplicate and the standard deviations of the three independent assays were calculated. Cell-based assays were performed by Colleen Connelly.

The SAR study of the lead compound **51** was encouraging given a few analogs with activities comparable to **51** (**102**, **103**, **107**, and **119**) or even slightly higher (**109**, **111**, **118**, and **120**) were identified. A 20% and 16% increases in the potency were achieved with the inhibitors **118** and **109**, respectively. Next, the selectivity of the oxadiazole inhibitors was investigated based on the study of the hit compound **51**. The oxadiazole **51** was tested at 10 μM in the miR-122 assay. This compound did not show any effect on neither the *Renilla* nor the firefly signal (Figure 2.16A). The luminescence reads out were slightly lower for **51** than for the DMSO control due to some toxicity. These data indicated that **51** did not inhibit miR-122, and therefore is not a general inhibitor of the miRNA pathway. These data also suggested that the inhibitor **51** does not stabilize the firefly enzyme, as no increase in FLuc was observed in the miR-122 assay

(Figure 2.16A). Given some oxadiazole containing compounds have been previously identified as FLuc inhibitors,[126] the hit compound **51** and the most potent analogs of this series were tested in the *in vitro* FLuc assay to determine whether they affect the FLuc enzyme (Figure 2.16B). The analogs **103**, **107**, **118**, **120**, and **121** showed a moderate inhibition of the firefly luciferase enzyme as they reduced luminescence by 33-52%. The hit compound **51** only slightly modified the luciferase signal in the *in vitro* assay (Figure 2.16B). Since the furan and pyridine derivatives **118** and **120** showed 33% FLuc inhibition, their high activity in the miR-21 luciferase assay might be due to stabilization of the firefly luciferase rather than true miR-21 downregulation. This also validates the decision to maintain the thiophene group on the majority of the analogs, as this motif seems less prone to induce FLuc stabilization. The selectivity of these derivatives for miR-21 inhibition should be further investigated. For example, the treatment of HeLa cells with the most promising oxadiazole inhibitors, followed by qRT-PCR measurement of the expression levels of several miRNAs will bring important knowledge regarding the selectivity profile of these compounds.

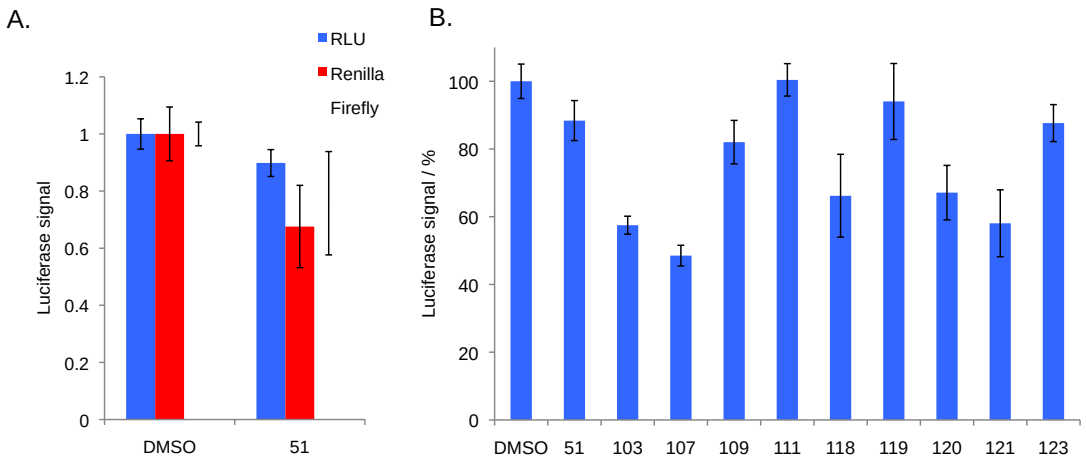

Figure 2.16: Evaluation of the selectivity of the oxadiazole miR-21 inhibitors.
A. Dual Luciferase Assay of Huh7-psiCHECK-miR-122 cells treated with the hit compound **51** at 10 μM. The luciferase signal was normalized to a DMSO control. **B**. *In vitro* FLuc assay. The compounds (10 μM) were incubated for 30 min with the recombinant firefly luciferase enzyme and the luminescence was measured using a Bright glo assay (Promega). The data are relative to the DMSO control. Experiments were performed in triplicate and the standard deviations of the three independent assays were calculated.

2.3.4 Validation of Potential Aryl-amide miR-21 Inhibitors (53 & 54)

The aryl-amide chemotype was found in several compounds identified in the HTS (Figure 2.4). The hit compounds **53** and **54** were re-synthesized to confirm their activity as miR-21 inhibitors. They were both synthesized in three steps from commercially available starting materials (Scheme 2.9).

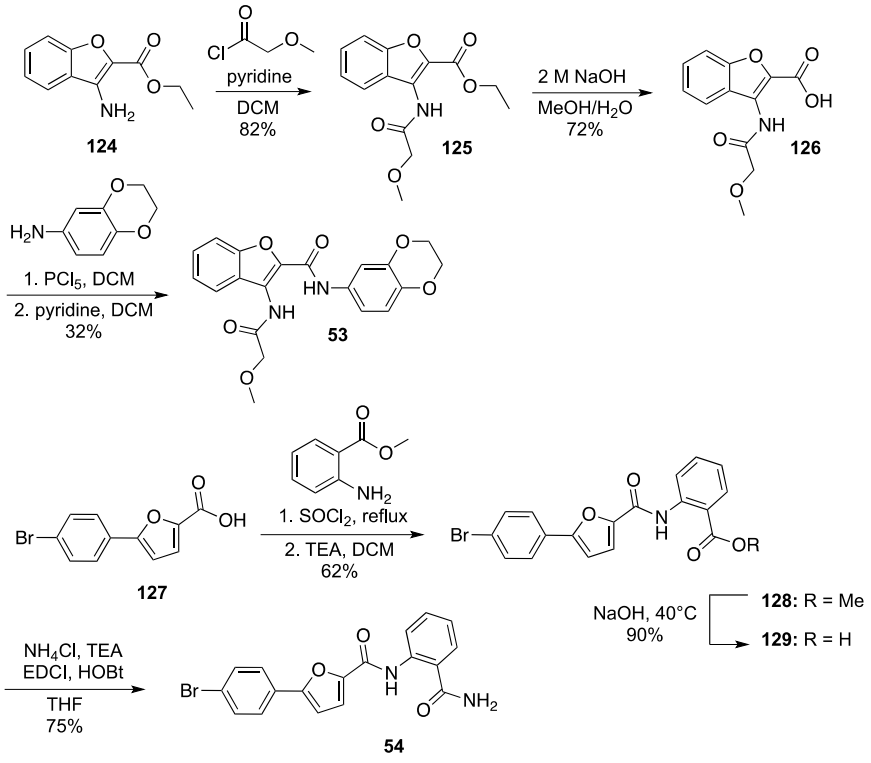

Scheme 2.9: Synthetic route to the aryl-amide hit compounds **53** and **54.**

.

For the synthesis of hit compound **53**, the aminobenzofuran **124** was treated with 2-methoxyacetyl chloride and pyridine in DCM,[136] followed by hydrolysis of the ethyl ester (**125**). Treatment of the ester **125** with 2 equivalents of 2 M LiOH (lithium hydroxide) at rt in dioxane, with 2 M KOH in EtOH,[137] or with 2 M LiOH at 60 °C in a mixture of THF/H_2O were unsuccessful in delivering the expected acid **126**. In fact, the heat caused the decomposition of the intermediate **125**. The ester was successfully converted to the carboxylic acid **126** using 10

equivalents of NaOH in a mixture of MeOH/H_2O at rt for 2 h (Scheme 2.9). Several different conditions were screened in order to perform the amide coupling reaction in the final step. Only starting material was recovered when the carboxylic acid intermediate **126** was treated with 1,4-benzodioxan-6-amine in the presence of different peptide coupling reagents such as EDCI, DMAP, and TEA in DCM[138] or HATU, DIPEA, and with/without HOBt in DMF. The coupling was also unsuccessful when the carboxylic acid **126** was heated to reflux with $SOCl_2$ (thionyl chloride) for 1 h, followed by evaporation of the excess $SOCl_2$ and subsequent reaction of the resulting acyl chloride with the amine in DCM. Finally, compound **53** was successfully obtained upon activation of **126** with phosphorus pentachloride at 0 °C, followed by treatment with 1,4-benzodioxan-6-amine and pyridine in DCM (Scheme 2.9).[139]

The synthesis of **54** started with the treatment of 5-(4-bromophenyl)-2-furoic acid (**127**) with $SOCl_2$ at reflux for 1 h, followed by the reaction of the corresponding acyl chloride with methyl anthranilate and TEA in DCM. The resulting methyl-ester **128** was then converted to the carboxylic acid **129** after treatment with 10 equivalents of NaOH in a 1:1 mixture of MeOH/H_2O at 40 °C for 1 h. The first failed attempt to compound **54** consisted in treating the acid **129** with oxalyl chloride in DCM and a catalytic amount of DMF, the resulting acyl chloride was taken up into $CHCl_3$ (chloroform) and stirred in presence of a solution of aqueous ammonia.[140] The next attempt relied in stirring the precursor **129** with TEA, EDCI, HOBt, and a solution of ammonium chloride in THF,[141] and successfully delivered **54** in 75% yield (Scheme 2.9).

Both re-synthesized hit compounds **53** and **54**, as well as the precursors **128** and **129** were tested in the miR-21 luciferase assay by Colleen Connelly. Unfortunately the two aryl-amides identified in the HTS, **53** and **54**, did not look very promising (Figure 2.17). Compound **53** exhibited an activity 32% lower than the reference miR-21 inhibitor **24**. Similarly, **54** showed a

38% reduced activity in comparison with **24**. The methyl ester and carboxylic acid precursors (**129** and **130**) were completely inactive (Figure 2.17). Given the low activity of these small molecules in the miR-21 assay, it was chosen not to investigate them more thoroughly and moved on to the study of another aryl-amide hit compound identified in the HTS (Figure 2.4).

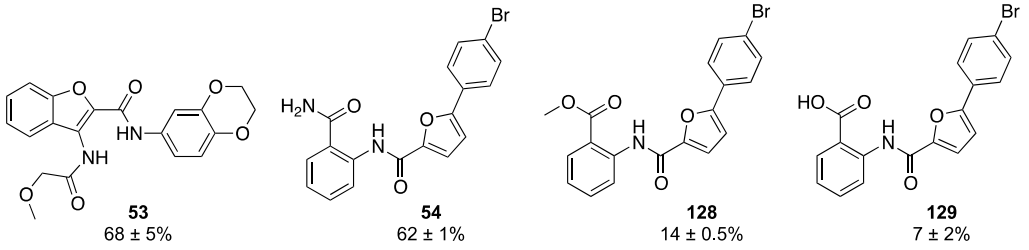

Figure 2.17: Activities of re-synthesized hit compounds **53**, **54**, and intermediates **128** and **129** in the miR-21 assay. The numbers represent the activity relative to **24** within the same assay. Experiments were performed in triplicate and the standard deviations of the three independent assays were calculated. Cell-based assays were performed by Colleen Connelly.

2.3.5 Validation of the Potential Aryl-amide miR-21 Inhibitor 55

The additional aryl-amide hit compound **55** identified in the HTS was re-synthesized by Matt Stephens and tested in the miR-21 luciferase assay by Yuta Naro. Even though this inhibitor showed a 20% reduced activity compared to **24**, it promoted a 36% increase in luciferase expression compared to DMSO (Figure 2.18), thus showing some potential miR-21 inhibition. A structure-activity relationship investigation was conducted to try to improve the potency (modifications from the parent compound shown in green, blue, or red in Figure 2.18). Replacement of the bulky piperidine group with a smaller acetyl (**130**) or methoxy (**131**) group resulted in ~47% and ~65% increase in activity compared to the parent compound **55**. Further modification of the *meta* position to a hydroxyl group (**132**) showed a more modest ~27% increase in activity, while complete removal of the *meta* substitution (**133**) completely abolished the activity. Very little change in activity was observed when an hydroxy group was introduced

in *meta* (**134**) or *para* (**135**) positions or upon removal of both substitutions (**136**). Interestingly, the 1,3-dihydroxy derivative (**137**) displayed a significant ~86% increase in activity. Replacement of a cyclohexene motif (**132**) with a cyclohexane (**138**) resulted in an ~57% increase in activity relative to **55**, while replacement with a benzene ring (**139**) or loss of the ring entirely (**140**) abolished the activity. Surprisingly, removal of the *meta*-hydroxy associated with substitution of the *p*-methoxy to an ethyl ether (**141**), propyl ether (**142**), benzyl ether (**143**), or to a free amine (**144**) rescued the activity (Figure 2.18).

Based on these observations, the *p*-methoxy was kept constant and modifications of the benzene motif were investigated. Increasing the size of the aliphatic linker by adding a carbon (**145**) resulted in a ~58% increase in activity compared to the parent compound **55**, while further extending or shortening the linker by an additional carbon (**146**, **147**) resulted in complete loss in activity. The introduction of 2-pyridine (**148**) resulted in a loss in activity, while modification with a naphthalene (**149**) or benzyl (**150**) groups partially recovered some activity. Completely removing the aliphatic linker (**151**) resulted in a gratifying ~103% increase in activity compared to **55** (Figure 2.18). Replacement of the benzene ring with a naphthalene (**152**), allyl (**153**) or free amino groups (**154**), led to reduced activities. Removal of the *p*-methoxy (**155**) from **151** resulted in a loss in inhibition, while having a *p*-methoxy group on both benzene rings (**156**) induced an important ~152% increase in activity over the original hit compound **55**. This SAR investigation led to the identification of four potent aryl amides miR-21 inhibitors (**131**, **137**, **151**, and **156** (Figure 2.18).

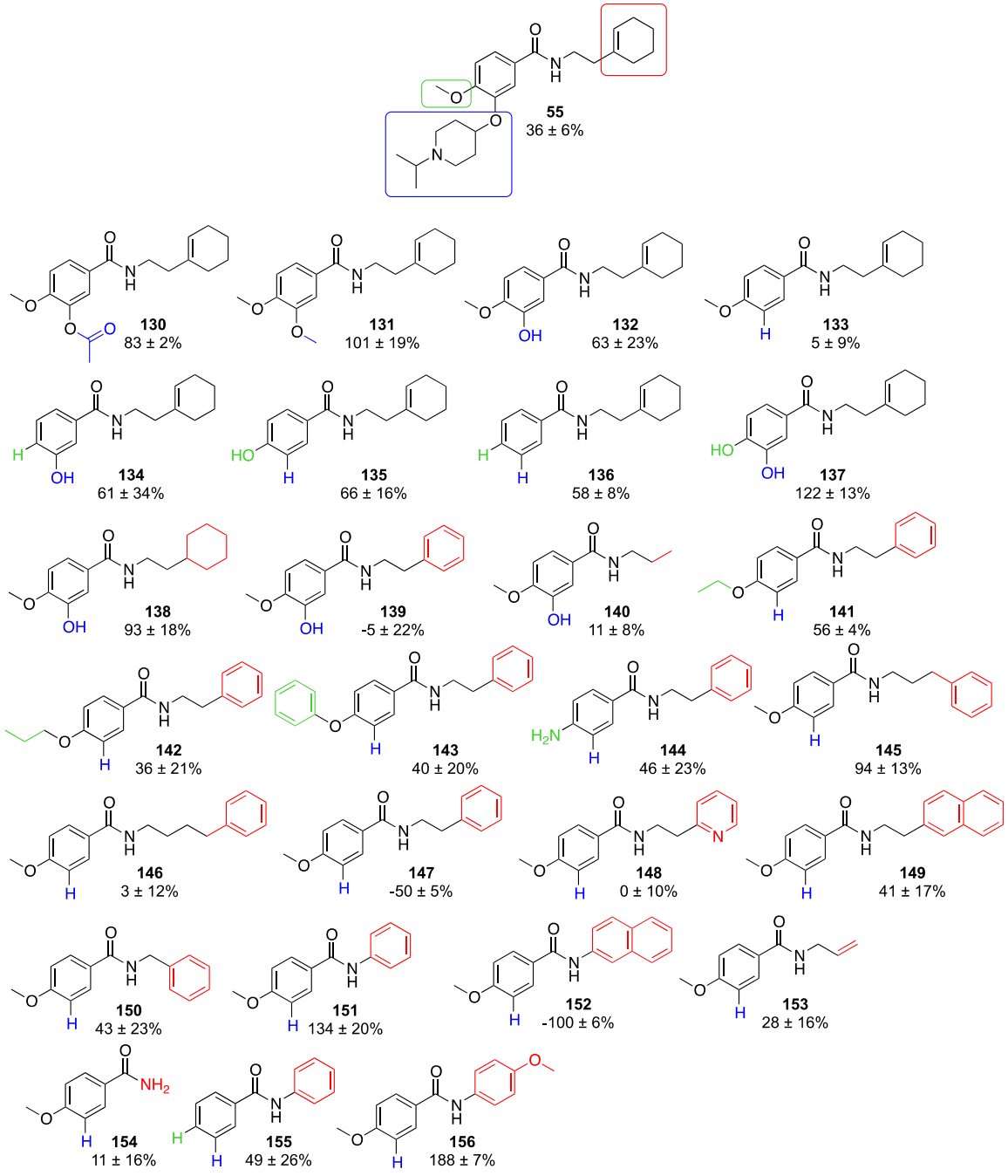

Figure 2.18: Activity of re-synthesized hit compound **55** in the miR-21 assay and SAR investigation.
Values represent percent change in luciferase signal normalized to cell viability and relative to DMSO control. Error calculated from the standard deviation of three independent measurements. Cell-based assays were performed by Yuta Naro and analogs were synthesized by Matt Stephens.

The four most promising aryl-amide analogs were further investigated to assess their potency and selectivity towards miR-21 inhibition. Yuta Naro tested the four inhibitors in dose-

response experiments using the miR-21 luciferase assay to calculate their EC_{50} values. Gratifyingly, **151** and **156**, which promoted the largest increase in firefly luminescence (Figure 2.18) were found to have EC_{50} values of 2.3 μM and 0.86 μM, respectively, which was comparable and even improved over the reference miR-21 inhibitor **24** (EC_{50} value of 2 μM). These inhibitors were tested in the miR-122 luciferase assay to determine their level of selectivity. Huh7-psiCHECK-miR122 cells were treated with the aryl-amide derivatives at 10 μM for 48 h and the *Renilla* luciferase expression was measured using a Dual Luciferase Assay (Promega). None of these inhibitors affected the expression of *Renilla* luciferase, suggesting some degree of selectively for miR-21 regulation (Figure 2.19).

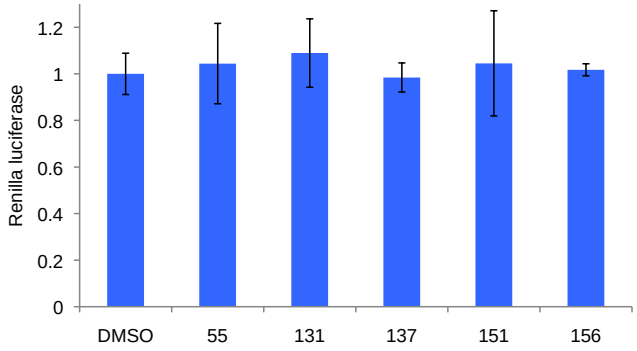

Figure 2.19: Evaluation of the selectivity of the aryl-amide inhibitors **55**, **131**, **137**, **151**, and **156** in the miR-122 assay.
Dual Luciferase Assay of Huh7-psiCHECK-miR-122 cells treated with the hit compound **55** and the most promising analogs at 10 μM. The luciferase signal was normalized to a DMSO control. Experiments were performed in triplicate and the standard deviations of the three independent assays were calculated.

To look more deeply into the selectivity of the aryl-amide inhibitors, the endogenous levels of three different miRNAs, in addition to miR-21, were measured by qRT-PCR after exposure to the compounds (Figure 2.20). HeLa cells were treated with the aryl-amide analogs **131**, **151**, and **156** at 10 μM for 48 h. The total RNA for each sample was isolated using the miRNeasy kit (qiagen), the concentration was measured on a Nanodrop, and all the samples were diluted to the same concentration (8 ng/μL) before being reverse transcribed using the TaqMan

microRNA Reverse Transcription Kit (Life Technologies) in combination with the corresponding TaqMan RT primers for RNU19 (endogenous control), miR-21, miR-125b, miR-17-5p, and miR-222 (Life Technologies). Quantitative Real Time PCR was conducted in triplicate for each RT reaction with the TaqMan 2x Universal PCR Master Mix and the TaqMan primers for RNU19 or the corresponding miRNAs on a CFX96 RT-PCR detection system (BioRad). Although, the derivative **131** did not show much inhibition, the aryl-amide **151** and **156** significantly reduced the miR-21 levels by 43 and 61%, respectively (Figure 2.20A). In contrast, the expression levels of miR-125b, miR-17-5p, and miR-222 were barely affected by the exposure to the inhibitors (Figure 2.20A). These data and the luciferase data (Figure 2.19) suggest that these compounds may be selective miR-21 inhibitors and not general inhibitors of the miRNA pathway.

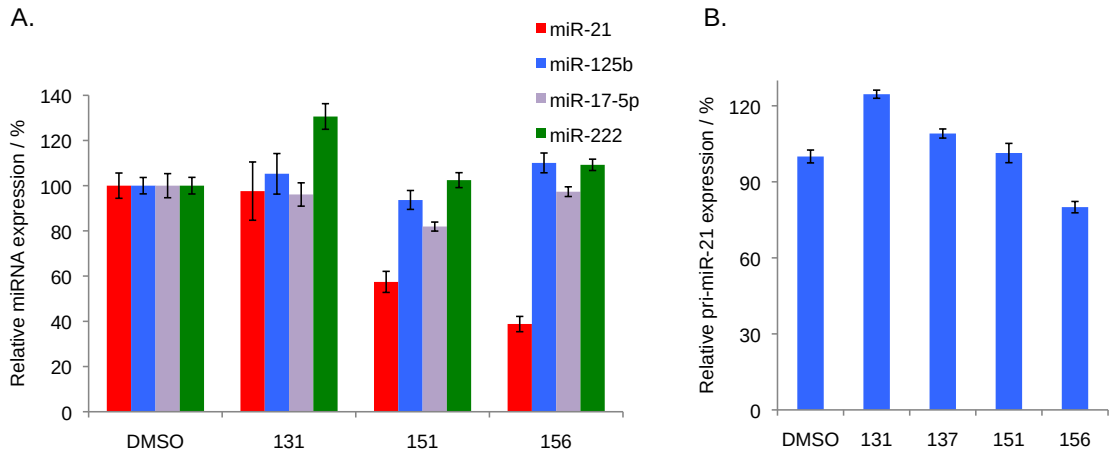

Figure 2.20: qRT-PCR measurements of miRNA expression levels after treatment with the potent aryl-amide miR-21 inhibitors **131**, **151**, and **156**.
HeLa cells were exposed to the inhibitors at 10 μM for 48 h. **A**. qRT-PCR of the intracellular levels of miRNAs miR-21, -125b, -17-5p, and -222. **B**. qRT-PCR of intracellular levels of pri-miR-21 after treatment with compounds at 10 μM for 48 h. The data were normalized to a DMSO control and the error bars indicate the standard deviation determined from three independent measurements.

The levels of primary pri-miR-21 were also measured by qRT-PCR after treatment with the compounds **131**, **137**, **151**, and **156**. In a similar way, HeLa cells were treated with the four

most potent aryl-amides at 10 μM for 48 h. The total RNA for each sample was isolated using the miRNeasy kit (qiagen), the concentration was measured on a Nanodrop, and all the samples were diluted to the same concentration (10 ng/μL) before being reverse transcribed using the iScript cDNA Synthesis kit (BioRad). Quantitative Real Time PCR was conducted in triplicate for each RT reaction with the TaqMan 2x Universal PCR Master Mix and the TaqMan primers for pri-miR-21 and the endogenous GAPDH control on a CFX96 RT-PCR detection system (BioRad). The levels of pri-miR-21 were normalized to the GAPDH control and the $2^{-\Delta\Delta Ct}$ method was used to determine the pri-miR-21 expression change in the treated samples relative to the DMSO control. In contrast to compound **24**, the aryl-amide inhibitors did not significantly modify the expression levels of pri-miR-21 (Figure 2.20B). These preliminary data suggest that the mechanism of action of these new inhibitors is fundamentally different from the mechanism of the previously discovered miR-21 inhibitor **24**. The aryl-amide inhibitors **151** and **156** do not target miR-21 at the transcriptional level, but rather may target some downstream processes involved in the maturation of miR-21. Further studies into their mechanism will be performed.

2.4 INVESTIGATION INTO THE MODE OF ACTION OF MIRNA INHIBITOR 51

2.4.1 Recovery of Inhibition by Transfection of Precursor miR-21

After studying a subset of the different chemotypes identified from the HTS (Figure 2.4), at least two new classes of inhibitors, the oxadiazole and the aryl-amide series based on **51** and **156**, respectively, delivered additional miR-21 inhibitors. The small molecule miR-21 inhibitors are therapeutically relevant as they can provide new lead structures for anticancer therapies, as

well as new probes to study the implication of miR-21 in the development of cancer. There are still a lot of unknowns to be discovered within the miRNA pathway and their participation in various diseases. Although there are some pieces of evidence showing that the oxadiazole **51** is a potent inhibitor of miR-21, nothing is known regarding its mechanism of action. Identifying the protein(s) specifically targeted by the small molecule miR-21 inhibitor **51** would not only increase the current knowledge but could also lead to potential new drug targets.

As discussed in Chapter 1.5, the small molecule inhibitors can potentially interfere with different steps of the biogenesis of miRNA. First, the effect of inhibitor **51** on miR-21 maturation was evaluated. Colleen Connelly transfected HeLa-miR-21-Luc cells, which were engineered to stably express the miR-21 reporter construct, with precursor pre-miR-21 (Figure 2.21). If the small molecule **51** interferes with the mature miR-21, either at the unwinding step, at the RISC loading step, or with the association of the miR-21 with the mRNA, or if **51** prevents the processing of pre-miR-21 into miR-21, introduction of exogenous pre-miR-21 should alleviate the inhibitory effect of **51**. Conversely, if the small molecule **51** acts at the transcriptional step, or blocks the processing of pri-miR-21, the exogenous pre-miR-21 should be processed properly through the miRNA pathway to produce mature miR-21. Transfection of HeLa-miR-21-Luc cells with xtremeGENE or precursor pre-miR-122 (used as a selectivity control) followed by exposure to DMSO did not have any effect on the luciferase expression; in comparison transfection with pre-miR-21 induced a 50% decrease in the firefly signal (Figure 2.21). This was due to the presence of additional mature miR-21, which further inhibited the translation of the firefly luciferase mRNA through binding to its target sequence. In the cells transfected with xtremeGENE (no precursor) or the control precursor pre-miR-122, treatment with the inhibitors **24** and **51** led to 50% increase in firefly expression, due to the inhibition of miR-21 by the small

molecules. However, in the cells transfected with the precursor pre-miR-21, treatment with **24** and **51** had virtually no effect on the luciferase expression compared to the DMSO control (Figure 2.21). This demonstrated that the precursor pre-miR-21 was correctly processed into mature miR-21, even in the presence of the small molecules **24** and **51**, and suggested that the inhibitors act at the transcriptional or the pre-transcriptional step. If the compounds would inhibit the miR pathway post-transcriptionally, an increase in firefly expression would be expected, because the processing of the precursor into mature miR-21 would be blocked by the inhibitors.

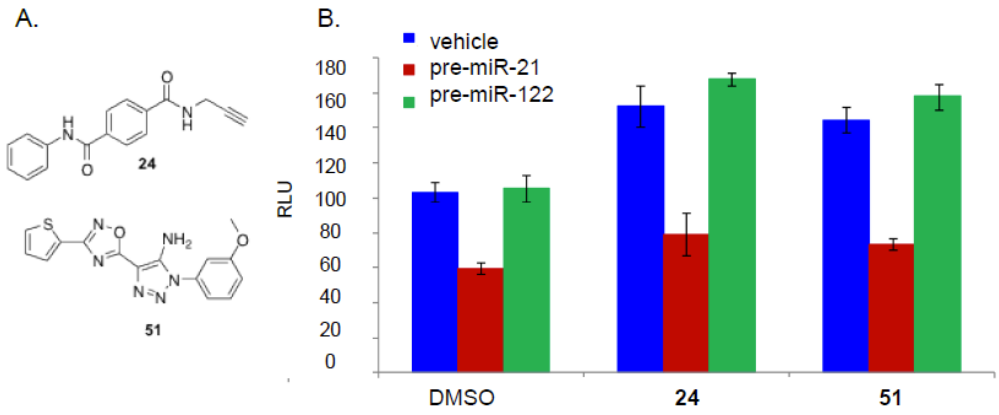

Figure 2.21: Recovery of the inhibitory activity of the miR-21 inhibitors **24** and **51** through transfection of a pre-miR-21 precursor.
A. Structure of the inhibitors **24** and **51**. **B**. Bright Glo Luciferase assay of HeLa-miR-21-Luc cells transfected with the precursors pre-miR-21 or pre-miR-122 and treated with DMSO, **24**, or **51** for 48 h. All experiments were conducted in triplicate and the data was normalized to the vehicle (xtremeGENE transfection reagent) control. The error bars indicate standard deviations determined from three independent experiments. Cell-based assays were performed by Colleen Connelly.

2.4.2 Target Identification Experiments for the Oxadiazole Inhibitor 51

Although the SAR studies of the hit compound **51** did not lead to the identification of a significantly more potent inhibitor, the knowledge collected during this investigation was very helpful in locating suitable positions where modifications were tolerated. In order to identify the cellular target of the inhibitor **51**, it was first opted to isolate the target protein via affinity-

purification (Figure 2.22).[142] This method relies on the attachment of the inhibitor "active pull-down probe" to a resin support. The cells are lysed and the cellular extract is incubated with the functionalized resin. This step is followed by a series of washes, elution of the target protein with free inhibitor, analysis by SDS-PAGE, and after excision from the gel, the protein is digested and analyzed by mass spectrometry to identify its identity (Figure 2.22). Some proteins might interact with the resin or the linker non-specifically and contrary to the unbound proteins, they might not be totally removed during the washing steps. That's why in addition to functionalizing the resin with an active ligand, the resin is also commonly modified with an inactive but structurally similar analog. That way the non-specific proteins appear on both "active" and "inactive" lanes on the gel, while the target protein is only visible on the active lane (Figure 2.22).[143]

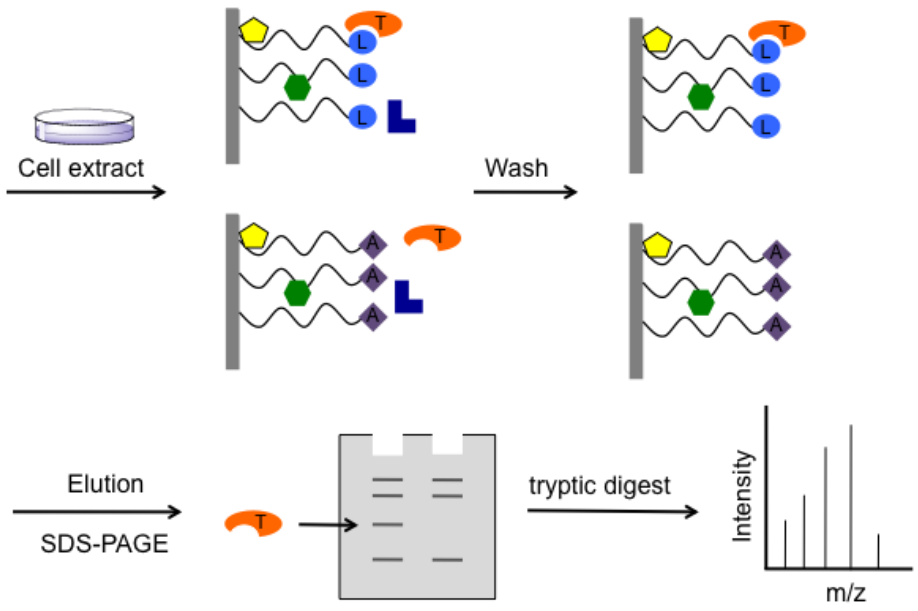

Figure 2.22: Representation of the affinity chromatography approach to target identification.
The active ligand (L) or a structurally similar inactive analog (A) are immobilized on a resin (shown in gray). The resin is incubated with cell lysate containing the target protein (T) and non-specific proteins (shown in green and yellow). Unbound proteins (shown in blue) are removed through a series of washes. The target protein is eluted by incubation of the resin with an excess of the unmodified active compound and separated by SDS-PAGE. The target protein is excised from the gel, digested, and finally analyzed by mass spectroscopy. Adapted from *Chem. Biol*. 17, Sato, S.; Murata, A.; Shirakawa, T.; Uesugi, M.; Biochemical Target Isolation for Novices: Affinity-Based Strategies, 616. Copyright (2010), with permission from Elsevier.

In order to isolate the target protein of **51** via affinity-purification, a nucleophilic handle needed to be introduced in the molecule to allow further attachment to a resin. Modification of the *para* position (**158**) with the hydroxymethylene group was well tolerated, while modifications of the *meta* (**157**) or *ortho* (**159**) positions led to 67% and 38% reduction in activity, respectively (Figure 2.23). To efficiently pull-down the target protein, it is important that the protein retains its affinity for the modified probe.[143] For example, attachment to the resin might block the approach of the protein or display the ligand in a conformation not anymore recognized by the protein. To address this concern, **160** was synthesized that contains a short PEG-linker (Figure 2.23). The introduction of a small linker was not tolerated as **160** suffered a 53% loss in activity.

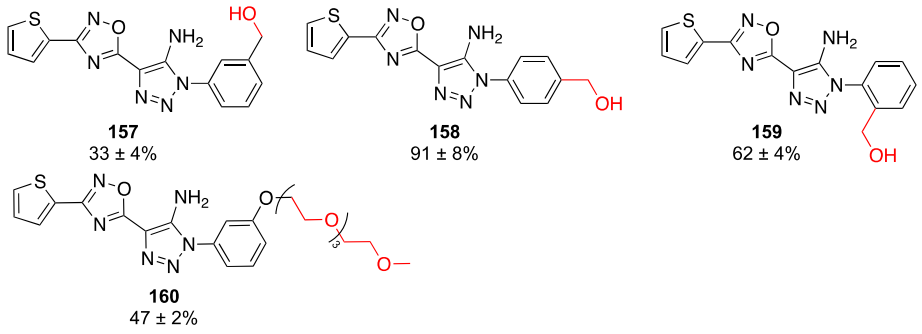

Figure 2.23: Structural modifications of the miR-21 inhibitor **51** aimed at identifying a probe suitable for affinity purification (variations to the original structure are shown in red).
The numbers represent the activity relative to **51** within the same miR-21 luciferase assay. All assays were conducted in triplicate and the error represents the standard deviation from the three independent experiments. Cell-based assays were performed by Colleen Connelly.

To synthesize the analog **160**, the aniline **161** was protected with a Boc protective group. The phenol **162** was alkylated with the short PEG linker after being heated to 60 °C in the presence of Cs_2CO_3 and **163** in DMA (dimethylacetamide). The corresponding product **164** was treated with 4 M HCl (hydrochloric acid) in dioxane to remove the protective group, and

subsequently treated with $NaNO_2$ and NaN_3 to afford the azide **166** (Scheme 2.10). Unfortunately, coupling of **166** with the nitrile derivative **99** failed to deliver the expected product. It was then decided to introduce the PEG linker directly on compound **112** using similar alkylation conditions with Cs_2CO_3 and DMA (Scheme 2.10).

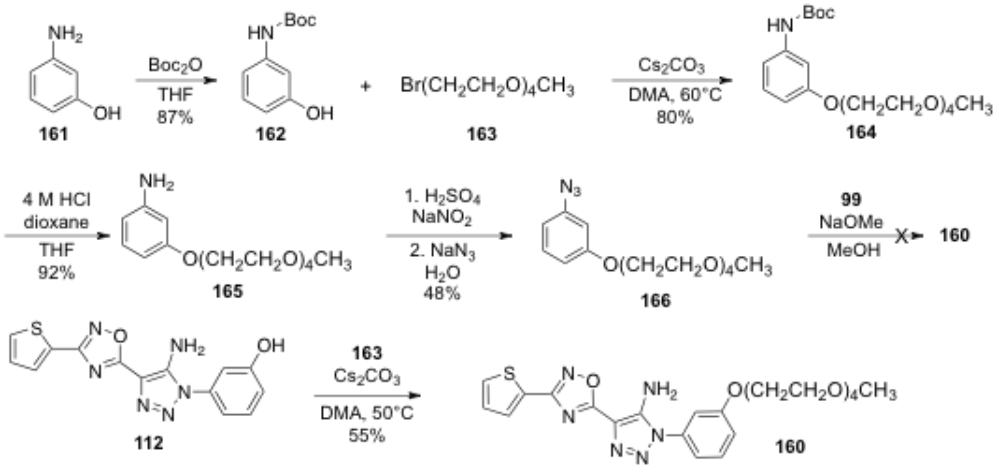

Scheme 2.10: Conditions tested to synthesize the pegylated-oxadiazole **160.**

Since **160** displayed a low activity, it did not seem that the affinity-purification would be successful in isolating the target protein. A different strategy, based on the photo-crosslinking method, was therefore envisioned. In this method a slight decrease in potency is more tolerated than in a pull-down experiment due to the formation of a covalent bond between the inhibitor and its target (Figure 2.24). To apply this strategy the inhibitor must be functionalized with two orthogonal motifs: 1) It must bear one photo-crosslinking group such as a diazirine, an aryl-azide, or a benzophenone group, which is capable of forming a covalent bond with the nearby target protein after a brief UV irradiation.[144] 2) An alkyne functionality is often introduced in order to add a fluorescent tag to the small molecule/protein complex via click reaction. Once such a modified compound is available, it is important to verify that these modifications do not

abolish the activity of the inhibitor. The cells (or cell lysate) are incubated with the inhibitor for a few hours, then exposed to UV light for a few minutes. After lysis of the cells, a click reaction is carried out to introduce a fluorophore or biotin tag to the probe/protein complex, in order to facilitate the subsequent analysis of the protein. After the click reaction, the cell lysate is analyzed by SDS-PAGE, from where the band corresponding to the target protein can be excised and further analyzed by mass spectrometry (Figure 2.24).

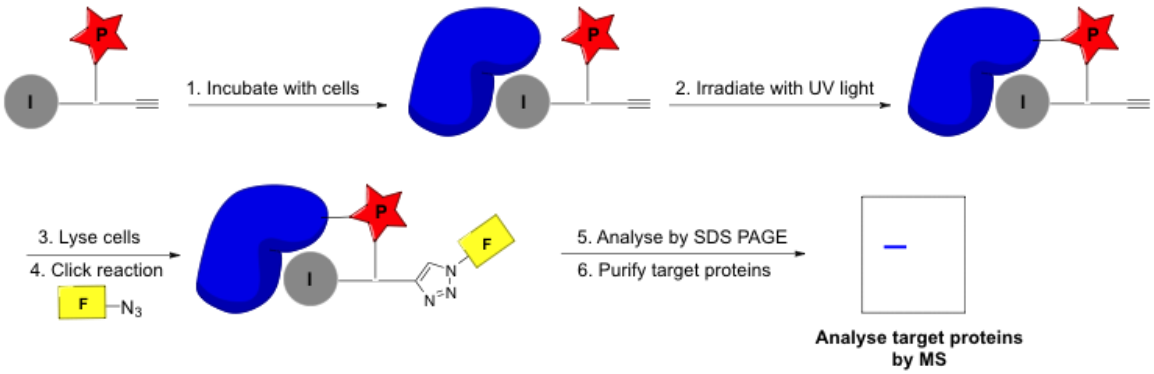

Figure 2.24: Schematic of the photo-crosslinking strategy to identify the target protein of **51.**
The inhibitor (I) is functionalized with an alkyne and a photo-probe (P). It is then incubated with live cells, and covalently linked to its target protein(s) upon UV irradiation. Following click reaction with an azido-fluorophore (F), the lysate is analyzed by SDS-PAGE and the target protein(s) can be easily detected when imaging for fluorescence. Adapted with permission from *J. Am. Chem. Soc.* **2012**, 134, 3001. Copyright 2012 American Chemical Society.

The inhibitor **51** was then modified with an alkyne or a benzophenone functionality to determine the feasibility of the photo-crosslinking method. Replacement of the *m*-methoxy (**51**) with *m*-propargyl (**167**) led to a slight increase in activity, whereas modification with a benzophenone in *meta* (**168**) or *ortho* (**170**) positions resulted in a 20% decrease in activity (Figure 2.25). Surprisingly, *para* substitution (**169**) could be well accommodated as very little change in activity was observed. Keeping the benzophenone in *meta* (**171**) or *para* (**172**) positions, an alkyne motif was introduced in place of the thiophene ring (Figure 2.25).

Gratifyingly these two photo-crosslinking probes still showed a good inhibition of miR-21, their activity was increased by 24% and 5%, respectively for **171** and **172**, compared to the parent compound **51**. Extension of the alkyne linker by four additional carbons (**173**) negatively affected the activity.

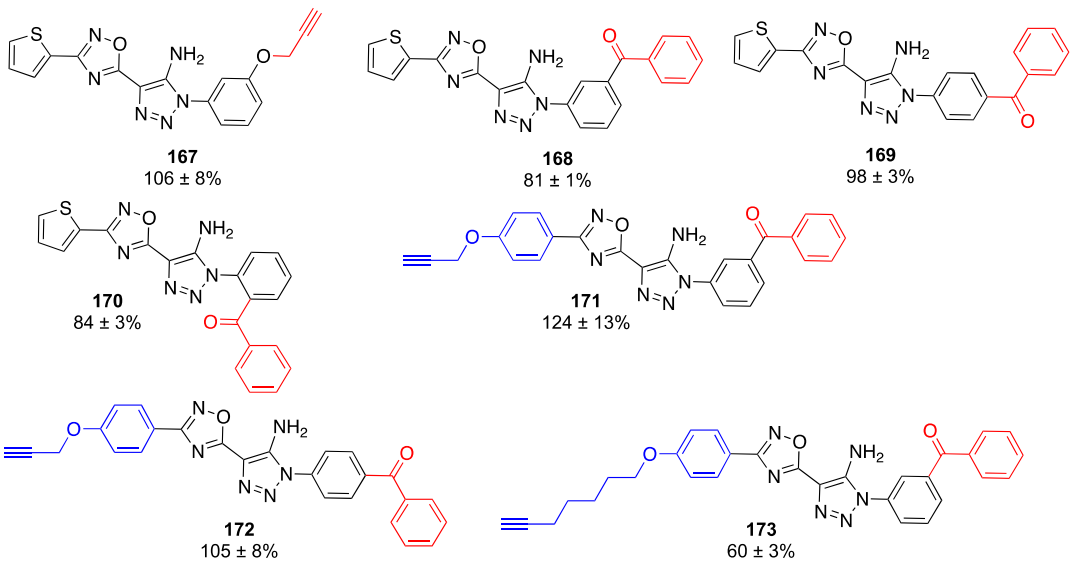

Figure 2.25: Structural modifications of the miR-21 inhibitor **51** aimed at identifying a probe suitable for photo-crosslinking (variations to the original structure are shown in red and blue).
The numbers represent the activity relative to **51** within the same miR-21 luciferase assay. All assays were conducted in triplicate and the error represents the standard deviation from the three independent experiments. Cell-based assays were performed by Colleen Connelly.

The analogs **167-170** were synthesized following the protocol described in Scheme 2.6 from the corresponding azides (**95**) and the intermediate **99**. The derivatives **171** and **172** were obtained using very similar conditions (Scheme 2.11). The alkylation of 4-hydroxybenzonitrile (**174**) with propargyl bromide and Cs_2CO_3 at 50 °C in acetone quantitatively delivered **175**. The nitrile **175** was then treated with Na_2CO_3 and $H_2NOH{\bullet}HCl$ to provide the hydroxamine **176** in 94% yield. This intermediate was condensed with **98** to form the oxadiazole precursor **177**, which was treated with the corresponding azides (**178**) to yield the probes **171** and **172** (Scheme

2.11). Similarly, **173** was obtained upon reaction of the azido-benzophenone **178** and the precursor **182**. The oxadiazole intermediate **182** was synthesized in three steps, starting from a Mitsunobu reaction between 4-hydroxybenzonitrile and the alcohol **179**, followed by treatment with Na_2CO_3 and $H_2NOH{\bullet}HCl$ to form the hydroxamine **181**. The precursor **181** was then heated to reflux with **98** to deliver **182** in moderate yield (Scheme 2.11).

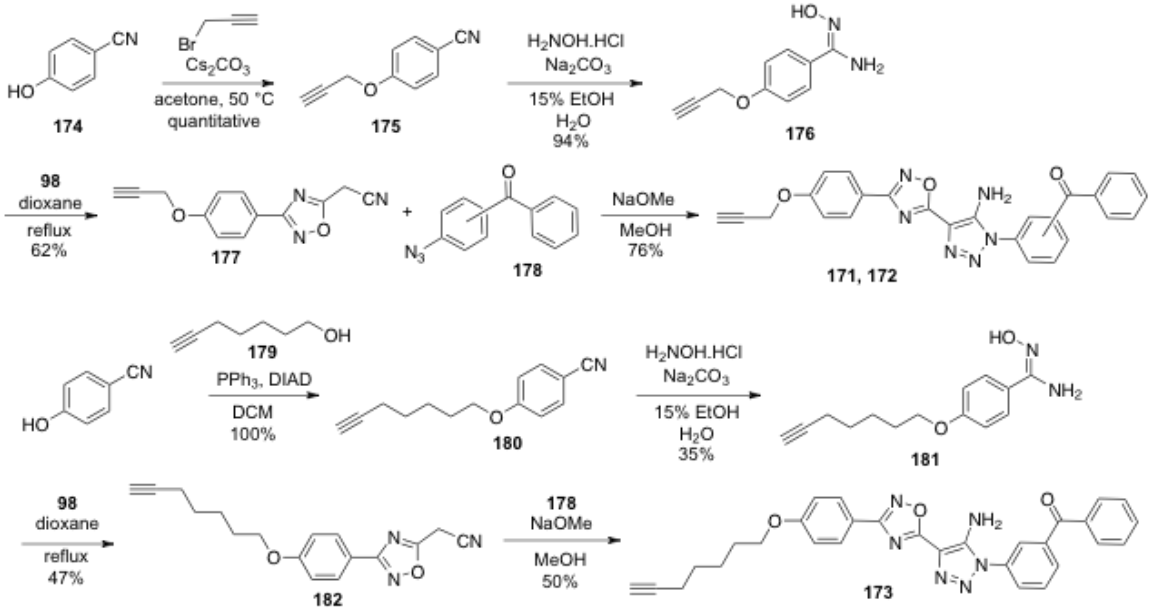

Scheme 2.11: Synthetic route to photo-crosslinking probes **171-173.**

Since the analogs **167**, **169**, and **171** showed satisfactory activity in the miR-21 luciferase assay, being comparable or slightly more potent than **51**, they were further tested in the *in vitro* FLuc assay. The less potent photoprobe **173** was also evaluated. None of these compounds inhibited the enzyme (Figure 2.26), which suggested that they display miRNA inhibition activity, and confirmed that they represent promising probes to investigate the mode of action of **51**.

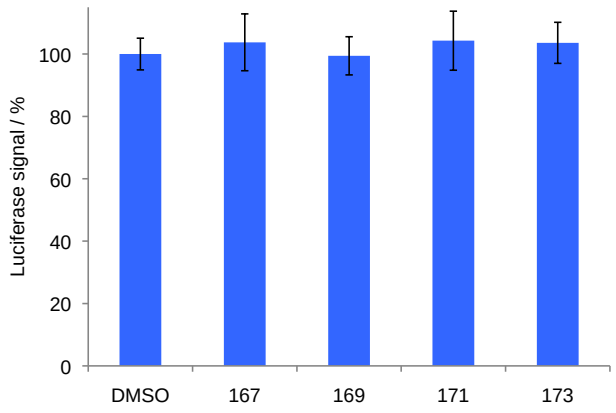

Figure 2.26: *In vitro* FLuc assay of the oxadiazole photoprobes.
The compounds **167**, **169**, **171**, and **173** (10 μM) were incubated for 30 min with the recombinant firefly luciferase enzyme and the luminescence was measured using a Bright glo assay (Promega). The data are relative to the DMSO control (1%). Three independent assays were averaged and error bars represent standard deviations.

The synthesis of the aryl-azide probe **188** was also undertaken. 4-Aminobenzonitrile was treated with $NaNO_2$ and NaN_3 to form the azide **184**. Different conditions were tested to synthesize **185** because the treatment with Na_2CO_3 and $H_2NOH{\bullet}HCl$, which was previously employed to obtain hydroxamine intermediates, failed to deliver the expected product. Instead, the nitrile **184** was heated to 50 °C in the presence of $H_2NOH{\bullet}HCl$ and a large excess of NMP (*N*-methylmorpholine). The intermediate **185** was then condensed with **98** to give the oxadiazole **186** in 79% yield. Although some of the expected azide **188** could be obtained after the cyclic addition of **186** and **187** (Scheme 2.13), it was contaminated with some impurities. In order to test and use the probe **188** in cell-based experiments different purification methods, such as trituration in DCM or hexanes and column chromatography, were tried to improve the purity of **188** but did not afford any pure compound. Given three interesting photo-crosslinking probes (**171**-**173**) were obtained, it was decided to test those in target identification experiments and to consider a different approach to the azide **188** only if the benzophenone probes failed to selectively react with the target protein.

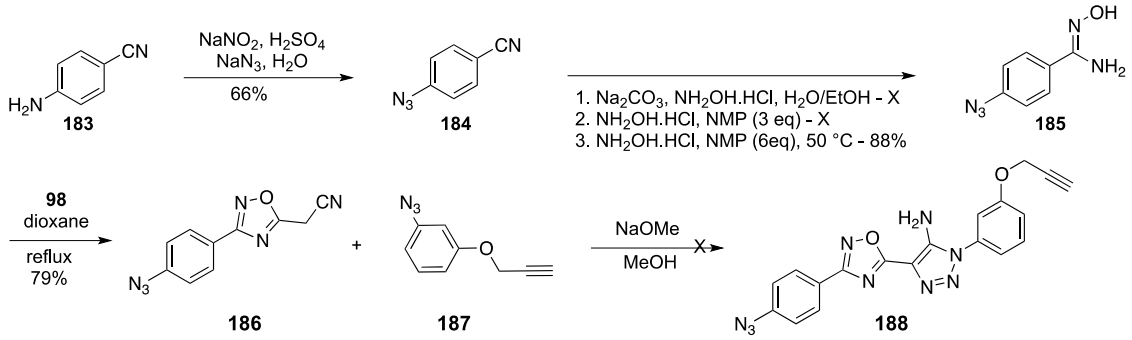

Scheme 2.12: Attempted synthesis of the azide photo-crosslinking probe **188.**

In the aim of facilitating the detection of the target protein(s), a fluorescein-azide was synthesized that could be introduced into the probe/protein complex via click reaction (Figure 2.24). 1,6-Dibromohexane was treated with NaN_3 to form 1,6-diazidohexane (**189**), and then a Staudinger reaction was carried out to reduce one azido group to the corresponding free amine **190**.[145] Fluorescein isothiocyanate was stirred overnight with DIPEA and **190** in DMF to deliver the azide **191** in 71% yield (Scheme 2.13).

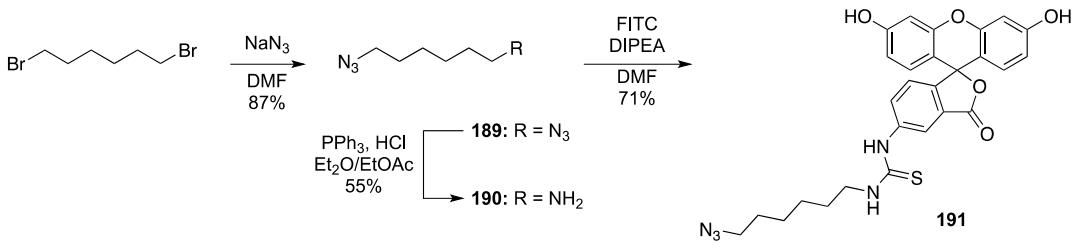

Scheme 2.13: Synthesis of the fluorescein-azide **191.**

Following the synthesis, the photo-crosslinking probes **171** and **173** were tested in live cell experiments by adapting a similar approach previously reported.[146] HeLa cells were treated with the inhibitors **171** and **173** (10 μM, 0.5% DMSO) or with DMSO (0.5%) for 16 h. The media was removed and the cells were quickly washed with 1 mL of PBS. The cells were

irradiated at 365 nm for 10 min, trypsinized, and pelleted by centrifugation. The proteins were extracted with 50 μL mammalian protein extraction buffer (GE healthcare) followed by 20 min incubation on ice, 5 min vortex, and 30 min centrifugation at 4 °C. The supernatant was extracted and the amount of proteins was determined using a Bradford assay. After dilution of each sample to the same concentration in PBS, the click reaction was performed with the fluorescein-azide (**191**), TCEP (tris(2-carboxyethyl)phosphine), copper (II) sulfate, and TBTA (tris[(1-benzyl-1H-1,2,3-triazol-4-yl)methyl]amine) for 2 h at room temperature. The final concentration of the fluorescein-azide was optimized to achieve successful labeling. After the click reaction an acetone precipitation was performed to remove the excess click reaction reagents, the proteins were re-suspended in PBS and analyzed by SDS-PAGE (Figure 2.27). Unfortunately, these experiments were not successful as the same fluorescently-labeled proteins were observed in lanes 3, 4, and 5 (Figure 2.27). In lane 3, the cells were only treated with DMSO (no alkyne-containing probe), therefore no fluorescently-tagged proteins were expected. These data suggest that the fluorescein-azide might non-specifically react with cellular components. In the future, to successfully detect the target protein the experimental design will need to be optimized, for example different UV irradiation times could be tested, the click reaction might be performed under denaturing conditions, and a different fluorophore probe could be synthesized.

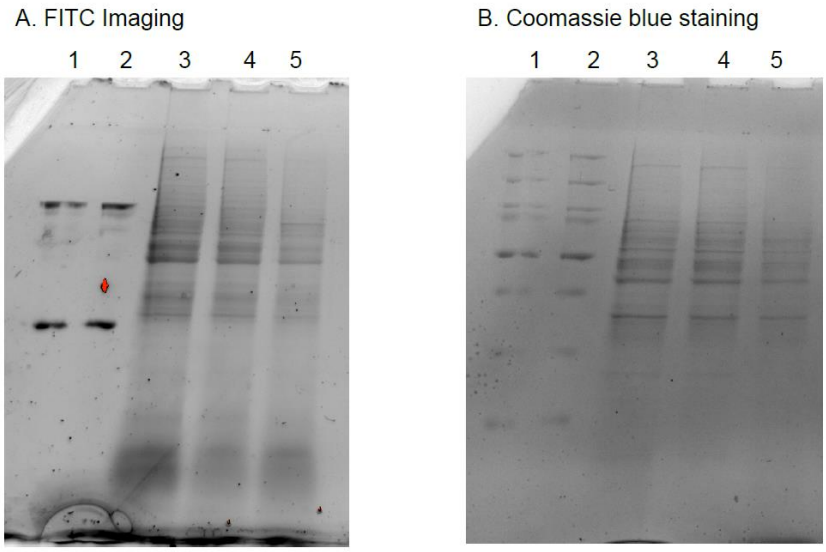

Figure 2.27: Example of a 12% SDS-PAGE of protein samples isolated from HeLa cells treated with the photoprobes **171** and 173 or the negative control DMSO, and labeled with the fluorescein-azide.
Lanes 1 & 2: Ladder, Lane 3: DMSO (0.5%), Lane 4: **171** (10 μM, 0.5% DMSO), Lane 5: **173** (10 μM, 0.5% DMSO). **A.** The gel was imaged on a ChemiDoc using the filter for FITC. **B.** The gel was non-specifically stained with coomassie blue.

2.5 THERAPEUTIC EVALUATION OF THE SMALL MOLECULE MIR-21 INHIBITORS IN LIVER CANCER CELLS

Hepatocellular carcinoma (HCC) is a primary cancer of the liver and is the third leading cause of cancer-related death worldwide.[147] Major risk factors include obesity, diabetes, and in 80% of cases infection with hepatitis B or C virus.[148] HCC is largely insensitive to most chemotherapeutics, only a few kinase inhibitors, such as sorafenib, help improving patients overall survival and reducing disease recurrence after surgery. However, metastasis and recurrence are still very common in 30-40% of cases.[147] The majority of patients are diagnosed at late stages of the diseases due to a lack of reliable biomarkers.[147] The molecular mechanisms

responsible for the pathogenesis of HCC have not been elucidated yet but would be of tremendous value in order to improve the diagnosis of HCC and find more effective treatments.

Some studies have recently linked miRNA misregulation with HCC. For example, the liver specific miR-122 is greatly downregulated in HCC cells; where it was shown to target Cyclin G1 (CCNG1) and the Bcl-2-family member Bcl-w, which results in chromosomal instability and enhanced anti-apoptotic activity.[149] Not surprisingly, miR-21 was found to be highly overexpressed in HCC cell lines compared to normal liver cells.[148] miR-21 was demonstrated to participate in the development of HCC, in part by repressing the tumor suppressor PDCD4,[150] and by suppressing both PTEN and human sulfatase-1 (hSulf-1), which leads to the activation of the AKT/ERK pathway.[151] Constitutive activation of the AKT pathway, reported in more than 40% cases of HCC, plays a critical role in the formation of metastasis and in drug-resistance.[152] Transfection with an AMO anti-miR-21 in various HCC cell lines was shown to promote significant reductions in cell viability.[148, 151] Interestingly, a recent study showed that the naturally occurring indole-3-carbinol (**21**, Figure 1.4) reduces the growth and clonogenic survival of HCC cell lines, via direct inhibition of miR-21, miR-221, and miR-222. Treatment of SNU-449 HCC cell lines with 200 μM indole-3-carbinol for 48 h elicited a 50% reduction in cell viability.[152] These results suggest that inhibiting miR-21 alone, or in combination with known drugs, represent a potentially attractive avenue to new HCC therapies.

Based on these observations, the ability of the miR-21 inhibitors **24** and **51** at promoting the death of HepG2 HCC cells was tested. HepG2 cells were treated with increasing concentrations of the compounds and incubated for 48 h, followed by measurement of cell viability using a CellTiter Glo assay (Promega). This luminescent assay measures the reduction in ATP levels, which correlates with the presence of metabolically active live cells. A dose-

dependent reduction of the cell viability was observed after treatment with either inhibitor (Figure 2.28). It is noteworthy that at a concentration of 50 μM, the inhibitors **24** and **51** displayed a 50% and 66% decrease in cell viability, respectively. This compares favorably with what was found with the natural product indole-3-carbinol and suggests that miR-21 inhibitors are effective at inducing apoptosis in HCC cells.

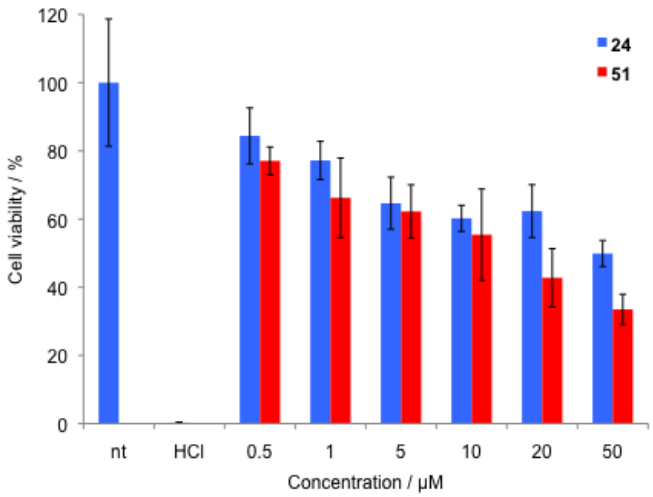

Figure 2.28: Cell viability assay of HepG2 cells treated with the miR-21 inhibitors **24** and **51.**
HepG2 cells were exposed to increasing concentrations of the inhibitors for 48 h and the cell viability was measured with a CellTiter Glo assay (Promega). The data were normalized to a non-treated control, and some cells were treated with 1 M HCl for 1 h as a positive control for cell death. All assays were conducted in triplicate and the error represents the standard deviation from the three independent experiments.

HepG2 cells that were transfected with a miR-122 overexpressing vector and treated with the anti-HCC reference drug sorafenib exhibited a significant reduction in cell viability, as well as a 35% increase in apoptosis, compared to sorafenib only exposed cells.[153] Given the scarcity of therapeutic agents for HCC and the poor efficacy of the available ones due to intrinsic drug-resistance,[154] there is an urgent need to identify new therapeutic approaches or combination therapies to improve patient outcome. In the future, it will be interesting to investigate the therapeutic potential associated with the co-treatment of HCC cells with the small molecule miR-

122 activator (**31**) and sorafenib, a small molecule miR-21 inhibitor (**24** or **51**) and the miR-122 activator **31**, or sorafenib with a small molecule miR-21 inhibitor (**24** or **51**).

2.6 SUMMARY AND OUTLOOK

Analogs of the previously identified miR-21 inhibitor **24** were synthesized to further improve its potency and replace the diazo linkage with more stable bonds. To that aim, four analogs were synthesized which introduced an amide bond in place of the diazo motif, but none of them showed noticeable improvements in activity.

Several hit compounds from a miR-21 high-throughput screen were re-synthesized and investigated through the synthesis and testing of analogs. Some of these re-synthesized hits did not show any activity in the miR-21 luciferase assay; as it was the case with the aryl-amides **53** and **54** and the ether-amides **47** and **48**. Five analogs of **47** were quickly synthesized in the hope to rescue some activity but since none of them showed any promising increase in luciferase expression in the miR-21 assay, this series was not pursued any further.

Even though the re-synthesized *N*-acylhydrazone hit compounds **49** and **50** were not very active, a few promising analogs were identified through preliminary SAR investigation (thirteen analogs total were synthesized). The best hydrazone derivatives **78** and **84** were subjected to secondary assays to investigate their selectivity. Although they had no effect on the expression of miR-122, they downregulated miR-21, -20a, -24, and -27b to the same extent, suggesting they are not selective towards miR-21 inhibition. Their selectivity profile would need to be further investigated via large scale profiling of miRNAs.

The re-synthesized oxadiazole hit compound **51** showed an encouraging 40% increase in activity compared to the reference inhibitor **24**. An SAR study was conducted via the synthesis of 34 analogs, where a few compounds were identified that displayed a comparable or slightly improved activity over **51**. Preliminary data indicated that the oxadiazole **51** targets miR-21 at a transcriptional or pre-transcriptional step. Different strategies have been attempted to identify the cellular target of **51**. Some efforts went into the synthesis of several photo-crosslinking probes, which exhibited the same level of activity as **51**, and will be used to isolate the target protein(s).

The last series of compounds studied was based on the hit aryl-amide **55**. In total, 28 analogs were synthesized (by Matt Stephens) that led to the identification of four promising inhibitors (**131**, **137**, **151**, and **156**). These compounds displayed a high level of selectivity for miR-21, and in contrast to the other miR-21 inhibitors discovered **24** and **51**, they seem to target downstream processes of miR-21 maturation. A more thorough investigation of their mode of action should be performed in the future.

miR-21 is a known oncomiR, which is highly expressed in almost all types of cancer. miR-21 inhibition has been shown to help inducing apoptosis, decreasing cell proliferation, and increasing the sensitivity of common chemotherapeutic agents.[104] The small molecule miR-21 inhibitors **24** and **51** induced a >50% decrease in cell viability of HepG2 cells at 20 μM. Further studies will investigate the therapeutic potential of the combination treatment of small molecule miR-21 inhibitors with either the small molecule miR-122 activator **31**, or known anticancer agents, specifically with sorafenib in HCC cells.

In conclusion, new small molecule miR-21 inhibitors were developed, which represent powerful tools to investigate miR-21 biogenesis, as well as miR-21 participation in carcinogenesis. More importantly, these small molecule miR-21 inhibitors provide new agents to

study the benefit of combination therapies and could aid in the development of new anticancer therapeutics.

2.7 EXPERIMENTALS

Cell culture. Experiments were performed using the HeLa cell line cultured in Dulbecco's Modified Eagle Medium (DMEM; Hyclone) supplemented with 10% Fetal Bovine Serum (FBS; Seradigm premium grade, Lot #093B13) and 2% penicillin/streptomycin (VWR) and maintained at 37 °C in a 5% CO_2 atmosphere. Huh7-psiCHECK-miR122 cells were cultured in Dulbecco's Modified Eagle Medium (DMEM; Hyclone) supplemented with 10% fetal bovine serum (FBS; Seradigm premium grade, Lot #093B13), 500 μg/mL of G418 (Sigma Aldrich), and 2% penicillin/streptomycin (VWR) and maintained at 37 °C in a 5% CO_2 atmosphere. HepG2 cells were cultured in Eagle's Minimum Essential Medium (Hyclone) supplemented with 10% FBS (VWR), 2% streptomycin/ampicillin (VWR), and 0.5 mM sodium pyruvate and maintained at 37 °C in a 5% CO_2 atmosphere.

Assessment of the selectivity of the small molecule miR-21 inhibitors. Huh7-psiCHECK-miR122 cells (a stably transfected line harboring a miR-122 binding sequence in the 3′ UTR of a *Renilla* luciferase gene)[124] were seeded at a density of 5,000 cells per well in white, clear-bottom, 384-well plates (Greiner). After an overnight incubation in media (DMEM, 10% FBS, free of antibiotics and free of G418, 45 μL), the cells were treated with compounds at a concentration of 10 μM (addition of 5 μL of a 0.1 mM solution stock in 1% DMSO) or a DMSO control (0.1% DMSO final concentration) in triplicate. The cells were incubated for 48 h followed by analysis

with a Dual Luciferase Reporter Assay Kit (Promega) using 20 μL passive lysis buffer and 25 μL of each luciferase reagent. The luminescence was measured on a Tecan M1000 platereader with a measurement time of 1 s and a delay time of 2 s. All experiments were performed in triplicate, for each well the *Renilla* luciferase read out was normalized to the firefly luciferase read out, and the average for each sample was further normalized to the DMSO control.

Quantitative real time PCR analysis. Hela cells were seeded at a density of 100,000 cells per well in 6-well plates, grown overnight, and treated with compounds at 10 μM (20 μL of a 1 mM DMSO stock in 1980 μL media) or with DMSO (1% final DMSO concentration). The cells were incubated at 37 °C for 48 h (DMEM, antibiotics-free, 5% CO_2). The media was removed, and cells were washed with PBS buffer (1 mL, pH 7.4) followed by RNA isolation with the miRNeasy mini kit (Qiagen) according to the procedure described in the appendix 6.2. The RNA was quantified using a Nanodrop ND-1000 spectrophotometer, and 40 ng of each RNA sample were reverse transcribed using the TaqMan microRNA Reverse Transcription Kit (Life Technologies) in conjunction with the RNU19 (control) or one of the miR-21, miR-125b, miR-222, miR-17-5p TaqMan RT primer (16 °C, 30 min; 42 °C, 30 min; 85 °C, 5 min, 5 μL RNA per 15 μL reaction). Quantitative real time PCR was carried out with a TaqMan 2x Universal PCR Master Mix and the appropriate TaqMan miRNA assay (Life Technologies) on a BioRad CFX96 RT-PCR thermocycler (1.3 μL RT PCR product; 95 °C, 10 min; followed by 40 cycles of 95 °C, 15 s; 60 °C, 60 s). The triplicate threshold cycles (Ct) obtained for each small molecule treatment were used to determine the relative levels of miR-21 in small molecule treated cells relative to the DMSO control using the $2^{-\Delta\Delta Ct}$ method.[155] The samples were also analyzed by qRT-PCR to measure the expression levels of pri-miR-21. After RNA isolation, 50 ng of each RNA sample were reverse transcribed using the iScript cDNA synthesis kit (BioRad) (25 °C, 5 min; 42 °C, 30

min; 85 °C, 5 min, 20 μL reaction). Quantitative real time PCR was conducted with a TaqMan 2x Universal PCR Master Mix and the appropriate TaqMan primers for hsa-pri-miR-21 or the endogenous control GAPDH (Life Technologies) on a BioRad CFX96 RT-PCR thermocycler (2 μL RT PCR product; 95 °C, 10 min; followed by 40 cycles of 95 °C, 15 s; 60 °C, 60 s). The triplicate threshold cycles (Ct) obtained for each small molecule treatment were used to determine the relative levels of pri-miR-21 in small molecule treated cells relative to the DMSO control and normalized to the GAPDH control using the $2^{-\Delta\Delta Ct}$ method.

Cell viability assay. HepG2 cells were passaged into a 96-well plate at 15,000 cells/well in 98 μL media, and were grown overnight. The cells were treated with DMSO or the small molecules at a range of concentrations (0.5-50 μM) (1% final DMSO concentration, by addition of 2 μL compound dilution in 50% DMSO) in triplicate. The cells were incubated at 37 °C for 48 h and were then assayed for viability using a Cell Titer Glo assay (Promega). An equal volume of Cell Titer Glo reagent (100 μL) was added to the media, the plate was shaken for 2 min to lyse the cells, and incubated in the dark at rt for 10 min. The luminescence was recorded on a microplate reader (Tecan M200). The percent cell viability relative to the DMSO control, where DMSO represents 100% viability, was calculated for each of the triplicates, the data was averaged, and standard deviations were calculated.

Target identification experiments for the miR-21 inhibitor 51. HeLa cells were passaged into 10 cm plates and were grown to 80% confluency. The media was removed and the cells (in 9.95 mL DMEM media, antibiotics-free) were treated with either DMSO (50 μL; 0.5% DMSO final concentration), or the small molecule probes **171** and **173** (10 μM, 50 μL of 2 mM DMSO stock) and incubated overnight at 37 °C. After an overnight incubation at 37 °C, the media was

removed, the cells were washed with PBS (1 mL), and irradiated in PBS (5 mL) on a transilluminator (365 nm, 25 W, UVP TFML-20) for 10 min. The PBS was removed, mammalian protein extraction buffer (1 mL, GE Healthcare) was added, the plates were shaken while kept on ice for 10 min, the cells were detached by pipetting them up and down, transferred to a microcentrifuge tube, and pelleted by centrifugation at 12,000 x g for 20 min at 4 °C. The supernatants were collected, the protein concentrations were determined with a Bradford assay (absorbance measured at 595 nm on a Tecan M1000), and an equal amount of proteins (100 μg) for each sample was treated with 33 μL of freshly prepared "click reaction cocktail"[146] containing the fluorescein-azide **191** (see the appendix 6.3.1 for the recipe of cocktail). The click reaction was performed at room temperature for 2 h. The proteins were subsequently isolated via acetone precipitation, 600 μL of prechilled acetone was added into the click reaction mixtures, which were then incubated for 60 min at −20 °C. The proteins were pelleted by centrifugation (13,000 x g for 10 min at 4 °C), the supernatants were discarded and the pellets were washed twice with prechilled MeOH (200 μL, 4 min centrifugation at 10,000 x g) and finally air dried at rt for 10 min. The pellets were re-suspended in PBS (40 μL), denaturing loading dye (5x) was added (10 μL) and the samples were heated to 95 °C for 5 min. The samples (40 μL) were then analyzed by a 12% SDS-PAGE (4% stacking gel) at 60 V for 30 min followed by 150 V for 90 min. The fluorescence was detected on a ChemiDoc (BioRad, setting: Filter 4: 530/28 nm, light: blue epi illumination).

Synthetic protocol

All reactions were performed in flame-dried glassware under a nitrogen atmosphere and stirred magnetically. Reactions were followed by thin layer chromatography (TLC) using glass-backed silica gel plates (Sorbent technologies, 250 μm thickness). Tetrahydrofuran and DCM were

obtained from a dry solvent delivery system. MeCN, EtOH, MeOH and pyridine were distilled from calcium hydride and stored over 4 Å molecular sieves. Other reagents and solvents were obtained from commercial sources (Sigma, VWR, Fisher, Accros), stored under nitrogen and used directly without further purification. Yields refer to pure compounds unless otherwise stated. Flash chromatography was performed on silica gel (60 Å, 40-63 μm (230 × 400 mesh), Sorbtech) as a stationary phase. High resolution mass spectral analysis (HRMS) was performed at the University of Pittsburgh. The ^{1}H NMR and ^{13}C NMR spectra were recorded on a 300 MHz or a 400 MHz Varian or Brucker NMR spectrometers. Chemical shifts are given in δ units (ppm) for NMR spectra.

Synthesis of analogs 38-41

Methyl 4-(phenylcarbamoyl)benzoate (43). TEA (2.8 ml, 20.12 mmol) was added to a solution of aniline (0.55 ml, 6.04 mmol) in DCM (10 ml) at 0 °C. The reaction mixture was stirred at 0 °C for 10 min and terephthalic acid monomethyl ester chloride (**42**) (1 g, 5.03 mmol) was added. The resulting mixture was slowly allowed to warm up to rt and stirred for 4 h. The solution was slowly neutralized with 1 M HCl (2 mL) and H_2O (20 mL) was added. The aqueous layer was extracted with DCM (2 x 15 mL). The combined organic layers were washed with H_2O (3 x 12 mL) and brine (8 mL). The organic layers were combined, dried with Na_2SO_4, filtered, and concentrated delivering **43** as a white solid (990 mg, 77%) that was used without further purification. ^{1}H NMR (300 MHz, chloroform-d) δ 8.15 (d, *J* = 8.5 Hz, 2H), 7.91 (d, *J* = 8.6 Hz, 2H), 7.89 (s, 1H), 7.64 (d, *J* = 7.6 Hz, 2H), 7.38 (t, *J* = 7.5 Hz, 2H), 7.20 (t, *J* = 7.5 Hz, 1H), 3.95 (s, 3H). The analytical data matched literature reports.[156]

4-(Phenylcarbamoyl)benzoic acid (44). A solution of the ester **43** (50 mg, 0.19 mmol) in MeOH (0.5 ml) was added to a solution of potassium hydroxide (33 mg, 0.59 mmol) in H_2O (0.2

ml). The resulting mixture was stirred under reflux for 1 h. After allowing the mixture to cool to room temperature, H_2O (5 ml) was added and the aqueous solution was washed with EtOAc (4 ml). The aqueous layer was acidified with 1 M HCl until pH ~ 3 and extracted with Et_2O (3 x 6 mL). The organic layers were combined, dried with Na_2SO_4, filtered, and concentrated to deliver **44** as a white solid (44 mg, 97%) that was used without further purification. ^{1}H NMR (300 MHz, DMSO-d6) δ 10.37 (s, 1H), 8.03 (t, *J* = 2.4 Hz, 4H), 7.75 (d, *J* = 7.5 Hz, 2H), 7.34 (t, *J* = 7.5 Hz, 2H), 7.15 (t, *J* = 7.5 Hz, 1H).

***N*^{1}-Phenyl-*N*^{4}-(prop-2-yn-1-yl)terephthalamide (38)**. EDCI (66 mg, 0.34 mmol) and HOBt (28 mg, 0.21 mmol) were added to a solution of **44** (45 mg, 0.19 mmol) in DCM (0.6 mL). The mixture was stirred at rt for 40 min, propargylamine (0.026 ml, 0.38 mmol) was added, and stirring was continued at rt overnight (ON). The reaction mixture was poured into H_2O (4 ml) and extracted with DCM (3 x 5 mL). The combined organic layers were washed with saturated $NaHCO_3$, brine, dried over Na_2SO_4, filtered, and concentrated. The residue was purified by flash chromatography on silica gel, eluting with 5% MeOH:DCM to give **38** as a brown solid (8 mg, 19%). ^{1}H NMR (300 MHz, DMSO-d6) δ 10.34 (s, 1H), 9.09 (s, 1H), 8.04 - 7.98 (m, 4H), 7.76 (d, *J* = 7.5 Hz, 2H), 7.35 (t, *J* = 7.2 Hz, 2H), 7.10 (t, *J* = 7.5 Hz, 1H), 4.08 - 4.05 (m, 2H), 3.15 - 3.13 (m, 1H). HRMS (ESI$^+$) calcd for $C_{17}H_{14}N_2O_2$ $(M+Na)^+$ 301.2950, found 301.0956.

***N*-Benzyl-*N*-phenylterephthalamide (39)**. Same procedure as **38** using benzylamine (39 mg, 0.37 mmol) as the starting material. The residue was purified by flash chromatography on silica gel, eluting with 5% MeOH:DCM to give **39** as a white solid (11 mg, 19%). ^{1}H NMR (300 MHz, DMSO-d6) δ 10.34 (s, 1H), 9.19 - 9.17 (m, 1H), 8.02 - 7.98 (m, 3H), 7.76 (d, *J* = 7.5 Hz, 2H),

7.37 - 7.22 (m, 7H), 7.10 (t, *J* = 7.5 Hz, 1H), 4.48 - 4.41 (m, 2H). HRMS (ESI^+) calcd for $C_{21}H_{18}N_2O_2$ $(M+Na)^+$ 353.3696, found 353.1269.

Methyl 4-(prop-2-yn-1-ylcarbamoyl)benzoate (45). Same procedure as **43** using terephthalic monomethyl ester chloride (500 mg, 2.5 mmol) and propargyl amine (0.194 ml, 3.02 mmol) as the starting materials. The compound **45** was obtained as a yellow solid (517 mg, 95%) that was used without further purification. ^1H NMR (300 MHz, DMSO-d6) δ 9.18 (s, 1H), 8.02 (d, *J* = 6.6 Hz, 2H), 7.96 (d, *J* = 6.5 Hz, 2H), 4.06 - 4.02 (m, 2H), 3.86 (s, 3H), 3.14 (s, 1H).

4-(Prop-2-yn-1-ylcarbamoyl)benzoic acid (46). Same procedure as **44** using **45** (50 mg, 0.23 mmol) as the starting material. The compound **46** was obtained as a white solid (38 mg, 84%) that was used without further purification. ^1H NMR (300 MHz, DMSO-d6) δ 9.18 (s, 1H), 7.98 (d, *J* = 6.6 Hz, 2H), 7.93 (d, *J* = 6.5 Hz, 2H), 4.06 - 4.02 (m, 2H), 3.14 (s, 1H).

***N*-(4-Iodophenyl)-*N*-(prop-2-yn-1-yl)terephthalamide (41)**. HATU (273 mg, 0.72 mmol) and 4-iodoaniline (65 mg, 0.29 mmol) were added to a solution of **46** (50 mg, 0.24 mmol) and DIPEA (0.25 ml, 1.44 mmol) in DMF (0.3 ml). The resulting mixture was stirred overnight at rt. The reaction mixture was poured into H_2O (4 ml) and extracted with Et_2O (3 x 5 mL). The combined organic layers were washed with brine (5 mL), dried over Na_2SO_4, filtered, and concentrated. The residue was purified by flash chromatography on silica gel, eluting with hexanes/EtOAc (1:1) to give **41** as a white-off solid (7 mg, 10%). ^1H NMR (300 MHz, chloroform-d) δ 8.01 (d, *J* = 9 Hz, 2H), 7.95 (d, *J* = 8.7 Hz, 2H), 7.80 (s, 1H), 7.67 (d, *J* = 9 Hz, 2H), 7.44 (d, *J* = 8.7 Hz, 2H), 6.89 (s, 1H), 2, 42 (s, 2H), 1.58 (s, 1H). HRMS (ESI^+) calcd for $C_{17}H_{14}IN_2O_2$ $(M+H)^+$ 405.2097, found 405.2651.

***N*-(4-Benzoylphenyl)-*N*-(prop-2-yn-1-yl)terephthalamide (40).** Same procedure as **41** using **46** (37 mg, 0.18 mmol) and 3-aminobenzophenone (71 mg, 0.36 mmol) as the starting materials. The residue was purified by flash chromatography on silica gel, eluting with hexanes/EtOAc (2:1) to give **40** as a yellow solid (5 mg, 8%). ^{1}H NMR (300 MHz, DMSO-d6) δ 9.98 (s, 1H), 8.30 - 8.21 (m, 3H), 8.12 - 7.85 (m, 3H), 7.84 - 7.81 (m, 2H), 7.60 - 7.55 (m, 5H), 4.23 - 4.20 (m, 2H), 2.71 - 2.69 (m, 1H). HRMS (ESI$^+$) calcd for $C_{24}H_{18}N_2O_3$ $(M+H)^+$ 383.4193, found 383.1391.

Synthesis of ether-amide analogs

2-(4-Nitrophenyl)benzo[*d*]thiazole (62). 4-Nitrobenzoyl chloride (312 mg, 1.7 mmol) was added to a solution of 2-aminothiophenol (0.180 mL, 1.7 mmol) in pyridine (4.2 mL), and the reaction mixture was heated to reflux for 3 h. After completion of the reaction, as confirmed by TLC, the mixture was poured into H_2O (6 mL). The product was isolated by filtration and washed with H_2O (2 x 3 mL). The crude product was purified by trituration in MeOH to give **62** as a yellow solid (256 mg, 59%). ^{1}H NMR (300 MHz, chloroform-d) δ 8.37 - 8.26 (m, 4H), 8.13 (d, *J* = 8.1 Hz, 2H), 7.96 (d, *J* = 8.1 Hz, 1H), 7.59 - 7.44 (m, 2H).

4-(Benzo[*d*]thiazol-2-yl)aniline (63). Tin(II) chloride (945 mg, 5.0 mmol) was added to a solution of **62** (256 mg, 1.0 mmol) in EtOH (3.3 mL). The mixture was stirred at reflux for 2 h, and the solvent was removed under vacuum. The residue was suspended in EtOAc (10 mL) and washed with 2 M NaOH (3 x 7 mL) and H_2O (2 x 7 mL). The organic layer was dried over Na_2SO_4, filtered, and concentrated. Trituration in MeOH afforded **63** as a yellow solid (187 mg, 83%). ^{1}H NMR (300 MHz, DMSO-d6) δ 8.00 (d, *J* = 7.9 Hz, 1H), 7.87 (d, *J* = 6 Hz, 1H), 7.74

(d, *J* = 8.4 Hz, 2H), 7.44 (td, *J* = 6.1, 2.9 Hz, 1H), 7.32 (td, *J* = 7.2, 2.9 Hz, 1H), 6.66 (d, *J* = 8.7 Hz, 2H), 5.88 (s, 2H). The analytical data matched literature reports.[157]

***tert*-Butyl 2-(2-iodophenoxy)acetate (57).** Cesium carbonate (150 mg, 0.46 mmol) was added to a solution of 2-iodophenol (50 mg, 0.23 mmol) in acetone (4.4 mL). The resulting mixture was stirred at 65 °C for 30 min. *tert*-Butylbromoacetate (0.037 mL, 0.23 mmol) was added and the solution was stirred for an additional hour. The reaction mixture was allowed to cool to rt and was filtered through a cotton plug. The residue was washed with acetone (2 x 5 mL) and the filtrate was concentrated. The residue was purified by flash chromatography on silica gel, eluting with hexanes/EtOAc (10:1) to give **57** as a yellow oil (66 mg, 86%). ^{1}H NMR (300 MHz, chloroform-d) δ 7.79 (d, *J* = 7.7 Hz, 1H), 7.26 (t, *J* = 7.5 Hz, 1H), 6.75 - 6.67 (m, 2H), 4.58 (s, 2H), 1.50 (s, 12H). The analytical data matched literature reports.[158]

2-(2-Iodophenoxy)acetic acid (58). TFA (7.9 mL) was added to a solution of **57** (66 mg, 0.20 mmol) in DCM (7.9 mL). The reaction mixture was stirred at rt for 2 h and concentrated under vacuum to give **58** as a yellow solid (49 mg, 90%). ^{1}H NMR (300 MHz, chloroform-d) δ 7.81 (d, *J* = 7.8 Hz, 1H), 7.32 (t, *J* = 7.5 Hz, 1H), 6.84 - 6.77 (m, 2H), 4.72 (s, 2H). The analytical data matched literature reports.[159]

2-(2-Iodophenoxy)acetyl chloride (59). Oxalyl chloride (0.3 mL, 3.45 mmol) and 2 drops of DMF were added to a solution of **58** (639 mg, 2.30 mmol) in DCM (6 mL) at 0 °C. The resulting mixture was slowly allowed to warm up to rt and stirred for 2 h. The solvent was removed under vacuum to deliver **59** as a brown solid that was used without further purification (652 mg, 96%). ^{1}H NMR (400 MHz, chloroform-d) δ 7.82 (d, *J* = 7.8 Hz, 1H), 7.32 - 7.29 (m, 1H), 6.81 (t, *J* = 6.0 Hz, 1H), 6.74 (d, *J* = 6.0 Hz, 1H), 5.01 (s, 2H).

***N*-(4-(Benzo[*d*]thiazol-2-yl)phenyl)-2-(2-iodophenoxy)acetamide (47).** The acyl chloride **59** (129 mg, 0.44 mmol) was added to a solution of **63** (50 mg, 0.22 mmol) and DIPEA (0.06 mL, 0.34 mmol) in DCM (3 mL). The resulting mixture was stirred at rt for 1.5 h, and then was filtered through a cotton plug. The filtrate was diluted with DCM (6 mL) and washed with 1 M HCl (2 x 5 mL), saturated $NaHCO_3$ (2 x 5 mL), brine (4 mL), dried over Na_2SO_4, filtered, and concentrated. The residue was purified by flash chromatography on silica gel, eluting with hexanes/EtOAc (2:1) to give **47** as a yellow solid (58 mg, 39%). ^{1}H NMR (300 MHz, chloroform-d) δ 9.04 (s, 1H), 8.12 - 8.05 (dd, *J* = 8.7, 7.5 Hz, 3H), 7.94 - 7.80 (m, 4H), 7.56 (t, *J* = 7.5 Hz, 1H), 7.41 (t, *J* = 7.8 Hz, 2H), 6.88 - 6.84 (m, 2H), 4.68 (s, 2H). HRMS (ESI^+) calcd for $C_{21}H_{15}IN_2O_2S$ $(M+H)^+$ 486.9972, found 487.0098.

The acyl chlorides used to synthesize the analogs **64** and **65** were prepared from the corresponding phenols following the same protocol described for **59**:

2-(4-Methoxyphenoxy)acetyl chloride. Same procedure as **59** using 2-(4-methoxyphenoxy)acetic acid (586 mg, 3.22 mmol) as the starting material. The compound was obtained as a brown oil (64 mg, 99%) and was used without further purification. ^{1}H NMR (400 MHz, chloroform-d) δ 6.85 (m, 4H), 4.90 (s, 2H), 3.78 (s, 3H).

2-Phenoxyacetyl chloride. Same procedure as **59** using 2-phenoxyacetic acid (728 mg, 4.79 mmol) as the starting material. The compound was obtained as a brown oil (80 mg, 98%) and was used without further purification. ^{1}H NMR (400 MHz, chloroform-d) δ 7.28 (t, *J* = 7.2 Hz, 2H), 7.01 (t, *J* = 6.8 Hz, 1H), 6.84 (d, *J* = 8.0 Hz, 2H), 4.91 (s, 2H). The analytical data matched literature reports.[160]

Analogs **64** and **65** were prepared from **63** and the corresponding acyl chlorides using the procedure described for **47**:

***N*-(4-(Benzo[d]thiazol-2-yl)phenyl)-2-(4-methoxyphenoxy)acetamide (64).** Same procedure as **47** using **63** (40 mg, 0.18 mmol) and 2-(4-methoxyphenoxy)acetyl chloride (72 mg, 0.36 mmol) as the starting materials. The residue was purified by flash chromatography on silica gel, eluting with DCM/EtOAc (7:1) to afford **64** as a yellow solid (35 mg, 50%). ^{1}H NMR (300 MHz, chloroform-d) δ 8.46 (s, 1H), 8.11 (dd, *J* = 8.7, 7.8 Hz, 3H), 7.91 (d, *J* = 7.5 Hz, 1H), 7.76 (d, *J* = 8.7 Hz, 2H), 7.49 (t, *J* = 8.3 Hz, 1H), 7.32 (t, *J* = 7.6 Hz, 1H), 7.00 - 6.88 (m, 4H), 4.60 (s, 2H), 3.80 (s, 3H). HRMS (ESI$^+$) calcd for $C_{21}H_{16}N_2O_2S$ $(M+H)^+$ 361.1005, found 361.1029.

***N*-(4-(Benzo[d]thiazol-2-yl)phenyl)-2-phenoxyacetamide (65).** Same procedure as **47** using **63** (40 mg, 0.18 mmol) and 2-phenoxyacetyl chloride (61 mg, 0.36 mmol) as the starting materials. The residue was purified by flash chromatography on silica gel, eluting with DCM/EtOAc (2:1) to afford **65** as a yellow solid (40 mg, 62%). ^{1}H NMR (300 MHz, chloroform-d) δ 8.45 (s, 1H), 8.01 (dd, *J* = 8.4, 7.6 Hz, 3H), 7.91 (d, *J* = 7.7 Hz, 1H), 7.77 (d, *J* = 8.6 Hz, 2H), 7.54 (t, *J* = 7.5 Hz, 1H), 7.38 (t, *J* = 7.8 Hz, 2H), 7.11 (t, *J* = 7.5 Hz, 1H), 7.03 (d, *J* = 8.7 Hz, 3H), 4.66 (s, 2H). HRMS (ESI$^+$) calcd for $C_{21}H_{16}N_2O_2S$ $(M+H)^+$ 361.1005, found 361.1029.

Synthesis of analogs 70-72

***N*-(2-Hydroxyphenyl)-4-nitrobenzamide (67).** 4-Nitrobenzoylchloride (1.7 g, 9.17 mmol) was added to a solution of 2-aminophenol (1.0 g, 9.17 mmol) and TEA (2 mL, 13.5 mmol) in THF (11 mL) at 0 °C. The resulting mixture was allowed to warm to rt and stirred for 20 h. After completion of the reaction (TLC), the mixture was dissolved in EtOAc (16 mL), washed successively with H_2O (2 x 8 mL), 1 M HCl (8 mL), brine (6 mL), dried over Na_2SO_4, filtered,

and concentrated to deliver **67** as a light brown solid (2.4 g, 90%) which was used without further purification. ^{1}H NMR (300 MHz, DMSO-d6) δ 9.83 (s, 1H), 9.71 (s, 1H), 8.34 (d, *J* = 7.2 Hz, 2H), 8.18 (d, *J* = 9 Hz, 2H), 7.60 (d, *J* = 7.7 Hz, 1H), 7.06 (dd, *J* = 8.1, 7.3 Hz, 1H), 6.92 (d, *J* = 8.1 Hz, 1H), 6.83 (t, *J* = 7.6 Hz, 1H).

2-(4-Nitrophenyl)benzo[*d*]oxazole (68). Acid *para*-toluenesulfonic (PTSA) (778 mg, 4.09 mmol) was added to a solution of **67** (500 mg, 1.95 mmol) in xylene (19 mL). The reaction mixture was heated to reflux for 4 h. After cooling down, the solution was diluted with EtOAc (15 mL), washed with saturated $NaHCO_3$ (2 x 8 mL), H_2O (2 x 8 mL). The combined aqueous layer was re-extracted with EtOAc (8 mL). The combined organic layers were washed with brine (5 mL), dried over Na_2SO_4, filtered, and concentrated. The residue was purified by flash chromatography on silica gel, eluting with hexanes/EtOAc (4:1) to give **68** as a yellow solid (148 mg, 32%). ^{1}H NMR (300 MHz, DMSO-d6) δ 8.44 (d, *J* = 1.7 Hz, 4H), 7.87 (t, *J* = 8.0 Hz, 2H), 7.55 - 7.42 (m, 2H).

4-(Benzo[*d*]oxazol-2-yl)aniline (69). Tin(II) chloride (3.7 g, 19.8 mmol) was added to a solution of the nitro **68** (950 mg, 3.9 mmol) in ethanol (20 mL). The mixture was stirred at reflux for 2 h. The solvent was removed under vacuum. The residue was diluted in EtOAc (18 mL) and washed with H_2O (2 x 10 mL) and brine (6 mL). The organic layer was dried over Na_2SO_4, filtered, and concentrated. Trituration in MeOH afforded **69** as a yellow solid (2.2 mg, 100%). ^{1}H NMR (300 MHz, DMSO-d6) δ 7.83 (d, *J* = 8.4 Hz, 2H), 7.66 – 7.63 (m, 2H), 7.33 - 7.27 (m, 2H), 6.67 (d, *J* = 8.7 Hz, 2H), 6.00 (s, 2H). The analytical data matched literature reports.[161]

***N*-(4-(Benzo[d]oxazol-2-yl)phenyl)-2-(2-iodophenoxy)acetamide (70).** The acyl chloride 5**9** (140 mg, 0.48 mmol) was added to a solution of **69** (50 mg, 0.24 mmol) and pyridine (0.03 mL, 0.37 mmol) in DCM (2 mL). The resulting mixture was stirred at rt for 3 h. The reaction mixture was diluted with DCM (5 mL), washed with 1 M HCl (4 mL). The aqueous layer was washed with DCM (2 x 6 mL). The combined organic layers were washed with brine (5 mL), dried over Na_2SO_4, filtered, and concentrated. The residue was purified by flash chromatography on silica gel, eluting with hexanes/EtOAc (3:1) to give **70** as a pink solid (8.1 mg, 20%). ^{1}H NMR (300 MHz, chloroform-d) δ 9.07 (s, 1H), 8.28 (d, *J* = 8.8 Hz, 1H), 7.89 - 7.76 (m, 4H), 7.61 - 7.58 (m, 1H), 7.40 - 7.32 (m, 2H), 6.88 (t, *J* = 14.4 Hz, 2H), 6.83 - 6.76 (m, 2H), 4.69 (s, 2H). HRMS (ESI^+) calcd for $C_{21}H_{15}IN_2O_3$ $(M+H)^+$ 471.0206, found 471.0226.

Analogs **71** and **72** were prepared from **69** and the corresponding acyl chlorides using the procedure described for **70**:

***N*-(4-(Benzo[d]oxazol-2-yl)phenyl)-2-(4-methoxyphenoxy)acetamide (71).** Same procedure as **70** using **69** (90 mg, 0.43 mmol) and 2-(4-methoxyphenoxy)acetyl chloride (172 mg, 0.86 mmol) as the starting materials. The residue was purified by flash chromatography on silica gel, eluting with hexanes/EtOAc (1:1) to afford **71** as a white solid (11 mg, 9%). ^{1}H NMR (300 MHz, chloroform-d) δ 8.48 (s, 1H), 8.26 (d, *J* = 8.7 Hz, 2H), 7.82 - 7.76 (m, 3H), 7.61 - 7.55 (m, 1H), 7.38 - 7.33 (m, 2H), 6.97 - 6.87 (dd, *J* = 9.6, 6.0 Hz, 4H), 4.60 (s, 2H), 3.80 (s, 3H). HRMS (ESI^+) calcd for $C_{22}H_{18}N_2O_4$ $(M+H)^+$ 375.1345, found 375.1363.

***N*-(4-(Benzo[d]oxazol-2-yl)phenyl)-2-phenoxyacetamide (72).** Same procedure as **70** using **69** (80 mg, 0.38 mmol) and 2-phenoxyacetyl chloride (129 mg, 0.76 mmol) as the starting materials. The residue was purified by flash chromatography on silica gel, eluting with hexanes/EtOAc

(3:1) to afford **72** as a white solid (11.2 mg, 9%) ^{1}H NMR (300 MHz, chloroform-d) δ 8.47 (s, 1H), 8.26 (d, *J* = 8.7 Hz, 2H), 7.82 - 7.75 (m, 3H), 7.61 - 7.55 (m, 1H), 7.40 - 7.33 (m, 3H), 7.08 - 7.00 (dd, *J* = 15.6, 6.6 Hz, 3H), 4.66 (s, 2H). HRMS (ESI$^+$) calcd for $C_{21}H_{16}N_2O_3$ $(M+H)^+$ 345.1239, found 345.1269.

Synthesis of *N*-acylhydrazone hit compounds 49 and 50

Picolinohydrazide (74). Hydrazine (0.105 mL, 3.31 mmol) was added dropwise to a solution of ethyl picolinate (0.223 mL, 1.65 mmol). The resulting mixture was heated to reflux for 18 h. After allowing the mixture to cool down, all volatiles were evaporated under vacuum and the residue was recrystallized from EtOH to give **74** as a white solid (111 mg, 25%). ^{1}H NMR (300 MHz, DMSO-d6) δ 9.85 (s, 1H), 8.59 (d, *J* = 4.7 Hz, 1H), 7.97 - 7.95 (m, 2H), 7.57 - 7.52 (m, 1H), 4.53 (s, 2H). The analytical data matched literature reports.[162]

***(E)*-*N*-(2-Methoxyphenyl)-3-(2-picolinoylhydrazono)butanamide (50).** A solution of **74** (40 mg, 0.29 mmol) in EtOH (0.7 mL) was added to a solution of acetanilide (60.1 mg, 0.29 mmol) in MeOH (0.7 mL). The resulting mixture was heated to reflux for 5 h. The solvents were removed under vacuum and the residue was triturated in hexanes to give **50** as a light brown solid (76 mg, 81%). ^{1}H NMR (300 MHz, chloroform-d) δ 10.88 (s, 1H), 8.56 (d, *J* = 4.5 Hz, 1H), 8.31 (d, *J* = 8.1 Hz, 3H), 7.90 (t, *J* = 7.7 Hz, 1H), 7.49 (t, *J* = 7.6 Hz, 1H), 7.04 – 6.34 (m, 3H), 3.86 (s, 3H), 3.59 (s, 2H), 2.24 (s, 3H). HRMS (ESI$^+$) calcd for $C_{17}H_{18}N_4O_8$ $(M+Na)^+$ 349.1277, found 349.1261.

2-Methylfuran-3-carbohydrazide (82). Hydrazine (0.113 mL, 3.57 mmol) was added to a stirred solution of methyl-2-methyl-3-furancarboxylate (0.224 mL, 1.78 mmol) in MeOH (3 mL) and heated to reflux overnight. After allowing the mixture to cool down, the solvent was

removed under vacuum to give **82** as a yellow solid (274 mg, 100%). ^{1}H NMR (300 MHz, DMSO-d6) δ 9.26 (s, 1H), 7.47 (sd, *J* = 1.8 Hz, 1H), 6.78 (sd, *J* = 1.8 Hz, 1H), 4.33 (s, 2H), 2.48 (s, 3H).

***N*-(4-Acetylphenyl)nicotinamide (81).** A solution of nicotinoyl chloride hydrochloride (250 mg, 1.77 mmol) in THF (1 mL) was added to a solution of 4-aminoacetophenone (286 mg, 2.12 mmol) and TEA (0.5 mL, 3.54 mmol) in THF (5 mL). The resulting mixture was stirred for 3 h at rt. The solvent was removed under vacuum and the residue was purified by flash chromatography on silica gel, eluting with 10% MeOH in DCM to give **81** as a pink solid (93 mg, 23%). ^{1}H NMR (300 MHz, chloroform-d) δ 9.11 (d, *J* = 2.4, 1H), 8.83 - 8.79 (m, 1H), 8.22 (d, *J* = 7.9 Hz, 1H), 8.01 (d, *J* = 8.7 Hz, 2H), 7.76 (d, *J* = 8.7, 2H), 7.47 (m, 1H), 2.61 (s, 3H).

(*E*)-*N*-(4-(1-(2-(2-Methylfuran-3-carbonyl)hydrazono)ethyl)phenyl)nicotinamide (49). The methyl ketone **81** (28 mg, 0.12 mmol) was added to a solution of **83** (16 mg, 0.12 mmol) in EtOH (0.3 mL). The reaction mixture was heated to reflux for 4 h. Upon cooling down the product precipitated out and was isolated by filtration and washed with cold Et_2O (2 x 4 mL) to afford **49** as a yellow solid (20 mg, 45%). ^{1}H NMR (400 MHz, DMSO-d6) δ 10.60 (s, 1H), 9.11 (s, 1H), 8.76 (sd, *J* = 3.2 Hz, 1H), 8.30 (m, 1H), 8.00 - 7.83 (m, 5H), 7.58 (d, *J* = 4.8 Hz, 2H), 6.94 (s, 1H), 2.51 (s, 3H), 2.31 (s, 3H). HRMS (ESI$^+$) calcd for $C_{20}H_{18}N_4O_3$ $(M+Na)^+$ 385.1277, found 385.1267.

The analogs **78** and **83**-**91** were prepared from the corresponding starting materials according to the procedure described for **49**:

(*E*)-*N'*-(1-(*p*-Tolyl)ethylidene)furan-2-carbohydrazide (78). Same procedure as **49** using 2-furoic hydrazide (50 mg, 0.39 mmol) and 4-methylacetophenone (53 mg, 0.39 mmol) as the starting materials. The residue was purified via recrystallization in EtOH to provide **78** as a white solid (67 mg, 70%). ^{1}H NMR (300 MHz, DMSO-d6) δ 7.92 (s, 1H), 7.71 (d, *J* = 7.8 Hz, 2H), 7.34 (s, 1H), 7.24 (d, *J* = 8.1 Hz, 2H), 6.68 (d, *J* = 3.5 Hz, 1H), 2.33 (s, 3H), 2.31 (s, 3H). HRMS (ESI$^+$) calcd for $C_{14}H_{14}N_2O_2$ $(M+H)^+$ 243.2811, found 243.1135. The analytical data matched literature reports.[163]

(*E*)-*N'*-Benzylidenefuran-2-carbohydrazide (83). Same procedure as **49** using 2-furoic hydrazide (50 mg, 0.39 mmol) and benzaldehyde (0.04 μL, 0.40 mmol) as the starting materials. The residue was purified via recrystallization in EtOH to provide **83** as a white solid (63 mg, 74%). ^{1}H NMR (300 MHz, DMSO-d6) δ 11.82 (s, 1H), 8.44 (s, 1H), 7.93 (s, 1H), 7.88 (dd, *J* = 6.9, 2.7 Hz, 2H), 7.48 - 7.42 (m, 2H), 7.29 (s, 1H), 6.69 (s, 1H). HRMS (ESI$^+$) calcd for $C_{12}H_{10}N_2O_2$ $(M+Na)^+$ 237.0640, found 237.0639. The analytical data matched literature reports.[164]

(*E*)-*N'*-(1-(Pyridin-2-yl)ethylidene)furan-2-carbohydrazide (84). Same procedure as **49** using 2-furoic hydrazide (52 mg, 0.41 mmol) and 2-acetylpyridine (0.046 μL, 0.41 mmol) as the starting materials. The residue was purified via recrystallization in EtOH to provide **84** as a white solid (2 mg, 5%) ^{1}H NMR (300 MHz, DMSO-d6) δ 8.60 (s, 1H), 8.08 - 7.80 (m, 3H), 7.42 (s, 2H), 6.70 (s, 1H), 2.42 (s, 3H). HRMS (ESI$^+$) calcd for $C_{12}H_{11}N_3O_2$ $(M+H)^+$ 252.0749, found 252.0751. The analytical data matched literature reports.[165]

(*E*)-3-(2-(Furan-2-carbonyl)hydrazono)-*N*-(2-methoxyphenyl)butanamide (85). Same procedure as **49** using 2-furoic hydrazide (50 mg, 0.39 mmol) and *o*-acetanisidine (90 mg, 0.44 mmol) as the starting materials. The residue was purified via recrystallization in Et_2O to provide **85** as a white solid (7.5 mg, 10%). ^{1}H NMR (300 MHz, methanol-d) δ 8.13 (dd, *J* = 1.6, 7.9 Hz, 1H), 7.73 (d, *J* = 1.5 Hz, 1H), 7.24 (d, *J* = 3.6 Hz, 1H), 7.20 - 6.90 (m, 3H), 6.65 (d, *J* = 3.5 Hz, 1H), 4.89 (s, 2H), 3.94 (s, 3H), 3.31 (s, 3H). HRMS (ESI^+) calcd for $C_{16}H_{17}N_3O_4$ $(M+Na)^+$ 338.3136, found 338.3432.

(*E*)-*N*'-Pentylidenefuran-2-carbohydrazide (86). Same procedure as **49** using 2-furoic hydrazide (59 mg, 0.47 mmol) and valeraldehyde (0.05 μL, 0.47 mmol) as the starting materials. The residue was purified via recrystallization in MeOH to provide **86** as a white solid (28 mg, 31%) ^{1}H NMR (300 MHz, methanol-d) δ 7.71 - 7.68 (m, 2H), 7.22 (d, *J* = 3.6 Hz, 1H), 6.61 (dd, *J* = 1.8, 3.6 Hz, 1H), 4.89 (s, 1H), 2.38 - 2.31 (m, 2H), 1.57 - 1.52 (m, 2H), 1.44 - 1.38 (m, 2H), 0.95 (t, *J* = 7.5 Hz, 3H). HRMS (ESI^+) calcd for $C_{10}H_{14}N_2O_2$ $(M+H)^+$ 195.2383, found 195.1126.

(*E*)-*N*'-([1,1'-Biphenyl]-4-ylmethylene)furan-2-carbohydrazide (87). Same procedure as **49** using 2-furoic hydrazide (59 mg, 0.47 mmol) and 4-biphenylcarboxaldehyde (87 mg, 0.47 mmol) as the starting materials. The residue was purified via recrystallization in Et_2O to provide **87** as a yellow solid (40 mg, 29%). ^{1}H NMR (400 MHz, DMSO-d6) δ 11.88 (s, 1H), 8.47 (s, 1H), 7.95 (s, 1H), 7.78 (d, *J* = 3.2 Hz, 4H), 7.75 - 7.71 (m, 4H), 7.50 - 7.46 (m, 2H), 7.40 - 7.36 (m, 1H), 6.70 (s, 1H). HRMS (ESI^+) calcd for $C_{18}H_{14}N_2O_2$ $(M+H)^+$ 291.3239, found 291.1122.

(*E*)-*N*'-(1-(Naphthalen-2-yl)ethylidene)furan-2-carbohydrazide (88). Same procedure as **49** using 2-furoic hydrazide (59 mg, 0.47 mmol) and 2-acetylnaphtalene (80 mg, 0.47 mmol) as the starting materials. The residue was purified via recrystallization in MeOH to provide **88** as a

white solid (51 mg, 41%). ^{1}H NMR (300 MHz, DMSO-d6) δ 8.30 (s, 1H), 8.10 - 7.92 (m, 5H), 7.46 (m, 2H), 7.40 (s, 1H), 6.60 (s, 1H), 3.32 (s, 3H).

***(E)*-2-Methyl-*N*'-(1-(p-tolyl)ethylidene)furan-3-carbohydrazide (89).** Same procedure as **49** using **82** (40 mg, 0.28 mmol) and 4-methylacetophenone (38 mg, 0.28 mmol) as the starting materials. The compound **89** was obtained as a white solid (22 mg, 31%) and was used without further purification. ^{1}H NMR (300 MHz, DMSO-d6) δ 10.29 (s, 1H), 7.60 (s, 2H), 7.56 (s, 1H), 7.21 (d, *J* = 7.9 Hz, 2H), 6.91 (s, 1H), 3.30 (s, 3H), 2.32 (s, 3H), 2.27 (s, 3H). HRMS (ESI^+) calcd for $C_{15}H_{16}N_2O_2$ $(M+H)^+$ 257.1290, found 257.1294.

(*E*)-*N*'-Benzylidenebenzohydrazide (90). Same procedure as **49** using phenylhydrazine (60 mg, 0.44 mmol) and benzaldehyde (0.045 μL, 0.44 mmol) as the starting materials. The residue was purified via recrystallization in MeOH to provide **90** as a white solid (45 mg, 45%). ^{1}H NMR (300 MHz, DMSO-d6) δ 11.80 (s, 1H), 8.44 (s, 1H), 7.90 (d, *J* = 9.6 Hz, 2H), 7.72 - 7.70 (m, 2H), 7.56 - 7.7.43 (m, 6H). HRMS (ESI^+) calcd for $C_{14}H_{12}N_2O$ $(M+H)^+$ 225.2658, found 225.1024. The analytical data matched literature reports.[166]

Ethyl benzofuran-2-carboxylate. Oxalyl chloride (0.13 mL, 1.48 mmol) and a catalytic amount of DMF were added to a solution of benzofuran-2-carbacid (200 mg, 1.23 mmol) in DCM (0.5 mL) at 0 °C, and the suspension was stirred overnight at rt. After removal of the solvents under vacuum, the residue was dissolved in EtOH (2 mL) and TEA (0.172 mL, 1.23 mmol) was added. The resulting mixture was heated under reflux for 4 h, after allowing the solution to cool to rt, H_2O (6 mL) was added and the product was extracted with DCM (3 x 5 mL). The combined organic layers were washed with $NaHCO_3$ (6 mL), brine (6 mL), dried over Na_2SO_4, filtered, and concentrated. The residue was purified by flash chromatography on silica gel, eluting with

hexanes/EtOAc (9:1) to deliver a white solid (138 mg, 59%). ^{1}H NMR (300 MHz, chloroform-d) δ 7.69 (dd, *J* = 0.9, 7.5 Hz, 1H), 7.61 (d, *J* = 7.5 Hz, 1H), 7.53 (d, *J* = 1.2 Hz, 1H), 7.46 (t, *J* = 7.2 Hz, 1H), 7.33 - 7.27 (m, 1H), 4.44 (q, *J* = 7.2 Hz, 2H), 1.43 (t, *J* = 7.2 Hz, 3H). The analytical data matched literature reports.[167]

Benzofuran-2-carbohydrazide. Hydrazine hydrate (0.072 mL, 1.45 mmol) was added to a solution of ethyl benzofuran-2-carboxylate (55 mg, 0.29 mmol) in EtOH (0.55 mL) and the resulting mixture was stirred under reflux for 3 h. After allowing the solution to cool to rt the product precipitated out and was collected by filtration. The crude product was recrystallized from EtOH to deliver a white solid (35 mg, 70%). ^{1}H NMR (300 MHz, methanol-d) δ 7.70 (d, *J* = 7.5 Hz, 1H), 7.57 (dd, *J* = 0.9, 8.4 Hz, 1H), 7.47 - 7.41 (m, 2H), 7.30 (t, *J* = 8.1 Hz, 1H).

(*E*)-*N*'-Benzylidenebenzofuran-2-carbohydrazide (91). Same procedure as **49** using benzofuran-2-carbohydrazide (26 mg, 0.15 mmol) and benzaldehyde (0.015 μL, 0.15 mmol) as the starting materials. The residue was purified via recrystallization in MeOH to provide **91** as a white solid (8 mg, 23%). ^{1}H NMR (300 MHz, methanol-d) δ 8.44 (s, 1H), 7.88 - 7.84 (m, 2H), 7.78 (d, *J* = 7.8 Hz, 1H), 7.69 - 7.64 (m, 2H), 7.53 (dd, *J* = 1.2, 7.2 Hz, 1H), 7.48 - 7.44 (m, 3H), 7.35 (t, *J* = 8.1 Hz, 1H). HRMS (ESI$^+$) calcd for $C_{16}H_{12}N_2O_2$ $(M+H)^+$ 265.2866, found 265.0968.

***N*-Phenethylfuran-2-carboxamide (92)**. EDCI (171 mg, 0.89 mmol), DMAP (136 mg, 1.11 mmol), and phenetylamine (0.056 mL, 0.44 mmol) were added to a solution of 2-furoic acid (50 mg, 0.44 mmol) and TEA (0.186 mL, 1.33 mmol) in DMF (1 mL). The reaction mixture was stirred overnight at rt, and then diluted with Et_2O (5 mL), washed with H_2O (2 x 5 mL), 10% HCl (3 mL), $NaHCO_3$ (3 mL), and brine (3 mL). The combined organic layers were dried over Na_2SO_4, filtered, and concentrated. The residue was purified by flash chromatography on silica

gel, eluting with hexanes/EtOAc (2:1) to give **92** as a colorless oil (7 mg, 10%). ^{1}H NMR (300 MHz, chloroform-d) δ 7.42 - 7.38 (m, 1H), 7.36 - 7.32 (m, 2H), 7.28 - 7.22 (m, 3H), 7.10 (dd, *J* = 1.9, J = 5.4 Hz, 1H), 6.50 - 6.48 (m, 1H), 3.68 (q, *J* = 6.6 Hz, 2H), 2.91 (t, *J* = 6.4 Hz, 2H). HRMS (ESI$^+$) calcd for $C_{13}H_{13}NO_2$ $(M+H)^+$ 216.2528, found 216.1029. The analytical data matched literature reports.[168]

Synthesis of the oxadiazole hit compound 51

1-Azido-3-methoxybenzene (95). Sulfuric acid (2.25 mL) was slowly added to a stirred solution of *m*-anisidine (1.05 mL, 8.5 mmol) in H_2O (6 mL) at 0 °C. A solution of sodium nitrite (762 mg, 11.0 mmol) in H_2O (1.2 mL) was added dropwise, and the resulting mixture was stirred for 30 min at 0 °C. A solution of sodium azide (884 mg, 13.6 mmol) in H_2O (1.6 mL) was added slowly. The reaction mixture was slowly allowed to warm to rt and stirred overnight. The mixture was poured into $NaHCO_3$ (10 mL) and extracted with DCM (3 x 10 mL). The combined organic layers were washed with brine (6 mL), dried over Na_2SO_4, filtered, and concentrated. The residue was purified by flash chromatography on silica gel, eluting with hexanes/EtOAc (9:1) to give **95** as a yellow oil (1.06 g, 84%). ^{1}H NMR (300 MHz, chloroform-d) δ 7.25 (t, *J* = 6.1 Hz, 1H), 6.71 – 6.63 (m, 2H), 6.55 (t, *J* = 2.3 Hz, 1H), 3.81 (s, 3H). The analytical data matched literature reports.[169]

(*E*)-*N*'-Hydroxythiophene-2-carboximidamide (97). A solution of hydroxylamine hydrochloride (4.5 g, 64.5 mmol) and sodium carbonate (4.5 g, 43 mmol) in H_2O (20 mL) was slowly added to a solution of 2-thiophenecarbonitrile (2 mL, 21.5 mmol) in a mixture of H_2O:15% EtOH (40:9 mL). The reaction mixture was stirred at rt for 24 h. The product was extracted with EtOAc (3 x 12 mL). The combined organic layers were washed with saturated $NaHCO_3$ (6 mL), brine (6 mL), dried over Na_2SO_4, filtered, and concentrated to afford **97** as a

white solid (12.9 g, 97%), which was used without further purification. ^{1}H NMR (300 MHz, DMSO-d6) δ 10.81 (s, 1H), 7.34 - 7.17 (m, 2H), 6.62 - 6.47 (m, 2H), 5.12 (s, 2H). The analytical data matched literature reports.[170]

2-(3-(Thiophen-2-yl)-1,2,4-oxadiazol-5-yl)acetonitrile (99). 1-Cyanoacetyl-3,5-dimethylpyrazole (1.4 g, 8.45 mmol) was added to a solution of **97** (1.0 g, 7.04 mmol) in dioxane and heated to reflux for 24 h. After allowing the mixture to cool to rt, the dioxane was removed under vacuum. The residue was dissolved in DCM (16 mL) and washed with saturated $NaHCO_3$ (2 x 10 mL), brine (6 mL), dried over Na_2SO_4, filtered, and concentrated. The residue was purified by flash chromatography on silica gel, eluting with hexanes/EtOAc (2:1) to give a yellow solid (1.8 g, 60%). ^{1}H NMR (300 MHz, chloroform-d) δ 7.83 (d, *J* = 3.7 Hz, 1H), 7.56 (d, *J* = 4.8 Hz, 1H), 7.18 (t, *J* = 5.0 Hz, 1H), 4.12 (s, 2H).

1-(3-Methoxyphenyl)-4-(3-(thiophen-2-yl)-1,2,4-oxadiazol-5-yl)-1*H*-1,2,3-triazol-5-amine (51). A solution of sodium methylate (102 mg, 1.89 mmol) in MeOH (3 mL) was added to **99** (120 mg, 0.63 mmol) in MeOH (1.5 mL). The resulting mixture was stirred at rt for 15 min, then the azide **95** (94 mg, 0.63 mmol) was added and the reaction mixture was stirred at 60 °C overnight. After allowing the solution to cool to room temperature, a few drops of H_2O were added. The precipitate was isolated by filtration and triturated into hexanes to give **51** as a brown solid (136 mg, 63%). ^{1}H NMR (300 MHz, DMSO-d6) δ 8.03 (d, *J* = 3.9 Hz, 1H), 7.91 (d, *J* = 4.8 Hz, 1H), 7.57 (t, *J* = 8.3 Hz, 1H), 7.30 (t, *J* = 5.2 Hz, 1H), 7.22 - 7.14 (m, 3H), 6.92 (s, 2H), 3.86 (s, 3H). LRMS calcd for $C_{15}H_{12}N_6O_2S$ $(M+Na)^+$ 363.06, found: 363.10.

The analogs **100-112** were prepared from **99** and the corresponding arylazides following the procedure and purification described for **51** unless otherwise indicated:

1-Azido-3-ethylbenzene. Same procedure as **95** using ethylaniline (0.26 mL, 2.06 mmol) as the starting material. The compound was obtained as an orange oil (250 mg, 80%) and was used without further purification. ^{1}H NMR (400 MHz, chloroform-d) δ 7.31 - 7.25 (m, 1H), 6.99 (d, *J* = 7.8 Hz, 1H), 6.87 (d, *J* = 6.8 Hz, 2H), 2.66 (q, *J* = 7.6 Hz, 2H), 1.31 (t, *J* = 8 Hz, 3H).

1-(3-Ethylphenyl)-4-(3-(thiophen-2-yl)-1,2,4-oxadiazol-5-yl)-1*H*-1,2,3-triazol-5-amine (102). Same procedure as **51** using 1-azido-3-ethylbenzene (54 mg, 0.37 mmol) and **99** (71 mg, 0.37 mmol) as the starting materials. The compound **102** was obtained as a brown solid (48 mg, 49%). ^{1}H NMR (300 MHz, DMSO-d6) δ 8.01 (d, *J* = 3.7 Hz, 1H), 7.89 (dd, *J* = 5.0, 1.2 Hz, 1H), 7.54 (t, *J* = 6.8 Hz, 1H), 7.50 - 7.41 (m, 3H), 7.29 (dd, *J* = 5.0, 3.7 Hz, 1H), 6.86 (s, 2H), 2.73 (q, *J* = 7.6 Hz, 2H), 1.24 (t, *J* = 7.6 Hz, 3H). HRMS (ESI$^+$) calcd for $C_{16}H_{14}N_6OS$ $(M+Na)^+$ 361.0847, found 361.0829.

3-Azido-*N*,*N*-dimethylaniline. Same procedure as **95** using 3-*N*,*N*-dimethyaniline (300 m, 2.2 mmol) as the starting material. The residue was purified by flash chromatography on silica gel, eluting with hexanes/EtOAc (9:1) to afford a light red oil (53 mg, 44%). ^{1}H NMR (300 MHz, chloroform-d) δ 7.22 (t, *J* = 8.1 Hz, 1H), 6.50 (d, *J* = 8.4 Hz, 1H), 6.42 (dd, *J* = 7.8, 2.1 Hz, 1H), 6.31 - 6.29 (m, 1H), 2.95 (s, 6H).

1-(3-(Dimethylamino)phenyl)-4-(3-(thiophen-2-yl)-1,2,4-oxadiazol-5-yl)-1*H*-1,2,3-triazol-5-amine (103). Same procedure as **51** using 3-azido-*N*,*N*-dimethylaniline (34 mg, 0.21 mmol) and **99** (40 mg, 0.21 mmol) as the starting materials. The compound **103** was obtained as a brown solid (26 mg, 35%). ^{1}H NMR (300 MHz, DMSO-d6) δ 8.0 (d, *J* = 2.4 Hz, 1H), 7.88 (d, *J* = 5.1

Hz, 1H), 7.42 (t, *J* = 8.1 Hz, 1H), 7.31 - 7.26 (m, 1H), 6.98 - 6.80 (m, 3H), 6. 79 (s, 2H), 2.97 (s, 6H). HRMS (ESI^+) calcd for $C_{16}H_{15}N_7OS$ $(M+H)^+$ 354.1, found 354.1.

1-Azido-3-isopropylbenzene. Same procedure as **95** using 3-isopropylaniline (0.365 mL, 2.59 mmol) as the starting material. The compound was obtained as a yellow oil (40 mg, 80%) and was used without further purification. ^1H NMR (300 MHz, chloroform-d) δ 7.26 (q, *J* = 6.8 Hz, 1H), 7.01 (d, *J* = 7.0 Hz, 1H), 6.85 (s, 2H), 2.85 (m, 1H), 1.23 (d, *J* = 7.5 Hz, 6H).

1-(3-Isopropylphenyl)-4-(3-(thiophen-2-yl)-1,2,4-oxadiazol-5-yl)-1*H*-1,2,3-triazol-5-amine (104). Same procedure as **51** using 1-azido-3-isopropylbenzene (34 mg, 0.21 mmol) and **99** (40 mg, 0.21 mmol) as the starting materials. The compound **104** was obtained as a brown solid (24 mg, 32%). ^1H NMR (300 MHz, DMSO-d6) δ 8.01 (d, *J* = 4.2 Hz, 1H), 7.90 (d, *J* = 5.0 Hz, 1H), 7.57 (t, *J* = 7.8 Hz, 1H), 7.51 - 7.42 (m, 3H), 7.29 (d, *J* = 5.0 Hz, 1H), 6.88 (s, 2H), 3.28 – 3.24 (m, 1H), 1.26 (d, *J* = 6.9 Hz, 6H). HRMS (ESI^+) calcd for $C_{17}H_{16}N_6OS$ $(M+H)^+$ 353.1, found 353.1.

1-Azido-3-(trifluoromethyl)benzene. Same procedure as **95** using 3-aminobenzotrifluoride (0.27 mL, 2.17 mmol) as the starting material. The residue was purified by flash chromatography on silica gel, eluting with pentane/Et_2O (8:1) to afford a light green oil (95 mg, 23%). ^1H NMR (300 MHz, chloroform-d) δ 7.48 (t, *J* = 8.1 Hz, 1H), 7.39 (d, *J* = 8.4 Hz, 1H), 7.22 (m, 2H).

4-(3-(Thiophen-2-yl)-1,2,4-oxadiazol-5-yl)-1-(3-(trifluoromethyl)phenyl)-1*H*-1,2,3-triazol-5-amine (105). Same procedure as **51** using 1-azido-3-(trifluoromethyl)benzene (51 mg, 0.27 mmol) and **99** (52 mg, 0.27 mmol) as the starting materials. The compound **105** was obtained as a grey solid (37 mg, 36%). ^1H NMR (300 MHz, DMSO-d6) δ 8.07 - 8.01 (m, 2H), 7.96 (d, *J* =

8.7 Hz, 2H), 7.88 (d, *J* = 4.8 Hz, 2H), 7.29 (t, *J* = 5.1 Hz, 1H), 7.08 (s, 2H). HRMS (ESI^+) calcd for $C_{15}H_9F_3N_6OS$ $(M+H)^+$ 379.1, found 379.1.

1-Azido-3-(trifluoromethoxy)benzene. Same procedure as **95** using 3-(trifluoromethoxy)aniline (0.227 mL, 1.69 mmol) as the starting material. The residue was purified by flash chromatography on silica gel, eluting with hexanes/EtOAc (8:1) to afford a yellow oil (53 mg, 44%). ^1H NMR (300 MHz, chloroform-d) δ 7.38 (t, *J* = 8.2 Hz, 1H), 6.99 (t, *J* = 8.0 Hz, 2H), 6.92 - 6.85 (m, 1H).

4-(3-(Thiophen-2-yl)-1,2,4-oxadiazol-5-yl)-1-(3-(trifluoromethoxy)phenyl)-1*H*-1,2,3-triazol-5-amine (106). Same procedure as **51** using 1-azido-3-(trifluoromethoxy)benzene (53 mg, 0.26 mmol) and **99** (50 mg, 0.26 mmol) as the starting materials. The compound **106** was obtained as a grey solid (19 mg, 20%). ^1H NMR (300 MHz, DMSO-d6) δ 8.02 (d, *J* = 3.6 Hz, 1H), 7.89 (d, *J* = 4.9 Hz, 1H), 7.78 (d, *J* = 8.3 Hz, 1H), 7.72 (s, 2H), 7.63 (d, *J* = 8.5 Hz, 1H), 7.44 – 7.46 (m, 1H), 7.03 (s, 2H). HRMS (ESI^+) calcd for $C_{15}H_9F_3N_6O_2S$ $(M+H)^+$ 395.0, found 395.0.

1-Azido-3-fluorobenzene. Same procedure as **95** using 3-fluoroaniline (0.105 mL, 1.08 mmol) as the starting material. The residue was purified by flash chromatography on silica gel, eluting with hexanes/EtOAc (8:1) to afford a yellow oil (250 mg, 41%). ^1H NMR (300 MHz, chloroform-d) δ 7.43 - 7.24 (m, 1H), 6.95 - 6.80 (m, 2H), 6.81 - 6.70 (m, 1H). The analytical data matched literature reports.[171]

1-(3-Fluorophenyl)-4-(3-(thiophen-2-yl)-1,2,4-oxadiazol-5-yl)-1*H*-1,2,3-triazol-5-amine (107). Same procedure as **51** using 1-azido-3-fluorobenzene (36 mg, 0.26 mmol) and **99** (50 mg, 0.26 mmol) as the starting materials. The compound **107** was obtained as a brown solid (33 mg, 45%). ^1H NMR (300 MHz, DMSO-d6) δ 8.04 (d, *J* = 3.8 Hz, 1H), 7.89 (d, *J* = 5.2 Hz, 1H), 7.75

- 7.64 (m, 1H), 7.60 (d, *J* = 9.3 Hz, 1H), 7.56 - 7.41 (m, 3H), 7.01 (s, 2H). HRMS (ESI^+) calcd for $C_{14}H_9FN_6OS$ $(M+Na)^+$ 351.0440, found 351.0528.

1-Azido-2-methoxybenzene. Same procedure as **95** using *o*-anisidine (0.46 mL, 4.06 mmol) as the starting material. The residue was purified by flash chromatography on silica gel, eluting with hexanes/EtOAc (5:1) to afford an orange oil (90 mg, 86%). ^1H NMR (400 MHz, chloroform-d) δ 7.07 (d, *J* = 7.6 Hz, 1H), 7.02 (d, *J* = 7.8 Hz, 1H), 6.97 - 6.87 (m, 2H), 3.87 (s, 3H). The analytical data matched literature reports.[169]

1-(2-Methoxyphenyl)-4-(3-(thiophen-2-yl)-1,2,4-oxadiazol-5-yl)-1*H*-1,2,3-triazol-5-amine (108). Same procedure as **51** using 1-azido-2-methoxybenzene (108 mg, 0.72 mmol) and **99** (166 mg, 0.87 mmol) as the starting materials. The residue was purified by flash chromatography on silica gel, eluting with hexanes/acetone (1:2) to afford **108** as a brown solid (41 mg, 18%). ^1H NMR (300 MHz, acetone-d6) δ 7.96 (d, *J* = 3.7 Hz, 1H), 7.84 (d, *J* = 4.8 Hz, 1H), 7.63 (t, *J* = 8.4 Hz, 1H), 7.55 (d, *J* = 7.8 Hz, 1H), 7.37 - 7.25 (m, 2H), 7.20 (t, *J* = 7.7 Hz, 1H), 6.42 (s, 2H), 3.93 (s, 3H). HRMS (ESI^+) calcd for $C_{15}H_{12}N_6O_2$ $(M+H)^+$ 341.3677, found 341.0833.

1-Azido-4-methoxybenzene. Same procedure as **95** using *p*-anisidine (0.47 mL, 4.06 mmol) as the starting material. The compound was obtained as a yellow solid (437 mg, 90%) and was used without further purification. ^1H NMR (300 MHz, chloroform-d) δ 6.90 (dd, *J* = 6.6, 12.9 Hz, 4H), 3.80 (s, 3H).

1-(4-Methoxyphenyl)-4-(3-(thiophen-2-yl)-1,2,4-oxadiazol-5-yl)-1*H*-1,2,3-triazol-5-amine (109). Same procedure as **51** using 1-azido-4-methoxybenzene (108 mg, 0.72 mmol) and **99** (166 mg, 0.87 mmol) as the starting materials. The compound **109** was obtained as a brown solid (57 mg, 73%). ^1H NMR (300 MHz, DMSO-d6). δ 8.02 (dd, *J* = 1.5, 3.9 Hz, 1H), 7.90 (dd, *J* = 1.5,

5.4 Hz, 1H), 7.54 (d, *J* = 9.0 Hz, 2H), 7.30 - 7.28 (m, 1H), 7.19 (d, *J* = 9.0 Hz, 2H), 6.81 (s, 2H), 3.58 (s, 3H). HRMS (ESI^+) calcd for $C_{15}H_{12}N_6O_2$ $(M+H)^+$ 341.3677, found 341.0828.

2-Azidonaphthalene. Same procedure as **95** using 2-naphthylamine (85 mg, 0.59 mmol) as the starting material. The residue was purified by flash chromatography on silica gel, eluting with hexanes/EtOAc (9:1) to afford an orange solid (35 mg, 35%). ^1H NMR (300 MHz, chloroform-d) δ 7.85 - 7.76 (m, 3H), 7.54 - 7.45 (m, 3H), 7.17 (dd, *J* = 2.4, 8.7 Hz, 1H). The analytical data matched literature reports.[172]

1-(Naphthalen-2-yl)-4-(3-(thiophen-2-yl)-1,2,4-oxadiazol-5-yl)-1*H*-1,2,3-triazol-5-amine (110). Same procedure as **51** using 2-azidonaphthalene (30 mg, 0.17 mmol) and **99** (34 mg, 0.17 mmol) as the starting materials. The compound **110** was obtained as a red solid (38 mg, 63%). ^1H NMR (300 MHz, DMSO-d6) δ 8.26 (d, *J* = 1.5 Hz, 1H), 8.20 (d, *J* = 8.4 Hz, 1H), 8.12 - 8.08 (m, 2H), 8.04 (d, *J* = 3.6 Hz, 1H), 7.90 (dd, *J* = 0.6, 4.8 Hz, 1H), 7.75 (dd, *J* = 1.8, 8.4 Hz, 1H), 7.69 - 7.66 (m, 2H), 7.31 - 7.29 (m, 1H), 7.01 (s, 2H). HRMS (ESI^+) calcd for $C_{18}H_{12}N_6OS$ $(M+H)^+$ 361.4004, found 361.0879.

3-Azido-1,1'-biphenyl. Azidotrimethylsilane (0.19 mL, 1.42 mmol) was added dropwise to a solution of 3-aminobiphenyl (200 mg, 1.18 mmol) and *tert*-butyl nitrite (0.21 mL, 1.77 mmol) in ACN (2 mL) at 0 °C. The reaction mixture was then slowly allowed to warm to rt and was stirred for 4 h. After completion of the reaction, Et_2O (8 mL) and H_2O (6 mL) were added, the organic layer was separated and further washed with H_2O (2 x 5 mL), brine (4 mL), dried over Na_2SO_4, filtered and concentrated. The residue was purified by flash chromatography on silica gel, eluting with hexanes/EtOAc (11:1) to deliver a light yellow oil (207 mg, 80%). ^1H NMR (300 MHz,

chloroform-d) δ 7.58 (d, *J* = 8.7 Hz, 2H), 7.48 - 7.35 (m, 5H), 7.25 - 7.23 (m, 1H), 7.03 - 7.00 (m, 1H). The analytical data matched literature reports.[173]

1-([1,1'-Biphenyl]-3-yl)-4-(3-(thiophen-2-yl)-1,2,4-oxadiazol-5-yl)-1*H*-1,2,3-triazol-5-amine (111). Same procedure as **51** using 3-azido-1,1'-biphenyl (32 mg, 0.16 mmol) and **99** (31 mg, 0.16 mmol) as the starting materials. The compound **111** was obtained as an orange solid (28 mg, 46%). ^{1}H NMR (300 MHz, DMSO-d6) δ 8.00 (dd, *J* = 0.9, 4.8 Hz, 1H), 7.89 (d, *J* = 6.9 Hz, 3H), 7.78 (d, *J* = 7.5 Hz, 2H), 7.72 (d, *J* = 8.1 Hz, 1H), 7.62 (d, *J* = 7.5 Hz, 1H), 7.49 (t, *J* = 7.2 Hz, 2H), 7.42 (d, *J* = 7.5 Hz, 1H), 7.30 - 7.26 (m, 1H), 6.99 (s, 2H). HRMS (ESI$^+$) calcd for $C_{20}H_{14}N_6OS$ $(M+H)^+$ 387.4377, found 387.1016.

3-(5-Amino-4-(3-(thiophen-2-yl)-1,2,4-oxadiazol-5-yl)-1*H*-1,2,3-triazol-1-yl)phenol (112). Boron tribromide (1 M solution in DCM, 0.62 mL, 0.62 mmol) was added dropwise to a solution of **51** (84 mg, 0.25 mmol) in DCM (1.3 mL) at 0 °C. The reaction mixture was slowly allowed to warm to rt and stirred overnight. H_2O was added (1.5 mL) and the product precipitated out, it was isolated by filtration, washed with H_2O (2 mL) and hexanes (3 x 2 mL), then it was dried under vacuum to afford **112** as a brown solid (57 mg, 73%). ^{1}H NMR (300 MHz, DMSO-d6). δ 10.11 (s, 1H), 8.02 (d, *J* = 3.6 Hz, 1H), 7.89 (d, *J* = 5.1 Hz, 1H), 7.43 (t, *J* = 8.1 Hz, 1H), 7.34 – 7.25 (m, 1H), 7.08 - 6.92 (m, 3H), 6.87 (s, 2H).

(1-(3-Methoxyphenyl)-1*H*-1,2,3-triazol-4-yl)methanol (113). Sodium ascorbate (58 mg, 0.29 mmol) and copper pentahydrate (18 mg, 0.07 mmol) were added to a solution of the azide **95** (56 mg, 0.37 mmol) and propargyl alcohol (0.024 mL, 0.41 mmol) in a solution of tBuOH:H_2O (0.2:0.2 mL) at rt. The resulting mixture was stirred overnight. The solvents were removed under vacuum. The residue was purified by flash chromatography on silica gel, eluting with 5% MeOH

in DCM to deliver **113** as a white solid (34 mg, 64%). ^{1}H NMR (300 MHz, DMSO-d6) δ 8.71 (s, 1H), 7.46 (d, *J* = 7.2 Hz, 4H), 7.04 – 6.98 (m, 1H), 5.33 (t, *J* = 5.5 Hz, 1H), 4.59 (d, *J* = 5.4 Hz, 2H), 3.84 (s, 3H). The analytical data matched literature reports.[174]

1-(3-Methoxyphenyl)-1*H*-1,2,3-triazole-4-carboxylic acid (114). A solution of 2.7 M Jones' reagent (0.25 mL) was added dropwise to a solution of **113** (34 mg, 0.16 mmol) in acetone (2 mL) at 0 °C and stirred for 10 min. The reaction mixture was allowed to warm up to rt and stirred for 1 h at rt. 2-Propanol was added slowly until the orange color of the excess of Jones' reagent was discharged. The reaction mixture was poured over ice, the product precipitated out, it was collected by filtration, washed with H_2O (3 mL), and dried under vacuum to give **114** as a light blue solid (25 mg, 71%). ^{1}H NMR (300 MHz, DMSO-d6) δ 9.42 (s, 1H), 7.58 – 7.42 (m, 4H), 7.08 (s, 1H), 3.85 (s, 3H). The analytical data matched literature reports.[175]

5-(1-(3-Methoxyphenyl)-1*H*-1,2,3-triazol-4-yl)-3-(thiophen-2-yl)-1,2,4-oxadiazole (115). EDCI (19 mg, 0.10 mmol) and **97** (15 mg, 0.10 mmol) were added to a solution of acid **114** (19 mg, 0.09 mmol) in ACN at rt. The mixture was stirred at rt for 30 min and then was heated to 120 °C overnight. After allowing the solution to cool to rt, the solvent was removed under vacuum. The residue was suspended into EtOAc (5 mL), washed with saturated $NaHCO_3$ (2 x 4 mL), dried over Na_2SO_4, filtered, and concentrated. The residue was purified by flash chromatography on silica gel, eluting with hexanes/EtOAc (2:1) to give **115** as a dark oil (13 mg, 46%). ^{1}H NMR (300 MHz, chloroform-d) δ 8.71 (s, 1H), 7.93 (d, *J* = 3.7 Hz, 1H), 7.55 (d, *J* = 5.0 Hz, 1H), 7.48 (t, *J* = 8.1 Hz, 1H), 7.46 – 7.40 (m, 1H), 7.34 (d, *J* = 8.8 Hz, 1H), 7.20 (t, *J* = 4.8 Hz, 1H), 7.06 (d, *J* = 8.2 Hz, 1H), 3.92 (s, 3H). HRMS (ESI^+) calcd for $C_{15}H_{11}N_5O_2S$ $(M+H)^+$ 326, found 326.

The analogs **116** and **117** were synthesized from intermediate **97** and the corresponding azides following the procedure described for **115**:

Azidobenzene. Same procedure as **95** using aniline (0.34 mL, 3.76 mmol) as the starting material. The compound was obtained as an orange oil (39 mg, 82%) and was used without further purification. ^{1}H NMR (300 MHz, chloroform-d) δ 7.36 (t, *J* = 8.1 Hz, 2H), 7.22 (t, *J* = 7.9 Hz, 1H), 7.02 (d, *J* = 7.5 Hz, 2H). The analytical data matched literature reports.[169]

(1-Phenyl-1*H*-1,2,3-triazol-4-yl)methanol. Same procedure as **113** using azidobenzene (87 mg, 0.73 mmol) as the starting material. The residue was purified by flash chromatography on silica gel, eluting with 5% MeOH in DCM to deliver a yellow solid (76 mg, 60%) ^{1}H NMR (300 MHz, DMSO-d6) δ 8.68 (s, 1H), 7.91 (d, *J* = 7.5 Hz, 2H), 7.58 (t, *J* = 8.4 Hz, 2H), 7.45 (d, *J* = 8.2 Hz, 1H), 5.33 (t, *J* = 5.6 Hz, 1H), 4.60 (d, *J* = 5.5 Hz, 2H). The analytical data matched literature reports.[174]

1-Phenyl-1*H*-1,2,3-triazole-4-carboxylic acid. Same procedure as **114** using (1phenyl-1*H*-1,2,3-triazol-4-yl)methanol (77 mg, 0.44 mmol) as the starting material. The compound was obtained as a yellow solid (21 mg, 25%). ^{1}H NMR (400 MHz, DMSO-d6) δ 9.38 (s, 1H), 7.95 (d, *J* = 8.4 Hz, 2H), 7.60 (t, *J* = 7.7 Hz, 2H), 7.52 (t, *J* = 8.0 Hz, 1H). The analytical data matched literature reports.[176]

5-(1-Phenyl-1*H*-1,2,3-triazol-4-yl)-3-(thiophen-2-yl)-1,2,4-oxadiazole (116). Same procedure as **115** using 1-phenyl-1*H*-1,2,3-triazole-4-carboxylic acid (20 mg, 0.11 mmol) and **97** (18 mg, 0.13 mmol) as the starting materials. The residue was purified by flash chromatography on silica gel, eluting with hexanes/EtOAc (3:1) to afford **116** as a white solid (8 mg, 25%). ^{1}H NMR (300 MHz, chloroform-d) δ 8.74 (s, 1H), 7.92 (d, *J* = 3.7 Hz, 1H), 7.82 (d, *J* = 12 Hz, 2H), 7.65 - 7.51

(m, 4H), 7.19 (t, *J* = 5.1 Hz, 1H). HRMS (ESI^+) calcd for $C_{14}H_9N_5OS$ $(M+Na)^+$ 318.0, found 318.0.

(1-(3-Fluorophenyl)-1*H*-1,2,3-triazol-4-yl)methanol. Same procedure as **113** using 1-azido-3-fluorobenzene (74 mg, 0.53 mmol) as the starting material. The residue was purified by flash chromatography on silica gel, eluting with 5% MeOH in DCM to deliver a yellow solid (57 mg, 56%). ^{1}H NMR (300 MHz, chloroform-d) δ 8.01 (s, 1H), 7.63 - 7.40 (m, 3H), 7.15 (m, 1H), 4.90 (s, 2H).

1-(3-Fluorophenyl)-1*H*-1,2,3-triazole-4-carboxylic acid. Same procedure as **114** using (1-(3-fluorophenyl)-1*H*-1,2,3-triazol-4-yl)methanol (57 mg, 0.29 mmol) as the starting material. The compound was obtained as a white solid (44 mg, 73%). ^{1}H NMR (300 MHz, DMSO-d6) δ 9.44 (s, 1H), 7.93 (t, *J* = 2.2 Hz, 1H), 7.91 - 7.83 (m, 2H), 7.66 (m, 1H), 7.38 (t, *J* = 8.4 Hz, 1H).

5-(1-(3-Fluorophenyl)-1*H*-1,2,3-triazol-4-yl)-3-(thiophen-2-yl)-1,2,4-oxadiazole (117). Same procedure as **115** using 1-(3-fluorophenyl)-1*H*-1,2,3-triazole-4-carboxylic acid (44 mg, 0.21 mmol) and **97** (36 mg, 0.25 mmol). The residue was purified by flash chromatography on silica gel, eluting with hexanes/EtOAc (3:1) to afford **117** as a yellow solid (19 mg, 28%). ^{1}H NMR (300 MHz, DMSO-d6) δ 9.96 (s, 1H), 8.05 - 7.87 (m, 5H), 7.71 (td, *J* = 8.3, 6.2 Hz, 1H), 7.48 - 7.39 (m, 1H), 7.31 (dd, *J* = 5.0, 3.7 Hz, 2H). HRMS (ESI^+) calcd for $C_{14}H_8FN_5OS$ $(M+H)^+$ 314.05, found 314.05.

The analogs **119-121** were synthesized from the corresponding azides and hydroximes following the procedure and purification described for **51** unless otherwise indicated:

***N*-Hydroxybenzimidamide.** Same procedure as **97** using benzonitrile (0.55 mL, 5.34 mmol) as the starting material. The compound was obtained as a yellow oil (397 mg, 56%). ^{1}H NMR (300

MHz, chloroform-d) δ 7.76 - 7.55 (m, 3H), 7.56 - 7.34 (m, 2H), 4.90 (s, 1H). The analytical data matched literature reports.[177]

2-(3-Phenyl-1,2,4-oxadiazol-5-yl)acetonitrile. Same procedure as **99** using *N*-hydroxybenzimidamide (152 mg, 1.11 mmol) and **98** (91 mg, 0.56 mmol) as the starting materials. The compound was obtained as a white solid (41 mg, 41%). ^{1}H NMR (300 MHz, chloroform-d) δ 8.07 (d, *J* = 8.0 Hz, 2H), 7.67 - 7.43 (m, 3H), 4.12 (s, 2H). The analytical data matched literature reports.[178]

1-(3-Methoxyphenyl)-4-(3-phenyl-1,2,4-oxadiazol-5-yl)-1*H*-1,2,3-triazol-5-amine (119). Same procedure as **51** using **95** (33 mg, 0.22 mmol) and 2-(3-phenyl-1,2,4-oxadiazol-5-yl)acetonitrile (41 mg, 0.22 mmol) as the starting materials. The compound was obtained as a brown solid (33 mg, 45%). ^{1}H NMR (300 MHz, chloroform-d) δ 8.15 (d, *J* = 8.0 Hz, 1H), 7.53 (d, *J* = 1.6 Hz, 4H), 7.23 - 7.06 (m, 4H), 5.49 (s, 1H), 3.90 (s, 3H). HRMS (ESI$^+$) calcd for $C_{17}H_{14}N_6O_2$ $(M+H)^+$ 335.1256, found 335.1342.

***N*-Hydroxypicolinimidamide**. Same procedure as **97** using 2-cyanopyridine (200 mg, 1.92 mmol) as the starting material. The compound was obtained as a light yellow solid (66 mg, 80%). ^{1}H NMR (300 MHz, DMSO-d6) δ 10.38 (s, 1H), 8.62 (d, *J* = 4.3 Hz, 1H), 7.99 - 7.84 (m, 2H), 7.57 - 7.43 (m, 1H), 6.85 (s, 2H). The analytical data matched literature reports.[179]

2-(3-(Pyridin-2-yl)-1,2,4-oxadiazol-5-yl)acetonitrile. Same procedure as **99** using *N*-hydroxypicolinimidamide (100 mg, 0.73 mmol) and **98** (143 mg, 0.87 mmol) as the starting materials. The residue was purified by flash chromatography on silica gel, eluting with hexanes/EtOAc (1:1) to afford a yellow solid (67 mg, 50%). ^{1}H NMR (300 MHz, DMSO-d6) δ 8.77 (d, *J* = 4.8 Hz, 1H), 8.14 - 7.98 (m, 2H), 7.64 - 7.60 (m, 1H), 4.81 (s, 2H).

1-(3-Methoxyphenyl)-4-(3-(pyridin-2-yl)-1,2,4-oxadiazol-5-yl)-1*H*-1,2,3-triazol-5-amine (120). Same procedure as **51** using **95** (45 mg, 0.30 mmol) and 2-(3-(pyridin-2-yl)-1,2,4-oxadiazol-5-yl)acetonitrile (57 mg, 0.30 mmol) as the starting materials. The compound was obtained as a light brown solid (24 mg, 25%). ^{1}H NMR (300 MHz, DMSO-d6) δ 8.77 (d, *J* = 4.0 Hz, 1H), 8.36 (d, *J* = 7.9 Hz, 1H), 8.04 (t, *J* = 5.8 Hz, 1H), 7.66 - 7.51 (m, 2H), 7.25 - 7.13 (m, 3H), 6.95 (s, 2H), 3.85 (s, 3H). HRMS (ESI$^+$) calcd for $C_{16}H_{13}N_7O_2$ $(M+H)^+$ 336.0, found 336.0.

1-(3-Fluorophenyl)-4-(3-(pyridin-2-yl)-1,2,4-oxadiazol-5-yl)-1*H*-1,2,3-triazol-5-amine (121). Same procedure as **51** using 1-azido-3-fluorobenzene (25 mg, 0.13 mmol) and 2-(3-(pyridin-2-yl)-1,2,4-oxadiazol-5-yl)acetonitrile (18 mg, 0.13 mmol) as the starting materials. The compound was obtained as a light orange solid (19 mg, 45%). ^{1}H NMR (300 MHz, DMSO-d6) δ 8.78 (d, *J* = 3.9 Hz, 1H), 8.37 (d, *J* = 7.8 Hz, 1H), 8.04 (t, *J* = 7.8 Hz, 1H), 7.76 - 7.57 (m, 3H), 7.53 - 7.50 (m, 2H), 7.04 (s, 2H). HRMS (ESI$^+$) calcd for $C_{15}H_{10}FN_7O$ $(M+Na)^+$ 346.2744, found 346.0810.

The analogs **122** and **123** were obtained following the protocol described for **115**:

***N*-Hydroxypentanimidamide.** Same procedure as **97** using valeronitrile (0.5 mL, 4.81 mmol) as the starting material. The compound was obtained as a colorless oil (40 mg, 25%). ^{1}H NMR (300 MHz, chloroform-d) δ 4.54 (s, 2H), 2.34 (t, *J* = 7.1 Hz, 2H), 2.13 (t, *J* = 8.1 Hz, 2H), 1.73 - 1.28 (m, 2H), 0.93 (t, *J* = 7.3 Hz, 3H). The analytical data matched literature reports.[180]

3-Butyl-5-(1-(3-methoxyphenyl)-1*H*-1,2,3-triazol-4-yl)-1,2,4-oxadiazole (122). Same procedure as **115** using *N*-hydroxypentanimidamide (60 mg, 0.52 mmol) and **114** (25 mg, 0.11 mmol) as the starting materials. The residue was purified by flash chromatography on silica gel, eluting with hexanes/EtOAc (2:1) to afford **122** as a white solid (7 mg, 22%). ^{1}H NMR (300 MHz, chloroform-d) δ 8.63 (s, 1H), 7.47 (t, *J* = 8.2 Hz, 1H), 7.39 (t, *J* = 2.2 Hz, 1H), 7.32 (d, *J* =

7.9 Hz, 1H), 7.05 (dd, *J* = 8.3, 2.5 Hz, 1H), 3.90 (s, 3H), 2.83 (t, *J* = 7.5 Hz, 2H), 1.81 (m, 2H), 1.44 (m, 2H), 0.96 (t, *J* = 7.3 Hz, 3H). HRMS (ESI^+) calcd for $C_{15}H_{17}N_5O_2$ $(M+Na)^+$ 322.1280, found 322.1258.

Benzo[*b*]thiophene-2-carbonitrile. Ammonium hydroxide (0.7 ml) and iodine (370 mg, 1.45 mmol) were added to a stirred solution of benzothiophene-2-carboxaldehyde (200 mg, 1.23 mmol) in THF (4 ml). The reaction mixture was stirred overnight under refluxing condition. The mixture was then treated with 5% aqueous solution of $Na_2S_2O_3$ (5 ml) and the product was extracted with EtOAc (2 x 6 mL). The combined organic layers were washed with brine, dried over Na_2SO_4, filtered, and concentrated. The product was obtained as a yellow oil (130 mg, 70%) and used without further purification. ^{1}H NMR (300 MHz, chloroform-d). δ 7.89 (m, 2H), 7.58 (d, *J* = 7.5 Hz, 1H), 7.49 (d, *J* = 7.0 Hz, 1H), 7.44 (m, 1H). The analytical data matched literature reports.[128]

***N*-Hydroxybenzo[*b*]thiophene-2-carboximidamide.** Same procedure as **97** using benzo[*b*]thiophene-2-carbonitrile (80 mg, 0.5 mmol) as the starting material. The compound was obtained as a white solid (64 mg, 67%). ^{1}H NMR (300 MHz, DMSO-d6) δ 9.93 (s, 1H), 7.87 (m, 2H), 7.65 - 7.50 (m, 1H), 7.40 - 7.30 (m, 2H), 6.05 (s, 2H).

3-(Benzo[*b*]thiophen-2-yl)-5-(1-(3-methoxyphenyl)-1*H*-1,2,3-triazol-4-yl)-1,2,4-oxadiazole (123). Same procedure as **115** using *N*-hydroxybenzo[*b*]thiophene-2-carboximidamide (42 mg, 0.22 mmol) and **114** (40 mg, 0.18 mmol) as the starting materials. The residue was purified by flash chromatography on silica gel, eluting with hexanes/EtOAc (3:1) to afford **123** as a light yellow solid (12 mg, 18%). ^{1}H NMR (300 MHz, DMSO-d6) δ 9.96 (s, 1H), 8.29 (s, 1H), 8.15 - 8.03 (m, 2H), 7.64 (d, *J* = 6.6 Hz, 1H), 7.61 - 7.47 (m, 3H), 7.13 (d, *J* = 9.4 Hz, 1H), 3.88 (s, 3H).

Synthesis of hit compounds 53 and 54

Ethyl-3-(2-methoxyacetamido)benzofuran-2-carboxylate (125). 2-Methoxyacetyl chloride (0.267 mL, 2.92 mmol) was added dropwise to a solution of ethyl 3-aminobenzofuran-2-carboxylate (200 mg, 0.97 mmol) and pyridine (0.236 mL, 2.92 mmol) in DCM (4.9 mL) at 0 °C. The resulting mixture was allowed to warm to rt and stirred for 2 h. The mixture was diluted with DCM (5 mL), and washed with H_2O (3 x 4 mL). The organic layer was dried over Na_2SO_4, filtered, and concentrated. The residue was purified by flash chromatography on silica gel, eluting with hexanes/EtOAc (3:2) to give **125** as a white solid (211 mg, 82%). ^{1}H NMR (400 MHz, chloroform-d) δ 10.22 (s, 1H), 8.49 - 8.44 (d, *J* = 12 Hz, 1H), 7.55 - 7.44 (m, 2H), 7.30 (t, *J* = 8 Hz, 1H), 4.50 (q, *J* = 7.1, 2H), 4.14 (s, 2H), 3.59 (s, 3H), 1.47 (t, *J* = 7.1, 3H).

3-(2-Methoxyacetamido)benzofuran-2-carboxylic acid (126). A 2 M solution of LiOH (2.94 mL) was added to the ester **125** (125 mg, 0.47 mmol) in a mixture of THF:MeOH (3 mL:1 mL). The reaction mixture was stirred at rt for 1h30. H_2O was added (6 mL) and the aqueous layer was washed with EtOAc (8 mL). The aqueous layer was acidified with 1 M HCl (pH ~ 3) and extracted with EtOAc (3 x 6 mL). The combined organic layers were dried over Na_2SO_4, filtered, and concentrated to give **126** as a light yellow solid (90 mg, 77%). ^{1}H NMR (300 MHz, chloroform-d) δ 10.20 (s, 1H), 8.48 (d, *J* = 8.2 Hz, 1H), 7.49 (s, 2H), 7.30 (m, 1H), 4.14 (s, 2H), 3.55 (s, 3H).

***N*-(2,3-Dihydrobenzo[*b*][1,4]dioxin-6-yl)-3-(2-methoxyacetamido)benzofuran-2-carboxamide (53).** PCl_5 (167 mg, 0.8 mmol) was added portionwise to a suspension of the acid **126** (40 mg, 0.16 mmol) in DCM (1.2 mL) at 0 °C. After the mixture turned clear, the reaction mixture was allowed to warm up to rt and stirred for 2 h. The solvent was removed under

vacuum and the residue was suspended in DCM (0.2 mL). This solution was added dropwise to a cold solution of 1,4-benzodioxan-6-amine (0.016 mL, 0.13 mmol) in pyridine (0.16 mL). After completion of the addition, the reaction mixture was stirred at rt ON. The mixture was diluted with DCM (6 mL) and washed with 1 M HCl (2 mL), H_2O (2 x 8 mL), 0.1 M NaOH (2 mL), brine (3 mL), dried over Na_2SO_4, filtered, and concentrated. The residue was purified by flash chromatography on silica gel, eluting with hexanes/EtOAc (1:1) to give **53** as a white solid (20 mg, 32%). ^{1}H NMR (300 MHz, chloroform-d) δ 8.16 (d, *J* = 7.8 Hz, 1H), 7.68 (d, *J* = 8.4 Hz, 1H), 7.61 (t, *J* = 6.9 Hz, 1H), 7.46 (t, *J* = 8.0 Hz, 1H), 7.03 (d, *J* = 8.5 Hz, 1H), 6.85 (sd, *J* = 2.5 Hz, 1H), 6.79 (dd, *J* = 8.5, 2.6 Hz, 1H), 4.39 - 4.29 (m, 4H), 4.24 (s, 2H), 3.38 (s, 3H).

Methyl-2-(5-(4-bromophenyl)furan-2-carboxamido)benzoate (128). Thionyl chloride (0.142 mL, 1.96 mmol) was added to a suspension of 5-(4-bromophenyl)-2-furoic acid (150 mg, 0.56 mmol). The mixture was heated to reflux for 1 h. The excess of thionyl chloride was removed under vacuum. The residual liquid was cooled to 0 °C in an ice bath and a solution of methyl-2-aminobenzoate (0.145 mL, 1.12 mmol) and TEA (0.098 mL, 0.7 mmol) in DCM (1.1 mL) was added slowly. The resulting mixture was heated to reflux for 1 h. It was then treated with a saturated sodium bicarbonate solution until the aqueous layer was slightly basic (pH ~ 8). The phases were separated and the organic layer was washed with H_2O (2 x 10 mL), dried over Na_2SO_4, filtered, and concentrated. The crude product was purified by recrystallization in refluxing EtOH to give **128** as a white solid (139 mg, 62%). ^{1}H NMR (300 MHz, chloroform-d) δ 12.34 (s, 1H), 8.87 (d, *J* = 8.6 Hz, 1H), 8.10 (d, *J* = 8.0 Hz, 1H), 7.83 - 7.73 (m, 2H), 7.60 (m, 3H), 7.31 (d, *J* = 10.8 Hz, 1H), 7.13 (t, *J* = 7.5 Hz, 1H), 6.80 (sd, *J* = 3.6 Hz, 1H), 4.01 (s, 3H).

2-(5-(4-Bromophenyl)furan-2-carboxamido)benzoic acid (129). NaOH (295 mg, 7.34 mmol) was added to a solution of the ester **128** (295 mg, 0.74 mmol) in MeOH:H_2O (2:1.2 mL). The

reaction was heated to reflux for 2.5 h. The reaction mixture was diluted with H_2O (6 mL) and extracted with EtOAc (5 mL). The aqueous layer was acidified to a pH of ~3 with 1 M HCl (2.5 mL) and extracted with EtOAc (3 x 6 mL). The combined organic layers were dried over Na_2SO_4, filtered, and concentrated to give **129** as a white solid (256 mg, 90%). ^{1}H NMR (300 MHz, DMSO-d6) δ 12.4 (s, 1H), 9.72 (d, *J* = 8.7 Hz, 1H), 8.12 (d, *J* = 8.4 Hz, 1H), 7.85 (d, *J* = 8.7 Hz, 2H), 7.68 (d, *J* = 8.7 Hz, 3H), 7.38 (sd, *J* = 3.6 Hz, 1H), 7.29 (sd, *J* = 3.9 Hz, 1H), 7.21 (t, *J* = 6.9 Hz, 1H).

5-(4-Bromophenyl)-*N*-(2-carbamoylphenyl)furan-2-carboxamide (54). EDCI (67 mg, 0.35 mmol), HOBt (49 mg, 0.36 mmol), and ammonium chloride (63 mg, 1.17 mmol) were added to a solution of **129** (45 mg, 0.12 mmol) and TEA (0.163 mL, 1.17 mmol) in THF (0.5 mL). The reaction mixture was stirred at rt overnight, and poured into H_2O (5 mL) and extracted with EtOAc (3 x 5 mL). The combined organic layers were washed with saturated $NaHCO_3$ (4 mL), brine (4 mL), dried over Na_2SO_4, filtered, and concentrated. The residue was purified by flash chromatography on silica gel, eluting with hexanes/EtOAc (2:1) to give **54** as a white solid (57 mg, 75%). ^{1}H NMR (300 MHz, DMSO-d6) δ 8.65 (d, *J* = 9.0 Hz, 1H), 8.41 (s, 1H), 7.89 (td, *J* = 8.1, 1.8 Hz, 3H), 7.70 (dd, *J* = 8.4, 2.1 Hz, 2H), 7.57 (t, *J* = 7.2 Hz, 1H), 7.35 – 7.28 (m, 2H), 7.18 (t, *J* = 7.5 Hz, 1H). HRMS (ESI$^+$) calcd for $C_{18}H_{13}BrN_2O_3$ $(M+Na)^+$ 408.2, found 409.0.

Synthesis of oxadiazole probes for target Identification

The analogs **157-159** were synthesized from intermediate **99** and the corresponding azides following the procedure described for **51**:

(3-Azidophenyl)methanol. Same procedure as **95** using 3-aminobenzylalcohol (200 mg, 1.62 mmol) as the starting material. The compound was obtained as a brown oil (52 mg, 78%). ^{1}H

NMR (300 MHz, DMSO-d6) δ 8.02 (d, *J* = 3.6 Hz, 1H), 7.89 (d, *J* = 5.0 Hz, 1H), 7.65 - 7.59 (m, 1H), 7.29 (d, *J* = 5.0 Hz, 1H), 5.42 (s, 1H), 4.62 (s, 2H). The analytical data matched literature reports.[181]

(3-(5-Amino-4-(3-(thiophen-2-yl)-1,2,4-oxadiazol-5-yl)-1*H*-1,2,3-triazol-1-yl)phenyl)methanol (157). Same procedure as **51** using **99** (48 mg, 0.25 mmol) and (3-azidophenyl)methanol (37 mg, 0.25 mmol) as the starting materials. The compound **157** was obtained as a brown solid (54 mg, 63%). ^{1}H NMR (300 MHz, DMSO-d6) δ 8.02 (d, *J* = 3.6 Hz, 1H), 7.89 (d, *J* = 4.8 Hz, 1H), 7.60 - 7.51 (m, 4H), 7.28 (t, *J* = 4.8 Hz, 1H), 6.89 (s, 2H), 5.48 (s, 1H), 4.62 (s, 2H). HRMS (ESI$^+$) calcd for $C_{15}H_{12}N_6O_2S$ $(M+H)^+$ 341.3677, found 341.0789.

(4-Azidophenyl)methanol. Same procedure as **95** using 4-aminobenzylalcohol (300 mg, 2.44 mmol) as the starting material. The residue was purified by flash chromatography on silica gel, eluting with hexanes/EtOAc (4:1) to deliver a brown oil (360 mg, 90%). ^{1}H NMR (300 MHz, chloroform-d) δ 7.16 (d, *J* = 8.6 Hz, 2H), 6.68 (d, *J* = 8.5 Hz, 2H), 4.55 (s, 2H). The analytical data matched literature reports.[173]

(4-(5-Amino-4-(3-(thiophen-2-yl)-1,2,4-oxadiazol-5-yl)-1*H*-1,2,3-triazol-1-yl)phenyl)methanol (158). Same procedure as **51** using **99** (50 mg, 0.26 mmol) and (4-azidophenyl)methanol (39 mg, 0.26 mmol) as the starting materials. The compound **158** was obtained as a brown solid (46 mg, 53%). ^{1}H NMR (300 MHz, DMSO-d6) δ 8.03 (s, 1H), 7.90 (m, 2H), 7.58 (s, 3H), 7.29 (s, 1H), 6.89 (s, 2H), 5.44 (s, 1H), 4.62 (s, 2H). HRMS (ESI$^+$) calcd for $C_{15}H_{12}N_6O_2S$ $(M+H)^+$ 341.3677, found 341.0794.

(2-Azidophenyl)methanol. Same procedure as **95** using 2-aminobenzylalcohol (200 mg, 1.62 mmol) as the starting material. The compound was obtained as a brown oil (90 mg, 98%). ^{1}H

NMR (300 MHz, chloroform-d) δ 7.34 (d, *J* = 8.6 Hz, 2H), 7.01 (d, *J* = 8.5 Hz, 2H), 4.66 (s, 2H). The analytical data matched literature reports.[182]

(2-(5-Amino-4-(3-(thiophen-2-yl)-1,2,4-oxadiazol-5-yl)-1*H*-1,2,3-triazol-1-yl)phenyl)methanol (159). Same procedure as **51** using **99** (50 mg, 0.26 mmol) and (2-azidophenyl)methanol (39 mg, 0.26 mmol) as the starting materials. The residue was purified by flash chromatography on silica gel, eluting with hexanes/EtOAc (4:1) to deliver **159** as a brown solid (22 mg, 48%). ^{1}H NMR (300 MHz, DMSO-d6) δ 8.01 (d, *J* = 3.7 Hz, 1H), 7.88 (d, *J* = 5.0 Hz, 1H), 7.74 (d, *J* = 7.6 Hz, 1H), 7.65 (t, *J* = 6.8 Hz, 1H), 7.52 (t, *J* = 7.5 Hz, 1H), 7.45 (d, *J* = 7.2 Hz, 1H), 7.29 – 7.26 (m, 1H), 6.79 (s, 2H), 5.37 (t, *J* = 5.4 Hz, 1H), 4.32 (d, *J* = 5.3 Hz, 2H). HRMS (ESI$^+$) calcd for $C_{15}H_{12}N_6O_2S$ $(M+H)^+$ 341.3677, found 341.0809.

***tert*-Butyl (3-hydroxyphenyl)carbamate (162).** di-*tert*-Butyl-dicarbonate (1.8 g, 8.2 mmol) was added to a solution of 3-aminophenol (600 mg, 5.5 mmol) in THF (6 ml). The reaction mixture was heated to reflux for 4 h. The mixture was diluted in EtOAc (15 ml) and washed with 1% HCl (5 mL) and H_2O (2 x 10 mL). The combined organic layers were further washed with brine (5 mL), dried over $MgSO_4$, filtered, and concentrated to give **162** as a white solid (852 mg, 87%). ^{1}H NMR (300 MHz, chloroform-d). δ 7.12 - 7.07 (m, 1H), 6.73 (d, *J* = 8.1 Hz, 1H), 6.60 - 6.52 (m, 2H), 3.54 - 3.50 (m, 1H), 1.51 (m, 9H). The analytical data matched literature reports.[175]

***tert*-Butyl (3-(2,5,8,11-tetraoxatridecan-13-yloxy)phenyl)carbamate (164).** Cs_2CO_3 (189 mg, 0.58 mmol) and triethyleneglycol-2-bromoethylmethylether (0.070 mL, 0.32 mmol) were added to a solution of the alcohol **162** (62 mg, 0.29 mmol) in DMA (0.5 mL). The resulting mixture was stirred at 60 °C overnight. After allowing the solution to cool to rt, H_2O (5 mL) was added and the product was extracted with Et_2O (2 x 6 mL). The combined organic layers were washed

with brine (4 mL), dried over Na_2SO_4, filtered, and concentrated. The residue was purified by flash chromatography on silica gel, eluting with hexanes/EtOAc (3/1) to afford **164** as a yellow oil (100 mg, 87%). ^{1}H NMR (300 MHz, chloroform-d). δ 7.16 - 7.10 (m, 1H), 6.80 (d, *J* = 8.6 Hz, 1H), 6.60 - 6.58 (m, 2H), 4.10 (t, *J* = 4.2 Hz, 2H), 3.82 (t, *J* = 5.1 Hz, 2H), 3.70 - 3.62 (m, 10H), 3.55 - 3.53 (m, 2H), 3.36 (s, 3H), 1.50 (s, 9H).

3-(2,5,8,11-Tetraoxatridecan-13-yloxy)aniline (165). A solution of 4 M HCl in dioxane (0.19 mL, 0.08 mmol) was added to a solution of the amine **164** (51 mg, 0.13 mmol) in THF (0.9 mL). The reaction mixture was stirred overnight at rt. The solvents were removed under pressure, the residue was dissolved in DCM (5 ml) and washed with H_2O (2 x 4 ml) and brine (4 mL). The organic layer was dried over Na_2SO_4, filtered, and concentrated to give **165** as an oil (35 mg, 92%). ^{1}H NMR (300 MHz, chloroform-d) δ 7.10 (t, *J* = 8.5 Hz, 1H), 6.30 - 6.25 (m, 3H), 4.10 (t, *J* = 4.2 Hz, 2H), 3.82 (t, *J* = 5.1 Hz, 2H), 3.70 - 3.56 (m, 12H), 3.36 (s, 3H).

13-(3-Azidophenoxy)-2,5,8,11-tetraoxatridecane (166). Same procedure as **95** using **165** (67 mg, 0.22 mmol) as the starting material. The residue was purified by flash chromatography on silica gel, eluting with DCM/EtOAc (1:1) to afford **166** as a yellow oil (34 mg, 48%). ^{1}H NMR (400 MHz, chloroform-d) δ 7.21 (t, *J* = 8.5 Hz, 1H), 6.68 (d, *J* = 9 Hz, 1H), 6.64 (d, *J* = 8.6 Hz, 1H), 6.55 (s, 1H), 3.84 - 3.81 (m, 2H), 3.71 - 3.61 (m, 12H), 3.60 - 3.56 (m, 2H), 3.36 (s, 3H).

1-(3-(2,5,8,11-Tetraoxatridecan-13-yloxy)phenyl)-4-(3-(thiophen-2-yl)-1,2,4-oxadiazol-5-yl)-1*H*-1,2,3-triazol-5-amine (160). Cs_2CO_3 (70 mg, 0.21 mmol) and triethyleneglycol-2-bromoethylmethylether (0.022 mL, 0.11 mmol) were added to a solution of the alcohol **112** (35 mg, 0.11 mmol) in DMA (0.3 mL). The resulting mixture was stirred at 50 °C overnight. After allowing the solution to cool to rt, H_2O (5 mL) was added and the product was extracted with

Et_2O (2 x 6 mL). The combined organic layers were washed with brine (4 mL), dried over Na_2SO_4, filtered, and concentrated. The residue was purified by flash chromatography on silica gel, eluting with methanol/DCM (5% MeOH) to give **160** as a yellow oil (28 mg, 55%). ^{1}H NMR (300 MHz, acetone-d6) δ 7.92 (m, 1H), 7.82 (m, 1H), 7.55 (m, 1H), 7.30 - 7.22 (m, 4H), 4.27 (t, *J* = 6.0 Hz, 2H), 3.87 (t, *J* = 3.9 Hz, 2H), 3.67 - 3.37 (m, 14H), 3.28 - 3.24 (m, 2H), 2.99 (s, 3H). HRMS (ESI^+) calcd for $C_{23}H_{28}N_6O_6S$ $(M+H)^+$ 517.1869, found 517.1908.

1-(3-(prop-2-yn-1-yloxy)phenyl)-4-(3-(thiophen-2-yl)-1,2,4-oxadiazol-5-yl)-1*H*-1,2,3-triazol-5-amine (167). Same procedure as **160** using **112** (23 mg, 0.07 mmol) and propargyl bromide (80% in toluene, 0.08 mL, 0.07 mmol) as the starting materials. The residue was purified by flash chromatography on silica gel, eluting with hexanes/EtOAc (3:1) to afford **167** as a white solid (5 mg, 20%). ^{1}H NMR (300 MHz, acetone-d) δ 7.95 (dd, *J* = 0.9, 3.3 Hz, 1H), 7.81 (d, *J* = 4.8 Hz, 1H), 7.62 - 7.57 (m, 1H), 7.34 - 7.24 (m, 4H), 6.61 (s, 2H), 4.94 (d, *J* = 2.4 Hz, 2H), 3.19 (t, *J* = 2.4 Hz, 1H). HRMS (ESI^+) calcd for $C_{17}H_{12}N_6O_2S$ $(M+H)^+$ 365.3891, found 365.0829.

The analogs **168-170** were synthesized from intermediate **99** and the corresponding azides following the procedure and purification described for **51**:

(3-Azidophenyl)(phenyl)methanone. Concentrated sulfuric acid (0.1 mL) was added to a solution of 3-aminobenzophenone (50 mg, 0.25 mmol) in acetic acid (0.34 mL) at 0 °C, then a solution of sodium nitrite (100 mg, 1.45 mmol) in H_2O (2 mL) was slowly added over 30 min. The resulting mixture was stirred at 0 °C for 2 h and a solution of sodium azide (162 mg, 2.5 mmol) in H_2O (3 mL) was added dropwise. The reaction mixture was stirred at 0 °C for 1 h and then it was diluted with H_2O (6 mL) and extracted with EtOAc (2 x 6 mL). The combined organic layers were further washed with H_2O (2 x 5 mL), $NaHCO_3$ (5 mL), brine (4 mL), dried over Na_2SO_4, filtered, and concentrated. The residue was purified by flash chromatography on

silica gel, eluting with hexanes/EtOAc (9:1) to deliver a yellow solid (52 mg, 95%) ^{1}H NMR (300 MHz, Chloroform-d) δ 7.79 (dt, *J* = 1.5, 81 Hz, 2H), 7.61 (t, *J* = 1.5, 7.5 Hz, 1H), 7.54 - 7.44 (m, 5H), 7.25 - 7.22 (m, 1H).

(3-(5-Amino-4-(3-(thiophen-2-yl)-1,2,4-oxadiazol-5-yl)-1*H*-1,2,3-triazol-1-yl)phenyl)(phenyl)methanone (168). Same procedure as **51** using **99** (25 mg, 0.13 mmol) and (3-azidophenyl)(phenyl)methanone (30 mg, 0.13 mmol) as the starting materials. The compound **168** was obtained as a brown solid (25 mg, 47%). ^{1}H NMR (300 MHz, DMSO-d6) δ 8.02 - 1.98 (m, 1H), 7.96 - 7.94 (m, 2H), 7.91 - 7.87 (m, 2H), 7.82 (d, *J* = 7.2 Hz, 3H), 7.70 (t, *J* = 7.0 Hz, 1H), 7.58 (t, *J* = 7.5 Hz, 2H), 7.30 - 7.28 (m, 1H), 7.02 (s, 2H). HRMS (ESI$^+$) calcd for $C_{21}H_{14}N_6O_2S$ $(M+H)^+$ 415.4478, found 415.0990.

(4-Azidophenyl)(phenyl)methanone. A solution of sodium nitrite (17.5 mg, 0.25 mmol) in H_2O (0.1 mL) was added to a solution of 4-aminobenzophenone (50 mg, 0.25 mmol) in 10% HCl (0.37 mL) at 0 °C and the resulting mixture was stirred for 30 min. A solution of sodium azide (18 mg, 0.28 mmol) in H_2O (0.3 mL) was added and the reaction mixture was stirred at 0 °C for another hour, allowed to warm up to rt and stirred for 1 h. The reaction mixture was then diluted with H_2O (4 mL) and extracted with EtOAc (2 x 5 mL). The combined organic layers were further washed with H_2O (2 x 4 mL), $NaHCO_3$ (4 mL), brine (4 mL), dried over Na_2SO_4, filtered, and concentrated. The residue was purified by flash chromatography on silica gel, eluting with hexanes/EtOAc (8:1) to deliver a yellow solid (44 mg, 80%). ^{1}H NMR (300 MHz, Chloroform-d) δ 7.87 - 7.75 (m, 4H), 7.59 (t, *J* = 7.5 Hz, 1H), 7.50 (t, *J* = 7.8 Hz, 2H), 7.12 (dt, *J* = 2.1, 4.2 Hz, 2H).

(4-(5-Amino-4-(3-(thiophen-2-yl)-1,2,4-oxadiazol-5-yl)-1*H*-1,2,3-triazol-1-yl)phenyl)(phenyl)methanone (169). Same procedure as **51** using **99** (25 mg, 0.13 mmol) and (4-azidophenyl)(phenyl)methanone (30 mg, 0.13 mmol) as the starting materials. The compound **169** was obtained as an orange solid (46 mg, 87%). ^{1}H NMR (300 MHz, DMSO-d6) δ 8.03 (dd, *J* = 0.9, 3.3 Hz, 1H), 7.96 (d, *J* = 8.4 Hz, 2H), 7.90 - 7.87 (m, 2H), 7.85 - 7.79 (m, 3H), 7.72 (t, *J* = 7.5 Hz, 1H), 7.60 (t, *J* = 7.5 Hz, 2H), 7.29 (td, *J* = 1.2, 5.1 Hz, 1H), 7.09 (s, 2H). HRMS (ESI$^+$) calcd for $C_{21}H_{14}N_6O_2S$ $(M+H)^+$ 415.4478, found 415.0933.

(2-Azidophenyl)(phenyl)methanone. Same procedure as (3-azidophenyl)(phenyl)methanone using 2-aminobenzophenone (150 mg, 0.76 mmol) as the starting material. The compound was obtained as a yellow solid (156 mg, 53%). ^{1}H NMR (300 MHz, chloroform-d) δ 7.80 (dd, *J* = 0.9, 8.1 Hz, 2H), 7.59 (tt, *J* = 1.5, 8.7 Hz, 1H), 7.54 - 7.43 (m, 3H), 7.38 (dd, *J* = 1.8, 7.8 Hz, 1H), 7.27 - 7.20 (m, 2H). The analytical data matched literature reports.[183]

(2-(5-Amino-4-(3-(thiophen-2-yl)-1,2,4-oxadiazol-5-yl)-1*H*-1,2,3-triazol-1-yl)phenyl)(phenyl)methanone (170). Same procedure as **51** using **99** (25 mg, 0.13 mmol) and (2-azidophenyl)(phenyl)methanone (30 mg, 0.13 mmol) as the starting materials. The compound **170** was obtained as an brown solid (53 mg, 94%) ^{1}H NMR (300 MHz, DMSO-d6) δ 8.85 (d, *J* = 8.1 Hz, 1H), 8.28 (t, *J* = 7.2 Hz, 1H), 8.16 (d, *J* = 8.4 Hz, 1H), 7.95 - 7.89 (m, 3H), 7.86 - 7.83 (m, 2H), 7.71 - 7.69 (m, 3H), 7.30 (td, *J* = 0.9, 3.9 Hz, 1H), 7.11 (s, 2H). HRMS (ESI$^+$) calcd for $C_{21}H_{14}N_6O_2S$ $(M+H)^+$ 415.4478, found 415.0933.

4-(Prop-2-yn-1-yloxy)benzonitrile (175). Cs_2CO_3 (2.73 g, 8.38 mmol) and propargyl bromide (80% in toluene, 0.467 mL, 4.19 mmol) were added to a solution of 4-cyanophenol (500 mg, 4.19 mmol) in acetone (10 mL). The reaction mixture was heated to reflux for 2 h. After cooling

to rt, the reaction mixture was filtered through celite, the solid was washed with acetone (2 x 5 mL) and the filtrate was concentrated. The residue was purified by flash chromatography on silica gel, eluting with hexanes/acetone (4:1) to deliver **175** as a light yellow solid (662 mg, 100%). ^{1}H NMR (300 MHz, chloroform-d) δ 7.60 (d, *J* = 9.0 Hz, 2H), 7.02 (d, *J* = 9.0 Hz, 2H), 4.75 (d, *J* = 2.4 Hz, 2H), 2.57 (t, *J* = 2.1 Hz, 1H). The analytical data matched literature reports.[184]

***N*-Hydroxy-4-(prop-2-yn-1-yloxy)benzimidamide (176)**. Same protocol as **97** using **175** (100 mg, 0.64 mmol) as the starting material. The compound **176** was obtained as a yellow solid (114 mg, 94%). ^{1}H NMR (300 MHz, acetone-d) δ 7.66 (d, *J* = 8.7 Hz, 2H), 6.99 (d, *J* = 9.0 Hz, 2H), 4.81 (d, *J* = 2.4 Hz, 2H), 3.10 (t, *J* = 2.4 Hz, 1H), 2.87 (s, 2H).

2-(3-(4-(Prop-2-yn-1-yloxy)phenyl)-1,2,4-oxadiazol-5-yl)acetonitrile (177). Same protocol as **99** using **98** (113 mg, 0.69 mmol) and **176** (111 mg, 0.58 mmol) as the starting materials. The residue was purified by flash chromatography on silica gel, eluting with hexanes/acetone (3:1) to deliver **177** as a yellow solid (84 mg, 62%). ^{1}H NMR (300 MHz, chloroform-d). δ 8.03 (dd, *J* = 2.1, 6.9 Hz, 2H), 7.07 (dd, *J* = 2.1, 6.9 Hz, 2H), 4.77 (d, *J* = 2.4 Hz, 2H), 4.11 (s, 2H), 2.56 (t, *J* = 2.4 Hz, 1H).

(3-(5-Amino-4-(3-(4-(prop-2-yn-1-yloxy)phenyl)-1,2,4-oxadiazol-5-yl)-1*H*-1,2,3-triazol-1-yl)phenyl)(phenyl)methanone (171). Same protocol as **51** using **177** (31 mg, 0.13 mmol) and (3-azidophenyl)(phenyl)methanone (29 mg, 0.13 mmol) as the starting materials. The compound **171** was obtained as a brown solid (45 mg, 76%). ^{1}H NMR (300 MHz, DMSO-d6) δ 8.14 (dd, *J* = 1.8, 6.9 Hz, 2H), 7.97 - 7.93 (m, 3H), 7.87 - 7.83 (m, 3H), 7.71 (t, *J* = 7.5 Hz, 1H), 7.61 (t, *J* =

8.1 Hz, 2H), 7.17 (dd, *J* = 1.8, 6.9 Hz, 2H), 7.06 (s, 2H), 4.90 (d, *J* = 2.4 Hz, 2H), 3.63 (t, *J* = 2.1 Hz, 1H). HRMS (ESI^+) calcd for $C_{26}H_{18}N_6O_3$ $(M+H)^+$ 463.4675, found 463.1508.

(4-(5-amino-4-(3-(4-(prop-2-yn-1-yloxy)phenyl)-1,2,4-oxadiazol-5-yl)-1*H*-1,2,3-triazol-1-yl)phenyl)(phenyl)methanone (172). Same protocol as **51** using **177** (27 mg, 0.11 mmol) and (4-azidophenyl)(phenyl)methanone (25 mg, 0.11 mmol) as the starting materials. The compound **172** was obtained as a brown solid (38 mg, 76%). ^1H NMR (300 MHz, DMSO-d6) δ 8.16 (d, *J* = 8.7 Hz, 2H), 7.98 (d, *J* = 8.4 Hz, 2H), 7.88 - 7.79 (m, 4H), 7.75 - 7.72 (m, 1H), 7.63 (t, *J* = 8.1 Hz, 2H), 7.16 (d, *J* = 9.0 Hz, 2H), 7.11 (s, 2H), 4.90 (d, *J* = 2.4 Hz, 2H), 3.63 (t, *J* = 2.4 Hz, 1H). HRMS (ESI^+) calcd for $C_{26}H_{18}N_6O_3$ $(M+H)^+$ 463.4675, found 463.1529.

4-(Hept-6-yn-1-yloxy)benzonitrile (180). DIAD (635 mg, 3.14 mmol), triphenylphosphine (713 mg, 2.71 mmol), and 6-heptyn-1-ol (0.39 ml, 3.14 mmol) were added to a solution of 4-cyanophenol (250 mg, 2.09 mmol) in DCM (5 ml) at 0°C. The reaction mixture was allowed to warm up to rt and stirred overnight. The solvent was removed under vacuum and the residue was purified by flash chromatography on silica gel, eluting with hexanes/EtOAc (7:1) to deliver **180** as a light yellow solid (548 mg, 100%). ^1H NMR (300 MHz, chloroform-d) δ 7.56 (d, *J* = 8.7 Hz, 2H), 6.92 (d, *J* = 8.7 Hz, 2H), 4.00 (t, *J* = 6.3 Hz, 2H), 2.22 - 2.18 (m, 2H), 1.95 (t, *J* = 2.7 HZ, 1H), 1.87 - 1.78 (m, 2H), 1.61 - 1.50 (m, 4H), 1.41 (d, *J* = 6.3 Hz, 2H).

(*E*)-4-(Hept-6-yn-1-yloxy)-*N*'-hydroxybenzimidamide (181). Same protocol as **97** using **180** (200 mg, 0.94 mmol) as the starting material. The compound **181** was obtained as a white solid (75 mg, 35%). ^1H NMR (300 MHz, chloroform-d) δ 7.77 (d, *J* = 9 Hz, 2H), 6.82 (d, *J* = 8.7 Hz, 2H), 3.86 (t, *J* = 6.3 Hz, 2H), 2.24 - 2.20 (m, 2H), 1.97 - 1.94 (m, 1H), 1.87 - 1.78 (m, 2H), 1.61 - 1.53 (m, 4H).

2-(3-(4-(Hept-6-yn-1-yloxy)phenyl)-1,2,4-oxadiazol-5-yl)acetonitrile (182). Same protocol as **99** using **181** (39 mg, 0.16 mmol) and **98** (28 mg, 0.17 mmol). The residue was purified by flash chromatography on silica gel, eluting with hexanes/EtOAc (5:1) to deliver **182** as a light yellow solid (21 mg, 47%). ^{1}H NMR (300 MHz, chloroform-d) δ 8.01 (d, *J* = 6.9 Hz, 2H), 6.98 (d, *J* = 6.9 Hz, 2H), 4.10 (s, 2H), 4.01 (t, *J* = 6.3 Hz, 2H), 2.24 - 2.20 (m, 2H), 1.97 - 1.94 (m, 1H), 1.87 - 1.78 (m, 2H), 1.64 - 1.60 (m, 4H).

(3-(5-Amino-4-(3-(4-(hept-6-yn-1-yloxy)phenyl)-1,2,4-oxadiazol-5-yl)-1*H*-1,2,3-triazol-1-yl)phenyl)(phenyl)methanone (173). Same protocol as **51** using **178** (11 mg, 0.05 mmol) and **182** (14 mg, 0.05 mmol) as the starting materials. The compound **173** was obtained as a brown solid (12 mg, 50%). ^{1}H NMR (300 MHz, DMSO-d6) δ 8.10 (d, *J* = 9 Hz, 2H), 7.95 - 7.93 (m, 3H), 7.86 - 7.82 (m, 3H), 7.71 - 7.68 (m, 1H), 7.62 - 7.56 (m, 2H), 7.09 (d, *J* = 8.7 Hz, 2H), 7.05 (s, 2H), 4.05 (t, *J* = 6.6 Hz, 2H), 2.75 (t, *J* = 2.4 Hz, 1H), 2.19 - 2.17 (m, 2H), 1.76 - 1.72 (m, 2H), 1.54 - 1.48 (m, 4H). HRMS (ESI$^+$) calcd for $C_{30}H_{26}N_6O_3$ $(M+H)^+$ 519.5738, found 519.2138.

Attempted synthesis of the azide 189

4-Azidobenzonitrile (184). Same protocol as **95** using 4-aminobenzonitrile (600 mg, 5.07 mmol) as the starting material. The residue was purified by flash chromatography on silica gel, eluting with hexanes/EtOAc (9:1) to deliver **184** as a light yellow solid (486 mg, 66%). ^{1}H NMR (300 MHz, chloroform-d) δ 7.64 (d, *J* = 9 Hz, 2H), 7.10 (d, *J* = 8.4 Hz, 2H). The analytical data matched literature reports.[173]

4-Azido-*N*-hydroxybenzimidamide (185). H_2NOH•HCl (86 mg, 0.12 mmol) and NMP (0.136 mL, 0.12 mmol) were added to a solution of **184** (30 mg, 0.2 mmol) in MeOH (1 mL). The reaction mixture was strirred overnight at 50 °C. The solvent was removed under vacuum and the

residue was suspended in EtOAc (4 mL). The organic layer was washed with saturated $NaHCO_3$ (3 mL), brine (3 mL), dried over Na_2SO_4, filtered, and concentrated to afford **185** as a white solid (32 mg, 88%). ^{1}H NMR (300 MHz, DMSO-d6) δ 9.23 (s, 1H), 7.67 (d, *J* = 9 Hz, 2H), 7.10 (d, *J* = 8.4 Hz, 2H), 5.81 (s, 2H).

2-(3-(4-Azidophenyl)-1,2,4-oxadiazol-5-yl)acetonitrile (186). Same protocol as **99** using **98** (79 mg, 0.48 mmol) and **185** (72 mg, 0.40 mmol) as the starting materials. The residue was purified by flash chromatography on silica gel, eluting with hexanes/EtOAc (6:1) to deliver **186** as a light orange solid (72 mg, 79%). ^{1}H NMR (300 MHz, chloroform-d) δ 8.06 (d, *J* = 9 Hz, 2H), 7.13 (d, *J* = 8.4 Hz, 2H), 4.13 (s, 2H).

Synthesis of fluorescein-azide 191

1,6-Diazidohexane (189). Sodium azide (676 mg, 10.4 mmol) was added to a solution of 1,6-dibromohexane (0.4 mL, 2.59 mmol) in DMF (2 mL). The resulting mixture was stirred overnight at 60 °C. The solvent was removed under vacuum, the residue was diluted in Et_2O (6 mL), the organic layer was washed with $NaHCO_3$ (2 x 5 mL). The aqueous layer was extracted with Et_2O (2 x 6 mL), the organic layers were combined, dried with Na_2SO_4, filtered, and concentrated. The residue was purified by flash chromatography on silica gel, eluting with hexanes/EtOAc (3:2) to give **189** as a white solid (211 mg, 82%). ^{1}H NMR (300 MHz, chloroform-d) δ 3.27 (t, *J* = 6.8 Hz, 4H), 1.66 - 1.55 (m, 4H), 1.47 - 1.37 (m, 4H). The analytical data matched literature reports.[145]

6-Azidohexan-1-amine (190). A solution of 1 M HCl (1.6 mL) was added to a solution of 1,6-diazidohexane (286 mg, 1.7 mmol) in Et_2O/EtOAc (1/1 mL). The mixture was cooled in an ice-bath and stirred vigorously. Triphenylphosphine (446 mg, 1.7 mL) was introduced portion wise

during 20 min. After stirring for 4 h at rt, the two layers were separated. The aqueous layer was extracted with Et_2O (2 x 5 mL). The combined aqueous layers were basified with NaOH 1 M until pH ~12 and extracted with Et_2O (3 x 6 mL). The organic layers were combined, dried with Na_2SO_4, filtered, and concentrated. The residue was purified by flash chromatography on silica gel, eluting with 10% MeOH, 1% NH_4OH in DCM to give **190** as a colorless oil (104 mg, 43%). ^{1}H NMR (300 MHz, chloroform-d) δ 3.25 (t, *J* = 6.8 Hz, 2H), 2.69 (t, *J* = 6.9 Hz, 2H), 1.65 - 1.44 (m, 2H), 1.52 - 1.29 (m, 6H). The analytical data matched literature reports.[145]

1-(6-Azidohexyl)-3-(3',6'-dihydroxy-3-oxo-3*H*-spiro[isobenzofuran-1,9'-xanthen]-5-yl)thiourea (191). The amine **190** (13.7 mg, 0.09 mmol) was added to a solution of fluorescein isothiocyanate (25 mg, 0.06 mmol) and DIPEA (0.021 mL, 0.12 mmol) in DMF (1 mL). The suspension was stirred overnight at rt. The reaction mixture was partitioned between EtOAc (4 mL) and 1 M HCl (3 mL), the organic layer was separated and washed further with 1 M HCl (2 x 4 mL) and brine (4 mL), the organic layers were combined, dried over Na_2SO_4, filtered, and concentrated. The residue was purified by flash chromatography on silica gel, eluting with 5% MeOH in DCM to give **191** as a bright yellow solid (22 mg, 71%). ^{1}H NMR (300 MHz, methanol-d) δ 8.10 (d, *J* = 1.5 Hz, 1H), 7.40 (dd, *J* = 1.8, 8.1 Hz, 1H), 7.14 (d, *J* = 8.4 Hz, 1H), 6.69 - 6.66 (m, 4H), 6.50 (dd, *J* = 2.4, 8.4 Hz, 2H), 3.61 (s, 2H), 1.70 - 1.63 (m, 5H), 1.46 - 1.43 (m, 5H). HRMS (ESI^+) calcd for $C_{27}H_{25}N_5O_5S$ $(M+H)^+$ 532.5908, found 532.1669.

3.0 DEVELOPMENT OF SMALL MOLECULE INHIBITORS OF MIR-122

3.1 INTRODUCTION TO MIRNA-122[a]

The microRNA miR-122, a liver-specific miRNA, is highly expressed in the liver at approximately 66,000 copies per cell, accounting for 70% of the total miRNAs in this tissue.[185] miR-122 is expressed in 18 species, such as mice, frogs, and zebrafish, where the entire sequence of mature miR-122 is highly conserved, suggesting that the whole sequence is necessary for the biological functions of miR-122.[185] miR-122 is involved in the regulation of important processes such as lipid and cholesterol metabolism, liver development, and systemic iron homeostasis.[185]

Krutzfeldt *et al.* were the first to show that complete loss of miR-122 activity was observed in mice injected with a miR-122 antagomir at a dose of 240 mg/kg body weight. The silencing effect was sustained for 23 days and was accompanied by a 40% decrease in plasma cholesterol levels. Gene expression analysis revealed that at least 11 genes involved in cholesterol biosynthesis, such as 3-hydroxy-3-methylglutaryl-coenzyme A reductase (HMGCR), 7-dehydrocholesterol reductase (DHCR7), mevalonate kinase (MVK), 3-hydroxy-3-methylglutaryl-coenzyme A synthase 1 (HMGCS1), and farnesyl diphosphate synthetase (FDPS), were downregulated following miR-122 silencing.[186] Similarly, using an anti-miR-122

[a] Part of this chapter was reprinted from *Curr. Med. Chem.* Thomas, M.; Deiters, A. MicroRNA miR-122 as a Therapeutic Target for Oligonucleotides and Small Molecules, 2013, 20, 29, 3629, with permission from Bentham Science Publishers.

2′-*O*-methoxyethyl phosphorothioate-modified oligonucleotide (miR-122 2′-MOE) in cell culture and in mice, Esau *et al.* treated mice twice weekly for four weeks with intraperitoneal injections of the 2′-MOE at doses ranging from 12.5 to 75 mg/kg, leading to a 3- to 10-fold reduction of miR-122 levels. [187] Plasma cholesterol and triglyceride levels were lowered and several genes associated with cholesterol metabolism, fatty-acid synthesis, and fatty-acid oxidation were reduced, including PMVK (phosphomevalonate kinase), FASN (fatty acid synthase), ACC (acetyl-CoA carboxylase) ACC1, ACC2, SCD1 (stearoyl-CoA desaturase-1) and ACLY (ATP citrate lyase).[187]

A correlation between the levels of miR-122 and the expression of four liver-enriched transcription factors (LETFs), notably C/EBPα (CCAA T/enhancer-binding proteins), and HNF4α (nuclear factor 4α), was identified.[188] Overexpression of these four LETFs in HCC-derived cells resulted in a significant up-regulation of miR-122, implying their involvement in the transcriptional regulation of miR-122. Furthermore, a binding site for HNF4α was recently discovered in the miR-122 promoter region.[189] Concomitant expressions of LETFs and miR-122 gradually increase in mice from embryonic day 12.5 until birth when the expression levels plateau. This period corresponds with the differentiation of bipotential hepatoblasts into mature hepatocytes. Since miR-122 is primarily expressed in hepatocytes, this finding suggests a role for miR-122 in liver development.[188] Additionally, a feedback loop between the LETF HNF6 and miR-122 was identified that tightly controls hepatocyte differentiation. HNF6 binds to the miR-122 promoter to stimulate the expression of miR-122, which subsequently results in the stimulation of the core LETFs, including HNF6, and the regulation of hepatocyte-specific genes.[190] In a similar fashion, a link between CUTL1, a transcriptional repressor of genes that

specifies terminal differentiation, and miR-122 was established, notably in the regulation of liver development and maintenance of the adult liver phenotype.[188]

In addition to being a key-regulator in the proliferation and differentiation of hepatocytes, as well as in the modulation of lipid and cholesterol metabolisms, miR-122 plays a significant role in the appearance and progression of several diseases (Figure 3.1).

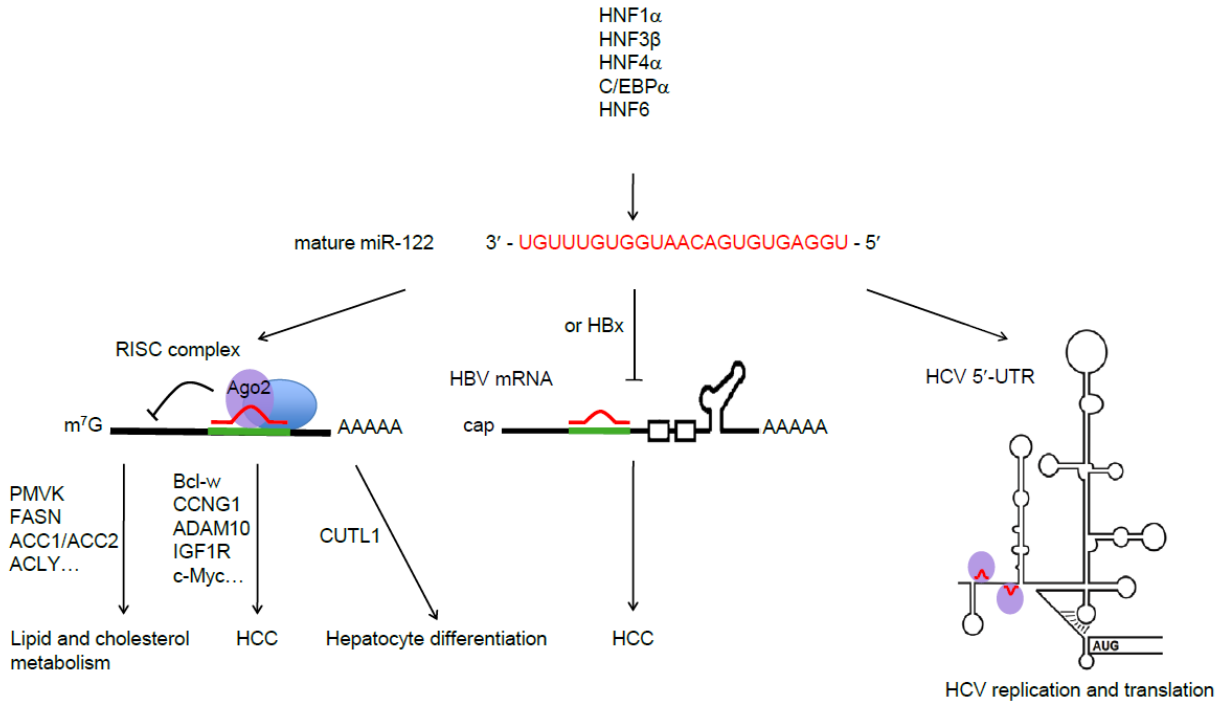

Figure 3.1: Biological roles of miR-122 and involvement in liver diseases.
miR-122 is controlled by the transcription factors HNF1α, HNF3β, HNF4α, HNF6, and C/EBPα, and regulates lipid and cholesterol metabolisms, as well as hepatocyte differentiation and proliferation. Down-regulation of miR-122 is found in HCC and interaction of miR-122 with the HCV genome enhances HCV replication and translation. Adapted from *Curr. Med. Chem.* 2013, 20, 3629.[b]

[b] HCV genome adapted from *FEBS Letters*, 584, C. Bung, Z. Bochkaeva, I. Terenin, R. Zinovkin, I. N. Shatsky, M. Niepmann, Influence of the hepatitis C virus 3′-untranslated region on IRES-dependent and cap-dependent translation initiation, 837. Copyright (2010), with permission from Elsevier. HBV mRNA adapted from *J. Virol*. **2000**, 74, 12, 5502, with permission from American Society for Microbiology.

3.1.1 Implication of miR-122 in HCC

Functional studies and miRNA profiling experiments of cell lines and patient tissues established a link between miR-122 and several hepatic disorders. Specifically, miR-122 downregulation is associated with hepatocellular carcinoma, chronic inflammation, cirrhosis, and nonalcoholic steatohepatitis.[191] HCC is among the five most common cancers; it is often detected at a late stage and due to a limited choice of current therapies a poor prognosis is typically observed.

Experiments in mice, which had a germline (KO) or a liver-specific (LKO) deletion of miR-122 introduced, resulted in a 30% reduction of total cholesterol and an accumulation of triglycerides in the liver. More precisely, miR-122 depletion induced a 57% decrease in low-density lipoprotein (LDL) cholesterol and a 25% decrease in high-density lipoprotein cholesterol.[191a] Similarly, miR-122 inhibition in chimpanzees treated with a locked nucleic acid (LNA)-modified phosphorothioate oligonucleotide, resulted in a pronounced decrease in LDL cholesterol.[192] Aging KO and LKO mice developed steatohepatitis and HCC as a result of an increased level of pro-inflammatory and tumor-promoting cytokines interleukin-6 and tumor necrosis factor.[191a] The loss of miR-122 function also prompted hepatocarcinogenesis through a different pathway by targeting CCNG1 (cyclin G1) and Bcl-w (Figure 3.1), which induced chromosomal instability and increased anti-apoptotic activity.[149] Additional miR-122 targets include ADAM10 (disintegrin and metalloprotease), IGF1R (insulin-like growth factor-1 receptor), SRF (serum response factor), c-Myc, pituitary tumour-transforming gene 1-binding factor (PTTG1), and the proto-oncogene Wnt1; all of those have been reported to participate in hepatocarcinogenesis through the deregulation of epithelial-mesenchymal transition, apoptosis, tumor cells proliferation, and migration.[193] Mice lacking miR-122 expression suffered from

HCC, with a 4:1 male-to-female ratio,[194] matching the gender distribution found in humans.[195] Hydrodynamic injection of miR-122 mimic recovered miR-122 expression and produced a significant reduction in angiogenesis, tumor occurrence, and tumor size.[194] A study performed in HCC-derived cell lines demonstrated that restoring miR-122 expression led to the recovery of *Bcl-w* function and increased the sensitivity of the cancer cells to the chemotherapeutic agent sorafenib.[153]

As previously mentioned, HBV infection represents one of the major risk factors for HCC. Although the precise molecular mechanisms responsible for the development of HCC have not been fully deciphered yet, recent evidence started to unveil a role for miR-122 in HBV-induced HCC.[196] Since it was demonstrated that the viral load and miR-122 expression are inversely correlated in HBV-infected patients, several mechanisms have been proposed to explain HBV-mediated suppression of miR-122.[196] One study reported that all HBV mRNAs possess a miR-122 binding site, and thus act as sponges to bind and sequester miR-122.[197] In addition, the hepatitis B virus protein X (HBx) was shown to inhibit miR-122 transcription via direct binding to the transcription factor Peroxisome proliferator activated receptor-gamma (PPARδ).[198] Monoadenylation of miR-122 by the cytoplasmic poly(A) RNAse polymerase Germline development 2 (Gld2) promotes the specific stabilization of miR-122 in human fibroblasts. Another insight into the HBV-induced miR-122 silencing, revealed that HBx negatively regulates the transcription of Gld2 which results in reduced miR-122 levels in HBV cells.[199]

Taken together, these results demonstrate that downregulation of miR-122 largely increases the risks of inflammation and HCC manifestations and, more importantly, that re-activation of miR-122 helps counteracting the progression of the disease.

3.1.2 Role of miR-122 in HCV

It is estimated that 185 million people are infected with HCV worldwide.[200] Acute infection causes jaundice and clinical symptoms such as fever, fatigue, and abdominal pain. About 55% to 85% of patients suffering from acute illness develop chronic HCV infection.[201] Even though in some cases chronic hepatitis C is asymptomatic, often it slowly progresses and generates extra hepatic diseases or causes chronic liver disorders,[201] such as cirrhosis (in 27% of cases) or HCC (25%).[202] The standard care for HCV, pegylated interferon-α (IFN) and ribavirin, are only effective in 50% of cases and are accompanied with severe side effects.[203] In addition, of the six different HCV genotypes, these treatments predominantly target genotype 1.[204] In 2011 the FDA approved two new protease inhibitors, boceprevir and telaprevir, which target the viral nonstructural protein 3 (NS3) or the enzyme NS3.4A serine protease, respectively. These new drugs complemented the current treatments, and even though they did not abolish the side effects and were only indicated toward HCV genotype 1, they significantly increased the cure rate (to about 70%).[205] In 2013, a second-generation NS3.4A serine protease inhibitor, simeprevir, was approved for use in combination with IFNα and ribavirin.[206] Even though this new treatment was only beneficial against genotype 1, it reduced the duration of the therapy from 48 weeks to only 24 weeks. Also in 2013, the nucleotide analog sofosbuvir, an inhibitor of the viral RNA polymerase NS5B, was approved as a 12-week combination therapy to treat genotypes 1 and 4, and allowed for the first time the formulation of an IFN-free regimen against genotypes 2 and

3.[206] Given the inconveniences accompanied with IFN treatment, subcutaneous administration and serious side-effects, the discovery of new directly acting antiviral agents, orally available and bypassing the necessity of IFN has revolutionized HCV therapies.[207] In 2014, new oral IFN-free regimens for genotype 1 were approved, which included the combination of sofosbuvir with either a second-generation NS3/4A protease inhibitor (ledipasvir) or an NS5A replication complex inhibitor (ombitasvir) with or without ribavirin. While these new treatments provide impressive cure rates (up to 90%), fewer side-effects, and greatly reduced duration of therapy (12-24 weeks versus 48 weeks previously), they still mostly target HCV genotype 1 and the occurrence of resistance has not been fully documented.[206]

The HCV genome contains two miR-122 binding sites, S1 and S2, near its 5′-end and it has been reported that the presence of mature miR-122 is necessary for HCV replication and translation (Figure 3.1).[208] Although the precise mechanisms by which miR-122 impacts the HCV life cycle is not clearly understood yet, recent studies suggest that miR-122 stabilizes the viral RNA.[209] Furthermore, the direct interaction between miR-122 and its targets S1 and S2 is thought to stimulate the translation by facilitating the association of the viral RNA and ribosomes.[210] In total contradiction with this hypothesis, another study unveiled a new mechanism for miR-122 participation in HCV, where miR-122 stimulates HCV RNA synthesis by competing with the ribonuclear protein PCBP2 for binding to the viral RNA, which prevents translation while simultaneously enhancing the amount of viral RNAs available for template RNA viral synthesis.[211] Despite the fact that contradictory results have been reported in the literature regarding the participation of Ago2 in HCV replication,[212] recent studies demonstrated that miR-122 interacts with the HCV RNA as a complex with Ago2 (Figure 3.1).[209b] Since miR-122 binds to the 5′-end of the viral RNA and it is well known that an RNA molecule can be

degraded from its 5′-end after cleavage of the monomethyl guanosine (m7G) cap, it was hypothesized that the complex formed by miR-122 and Ago2 could act as a cap, protecting the viral RNA from 5′ exonuclease degradation, more specifically by the exonuclease Xrn1.[209a] Experiments in murine embryonic fibroblasts transfected with synthetic HCV RNAs with or without a m7G cap and in the presence or absence of miR-122 duplex validated this hypothesis. The degradation rate of the 5′ capped RNA was not affected by the presence of miR-122 whereas the degradation rate of the 5′ uncapped RNA was significantly slower when co-transfected with miR-122 mimics.[209b] However, miR-122 is specifically required for viral replication even in cells lacking the exonuclease Xrn1,[213] indicating additional functions for miR-122 such as promoting viral RNA synthesis.[211] Similarly to HBV infection, it has been proposed that the HCV genome acts as a sponge for miR-122, and that binding to miR-122 to either S1 or S2 results in miR-122 sequestration and prompts global up-regulation of host miR-122 targets, thus providing a favorable environment for carcinogenesis.[214]

Most importantly the two miR-122 binding sites are conserved across the different HCV genotypes, which reinforces the therapeutic potential of targeting miR-122, as there is a critical necessity for new and broader antiviral therapies.[204, 215] Li *et al.* developed an assay in Huh7.5 cells where genotypes 1-6 HCV are expressed. They found that transfection of Miravirsen, the well-established fully phosphorothioate-modified DNA/LNA mixmer targeting miR-122 (LNA-antimiR-122), yielded an efficient, dose-dependent reduction of the infection in all six genotypes.[71] Using the same LNA-antimiR-122, Lanford *et al.* treated HCV-infected chimpanzees through injections once a week for 12 weeks.[192] They observed a significant decrease in the viral RNA load after 3 weeks with a maximum decrease reached 2 weeks after the end of the treatment. The reduction in the levels of HCV-infected RNA was not accompanied

with any rebound in viremia, either during the dosing phase or even up to 6 weeks after the end of the treatment. Overall, exposure to the LNA-antimiR-122 oligonucleotide led to a long-lasting effect, no noticeable toxicity, no viral resistance, and no side effects.[192] In addition deep sequencing of the 5′ noncoding region of the HCV genome of the high-dose animals demonstrated that no adaptive mutations occurred in the S1 and S2 miR-122 recognition sites. This result was in strong opposition to another study which observed 67% of HCV clones presenting mutations within 2 days after administration of a non-nucleoside polymerase inhibitor.[192] Another pre-clinical study aimed at investigating the effects caused by treatment with Miravirsen was conducted on cynomolgus monkeys at pharmacologic and supra-pharmacologic doses. The monkeys were injected with the LNA-antimiR-122 twice weekly for 4 weeks and a dose-dependent decrease in total serum cholesterol was observed. The LNA was rapidly cleared from plasma ($t_{1/2}$ ~ 10 - 36 min) but was accumulated in the liver and the kidneys where elimination occurred at a much slower rate ($t_{1/2}$ ~ 37 - 20 days). These effects were not associated with any evident toxicity, even at the highest dose, which largely went beyond the dose needed for maximal miR-122 inhibition.[216] As previously mentioned, Miravirsen is currently investigated in clinical trials as a new HCV therapy, and promising results in phase 2a trials revealed that four out of the nine patients who received the drug for 4 weeks exhibited a complete reduction in HCV levels with no signs of viral resistance.[72] One of the main challenges in creating new and effective HCV therapeutics stems from the fact that the HCV genome evades selection pressure through rapid mutation due to the lack of error-proofing of the viral RNA polymerase.[201] Consequently, targeting a host factor at the miRNA-mRNA interface, rather than a viral component, could feature a novel and efficient anti-viral strategy since it is less likely to induce viral resistance.

Since interferon has long been the standard agent for HCV treatment, its effect on miR-122 function was studied extensively. The levels of miR-122 in Huh7 cells treated with interferon-β were reduced by 80%.[217] However, studies carried out on samples isolated from chronic hepatitis C (CHC) infected patients, where the miR-122 levels were evaluated before and 4 hours after treatment with interferon-α, showed no modifications of the miR-122 levels.[218] No effect of IFN on miR-122 levels was also observed in mice, indicating discrepancies between *in vitro* and *in vivo* experiments.[218] Though no correlation could be established between serum levels of miR-122 and HCV RNA, a previous report suggested that miR-122 provides a practical biomarker for liver injuries, since its levels in CHC infected patients are higher than in healthy individuals.[219] There were no differences noted, however, when comparing miR-122 levels in the serum of patients who responded well to IFN therapy and patients who did not.[220] In contrast, liver biopsies revealed that subjects who did not respond to IFN displayed considerably lower pretreatment miR-122 levels than patients who responded well to the treatment.[218] These results are somewhat surprising since miR-122 inhibition with LNA-antimiR-122 appeared effective in significantly reducing the HCV RNA infection in both responding and non-responding patients. This could suggest that even low miR-122 levels are sufficient to promote the replication and translation of HCV.[218] Moreover, whereas five known IFN-regulated genes (IRGs) were strongly up-regulated in responding patients after administration of IFN-α, no effects were noticed in expression of IRGs in the non-responding population.[218] Interestingly, chimpanzees treated with Miravirsen displayed a pronounced decrease in the expression levels of IRGs.[192] This observation is important since patients who do not respond to current interferon-α therapies display particularly high IRG levels. Thus by normalizing the levels of IFN-regulated genes,

miR-122 antagonist-based therapies raise the possibility to sensitize IFN non-responding patients to IFN treatment.[192]

These results provide additional evidence of the beneficial effects of targeting miR-122 and, more importantly, suggest the possibility of developing more effective combination therapies. In conclusion, agents that can specifically regulate miR-122 activity constitute new tools to elucidate the involvement of miR-122 in HCC and in HCV infection and could provide potential new anticancer and antiviral therapies.

3.2 PREVIOUS WORK

The discovery of the first small molecule inhibitor of miR-21, the diazobenzene **24**, was a successful proof-of-principle for the development of small molecules that selectively modulate the function of a miRNA of interest. A reporter assay was similarly developed to screen for small molecule modifiers of miR-122[124] and the Deiters lab identified two inhibitors (**29**, **30**) and one activator (**31**) of miR-122 function (Figure 1.5).[98] In comparison with the previously described miR-21 assay, the miR-122 reporter construct was based on the psiCHECK-2 plasmid (Promega) and possesses two luciferase genes, *Renilla* and firefly luciferases. The miR-122 target sequence was inserted downstream of the *Renilla* luciferase gene, while the firefly expression serves as an internal control for normalization purposes and to account for variation in transfection efficiency and cell viability. This sensor can be used in cells to detect both a miR-122 inhibitor, indicated by an increase in the *Renilla* expression, and a miR-122 activator, indicated by a reduction in the *Renilla* signal.[98] A pilot screen of 1,364 compounds, from the NCI Developmental Therapeutics Program (Diversity Set II) was performed in Huh7 cells stably expressing the psiCHECK-miR-

122 reporter construct. The cells were exposed to 10 μM of each small molecule for 48 h and assayed using a Dual Luciferase Assay Kit (Promega). Two miR-122 inhibitors were identified through this screen, compounds **29** and **30** which induced a 773 ± 38% and a 1251 ± 125% increase in the relative luciferase signal, respectively (Figure 3.2).[98]

To validate the effect of these inhibitors on miR-122 expression, Huh7 cells were transfected with the psiCHECK-empty reporter (where the miR-122 binding site was replaced with a linker not targeted by any known miRNAs) and exposed to 10 μM of **29** and **30** for 48 h. The luciferase signal was not affected by either compound, which confirmed that they did not interact with the luciferase reporter in a non-miRNA specific pathway. The inhibitors **29** and **30** were also tested in the miR-21 luciferase assay in HeLa cells and did not exhibit any activity, indicating some selectivity of both of these small molecules for miR-122.[98] Dose-response experiments were performed with **29** and **30** in the miR-122 luciferase assay, and their EC_{50} values were determined as 3 and 0.6 μM, respectively. Both inhibitors were investigated by preliminary structure-activity relationship studies to understand the molecular requirements for miR-122 inhibition. Modifications in the amide linkage of **29** (shown in magenta in Figure 3.2) or replacement of the naphtyl group with diverse aromatic rings (shown in blue in Figure 3.2) resulted in significant decreases in activity. Attempts to modify the benzene substituents of **29** (shown in red in Figure 3.2) led to similar losses in activity. Likewise, modifications were made on **30** to investigate the importance of the *trans*-decahydroquinoline motif (shown in blue in Figure 3.2).

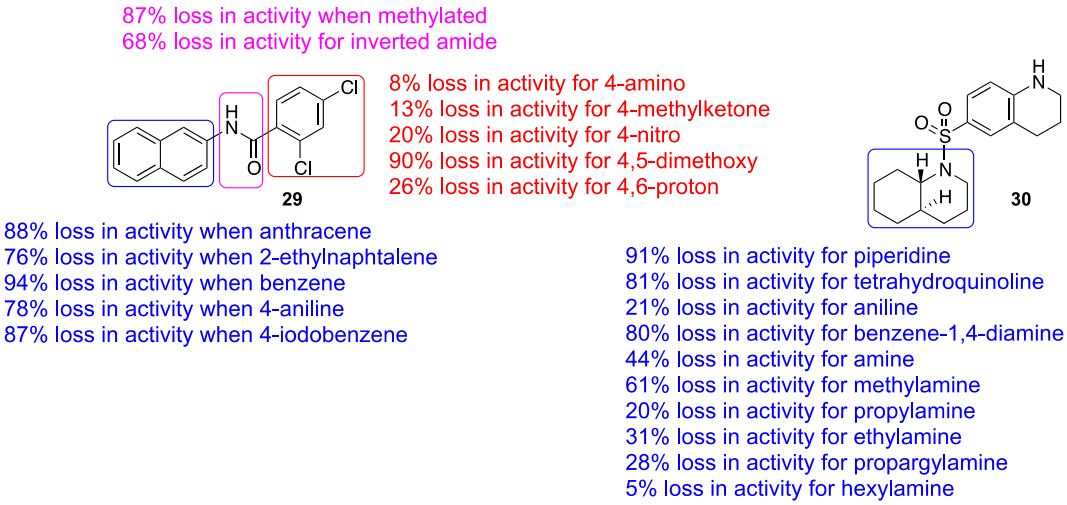

Figure 3.2: Summary of the preliminary SAR studies of the miR-122 inhibitors **29** (right) and **30** (left). The data were adapted from *J. Am. Chem. Soc.*, **2010**, *132*, 7976.

Given that miR-122 is greatly downregulated in HCC, small molecules capable of restoring miR-122 function in cancer cells may have a therapeutic effect. The psiCHECK-miR122 reporter was consequently used to screen for small molecule activators of miR-122. Among the same initial set of 1,364 compounds, the small molecule **31** was found to be a miR-122 activator, it induced a 90% decrease in the *Renilla* luciferase signal, whereas no changes in luminescence were observed in Huh7 cells transfected with the control reporter, psiCHECK-empty.[98] In addition, the compound **31** was tested in the miR-21 assay and did not perturb luciferase expression, thus validating that **31** is not a general activator of the miRNA pathway but rather may be specific toward miR-122 upregulation.[98] The miR-122 activator **31** displayed an IC_{50} value of 3 μM when tested in dose-response in the miR-122 luciferase assay. SAR studies of **31** indicted that the amino group on the fused rings (shown in red in Figure 3.3) appeared to be critical since removal or replacement with a nitro group induced decrease in activities. Substitutions of the *N*,*N*-dimethylpropanamine motif (shown in blue in Figure 3.3) with different functional groups drastically reduced the activity.[98]

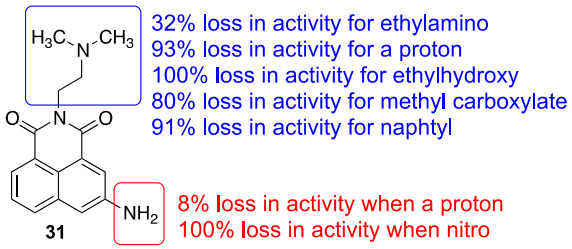

Figure 3.3: Summary of the SAR studies of the miR-122 activator **31.**
The data were adapted from *J. Am. Chem. Soc*. **2010**, *132*, 7976.

The intracellular levels of miR-122 were measured by qRT-PCR following exposure to these 3 small molecule modifiers of miR-122. Huh7 cells were treated with **29**, **30**, and **31** at 10 μM for 48 h. The activator **31** induced a 438% increase in miR-122 expression level in comparison with DMSO treated cells, whereas the inhibitors **30** and **29** exhibited a 72% and 45% knock-down of mature miR-122 levels relative to DMSO treated cells, respectively (Figure 3.4).[98] This was consistent with the higher activity of the sulfonamide **30** in the luciferase assay. To assess the specificity of these small molecules, the levels of mature miR-21 in HeLa cells treated with the three compounds at 10 μM were also measured by qRT-PCR. None of the three modifiers perturbed miR-21 expression levels (Figure 3.4), suggesting that these small molecules displayed some degree of selectivity towards the regulation of miR-122.

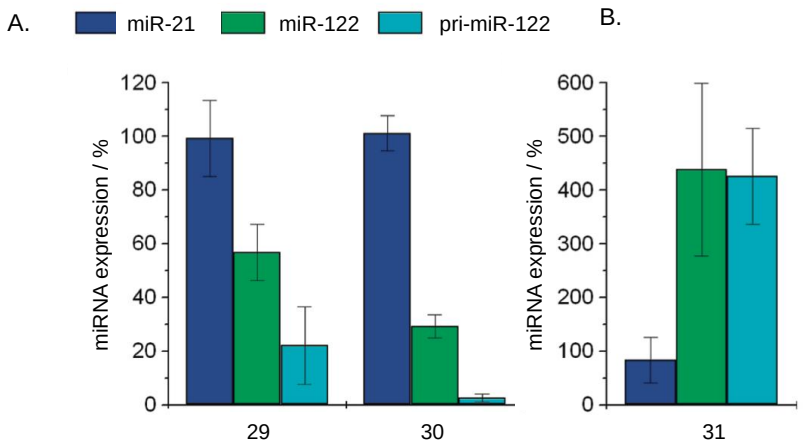

Figure 3.4: qRT-PCR measurements of endogenous levels of miR-122 in Huh7 cells and miR-21 in HeLa cells after 10 μM treatment with **A**. the miR-122 inhibitors **29** and **30** or **B**. the miR-122 activator **31**. Adapted from *J. Am. Chem. Soc*. **2010**, *132*, 7976. Copyright (2010) American Chemical Society.

In order to learn more about the mechanisms of these small molecules, the intracellular levels of primary miR-122 (pri-miR-122) were similarly measured by qRT-PCR (Figure 3.4A). The amide **29** and the sulfonamide **30** induced a 78% and 97% decrease in pri-miR-122 levels in comparison to DMSO treated cells, respectively. Conversely, upon treatment with the activator **31** an increase in pri-miR-122 levels was observed (Figure 3.4B). Since the levels of pri-miR-122 were significantly reduced following exposure to the inhibitors **29** and **30** (Figure 3.4A), it was hypothesized that, similarly to the miR-21 inhibitor **24**, the small molecule miR-122 inhibitors act at the post-transcriptional or transcriptional step rather than at any downstream processes of the miRNA pathway.[98]

In addition, melting experiments were performed to investigate an eventual direct interaction of the small molecule miR-122 inhibitor **30** with the miR-122 oligonucleotide itself. The thermal stability of pre-miR-122 was analyzed in the absence and in the presence of the miR-122 inhibitor **30** as well as with the known RNA binder tobramycin.[98] A variation of 10 °C was observed in the melting temperatures of pre-miR-122 in the absence and in the presence of tobramycin, which indicated a stabilization of the RNA upon direct interaction with tobramycin;

whereas the melting temperature was 60 °C regardless of the absence of presence of **30** (Figure 3.5). This confirmed that the inhibition observed in the previous experiments (Figure 3.2 and Figure 3.4) was not due to the direct binding of the small molecule **30** to the miR-122 oligonucleotide.

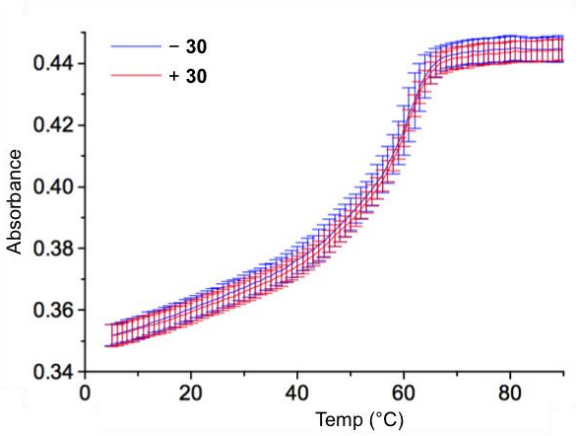

Figure 3.5: Melting curves of pre-miR-122 in the absence and presence of the small molecule miR-122 inhibitor **30.** Adapted from *J. Am. Chem. Soc*. **2010**, *132*, 7976. Copyright (2010) American Chemical Society.

Subsequent experiments were performed to illustrate the therapeutic importance of these small molecule regulators of miR-122. Since the inhibitors **29** and **30** were shown to efficiently downregulate miR-122 expression, their ability to inhibit HCV replication was evaluated (Figure 3.6A). Following transfection of Huh7 cells with genotype 1a H77c RNA, the cells were subsequently exposed for 48 h to either a miR-122 antagomir (positive control) or to the small molecules **29** and **30** (10 μM) and DMSO (negative control).[98] Consistent with what has been reported in the literature, the HCV RNA levels were reduced by 80% upon treatment with the miR-122 antagomir, as determined by qRT-PCR (Figure 3.6A).[71] Treatment with the small molecule miR-122 inhibitors **29** and **30** reduced by 52% and 53% the levels of HCV RNA, respectively (Figure 3.6A).[98]

On the other hand, an aberrantly low level of endogenous miR-122 has been found to promote HCC. In HCC-derived cell lines, Hep3B and HepG2, miR-122 is highly downregulated and as a consequence, its direct targets, such as *Bcl-w,* are abnormally upregulated.[149] Treatment of HepG2 cells with a miR-122 duplex, mimicking an increase in endogenous miR-122 levels, led to a significant reduction of the *Bcl-w* protein expression. Repression of the gene *Bcl-w* by miR-122 was later shown to trigger apoptosis in diseased cells by restoring capase-3 activity.[149] To verify the positive effect of **31**, which was hypothesized to stimulate miR-122 expression and to induce apoptosis of cancer cells, Huh7 and HepG2 cells were treated with the small molecule miR-122 activator at 10 and 20 μM and the cell viability was measured after 48 hours. Treatment with the miR-122 activator **31** resulted in a 70% reduction in cell viability of HepG2 cells which express miR-122 at a greatly reduced level (≥99%), compared to only a 10% reduction in cell viability of Huh7 cells which express ≤85% miR-122 levels, compared to primary hepatocytes (Figure 3.6B).[98, 221]

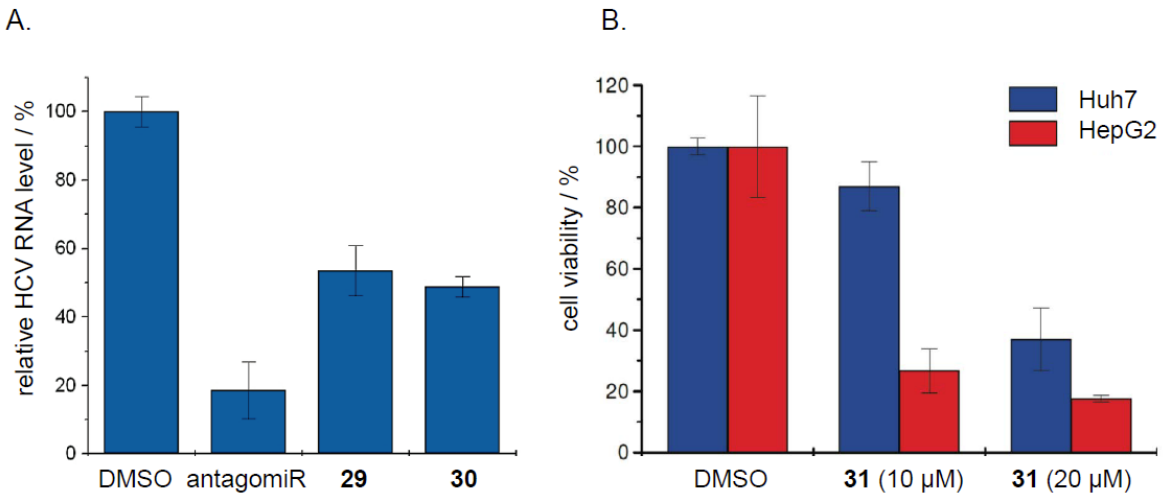

Figure 3.6: Demonstration of the therapeutic potential of the small molecule miR-122 modifiers.
A. Small molecule miR-122 inhibitors **29** and **30** significantly reduced the levels of viral RNA. **B.** The small molecule miR-122 activator **31** triggered apoptosis in cancer cells expressing low miR-122 levels. Adapted from *J. Am. Chem. Soc*. **2010**, *132*, 7976. Copyright (2010) American Chemical Society.

Together these results highlighted, for the first time, the therapeutic potential of small molecule modifiers of specific disease-causing microRNA.

3.3 SYNTHESIS OF SMALL MOLECULE MIR-122 INHIBITORS

Following the initial discovery of the miR-122 inhibitor **30**,[98] further SAR studies were conducted through the synthesis and testing of analogs in order to further optimize the activity and to better understand the molecular requirements for miR-122 inhibition. Three different series of analogs were investigated, through modifications of the *trans*-decahydroquinoline moiety, the sulfonamide linkage, or the aniline motif.

3.3.1 SAR Studies of Inhibitor 30 through Modifications of the *trans*-decahydroquinoline

The sulfonamide derivatives **202-226** were prepared according to a procedure developed by Colleen Connelly and further optimized to increase the product yields (Scheme 3.1). The analogs **196-198**, **200**, **206**, **207**, and **213** were synthesized by Colleen Connelly.[98] Trifluoroacetic anhydride (TFAA) was added to a solution of the tetrahydroquinoline **192** and TEA in Et_2O at 0 °C and stirred overnight. The protected amine **193** was refluxed in chlorosulfonic acid for 2 hours to yield the *para*-substituted sulfonyl chloride **194**. Although the major product obtained was the *para*-substituted compound, the yield of the reaction was somewhat variable (50 to 69%), due to the formation of other regioisomers. The sulfonyl chloride intermediate **194** was treated with different amines and TEA in DCM to provide the

diverse analogs (Scheme 3.1). The reaction time of the sulfonamide-coupling step had to be carefully optimized and monitored since the TFA protecting group would fall off if exposed to a primary amine for too long. The sulfonamide **195** was deprotected in the last step upon treatment with K_2CO_3 in a mixture of MeOH/H_2O (Scheme 3.1).

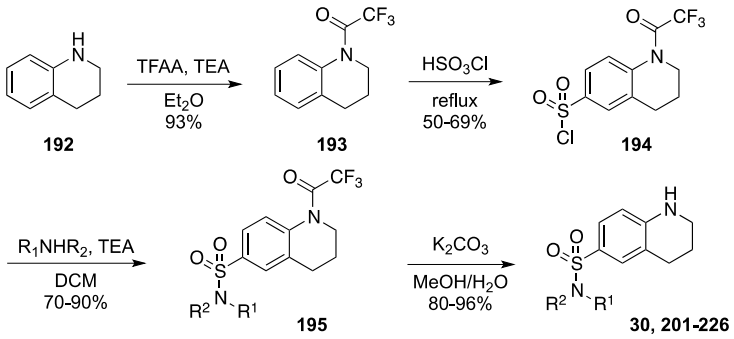

Scheme 3.1: Synthesis of sulfonamide **30** and analogs **200-226.**
See Figures 3.9 and 3.10 for definition of R groups.

First, an attempt was made to simplify the *trans*-decahydroquinoline ring, which was substituted with various linear amines of increasing sizes (Figure 3.7). The resulting analogs were tested in the miR-122 luciferase assay (10 μM for 48 h) by Colleen Connelly, and their activities were compared to **30**. A correlation was observed between the number of carbons in the amine chains and the activity. Indeed, the simplest free amine derivative **196** exhibited a 71% decrease in activity compared to **30**, while extending the size of the linker by one (**197**) or three (**198**) additional carbons progressively restored some activity. This trend was observed in analogs bearing a chain of up to 4 carbons, the best one, **199**, displayed a similar potency as the parent compound **30**. The opposite trend was observed when the size of the linear amine was being further extended; substitution with hexylamine (**200**), octylamine (**201**), decanamine (**202**), and dodecylamine (**203**) functionalities resulted in a progressive reduction in the activity (Figure 3.7). Since an amine chain of 4 carbons seemed to be optimal, the isobutyl (**204**) and the methylcyclopropyl (**205**) derivatives were designed to examine the importance of the linear alkyl

chain. Although the isobutyl group (**204**) was well tolerated since **204** was slightly more potent than **30**, introduction of a cyclopropane (**205**) decreased the activity by 26% (Figure 3.7). Compounds **206** and **207** were designed with short 3-carbon linkers and functionalities allowing for further derivatization. For example, **207** was used in a "click reaction" with 1-azidopropanol to give the triazole **208**. Modification with an allyl (**206**), a propargyl (**207**), or a triazole (**208**) motif resulted in a 31%, 28%, and 63% reduction in the activity relative to **30**, respectively. Since the parent compound **30** is substituted with a tertiary amine, tertiary amine analogs of **199**, **204**, and **207** were synthesized. Introduction of a methyl (**210** and **211**) or a second propargyl group (**209**) led to significant losses in activity. Surprisingly, the addition of a second butylamine group (**212**) led to a slight improvement over the monoalkylated analog **201**, and yielded a 10% increase in activity compared to **30** (Figure 3.7). Simplification of the *trans*-decahydroquinoline with the smallest piperidine ring (**213**) abolished the activity. Based on the promising data for **212**, the macrocycles **214** and **215** were synthesized to determine if a rigidified cyclic structure would be beneficial. Introduction of a 7-member ring (**214**) or an 8-member ring (**215**) was not tolerated as the activity drastically dropped to 37% and 58%, respectively.

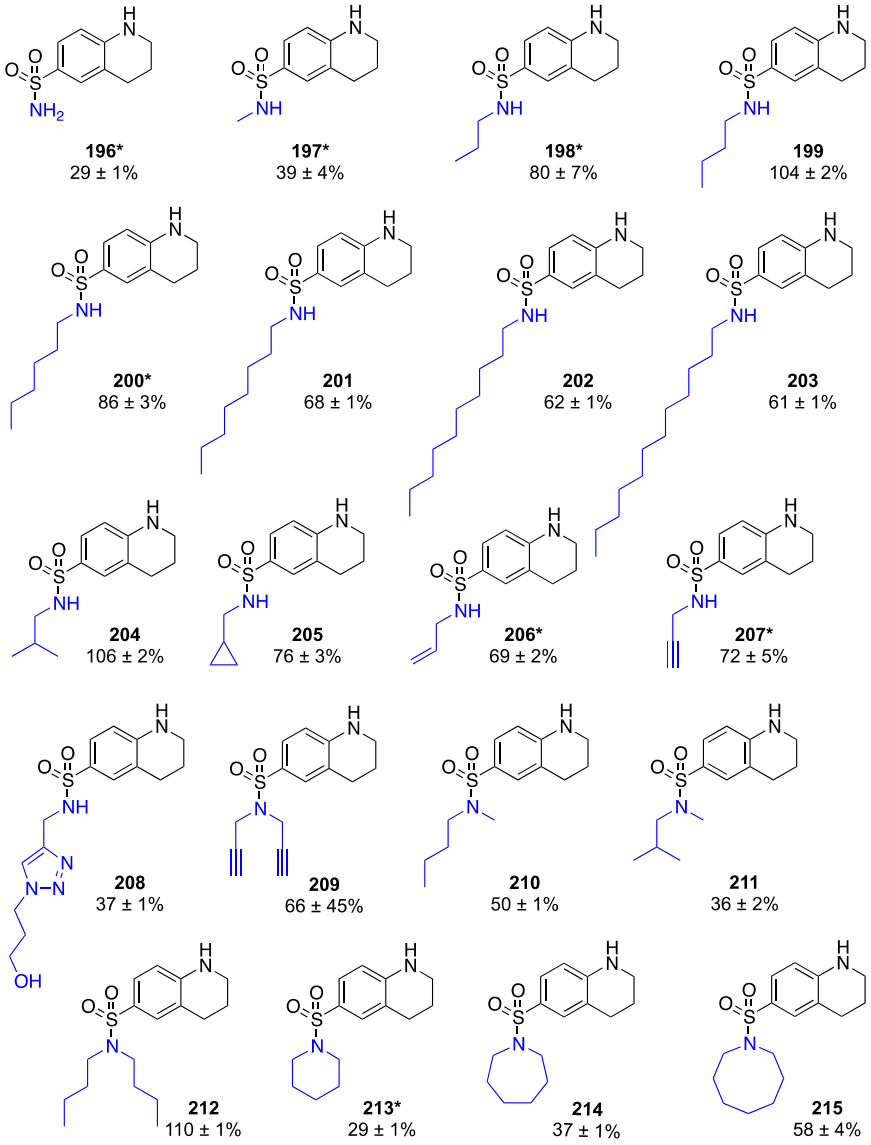

Figure 3.7: SAR investigation of the miR-122 inhibitor **30** through modification of the trans-decahydroquinoline ring (variations to the original structure are shown in blue).
The numbers represent the activity (in percent) relative to **30** within the same miR-122 luciferase assay. Experiments were performed in triplicate and the standard deviations of the three independent assays were calculated. Syntheses of labeled analogs (*)[98] and cell-based assays were performed by Colleen Connelly.

The *trans*-decahydroquinoline ring was then replaced with a tetrahydroquinoline ring (**216**) to examine the effect on the activity upon the introduction of a planar unsaturated group, which resulted in a reduction of activity to 49% (relative to **30**). Modification with a benzylamine (**217**), a 4-methylpyridine (**218**), or a benzothiazol-2-amine (**220**) moiety similarly reduced the activity. Surprisingly, introduction of a methoxy group on the benzothiazole ring

(**221**) rescued some activity, and substitution with a methyl-tetrahydropyran (**219**) led to slightly enhanced potency compared to **30** (Figure 3.8).

The derivatives **222-225** were designed to introduce a nucleophilic handle in the small molecule that could be further used for other applications such as pull-down assays (Figure 2.24).[222] Modifications with a hydroxyl (**222-224**) or an amino (**225**) functionality resulted in >60% reductions in activity compared to **30** (Figure 3.8). Treatment of the sulfonyl chloride **194** with 3 equivalents of hexane-1,6-diamine (Scheme 3.1) delivered the inactive dimer **226** as the major product. The expected product **225**, was obtained using a large excess of the amine and keeping the reaction mixture at 0 °C. Unlike the other analogs in this series (Figure 3.8), the alcohol derivative **224** was obtained after treatment of **194** with 6-aminohexanol and pyridine.[223]

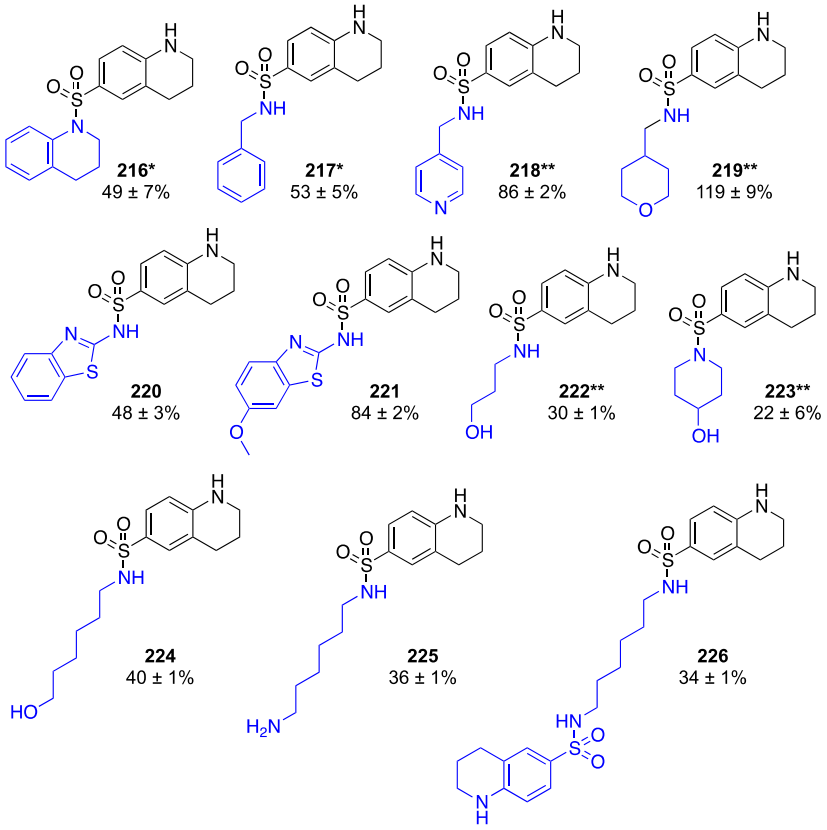

Figure 3.8: Structure-activity relationship investigation of the miR-122 inhibitor 30 through modification of the trans-decahydroquinoline ring (variations to the original structure are shown in blue).
The numbers represent the activity (in percent) relative to **30** within the same miR-122 luciferase assay. Experiments were performed in triplicate and the standard deviations of the three independent assays were calculated. Syntheses of labeled analogs (*) and cell-based assays were performed by Colleen Connelly,[98] the labeled analogs (**) were synthesized by Rohan Kumbhare.

After structural modifications of the miR-122 inhibitor **30** through substitutions with linear and aliphatic amine functionalities, aromatic rings were introduced (Figure 3.9). Treatment of **194** with TEA and diverse anilines as described in Scheme 3.1 only gave low product yields; new conditions had to be implemented in order to synthesize the aromatic analogs **229**-**237** in satisfactory yields. Instead, the sulfonyl chloride **194** was heated to reflux overnight in presence of the aniline derivatives and pyridine. The intermediate **227** was then deprotected with K_2CO_3 to afford the aromatic analogs **229**-**237** in high yields (Scheme 3.2).

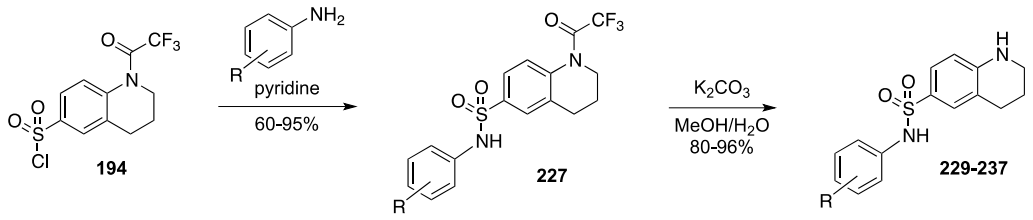

Scheme 3.2: Synthesis of sulfonamide analogs **230**-**238.**
See Figure 3.8 for definition of R groups.

Replacement of the *trans*-decahydroquinoline with a benzene ring (**228**) did not affect the activity. Substitution with a 3-naphtalene motif (**229**) to resemble the configuration of parent compound **30**, reduced the activity by 22%, whereas substitution with a 2-napthalene motif (**230**) yielded a 46% increase in activity over **30**. Introduction of the bulkier anthraquinone motif was well tolerated, as **231** was 9% more potent than **30**, however this analog suffered from poor solubility. Modification with a 3-pyridine motif (**232**) resulted in ~50% loss in activity, as did substitution of the two *meta* positions with methoxy groups (**233**). Likewise, introduction of a nitro (**234**) or an amino (**235**) group in the *para* position negatively affected the activity. However, *para* modifications with the bulky *tert*-butyl group (**236**) or with an acetyl group (**237**) recovered the activity. The acetyl derivative **237** displayed a 10% increase in activity compared to **30** (Figure 3.9). These results (Figure 3.7, Figure 3.8, and Figure 3.9) suggested that either a short (<4 carbons) linear amine or a bulky aniline functionality is optimal for miR-122 inhibition.

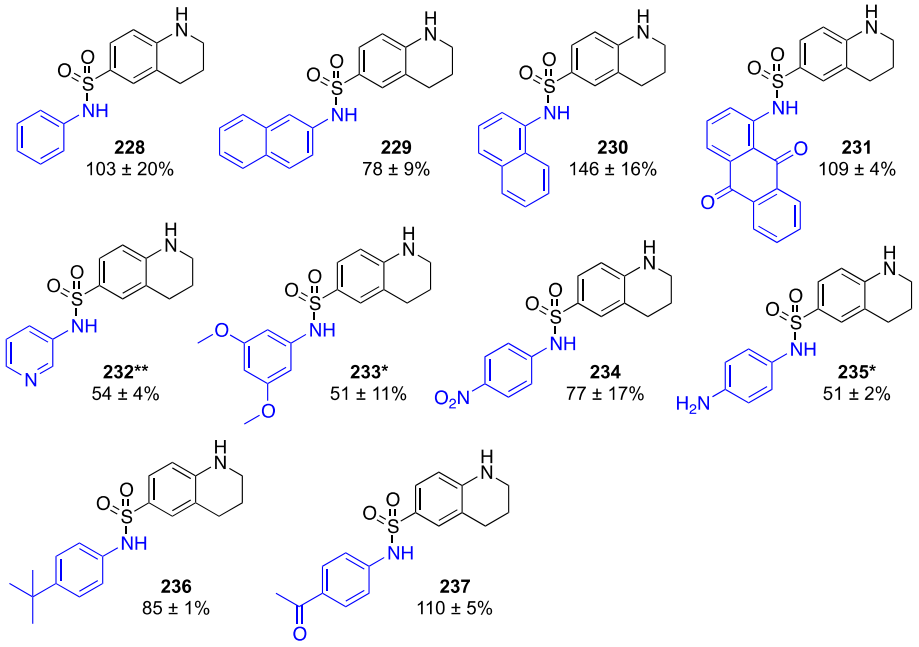

Figure 3.9: Structure-activity relationship investigation of the miR-122 inhibitor **30** through modification of the trans-decahydroquinoline ring (variations to the original structure are shown in blue).
The numbers represent the activity (in percent) relative to 30 within the same miR-122 luciferase assay. Experiments were performed in triplicate and the standard deviations of the three independent assays were calculated. Syntheses of analogs labeled with an asterisk (*) and cell-based assays were performed by Colleen Connelly.[98] Analogs labeled by a double-asterisk (**) were synthesized by Rohan Kumbhare.

3.3.2 SAR Studies of Inhibitor 30 through Modifications of the Sulfonamide Linkage

In order to determine whether the sulfonamide linkage is necessary for the miR-122 inhibitory activity, it was replaced with a carboxamide group (Scheme 3.3). The amide **240** was synthesized in two steps (Scheme 3.3). The carboxylic acid **238** was stirred with *trans*-decahydroquinoline in the presence of TEA and the peptide coupling reagents HOBt and EDCI in DCM to deliver the amide precursor **239**. Reduction of the pyridine ring was performed with palladium on carbon (Pd/C) and ammonium formate in refluxing MeOH, and afforded **240** in 55% yield (Scheme 3.3).[224] Other conditions using platinum oxide and hydrogen in TFA were

tested but failed to deliver the expected product **240**.[225] Both amide derivatives **239** and **240** were completely inactive in the miR-122 luciferase assay (Scheme 3.3), validating the importance of the sulfonamide motif to maintain miR-122 activity.

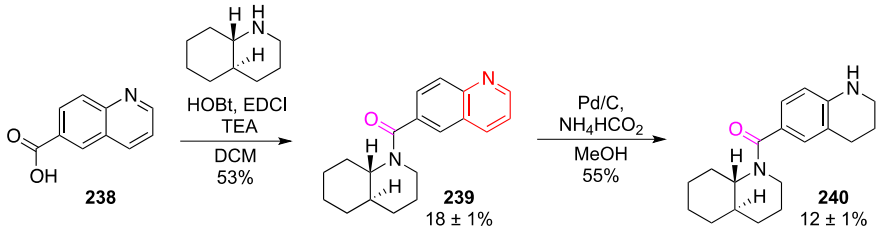

Scheme 3.3: Synthesis of the amide analog of **30.**
The numbers represent the activity (in percent) relative to **30** within the same miR-122 luciferase assay. Experiments were performed in triplicate and the standard deviations of the three independent assays were calculated. The cell-based assays were performed by Colleen Connelly.

3.3.3 SAR Studies of Inhibitor 30 through Modifications of the Tetrahydroquinoline

Lastly, structural modifications around the tetrahydroquinoline ring were investigated (Figure 3.10). To determine whether the cyclic structure of the tetrahydroquinoline motif is necessary to maintain miR-122 inhibition, the free aniline **244** was synthesized and further tested in the miR-122 luciferase assay. The synthesis started with the protection of the aniline with a phthalic protecting group under microwave conditions (Scheme 3.4).[226] The intermediate **241** was refluxed in chlorosulfonic acid for 2 hours to yield the *para* sulfonyl chloride **242**, which was subsequently treated with *trans*-decahydroquinoline to give compound **243** in 63% yield. The final compound **244** was obtained in 69% yield after removal of the protecting group with hydrazine (Scheme 3.4).[227] Both the protected and deprotected analogs **243** and **244** were tested

in the miR-122 luciferase assay and were totally inactive (Figure 3.10). The same results were observed for the aniline **245**, which was synthesized as described in Scheme 3.4.

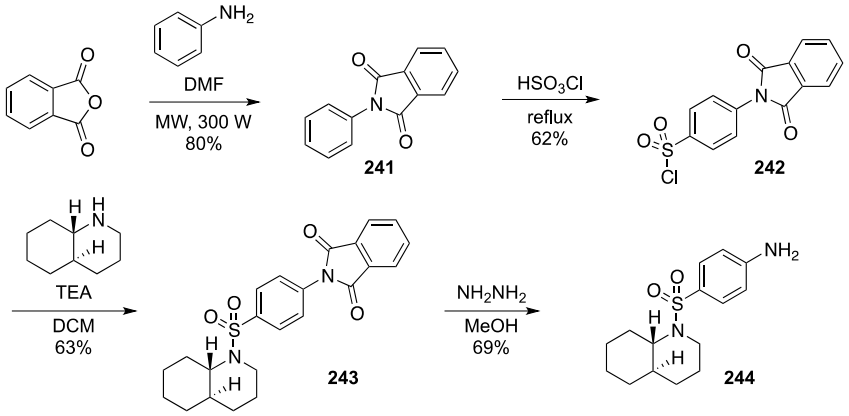

Scheme 3.4: Synthesis of aniline derivative **244.**

Substitution with a smaller 5-member ring was also envisioned, and analog **246** was synthesized according to the procedure previously discussed (Scheme 3.3) starting from the commercially available indoline. Compound **246** displayed an activity equivalent to **30** demonstrating that a smaller but more strained ring can be well accommodated in the binding pocket of the putative target protein. Modifications with a hydroxylamine (**247**) or a sulfonamide (**248**) motif led to reductions in the activity. The methylated analog **249** was designed to assess the importance of having a hydrogen-bond donor functionality on the tetrahydroquinoline ring (Figure 3.10). An initial attempt was made to methylate the amine on the tetrahydroquinoline ring with acetic acid, formaldehyde (37%), and zinc but the product was not recovered. Instead, **249** was obtained by reductive amination of **30** upon treatment with formaldehyde (37%) and sodium cyanoborohydrate in MeOH (Scheme 3.5).[228] Introduction of a small methyl group (**249**) led to an 11% increase in activity over the parent compound **30** (Figure 3.10). Analogs **250**, **251**, **252**, and **253** were then synthesized to determine whether introducing additional hydrophobic

interactions by extending the aliphatic group on the tetrahydroquinoline would be beneficial for the activity (Figure 3.10). The sulfonamide **30** was alkylated with an allyl (**250**), a propargyl (**251**), and a butyl group (**252**) at elevated temperature in the presence of the corresponding alkylbromide and DIPEA (Scheme 3.5).[229] The benzyl derivative **253** was obtained after treatment of **30** with benzyl chloride and K_2CO_3 in refluxing DMF.[229] Extending the aliphatic linker by three additional carbons did not further increase the activity but was well tolerated, as **250** and **251** displayed a similar activity as **30** in the miR-122 luciferase assay. However, substitutions with a longer butyl (**252**) and bulkier benzyl (**253**) groups led to increasing reductions in the activity (Figure 3.10). Given the conditions used to perform the alkylation of the secondary amine delivered low yields, another route was envisioned to conveniently access diverse propargylated analogs (Scheme 3.5). This was deemed advantageous since the propargyl group would be installed on the tetrahydroquinoline ring at an earlier stage of the synthesis, thus bypassing the need for any protecting group and shortening the synthesis by two steps (Scheme 3.5). Although, **260** was obtained in 87% yield after treating **192** with propargyl bromide and DIPEA, efforts to introduce the sulfonyl chloride functionality were all unsuccessful. The propargylated intermediate **260** was treated with varying equivalents of chlorosulfonic acid, at different temperatures, and in different co-solvents but none of these conditions delivered the desired product **261**. Instead, it seemed that due to the presence of the activating propargyl amine on the ring (compared to the trifluoroacetyl protecting group commonly used), a mixture of *ortho* and *para* substituted products was formed and the desired *para*-substituted sulfonyl chloride **261** could not be isolated.[230] Other conditions consisting of installing the sulfonic acid on the ring first and then adding the chloride group upon treatment with phosphorus chloride similarly failed to deliver **261**.

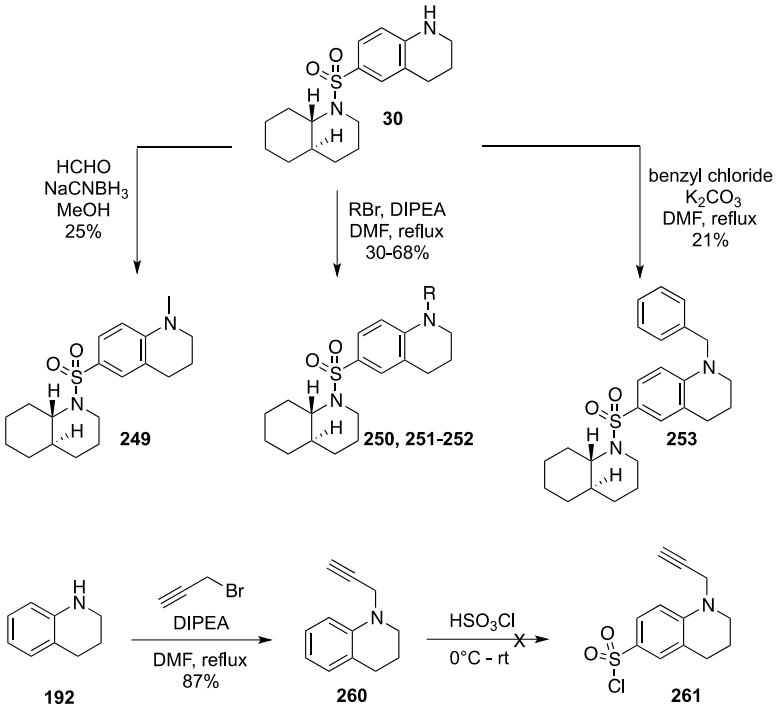

Scheme 3.5: Conditions used and attempted to synthesize the alkylated analogs **249-253.**
The R groups are shown in Figure 3.10.

The derivatives **254-256** were designed with functional groups susceptible to form a covalent bond upon reaction with a nucleophilic residue (i.e., cysteine) within a putative binding pocket. Not surprisingly, the chlorine (**254**) and alkene (**255**) analogs were highly toxic and no assay data could be generated for these compounds. The compound **256** was less toxic but did not show any activity in the miR-122 luciferase assay (Figure 3.10).

The analog **257** was synthesized to investigate if a structure different from the fused tetrahydroquinoline ring could be tolerated. The commercially available iodobenzene was treated with chlorosulfonic acid to give a mixture of the *ortho* and *para* substituted sulfonyl chloride **262**. This mixture was stirred in the presence of *trans*-decahydroquinoline and TEA in DCM to deliver **263**. Although the intermediate **263** was obtained as a mixture of *ortho*- and *para*-sulfonamide analogs, it was still submitted to the copper catalyzed coupling reaction.

Gratifyingly, after irradiation of **263** under microwave conditions at 130 °C for 10 minutes in the presence of pyrrole, copper acetate, and diazabicycloundecene (DBU) in DMF the desired *para*-substituted derivative **257** was obtained (Scheme 3.6).[231] The synthesis of **257** was generally low yielding but since this compound did not show any miR-122 inhibition (Figure 3.10), no further optimization was performed.

The amide **258** was designed to investigate whether installing either a less basic functionality or a hydrogen bond acceptor onto the ring would be beneficial for activity. The analog **258** was synthesized using the conditions depicted in Scheme 3.1, starting from the commercially available dihydroquinolinone. Since the basicity of the cyclic amine was lowered by the presence of the carbonyl group on the ring, **258** could be obtained in 2 steps without the need for any protecting group. Dihydroquinolinone was refluxed in chlorosulfonic acid for 3 hours to give the sulfonyl chloride intermediate in 76% yield. This precursor was then stirred in pyridine at 40 °C in presence of *trans*-decahydroquinoline to give the analog **258**. Introduction of an amide motif (**258**) on the tetrahydroquinoline ring drastically reduced the activity (Figure 3.10).

Lastly, **259** was synthesized to test if a quinoline would be tolerated. Oxidation of the piperidine ring was first tested on the commercially available tetrahydroquinoline. First, tetrahydroquinoline was treated with potassium iodide and *tert*-butylhydroperoxide (70% in H_2O) in ACN but an inseparable mixture of the expected product and the partially oxidized compound was obtained.[232] Tetrahydroquinoline was also heated to reflux in dioxane in the presence of 2,3-dichloro-5,6-dicyanobenzoquinone (DDQ) to afford the expected product in 30% yield.[233] Some product was also obtained, in lower yield, under microwave irradiation (300 W) of the tetrahydroquinoline and DDQ in toluene. Since both of these reactions showed total and

clean conversion by TLC, it was hypothesized that the low yields were due to the loss of some material during the extraction phase as the obtained quinoline was somewhat soluble in the aqueous layer. Under the same conditions, **30** was oxidized with DDQ to deliver the analog **259** in 87% yield (Scheme 3.6). Oxidation of the tetrahydroquinoline ring led to a 58% loss in activity compared to the reference inhibitor **30** (Figure 3.10).

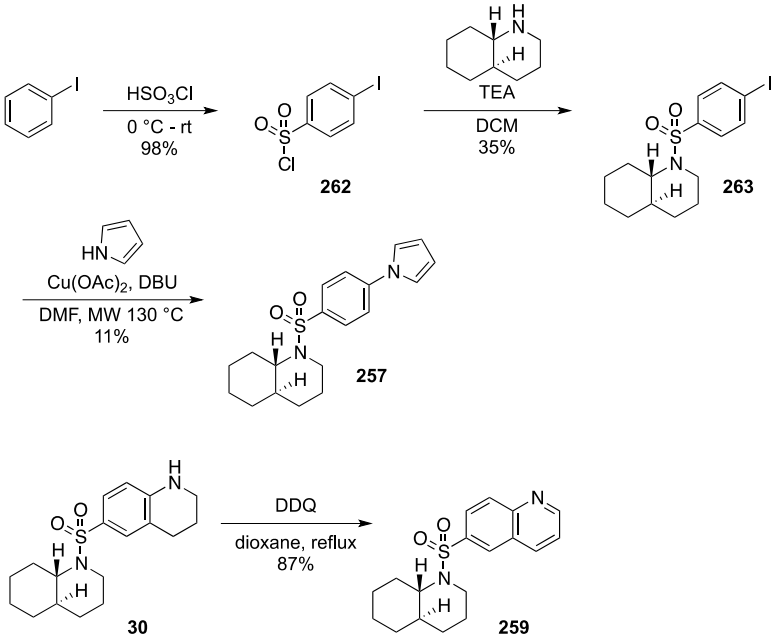

Scheme 3.6: Syntheses of pyrrole and quinoline analogs **257** and **259.**

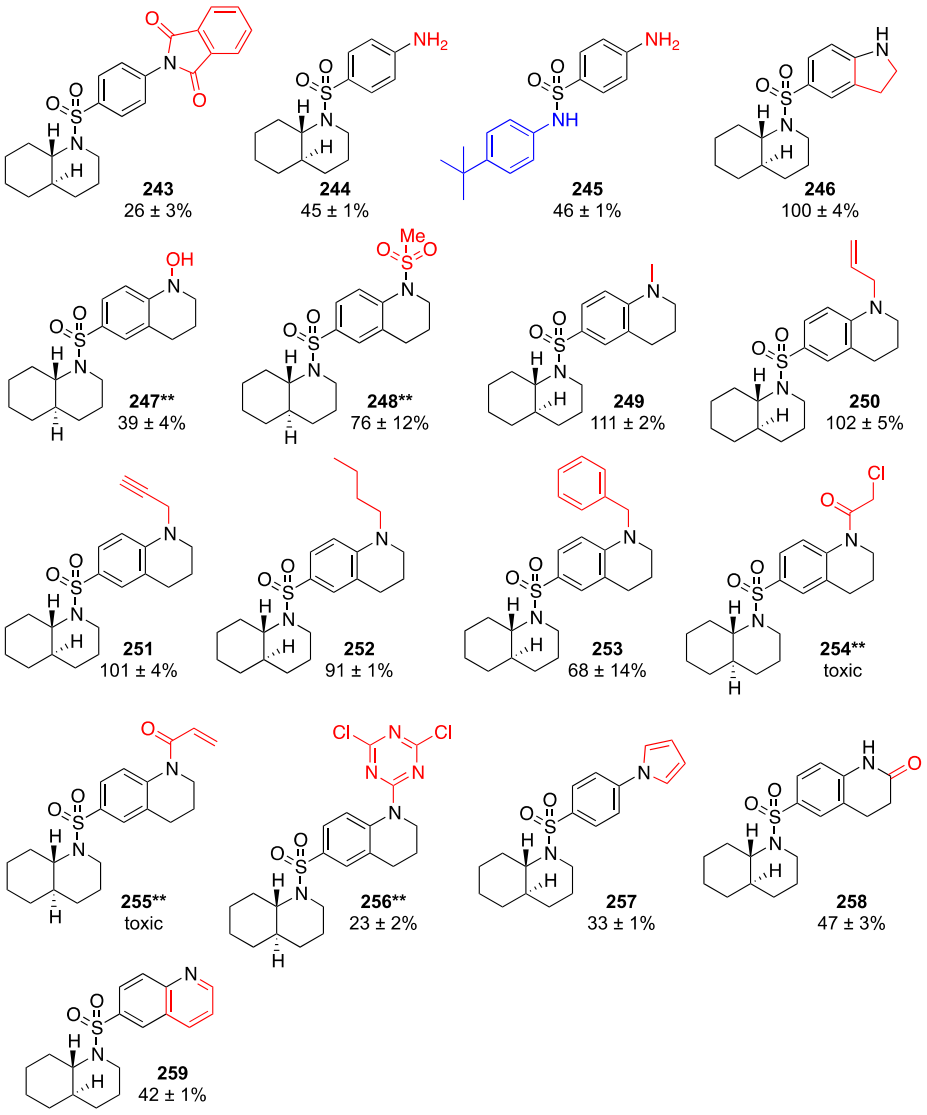

Figure 3.10: Structure-activity relationship studies of the miR-122 inhibitor **30** through modification of the tetrahydroquinoline motif (variations to the original structure are shown in red).
The numbers represent the activity (in percent) relative to **30** within the same miR-122 luciferase assay. Experiments were performed in triplicate and the standard deviations of three independent assays were calculated. The cell-based assays were performed by Colleen Connelly and the analogs labeled (**) were synthesized by Rohan Kumbhare.

Overall, only the introduction of a short aliphatic group (up to 3-carbons long) was tolerated and gave analogs of similar potency as **30**; every other modification of the tetrahydroquinoline motif resulted in a reduction of activity (Figure 3.8, Figure 3.9, and Figure 3.10).

3.4 HIGH-THROUGHPUT SCREENING FOR SMALL MOLECULE MIR-122 INHIBITORS

A cell line stably expressing the luciferase reporter for miR-122, Huh7-psiCHECK-miR122, was generated by Colleen Connelly in order to facilitate the high-throughput screening of a large number of small molecules.[124] Since the reporter is stably expressed there is no need for transfection, which greatly improves the reproducibility and robustness of the assay. After the stable cell line was validated, it was submitted to the Broad Institute's Probe Development Center (BIPDeC) for high-throughput screening of more than 300,000 small molecule miR-122 modifiers, followed by several secondary assays to determine the specificity and selectivity of the hit compounds (Figure 3.11). The BIPDeC screened 336,006 compounds from the Broad Institute's Diversity Oriented Synthesis (DOS) collection (71,424 compounds) and the NIH's Molecular Libraries Probe Production Center Network library (MLPCN, 264,582 compounds) in a primary assay using the Huh7-psiCHECK-miR122 cell line. The previously discovered miR-122 inhibitor **30** was used as a positive control throughout the assay. The cells were plated in 384-well plates, treated with the small molecules at 10 μM for 48 hours and the luminescence was measured with a *Renilla*-Glo reporter kit (Promega). Since the transfection is bypassed when using the stable cell line, it is not necessary to perform a Dual luciferase assay, so only the *Renilla* luciferase signal was recorded during the HTS.

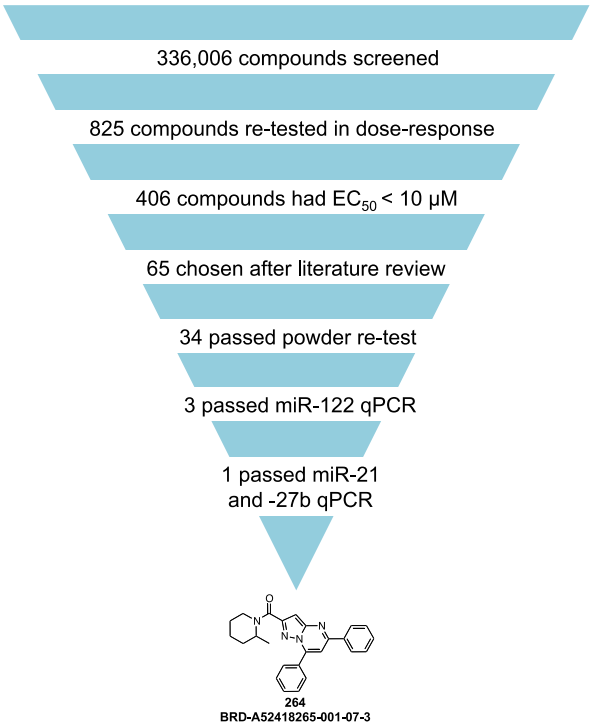

Figure 3.11: Screening flow chart indicating the number of compounds that successfully passed each round of screening, leading to the preliminary hit compound **264.**

Following the primary screen, small molecules displaying an activity greater or equal to 90% relative to the activity of **30** were considered as active and further investigated. From the 336,006 compounds tested in the primary screen, 1,023 compounds (179 compounds from the DOS collection and 844 from the MLPCN library) were identified as active inhibitors, constituting a hit rate of 0.3%. The primary screen was performed in duplicate for each compound to verify the reproducibility (Figure 3.12). Figure 3.12B shows all compounds aligned along the diagonal, indicating a good correlation between the results obtained in both assays.

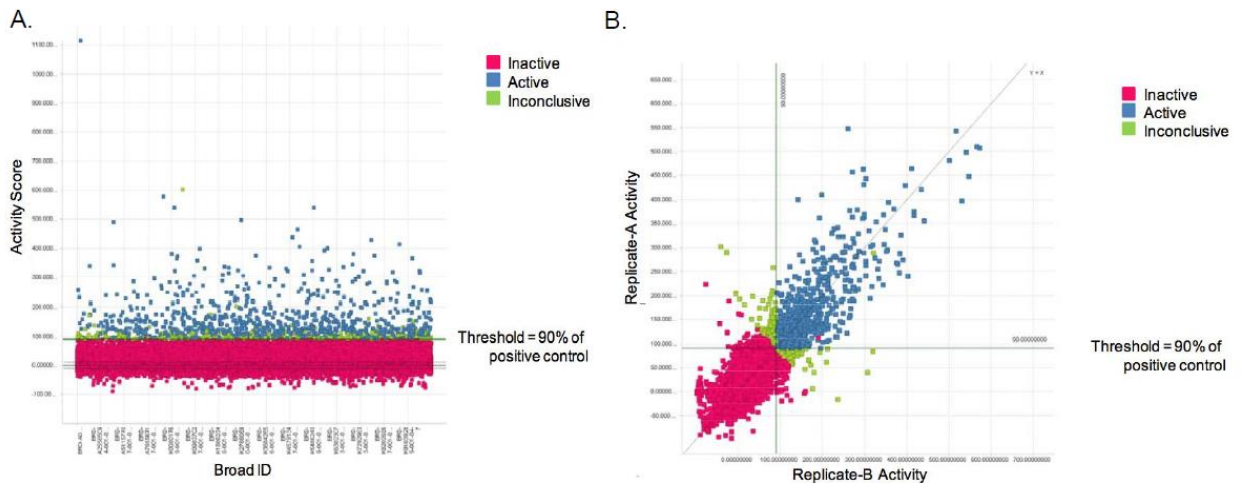

Figure 3.12: Results of the HTS performed in Huh7-psiCHECK-miR122 cells by the Broad Institute's Probe Development Center.
A. Activity data for all small molecules screened in the primary assay, where each point represents one compound. **B.** Activity comparison of two replicates (A and B) for each compound. Data was provided by Kate Hartland (BIPDeC).

Following the primary screen, BIPDeC analyzed the list of active compounds to eliminate any potential false-positives by: 1) removing any pan-assay interference compounds or "PAINs" which are known to be promiscuous in many biological assays;[234] and 2) discarding any compounds with chemically reactive groups, metabolically labile groups, pH sensitive or hydrolytically unstable groups, or other groups not amenable to SAR studies. The 825 remaining compounds were tested in an 8-point dose-response assay in the Huh7-psiCHECK-miR122 cell line, and 406 compounds were selected that displayed EC_{50} values of less than 10 μM. The specificity of these compounds was then investigated by cross-referencing the active compounds with the compounds tested in an HTS assay for miR-21 inhibitors (PubChem AID 2289). The derivatives found active in both the miR-122 and miR-21 assays were disregarded as they were not considered miR-122 specific, but more likely represent general inhibitors of the miRNA pathway.

Solid samples of the 65 compounds selected after the cross-analysis were obtained from the MLPCN and re-tested in the Huh7-psiCHECK-miR122 assay. Only 34 compounds displayed the expected activity and were tested in dose-response in Huh7 cells by qRT-PCR to measure their effect on the miR-122 expression levels. Three compounds induced a significant reduction in miR-122 expression and were subsequently examined in their selectivity based on the expression levels of miR-21 and miR-27b in Huh7 cells treated with the 3 derivatives. After this series of secondary assays, compound **264** was identified as an active hit: **264** has an EC_{50} value of 832 nM and selectively reduced miR-122 expression by 1.5-fold (Figure 3.11).

3.4.1 Investigation of Hit Compounds Identified in the Primary Screen

The four most active compounds in the primary assay were re-synthesized and tested in the miR-122 luciferase assay at 10 μM (Figure 3.13) or in dose-response (Figure 3.14). Although **265** and **266** were 13% and 27% less potent than the reference inhibitor **30**, respectively at 10 μM, their EC_{50} values were equivalent (**265**) or improved (**266**) relative to **30** (EC_{50} value of 1 μM). The methyl ester **267** and the compound **268** showed an activity and EC_{50} comparable to **30**.

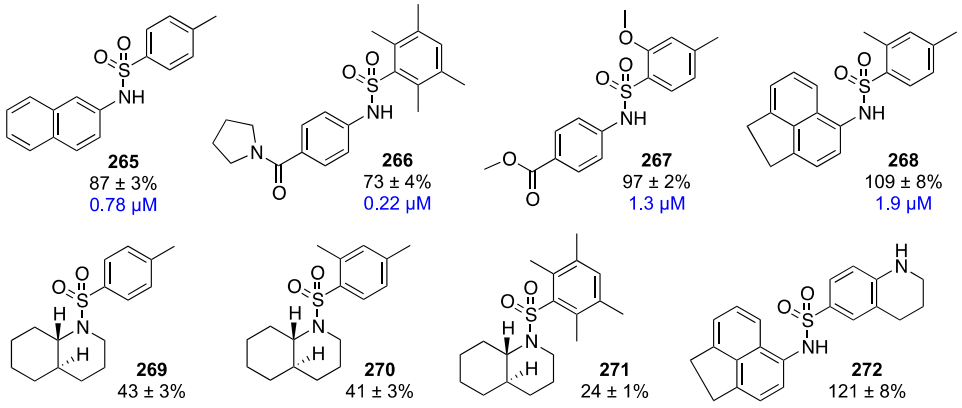

Figure 3.13: Structure of the best compounds identified in the primary assay and additional analogs.
The compounds were tested at 10 µM in Huh7-psiCHECK-miR122 cells. The numbers represent the activity (in percent) relative to **30** within the same assay. EC_{50} values are shown in blue. Experiments were performed in triplicate and the standard deviations of three independent assays were calculated.

A few analogs were also synthesized that combined structural motifs of both the reference inhibitor **30** and the newly identified hits (Figure 3.13). Combining the *trans*-decahydroquinoline motif of **30** with the benzene rings of **265**, **266**, and **268** led to the inactive analogs **269**, **270**, and **271**. Substituting the dimethylbenzene motif of **268** with the tetrahydroquinoline motif of **30** led to a 12% increase in activity (**272**).

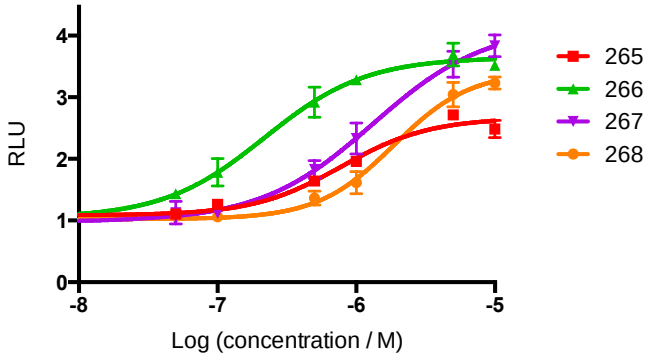

Figure 3.14: Dose-response curves in Huh7-psiCHECK-miR122 cells treated with the best compounds identified in the primary assay in the HTS.
All experiments were conducted in triplicate and normalized to a DMSO control. The error bars represent the standard deviation from three independent experiments.

The hit compound **265** was synthesized as described in Scheme 3.2, whereas the compound **266** was obtained in 3 steps (Scheme 3.7). 4-Nitrobenzoyl chloride (**61**) was treated with TEA and pyrrolidine in DCM to deliver **273** in 86% yield. The intermediate **273** was reduced to the corresponding amine **274** and subsequently heated to reflux with 2,3,5,6-tetramethylbenzene-1-sulfonyl chloride to afford **266**. 4-Aminobenzoic acid was heated to reflux in the presence of $SOCl_2$ in MeOH to yield the corresponding methyl ester and was further refluxed in pyridine with 2-methoxy-4-methylbenzene-1-sulfonyl chloride to deliver **267**. The derivative **268** was synthesized in 4 steps: 1,2-dihydroacenaphthylene was treated with acetic acid and nitric acid to give the nitro **275**, which was reduced with H_2 in the presence of palladium on carbon. 2,4-Dimethylbenzene-1-sulfonyl chloride was obtained using chlorosulfonic acid as described in Scheme 3.1 and added to a solution of the amine **276** in pyridine (Scheme 3.7). The analogs **269**-**271** were prepared according to the conditions depicted in the Scheme 3.1, and **272** was obtained following the route shown in Scheme 3.2.

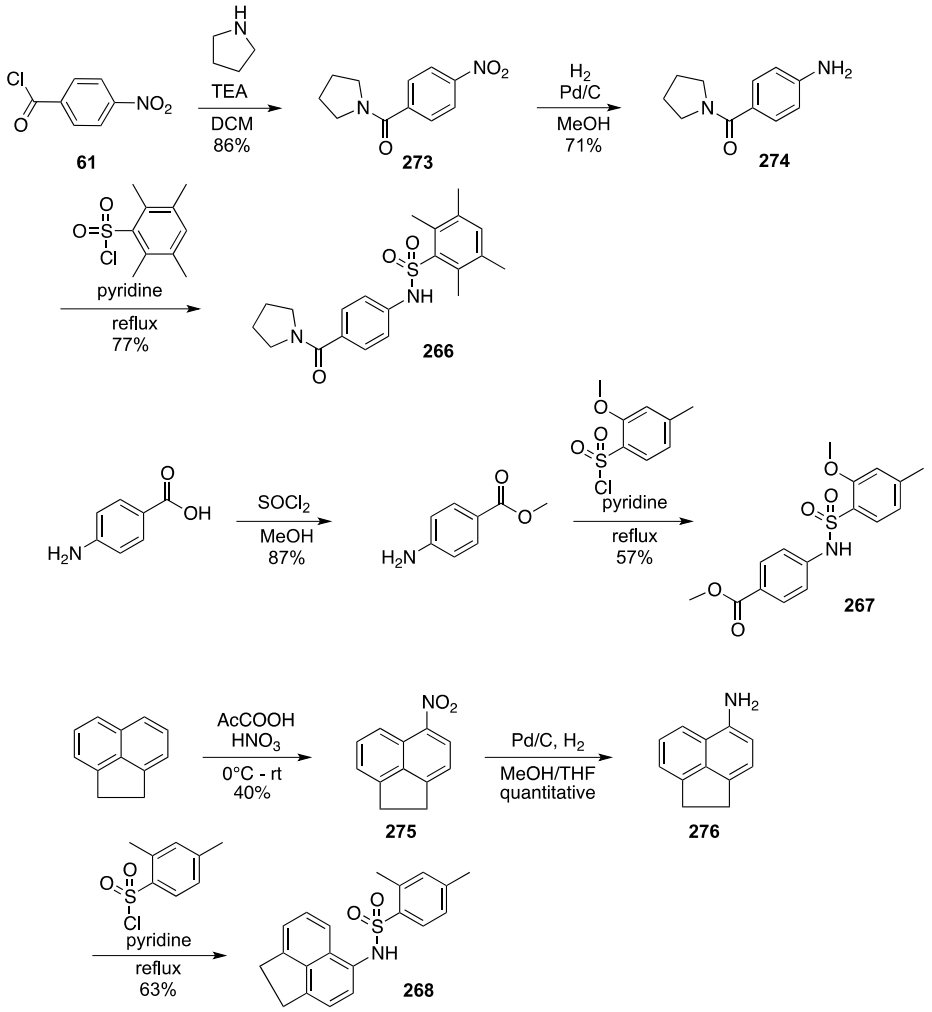

Scheme 3.7: Re-synthesis of best compounds identified in the primary assay of the HTS.

It was recently reported that similarly to the firefly luciferase, the *Renilla* luciferase is susceptible to undergo ligand-based stabilization by small molecule inhibitors leading to the accumulation of the protein in cell-based assays, and possibly creating false-positive hits in high-throughput screens.[235] Conversely, biochemical evaluation of these same inhibitors causes a significant decrease in luciferase signal. In addition, it was indicated that sulfonamide derivatives may be prone to stabilizing the *Renilla* luciferase, as was demonstrated with the compound **277**.[235] The sulfonamide **277** was synthesized in one step (Scheme 3.8) to provide a positive control in follow-up studies aimed to determine the effect of the promising compounds identified

in the HTS on *Renilla* luciferase. The derivative **277** was tested in Huh7-psiCHECK-miR122 cells at 10 μM and in dose-response, where it exhibited a 23% increased activity over **30** but an equivalent EC_{50} value (Scheme 3.8). Both **30** and **277** were further tested in dose-response experiments in an *in vitro Renilla* luciferase (RLuc) assay (Figure 3.15); **277** displayed similar EC_{50} values in both the *in vitro* assay (4.7 μM) and the miR-122 luciferase assay, while **30** showed a significantly higher EC_{50} value in the RLuc assay (21.8 μM) than in Huh7-psiCHECK-miR122 cells. These results validate previous reports that *Renilla* inhibitors might deliver false-positive hits in the HTS, as these compounds also induce an increase in *Renilla* luminescence. Given that **277** significantly increased the *Renilla* luciferase signal in the miR-122 luciferase assay, this highlights the necessity to investigate the promising compounds in the Huh7-psiCHECK-miR122 assay to validate that their activity is actually due to miR-122 inhibition and not *Renilla* luciferase stabilization.

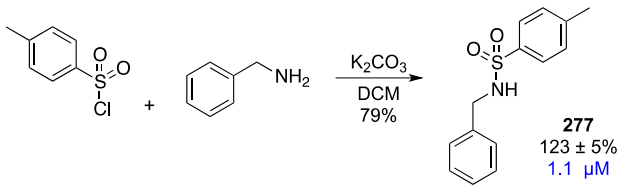

Scheme 3.8: Synthesis of the reported Renilla luciferase inhibitor **277.**
The numbers represent activity relative to **30** within the same miR-122 luciferase assay. EC_{50} value is shown in blue.

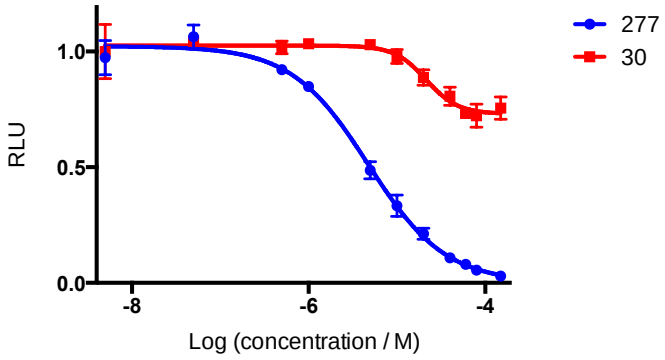

Figure 3.15: Dose-response curves for the sulfonamides **30** and **277** in the *in vitro* RLuc assay.
All experiments were conducted in triplicate and normalized to a DMSO control. The error bars represent the standard deviation from three independent experiments.

Except for compound **268**, none of these analogs, that displayed the highest activities in the primary screen, were identified as a hit compound. This suggested that these derivatives did not exhibit sufficient selectivity and specificity for miR-122 inhibition, and thus were not further pursued.

3.4.2 Preliminary SAR studies of the Hit Compounds 278-279 Identified in the HTS

After performing the HTS, the Broad Institute provided solid samples for the 34 compounds that passed their powder re-test in order to validate the results in our lab. Each compound was tested by Colleen Connelly in: 1) the Huh7-psiCHECK-miR122 assay to confirm miR-122 inhibition, 2) the psiCHECK-empty assay in Huh7 cells to assess the specificity, and 3) the HeLa-miR21-Luc assay to determine the selectivity for miR-122 inhibition. In these confirmatory experiments, the active compound **264** identified by the BIPDeC was found inactive, and instead the two sulfonamides **278** and **279** were identified as new hit compounds (Figure 3.16).

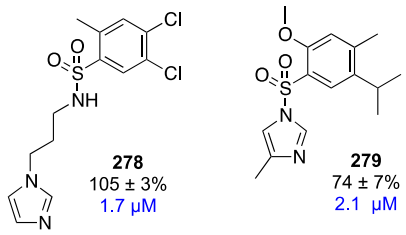

Figure 3.16: Structure of the best compounds identified in the HTS by Colleen Connelly.
The numbers represent the activity (in percent) relative to **30** within the same miR-122 luciferase assay. EC_{50} values are shown in blue. Experiments were performed in triplicate and the standard deviations of three independent assays were calculated. The analog **278** was re-synthesized by Haley Grimm.

These hit compounds were re-synthesized in collaboration with Haley Grimm (**278**) to allow for full characterization and further investigation. The hit **278** was prepared in 2 steps (Scheme 3.9). 1,2-Dichloro-4-methylbenzene was treated with chlorosulfonic acid to afford the sulfonyl chloride **280**, which was subsequently stirred in the presence of 1-(3-aminopropyl)imidazole and NaH to provide **278**. The derivative **279** was obtained in 3 steps (Scheme 3.9). 4-Isopropyl-3-methylphenol was converted to the corresponding methylether, which was heated to reflux in the presence of chlorosulfonic acid to deliver **281**. The sulfonyl chloride **281** was treated with 4-methylimidazole to afford **279** in 79% yield (Scheme 3.9). These two hit compounds were tested in the miR-122 luciferase assay at 10 μM (Figure 3.16) and in dose-response experiments (Figure 3.21 and Figure 3.25). They both displayed an EC_{50} value comparable to that of **30**, but at a concentration of 10 μM, **278** exhibited a similar activity to **30** while **279** was found 26% less potent. Subsequent examination of these compounds in the *in vitro* RLuc assay revealed that while **279** did not interact with the *Renilla* luciferase, **278** potently inhibited it.

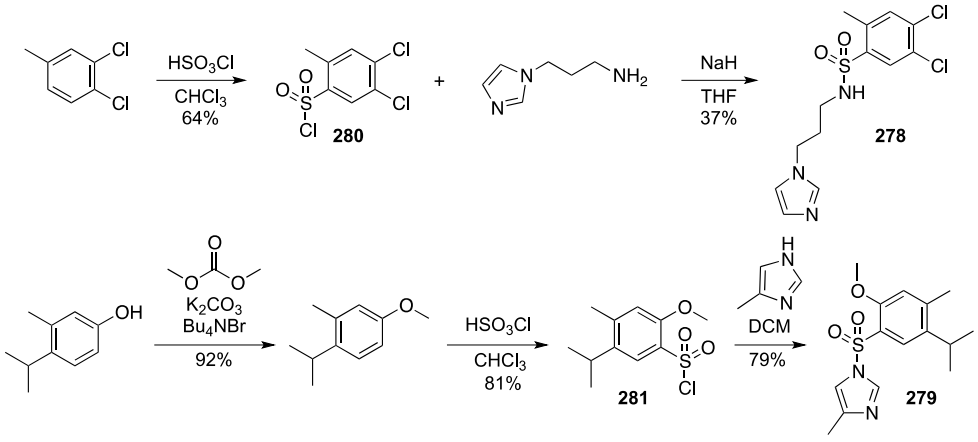

Scheme 3.9: Re-synthesis of the hit compounds **278** and **279** identified in the HTS.

Since the two hit compounds identified in the HTS belong to the sulfonamide-class, the Broad Institute provided a series of additional sulfonamide derivatives to start preliminary SAR

studies. The analogs **282**-**297** were tested in the miR-122 luciferase assay at 10 μM (Figure 3.17). Most of these 16 compounds were inactive and only 7 showed an activity 10 to 49% higher than **30**.

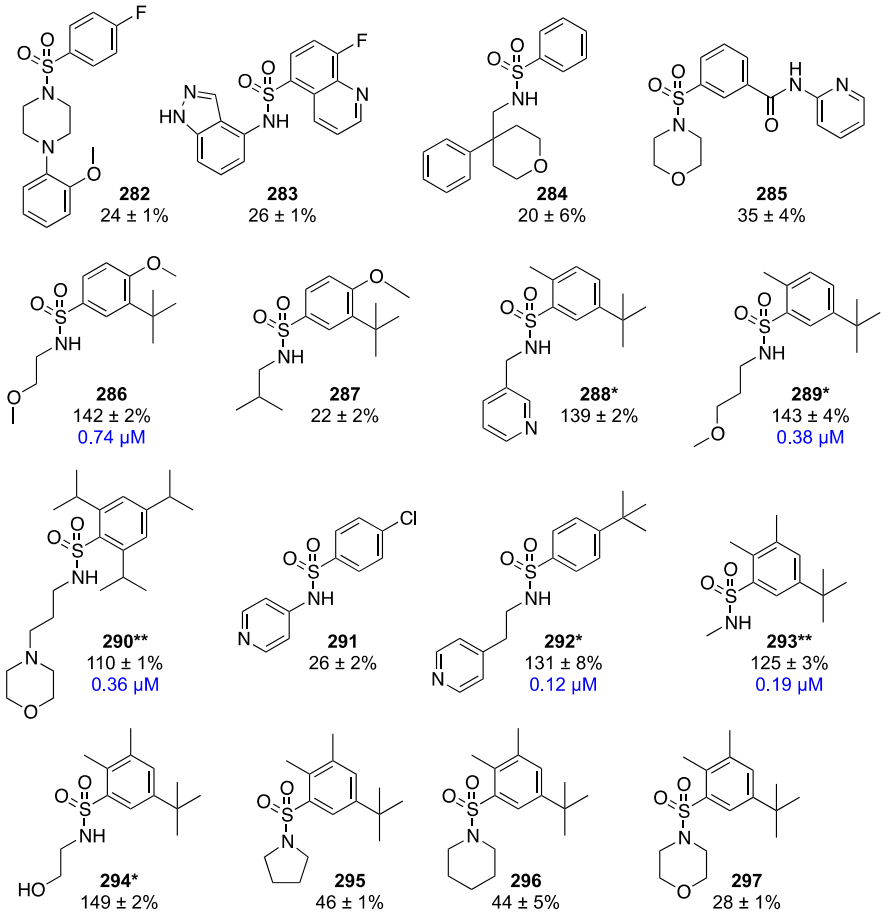

Figure 3.17: Structure of additional sulfonamides for preliminary SAR studies of the best compounds identified in the HTS.
The numbers represent the activity (in percent) relative to **30** within the same miR-122 luciferase assay. EC_{50} values are shown in blue. Experiments were performed in triplicate and the standard deviations of three independent assays were calculated. The best analogs, labeled with one or two asterixes (* or **), were re-synthesized by me or by Haley Grimm, respectively.

The derivatives **286**, **289**, **290**, **292**, and **293** were tested in dose-response in Huh7-psiCHECK-miR122 cells (Figure 3.18), and all displayed a satisfying EC_{50} value less than 1 μM.

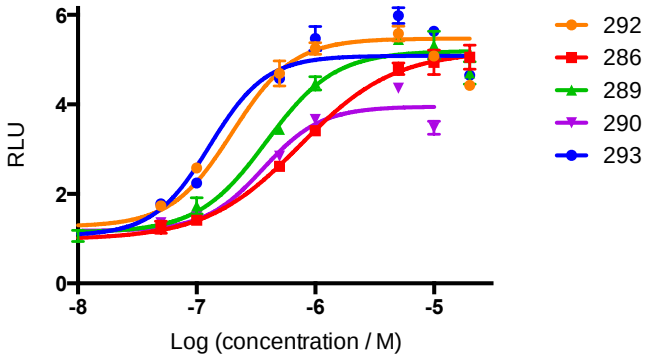

Figure 3.18: Dose-response curves in Huh7-psiCHECK-miR122 cells treated with the best sulfonamide analogs identified by the HTS after preliminary SAR.
All assays were conducted in triplicate and normalized to a DMSO control. The error bars represent the standard deviation from three independent experiments.

As previously mentioned, *Renilla* luciferase inhibitors are likely to create false-positive hits in the miR-122 luciferase assay.[235] Stabilization of the enzyme leads to the accumulation of the protein and therefore an increase in the *Renilla* luminescence signal at the time of readout. In order to determine the specificity for miR-122 inhibition, the best analogs were re-synthesized and submitted to secondary assays to evaluate their effect on *Renilla* luciferase (Figure 3.19). The most promising compounds **286**, **288**, **289**, **290**, **292**, **293**, and **294** were tested at 10 μM in either an *in vitro* RLuc assay (Figure 3.19A) or in Huh7 cells using the control reporter (Figure 3.19B). The previously reported *Renilla* luciferase inhibitor **277** was used as a positive control. In the RLuc assay, **277** induced an 80% decrease in the luminescence signal, and all compounds tested showed a greater or equal reduction in luminescence, indicating strong *Renilla* luciferase inhibition (Figure 3.19A). The analogs were also assayed in the control experiment in Huh7 cells transfected with the psiCHECK-empty reporter construct (Figure 3.19B). The compounds elicited a 3- to 8-fold increase in luminescence, suggesting that the high activity observed in the miR-122 luciferase assay might be due to a non-specific interaction of the compounds with the *Renilla* luciferase enzyme, rather than to their ability to inhibit miR-122.

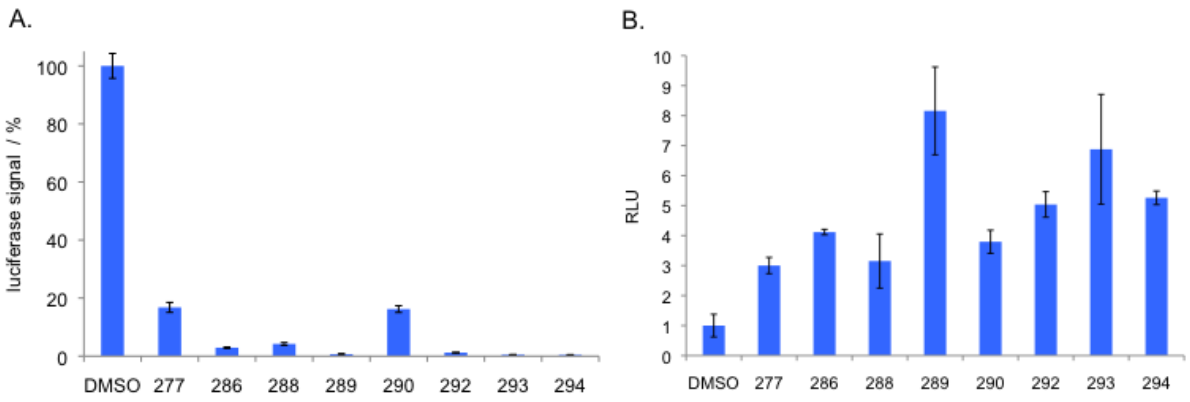

Figure 3.19: Secondary assays to determine the selectivity of the best sulfonamide analogs identified by the HTS after preliminary SAR.
A. *In vitro* RLuc assay, the compounds were tested at 10 μM. **B**. Dual Luciferase assay of Huh7 cells transfected with psiCHECK-empty and treated with the analogs at 10 μM for 48 h. The luciferase signal was normalized to a DMSO control. The error bars indicate the standard deviations determined from three independent measurements.

3.4.3 Validation of the Hit Compound 278 Identified in the HTS

Along with the previous set of sulfonamides (Figure 3.17), the Broad Institute provided analogs of the two hit compounds **278** and **279** for SAR investigation. Simplifying the 3-propanamine-imidazole motif with an ethyl (**299**) or propyl (**300**) group led to ~10% decreased activities (Figure 3.20) compared to the hit compound **278**. Replacing the 2 chlorine atoms with 2 methyl groups (**301**) restored the activity, but modification with a hydroxyethyl group (**302** and **303**) yielded a significant reduction in activity. Similarly, replacing the 3-propanamine-imidazole moiety with an isobutyl (**304**), a cyclopentyl (**305**), or a morpholine group (**306**) negatively affected the activity. Substitution of the 4,5-dichloro-2-methylbenzene-1-sulfonyl chloride (**278**) with the tetra-methylbenzene-sulfonyl chloride (**307**) or with the 3,5-dichloro-2-methylbenzene-1-sulfonyl chloride (**308**) slightly increased the activity. Conversely, replacement with the 4-fluoro-2-methylbenzene-1-sulfonyl chloride (**309**) induced a 70% decrease in activity compared

to **278**. Similarly, introduction of a benzimidazole motif (**310**) abolished the activity (Figure 3.20).

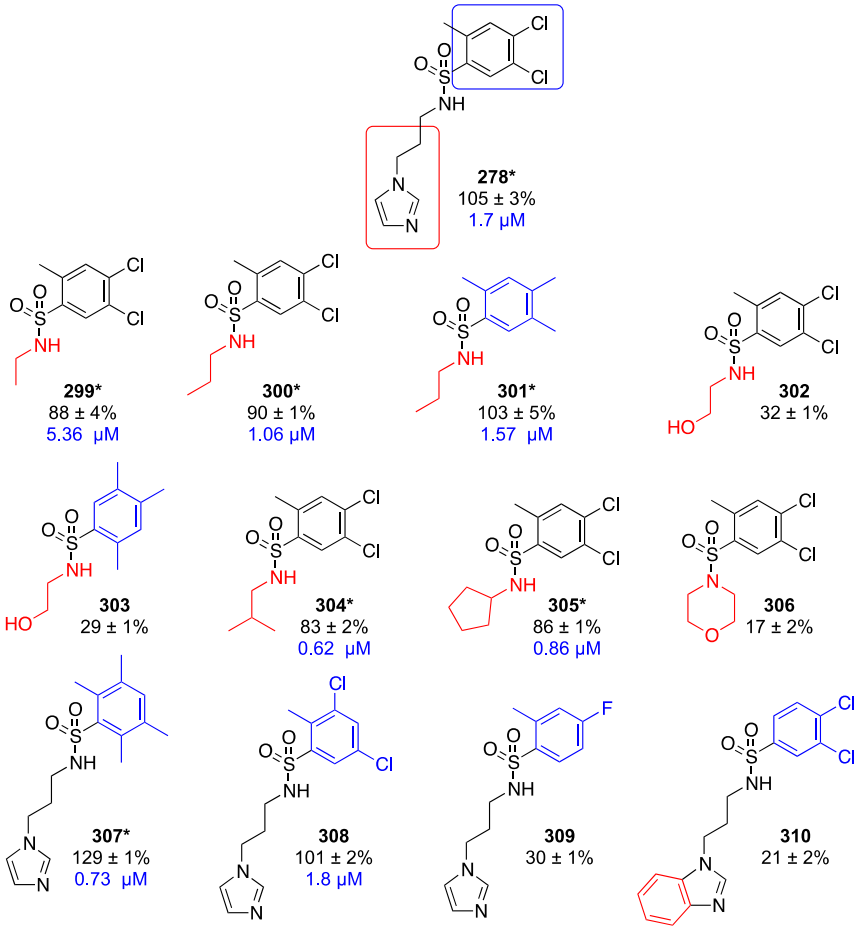

Figure 3.20: Structure-activity relationship studies of the hit compound **278** through modification of the ring substituents or the amine motif (variations to the original structure are shown in blue and red).
The numbers represent the activity (in percent) relative to **278** within the same miR-122 luciferase assay. EC_{50} values are shown in blue. Experiments were performed in triplicate and the standard deviations of three independent assays were calculated. The analogs labeled with an asterix (*) were re-synthesized by Haley Grimm.

The best analogs **299**, **300**, **301**, **304**, **305**, **307**, and **308** were tested in dose-response in Huh7-psiCHECK-miR122 cells (Figure 3.21). All the analogs displayed similar EC_{50} values to **278** (~1 µM), except **299**, which had an EC_{50} value of 5.4 µM.

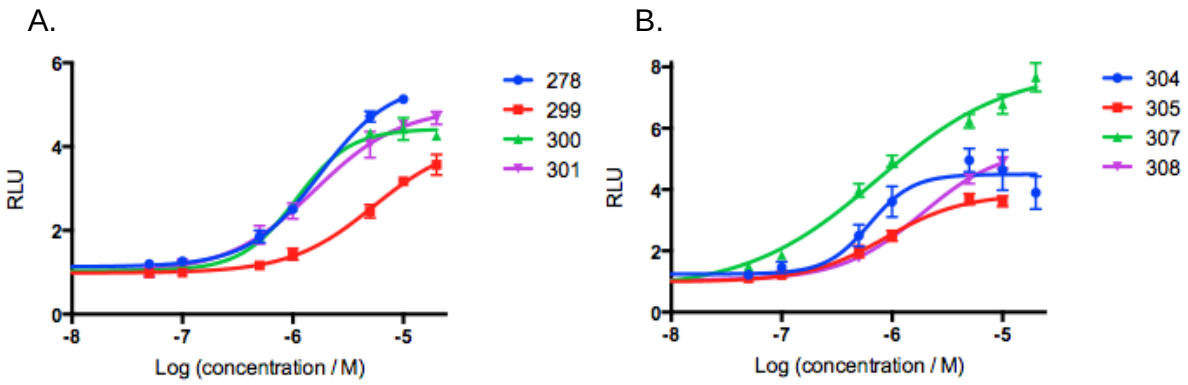

Figure 3.21: Dose response curves in Huh7-psiCHECK-miR122 cells treated with the best analogs of hit compound **278.**
A. Compounds **299**, **300**, **301**, and the hit compound **278**. **B**. Compounds **304**, **305**, **307**, and **308**. All assays were conducted in triplicate and normalized to a DMSO control. The error bars represent the standard deviation from three independent experiments.

The specificity of the best analogs was further investigated. Unfortunately, as Figure 3.22 shows, all of these compounds are potent *Renilla* luciferase inhibitors. They significantly reduced the *Renilla* luminescence (≥80%) in the *in vitro* RLuc assay (Figure 3.22A), and increased the signal by 3- to 8-fold in the control experiment using psiCHECK-empty (Figure 3.22B). These results suggest that the high activities of these analogs observed in the miR-122 luciferase assay, were mostly due to stabilization of the *Renilla* luciferase enzyme and not due to the perturbation of miR-122 expression. In fact, the compound **278** consisted in a false-positive hit in the HTS.

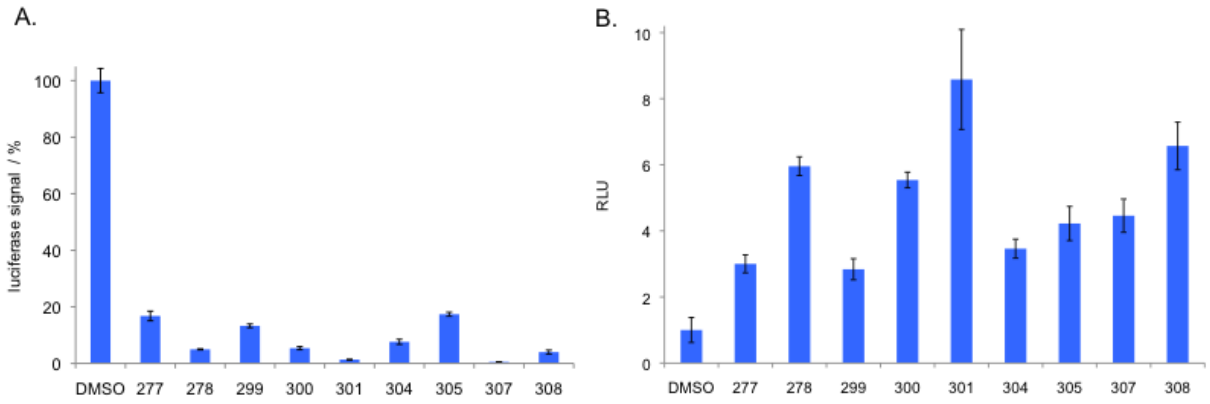

Figure 3.22: Secondary assays to determine the selectivity of the best analogs of hit **278** identified in the HTS. **A**. *In vitro* RLuc assay, the compounds were tested at 10 μM. **B.** Dual Luciferase assay of Huh7 cells were transfected with psiCHECK-empty and treated with the analogs at 10 μM for 48 h. The luciferase signal was normalized to a DMSO control. The error bars indicate the standard deviations determined from three independent measurements.

3.4.4 Validation of the Hit Compound 279 Identified in the HTS

Structural modifications were made on the hit compound **279** in an attempt to improve its potency. First, the 4-methylimidazole motif was simplified with a hydroxy (**311**), a dimethylamine (**312**), or an ethylamine group (**313**), all of which resulted in a significant loss in activity (Figure 3.23). Introduction of an ethanolamine motif (**314**) greatly increased the activity by 212%. Replacing the 4-methylimidazole ring on **279** with a 4-methylpyrazole (**315**), 4,5-dichloro-imidazole (**316**), imidazole (**317**), or pyrrole (**318**) motifs abolished the activity. Modification with a 4-methylpyrrole group (**319**) led to a 35% decrease in activity compared to **279**, highlighting the importance of the 4-methylimidazole ring to maintain miR-122 inhibition. Replacement of the methyl with a phenyl group (**320**) significantly reduced the activity. Modifications with the bulky benzimidazole (**321**) or indole (**322**) led to a 33% and 45% decrease in activity compared to **279**, respectively. Introduction of a benzoimidazole-2-amine (**323**) or *trans*-decahydroquinoline (**325**) motifs negatively affected the activity. Surprisingly,

substitution with a benzotriazole (**324**) group delivered a compound as potent as **279** (Figure 3.23).

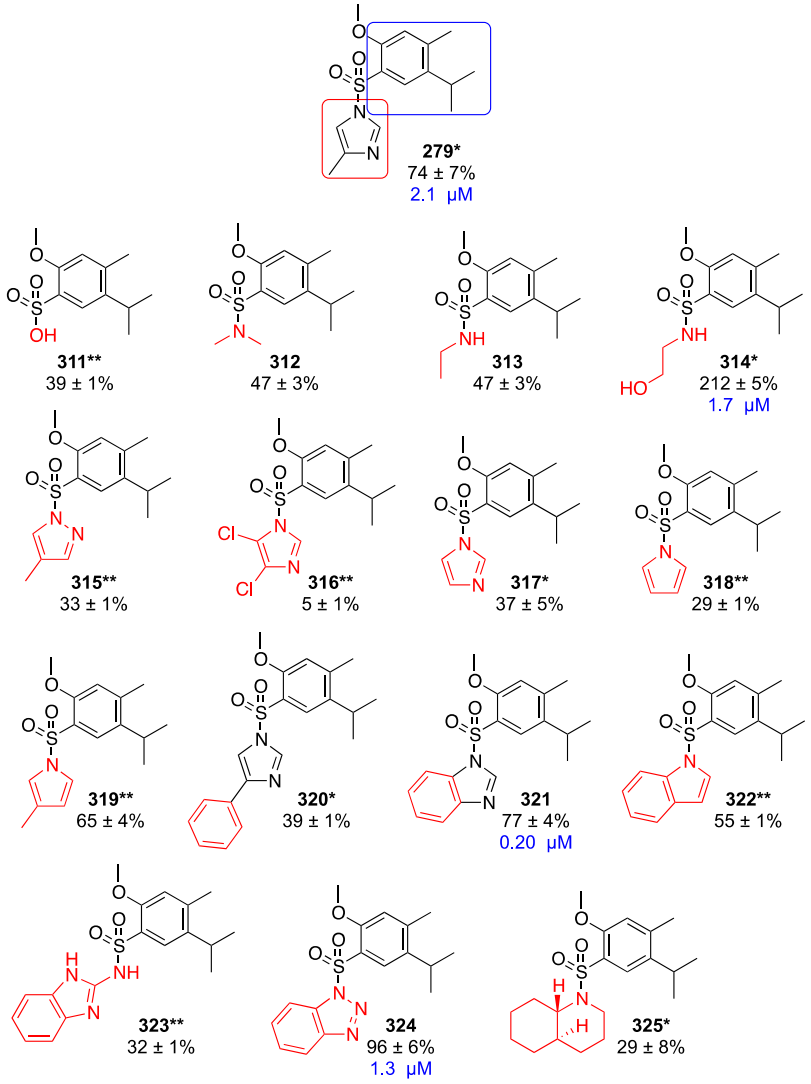

Figure 3.23: Structure-activity relationship studies of the hit compound **279** through modification of the 4-methyl-imidazole motif (variations to the original structure are shown in red).
The numbers represent the activity (in percent) relative to **279** within the same miR-122 luciferase assay. EC_{50} values are shown in blue. Experiments were performed in triplicate and the standard deviations of three independent assays were calculated. The compounds were provided by the Broad Institute, excepted the analogs labeled with one or two asterixes (* or **), which were synthesized by me or by Rohan Kumbhare, respectively.

Removal of the isopropyl group (**326** and **327**) or replacement with a methyl group (**328**) abrogated the activity. Removal of the methyl in the *meta* position, however, seemed to be more tolerated as the activity was only slightly decreased by 12% and 16% for **329** and **330** compared

to **279**, respectively. Modifications of the methoxy group with an ethoxy (**331**) or a propargyl motif (**332**) induced an 18% and 44% loss in activity, respectively. As expected, the benzotriazole analog substituted with a propargyl (**333**) motif instead of the methoxy (**324**) group exhibited a significant loss in potency. Substitution of the benzene ring with a tetrahydroquinoline motif as in **30**, or with 4,5-dichloro-2-methylbenzene similarly to **278**, resulted in drastic reductions in activity (Figure 3.24).

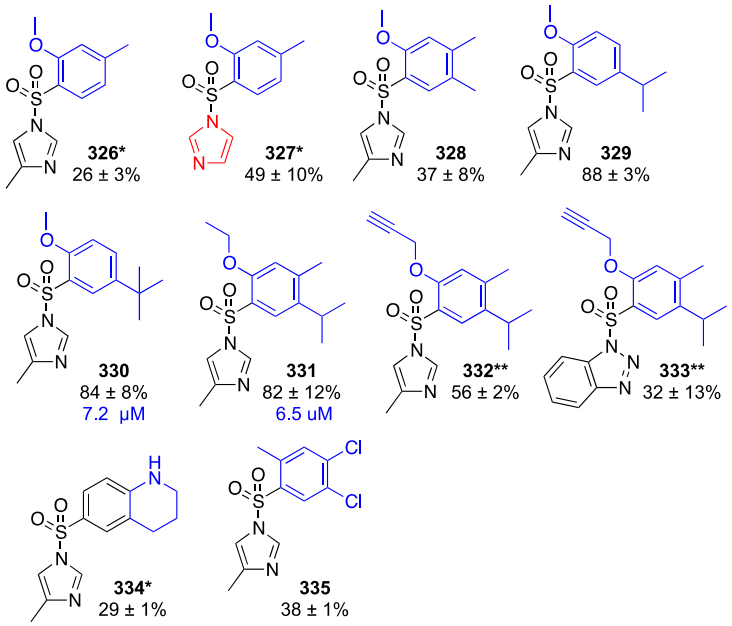

Figure 3.24: Structure-activity relationship studies of the hit compound **279** through modification of the benzene ring substituents (variations to the original structure are shown in blue).
The numbers represent activity relative to **279** within the same miR-122 luciferase assay. EC_{50} values are shown in blue. Experiments were performed in triplicate and the standard deviations of three independent assays were calculated. The compounds were provided by the Broad Institute, excepted the analogs labeled with one or two asterixes (* or **), which were synthesized by me or by Rohan Kumbhare, respectively.

The best analogs identified through structural modifications of **279**, were tested in dose-response in Huh7-psiCHECK-miR122 cells (Figure 3.25). Analogs **330** and **331** were less potent than **279** with EC_{50} values of ~7 µM. The compounds **314** and **324** displayed EC_{50} values equivalent to **279**. Surprisingly, the indole derivative **321**, which exhibited a 23% reduced

activity compared to **279** in the miR-122 luciferase assay (at 10 μM), was found 10 times more potent than **279** when tested in dose-response (Figure 3.25).

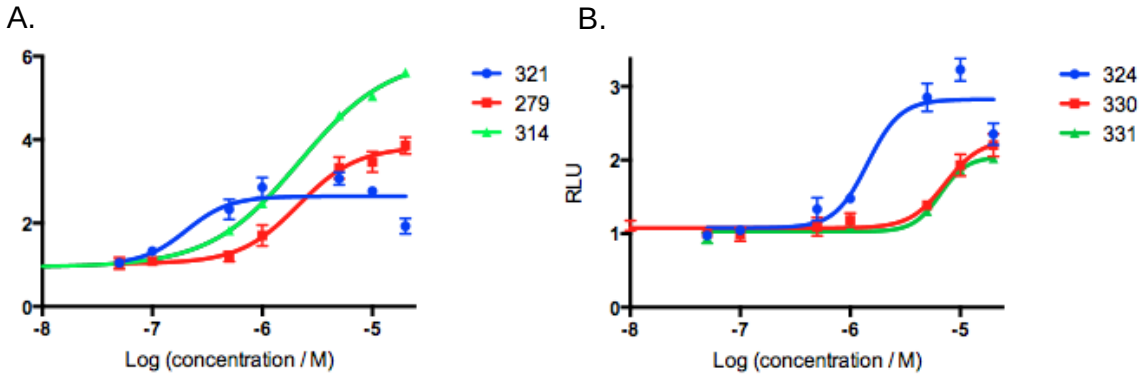

Figure 3.25: Dose-response curves in Huh7-psiCHECK-miR122 cells treated with the best analogs of hit compound **279.**
A. Compounds **314**, **321**, and hit compound **279**. **B**. Compounds **324**, **330**, and **331**. All assays were conducted in triplicate and normalized to a DMSO control. The error bars represent the standard deviation from three independent experiments.

To verify the specificity of these analogs for miR-122 inhibition, they were submitted to secondary assays (Figure 3.26). The compounds **279**, **314**, **321**, **324**, **329**, **330**, and **331** were tested in the *in vitro* RLuc assay; **314**, **321**, **330**, and **331** induced ≥30% decrease in *Renilla* luminescence, while the analogs **279**, **324**, and **329** only modestly affected the enzyme, with ≤20% inhibition observed (Figure 3.26A). Not surprisingly, **314**, which induced the most Rluc inhibition *in vitro*, most strongly affected the luminescence signal in the psiCHECK-empty assay (Figure 3.26B). The compounds **324**, **329**, **330**, and **331** induced a 2- to 2.5-fold increase in the psiCHECK-empty assay. The derivatives **279** and **321** did not perturb the luminescence signal in the control assay (Figure 3.26B), suggesting some level of specificity for miRNA inhibition.

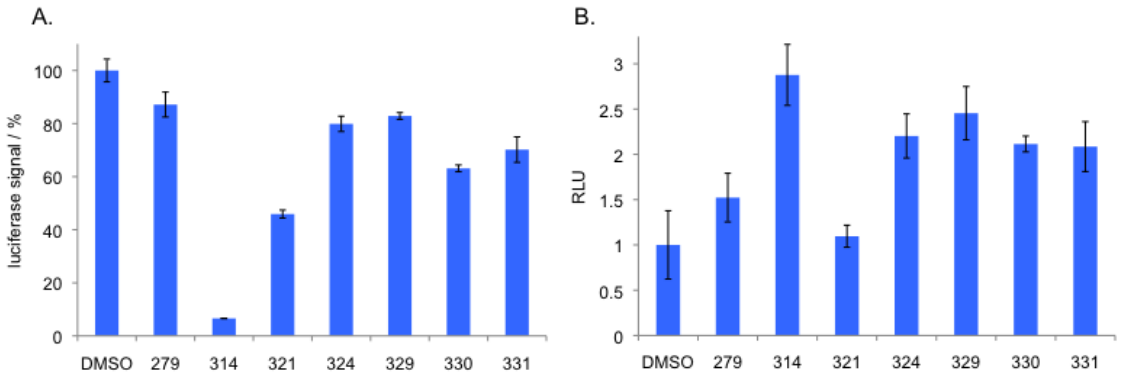

Figure 3.26: Secondary assays to determine the selectivity of the best analogs of hit 279 identified in the HTS. **A**. *In vitro* RLuc assay, the compounds were tested at 10 μM. **B**. Dual Luciferase assay of Huh7 cells transfected with psiCHECK-empty and treated with the analogs at 10 μM for 48 h. The luciferase signal was normalized to a DMSO control. The error bars indicate the standard deviations determined from three independent measurements.

The most promising inhibitors **279**, **321**, and **324** were tested in qRT-PCR experiments (Figure 3.27). Huh7 cells were exposed to a DMSO control or to the inhibitors at 10 μM for 48 hours. The total RNA was isolated using the miRNeasy kit (Qiagen), and the qRT-PCR was performed in triplicate using TaqMan probes for miR-122 and RNU19 (control). The data was then normalized to the DMSO and RNU19 controls using the $2^{-\Delta\Delta Ct}$ method.[155] The 2 most promising inhibitors **279** and **321** reduced the level of miR-122 expression by 43% and 23% compared to the DMSO control, respectively. The benzotriazole analog **324**, unfortunately, did not induce any down-regulation of miR-122 expression (Figure 3.27). Follow-up studies will be performed in the future to investigate the selectivity of **279** and **321**, as well as their mode of action.

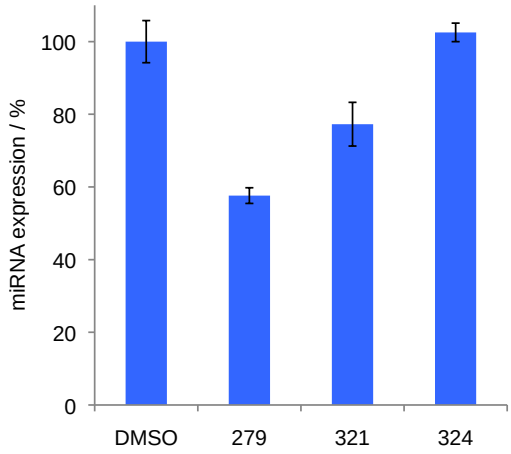

Figure 3.27: qRT-PCR measurements of mature miR-122 levels in Huh7 cells treated with the hit compound **279** and the best analogs (10 μM).
The relative expression of miR-122 for small molecule treated cells was normalized to a DMSO control (100% expression) and RNU19 expression. The error bars indicate the standard deviation determined from three independent measurements.

3.4.5 Re-examination of the 34 Hit Compounds Identified in the HTS

Since the sulfonamide chemotype was observed in the majority of the active compounds identified in the HTS, and most of them were found to be potent *Renilla* luciferase inhibitors, it was decided to re-investigate the top 34 hit compounds provided by the Broad Institute, which included 6 non-sulfonamide derivatives (**264**, **336**, **337**, **338**, **347**, and **362** Figure 3.28 and Figure 3.29). All the analogs were re-tested in the miR-122 luciferase assay. Only 18 compounds were found as active or more active than **30** in the Huh7-psiCHECK-miR122 assay. The derivatives **341** and **360** were as active as **30**; compounds **338**, **342**, **344**, **349**, **350**, **351**, **353-356**, **359**, and **362** elicited a 10 to 50% increase in activity. The analogs **268** and **346** induced ≥200% increase in activity and compounds **348** and **352** promoted a significant ≥300% enhancement in activity. It is noteworthy that **338** and **362** were the only active compounds not presenting a

sulfonamide scaffold. The analog **268**, which was one of the top 4 most active compounds in the primary screen, was the only one remaining after all the secondary assay studies.

These compounds were then tested in the *in vitro* RLuc assay to determine their effect on *Renilla* luciferase (Figure 3.28 and Figure 3.29). Unfortunately, most of the derivatives showed a strong *Renilla* luciferase inhibition. Only **336**, **339**, **357**, **362**, and **363** elicited a modest (≤50%) interaction with the enzyme. The compounds **336** and **357** were disregarded because they were inactive in the miR-122 luciferase assay. The analogs **339**, **362**, and **363** were further investigated; **339** showed an activity comparable to **279** in Huh7-psiCHECK-miR122 cells, and **362** exhibited an 18% increased activity compared to **30**.

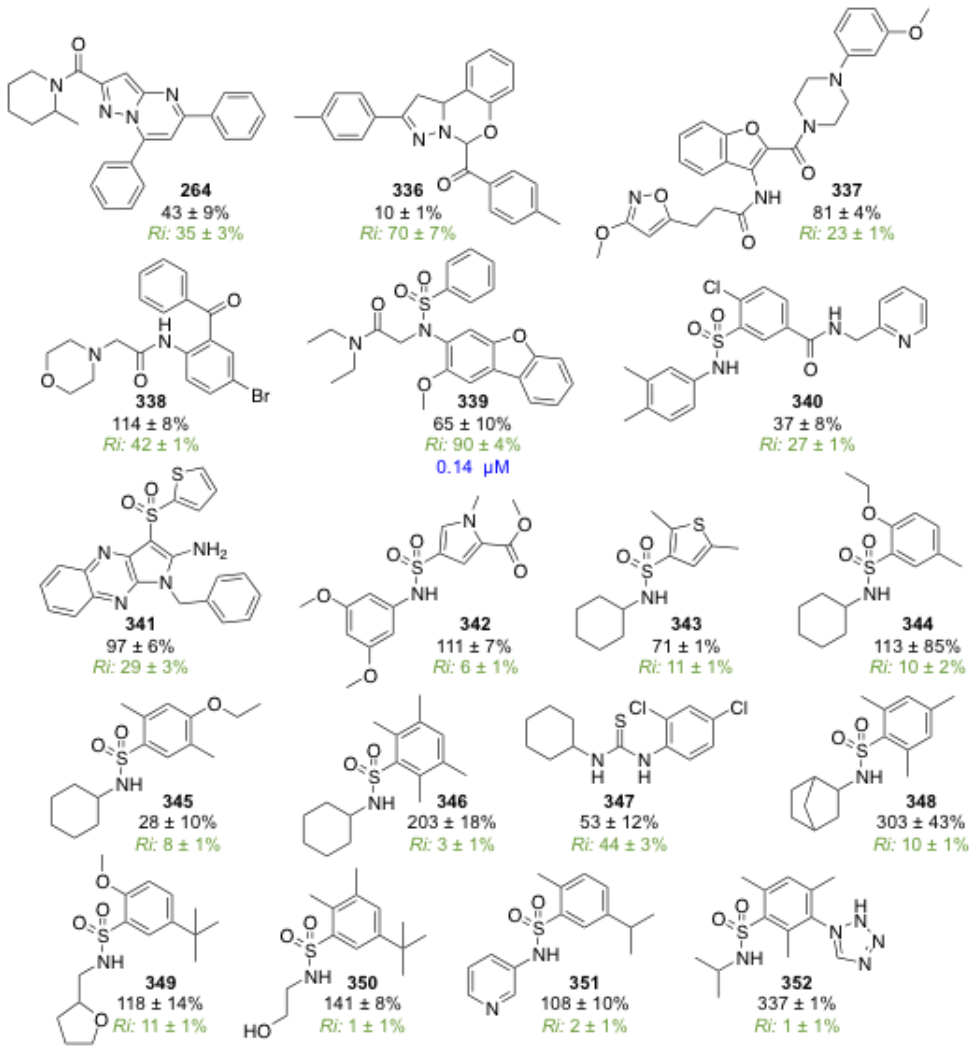

Figure 3.28: Structure of best 34 compounds identified in the HTS.
The numbers in black represent the activity (in percent) relative to **30** within the same miR-122 luciferase assay. *Ri* values (in green) represent *Renilla* luciferase *in vitro* activity (in percent) relative to a DMSO control (100%). Lower numbers indicate a stronger inhibition. EC_{50} values are shown in blue. Experiments were performed in triplicate and the standard deviations of three independent assays were calculated.

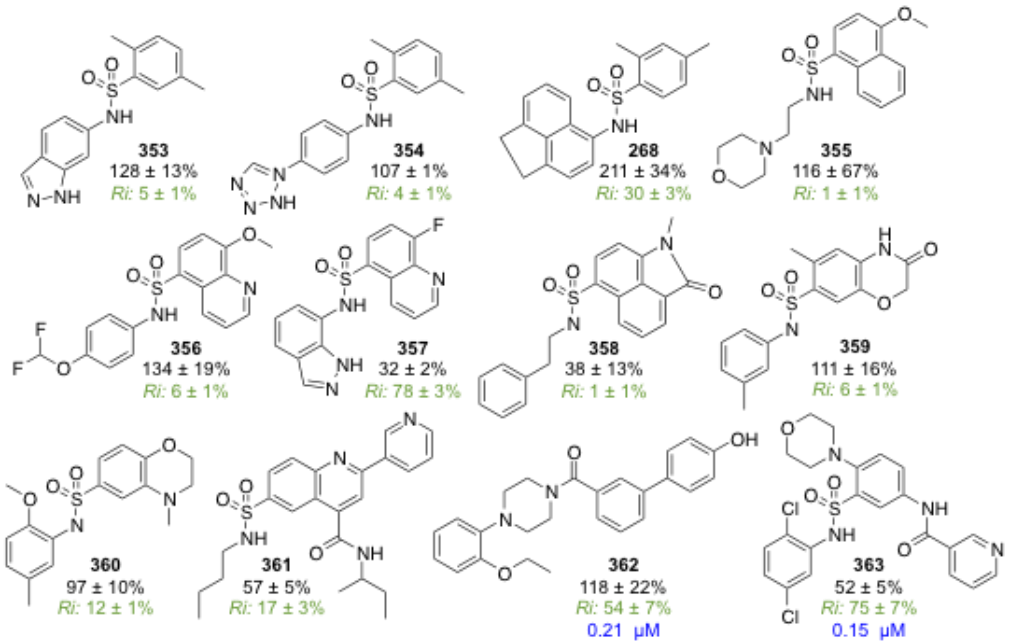

Figure 3.29: Structure of best 34 compounds identified in the HTS – continued.
The numbers in black represent the activity (in percent) relative to **30** within the same miR-122 luciferase assay. *Ri* values (in green) represent *Renilla* luciferase *in vitro* activity (in percent) relative to a DMSO control (100%). Lower numbers indicate a stronger inhibition. EC_{50} values are shown in blue. Experiments were performed in triplicate and the standard deviations of three independent assays were calculated.

The best 3 compounds **339**, **362**, and **363** were tested in dose-response in Huh7-psiCHECK-miR122 cells (Figure 3.30), and displayed significantly lower EC_{50} values (≤10-fold) than **30**.

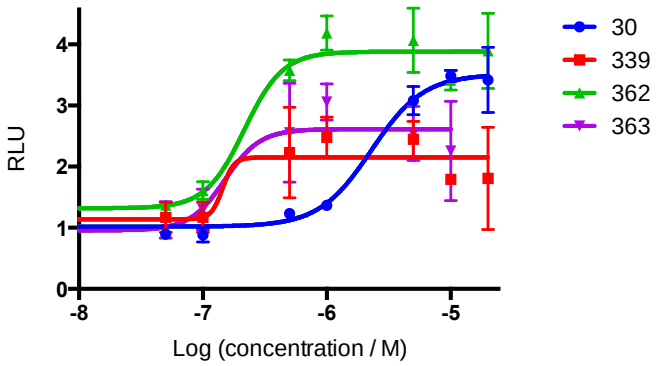

Figure 3.30: Dose response curves in Huh7-psiCHECK-miR122 cells treated with the most promising hit compounds identified in the HTS (**339, 362**, and **362**) and the positive control **30.**
All assays were conducted in triplicate and normalized to a DMSO control. The error bars represent the standard deviation from three independent experiments.

These three analogs, along with the two non-sulfonamide derivatives **264** and **338** were further evaluated in Huh7 cells transfected with the psiCHECK-empty reporter (Figure 3.31). The hit compound **264**, identified by the Broad Institute, but deemed inactive in subsequent assays, did not show any effect on the luminescence signal in the reporter assay, similarly to **363**. Conversely, the sulfonamide **339** and the two amide derivatives **338** and **362** induced a 2- and 2.5-fold increase in the signal over the DMSO control, respectively. These results indicated that the compounds **338**, **339**, **362**, and **363** might lack specificity for miR-122, as they induced an increase in the luminescence signal of the control reporter. However, since the *in vitro* data indicated a modest inhibition of the *Renilla* luciferase by **338** and **362**, and only a weak inhibition by **339** and **363**, the direct effect of these compounds on miR-122 regulation should be examined.

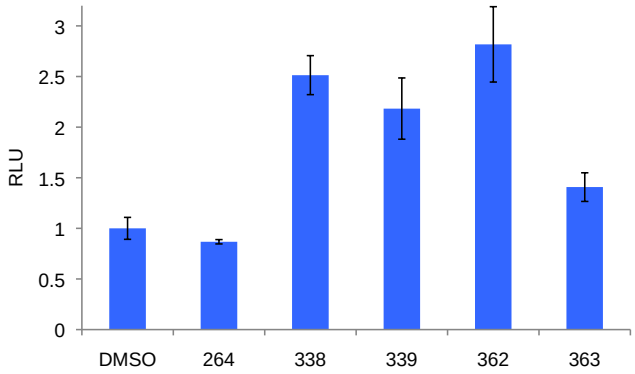

Figure 3.31: Specificity study of interesting compounds from the HTS.
Dual Luciferase assay of Huh7 cells transfected with psiCHECK-empty and treated with the analogs **264**, **338**, **339**, **362**, and **363** at 10 μM for 48 h. The luciferase signal was normalized to a DMSO control. The error bars indicate the standard deviations determined from three independent measurements.

These five compounds were also tested in qRT-PCR experiments to directly measure their effect on miR-122 expression levels (Figure 3.32). Huh7 cells were treated with DMSO or the inhibitors at 10 μM for 48 hours. The total RNA was isolated with the miRNeasy kit and

used in qRT-PCR experiments in conjunction with the TaqMan probes for miR-122 or the control RNU19. Although **338** and **363** displayed a relatively high activity in the miR-122 luciferase assay, they did not reduce miR-122 expression. In agreement with what had been observed in the luciferase assay (Figure 3.28), **264** did not affect miR-122 expression. The sulfonamide **339** similarly did not induce any change in the intracellular levels of miR-122. Interestingly, the amide **362** showed a somewhat promising 24% reduction in miR-122 expression levels. Extensive re-analysis of the hit compounds identified by the Broad Institute revealed that most of these derivatives are *Renilla* luciferase inhibitors (Figure 3.28 and Figure 3.29), and do not actually affect miR-122 activity.

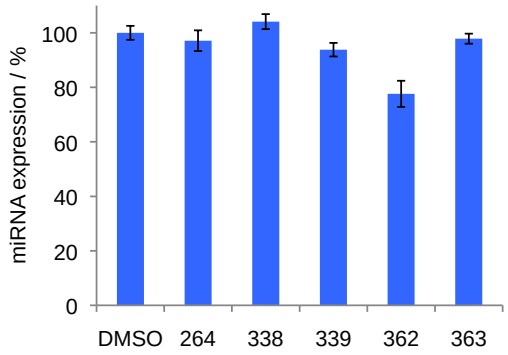

Figure 3.32: qRT-PCR measurements of mature miR-122 levels in Huh7 cells treated with **264, 338-339**, and **362-363** at 10 μM.
The relative expression of miR-122 for small molecule treated cells was normalized to a DMSO control (100% expression) and RNU19 expression. The error bars indicate the standard deviation determined from three independent measurements.

3.5 SUMMARY AND OUTLOOK

The previously identified miR-122 inhibitor **30** was extensively investigated through SAR studies. A total of 43 analogs were synthesized in order to better understand the molecular

requirement for miR-122 inhibition. A few compounds displayed activities comparable to **30** or slightly higher, but unfortunately this SAR investigation did not provide any analog significantly more potent than the inhibitor **30**.

A recent HTS of >300,000 compounds was conducted in collaboration with the Broad Institute to identify additional small molecule miR-122 inhibitors. From the 336,006 compounds tested in the primary screen, 1,023 compounds that displayed an activity ≥90% relative to **30** (at 10 μM) were identified as active. Following dose-response experiments, removal of compounds structurally problematic, known to be promiscuous, or that were also found as active in an unrelated HTS for miR-21 inhibitors, and powder re-test, only 34 small molecules remained. These were re-tested in the miR-122 luciferase assay and in qRT-PCR experiments to measure the levels of expression of miR-122, miR-21, and miR-27b. Subsequent validation of the hit compounds identified in the HTS led to the discovery of the two potent sulfonamide inhibitors **278** and **279**. Preliminary SAR studies were performed for both compounds to further improve their activity. The best analogs of both series were tested in dose-response and submitted to secondary assays to evaluate their specificity. All the analogs of **278**, along with **278**, were found to be potent *Renilla* luciferase inhibitors. Gratifyingly, **279** and its analog **321** showed some specificity for miR-122 inhibition and induced a significant reduction in miR-122 expression, as found in qRT-PCR experiments. The compound **279** had an EC_{50} value equivalent to **30**, and **321** was found to be 10 times more potent. Follow-up studies need to be performed to further investigate the selectivity of **279** and **321** for miR-122 inhibition and determine their mechanism of action.

Additionally, careful re-investigation of the hits identified in the HTS, suggested that most of the compounds represent potent inhibitors of the *Renilla* luciferase enzyme rather than

actual miR-122 inhibitors. This highlights the importance of conducting secondary assays to distinguish compounds that showed activity by inhibiting the target of interest (miR-122), from non-specific compounds, which interfered with the assay read out. It would have been helpful to include the *in vitro* RLuc assay as a control, following the primary screen of 336,006 compounds in the HTS. Nonetheless, this study also revealed the structurally diverse **362** as a promising new miR-122 inhibitor. It displayed an improved EC_{50} value of 0.2 μM and, more importantly, reduced the expression levels of miR-122 by 24% compared to a DMSO control. Of note, the amide **362** exhibited some degree of non-specificity as it showed 46% inhibition in the RLuc assay. SAR studies need to be conducted to improve the activity and specificity of **362** for miR-122 inhibition.

More importantly, miR-122 represents an attractive therapeutic target, since it is required for HCV replication. Exposure of infected liver cells to the previously identified small molecule miR-122 inhibitors **29** and **30** resulted in >50% reduction of HCV RNA levels.[98] Once the selectivity profile of the newly identified miR-122 inhibitors is determined, these compounds **279**, **321**, and **362** need to be tested for their ability to reduce HCV replication in liver cells.

In conclusion, additional small molecule inhibitors of miR-122 have been identified through HTS, that could provide potential new tools to elucidate the involvement of miR-122 in HCV as well as new antiviral therapies.

3.6 EXPERIMENTALS

Cell culture. Experiments were performed using the Huh7 cell line (gift from Dr. Asokan, UNC) cultured in Dulbecco's Modified Eagle Medium (DMEM; Hyclone) supplemented with 10% Fetal Bovine Serum (FBS; Seradigm catalog number 97068-085, lot #093B13) and 2% penicillin/streptomycin (VWR) and maintained at 37 °C in a 5% CO_2 atmosphere. Huh7-psiCHECK-miR122 cells[124] were cultured in Dulbecco's Modified Eagle Medium (DMEM; Hyclone) supplemented with 10% fetal bovine serum (FBS; Seradigm catalog number 97068-085, lot #093B13), 500 μg/mL of G418 (Sigma Aldrich), and 2% penicillin/streptomycin (VWR) and maintained at 37 °C in a 5% CO_2 atmosphere.

Screening of the compounds in the miR-122 luciferase assay. Huh7-psiCHECK-miR122 cells were seeded at a density of 5,000 cells per well in white, clear-bottom, 384-well plates (Greiner). After an overnight incubation in media (DMEM, 10% FBS, free of antibiotics and free of G418, 45 μL), the cells were treated with compounds at a concentration of 10 μM (by addition of 5 μL of a 0.1 mM solution stock in 1% DMSO) or a DMSO control (0.1% DMSO final concentration) in triplicate. The cells were incubated for 48 h followed by analysis with a Dual Luciferase Reporter Assay Kit (Promega) using 20 μL passive lysis buffer and 25 μL of each luciferase reagent. The luminescence was measured on a Tecan M1000 platereader with a measurement time of 1 s and a delay time of 2 s. All experiments were performed in triplicate, for each well the *Renilla* luciferase read out was normalized to the firefly luciferase read out, and the average for each sample was further normalized to the DMSO control.

Quantitative real time PCR analysis. Huh7 cells were seeded at a density of 150,000 cells per well in 6-well plates and grown overnight. The media was replaced with 1,98 mL DMEM and

the cells were treated with compounds at a 10 μM concentration (20 μL of 1 mM DMSO stock) or with DMSO (1% final DMSO concentration). The cells were incubated at 37 °C for 48 h (DMEM, antibiotics-free, 5% CO_2, 2 mL final volume). The media was removed, and the cells were washed with PBS buffer (1 mL, pH 7.4) followed by RNA isolation with a miRNeasy mini kit (Qiagen) using the procedure described in the appendix 6.2. Following quantification, the RNA samples were diluted to 3 ng/μL in RNAse-free water, and 15 ng (5 μL) of each sample were reverse transcribed using the TaqMan microRNA Reverse Transcription Kit (Life Technologies) in conjunction with the RNU19 (control) or the miR-122 TaqMan RT primer. The real time PCR was then carried out with a TaqMan 2x Universal PCR Master Mix and the appropriate TaqMan miRNA assay for miR-122 and RNU19 (Life Technologies). The triplicate threshold cycles (Ct) obtained for each small molecule treatment were used to determine the relative levels of miR-122 in small molecule treated cells relative to the DMSO control using the $2^{-\Delta\Delta Ct}$ method.[155]

Assessment of the specificity of the inhibitors using the psiCHECK-empty reporter. Huh7 cells were seeded at a density of 15,000 cells per well in a white clear-bottom 96-well plates (VWR), in 200 μL media (DMEM, 10% FBS, no-antibiotics) and grown overnight. The cells were transfected with 40 ng of psiCHECK-empty using Lipofectamine 2000 (Life Technologies) in 200 μL OptiMEM (Life Technologies). After 2 h incubation at 37 °C, the media was replaced with DMEM (198 μL, 10% FBS, no antibiotics) supplemented with the compounds at 10 μM (2 μL of a 1 mM 10% DMSO stock) or DMSO control (0.1% DMSO final concentration). The cells were incubated for 48 h followed by analysis with a Dual Luciferase Reporter Assay Kit (Promega) using 30 μL passive lysis buffer and 50 μL of each luciferase reagent. The luminescence was measured on a Tecan M1000 platereader with a measurement time of 1 s and a

delay time of 2 s. All experiments were performed in triplicates, for each well the *Renilla* read out was normalized to the firefly luciferase read out, and the average for each sample was further normalized to the DMSO control.

***In vitro* RLuc inhibition assay**. The protocol was adapted from previous reports.[235] The experiment was performed in a white 384-well plate in triplicate. The compounds were diluted at 50 μM (20% final DMSO concentration) in PBS (6 μL of a 250 μM DMSO stock in 24 μL of PBS). The recombinant *Renilla* luciferase enzyme (RayBiotech, 9 μL of a 0.3 mg/L PBS stock) was added to each well. The compounds were added to obtain a final concentration of 10 μM (4% final DMSO concentration, addition of 6 μL of the 50 μM stock). Then, 15 μL of *Renilla*-glo buffer (Promega) supplemented with the substrate (10 μL of substrate per 1 mL of buffer) was added to each well. The plate was quickly centrifuged at 1,000 x g for 1 min and shaken in the dark for 10 min. The luminescence was measured on a Tecan M1000 luminometer with a measurement time of 1 s. All experiments were performed in triplicates, and the average for each sample was normalized to the DMSO control.

Organic synthesis.

All reactions were performed in flame-dried glassware under a nitrogen atmosphere and stirred magnetically. Reactions were followed by thin layer chromatography (TLC) using glass-backed silica gel plates (Sorbent technologies, 250 μm thickness). Tetrahydrofuran and DCM were obtained from a dry solvent delivery system. MeCN, EtOH, MeOH and pyridine were distilled from calcium hydride and stored over 4 Å molecular sieves. Other reagents and solvents were obtained from commercial sources (Sigma, VWR, Fisher, Accros), stored under nitrogen and used directly without further purification. Yields refer to pure compounds unless otherwise

stated. Flash chromatography was performed on silica gel (60 Å, 40-63 μm (230 × 400 mesh), Sorbtech) as a stationary phase. High-resolution mass spectral analysis (HRMS) was performed at the University of Pittsburgh on a Q-Exactive (Thermo Scientific) mass spectrometer. The ^{1}H NMR and ^{13}C NMR spectra were recorded on a 300 MHz or a 400 MHz Varian or Bruker NMR spectrometers. Chemical shifts are given in δ units (ppm) for NMR spectra.

1-(3,4-Dihydroquinolin-1(2*H*)-yl)-2,2,2-trifluoroethanone (193). TEA (6.3 mL, 45.3 mmol) was added to a stirred solution of tetrahydroquinoline (1.9 mL, 15.1 mmol) in Et_2O (10 mL). The solution was cooled to 0 °C and TFAA (4.23 mL, 30.2 mmol in 5 mL of Et_2O) was added drop-wise. The resulting mixture was allowed to warm up to room temperature and was stirred overnight. The mixture was diluted with Et_2O (5 mL), washed with H_2O (3 x 20 mL) and brine (16 mL), dried over Na_2SO_4, filtered, and concentrated. The residue was purified by flash chromatography on silica gel, eluting with hexanes/EtOAc (6:1) to give **193** as a yellow solid (3.1 g, 88%). ^{1}H NMR (300 MHz, chloroform-d) δ 7.62 (d, *J* = 9.6 Hz, 1H), 7.22 (d, *J* = 6.3 Hz, 2H), 3.84 (t, *J* = 6.2 Hz, 2H), 2.86 (t, *J* = 6.9 Hz, 2H), 2.07 (t, *J* = 6.6 Hz, 2H). The analytical data is in agreement with literature reports.[98]

1-(2,2,2-Trifluoroacetyl)-1,2,3,4-tetrahydroquinoline-6-sulfonyl chloride (194). The intermediate **193** (200 mg, 0.87 mmol) was added to chlorosulfonic acid (0.3 mL, 4.4 mmol) at 0 °C. The reaction mixture was slowly allowed to warm up to room temperature over 30 min and heated to reflux for 2.5 h. The solution was cooled down to 0 °C in an ice bath and ice-cold water (3 mL) was slowly added, followed by EtOAc (5 mL). The layers were separated, the aqueous layer was extracted with EtOAc (3 x 5 mL), the organic layers were combined, washed with H_2O (3 x 10 mL) and brine (8 mL), dried over Na_2SO_4, filtered, and concentrated. The residue was

purified by flash chromatography on silica gel, eluting with hexanes/EtOAc (5:1) to give **194** as a yellow solid (199 mg, 69%). ^{1}H NMR (300 MHz, chloroform-d) δ 7.99 (d, *J* = 9.6 Hz, 1H), 7.89 (dd, *J* = 7.2, 2.2 Hz, 2H), 3.91 (m, 2H), 3.02 (dd, *J* = 7.7, 6.1 Hz, 2H), 2.16 (td, *J* = 7.0, 5.8 Hz, 2H). The analytical data is in agreement with literature reports.[98]

2,2,2-Trifluoro-1-(6-(((4a*R*,8a*S*)-octahydroquinolin-1(2*H*)-yl)sulfonyl)-3,4-dihydroquinolin-1(2*H*)-yl)ethanone (195). TEA (0.306 mL, 2.19 mmol) was added to a solution of *trans*-decahydroquinoline (102 mg, 0.73 mmol) in DCM (6 mL) at 0 °C. A solution of **194** (120 mg, 0.37 mmol) in DCM (3 mL) was added drop-wise. The reaction mixture was allowed to warm to room temperature and stirred for 3 h. A 1 M HCl solution (2 mL) and DCM (6 mL) were added, the layers were separated, the aqueous layer was extracted with DCM (2 x 6 mL), the organic layers were combined, washed with H_2O (2 x 5 mL) and brine (4 mL), dried over Na_2SO_4, filtered, and concentrated. The residue was purified by flash chromatography on silica gel, eluting with hexanes/EtOAc (4:1) to give **195** as a white solid (97 mg, 61%). ^{1}H NMR (400 MHz, chloroform-d) δ 7.82 (s, 1H), 7.68 - 7.55 (m, 2H), 4.08 (m, 1H), 3.85 (dd, *J* = 6.9, 5.0 Hz, 2H), 2.93 (t, *J* = 6.9 Hz, 2H), 2.75 (ddd, *J* = 13.2, 7.9, 6.0 Hz, 1H), 2.49 (ddd, *J* = 11.4, 10.0, 3.6 Hz, 1H), 2.23 - 2.05 (m, 3H), 1.80 - 1.37 (m, 6H), 1.31 - 0.87 (m, 3H). The analytical data is in agreement with literature reports.[98]

6-(((4a*R*,8a*S*)-Octahydroquinolin-1(2*H*)-yl)sulfonyl)-1,2,3,4-tetrahydroquinoline (30). K_2CO_3 (540 mg, 4.12 mmol) was added to a solution of **195** (93 mg, 0.21 mmol) in MeOH:H_2O (3.9:1.6 mL), and the reaction mixture was stirred for 2 h at rt. The solvents were removed under vacuum, the residue was dissolved in H_2O (5 mL), the product was extracted with DCM (3 x 8 mL), and the combined organic layers were washed with brine (6 mL), dried over Na_2SO_4,

filtered, and concentrated. The residue was purified by flash chromatography on silica gel, eluting with hexanes/EtOAc (4:1) to afford **30** as a white solid (49 mg, 72%). ^{1}H NMR (400 MHz, chloroform-d) δ 7.31 - 7.21 (m, 2H), 6.41 - 6.34 (m, 1H), 4.40 (s, 1H), 4.04 - 3.94 (m, 1H), 3.30 (t, *J* = 5.6 Hz, 2H), 2.71 (t, *J* = 6.3 Hz, 2H), 2.65 - 2.54 (m, 1H), 2.37 - 2.25 (m, 2H), 1.93 - 1.82 (m, 2H), 1.75 - 1.31 (m, 8H), 1.23 - 1.00 (m, 2H), 1.00 - 0.81 (m, 2H); ^{13}C NMR (400 MHz, chloroform-d) δ 148.265, 128.856, 126.861, 126.248, 120.528, 112.949, 65.097, 48.993, 41.810, 41.403, 33.746, 32.146, 32.046, 27.225, 26.186, 25.702, 25.459, 21.372. The analytical data is in agreement with literature reports.[98]

The compounds **201**-**215** and **220**-**221** were prepared from **194** and the corresponding amines using the procedure described for **30**:

***N*-Butyl-1,2,3,4-tetrahydroquinoline-6-sulfonamide (199)**. Same procedure as **195** using butylamine (0.051 mL, 0.52 mmol) and **194** (85 mg, 0.26 mmol) as the starting materials. The residue was purified by flash chromatography on silica gel, eluting with hexanes/EtOAc (4:1) to deliver **199** as a white solid (45 mg, 86%). ^{1}H NMR (300 MHz, chloroform-d) δ 7.45 - 7.37 (m, 2H), 6.43 (d, *J* = 9.0 Hz, 1H), 4.35 (s, 1H), 4.12 (t, *J* = 6.2 Hz, 1H), 3.40 - 3.32 (m, 2H), 2.90 (q, *J* = 6.7 Hz, 2H), 2.77 (t, *J* = 6.3 Hz, 2H), 1.95 - 1.90 (m, 2H), 1.49 - 1.37 (m, 2H), 1.33 - 1.25 (m, 4H), 0.86 (t, *J* = 7.2 Hz, 3H). The analytical data is in agreement with literature reports.[98]

***N*-Octyl-1,2,3,4-tetrahydroquinoline-6-sulfonamide (201).** Same procedure as **195** using octylamine (0.075 mL, 0.45 mmol) and **194** (50 mg, 0.15 mmol) as the starting materials. The residue was purified by flash chromatography on silica gel, eluting with hexanes/EtOAc (6:1) to deliver **201** as a colorless oil (20 mg, 31%). ^{1}H NMR (300 MHz, chloroform-d) δ 7.46 - 7.38 (m,

2H), 6.43 (d, *J* = 8.2 Hz, 1H), 4.37 (s, 1H), 4.22 (bs, 1H), 3.36 (t, *J* = 6.0 Hz, 2H), 2.92 - 2.85 (m, 2H), 2.76 (t, *J* = 6.4 Hz, 2H), 1.95 - 1.91 (m, 2H), 1.42 (t, *J* = 6.6 Hz), 1.28 - 1.22 (m, 10H), 0.86 (t, *J* = 6.4 Hz, 3H). HRMS (ESI^+) calculated for $C_{17}H_{28}N_2O_2S$ $(M+Na)^+$ 347.1769, found 347.1739.

***N*-Decyl-1,2,3,4-tetrahydroquinoline-6-sulfonamide (202)**. Same procedure as **30** using 1-aminodecane (0.091 mL, 0.45 mmol) and **194** (50 mg, 0.15 mmol) as the starting materials. The residue was purified by flash chromatography on silica gel, eluting with hexanes/EtOAc (6:1) to afford **202** as a white solid (19 mg, 40%). ^1H NMR (300 MHz, chloroform-d) δ 7.42 - 7.39 (m, 2H), 6.42 (d, *J* = 9.0 Hz, 1H), 4.35 (s, 1H), 4.16 (t, *J* = 6.1 Hz, 1H), 3.36 (t, *J* = 5.4 Hz, 2H), 2.89 (q, *J* = 7.0 Hz, 2H), 2.77 (t, *J* = 6.2 Hz, 2H), 1.95 - 1.91 (m, 2H), 1.43 (t, *J* = 6.7 Hz, 2H), 1.22 (s, 14H), 0.87 (t, *J* = 6.8 Hz, 3H). HRMS (ESI^+) calculated for $C_{19}H_{32}N_2O_2S$ $(M+Na)^+$ 375.2082, found 375.2046.

***N*-Dodecyl-1,2,3,4-tetrahydroquinoline-6-sulfonamide (203)**. Same procedure as **195** using dodecylamine (0.104 mL, 0.45 mmol) and **194** (50 mg, 0.15 mmol) as the starting materials. The residue was purified by flash chromatography on silica gel, eluting with hexanes/EtOAc (8:1) to deliver **203** as a white solid (8 mg, 25%). ^1H NMR (300 MHz, chloroform-d) δ 7.41 - 7.39 (m, 2H), 6.42 (d, *J* = 9.0 Hz, 1H), 4.33 (s, 1H), 4.12 (t, *J* = 6.2 Hz, 1H), 3.36 (t, J = 6.0 Hz, 2H), 2.89 (q, *J* = 6.8 Hz, 2H), 2.77 (t, *J* = 6.3 Hz, 2H), 1.97 - 1.91 (m, 2H), 1.43 (t, *J* = 7.0 Hz, 2H), 1.23 (d, *J* = 7.8 Hz, 18H), 0.88 (t, *J* = 6.7 Hz, 3H). HRMS (ESI^+) calculatedd for $C_{21}H_{36}N_2O_2S$ $(M+H)^+$ 381.2576, found 381.2545.

***N*-Isobutyl-1,2,3,4-tetrahydroquinoline-6-sulfonamide (204).** Same procedure as **195** using isobutylamine (0.051 mL, 0.52 mmol) and **194** (85 mg, 0.26 mmol) as the starting materials. The

residue was purified by flash chromatography on silica gel, eluting with hexanes/EtOAc (7:1) to deliver **204** as a colorless oil (35 mg, 75%). ^{1}H NMR (300 MHz, chloroform-d) δ 7.41 - 7.39 (m, 2H), 6.42 (d, *J* = 9.0 Hz, 1H), 4.35 (s, 1H), 4.24 (t, *J* = 6.5 Hz, 1H), 3.36 (t, *J* = 4.8 Hz, 2H), 2.77 (t, *J* = 6.3 Hz, 2H), 2.70 (t, *J* = 6.7 Hz, 2H), 1.95 - 1.91 (m, 2H), 1.75 - 1.71 (m, 1H), 0.87 (d, *J* = 6.7 Hz, 6H).

***N*-(Cyclopropylmethyl)-1,2,3,4-tetrahydroquinoline-6-sulfonamide (205)**. Same procedure as **195** using cyclopropanemethylamine (0.026 mL, 0.30 mmol) and **194** (50 mg, 0.15 mmol) as the starting materials. The residue was purified by flash chromatography on silica gel, eluting with hexanes/EtOAc (8:1) to deliver **205** as a colorless oil (28 mg, 83%). ^{1}H NMR (400 MHz, chloroform-d) δ 7.48 - 7.34 (m, 2H), 6.41 (d, *J* = 9.1 Hz, 1H), 4.50 (t, *J* = 5.9 Hz, 1H), 3.34 (t, *J* = 5.2 Hz, 2H), 2.77 - 2.72 (m, 4H), 1.94 - 1.88 (m, 2H), 0.90 - 85 (m, 2H), 0.44 (q, *J* = 5.4 Hz, 2H), 0.08 (q, *J* = 5.1 Hz, 2H). HRMS (ESI$^+$) calculated for $C_{13}H_{18}N_2O_2S$ $(M+H)^+$ 267.3672, found 267.1152.

***N*-(Prop-2-yn-1-yl)-1-(2,2,2-trifluoroacetyl)-1,2,3,4-tetrahydroquinoline-6-sulfonamide**. Same procedure as **195** using propargylamine (0.059 mL, 0.91 mmol) and **194** (100 mg, 0.30 mmol) as the starting materials. The residue was purified by flash chromatography on silica gel, eluting with hexanes/EtOAc (2:1) to deliver a white solid (71 mg, 67%). ^{1}H NMR (300 MHz, chloroform-d) δ 7.76 (s, 1H), 7.73 (d, *J* = 7.8 Hz, 2H), 4.66 - 4.64 (m, 1H), 3.89 - 3.85 (m, 2H), 2.94 (t, *J* = 6.9 Hz, 2H), 2.14 - 2.12 (m, 2H).

***N*-((1-(3-Hydroxypropyl)-1*H*-1,2,3-triazol-4-yl)methyl)-1-(2,2,2-trifluoroacetyl)-1,2,3,4-tetrahydroquinoline-6-sulfonamide**. Sodium ascorbate (13.7 mg, 0.07 mmol) and copper

sulfate pentahydrate (4.3 mg, 0.01 mmol) were added to a solution of 3-azidopropanol (10.5 mg, 0.10 mmol) and *N*-(prop-2-yn-1-yl)-1-(2,2,2-trifluoroacetyl)-1,2,3,4-tetrahydroquinoline-6-sulfonamide (30 mg, 0.09 mmol) in tBuOH:H2O (0.5:0.5 mL). The resulting mixture was stirred at room temperature overnight. The solvents were removed under vacuum and the residue was purified by flash chromatography on silica gel, eluting with 5% MeOH in DCM to give a white oil (24 mg, 78%). ^{1}H NMR (300 MHz, chloroform-d) δ 7.80 (d, *J* = 8.1 Hz, 1H), 7.70 - 7.66 (m, 2H), 7.48 (s, 1H), 5.81 (t, *J* = 6.3 Hz, 1H), 4.33 (t, *J* = 6.6 Hz, 2H), 4.27 (d, *J* = 6.0 Hz, 2H), 3.88 - 3.84 (m, 2H), 3.57 (t, *J* = 5.7 Hz, 2H), 2.96 - 2.91 (t, *J* = 6.9 Hz, 2H), 2.15 - 2.04 (m, 4H). HRMS (ESI$^+$) calculated for $C_{17}H_{20}F_3N_5O_4S$ $(M+Na)^+$ 370.1086, found 370.1095.

***N*-((1-(3-Hydroxypropyl)-1*H*-1,2,3-triazol-4-yl)methyl)-1,2,3,4-tetrahydroquinoline-6-sulfonamide (208)**. Same procedure as **30** using *N*-((1-(3-hydroxypropyl)-1*H*-1,2,3-triazol-4-yl)methyl)-1-(2,2,2-trifluoroacetyl)-1,2,3,4-tetrahydroquinoline-6-sulfonamide (7 mg, 0.015 mmol) and K_2CO_3 (41 mg, 0.29 mmol) as the starting materials. The residue was purified by flash chromatography on silica gel, eluting with 5% MeOH in DCM to afford **208** as a white oil (4 mg, 60%). ^{1}H NMR (300 MHz, acetone-d) δ 7.62 (s, 1H), 7.35 - 7.32 (m, 2H), 6.51 (d, *J* = 9.3 Hz, 1H), 6.40 (s, 1H), 5.80 (s, 1H), 4.43 (t, *J* = 6.9 Hz, 2H), 4.10 (s, 2H), 3.54 (t, *J* = 6.0 Hz, 2H), 3.36 - 3.32 (m, 2H), 2.82 - 2.76 (m, 2H), 2.75 (t, *J* = 6.3 Hz, 2H), 1.99 - 1.87 (m, 2H). HRMS (ESI$^+$) calculated for $C_{15}H_{21}N_5O_3S$ $(M+H)^+$ 352.4319, found 352.1454.

***N*,*N*-Di(prop-2-yn-1-yl)-1-(2,2,2-trifluoroacetyl)-1,2,3,4-tetrahydroquinoline-6-sulfonamide.** Same procedure as **195** using dipropargylamine (0.066 mL, 0.64 mmol) and **194** (70 mg, 0.21 mmol) as the starting materials. The residue was purified by flash chromatography on silica gel, eluting with hexanes/EtOAc (2:1) to deliver a colorless oil (45 mg, 56%). ^{1}H NMR (300 MHz,

chloroform-d) δ 7.82 (s, 1H), 7.67 (d, *J* = 7.8 Hz, 2H), 4.16 (s, 4H), 3.85 (t, *J* = 4.5 Hz, 2H), 2.94 (t, *J* = 5.1 Hz, 2H), 2.18 (s, 2H), 2.12 - 2.10 (m, 2H).

***N*,*N*-Di(prop-2-yn-1-yl)-1,2,3,4-tetrahydroquinoline-6-sulfonamide (209).** Same procedure as **30** using *N*,*N*-di(prop-2-yn-1-yl)-1-(2,2,2-trifluoroacetyl)-1,2,3,4-tetrahydroquinoline-6-sulfonamide (45 mg, 0.12 mmol) and K_2CO_3 (315 mg, 2.28 mmol) as the starting materials. The residue was purified by flash chromatography on silica gel, eluting with hexanes/EtOAc (3:1) to deliver **209** as a yellow oil (24 mg, 71%). ^{1}H NMR (300 MHz, chloroform-d) δ 7.36 - 7.34 (m, 2H), 6.40 (d, *J* = 9.1 Hz, 1H), 4.44 (s, 1H), 4.11 (s, 4H), 3.34 (t, *J* = 5.7 Hz, 2H), 2.74 (t, *J* = 6.3 Hz, 2H), 2.17 (s, 2H), 1.93 - 1.86 (m, 2H). HRMS (ESI$^+$) calculated for $C_{15}H_{16}N_2O_2S$ $(M+H)^+$ 289.1011, found 289.1003.

***N*-Butyl-*N*-methyl-1-(2,2,2-trifluoroacetyl)-1,2,3,4-tetrahydroquinoline-6-sulfonamide.** Same procedure as **195** using *N*-methyl-butylamine (0.09 mL, 0.78 mmol) and **194** (85 mg, 0.26 mmol) as the starting materials. The residue was purified by flash chromatography on silica gel, eluting with hexanes/EtOAc (2:1) to deliver a white solid (47 mg, 48%). ^{1}H NMR (300 MHz, chloroform-d) δ 7.76 (s, 1H), 7.60 (d, *J* = 7.8 Hz, 2H), 3.86 (t, *J* = 4.2 Hz, 2H), 3.01 - 2.94 (m, 4H), 2.71 (s, 3H), 2.12 - 2.09 (m, 2H), 1.52 - 1.48 (m, 2H), 1.36 - 1.33 (m, 2H), 0.9 (t, *J* = 5.4 Hz, 3H).

***N*-Butyl-*N*-methyl-1,2,3,4-tetrahydroquinoline-6-sulfonamide (210)**. Same procedure as **30** using *N*-butyl-*N*-methyl-1-(2,2,2-trifluoroacetyl)-1,2,3,4-tetrahydroquinoline-6-sulfonamide (47 mg, 0.12 mmol) and K_2CO_3 (315 mg, 2.28 mmol) as the starting materials. The residue was purified by flash chromatography on silica gel, eluting with hexanes/EtOAc (5:1) to deliver **210** as a colorless oil (47 mg, 48%). ^{1}H NMR (300 MHz, chloroform-d) δ 7.30 (d, *J* = 6.6 Hz, 2H),

6.42 (d, *J* = 9.1 Hz, 1H), 4.41 (s, 1H), 3.33 (t, *J* = 5.4 Hz, 2H), 2.92 (t, *J* = 7.1 Hz, 2H), 2.74 (t, *J* = 6.3 Hz, 3H), 2.64 (s, 3H), 1.94 - 1.90 (m, 2H), 1.50 - 1.45 (m, 2H), 1.38 - 1.29 (m, 2H), 0.90 (t, *J* = 7.2 Hz, 3H). HRMS (ESI^+) calculated for $C_{14}H_{22}N_2O_2S$ $(M+H)^+$ 283.1480, found 283.1496.

***N*-Isobutyl-*N*-methyl-1-(2,2,2-trifluoroacetyl)-1,2,3,4-tetrahydroquinoline-6-sulfonamide.** Same procedure as **195** using *N*-methylisobutylamine (0.05 mL, 0.51 mmol) and **194** (85 mg, 0.26 mmol) as the starting materials. The residue was purified by flash chromatography on silica gel, eluting with hexanes/EtOAc (2:1) to deliver a white solid (37 mg, 37%). ^1H NMR (300 MHz, chloroform-d) δ 7.86 (s, 1H), 7.58 (d, *J* = 7.8 Hz, 2H), 3.90 - 3.84 (m, 2H), 2.97 - 2.92 (m, 2H), 2.81 - 2.71 (m, 5H), 2.16 - 2.09 (m, 2H), 1.90 - 1.83 (m, 2H), 0.95 - 0.90 (m 5H).

***N*-Isobutyl-*N*-methyl-1,2,3,4-tetrahydroquinoline-6-sulfonamide (211).** Same procedure as **30** using *N*-isobutyl-*N*-methyl-1-(2,2,2-trifluoroacetyl)-1,2,3,4-tetrahydroquinoline-6-sulfonamide (36 mg, 0.09 mmol) and K_2CO_3 (251 mg, 1.8 mmol) as the starting materials. The residue was purified by flash chromatography on silica gel, eluting with hexanes/EtOAc (3:1) to deliver **211** as a colorless oil (15 mg, 60%). ^1H NMR (300 MHz, chloroform-d) δ 7.32 (d, *J* = 6.6 Hz, 2H), 6.42 (d, *J* = 9 Hz, 1H), 4.36 (s, 1H), 3.42 - 3.33 (m, 2H), 2.84 - 2.64 (m, 7H), 2.00 - 1.77 (m, 3H), 0.94 (d, *J* = 5.1 Hz, 6H). HRMS (ESI^+) calculated for $C_{14}H_{22}N_2O_2S$ $(M+H)^+$ 283.1480, found 283.1562.

***N*,*N*-Dibutyl-1-(2,2,2-trifluoroacetyl)-1,2,3,4-tetrahydroquinoline-6-sulfonamide.** Same procedure as **195** using dibutylamine (0.13 mL, 0.78 mmol) and **194** (85 mg, 0.26 mmol) as the starting materials. The residue was purified by flash chromatography on silica gel, eluting with hexanes/EtOAc (6:1) to deliver a white solid (55 mg, 50%). ^1H NMR (400 MHz, chloroform-d) δ 7.72 (s, 1H), 7.63 (d, *J* = 7.8 Hz, 2H), 3.85 (t, *J* = 6.4 Hz, 2H), 3.12 - 3.08 (m, 4H), 2.93 (t, *J* =

6.9 Hz, 2H), 2.12 - 2.09 (m, 2H), 1.52 - 1.48 (m, 4H), 1.28 - 1.26 (m, 4H), 0.89 (t, *J* = 7.6 Hz, 6H).

***N*,*N*-Dibutyl-1,2,3,4-tetrahydroquinoline-6-sulfonamide (212).** Same procedure as **30** using *N*,*N*-dibutyl-1-(2,2,2-trifluoroacetyl)-1,2,3,4-tetrahydroquinoline-6-sulfonamide (55 mg, 0.13 mmol) and K_2CO_3 (341 mg, 2.1 mmol) as the starting materials. The residue was purified by flash chromatography on silica gel, eluting with hexanes/EtOAc (3:1) to deliver **212** as a colorless oil (14 mg, 32%). ^{1}H NMR (300 MHz, chloroform-d) δ 7.34 (d, *J* = 6.6 Hz, 2H), 6.41 (d, *J* = 9.0 Hz, 1H), 4.31 (s, 1H), 3.35 (t, *J* = 5.7 Hz, 2H), 3.04 (t, *J* = 7.5 Hz, 4H), 2.76 (t, *J* = 6.3 Hz, 2H), 1.96 - 1.90 (m, 2H), 1.57 - 1.44 (m, 4H), 1.34 - 1.23 (m, 4H), 0.90 (t, *J* = 7.3 Hz, 6H). HRMS (ESI$^+$) calculated for $C_{17}H_{28}N_2O_2S$ $(M+H)^+$ 325.4894, found 325.1957.

1-(6-(Azepan-1-ylsulfonyl)-3,4-dihydroquinolin-1(2*H*)-yl)-2,2,2-trifluoroethanone. Same procedure as **195** using hexamethyleneimine (0.038 mL, 0.33 mmol) and **194** (55 mg, 0.17 mmol) as the starting materials. The residue was purified by flash chromatography on silica gel, eluting with hexanes/EtOAc (3:1) to deliver a white solid (52 mg, 84%). ^{1}H NMR (300 MHz, chloroform-d) δ 7.76 (s, 1H), 7.60 (d, *J* = 7.8 Hz, 2H), 3.87 (t, *J* = 6 Hz, 2H), 3.27 (t, *J* = 5.7 Hz, 4H), 2.94 (t, *J* = 6.9 Hz, 2H), 2.14 - 2.12 (m, 2H), 1.73 - 1.58 (m, 8H).

6-(Azepan-1-ylsulfonyl)-1,2,3,4-tetrahydroquinoline (214). Same procedure as **30** using 1-(6-(azepan-1-ylsulfonyl)-3,4-dihydroquinolin-1(2*H*)-yl)-2,2,2-trifluoroethanone (52 mg, 0.13 mmol) and K_2CO_3 (349 mg, 2.5 mmol) as the starting materials. The residue was purified by flash chromatography on silica gel, eluting with hexanes/EtOAc (5:1) to deliver **214** as an off-white solid (42 mg, 90%). ^{1}H NMR (300 MHz, chloroform-d) δ 7.39 - 7.28 (m, 2H), 6.42 (d, *J* = 9.0 Hz, 1H), 4.15 (s, 1H), 3.33 (t, *J* = 5.4 Hz, 2H), 3.20 (t, *J* = 6.0 Hz, 4H), 2.74 (t, *J* = 6.3 Hz,

2H), 1.97 - 1.85 (m, 2H), 1.75 - 1.63 (m, 4H), 1.58 - 1.54 (m, 4H). HRMS (ESI^+) calculated for $C_{15}H_{22}N_2O_2S$ $(M+H)^+$ 295.4203, found 295.1474.

1-(6-(Azocan-1-ylsulfonyl)-3,4-dihydroquinolin-1(2*H*)-yl)-2,2,2-trifluoroethanone. Same procedure as **195** using heptamethyleneimine (0.038 mL, 0.30 mmol) and **194** (50 mg, 0.15 mmol) as the starting materials. The residue was purified by flash chromatography on silica gel, eluting with hexanes/EtOAc (2:1) to deliver a white solid (52 mg, 87%). ^1H NMR (300 MHz, chloroform-d) δ 7.65 (s, 1H), 7.60 (d, *J* = 7.8 Hz, 2H), 3.86 (t, *J* = 5.7 Hz, 2H), 3.14 (t, *J* = 5.4 Hz, 4H), 2.94 (t, *J* = 6.9 Hz, 2H), 2.15 - 2.09 (m, 2H), 1.73 - 1.63 (m, 10H).

6-(Azocan-1-ylsulfonyl)-1,2,3,4-tetrahydroquinoline (215). Same procedure as **30** using 1-(6-(azocan-1-ylsulfonyl)-3,4-dihydroquinolin-1(2*H*)-yl)-2,2,2-trifluoroethanone (48 mg, 0.12 mmol) and K_2CO_3 (314 mg, 2.3 mmol) as the starting materials. The residue was purified by flash chromatography on silica gel, eluting with hexanes/EtOAc (6:1) to deliver **215** as a white solid (20 mg, 54%). ^1H NMR (400 MHz, chloroform-d) δ 7.37 (d, *J* = 5.6 Hz, 2H), 6.51 (d, *J* = 9.0 Hz, 1H), 3.36 (t, *J* = 5.6 Hz, 2H), 3.10 (t, *J* = 6.0 Hz, 4H), 2.78 (t, *J* = 6.3 Hz, 2H), 1.98 - 1.94 (m, 2H), 1.74 - 1.63 (m, 10H). HRMS (ESI^+) calculated for $C_{16}H_{24}N_2O_2S$ $(M+H)^+$ 309.4469, found 309.1640.

***N*-(Benzo[*d*]thiazol-2-yl)-1-(2,2,2-trifluoroacetyl)-1,2,3,4-tetrahydroquinoline-6-sulfonamide.** Same procedure as **195** using 2-aminobenzothiazole (33 mg, 0.22 mmol) and **194** (52 mg, 0.22 mmol) as the starting materials. The residue was purified by flash chromatography on silica gel, eluting with DCM/EtOAc (1:1) to deliver a white solid (69 mg, 71%). ^1H NMR (300 MHz, CD_3OD) δ 7.78 (d, *J* = 9.6 Hz, 2H), 7.65 (d, *J* = 6.9 Hz, 1H), 7.39 - 7.25 (m, 4H), 3.86 (t, *J* = 5.7, 2H), 2.94 (t, *J* = 6.9 Hz, 2H), 2.09 - 2.00 (m, 2H).

***N*-(Benzo[*d*]thiazol-2-yl)-1,2,3,4-tetrahydroquinoline-6-sulfonamide (220)**. Same procedure as **30** using *N*-(benzo[*d*]thiazol-2-yl)-1-(2,2,2-trifluoroacetyl)-1,2,3,4-tetrahydroquinoline-6-sulfonamide (68 mg, 0.15 mmol) and K_2CO_3 (404 mg, 2.9 mmol) as the staring materials. The residue was purified by flash chromatography on silica gel, eluting with DCM/EtOAc (1:1) to deliver **220** as a white solid (7.3 mg, 15%). ^{1}H NMR (300 MHz, methanol-d4) δ 7.62 (d, *J* = 6.7 Hz, 1H), 7.40 - 7.19 (m, 5H), 6.45 (d, *J* = 7.7 Hz, 1H), 2.74 - 2.70 (m, 2H), 1.88 (t, *J* = 5.7 Hz, 2H), 1.26 - 1.18 (m, 2H). HRMS (ESI$^+$) calculated for $C_{16}H_{15}N_3O_2S_2$ $(M+H)^+$ 346.4471, found 346.0672.

***N*-(6-Methoxybenzo[*d*]thiazol-2-yl)-1-(2,2,2-trifluoroacetyl)-1,2,3,4-tetrahydroquinoline-6-sulfonamide**. Same procedure as **195** using 2-amino-6-methoxybenzothiazole (27 mg, 0.15 mmol) and **194** (50 mg, 0.15 mmol) as the starting materials. The residue was purified by flash chromatography on silica gel, eluting with DCM/acetone (1:1) to deliver a white solid (50 mg, 46%). ^{1}H NMR (300 MHz, acetone-d) δ 7.76 (s, 3H), 7.50 - 7.46 (m, 1H), 3.88 (t, *J* = 5.7 Hz, 2H), 3.84 (s, 3H), 3.14 (t, *J* = 5.4 Hz, 3H), 2.15 - 2.09 (m, 2H).

***N*-(6-Methoxybenzo[*d*]thiazol-2-yl)-1,2,3,4-tetrahydroquinoline-6-sulfonamide (221).** Same procedure as **30** using *N*-(6-methoxybenzo[*d*]thiazol-2-yl)-1-(2,2,2-trifluoroacetyl)-1,2,3,4-tetrahydroquinoline-6-sulfonamide (30 mg, 0.06 mmol) and K_2CO_3 (157 mg, 0.14 mmol) as the starting materials. The residue was purified by flash chromatography on silica gel, eluting with DCM/acetone (2:1) to deliver **221** as a white solid (16 mg, 54%). ^{1}H NMR (300 MHz, methanol-d) δ 7.58 - 7.46 (m, 2H), 7.44 (d, *J* = 7.6 Hz, 1H), 7.16 - 7.10 (m, 1H), 6.80 (d, *J* = 8.0 Hz, 1H), 6.42 (d, *J* = 7.8 Hz, 1H), 3.78 - 3.74 (m, 3H), 3.33 - 3.26 (m, 5H), 2.62 (t, *J* = 5.6 Hz, 2H), 1.92 - 1.86 (m, 2H). HRMS (ESI$^+$) calculated for $C_{17}H_{17}N_3O_3S_2$ $(M+H)^+$ 376.0790, found 376.0792.

***N*-(6-Hydroxyhexyl)-1-(2,2,2-trifluoroacetyl)-1,2,3,4-tetrahydroquinoline-6-sulfonamide.** 6-Aminohexanol (61 mg, 0.51 mmol) was added to a stirred solution of **194** (60 mg, 0.18 mmol) and pyridine (0.043 mL, 0.54 mmol) in DCM (1.4 mL). The reaction mixture was stirred at rt for 1 h, and H_2O (3 mL) was added. The organic layer was extracted with DCM (4 mL), the aqueous layer was further washed with DCM (3 x 4 mL). The combined organic layers were dried over $MgSO_4$, filtered, and concentrated. The compound was obtained as an oil (76 mg, 78%) and was used without further purification. ^{1}H NMR (400 MHz, chloroform-d) δ 7.80 (s, 1H), 7.66 (d, *J* = 6.4 Hz, 2H), 5.42 (s, 1H), 3.84 (t, *J* = 6.2 Hz, 2H), 3.60 - 3.57 (m, 2H), 2.93 - 2.90 (m, 4H), 2.12 - 2.04 (m, 2H), 1.54 - 1.39 (m, 8H).

***N*-(6-Hydroxyhexyl)-1,2,3,4-tetrahydroquinoline-6-sulfonamide (224)**. Same procedure as **30** using *N*-(6-hydroxyhexyl)-1-(2,2,2-trifluoroacetyl)-1,2,3,4-tetrahydroquinoline-6-sulfonamide (70 mg, 0.17 mmol) and K_2CO_3 (450 mg, 3.26 mmol) as the starting materials. The residue was purified by flash chromatography on silica gel, eluting with 5% MeOH in DCM to deliver **224** as a light yellow oil (42 mg, 79%). ^{1}H NMR (400 MHz, chloroform-d) δ 7.37 (d, *J* = 6.4 Hz, 2H), 6.42 (d, *J* = 9.1 Hz, 1H), 4.71 (t, *J* = 6.2 Hz, 1H), 3.56 (t, *J* = 6.6 Hz, 2H), 3.32 (t, *J* = 6.0 Hz, 2H), 2.85 (q, *J* = 6.8 Hz, 2H), 2.73 (t, *J* = 6.3 Hz, 2H), 2.04 - 1.87 (m, 2H), 1.54 - 1.39 (m, 4H), 1.33 - 1.18 (m, 4H). HRMS (ESI^+) calculated for $C_{15}H_{24}N_2O_3S$ $(M+Na)^+$ 335.1504, found 335.1398.

***N*-(6-aminohexyl)-1,2,3,4-tetrahydroquinoline-6-sulfonamide (225)**. Same procedure as **195** using 1,6-diaminohexane (105 mg, 0.91 mmol) and **194** (50 mg, 0.15 mmol) as the starting materials. The residue was purified by flash chromatography on silica gel, eluting with DCM/MeOH 5% to deliver **225** as a colorless oil (13 mg, 28%). ^{1}H NMR (300 MHz, chloroform-d) δ 7.44 - 7.35 (m, 2H), 6.42 (d, *J* = 9.0 Hz, 1H), 4.42 (s, 2H), 3.33 (d, *J* = 5.4 Hz,

2H), 2.88 (t, *J* = 7.1 Hz, 2H), 2.76 (t, *J* = 6.1 Hz, 2H), 2.66 - 2.62 (m, 2H), 1.96 - 1.88 (m, 2H), 1.58 - 1.24 (m, 8H). HRMS (ESI^+) calculated for $C_{15}H_{25}N_3O_2S$ $(M+H)^+$ 312.1746, found 312.1833.

***N*,*N*'-(hexane-1,6-diyl)bis(1,2,3,4-tetrahydroquinoline-6-sulfonamide) (226)**. Same procedure as **195** using 1,6-diaminohexane (53 mg, 0.45 mmol) and **194** (50 mg, 0.15 mmol. The residue was purified by flash chromatography on silica gel, eluting with 5% MeOH in DCM to deliver **226** as a white oil (17 mg, 20%). ^1H NMR (300 MHz, chloroform-d) δ 7.47 - 7.34 (m, 4H), 6.43 (d, *J* = 9.1 Hz, 2H), 4.43 (s, 2H), 4.34 (t, *J* = 6.3 Hz, 2H), 3.62 (t, *J* = 5.4 Hz, 4H), 2.86 (q, *J* = 6.6 Hz, 4H), 2.76 (t, *J* = 6.2 Hz, 4H), 1.92 (t, *J* = 6.2 Hz, 4H), 1.60 (s, 2H), 1.37 (t, *J* = 6.5 Hz, 2H), 1.26 - 1.11 (m, 2H). HRMS (ESI^+) calculated for $C_{24}H_{34}N_4O_2S_2$ $(M+H)^+$ 507.2100, found 507.2066.

***N*-Phenyl-1,2,3,4-tetrahydroquinoline-6-sulfonamide (228)**. Same procedure as **30** using *N*-phenyl-1-(2,2,2-trifluoroacetyl)-1,2,3,4-tetrahydroquinoline-6-sulfonamide (223 mg, 0.58 mmol) and K_2CO_3 (1.5 g, 11.5 mmol) as the starting materials. The residue was purified by flash chromatography on silica gel, eluting with hexanes/EtOAc (2:1) to deliver **228** as a yellow solid (150 mg, 90%). ^1H NMR (300 MHz, chloroform-d) δ 7.35 - 7.32 (m, 2H), 7.26 - 7.20 (m, 2H), 7.08 - 7.04 (m, 3H), 6.88 (s, 1H), 6.35 (d, *J* = 9.3 Hz, 1H), 3.32 (t, *J* = 5.4 Hz, 2H), 2.68 (t, *J* = 6.6 Hz, 2H), 1.91 - 1.82 (m, 2H). The analytical data is in agreement with literature reports.[98]

***N*-(Naphthalen-2-yl)-1-(2,2,2-trifluoroacetyl)-1,2,3,4-tetrahydroquinoline-6-sulfonamide.** 2-Naphtylamine (15 mg, 0.11 mmol) was added to a stirred solution of **194** (35 mg, 0.11 mmol) in pyridine (0.3 mL). The reaction mixture was refluxed overnight, and allowed to cool to room temperature. DCM (4 mL) and H_2O (3 mL) were added, the organic layer was washed with 1 M

HCl (3 mL), H_2O (3 x 4 mL) and brine (3 mL), dried over $MgSO_4$, filtered, and concentrated. The residue was purified by flash chromatography on silica gel, eluting with hexanes/EtOAc (3:1) to deliver a colorless oil (38 mg, 88%). ^{1}H NMR (300 MHz, chloroform-d) δ 7.67 - 7.65 (m, 5H), 7.56 (s, 1H), 7.45 - 7.36 (m, 3H), 7.38 - 7.25 (m, 1H), 3.77 (t, *J* = 6.0 Hz, 2H), 2.78 (t, *J* = 6.6 Hz, 2H), 2.05 - 1.98 (m, 2H).

***N*-(Naphthalen-2-yl)-1,2,3,4-tetrahydroquinoline-6-sulfonamide (229)**. Same procedure as **30** using *N*-(naphthalen-2-yl)-1-(2,2,2-trifluoroacetyl)-1,2,3,4-tetrahydroquinoline-6-sulfonamide (38 mg, 0.09 mmol) and K_2CO_3 (230 mg, 1.6 mmol) as the starting materials. The residue was purified by flash chromatography on silica gel, eluting with hexanes/EtOAc (2:1) to deliver **229** as a white solid (22 mg, 76%). ^{1}H NMR (300 MHz, chloroform-d) δ 7.75 - 7.69 (m, 3H), 7.53 (s, 1H), 7.45 - 7.40 (m, 3H), 7.38 - 7.25 (m, 1H), 7.02 (s, 1H), 6.44 - 6.39 (m, 1H), 3.30 (t, *J* = 6.0 Hz, 2H), 2.65 (t, *J* = 6.6 Hz, 2H), 1.90 - 1.82 (m, 2H). HRMS (ESI^+) calculated for $C_{19}H_{18}N_2O_2S$ $(M+H)^+$ 339.4314, found 339.1139.

***N*-(Naphthalen-1-yl)-1-(2,2,2-trifluoroacetyl)-1,2,3,4-tetrahydroquinoline-6-sulfonamide.** Same procedure as *N*-(naphthalen-2-yl)-1-(2,2,2-trifluoroacetyl)-1,2,3,4-tetrahydroquinoline-6-sulfonamide using 1-naphtylamine (0.027 mL, 0.21 mmol) and **194** (70 mg, 0.21 mmol) as the starting materials. The residue was purified by flash chromatography on silica gel, eluting with hexanes/EtOAc (2:1) to deliver a white solid (31 mg, 70%). ^{1}H NMR (300 MHz, chloroform-d) δ 7.88 - 7.75 (m, 3H), 7.50 - 7.52 (m, 1H), 7.48 - 7.44 (m, 5H), 6.73 (s, 1H), 3.78 (t, *J* = 5.7 Hz, 2H), 2.71 (t, *J* = 6.3 Hz, 2H), 2.01 - 1.88 (m, 2H).

***N*-(Naphthalen-1-yl)-1,2,3,4-tetrahydroquinoline-6-sulfonamide (230)**. Same procedure as **30** using *N*-(naphthalen-1-yl)-1-(2,2,2-trifluoroacetyl)-1,2,3,4-tetrahydroquinoline-6-sulfonamide

(31 mg, 0.07 mmol) and K_2CO_3 (187 mg, 1.35 mmol) as the staring materials. The residue was purified by flash chromatography on silica gel, eluting with hexanes/EtOAc (4:1) to deliver **230** as a white solid (23 mg, 96%). ^{1}H NMR (300 MHz, chloroform-d) δ 7.88 - 7.79 (m, 2H), 7.66 (t, *J* = 4.8 Hz, 1H), 7.48 - 7.44 (m, 2H), 7.36 - 7.32 (m, 3H), 7.28 - 7.26 (m, 1H), 6.73 (s, 1H), 6.40 (d, *J* = 8.7 Hz, 1H), 3.30 (t, *J* = 5.7 Hz, 2H), 2.65 (t, *J* = 6.3 Hz, 2H), 1.88 - 1.84 (m, 2H). HRMS (ESI⁻) calculated for $C_{19}H_{18}N_2O_2S$ $(M-H)^-$ 337.4155, found 337.1021.

***N*-(9,10-Dioxo-9,10-dihydroanthracen-1-yl)-1-(2,2,2-trifluoroacetyl)-1,2,3,4-tetrahydroquinoline-6-sulfonamide.** Same procedure as *N*-(naphthalen-2-yl)-1-(2,2,2-trifluoroacetyl)-1,2,3,4-tetrahydroquinoline-6-sulfonamide using 1-aminoanthraquinone (54 mg, 0.24 mmol) and **194** (80 mg, 0.24 mmol) as the starting materials. The residue was purified by flash chromatography on silica gel, eluting with hexanes/EtOAc (3:1) to deliver an orange solid (7 mg, 10%). ^{1}H NMR (300 MHz, acetone-d) δ 8.37 - 8.27 (m, 1H), 8.26 - 8.19 (m, 1H), 8.02 (d, *J* = 8.0 Hz, 1H), 7.95 - 7.85 (m, 3H), 7.82 (d, *J* = 8.4 Hz, 1H), 7.45 (s, 2H), 6.45 (d, *J* = 7.9 Hz, 1H), 3.27 (t, *J* = 6.0 Hz, 2H), 2.69 (t, *J* = 5.9 Hz, 2H), 1.82 - 1.76 (m, 2H).

***N*-(9,10-Dioxo-9,10-dihydroanthracen-1-yl)-1,2,3,4-tetrahydroquinoline-6-sulfonamide (231)**. Same procedure as **30** using *N*-(9,10-dioxo-9,10-dihydroanthracen-1-yl)-1-(2,2,2-trifluoroacetyl)-1,2,3,4-tetrahydroquinoline-6-sulfonamide (6.5 mg, 0.01 mmol) and K_2CO_3 (33 mg, 0.24 mmol) as the starting materials. The residue was purified by flash chromatography on silica gel, eluting with hexanes/EtOAc (2:1) to deliver **231** as an orange solid (4 mg, 78%). ^{1}H NMR (300 MHz, acetone-d) δ 8.37 - 8.27 (m, 1H), 8.26 - 8.19 (m, 1H), 8.02 (d, *J* = 8.0 Hz, 1H), 7.95 - 7.85 (m, 2H), 7.82 (d, *J* = 8.4 Hz, 1H), 7.45 (s, 3H), 6.45 (d, *J* = 7.9 Hz, 1H), 3.27 (t, *J* =

6.0 Hz, 2H), 2.69 (t, *J* = 5.9 Hz, 2H), 1.82 - 1.76 (m, 2H). HRMS (ESI^+) calculated for $C_{23}H_{18}N_2O_4S$ $(M+H)^+$ 419.4730, found 419.1080.

***N*-(4-nitrophenyl)-1-(2,2,2-trifluoroacetyl)-1,2,3,4-tetrahydroquinoline-6-sulfonamide.** Same procedure as *N*-(naphthalen-2-yl)-1-(2,2,2-trifluoroacetyl)-1,2,3,4-tetrahydroquinoline-6-sulfonamide using 4-nitroaniline (211 mg, 1.52 mmol) and **194** (500 mg, 1.52 mmol) as the starting materials. The residue was purified by flash chromatography on silica gel, eluting with DCM/acetone (8:1) to deliver a yellow solid (598 mg, 92%). ^{1}H NMR (300 MHz, acetone-d6) δ 8.16 (d, *J* = 9.3 Hz, 2H), 7.90 - 7.70 (m, 3H), 7.47 (d, *J* = 9.0 Hz, 2H), 3.90 (t, *J* = 5.2 Hz, 2H), 2.98 (t, *J* = 6.2 Hz, 2H), 1.89 - 1.79 (m, 2H).

***N*-(4-Nitrophenyl)-1,2,3,4-tetrahydroquinoline-6-sulfonamide (234)**. Same procedure as **30** using *N*-(4-nitrophenyl)-1-(2,2,2-trifluoroacetyl)-1,2,3,4-tetrahydroquinoline-6-sulfonamide (598 mg, 1.39 mmol) and K_2CO_3 (3.6 g, 26.5 mmol) as the staring materials. The residue was purified by flash chromatography on silica gel, eluting with hexanes/EtOAc (1:1) to deliver **234** as a yellow solid (455 mg, 98%). ^{1}H NMR (300 MHz, acetone-d6) δ 8.14 (d, *J* = 9.3 Hz, 2H), 7.42 (dd, *J* = 1.5, 7.8 Hz, 4H), 6.50 (d, *J* = 9.0 Hz, 1H), 6.02 (s, 1H), 3.36 - 3.27 (m, 2H), 2.71 (t, *J* = 6.2 Hz, 2H), 1.89 - 1.79 (m, 2H).

***N*-(4-(*tert*-Butyl)phenyl)-1-(2,2,2-trifluoroacetyl)-1,2,3,4-tetrahydroquinoline-6-sulfonamide.** Same procedure as *N*-(naphthalen-2-yl)-1-(2,2,2-trifluoroacetyl)-1,2,3,4-tetrahydroquinoline-6-sulfonamide using 4-*tert*-butylaniline (0.029 mL, 0.18 mmol) and **194** (60 mg, 0.18 mmol) as the starting materials. The residue was purified by flash chromatography on silica gel, eluting with hexanes/EtOAc (4:1) to deliver a yellow oil (72 mg, 90%). ^{1}H NMR (300 MHz, chloroform-d) δ 8.63 (d, *J* = 8.8 Hz, 1H), 7.73 - 7.71 (m, 2H), 7.61 - 7.59 (m, 1H), 7.31 -

7.23 (m, 1H), 7.01 (d, *J* = 8.6 Hz, 2H), 3.82 (t, *J* = 6.4 Hz, 2H), 2.81 (t, *J* = 6.2 Hz, 2H), 1.86 - 1.80 (m, 2H), 1.25 (s, 9H).

***N*-(4-(*tert*-Butyl)phenyl)-1,2,3,4-tetrahydroquinoline-6-sulfonamide (236).** Same procedure as **30** using *N*-(4-(*tert*-butyl)phenyl)-1-(2,2,2-trifluoroacetyl)-1,2,3,4-tetrahydroquinoline-6-sulfonamide (72 mg, 0.16 mmol) and K_2CO_3 (420 mg, 3.04 mmol) as the starting materials. The residue was purified by flash chromatography on silica gel, eluting with hexanes/EtOAc (1:1) to deliver **236** as a light yellow solid (39 mg, 71%). ^{1}H NMR (300 MHz, chloroform-d) δ 7.34 (d, *J* = 8.8 Hz, 2H), 7.22 (d, *J* = 8.6 Hz, 2H), 7.03 - 6.96 (m, 3H), 6.31 (d, *J* = 8.3 Hz, 1H), 3.27 (t, *J* = 6.4 Hz, 2H), 2.63 (t, *J* = 6.2 Hz, 2H), 1.86 - 1.80 (m, 2H), 1.24 (s, 9H). HRMS (ESI$^+$) calculated for $C_{19}H_{24}N_2O_2S$ $(M+H)^+$ 345.4795, found 345.1644.

***N*-(4-Acetylphenyl)-1-(2,2,2-trifluoroacetyl)-1,2,3,4-tetrahydroquinoline-6-sulfonamide.** Same procedure as *N*-(naphthalen-2-yl)-1-(2,2,2-trifluoroacetyl)-1,2,3,4-tetrahydroquinoline-6-sulfonamide using 4-aminoacetophenone (21 mg, 0.15 mmol) and **194** (50 mg, 0.15 mmol) as the starting materials. The residue was purified by flash chromatography on silica gel, eluting with hexanes/EtOAc (2:1) to deliver a yellow solid (45 mg, 71%). ^{1}H NMR (300 MHz, chloroform-d) δ 7.85 (d, *J* = 8.8 Hz, 3H), 7.69 - 7.7.67 (m, 2H), 7.15 (d, *J* = 8.8 Hz, 2H), 3.81 (t, *J* = 5.6 Hz, 2H), 2.87 (t, *J* = 6.0 Hz, 2H), 2.51 (s, 3H), 1.27 - 1.22 (m, 2H).

***N*-(4-Acetylphenyl)-1,2,3,4-tetrahydroquinoline-6-sulfonamide (237).** Same procedure as **30** using *N*-(4-acetylphenyl)-1-(2,2,2-trifluoroacetyl)-1,2,3,4-tetrahydroquinoline-6-sulfonamide (45 mg, 0.11 mmol) and K_2CO_3 (278 mg, 2.01 mmol) as the starting materials. The residue was purified by flash chromatography on silica gel, eluting with hexanes/EtOAc (1:1) to give **237** as a light orange solid (45 mg, 71%). ^{1}H NMR (400 MHz, chloroform-d) δ 7.81 (d, *J* = 8.8 Hz, 2H),

7.68 (s, 1H), 7.45 - 7.42 (m, 2H), 7.15 (d, *J* = 8.8 Hz, 2H), 6.35 (d, *J* = 9.2 Hz, 1H), 3.31 (t, *J* = 5.6 Hz, 2H), 2.68 (t, *J* = 6.0 Hz, 2H), 2.51 (s, 3H), 1.86 - 1.82 (m, 2H). HRMS (ESI^+) calcualted for $C_{17}H_{18}N_2O_3S$ $(M+H)^+$ 331.4094, found 331.1087.

((4a*R*,8a*S*)-Octahydroquinolin-1(2*H*)-yl)(quinolin-6-yl)methanone (239). TEA (0.16 mL, 1.15 mL), HOBt (171 mg, 1.26 mmol), and EDCI (242 mg, 1.26 mmol) were added to a stirred solution of 6-quinolinecarboxylic acid (200 mg, 1.15 mmol) in DCM (5 mL) at 0 °C. The suspension was slowly allowed to warm to rt and stirred for 1 h. *trans*-Decahydroquinoline (176 mg, 1.26 mmol) was added to the solution and the resulting mixture was stirred overnight at rt. The solvent was removed under vacuum and the residue was purified by flash chromatography on silica gel, eluting with 10% MeOH in DCM to deliver **239** as an orange solid (179 mg, 53%). ^{1}H NMR (300 MHz, chloroform-d) δ 8.87 - 8.85 (m, 1H), 8.16 - 8.02 (m, 2H), 7.82 (d, *J* = 1.9 Hz, 1H), 7.66 (dd, *J* = 8.6, 1.9 Hz, 1H), 7.39 - 7.34 (m, 1H), 3.53 - 3.48 (m, 1H), 3.40 - 3.31 (m, 2H), 2.27 - 2.25 (m, 1H), 1.78 - 1.48 (m, 4H), 1.39 - 1.02 (m, 6H).

***((4R, 8S)*-Octahydroquinolin-1(2*H*)-yl)(1,2,3,4-tetrahydroquinolin-6-yl)methanone (240).** Pd/C (10%, 40 mg) was added to a solution of **239** (66 mg, 0.22 mmol) and ammonium formate (222 mg, 3.52 mmol) in MeOH (1 mL). The reaction mixture was heated to reflux for 4 h. After allowing the mixture to cool down to rt, it was filtered through a pad of silica, washed with EtOAc (4 x 4 mL) and MeOH (2 x 4 mL), and the filtrate was concentrated. The residue was purified by flash chromatography on silica gel, eluting with hexanes:EtOAc (5:1) to afford **240** as a white solid (31 mg, 48%). ^{1}H NMR (300 MHz, chloroform-d) δ 7.09 - 6.98 (m, 2H), 6.37 (d, *J* = 8.0 Hz, 1H), 4.19 - 4.00 (m, 1H), 3.55 - 3.26 (m, 5H), 2.73 (t, *J* = 6.4 Hz, 2H), 2.25 - 2.22 (m, 1H), 1.98 - 1.83 (m, 2H), 1.81 - 1.50 (m, 6H), 1.50 - 1.33 (m, 2H), 1.36 - 0.96 (m, 4H).

2-Phenylisoindoline-1,3-dione (241). A solution of phthalic anhydride (486 mg, 3.28 mmol) and aniline (0.3 mL, 3.28 mmol) in DMF (6.5 mL) was irradiated under microwave conditions at 300 W for 1 h. The reaction mixture was poured into crushed ice (4 mL) and the precipitate was isolated by filtration, washed with cold H_2O (2 x 6 mL), and dried under vacuum affording **241** as a light brown solid (587 mg, 80%). ^{1}H NMR (300 MHz, chloroform-d) δ 8.02 - 7.94 (m, 2H), 7.81 - 7.78 (m, 2H), 7.57 - 7.38 (m, 5H). The analytical data is in agreement with literature reports.[236]

4-(1,3-Dioxoisoindolin-2-yl)benzene-1-sulfonyl chloride (242). Same procedure as **194** using **241** (200 mg, 0.89 mmol) as the starting material delivered **242** as a white solid (178 mg, 62%). ^{1}H NMR (300 MHz, DMSO-d6) δ 8.00 - 7.86 (m, 4H), 7.69 (dd, *J* = 6.6, 1.8 Hz, 2H), 7.43 - 7.35 (m, 2H). The analytical data is in agreement with literature reports.[237]

2-(4-(((4a*R*,8a*S*)-Octahydroquinolin-1(2*H*)-yl)sulfonyl)phenyl)isoindoline-1,3-dione (243). TEA (0.45 mL, 3.24 mmol) was added to a stirred solution of *trans*-decahydroquinoline (152 mg, 1.09 mmol) and **242** (175 mg, 0.54 mmol) in DCM (2.5 mL) at 0 °C. The reaction mixture was allowed to warm to rt and stirred overnight. The reaction mixture was diluted with DCM (6 mL), washed with 1 M HCl (4 mL), H_2O (2 x 5 mL) and brine (5 mL), dried over Na_2SO_4, filtered, and concentrated. The residue was purified by flash chromatography on silica gel, eluting with DCM/EtOAc (5:1) to deliver **243** as a white solid (145 mg, 63%). ^{1}H NMR (400 MHz, chloroform-d) δ 8.04 - 7.97 (m, 2H), 7.96 - 7.89 (m, 2H), 7.88 - 7.81 (m, 2H), 7.69 (m, 2H), 4.15 (d, *J* = 12.8 Hz, 2H), 2.79 (m, 2H), 2.61 - 2.51 (m, 2H), 2.24 - 2.20 (m, 2H), 1.82 - 1.58 (m, 4H), 1.48 - 1.33 (m, 2H), 1.30 - 0.91 (m, 2H). HRMS (ESI^+) calcd for $C_{23}H_{24}N_2O_4S$ $(M+H)^+$ 425.5206, found 425.1547.

4-(((*4R, 8S*)-Octahydroquinolin-1(2*H*)-yl)sulfonyl)aniline (244). Hydrazine monohydrate (0.1 mL, 3.25 mmol) was added to a solution of **243** (55 mg, 0.13 mmol) in MeOH (1 mL). The resulting solution was heated to 55 °C for 3 h. After allowing the mixture to cool down to rt, the precipitate was collected by filtration and washed with MeOH (2 x 4 mL). The filtrate was evaporated down, and the residue was suspended in DCM (4 mL), washed with H_2O (2 x 4 mL), $NaHCO_3$ (4 mL) and brine (4 mL), dried over Na_2SO_4, filtered, and concentrated to afford **244** as a white solid (26 mg, 69%). ^{1}H NMR (300 MHz, chloroform-d) δ 7.55 - 7.50 (m, 2H), 6.78 - 6.60 (m, 2H), 4.15 (s, 2H), 4.06 - 4.01 (m, 1H), 2.70 - 2.65 (m, 1H), 2.45 - 2.23 (m, 2H), 1.86 - 1.32 (m, 6H), 1.20 - 0.82 (m, 6H). HRMS (ESI^+) calcd for $C_{15}H_{22}N_2O_2S$ $(M+H)^+$ 295.4203, found 295.1488.

***N*-(4-(*tert*-butyl)phenyl)-4-(1,3-dioxoisoindolin-2-yl)benzenesulfonamide.** Same procedure as *N*-(naphthalen-2-yl)-1-(2,2,2-trifluoroacetyl)-1,2,3,4-tetrahydroquinoline-6-sulfonamide using *tert*-butylaniline (0.049 mL, 0.31 mmol) and **242** (100 mg, 0.31 mmol) as the starting materials. The residue was purified by flash chromatography on silica gel, eluting with DCM/EtOAc (3:1) to deliver an oil (81 mg, 60%). ^{1}H NMR (300 MHz, chloroform-d) δ 7.96 - 7.94 (m, 4H), 7.82 - 7.80 (m, 2H), 7.63 (d, *J* = 8.5 Hz, 2H), 7.27 - 7.24 (m, 2H), 7.22 - 7.20 (m, 2H), 6.31 (d, *J* = 8.3 Hz, 1H), 1.24 (s, 9H).

4-Amino-*N*-(4-(*tert*-butyl)phenyl)benzenesulfonamide (245). Same protocol as **244** using *N*-(4-(*tert*-butyl)phenyl)-4-(1,3-dioxoisoindolin-2-yl)benzenesulfonamide (81 mg, 0.19 mmol) as the starting material. The residue was purified by flash chromatography on silica gel, eluting with hexanes/EtOAc (1:1) to deliver 245 as a white solid (31 mg, 57%). ^{1}H NMR (300 MHz, chloroform-d) δ 7.54 (d, *J* = 8.6 Hz, 2H), 7.23 (d, *J* = 8.5 Hz, 2H), 6.97 (d, *J* = 8.5 Hz, 2H), 6.31

(t, *J* = 8.3 Hz, 2H), 1.24 (s, 9H). LRMS (ESI^+) calcd for $C_{16}H_{20}N_2O_2S$ $(M+Na)^+$ 327.1, found 327.1.

2,2,2-Trifluoro-1-(indolin-1-yl)ethanone. Same procedure as **193** using indoline (0.56 mL, 5.03 mmol) as the starting material. The compound was obtained as a white solid (1.1 g, 100%). ^1H NMR (300 MHz, chloroform-d) δ 8.20 (d, *J* = 8.6 Hz, 1H), 7.33 - 7.21 (m, 2H), 7.16 (d, *J* = 7.6 Hz, 1H), 4.28 (t, *J* = 8.2 Hz, 2H), 3.26 (t, *J* = 8.2 Hz, 2H). The analytical data is in agreement with literature reports.[238]

1-(2,2,2-Trifluoroacetyl)indoline-5-sulfonyl chloride. Same procedure as **194** using 2,2,2-trifluoro-1-(indolin-1-yl)ethanone (300 mg, 1.87 mmol) as the starting material. The residue was purified by flash chromatography on silica gel, eluting with hexanes/EtOAc (6:1) to deliver a brown solid (253 mg, 43%). ^1H NMR (300 MHz, chloroform-d) δ 8.42 (d, *J* = 8.6 Hz, 1H), 8.05 - 7.92 (m, 2H), 4.43 (t, *J* = 8.4 Hz, 2H), 3.40 (t, *J* = 8.5 Hz, 2H).

(4a*R*,8a*S*)-1-(Indolin-5-ylsulfonyl)decahydroquinoline (246). Same procedure as **30** using 1-(2,2,2-trifluoroacetyl)indoline-5-sulfonyl chloride (43 mg, 0.10 mmol) and K_2CO_3 (270 mg, 1.95 mmol) as the starting materials. The residue was purified by flash chromatography on silica gel, eluting with hexanes/EtOAc (2:1) to deliver **246** as a white solid (27 mg, 82%). ^1H NMR (400 MHz, chloroform-d) δ 7.43 (d, *J* = 8.6 Hz, 2H), 6.56 (d, *J* = 8.8 Hz, 1H), 4.19 (s, 1H), 4.09 - 3.99 (m, 1H), 3.66 (t, *J* = 8.6 Hz, 2H), 3.06 (t, *J* = 8.6 Hz, 2H), 2.73 - 2.62 (m, 1H), 2.45 - 2.26 (m, 2H), 1.74 - 1.72 (m, 1H), 1.70 - 1.37 (m, 6H), 1.33 - 1.04 (m, 2H), 1.03 - 0.85 (m, 3H). HRMS (ESI^+) calcd for $C_{17}H_{24}N_2O_2S$ $(M+H)^+$ 321.4576, found 321.1647.

1-Methyl-6-(((*4R,8S*)-octahydroquinolin-1(2*H*)-yl)sulfonyl)-1,2,3,4-tetrahydroquinoline (249). Sodium cyanoborohydride (165 mg, 2.63 mmol) and formaldehyde (37% in aqueous

solution, 0.11 mL) were added to a solution of **30** (24 mg, 0.07 mmol) in MeOH (0.5 mL). The reaction mixture was stirred at rt for 1 h. The solvent was removed under vacuum, the residue was suspended in EtOAc (6 mL), washed with H_2O (2 x 5 mL), $NaHCO_3$ (4 mL) and brine (4 mL), dried over Na_2SO_4, filtered, and concentrated. The residue was purified by flash chromatography on silica gel, eluting with hexanes/EtOAc (4:1) to give **249** as a colorless oil (6 mg, 25%). ^{1}H NMR (300 MHz, chloroform-d) δ 7.06 - 6.81 (m, 3H), 4.16 - 4.00 (m, 1H), 3.30 - 3.26 (m, 2H), 3.29 (s, 3H), 2.78 (t, *J* = 6.3 Hz, 2H), 2.74 - 2.62 (m, 1H), 2.52 - 2.30 (m, 2H), 2.04 - 1.95 (m, 2H), 1.82 - 1.35 (m, 6H), 1.34 - 1.07 (m, 4H), 1.08 - 0.82 (m, 2H). LRMS (ESI$^+$) calcd for $C_{19}H_{28}N_2O_2S$ $(M+H)^+$ 349.19, found 349.

1-Allyl-6-(((*4R,8S*)-octahydroquinolin-1(2*H*)-yl)sulfonyl)-1,2,3,4-tetrahydroquinoline (250). Same procedure as **252** using **30** (40 mg, 0.12 mmol) and allyl bromide (0.016 mL, 0.18 mmol) as the starting materials. The residue was purified by flash chromatography on silica gel, eluting with hexanes/EtOAc (3:1) to afford **250** as a white solid (30 mg, 68%). ^{1}H NMR (400 MHz, chloroform-d) δ 7.38 (dd, *J* = 8.8, 2.4 Hz, 1H), 7.29 (d, *J* = 2.4 Hz, 1H), 6.48 (d, *J* = 8.8 Hz, 1H), 5.81 - 5.77 (m, 1H), 5.21 - 5.11 (m, 2H), 4.10 - 4.03 (m, 1H), 3.95 (t, *J* = 5.6 Hz, 2H), 2.76 (t, *J* = 6.0 Hz, 2H), 2.67 - 2.59 (m, 1H), 2.42 - 2.30 (m, 2H), 1.96 (t, *J* = 8.7 Hz, 2H), 1.89 - 1.81 (m, 1H), 1.80 - 1.49 (m, 8H), 1.21 - 1.08 (m, 2H), 1.02 - 0.88 (m, 2H). LRMS (ESI$^+$) calcd for $C_{21}H_{30}N_2O_2S$ $(M+H)^+$ 375.21, found 375.2.

6-(((4a*R*,8a*S*)-Octahydroquinolin-1(2*H*)-yl)sulfonyl)-1-(prop-2-yn-1-yl)-1,2,3,4-tetrahydroquinoline (251). Same procedure as **252** using **30** (40 mg, 0.12 mmol) and propargyl bromide (0.02 mL, 0.18 mmol, 80% solution in toluene) as the starting materials. The residue was purified by flash chromatography on silica gel, eluting with hexanes/EtOAc (3:1) to afford

251 as a white solid (11 mg, 25%). ^{1}H NMR (300 MHz, chloroform-d) δ 7.47 (dd, *J* = 8.7, 2.3 Hz, 1H), 7.38 - 7.31 (m, 1H), 6.70 (d, *J* = 8.7 Hz, 1H), 4.12 - 3.98 (m, 3H), 3.41 (t, *J* = 6.7 Hz, 2H), 2.78 (t, *J* = 6.3 Hz, 2H), 2.71 - 2.60 (m, 1H), 2.44 - 2.26 (m, 2H), 2.21 (t, *J* = 2.4 Hz, 1H), 2.06 - 1.95 (m, 2H), 1.80 - 1.54 (m, 8H), 1.32 - 1.10 (m, 2H), 1.03 - 0.85 (m, 2H). HRMS (ESI$^+$) calcd for $C_{21}H_{28}N_2O_2S$ $(M+H)^+$ 373.5322, found 373.1959.

1-Butyl-6-(((*4R,8S*)-octahydroquinolin-1(2*H*)-yl)sulfonyl)-1,2,3,4-tetrahydroquinoline (252). DIPEA (0.028 mL, 0.16 mmol) and bromobutane (0.018 mL, 0.16 mmol) were added to a solution of **30** (37 mg, 0.11 mmol) in DMF (0.2 mL). The mixture was heated to reflux for 3 h. The reaction mixture was allowed to cool down to rt and diluted with Et_2O (5 mL), washed with H_2O (3 x 5 mL) and brine (4 mL), dried over Na_2SO_4, filtered, and concentrated. The residue was purified by flash chromatography on silica gel, eluting with hexanes/EtOAc (4:1) to give **252** as a white solid (13 mg, 31%). ^{1}H NMR (400 MHz, chloroform-d) δ 7.40 (dd, *J* = 8.8, 2.5 Hz, 1H), 7.28 (d, *J* = 2.4 Hz, 1H), 6.50 (d, *J* = 8.8 Hz, 1H), 4.08 - 4.00 (m, 1H), 3.35 (t, *J* = 5.6 Hz, 2H), 3.28 (t, *J* = 8.0 Hz, 2H), 2.75 (t, *J* = 6.3 Hz, 2H), 2.70 - 2.58 (m, 1H), 2.43 - 2.32 (m, 2H), 1.96 - 1.80 (m, 2H), 1.76 (d, *J* = 6.9 Hz, 1H), 1.70 - 1.50 (m, 8H), 1.49 - 1.30 (m, 3H), 1.30 - 1.06 (m, 3H), 1.03 - 0.90 (m, 3H). HRMS (ESI$^+$) calcd for $C_{22}H_{34}N_2O_2S$ $(M+H)^+$ 391.24, found 391.2.

1-Benzyl-6-(((*4R,8S*)-octahydroquinolin-1(2*H*)-yl)sulfonyl)-1,2,3,4-tetrahydroquinoline (253). K_2CO_3 (25 mg, 0.18 mmol) and benzyl chloride (0.021 mL, 0.18 mmol) were added to a solution of **30** (40 mg, 0.12 mmol) in DMF (0.1 mL). The resulting mixture was heated to reflux for 4 h. The reaction mixture was allowed to cool down to rt and diluted with Et_2O (5 mL), washed with H_2O (3 x 5 mL) and brine (4 mL), dried over Na_2SO_4, filtered, and concentrated.

The residue was purified by flash chromatography on silica gel, eluting with hexanes/EtOAc (3:1) to deliver **253** as a white solid (10 mg, 21%). ^{1}H NMR (400 MHz, chloroform-d) δ 7.36 - 7.26 (m, 5H), 7.22 (d, *J* = 6.8 Hz, 2H), 6.47 (d, *J* = 6.8 Hz, 1H), 4.55 (s, 2H), 4.09 - 3.99 (m, 1H), 3.42 (t, *J* = 6.0 Hz, 2H), 2.84 (t, *J* = 6.3 Hz, 2H), 2.83 - 2.65 (m, 1H), 2.39 - 2.32 (m, 2H), 2.06 - 2.01 (m, 2H), 1.80 - 1.37 (m, 7H), 1.30 - 1.05 (m, 3H), 1.04 - 0.85 (m, 2H). HRMS (ESI$^+$) calcd for $C_{25}H_{32}N_2O_2S$ $(M+H)^+$ 425.23, found 425.2.

4-Iodobenzene-1-sulfonyl chloride (262). Same procedure as **196** using iodobenzene (0.33 mL, 2.96 mmol) as the starting material. The residue was purified by flash chromatography on silica gel, eluting with hexanes/EtOAc (8:1) to deliver **262** as a yellow solid (875 mg, 98%). ^{1}H NMR (300 MHz, chloroform-d) (*ortho/para* mixture) δ 8.04 - 7.96 (m, 2H), 7.90 - 7.84 (m, 2H), 7.77 - 7.71 (m, 2H), 7.65 - 7.59 (m, 2H). The analytical data are in agreement with literature reports.[239]

(4a*R*,8a*S*)-1-((4-Iodophenyl)sulfonyl)decahydroquinoline (263). Same procedure as **195** using **262** (875 mg, 2.89 mmol) and *trans*-decahydroquinoline (1.2 g, 8.68 mmol) as the starting materials. The residue was purified by flash chromatography on silica gel, eluting with hexanes/EtOAc (6:1) to deliver **263** as a white solid (385 mg, 35%). ^{1}H NMR (400 MHz, chloroform-d) (*ortho/para* mixture) δ 7.91 - 7.81 (m, 4H), 7.65 - 7.59 (m, 2H), 7.54 - 7.47 (m, 2H), 4.12 - 4.05 (m, 2H), 2.82 - 2.71 (m, 2H), 2.49 - 2.45 (m, 2H), 2.14 - 2.12 (m, 2H), 1.79 - 1.49 (m, 6H), 1.49 - 1.40 (m, 2H), 1.29 - 1.04 (m, 2H), 1.04 - 0.87 (m, 2H).

(*4S,8R*)-1-((4-(1*H*-Pyrrol-1-yl)phenyl)sulfonyl)decahydroquinoline (257). Copper (II) acetate (76 mg, 0.42 mmol) and DBU (0.126 mL, 0.84 mmol) were added to a solution of pyrrole (0.035 mL, 0.5 mmol) and **263** (170 mg, 0.42 mmol) in DMF (0.6 mL). The reaction mixture was irradiated under microwave conditions at 130 °C for 10 min. After allowing the solution to cool

down, it was filtered through a cotton plug in a pasteur pipette, the filtrate was diluted with Et_2O (4 mL), washed with H_2O (3 x 4 mL) and brine (4 mL), dried over Na_2SO_4, filtered, and concentrated. The residue was purified by flash chromatography on silica gel, eluting with hexanes/EtOAc (6:1) to afford **257** as a white solid (16 mg, 11%). ^{1}H NMR (300 MHz, chloroform-d) δ 7.86 - 7.82 (m, 2H), 7.77 - 7.52 (m, 4H), 7.23 - 7.11 (m, 1H), 6.47 - 6.35 (m, 1H), 4.12 - 4.06 (m, 1H), 2.90 - 2.71 (m, 1H), 2.63 - 2.41 (m, 1H), 2.35 - 2.14 (m, 2H), 1.97 - 1.37 (m, 6H), 1.35 - 1.07 (m, 4H), 1.03 - 0.82 (m, 2H). HRMS (ESI^+) calcd for $C_{19}H_{24}N_2O_2S$ $(M+Na)^+$ 367.1456, found 367.1450.

2-Oxo-1,2,3,4-tetrahydroquinoline-6-sulfonyl chloride. Same procedure as **194** using 3,4-dihydroquinolin-2(1*H*)-one (100 mg, 0.68 mmol) as the starting material. The residue was purified by flash chromatography on silica gel, eluting with hexanes/EtOAc (1:1) to afford a light brown solid (126 mg, 76%). ^{1}H NMR (300 MHz, DMSO-d6) δ 10.11 (s, 1H), 7.41 - 7.28 (m, 2H), 6.75 (d, *J* = 8.1 Hz, 1H), 2.84 (t, *J* = 7.5 Hz, 2H), 2.42 (t, J = 7.8 Hz, 2H).

6-(((4a*R*,8a*S*)-Octahydroquinolin-1(2*H*)-yl)sulfonyl)-3,4-dihydroquinolin-2(1*H*)-one (258). 2-Oxo-1,2,3,4-tetrahydroquinoline-6-sulfonyl chloride (50 mg, 0.20 mmol) was added to a solution of *trans*-decahydroquinoline (28.4 mg, 0.20 mmol) in pyridine (1.6 mL). The resulting mixture was heated to 40 °C overnight. H_2O (4 mL) and EtOAc (5 mL) were added, the layers were separated, the combined organic layers were washed with 1 M HCl (4 mL), H_2O (4 mL) and brine (4 mL), dried over Na_2SO_4, filtered, and concentrated to deliver **258** as a light yellow solid (14.4 mg, 20%). ^{1}H NMR (300 MHz, chloroform-d) δ 8.61 (s, 1H), 7.61 (d, *J* = 7.1 Hz, 2H), 6.87 (d, *J* = 8.9 Hz, 1H), 4.10 (m, 1H), 3.04 (t, *J* = 7.6 Hz, 2H), 2.83 - 2.58 (m, 2H), 2.68 -

2.47 (m, 1H), 2.19 - 2.11 (m, 1H), 1.82 - 1.36 (m, 6H), 1.36 - 1.07 (m, 4H), 1.07 - 0.83 (m, 4H). HRMS (ESI^+) calcd for $C_{18}H_{24}N_2O_3S$ $(M+Na)^+$ 371.1405, found 371.1405.

6-(((*4S,8R*)-Octahydroquinolin-1(2*H*)-yl)sulfonyl)quinoline (259). DDQ (67 mg, 0.35 mmol) was added to a solution of **30** (47 mg, 0.14 mmol) in dioxane (0.6 mL). The resulting mixture was heated to reflux for 24 h. After allowing the mixture to cool down, the solvent was removed under vacuum, the residue was suspended in EtOAc (5 mL) and washed with $NaHCO_3$ (2 x 5 mL). The aqueous layer was extracted with EtOAc (2 x 5 mL), the combined organic layers were washed with brine (4 mL), dried over Na_2SO_4, filtered, and concentrated. The residue was purified by flash chromatography on silica gel, eluting with hexanes/EtOAc (2:1) to afford **259** as a green oil (40 mg, 87%). ^1H NMR (400 MHz, chloroform-d) δ 9.03 (d, *J* = 4.2 Hz, 1H), 8.35 (d, *J* = 2.1 Hz, 1H), 8.28 (dd, *J* = 8.5, 1.7 Hz, 1H), 8.20 (d, *J* = 8.9 Hz, 1H), 8.00 (dd, *J* = 8.9, 2.2 Hz, 1H), 7.53 - 7.50 (m, 1H), 4.20 - 4.15 (m, 1H), 2.90 - 2.84 (m, 1H), 2.61 - 2.55 (m, 1H), 2.23 - 2.12 (m, 1H), 1.76 - 1.41 (m, 8H), 1.17 - 0.83 (m, 4H). HRMS (ESI^+) calcd for $C_{18}H_{22}N_2O_2S$ $(M+H)^+$ 331.4524, found 331.1489.

1-(Prop-2-yn-1-yl)-1,2,3,4-tetrahydroquinoline (260). Same procedure as **252** using **192** (0.57 mL, 5.57 mmol) and propargyl bromide (0.74 mL, 8.36 mmol) as the starting materials. The residue was purified by flash chromatography on silica gel, eluting with hexanes/EtOAc (2:1) to deliver **260** as a dark oil (83 mg, 87%). ^1H NMR (300 MHz, chloroform-d) δ 7.10 (t, *J* = 1.8 Hz, 1H), 7.01 (d, *J* = 7.3 Hz, 1H), 6.79 - 6.67 (m, 2H), 4.04 (d, *J* = 2.4 Hz, 2H), 3.31 (t, *J* = 5.4 Hz, 2H), 2.80 (t, *J* = 6.5 Hz, 2H), 2.17 (t, *J* = 2.4 Hz, 1H), 2.09 - 1.97 (m, 2H). The analytical data are in agreement with literature reports.[240]

Analogs synthesized as part of the HTS investigation

4-Methyl-*N*-(naphthalen-2-yl)benzenesulfonamide (265). 2-Naphtylamine (0.02 mL, 0.18 mmol) was added to a stirred solution of 4-toluenesulfonyl chloride (35 mg, 0.18 mmol) in pyridine (0.3 mL). The reaction mixture was heated to reflux overnight. After allowing the mixture to cool down to rt, EtOAc (4 mL) was added. The organic layer was washed with 1 M HCl (2 mL), H_2O (2 x 3 mL) and brine (3 mL), dried over Na_2SO_4, filtered, and concentrated. The residue was purified by flash chromatography on silica gel, eluting with hexanes/EtOAC (6:1) to afford **265** as a red solid (20 mg, 38%). ^{1}H NMR (300 MHz, chloroform-d) δ 7.76 (m, 5H), 7.52 (d, *J* = 2.1 Hz, 1H), 7.45 - 7.40 (m, 2H), 7.26 - 7.17 (m, 3H), 6.90 (s, 1H), 2.34 (s, 3H). The analytical data is in agreement with literature reports.[241]

(4-Nitrophenyl)(pyrrolidin-1-yl)methanone (273). Pyrrolidine (0.111 mL, 1.35 mmol) and TEA (0.235 mL, 1.69 mmol) were added to a stirred solution of 4-nitrobenzoylchloride (300 mg, 1.61 mmol) in DCM (1.2 mL) at 0 °C. The mixture was stirred at 0 °C for 3 h and poured into H_2O (6 mL). The organic layer was separated and washed with 0.5 M HCl (2 x 5 mL), $NaHCO_3$ (6 mL) and brine (4 mL), dried over $MgSO_4$, filtered, and concentrated. The residue was purified by flash chromatography on silica gel, eluting with acetone/DCM (1:8) to deliver **273** as a yellow solid (256 mg, 86%). ^{1}H NMR (300 MHz, chloroform-d) δ 8.24 (d, *J* = 9.0 Hz, 2H), 7.67 (d, *J* = 8.7 Hz, 2H), 3.66 (t, *J* = 6.9 Hz, 2H), 3.37 (t, *J* = 6.6 Hz, 2H), 2.01 - 1.90 (m, 4H).

(4-Aminophenyl)(pyrrolidin-1-yl)methanone (274). A solution of **273** (235 mg, 1.07 mmol) in MeOH (1.4 mL) was stirred at rt, the reaction flask was purged with dry N_2 to remove oxygen and Pd/C (10%, 18 mg) was added. The flask was purged with H_2 and the reaction mixture was stirred overnight at rt under H_2 atmosphere. After completion of the reaction, the mixture was

filtered through a silica pad and washed with EtOAc (4 x 6 mL) and MeOH (2 x 5 mL). The filtrate was concentrated and the residue was purified by flash chromatography on silica gel, eluting with DCM/EtOAc (2:1) to give **274** as a yellow solid. ^{1}H NMR (300 MHz, chloroform-d) δ 7.43 - 7.38 (m, 2H), 6.75 - 6.69 (m, 2H), 3.90 (s, 2H), 3.60 - 3.46 (m, 4H), 4.22 - 4.16 (m, 4H). The analytical data is in agreement with literature reports.[242]

2,3,5,6-Tetramethyl-*N*-(4-(pyrrolidine-1-carbonyl)phenyl)benzenesulfonamide (266). Same protocol as **265** using **274** (16 mg, 0.09 mmol) and 2,3,5,6-tetramethylbenzenesulfonyl chloride (20 mg, 0.09 mmol) as the starting materials. The residue was purified by flash chromatography on silica gel, eluting with acetone/DCM (1:4) to afford **266** as a white solid (26 mg, 77%). ^{1}H NMR (300 MHz, DMSO-d6) δ 10.45 (s, 1H), 7.35 (d, *J* = 8.4 Hz, 2H), 7.21 (s, 1H), 6.90 (d, *J* = 8.4 Hz, 2H), 3.34 - 3.32 (m, 4H), 2.19 (s, 6H), 1.98 - 1.80 (m, 4H). HRMS (ESI$^+$) calcd for $C_{21}H_{26}N_2O_3S$ $(M+H)^+$ 387.5157, found 387.1754.

Methyl 4-aminobenzoate. Thionyl chloride (1 mL, 14.5 mmol) was slowly added to a stirred solution of 4-aminobenzoic acid (100 mg, 0.73 mmol) in MeOH (7 mL) at 0 °C. The resulting mixture was stirred at rt for 30 min and then heated to reflux for 6 h. After allowing the solution to cool down to rt, the solvent was removed under vacuum and the residue was suspended in H_2O (4 mL). The resulting solution was neutralized with K_2CO_3 (52 mg) and extracted with DCM (2 x 5 mL). The combined organic layers were dried over $MgSO_4$, filtered, and concentrated to afford a white solid (96 mg, 87%). ^{1}H NMR (300 MHz, DMSO-d6) δ 7.61 (d, *J* = 8.7 Hz, 2H), 6.53 (d, *J* = 6.6 Hz, 2H), 5.95 (s, 2H), 3.70 (s, 3H). The analytical data are in agreement with literature reports.[243]

Methyl 4-(2-methoxy-4-methylphenylsulfonamido)benzoate (267). Same procedure as **265** using methyl 4-aminobenzoate (14 mg, 0.09 mmol) and 2-methoxy-5-methylbenzene-1-sulfonyl chloride (20 mg, 0.09 mmol) as the starting materials. The residue was purified by flash chromatography on silica gel, eluting with hexanes/EtOAC (4:1) to afford **267** as a white solid (17 mg, 57%). ^{1}H NMR (300 MHz, chloroform-d) δ 7.88 (d, *J* = 8.7 Hz, 2H), 7.72 (d, *J* = 1.9 Hz, 1H), 7.28 - 7.22 (m, 1H), 7.11 (d, *J* = 9.0 Hz, 2H), 6.85 (d, *J* = 8.4 Hz, 1H), 3.97 (s, 3H), 3.82 (s, 3H), 2.28 (s, 3H). HRMS (ESI^{+}) calcd for $C_{16}H_{17}NO_5S$ $(M+H)^{+}$ 336.3828, found 336.0913.

5-Nitro-1,2-dihydroacenaphthylene (275). Acenaphtene (50 mg, 0.32 mmol) was dissolved in a solution of glacial acetic acid (0.38 mL). The solution was placed in an ice bath and cooled down to ~ 10 °C. Nitric acid (0.024 mL) was slowly added, the reaction mixture was kept at ~ 10 °C for 20 min and slowly allowed to warm to rt. The resulting mixture was stirred for 5 h, after completion of the reaction ice-cold H_2O (4 mL) was added and the product was extracted with EtOAc (3 x 4 mL). The combined organic layers were washed with $NaHCO_3$ (2 x 5 mL) and brine (4 mL), dried over Na_2SO_4, filtered, and concentrated. The residue was purified by flash chromatography on silica gel, eluting with hexanes/EtOAc (9:1) to give **275** as a yellow solid (25 mg, 40%). ^{1}H NMR (300 MHz, chloroform-d) δ 8.55 (dd, *J* = 0.6, 8.1 Hz, 2H), 7.73 (t, *J* = 6.9 Hz, 1H), 7.44 (d, *J* = 6.6 Hz, 1H), 7.32 (dd, *J* = 2.4, 7.8 Hz, 1H), 3.52 - 3.44 (m, 4H). The analytical data is in agreement with literature reports.[244]

1,2-Dihydroacenaphthylen-5-amine (276). Same procedure as **274** using **275** (80 mg, 0.41 mmol) as the starting material. The residue was purified by flash chromatography on silica gel, eluting with hexanes/EtOAc (4:1) to give **276** as a dark oil (21 mg, 100%). ^{1}H NMR (300 MHz, chloroform-d) δ 7.55 (d, *J* = 8.2 Hz, 1H), 7.70 (t, *J* = 8.4 Hz, 1H), 7.28 - 7.24 (m, 1H), 7.10 (d, *J*

= 7.2 Hz, 1H), 6.85 (d, *J* = 6.9 Hz, 1H), 3.41 - 3.30 (m, 4H). The analytical data is in agreement with literature reports.[245]

2,4-Dimethylbenzene-1-sulfonyl chloride. Chlorosulfonic acid (0.19 mL, 2.82 mmol) was added to a stirred solution of *m*-xylene (0.115 mL, 0.94 mmol) in $CHCl_3$ (0.3 mL) at 0 °C. The reaction mixture was slowly allowed to warm to room temperature and stirred for 1 h. The mixture was poured into ice-cold H_2O (4 mL) and the aqueous layer was extracted with $CHCl_3$ (3 x 5 mL). The combined organic layers were dried over Na_2SO_4, filtered, and concentrated to afford a yellow oil (139 mg, 72%). ^{1}H NMR (300 MHz, chloroform-d) δ 7.94 (d, *J* = 8.1 Hz, 1H), 7.26 - 7.20 (m, 2H), 2.74 (s, 3H), 2.43 (s, 3H). The analytical data are in agreement with literature reports.[246]

***N*-(1,2-Dihydroacenaphthylen-5-yl)-2,4-dimethylbenzenesulfonamide (268)**. Same procedure as **265** using **276** (20 mg, 0.12 mmol) and 2,4-dimethylbenzene-1-sulfonyl chloride (36 mg, 0.17 mmol) as the starting materials. The residue was purified by flash chromatography on silica gel, eluting with hexanes/EtOAc (4:1) to afford **268** as a yellow solid (26 mg, 63%). ^{1}H NMR (300 MHz, chloroform-d) δ 7.78 (d, *J* = 8.4 Hz, 1H), 7.54 (d, *J* = 8.1 Hz, 1H), 7.44 (t, *J* = 6.9 Hz, 1H), 7.29 - 7.26 (m, 1H), 7.17 (d, *J* = 7.2 Hz, 1H), 7.11 - 6.99 (m, 4H), 6.99 (s, 1H), 3.40 - 3.31 (m, 4H), 2.60 (s, 3H), 2.33 (s, 3H). HRMS (ESI$^+$) calcd for $C_{20}H_{19}NO_2S$ $(M+H)^+$ 338.4433, found 338.3430.

(4a*R*,8a*S*)-1-Tosyldecahydroquinoline (269). Same procedure as **195** from *trans*-decahydroquinoline (43 mg, 0.31 mmol) and 4-toluenesulfonyl chloride (30 mg, 0.15 mmol) as the starting materials. The residue was purified by flash chromatography on silica gel, eluting with hexanes/EtOAc (9:1) to deliver **269** as a colorless oil (34 mg, 77%). ^{1}H NMR (400 MHz,

chloroform-d) δ 7.66 (d, *J* = 8.1 Hz, 2H), 7.27 (d, *J* = 8.1 Hz, 2H), 4.12 - 4.08 (m, 1H), 2.76 - 2.71 (m, 1H), 2.42 (s, 3H), 2.26 - 2.22 (m, 1H), 1.65 - 25 (m, 9H), 1.20 - 1.02 (m, 2H), 0.98 - 0.91 (m, 2H). HRMS (ESI^+) calcd for $C_{16}H_{23}NO_2S$ $(M+H)^+$ 294.4323, found 294.1517.

(4a*R*,8a*S*)-1-((2,4-Dimethylphenyl)sulfonyl)decahydroquinoline (270). Same procedure as **195** using *trans*-decahydroquinoline (24 mg, 0.24 mmol) and 2,4-dimethylbenzene-1-sulfonyl chloride (25 mg, 0.12 mmol) as the starting materials. The residue was purified by flash chromatography on silica gel, eluting with hexanes/EtOAc (6:1) to deliver **270** as a light yellow solid (25 mg, 69%). ^1H NMR (300 MHz, chloroform-d) δ 7.80 (d, *J* = 8.4 Hz, 1H), 7.08 - 7.06 (m, 2H), 4.22 (m, 1H), 2.98 - 2.78 (m, 2H), 2.54 (s, 3H), 2.36 (s, 3H), 1.80 - 1.54 (m, 10H), 1.18 - 0.98 (m, 3H). HRMS (ESI^+) calcd for $C_{17}H_{25}NO_2S$ $(M+H)^+$ 308.4588, found 308.1669.

(4a*R*,8a*S*)-1-((2,3,5,6-Tetramethylphenyl)sulfonyl)decahydroquinoline (271). Same protocol as **195** from *trans*-decahydroquinoline (47 mg, 0.34 mmol) and 2,3,4,5-tetramethylsulfonyl chloride (40 mg, 0.17 mmol) as the starting materials. The residue was purified by flash chromatography on silica gel, eluting with hexanes/EtOAc (9:1) to deliver **271** as a white solid (16 mg, 61%). ^1H NMR (400 MHz, chloroform-d) δ 7.11 (s, 1H), 4.08 - 4.05 (m, 2H), 2.80 - 2.73 (m, 2H), 2.50 (s, 6H), 2.25 (s, 6H), 1.75 - 1.50 (m, 10H), 1.17 - 0.90 (m, 2H). HRMS (ESI^+) calcd for $C_{19}H_{29}NO_2S$ $(M+H)^+$ 336.5120, found 336.2005.

***N*-(1,2-dihydroacenaphthylen-5-yl)-1-(2,2,2-trifluoroacetyl)-1,2,3,4-tetrahydroquinoline-6-sulfonamide**. Same protocol as **195** from **276** (15 mg, 0.09 mmol) and **194** (30 mg, 0.09 mmol) as the starting materials. The residue was purified by flash chromatography on silica gel, eluting with hexanes/EtOAc (3:1) to deliver a white solid (28 mg, 68%). ^1H NMR (300 MHz, chloroform-d) δ 7.70 - 7.62 (m, 2H), 7.53 (s, 1H), 7.42 - 7.25 (m, 4H), 7.19 (d, *J* = 7.5 Hz, 1H),

6.92 (s, 1H), 3.79 (t, *J* = 5.7 Hz, 2H), 3.40 - 3.34 (m, 4H), 2.73 (t, *J* = 5.4 Hz, 2H), 2.01 (t, *J* = 6.6 Hz, 2H).

***N*-(1,2-Dihydroacenaphthylen-5-yl)-1,2,3,4-tetrahydroquinoline-6-sulfonamide (272).** Same protocol as **30** using *N*-(1,2-dihydroacenaphthylen-5-yl)-1-(2,2,2-trifluoroacetyl)-1,2,3,4-tetrahydroquinoline-6-sulfonamide (28 mg, 0.06 mmol) and K_2CO_3 (161 mg, 1.17 mmol) as the starting materials. The residue was purified by flash chromatography on silica gel, eluting with hexanes/EtOAc (2:1) to deliver **272** as a light yellow solid (19 mg, 86%). ^{1}H NMR (300 MHz, acetone-d) δ 8.40 (s, 1H), 7.81 (d, *J* = 8.4 Hz, 1H), 7.41 - 7.15 (m, 5H), 6.37 (d, *J* = 9.3 Hz, 1H), 5.82 (s, 1H), 3.35 - 3.25 (m, 4H), 2.80 (t, *J* = 7.0 Hz, 2H), 2.60 (t, *J* = 6.6 Hz, 2H), 1.85 - 1.76 (m, 2H). HRMS (ESI$^+$) calcd for $C_{21}H_{20}N_2O_2S$ $(M+H)^+$ 365.4686, found 365.1332.

***N*-Benzyl-4-methylbenzenesulfonamide (277).** Benzylamine (0.077 mL, 0.71 mmol) and K_2CO_3 (194 mg, 1.4 mmol) were added to a stirred solution of *p*-toluenesulfonyl chloride (68 mg, 0.36 mmol) in DCM (2 mL) at 0 °C. The mixture was allowed to warm to rt, stirred for 3 h and poured into H_2O (4 mL). The organic layer was separated and washed with H_2O (2 x 5 mL), $NaHCO_3$ (4 mL) and brine (4 mL), dried over $MgSO_4$, filtered, and concentrated. The residue was purified by flash chromatography on silica gel, eluting with hexanes/EtOAc (1:1) to deliver **277** as white solid (72 mg, 79%). ^{1}H NMR (400 MHz, chloroform-d) δ 7.84 (d, *J* = 8.4 Hz, 2H), 7.37 (d, *J* = 8 Hz, 2H), 7.34 - 7.33 (m, 3H), 7.28 - 7.26 (m, 2H), 4.68 (t, *J* = 5.6 Hz, 1H), 4.18 (d, *J* = 6 Hz, 2H), 2.51 (s, 3H). The analytical data are in agreement with literature reports.[247]

1-Isopropyl-4-methoxy-2-methylbenzene. Tetra-n-butylammonium bromide (536 mg, 1.66 mmol) and K_2CO_3 (459 mg, 3.32 mmol) were added to a solution of 4-isopropyl-3-methylphenol (500 mg, 3.32 mmol) in dimethylcarbonate (2.8 ml). The reaction mixture was stirred under

refluxing conditions overnight. After allowing the mixture to cool down to rt, H_2O (5 ml) and DCM (6 ml) were added. The organic layer was separated and further washed with $NaHCO_3$ (4 mL) and brine (4 mL), dried over $MgSO_4$, filtered, and concentrated. The residue was purified by flash chromatography on silica gel, eluting with hexanes/EtOAc (10:1) to afford a white solid (504 mg, 92%). ^{1}H NMR (300 MHz, chloroform-d) δ 7.15 (d, *J* = 8.4 Hz, 1H), 6.75 - 6.69 (m, 2H), 3.55 (s, 3H), 3.10 - 3.04 (m, 1H), 2.32 (s, 3H), 1.21 (d, *J* = 6.9 Hz, 6H).

5-Isopropyl-2-methoxy-4-methylbenzene-1-sulfonyl chloride (281). Chlorosulfonic acid (0.461 mL, 6.94 mmol) was added to a stirred solution of 1-isopropyl-4-methoxy-2-methylbenzene (380 mg, 2.31 mmol) in $CHCl_3$ (2.5 ml) at 0 °C. The reaction mixture was slowly allowed to warm to room temperature and stirred for 1 h. The suspension was cooled down to 0 °C in an ice bath and ice-cold water (5 mL) was slowly added. The aqueous layer was extracted with DCM (3 x 8 mL), the combined organic layers were then washed with H_2O (3 x 8 mL) and brine (4 mL), dried over $MgSO_4$, filtered, and concentrated to deliver **281** as a white solid (490 mg, 81%). ^{1}H NMR (300 MHz, chloroform-d) δ 7.76 (s, 1H), 6.87 (s, 1H), 4.01 (s, 3H), 3.10 - 3.04 (m, 1H), 2.43 (s, 3H), 1.22 (d, *J* = 6.8 Hz, 6H).

1-((5-Isopropyl-2-methoxy-4-methylphenyl)sulfonyl)-4-methyl-1*H*-imidazole (279). TEA (0.084 mL, 0.6 mmol) was added to a stirred solution of **281** (40 mg, 0.15 mmol) and 4-methylimidazole (25 mg, 0.30 mmol) in THF (0.6 mL) at 0 °C. The reaction mixture was slowly allowed to warm to rt and stirred for 2 h. The solvent was removed under vacuum and the residue was purified by flash chromatography on silica gel, eluting with acetone/DCM (1:12) to afford **279** as a white solid (20 mg, 66%). ^{1}H NMR (400 MHz, chloroform-d) δ 7.98 (s, 1H), 7.81 (s, 1H), 6.92 (s, 1H), 6.72 (s, 1H), 3.80 (s, 3H), 3.10 - 3.05 (m, 1H), 2.36 (s, 3H), 2.15 (s,

3H), 1.22 (d, *J* = 6.8 Hz, 6H). HRMS (ESI^+) calcd for $C_{15}H_{20}N_2O_3S$ $(M+H)^+$ 309.4938, found 309.1279.

5-(*tert*-Butyl)-2-methyl-*N*-(pyridin-3-ylmethyl)benzenesulfonamide (288). K_2CO_3 (87 mg, 0.63 mmol) and 5-(*tert*-butyl)-2-methylbenzene-1-sulfonyl chloride (39 mg, 0.16 mmol) were added to a stirred solution of 3-aminomethylpyridine (34 mg, 0.32 mmol) in DCM (2 ml) at 0 °C. The reaction mixture was stirred at rt for 2 h. The solvent was removed under vacuum. The residue was purified by flash chromatography on silica gel, eluting with 5% MeOH/DCM to afford **288** as a light yellow solid (35 mg, 74%). ^1H NMR (400 MHz, chloroform-d) δ 8.48 (s, 1H), 8.37 (s, 1H), 7.95 (s, 1H), 7.54 (d, *J* = 8 Hz, 1H), 7.45 (d, *J* = 8 Hz, 1H), 7.30 - 7.17 (m, 2H), 4.83 - 4.80 (m, 1H), 4.18 - 4.16 (m, 2H), 2.58 (s, 3H), 1.31 (s, 9H). HRMS (ESI^-) calcd for $C_{17}H_{22}N_2O_2S$ $(M-H)^-$ 317.1324, found 317.1337.

5-(*tert*-Butyl)-*N*-(3-methoxypropyl)-2-methylbenzenesulfonamide (289). Same procedure as **288** using 5-(*tert*-butyl)-2-methylbenzene-1-sulfonyl chloride (44 mg, 0.18 mmol) and 3-methoxypropylamine (0.036 mL, 0.36 mmol) as the starting materials. The residue was purified by flash chromatography on silica gel, eluting with hexanes:EtOAc (3:1) to afford **289** as a colorless oil (45 mg, 88%). ^1H NMR (400 MHz, chloroform-d) δ 7.87 (s, 1H), 7.45 (d, *J* = 7.6 Hz, 1H), 7.22 (d, *J* = 8 Hz, 1H), 5.30 - 5.28 (m, 1H), 3.48 (t, *J* = 6 Hz, 2H), 3.28 (s, 3H), 3.04 - 3.02 (m, 2H), 2.59 (s, 3H), 1.71 - 1.69 (m, 2H), 1.31 (s, 9H). ^{13}C NMR (300 MHz, Chloroform-d) δ 156.1, 149.3, 137.3, 133.7, 132.3, 129.5, 126.4, 71.9, 58.8, 42.1, 34.6, 31.2, 28.8, 19.6. HRMS (ESI^-) calcd for $C_{15}H_{25}NO_3S$ $(M-H)^-$ 298.4210, found 298.1487.

4-(*tert*-Butyl)-*N*-(2-(pyridin-4-yl)ethyl)benzenesulfonamide (292). Same procedure as **288** using 4-(*tert*-butyl)benzene-1-sulfonyl chloride (60 mg, 0.26 mmol) and 2-(pyridin-4-

yl)ethanamine (0.061 mL, 0.51 mmol) as the starting materials. The residue was purified by flash chromatography on silica gel, eluting with 5% MeOH in DCM to deliver **292** as a white solid (40 mg, 77%). ^{1}H NMR (400 MHz, chloroform-d) δ 8.42 (d, *J* = 6 Hz, 2H), 7.74 (d, *J* = 8.8 Hz, 2H), 7.50 (d, *J* = 8.8 Hz, 2H), 7.02 (d, *J* = 6 Hz, 2H), 4.44 (s, 1H), 3.28 - 3.26 (m, 2H), 2.80 (t, *J* = 7.8 Hz, 2H), 1.35 (s, 9H). HRMS (ESI$^-$) calcd for $C_{17}H_{22}N_2O_2S$ $(M-H)^-$ 317.4258, found 317.1334.

5-(*tert*-Butyl)-2,3-dimethylbenzene-1-sulfonyl chloride. Same procedure as **196** using 4-*tert*-butyl-*o*-xylene (200 mg, 1.23 mmol) as the starting material. The residue was purified by flash chromatography on silica gel, eluting with hexanes/EtOAc (4:1) to deliver a colorless oil (181 mg, 56%). ^{1}H NMR (300 MHz, chloroform-d) δ 7.93 (s, 1H), 7.51 (s, 1H), 2.85 (s, 3H), 2.39 (s, 3H), 1.33 (s, 9H).

5-(*tert*-Butyl)-*N*-(2-hydroxyethyl)-2,3-dimethylbenzenesulfonamide (294). Same procedure as **195** using 5-(*tert*-butyl)-2,3-dimethylbenzene-1-sulfonyl chloride (40 mg, 0.15 mmol) and ethanolamine (0.01 mL, 0.17 mmol) as the starting materials. The residue was purified by flash chromatography on silica gel, eluting with 5% MeOH/DCM to afford **294** as a colorless oil (77 mg, 90%). ^{1}H NMR (300 MHz, chloroform-d) δ 7.85 (s, 1H), 7.37 (s, 1H), 3.70 (t, *J* = 5.1 Hz, 2H), 3.08 (t, *J* = 4.8 Hz, 2H), 2.55 (s, 3H), 2.34 (s, 3H), 1.31 (s, 9H). HRMS (ESI$^-$) calcd for $C_{14}H_{23}NO_3S$ $(M-H)^-$ 284.3944, found 284.1329.

***N*-(2-Hydroxyethyl)-5-isopropyl-2-methoxy-4-methylbenzenesulfonamide (314).** Same procedure as **195** using **281** (45 mg, 0.17 mmol) and ethanolamine (0.029 mL, 0.48 mmol) as the starting materials. The residue was purified by flash chromatography on silica gel, eluting with 5% MeOH in DCM to deliver **314** as a colorless oil (7 mg, 15%). ^{1}H NMR (400 MHz, chloroform-d) δ 8.65 (s, 1H), 7.71 (s, 1H), 6.78 (s, 1H), 5.34 - 5.32 (m, 1H), 3.94 (s, 3H), 3.69 -

3.66 (m, 2H), 3.00 - 2.98 (m, 3H), 2.38 (s, 3H), 1.22 (d, *J* = 6.8 Hz, 6H). HRMS (ESI⁻) calcd for $C_{13}H_{21}NO_4S$ $(M-H)^-$ 286.3672, found 286.1122.

1-((5-Isopropyl-2-methoxy-4-methylphenyl)sulfonyl)-1*H*-imidazole (317). Imidazole (23 mg, 0.34 mmol) was added to a stirred solution of **281** (30 mg, 0.11 mmol) in DCM (0.3 mL) at 0 °C. The reaction mixture was allowed to warm to rt and further stirred for 3 h. The solvent was removed under vacuum and the residue was purified by flash chromatography on silica gel, eluting with acetone:DCM (1:8) to afford **317** as a white solid (26 mg, 79%). ^{1}H NMR (300 MHz, chloroform-d) δ 8.17 (s, 1H), 7.85 (s, 1H), 7.32 (s, 1H), 7.07 (s, 1H), 6.75 (s, 1H), 3.84 (s, 3H), 3.12 - 3.07 (m, 1H), 2.39 (s, 3H), 1.23 (d, *J* = 6.8 Hz, 6H). HRMS (ESI^+) calcd for $C_{14}H_{18}N_2O_3S$ $(M+H)^+$ 295.3773, found 295.1104.

1-((5-Isopropyl-2-methoxy-4-methylphenyl)sulfonyl)-4-phenyl-1*H*-imidazole (320). Same procedure as **317** using **281** (40 mg, 0.15 mmol) and 4-phenylimidazole (66 mg, 0.45 mmol) as the starting materials. The residue was purified by flash chromatography on silica gel, eluting with DCM to afford **320** as a white solid (54 mg, 96%). ^{1}H NMR (300 MHz, chloroform-d) δ 8.16 (s, 1H), 7.88 (s, 1H), 7.76 (d, *J* = 8.4 Hz, 2H), 7.71 (s, 1H), 7.40 (t, *J* = 8.7 Hz, 2H), 7.28 (t, *J* = 7.5 Hz, 1H), 6.74 (s, 1H), 3.84 (s, 3H), 3.13 - 3.08 (m, 1H), 2.38 (s, 3H), 1.28 (d, *J* = 6.9 HZ, 6H). HRMS (ESI^+) calcd for $C_{20}H_{22}N_2O_3S$ $(M+H)^+$ 371.4732, found 371.1416.

(4a*R*,8a*S*)-1-((5-Isopropyl-2-methoxy-4-methylphenyl)sulfonyl)decahydroquinoline (325). Same procedure as **195** using **281** (25 mg, 0.09 mmol) and *trans*-decahydroquinoline (26 mg, 0.19 mmol) as the starting materials. The residue was purified by flash chromatography on silica gel, eluting with hexanes:EtOAc (5:1) to afford **325** as a colorless oil (25 mg, 70%). ^{1}H NMR (300 MHz, chloroform-d) δ 7.71 (s, 1H), 6.72 (s, 1H), 4.15 - 4.10 (m, 1H), 3.88 (s, 3H), 3.08 -

3.03 (m, 1H), 2.85 - 2.65 (m, 1H), 2.64 - 2.35 (m, 1H), 2.34 (s, 3H), 2.04 - 2.02 (m, 2H), 1.69 - 1.59 (m, 6H), 1.20 (d, *J* = 6.8 Hz, 8H), 1.17 - 1.04 (m, 7H). HRMS (ESI^+) calcd for $C_{20}H_{31}NO_3S$ $(M+H)^+$ 366.5380, found 366.2091.

1-((2-Methoxy-4-methylphenyl)sulfonyl)-4-methyl-1*H*-imidazole (326). 6-Methoxy-m-toluenesulfonyl chloride (40 mg, 0.18 mmol) was added to a solution of 4-methylimidazole (45 mg, 0.54 mmol) in DCM (0.5 ml) at 0 °C. The reaction mixture was stirred at rt overnight. The solvent was removed under vacuum. The residue was purified by flash chromatography on silica gel, eluting with DCM/acetone (8:1) to deliver **326** as a white solid (45 mg, 85%). ^1H NMR (300 MHz, Chloroform-d) δ 8.04 (s, 1H), 7.82 (s, 1H), 7.42 (d, *J* = 8.4 Hz, 1H), 6.95 (s, 1H), 6.86 (d, *J* = 8.1 Hz, 1H), 3.85 (s, 3H), 2.36 (s, 3H), 2.14 (s, 3H). HRMS (ESI^+) calcd for $C_{12}H_{14}N_2O_3S$ $(M+H)^+$ 267.0803, found 267.0809.

1-((2-Methoxy-4-methylphenyl)sulfonyl)-1*H*-imidazole (327). Same procedure as **265** using 6-methoxy-*m*-toluenesulfonyl chloride (50 mg, 0.23 mg) and imidazole (15 mg, 0.23 mmol) as the starting materials. The residue was purified by flash chromatography on silica gel, eluting with 5% MeOH in DCM to afford **327** as a white solid (14 mg, 24%). ^1H NMR (300 MHz, chloroform-d) δ 8.09 (s, 1H), 7.84 (d, *J* = 2.1 Hz, 1H), 7.42 (dq, *J* = 0.6, 8.4 Hz, 1H), 7.28 (s, 1H), 7.04 (s, 1H), 6.87 (d, *J* = 8.4 Hz, 1H), 3.83 (s, 3H), 2.36 (s, 3H). HRMS (ESI^+) calcd for $C_{11}H_{12}N_2O_3S$ $(M+H)^+$ 253.2975, found 253.0638.

6-((4-Methyl-1*H*-imidazol-1-yl)sulfonyl)-1-(2,2,2-trifluoroacetyl)-1,2,3,4-tetrahydroquinoline. Same procedure as **195** using **194** (35 mg, 0.10 mg) and 4-methylimidazole (26 mg, 0.30 mmol) and as the starting materials. The residue was purified by flash chromatography on silica gel, eluting with acetone/DCM (1:11) to give a white solid (38

mg, 84%). ^{1}H NMR (300 MHz, chloroform-d) δ 7.98 - 7.91 (m, 2H), 7.77 - 7.74 (m, 2H), 6.99 (s, 1H), 3.86 (t, J = 6 Hz, 2H), 2.96 (t, J = 5.6 Hz, 2H), 2.20 (s, 3H), 2.14 - 2.10 (m, 2H).

6-((4-Methyl-1*H*-imidazol-1-yl)sulfonyl)-1,2,3,4-tetrahydroquinoline (334). Same procedure as **30** using 6-((4-Methyl-1*H*-imidazol-1-yl)sulfonyl)-1-(2,2,2-trifluoroacetyl)-1,2,3,4-tetrahydroquinoline (34 mg, 0.09 mmol) and K_2CO_3 (234 mg, 1.69 mmol) as the starting materials. The residue was purified by flash chromatography on silica gel, eluting with acetone/DCM (1:9) to deliver **334** as a white solid (17 mg, 67%). ^{1}H NMR (300 MHz, chloroform-d) δ 7.98 (s, 1H), 7.47 - 7.44 (m, 1H), 6.97 (s, 1H), 6.44 (d, *J* = 8.7 Hz, 1H), 4.80 (s, 1H), 3.88 (t, *J* = 5.4 Hz, 2H), 2.75 (t, *J* = 6.3 Hz, 2H), 2.22 (s, 3H), 1.94 - 1.90 (m, 2H).

4.0 MODE OF ACTION STUDIES OF THE MIR-122 INHIBITORS

Investigations into the biogenesis of miRNAs, as well as the molecular mechanisms responsible for their participation in various diseases, constitute an active field of research. Additional knowledge into the regulation of specific miRNAs will bring valuable insight to promote the development of miRNA-based therapeutics.[2] It is now well established that miR-122 intricately drives the replication of the HCV virus,[211] spurring interest in the development of new anti-HCV therapies based on miR-122 inhibition,[2] pioneered by the LNA anti-miR122 miravirsen.[72, 192] Additionally, small molecule miR-122 specific inhibitors represent promising new antiviral strategies since they can reduce HCV replication.[98] However, the mode of action of the small molecule miR-122 inhibitors has not been elucidated. Identifying the protein(s) specifically targeted by the small molecule miR-122 inhibitor **30** would not only expand the current knowledge of miR-122 biogenesis but could also lead to potential new drug targets for the treatment of HCV infection.

4.1 PREVIOUS WORK: RECOVERY OF INHIBITION BY TRANSFECTION OF PRECURSOR PRE-MIR-122

Preliminary experiments suggested that the regulatory effect of the small molecule **30** was not due to direct binding with the miRNA oligonucleotide (Figure 3.5). It was further

demonstrated by qRT-PCR experiments that exposure of Huh7 cells to 10 μM of compound **30** led to a 97% and a 72% knockdown of both pri-miR-122 and mature miR-122 expression levels, respectively (Figure 3.4).[98] These data indicated that **30** acts either at the transcriptional level, by inhibiting a necessary factor for the transcription of the miR-122 gene into the primary pri-miR-122 transcript, or at the pre-transcriptional level, by interfering with epigenetic events, such as DNA methylation or acetylation. To further validate this hypothesis, Huh7-psiCHECK-miR122 cells were exposed to both **30** and transfected with the precursor pre-miR-122. If the small molecule **30** acts upstream of the formation of the pri-miR-122 transcript, as hypothesized, introduction of exogenous precursor pre-miR-122 should recover the inhibitory activity of **30**. The proper processing of exogenous pre-miR-122 through the miRNA pathway should then deliver mature miR-122, capable of repressing their targets including the engineered miR-122 luciferase reporter.

As expected, transfection of Huh7-psiCHECK-miR122 cells with xtremeGENE (vehicle) or precursor pre-miR-21, followed by exposure to DMSO did not have any effect on the luciferase expression. The pre-miR-21 was used as a control in that experiment, to verify that the transfection of a precursor was not interfering with the activities of the small molecules independently of their miR-122 regulatory effect. In contrast, transfection with pre-miR-122 induced a 50% decrease in the *Renilla* luciferase signal (Figure 4.1). This was due to the presence of additional mature miR-122, which induced the silencing of the luciferase through specific binding to the mRNA. In the cells transfected with xtremeGENE (no precursor) or the control precursor pre-miR-21, treatment with the inhibitors **29** and **30** led to a 7- and 4-fold increase in *Renilla* luciferase expression over the DMSO control, respectively, due to the inhibition of miR-122 by the small molecules. However, in the cells treated with **29** and **30**, the

presence of precursor pre-miR-122 significantly reduced the *Renilla* luciferase signal, almost to the level of the DMSO control (Figure 4.1). This demonstrated that the precursor pre-miR-122 was correctly processed into mature miR-122, even in the presence of the small molecules **29** and **30**, and reinforced the hypothesis that the inhibitors act at the transcriptional or the pre-transcriptional step.

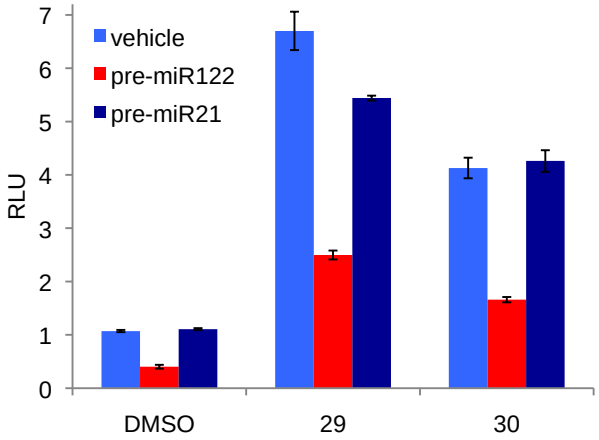

Figure 4.1: Recovery of the inhibitory activity of the miR-122 inhibitors **29** and **30** through transfection of a pre-miR-122 precursor.
Huh7-psiCHECK-miR122 cells were transfected with the precursors pre-miR-122 or pre-miR-21 and treated with DMSO, **29**, or **30** for 48 h. All experiments were conducted in triplicate and the data was normalized to the vehicle control (xtremeGENE transfection reagent). The error bars indicate standard deviations determined from three independent experiments. These experiments were performed by Colleen Connelly.

4.2 INVESTIGATION INTO THE PROTEIN TARGETED BY THE SMALL MOLECULE MIR-122 INHIBITOR

4.2.1 Synthesis of Small Molecule Probes

Although the SAR studies of the previously discovered miR-122 inhibitor **30** did not provide any significantly more potent inhibitors (Chapter 3.3), the knowledge collected during this investigation was crucial in locating suitable positions where modifications were tolerated. Since the introduction of a nucleophilic handle, such as the $(CH_2)_{4\text{-}6}OH$, $C_6H_4NH_2$, or $(CH_2)_6NH_2$ groups, in place of the *trans*-decahydroquinoline ring led to significant losses in activity (Figure 3.8 and Figure 3.9), applying a solid-phase immobilization of **30** for pull-down experiments (Figure 2.22) did not seem suitable. Instead, since it was shown that an alkyne functionality could be introduced into the tetrahydroquinoline motif without affecting the activity, and that some modifications on the benzene ring could be accommodated (Figure 3.9), a photo-crosslinking strategy was designed to identify the target protein of **30** (Figure 2.24).[248] It was envisioned that a small molecule photoprobe miR-122 inhibitor functionalized with an alkyne group could be synthesized to allow for covalent attachment to the target protein. Further derivatization with a fluorescent tag via a [3+2] cycloaddition would facilitate the detection of the protein.

A photoprobe consists of a bioactive small molecule substituted with a photoreactive group, which is able to form a covalent bond with the target protein after brief irradiation with UV light (Figure 2.24). Due to the formation of a covalent bond between the inhibitor and its cellular target, photoaffinity labeling is amenable to the detection of proteins with low abundance or with a low affinity for the modified small molecule. A good photoprobe must be reasonably

stable under ambient light, its excited state needs to have a short life-time to avoid non-specific binding, and it must be able to form a covalent bond with various residues.[144] The most commonly used photoactive groups are arylazides and diazirines because of their relative stability, small sizes, and ease of introduction into a molecule.[249] Benzophenones are also employed, as they are generally efficient and selective, they are stable under ambient light and protic solvent condition, and they preferentially react with unreactive C-H bonds.[114]

An additional SAR investigation of **30** was performed to determine which position on the small molecule could be substituted with a photo-crosslinking group, and which one would be more suitable. Since it was previously observed that a *para tert*-butyl (**237**) or acetyl (**238**) groups could be introduced, these compounds were further functionalized with a propargyl motif, which yielded the analogs **364** and **365** that were slightly more active than **30** (Figure 4.2). Based on these results, the *para* arylazide **366** was synthesized and displayed a promising 28% increase in activity over **30**. Modification with a small alkyne group was well tolerated, as **367** exhibited an activity comparable to **30**, thus representing a probe suitable for photo-crosslinking experiments. Since it was reported in the literature that 4-azidotetrafluoroaniline derivatives are often more efficient at photo-crosslinking than their arylazide counterparts,[250] **368** was synthesized to assess the effect of introducing highly electronegative fluorine. However, compound **368** showed a 25% loss in activity, suggesting that functionalization with fluoro groups might lead to an inactive photoprobe. In addition, a benzophenone photoactive group was installed in the *ortho* (**369**), *meta* (**370**), or *para* (**371**) positions. Modification in the *ortho* or *para* positions with the bulky benzophenone resulted in a 22% and 60% increase in activity compared to **30**, respectively. However, the *meta* substitution negatively affected the activity (Figure 4.2). The corresponding alkyne-derivatives of the potent **369** and **371** were synthesized,

but unfortunately significant reductions in activity were observed for **372** and **373**. The slightly smaller indoline analog **374** was designed with the hope that this compound might be better accommodated in the putative binding pocket of the target protein than **371**. Although **374** showed an activity equivalent to **30**, the subsequent introduction of an alkyne into **375**, similarly abolished the activity. Given that **30** is substituted with a tertiary sulfonamide, a methyl group was added to the *ortho*-benzophenone compound **369** to mimic the H-bond configuration of the reference inhibitor **30**. The analog **376** displayed a favorable 51% increase in activity relative to **30**, and furthermore, the propargyl derivative **377** showed an activity similar to the reference inhibitor **30**. The same strategy was applied to the arylazide analog **378**, which was totally inactive (Figure 4.2). The high activity exhibited by the benzophenone derivatives in the luciferase assay was somewhat surprising, and the results would need to be further confirmed by qRT-PCR experiments.

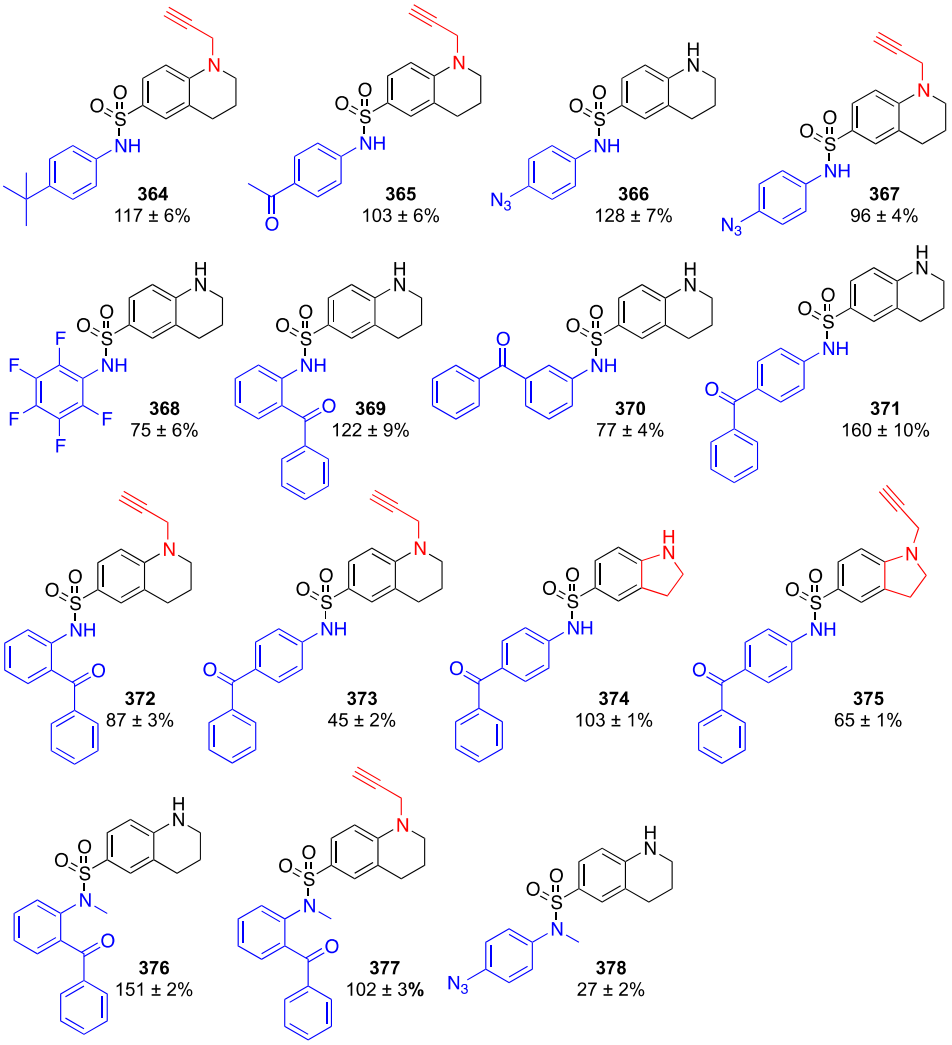

Figure 4.2: Structural modifications performed on **30** aimed towards the installation of functionalities necessary for photo-crosslinking experiments.
The modifications from the initial structure are shown in blue and red. The percentages represent luciferase activity relative to **30** within the same assay. Experiments were performed in triplicate and the standard deviations of the three independent assays were calculated. Cell-based assays were performed by Colleen Connelly.

The analogs **364**, **365**, **368-369**, **371-375** were synthesized according to Scheme 4.1. The sulfonyl chloride **194** was heated to reflux in pyridine in the presence of the corresponding anilines, and the TFA protecting group was subsequently removed with K_2CO_3 in MeOH/H_2O. The propargyl group was installed as previously described, through treatment with propargyl bromide and DIPEA in refluxing DMF.[251]

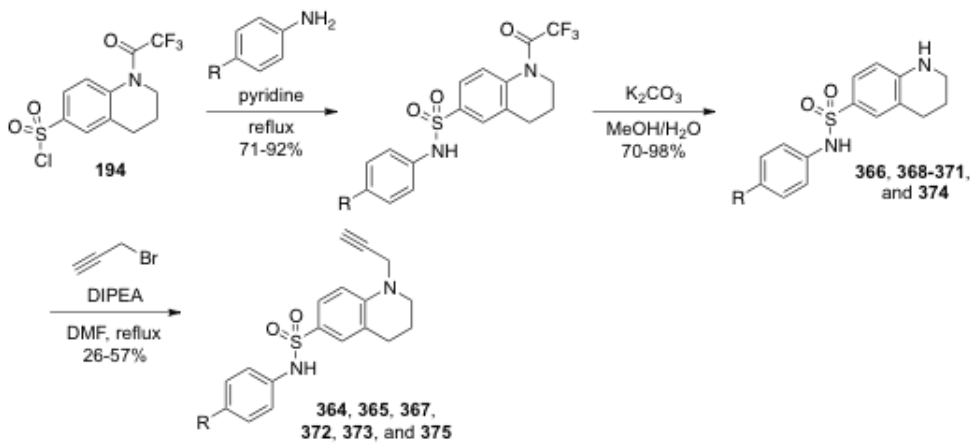

Scheme 4.1: Synthesis of analogs designed for use in photoaffinity labeling experiments.
For R groups see Figure 4.2.

The azide **366** was first synthesized from the nitro **379**, which was reduced with tin(II) chloride in refluxing EtOH (Scheme 4.2).[118] The intermediate **380** was converted to the corresponding azide through treatment with $NaNO_2$ and NaN_3 and subsequently deprotected with K_2CO_3 to deliver **366**. The propargylated analog **367** was similarly obtained from the nitro compound **381**, after successive treatments with tin(II) chloride, $NaNO_2$, and NaN_3 (Scheme 4.2). Since **367** acted as a potent small molecule miR-122 inhibitor possessing the two functionalities necessary to carry out 1) the photo-crosslinking experiments and 2) the subsequent "click reaction" with a fluorescent tag, the synthesis of **367** was scaled up to afford enough material for the biological studies. As the previous conditions used for the synthesis of **366** and **367** were generally low yielding, especially the step where the azido group was introduced, a different optimized route was designed (Scheme 4.2). 4-Nitroaniline was quantitatively protected using trifluoroacetic anhydride. Several conditions had to been screened for the reduction of the nitro **382** (Scheme 4.2), which was eventually carried out with H_2 and Pd/C in MeOH. Treatment of the aniline intermediate **383** at 0 °C sequentially with HCl, $NaNO_2$, and NaN_3 in H_2O delivered the corresponding azide in 98% yield, which was further exposed to K_2CO_3 to afford 4-azidoaniline. This intermediate **384** was then stirred at rt in pyridine for 2 h in the presence of

194 to deliver the TFA protected precursor **385** in 94% yield, which was further deprotected with K_2CO_3. Finally, **366** was treated with propargyl bromide to yield the photo-crosslinking probe **367** (Scheme 4.2). Unlike previous alkylation reactions, which were performed under refluxing conditions, the alkylation of **366** with propargyl bromide was carried out at 50 °C due to the decomposition of the starting material at higher temperatures.

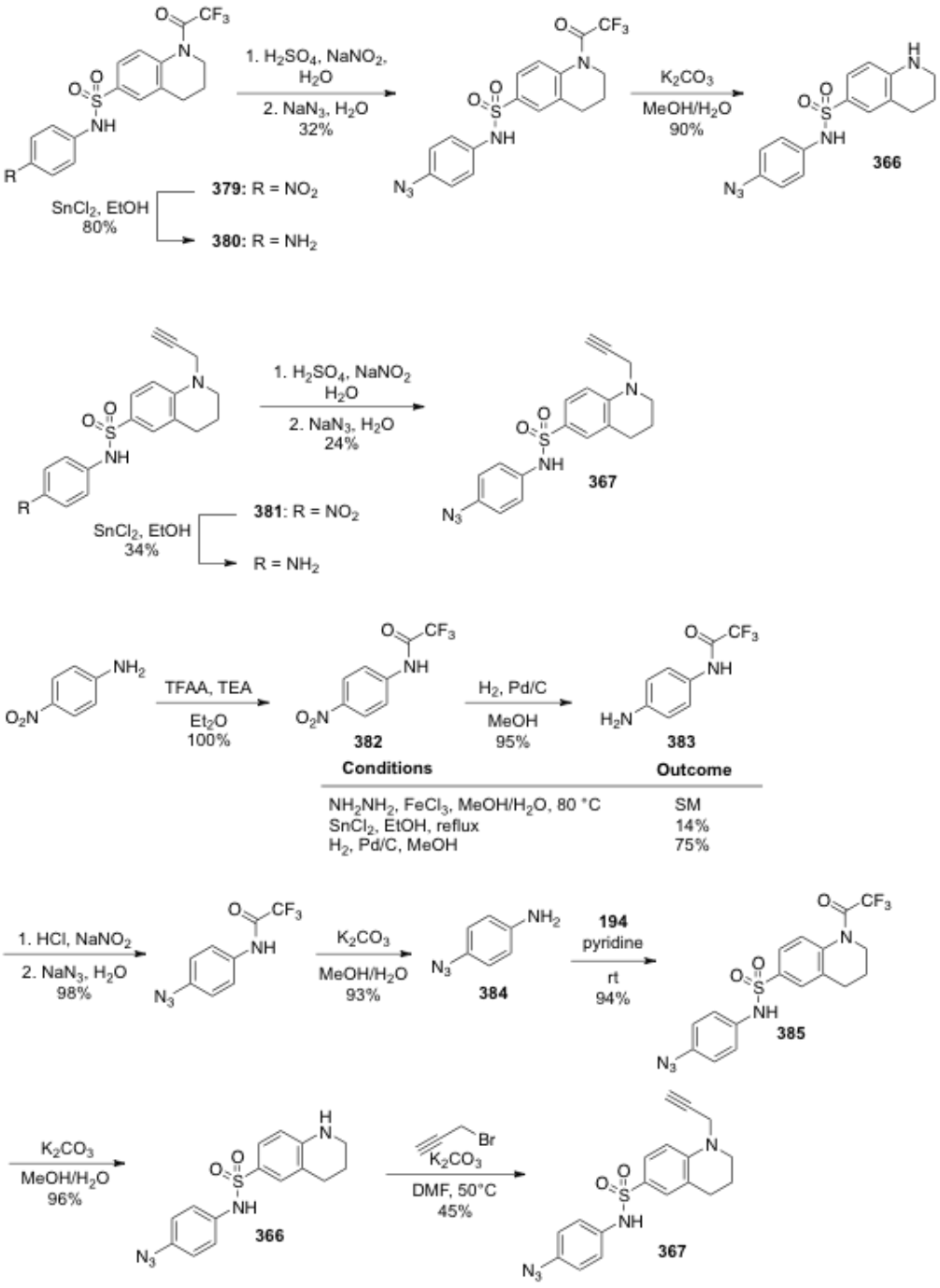

Scheme 4.2: Different synthetic approaches towards the azides **366** and **367**.

The *ortho*- and *para*-substituted benzophenone derivatives were synthesized as shown in Scheme 4.1. However, these conditions failed to deliver the *meta*-analog **370**. Several test reactions were performed using the commercially available *para*-toluenesulfonyl chloride and 3-

aminobenzophenone in order to optimize the coupling reaction, but were similarly unsuccessful in delivering the expected product. For example, when *p*-toluenesulfonyl chloride and 3-aminobenzophenone were treated with TEA in DCM, NaH in DMF,[252] or refluxed in pyridine,[253] only trace amount of the product was obtained. Similarly, only unreacted starting materials were observed following treatment with copper(II) oxide in ACN[254] or with pyridine in DCM at rt. It was then attempted to render the carbonyl group less electron withdrawing via protection of the ketone with ethylene glycol. 3-Aminobenzophenone was heated under Dean-Stark conditions in toluene, with ethylene glycol and *p*-toluene sulfonic acid, but the corresponding acetal was not obtained.[255] Another strategy was adopted, which aimed to transform the deactivating carbonyl group into a corresponding electron-donating hydroxyl group (Scheme 4.3). 3-Aminobenzophenone was heated to reflux in EtOH in presence of sodium borohydride to provide the alcohol **386** in 88% yield.[256] The intermediate **386** was treated with **194** in refluxing pyridine, which successfully delivered the *meta* sulfonamide derivative **387**. The alcohol was subsequently oxidized with pyridinium chlorochromate (PCC) in DCM.[257] Removal of the protecting group delivered the final analog **370** as a yellow solid in 81% yield (Scheme 4.3).

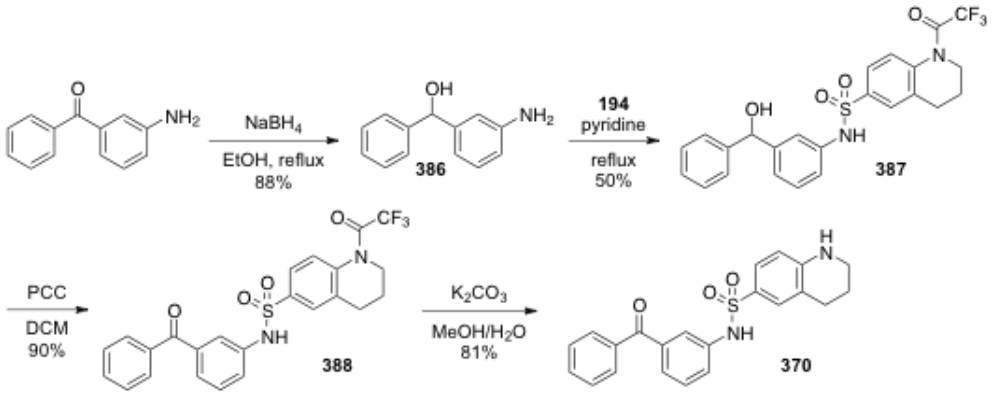

Scheme 4.3: Synthesis of the meta-benzophenone analog **370.**

Treatment of 2-aminobenzophenone with **194** in refluxing pyridine (Scheme 4.1) provided the TFA-protected derivative **389**, which was subsequently treated with iodomethane and K_2CO_3 to afford the methylated sulfonamide **390**.[258] Removal of the protecting group yielded **376**, which was further alkylated with propargyl bromide and K_2CO_3 to deliver **377** (Scheme 4.4). In summary, two small molecule inhibitors of miR-122 (**367** and **377**) have been successfully synthesized that contain either an arylazide or a benzophenone functionality that can be used in photo-crosslinking experiments.

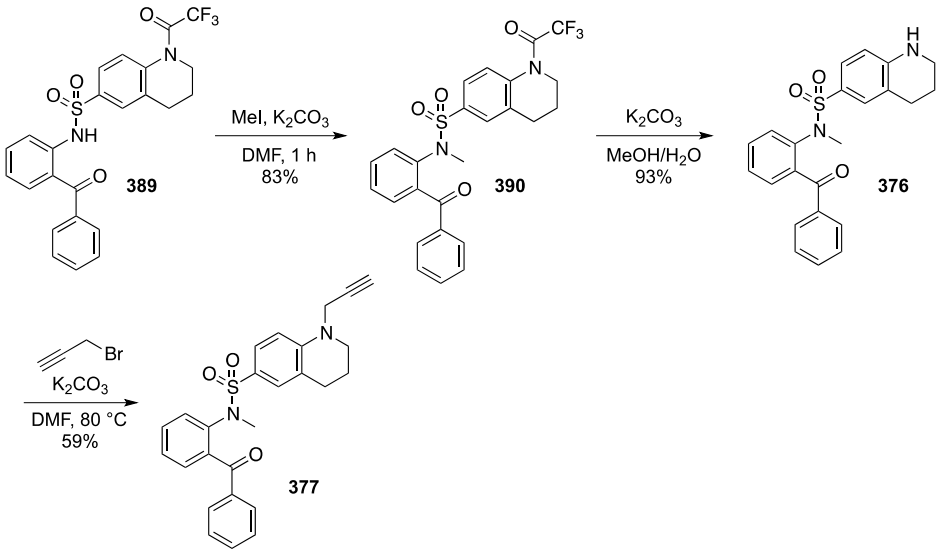

Scheme 4.4: Synthesis of benzophenone analogs **376** and **377.**

It was envisioned that a small molecule structurally similar to the active photoprobe, also substituted with the photo-crosslinking and the alkyne functional groups, but which does not exhibit any miR-122 inhibition would provide an important negative control for the photoaffinity labeling experiments, and help to distinguish the target protein from non-specific protein-small molecule interactions. Previously, it was observed that the amide analog of **30**, **240** was completely inactive in the luciferase reporter assay. Based on this observation, the amide **394** was synthesized as a negative control (Scheme 4.5). 6-Quinolinecarboxylic acid was protected as

a methylester after being heated to reflux in MeOH in presence of thionyl chloride.[259] The pyridine ring was reduced with Pd/C and ammonium formate in refluxing MeOH.[224] The amine **391** was alkylated with propargyl bromide and K_2CO_3 to deliver the propargylated intermediate **392** in 88% yield.[251] Hydrolysis of the ester was carried out with NaOH in a mixture of MeOH/H_2O for 4 h at 50 °C. Treatment of the acid **393** with 4-azidoaniline (**384**), the peptide coupling reagent HATU, and DIPEA afforded the amide derivative **394** (Scheme 4.5). As expected, **394** displayed very little miR-122 inhibitory activity, which validated its function as a negative control.

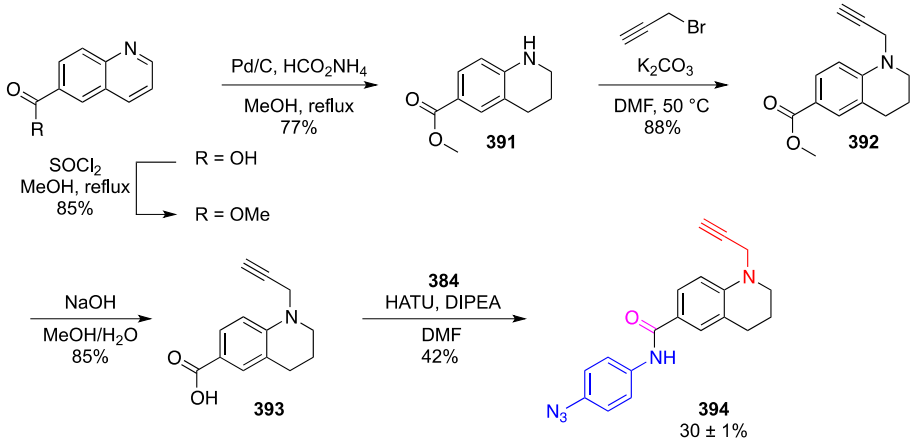

Scheme 4.5: Synthesis of the inactive small molecule probe **394.**
The alkyne functionality is shown in red, the arylazido photo-crosslinking group is shown in blue, and the amide deviation from the parent structure **30** is shown in magenta.

4.2.2 Target Identification Experiments with the Inhibitor 30

In order to selectively detect proteins crosslinked to **367**/**377**, the azido-rhodamine **396** was synthesized in 4 steps (Scheme 4.6) to perform [3+2] cycloaddition reactions.[260] 1,6-Dibromohexane was heated to 55 °C in DMF in the presence of NaN_3 to deliver 1-azido-6-bromohexane, following nucleophilic substitution of the bromine was achieved after treatment with methylamine in THF. Rhodamine B was heated to reflux in carbon tetrachloride (CCl_4) and

thionyl chloride, and the resulting acyl chloride was treated with the amine **395** and K_2CO_3 to afford the azido-rhodamine **396** as a bright pink powder (Scheme 4.6).[261] Since it was reported that when substituted with a secondary amide, the rhodamine can quickly undergo cyclization to form a non-fluorescent lactam derivative,[262] the azide-rhodamine **396** was modified with a tertiary methylamide to prevent the formation of the cyclic by-product.

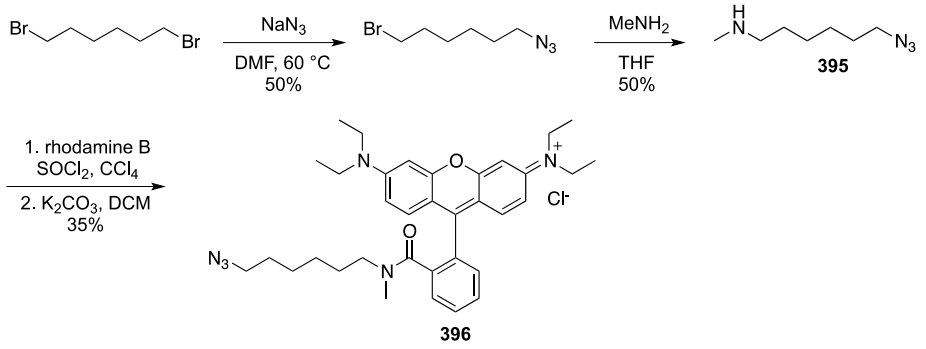

Scheme 4.6: Synthesis of the azido-rhodamine **396.**

The photo-crosslinking strategy employed using the developed photoprobes **367**, **377**, and **394** and the azido-rhodamine is outlined in Figure 4.3. Huh7 cells were passaged into 10 cm plates and were grown to 90% confluency. The cells were treated either with DMSO, the inhibitor **30**, the small molecule probes **367** and **377** or the inactive derivative **394** (10 μM, 0.5% DMSO). After overnight incubation at 37 °C, the cells were washed with PBS to remove any excess probe and irradiated for 10 min at 365 nm (based on literature reports; further optimization of the photocrosslinking experiment are discussed below). The cells were pelleted by centrifugation and lysis was carried out with mammalian protein extraction buffer, followed by incubation on ice for 20 min and vortexing every 5 min. After centrifugation, the supernatant containing the protein lysate was submitted to a [3+2] cycloaddition reaction with the azido-rhodamine **396**, in the presence of TCEP, copper (II) sulfate, and TBTA.[146] Each sample was

analyzed by SDS-PAGE and the gel was imaged on a phosphorimager (filter 580 nm, rhodamine B: excitation wavelength is 540 nm and emission wavelength is 625 nm).

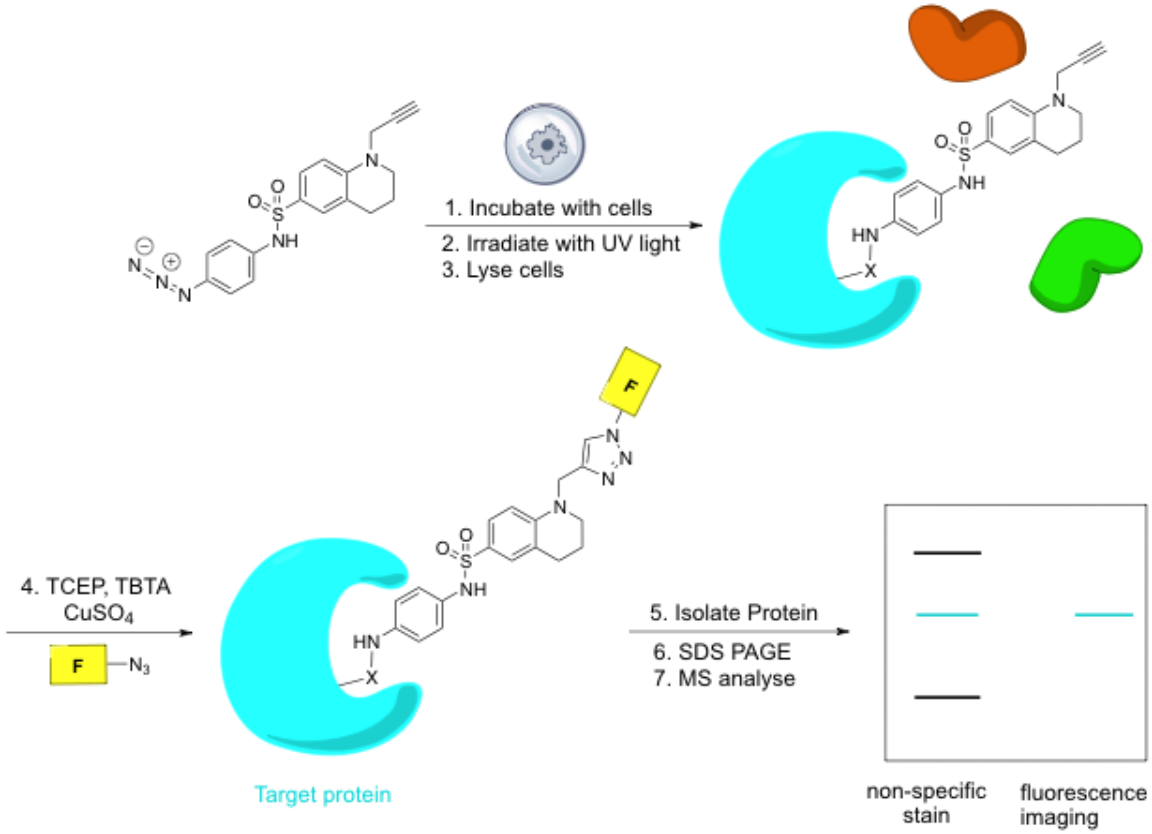

Figure 4.3: Representation of the photo-crosslinking strategy applied to detect the target protein(s) of the miR-122 inhibitor **30.**
The inhibitor was modified with a photoreactive group, incubated with live cells, and covalently linked to its target protein upon UV irradiation. Following click reaction with a fluorophore-azide (F), the lysate was analyzed by SDS-PAGE and the target protein was detected when the fluorescence was imaged. X represents the binding site residue of the target protein that covalently reacts with the photoprobe.

Figure 4.4 shows an example of a gel obtained after photoaffinity labeling experiments using the probes **367**, **377**, and the negative control **394** in conjunction with the azido-rhodamine **396**. As expected, there was no fluorescence detected when the cells were treated either with DMSO or the inhibitor **30**, which represents a negative control as it lacks a photoreactive group (lanes 2 and 3, Figure 4.4). However, two distinct bands were observed at ~50-60 kDa for the sample containing the photoactive probe **367** (lane 4, Figure 4.4). A competitive experiment was

also performed where the cells were exposed to both **367** (10 μM) and a 5-fold excess of **30** (50 μM). A slight decrease in fluorescence intensity was observed for the competition experiment (lane 5, Figure 4.4). Notably, the top band was less intense in lane 5 than in lane 4, indicating that the inhibitor **30** was able to successfully compete with the photoprobe **367** for binding to the target protein. In the sample treated with the negative-control probe **394**, which displayed only minimal miR-122 inhibitory activity, no fluorescence was detected (lane 6) indicating that the two fluorescently-labeled proteins observed in lane 4 are specific to the miR-122 inhibitor probe **367**. Although, the benzophenone **377** exhibited a higher potency than **367** in the luciferase assay, no protein labeling was achieved with this probe (lane 7). This lack of efficiency might be due to the substitution in the *ortho* position of the benzophenone moiety, which may lead to lower effectiveness of the probe **377**.[114] It was attempted to optimize the photoaffinity labeling of the benzophenone probe **377**. A time course experiment was performed where cells treated with **377** (10 μM) were irradiated with UV light for 10, 20, 30, or 45 min. The cells were lysed, treated with the azido-rhodamine, and analyzed by SDS-PAGE. Even with longer irradiation times, no fluorescence was detected, except for the 45 min time point where some fluorescent bands were visible. However, efforts to reproduce this data were unsuccessful. It was also attempted to treat the cells with higher concentrations of **377**, but even after treatment at 20 or 40 μM the photoaffinity labeling remained unsuccessful.

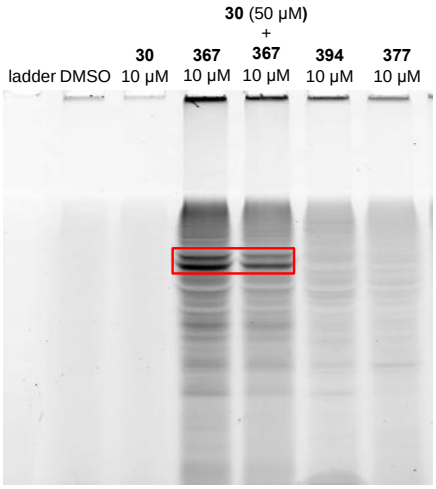

Figure 4.4: Fluorescence imaging of an SDS-PAGE of protein samples isolated from Huh7 cells treated with DMSO, the miR-122 inhibitor **30**, the photoprobes **367** and **377**, or the negative control **394.**
Fluorescence was imaged on a phosphorimager. The two fluorescently labeled proteins are indicated by a red box.

Since **367** was the only probe capable of selectively labeling the target proteins, it was used in subsequent target ID studies. Higher concentrations of **367** were tested, but due to toxicity, it only resulted in lower protein recovery. The cells were incubated with **367** either for 3 h or 16 h, but only a low level of fluorescence was detected after the 3 h incubation, suggesting the overnight incubation was favorable. The cells were irradiated with UV light at different wavelengths and the same two bands were detected after irradiation at 254 or 365 nm, but only the top band was detected - albeit very weakly - after irradiation at 302 nm. Since it was previously reported that the optimal wavelength for photolysis of aryl azides is >315 nm, given they absorb UV light in the 300-320 nm range, the subsequent photo-labeling experiments were performed at 365 nm.[263] The labeling experiment was also tested under denaturing conditions. The samples were heated to 95 °C for 10 min (in 1% SDS) prior to the click reaction, and analyzed by PAGE side by side with the corresponding non-denatured samples. The same two fluorescently labeled bands were detected in both lanes, indicating that the alkyne group of **367** was similarly accessible to the azido-rhodamine under native or denaturing conditions. In

another experiment, following exposure to **367**, the proteins were extracted with a nuclear protein extraction kit (NE-PER kit, Pierce), which allowed for the extraction of the nuclear and cytoplasmic proteins separately. The proteins issued from both fractions were submitted to the click reaction with the azido-rhodamine and analyzed by SDS-PAGE. No fluorescence was detected in the nuclear extract sample, however the two bands previously observed were present in the cytoplasmic fraction, indicating that the target proteins are localized in the cytoplasm.

The previous experiments with the rhodamine **396** represented a proof-of-principle for the successful realization of photoaffinity labeling and allowed for the detection of the protein targets of the inhibitor. However, the main goal is to identify the proteins through isolation and MS analysis. The proteins must be isolated in a high purity and quantity in order to be accurately identified. The azido-biotin **397**[264] was then synthesized from the azidoamine **190** and biotin-NHS (Scheme 4.7) to facilitate the isolation of the target proteins via affinity purification with a streptavidin resin. Since biotin and streptavidin have extremely high affinity for each other, the biotin group serves as a linker to attach the biotinylated probe/protein complex to the streptavidin resin, allowing non-specific proteins to be removed through a series of washes and enriching the target protein by elution from the resin.[222]

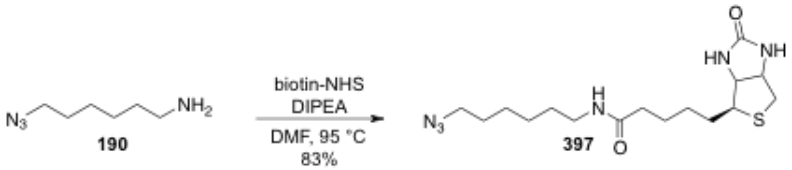

Scheme 4.7: Synthesis of the azido-biotin **397.**

The crosslinking experiments were repeated in Huh7 cells treated with **367**, except the azido-biotin **397** was used in the click reaction instead of the rhodamine **396** (Figure 4.5). Following the click reaction, an acetone precipitation was performed to remove any excess click

reagents and the proteins were re-dissolved in PBS supplemented with different amounts of the streptavidin resin and incubated at 4 °C overnight. The resins were thoroughly washed to remove any non-specific proteins and then suspended in SDS loading buffer, denatured at 95 °C for 15 min, and analyzed via a 12% SDS-PAGE. This experiment was repeated several times, using varying amounts of protein and the streptavidin resin, in attempts to improve the purification. A representative gel is shown in Figure 4.5. Unfortunately, lower amounts of streptavidin (<80 μL, lane 2) did not enable efficient pull-down of the target proteins, and higher amounts of resin (>100 μL, lanes 3-5) resulted in the isolation of a significant amount of non-specifically binding proteins.

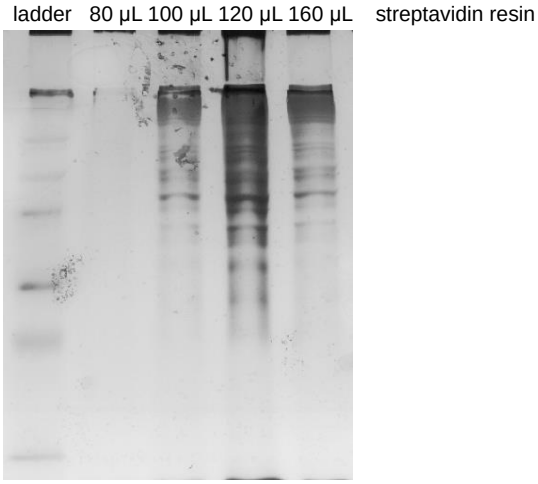

Figure 4.5: Example of a silver-stained 12% SDS-PAGE of protein samples isolated from Huh7 cells treated with the photoprobe **367,** labeled with the biotin-azide, and purified with various amounts of streptavidin resin.

The same results were observed with varying amounts of protein. When the experiment was carried out with 150 μg of protein, only one very faint band of the expected size (~50-60 kDa) was detected on the gel after silver staining. Although the protein was pure, it was obtained in a quantity too low for MS analysis. Subsequent attempts to increase the protein yield, by performing the labeling experiment with higher amounts of protein for example, resulted in the

isolation of many non-specific proteins, some of which were biotinylated (as determined by an anti-biotin Western blot). Since biotin binds to streptavidin with a high affinity, the conditions required for the elution of the biotinylated probe/protein complex were somewhat harsh: the protein samples were eluted after being heated in SDS loading buffer at 95 °C for 15 min. Therefore, any protein bound to the streptavidin resin was denatured and eluted along with the target protein(s).

Next, a different purification of the target protein(s) was attempted by using two-dimensional gel electrophoresis (2-D gel), which is a technique commonly employed to purify proteins from complex samples based on their isoelectric points and molecular weights. First the solubilized samples are loaded onto an IPG (immobilized pH gradient) strip, and an electric current is applied. The proteins separate as they migrate through the pH gradient until they reach their isoelectric point, which corresponds to the pH where the net charge of the protein becomes neutral.[265] The second dimension consists of a standard SDS-PAGE, where the proteins are separated based on their molecular weights in a perpendicular direction to the first dimension. The proteins are then separated and aligned along two axes: isoelectric points vs molecular weights. Although quite straightforward in theory, the 2-D gel technique required extensive optimization. Since the IPG strips are supplied dried, a critical step prior to running the isoelectric focusing consists in solubilizing the proteins in a compatible buffer in order to rehydrate the IPG strip. The rehydration step can be performed in two different ways: active rehydration is done in 30 min under low voltage current, whereas passive rehydration is often done overnight on a bench top. The experimental conditions, such as amounts of proteins used, rehydration method, and incubation time were extensively optimized. Although time consuming, 24 h passive rehydration was found to give the best results.

Huh7 cells were treated with the aryl azide probe **367** (10 μM) and incubated overnight at 37 °C. The cells were irradiated at 365 nm for 10 min and then lysed using mammalian protein extraction buffer supplemented with protease inhibitor cocktail. A Bradford assay was performed to quantify the protein extract, and 100 μg of total protein was used in a click reaction with the rhodamine-azide **396**, which was carried out in the presence of TCEP, $CuSO_4$, and TBTA for 2 h at room temperature.[146] A comprehensive optimization of the [3+2] cycloaddition reaction conditions was not conducted. An acetone precipitation was then performed to remove excess click reaction reagents, and the sample was analyzed by 2-D gel electrophoresis. The sample was loaded onto a pH 4-7 ReadyStrip IPG strip (Bio-Rad) through passive in-gel rehydration for 24 h at room temperature. The proteins were then separated according to their isoeletric points on a PROTEAN IEF Cell (Bio-Rad) following the manufacturer's protocol. The IPG strip was loaded onto a 12% SDS-PAGE and the proteins were further separated according to their molecular weights. The fluorescence was then visualized on a Typhoon 7000 phosphorimager, and the gel was silver stained to determine whether the target protein(s) could be selectively excised from the gel (Figure 4.6A). The procedure was repeated to obtain an additional non-stained gel for mass spectrometry analysis (Figure 4.6B).

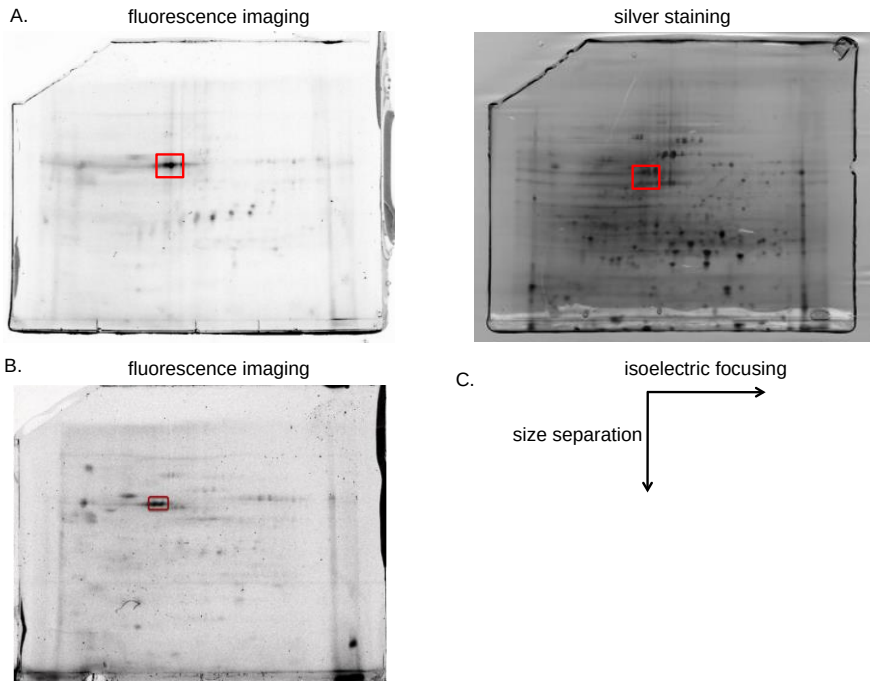

Figure 4.6: Representative gels obtained following 2-D gel experiments in Huh7 cells.
A. Fluorescence imaging and silver staining of a 2-D gel containing proteins isolated from Huh7 cells treated with the photoprobe **367** and labeled with the rhodamine-azide **396**. **B**. Fluorescence imaging of the 2-D gel containing proteins isolated from Huh7 cells treated with the photoprobe **367** and labeled with the rhodamine-azide **396** that was submitted for analysis by mass spectrometry. The fluorescently labeled proteins are indicated by a red box. **C**. The directions of the two separation steps are indicated.

The gel in Figure 4.6B was submitted to Nedyalka Dicheva at the UNC Michael Hooker Proteomics Center at UNC Chapel Hill for protein identification. At the Proteomics Center, the gel was stained with coomassie blue and the fluorescent proteins were excised in a single sample, as the two fluorescent spots were not resolved enough to be individually excised. The sample was destained and digested in-gel using trypsin (performed by Nedyalka Dicheva). The resulting peptide fragments were extracted from the gel and analyzed with an ABI 4800 MALDI-TOF/TOF MS. The identity of the target protein was determined upon examination of the resulting mass spectrum of the digest peptide products and comparison with theoretical peptide maps stored in publicly available database (Mascot). The results obtained for the mass spectrometry analysis are shown in Table 4.1. The “Peptide Count” refers to the number of

observed peptides matching the theoretical digest of the identified protein, the "MS & MS/MS score" is the combined score of the quality of the peptide-mass fingerprint match and MS/MS peptide fragment ion matches, the "Peptide Sequenced Ion Score" is the score of the quality of MS/MS peptide fragment ion matched only, and the "Scoring Threshold" is a threshold set to determine hits based on the "MS & MS/MS score" or "Ion score" where score above this value are considered a significant identification. The top hit for the target protein corresponded to β-tubulin, which is a ~50 kDa protein involved in the assembly of microtubules.

Protein	MW (Da)	Peptide count	MS & MS/MS score	Peptide sequenced ion score	Scoring threshold
tubulin beta	47736	21	983	850	71
tubulin beta-4B chain	49799	21	897	770	71
tubulin alpha-1C chain	49864	5		143	71
ATP synthase, H+ transporting	56525	25	1740	1558	71

Table 4.1: Protein identification results for mass spectrometry analysis of rhodamine-labeled target proteins excised from a 2-D gel (data provided by Nedyalka Dicheva, UNC Michael Hooker Proteomics Center).

To correlate the previous results, the 2-D gel experiment was repeated with the photoprobe **367**, and the gel was submitted to the UNC Michael Hooker Proteomics Center for protein identification, which was performed as previously described. Similarly to the previous experiment, the two fluorescent spots could not be separated and were analyzed in a single sample. β-Tubulin did not appear as a hit in this experiment. Instead, ATP synthase subunit beta (~56 kDa), 26S protease regulatory subunit 6B (~47 kDa), and the heat shock protein HSP-60 (~61 kDa) were identified (Table 4.2).

Protein	MW (Da)	Peptide count	MS & MS/MS score	Peptide sequenced ion score	Scoring threshold
ATP synthase subunit beta	56525	20	621	557	61
26S protease regulatory subunit 6B	47337	15	250	179	61
protein disulfide-isomerase A6	48091	9	104	79	61
60 kDa heat shock protein	61016	11	257	228	61

Table 4.2: Protein identification results for mass spectrometry analysis of rhodamine-labeled target proteins excised from a 2-D gel (data provided by Nedyalka Dicheva, UNC Michael Hooker Proteomics Center).

The same experiment was repeated: Huh7 cells were treated with the arylazide **367**, irradiated with UV light, lysed, conjugated with the azido-rhodamine **396**, and the lysate was analyzed on a 2-D gel. Two similar gels were obtained (Figure 4.7), the fluorescent areas (comprised of the 2 unresolved fluorescent protein spots) were excised and submitted to the Biomedical Mass Spectrometry Center at the University of Pittsburgh for comparison.

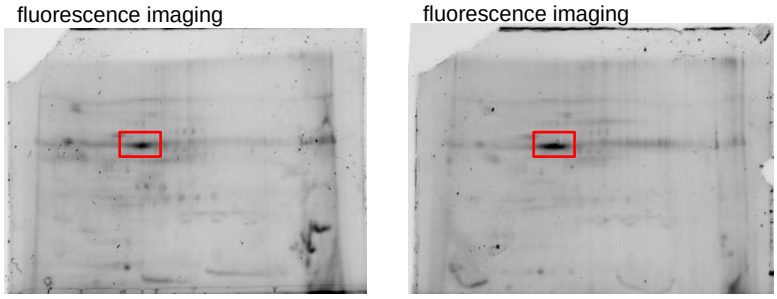

Figure 4.7: Fluorescence imaging of the 2-D gel containing proteins isolated from Huh7 cells treated with the photoprobe **367** and labeled with the rhodamine-azide **396** that were submitted for analysis by mass spectrometry. The fluorescently labeled proteins are indicated by a red box.

The samples were digested with trypsin and the tryptic peptides were analyzed by nano reverse phase HPLC interfaced with a mass spectrometer. The tandem mass spectra (MS/MS) were analyzed as previously with the search engine MASCOT and identified peptides and proteins were further statistically validated with the Scaffold software. A total of 66 putative

target proteins were identified, and the top "hits" from both samples were in good correlation (Table 4.3). The percent numbers represent the "sequence coverage" or the similitude between the theoretical sequence and the numbers of matching peptides from the analyzed sample. Although there was no correlation found between the 2 previous analyses (Table 4.1 and Table 4.2), the most probable protein identified in both new samples was β-tubulin and the third most probable was the ATP synthase subunit beta, which were previously detected in the first and second protein identification experiments, respectively. The second highly probable protein (>60% percent coverage) identified in both samples was vimentin (Table 4.3), a type III intermediate filament that is a major component of the cytoskeleton with tubulin and actin proteins. Other proteins were predicted with a lower probability, such as keratin, which probably resulted from contamination.

Protein	MW (kDa)	Sample 1 (%)	Sample 2 (%)
tubulin beta	50	74.3	70.5
vimentin	54	62.7	59
ATP synthase subunit beta	57	69.4	39.5
keratin, type II	66	51.7	15.5
keratin, type I	59	52.1	9.93
tubulin alpha-1B	50	42.4	55.9

Table 4.3: Protein identification results for mass spectrometry analysis of rhodamine-labeled target proteins excised from a 2-D gel (data provided by Biomedical Mass Spectrometry Center, University of Pittsburgh).

The identification of the binding partner of a small molecule drug/probe is critical in understanding the precise mechanism of the compound and in predicting its safety profile.[266] However, target identification is a challenging process, associated with multiple obstacles, and often represents the bottleneck in chemical genetics approaches. For example, the specific detection of low-abundant proteins is very difficult due to the presence of highly abundant non-specific binding proteins, such as cytoskeleton proteins tubulin, actin, and heat shock proteins, as

well as mitochondrial ATP synthases.[266] In fact, actin and tubulin proteins have been reported to commonly interfere with target identification analyses due to their high abundance and their molecular weight (42 and 50 kDa), which is similar to that of many putative target proteins.[267] Since β-tubulin was identified as a positive hit for the target protein in three out four analyses, follow-up experiments were implemented in order to evaluate β-tubulin as a real hit and confirm that it corresponds to one of the fluorescently-labeled proteins. Huh7 cells were treated with the photoprobe **367** (10 μM) and incubated overnight at 37 °C. The cells were irradiated at 365 nm for 10 min, lysed, submitted to a click reaction with the rhodamine-azide **396**, and acetone precipitated. The samples were run on a 12% SDS-PAGE, the fluorescence was imaged (Figure 4.8A), and the samples were further analyzed by Western Blot using β-tubulin and GAPDH (control) primary antibodies and a goat-anti-rabbit-IgG-HRP secondary antibody. The Western Blot was developed by HRP colorimetric staining and imaged on a phosphorimager (Figure 4.8A). These results suggested that the lightest band detected after photo-crosslinking with **367** may be β-tubulin. The same Western Blot analysis was also performed on a sample separated via 2-D gel, and validated that the fluorescently-labeled spot corresponded to β-tubulin (Figure 4.8B). The correct identification of β-tubulin as one of the fluorescently-tagged proteins, although promising, does not guarantee that β-tubulin is a real cellular target for **367**, and it still needs to be considered that its detection might be due to non-specific hydrophobic interactions with the probe or the fluorophore, or alternatively that the target protein simply has a similar molecular weight. One method to address this question would consist in depleting the cell lysate of any abundant non-specific binders prior to the click reaction. For instance, the cell lysate might be pre-cleared using an agarose resin before being used in the [3+2] cycloaddition

reaction,[267] and both conditions, ±lysate pre-clearing, can be analyzed side by side on an SDS-PAGE to examine for any differences in the proteins fluorescently-labeled.

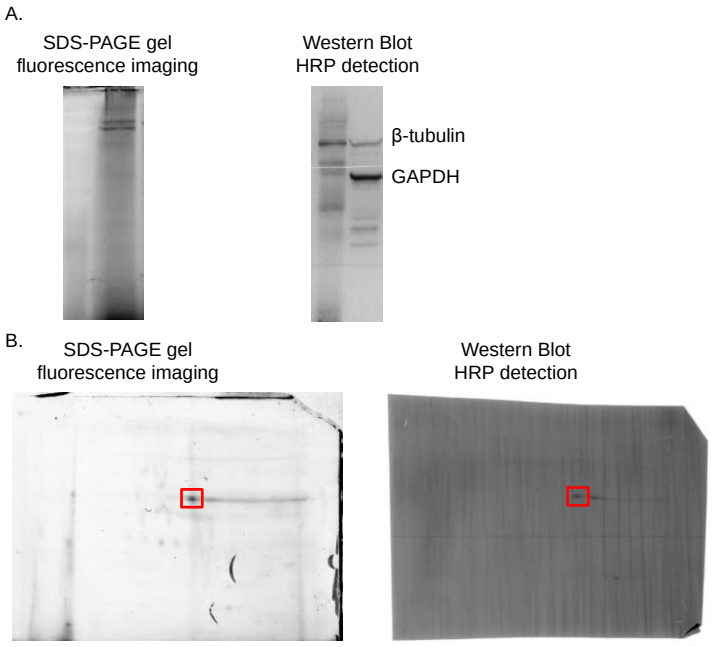

Figure 4.8: Validation studies of β-tubulin as a potential target for the miR-122 inhibitor **30.**
A. Fluorescence imaging of an SDS-PAGE containing proteins isolated from Huh7 cells treated with the photoprobe **367** and labeled with the rhodamine-azide **396** (left). Colorimetric HRP detection of β-tubulin by Western blot (right). Lane 1: Ladder, Lane 2: **367** (10 μM). **B.** Fluorescence imaging of a 2-D gel containing proteins isolated from Huh7 cells treated with the photoprobe **367** and labeled with the rhodamine-azide **396** (right). Colorimetric HRP detection of β-tubulin by Western blot (right). The fluorescently labeled proteins are indicated by a red box.

Given that one of the fluorescently-tagged proteins was identified as β-tubulin, a loss of function experiment was performed to determine whether inhibiting β-tubulin affected miR-122 expression. Huh7-psiCHECK-miR122 cells were transfected with an siRNA targeting β-tubulin (class 4B, Sigma Aldrich, NM_006088) at 50 or 100 pmol. Following transfection the cells were incubated at 37 °C for 48 h and the luminescence was analyzed with a dual luciferase assay (Promega). Figure 4.9 shows that the β-tubulin siRNA did not modify the intensity of the luciferase signal compared to the XtremeGENE control, suggesting that inhibiting β-tubulin did not promote the inhibition of miR-122. However, only the isotype 4B was targeted with the

siRNA (based on the MS analysis Table 4.1). Since β-tubulin has diverse isotypes, further experiments should be performed, with a pool of siRNA corresponding to the different isotypes for example, and the efficiency of the silencing should be confirmed either by Western Blot analysis or qRT-PCR measurements, before concluding that the inhibition of β-tubulin does not affect miR-122 regulation.

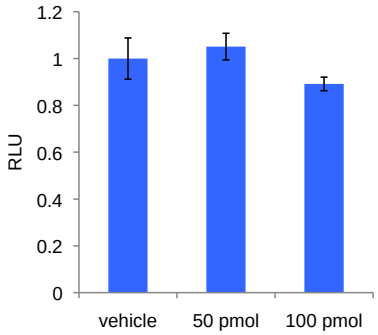

Figure 4.9: Assessment of the validity of β-tubulin as the target protein of the inhibitor **30.**
Huh7-psiCHECK-miR122 cells were transfected with an siRNA for β-tubulin at (50 or 100 pmol). Data were normalized to the vehicle (XtremeGENE transfection reagent) control. Experiments were performed in triplicate and the standard deviations of the three independent assays were calculated.

Due to the large number of putative proteins identified in the mass spectrometry analyses, it was hypothesized that the protein separation using 2-D gel did not afford samples with the desired/necessary purity. Indeed, the two fluorescent spots could not be resolved on the 2-D gel, and the protein spots were not detected after coomassie blue staining, which complicated the delicate step of band excision from the gel and increased the risk of including non-specific proteins. Another strategy was then designed to try to further purify the target proteins. Since pull-down experiments using biotin-streptavidin were unsuccessful due to the harsh elution conditions required, it was hypothesized that immunopurification might achieve efficient recovery of the target proteins since this method necessitates milder elution conditions.

It was then attempted to isolate the target proteins by immunopurification (IP) using the fluorescein-azide **191**. Huh7 cells were treated overnight with the aryl azide **367** or the negative

control **394** (10 μM), irradiated at 365 nm for 10 min, and lysed. Following the [3+2] cycloaddition reaction with the fluorescein-azide **191** and acetone precipitation (as previously described), the samples were re-suspended in tris-buffered saline (TBS) and incubated with a monoclonal anti-fluorescein IgG antibody (Sigma) at 4 °C overnight. The samples were then incubated with protein A/G agarose beads (Sigma) at 4 °C for 3 h. Proteins A/G are immunoglobulin (IgG)-binding proteins. Supported by the agarose resin they provide an affinity ligand for polyclonal and monoclonal IgG antibodies, therefore facilitating their purification (Figure 4.10). The mixtures were loaded onto spin columns and washed several times to remove any unbound proteins. Several conditions were tested for the elution of the target proteins, and only similar treatment as previously described for the biotin-streptavidin purification (95 °C for 15 min in SDS loading buffer followed by centrifugation) enabled the detection of proteins by SDS-PAGE. A representative gel is shown in Figure 4.11.

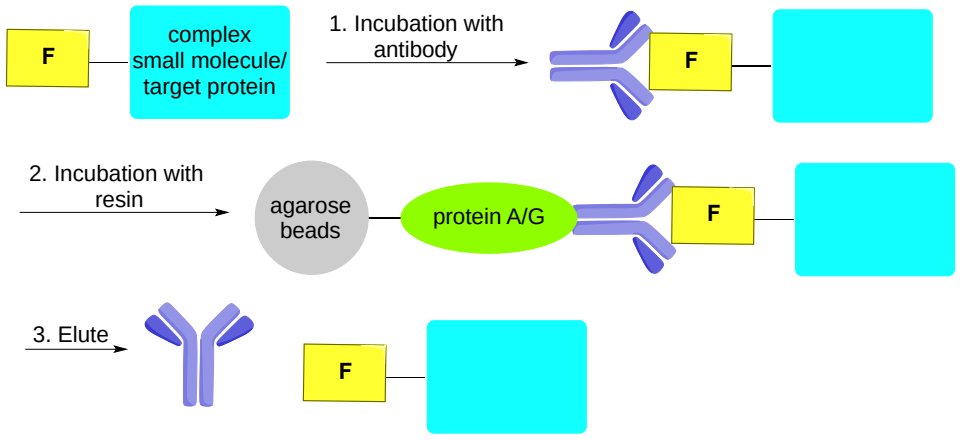

Figure 4.10: Representation of the immunopurification strategy.
F represents the fluorescein tag added to the complex of the small molecule/target protein via click reaction.

Again, several experimental conditions were tested, where the amounts of total protein subjected to the click reaction, the amounts of antibody, and the quantity of the agarose-protein

A/G beads were modified to improve the purification. Although the optimized conditions enabled the selective detection of only one fluorescently-labeled protein with the active photoprobe (lane 2, Figure 4.11), coomassie blue staining revealed that some other, non-labeled proteins were recovered as well. For example, no band was detected in lane 3 when the fluorescence was imaged, but the same bands were observed in both lanes 2 and 3 after coomassie staining. Similar to the purification using the streptavidin resin described previously, non-specific interactions between the protein A/G agarose beads and non-labeled proteins within the sample may occur. If the non-specific proteins are not effectively removed during the wash steps, these proteins will be eluted along the target proteins. Prior to the elution step the samples are denatured directly on the resin, which results in the co-elution of the target proteins and the antibody. Given that the molecular weight of IgG antibody heavy chain is ~50 kDa, it is possible that the heavy chains co-migrate with the target proteins on the SDS-PAGE gel, which may explain the detection of several bands around this area after coomassie staining (lanes 2 and 3, Figure 4.11).

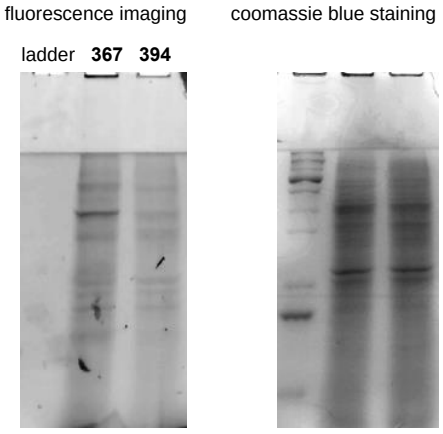

Figure 4.11: Imaging of a 12% SDS-PAGE containing protein samples isolated from Huh7 cells treated with the photoprobe **367** (10 µM) or the negative control **394** (10 µM), labeled with the fluorescein-azide, and purified with 7 µL of anti-fluorescein antibody and 80 µL protein A/G agarose beads.
Fluorescence was imaged on a phosphorimager.

Since one important drawback of the previous method lied in the co-migration of the target proteins and the heavy chains of the anti-fluorescein antibody due to their similar molecular weights, it was hypothesized that their isoelectric points might be different, and therefore they could be separated on a 2-D gel. The immunopurification procedure previously described was repeated, except the elution was performed using the rehydration buffer (BioRad) required for the proper rehydration of the IPG strip. Figure 4.12 shows a representative gel. Although some fluorescence was detected, the intensity was much weaker than previously observed, and after silver staining no spots were visible in the expected area of the target proteins (indicated with a red box), suggesting that the target protein was recovered in a quantity too low for accurate mass spectrometry analysis.

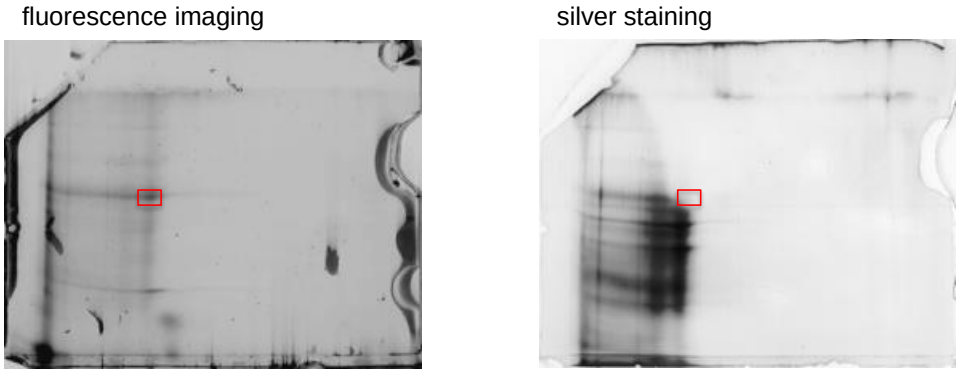

Figure 4.12: Imaging of a 2-D gel of protein samples isolated from Huh7 cells treated with the photoprobe **367,** labeled with the fluorescein-azide **191,** and purified with the anti-fluorescein antibody and the protein A/G agarose beads.
Fluorescence was imaged on a ChemiDoc.

Lastly, it was attempted to purify the target proteins using an aldehyde-activated resin to covalently immobilize the antibody on the agarose beads (Direct IP kit, Pierce), which would prevent the antibody interference previously described. The aldehyde-activated resin was incubated for 2 h at rt in the presence of the anti-fluorescein antibody and cyanoborohydride, which enabled the covalent attachment of the antibody to the agarose beads. Huh7 cells were

treated overnight with the aryl azide **367** or the negative control **394** (10 μM), irradiated at 365 nm for 10 min, and lysed. Following click reaction with the fluorescein-azide **191** and acetone precipitation (as previously described), the samples were re-suspended in 300 μL of IP lysis buffer supplemented with the protease inhibitors sodium fluoride and vanadate, and loaded onto spin columns containing the resin modified with the anti-FITC antibody. The samples were shaken overnight at 4 °C and thoroughly washed. The proteins were then eluted by incubation of 50 μL elution buffer at rt for 10 min followed by centrifugation. Most antibody-antigen binding interactions are optimal under physiological conditions (pH 7.4), and elution methods often rely on the alteration of the pH and/or ionic state of the environment to effectively dissociate these interactions. The elution buffer used in that study was a 0.1 M glycine•HCl solution (pH ~2.8). Another strategy, that should be tested, consists in the selective elution of the small molecule/protein complex via the addition of an excess of the free antigen (ie. fluorescein). The antigen would compete with the probe/protein complex for binding to the antibody, thus displacing and releasing the complex. The elution process was repeated three times and the isolated fractions were recovered separately. The samples were analyzed on a 12% SDS-PAGE. A representative gel is shown in Figure 4.13. Once again, the procedure was repeated several times varying the amount of total protein subjected to the click reaction, the quantity of antibody, and the quantity of the resin used in order to optimize the purification. A very intense fluorescently-labeled protein (top band in all lanes Figure 4.13) was observed across all the conditions tested (~70 kDa), and remains to be identified. The fractions containing the resin washes should be similarly analyzed by SDS-PAGE to determine whether this protein is already present or if it is being eluted off the column only at the same time as the target protein. The gel showed that the target proteins were efficiently eluted off the columns after two washes with

elution buffer, however the eluted fractions were still contaminated with non-specific proteins. More surprisingly, the target proteins were also detected in the sample treated with the negative control **394** (lane 3, Figure 4.13). This was in contrast to previous experiments, when samples from Huh7 cells treated with the photoprobe **367** or the negative control **394** (10 μM) were loaded on a SDS-PAGE following the acetone precipitation (no purification performed), the fluorescently-tagged target proteins were only detected in the sample treated with **367**, in a similar fashion to what was observed in Figure 4.4. Similarly to Figure 4.4, including a competitive experiment, where the cells are exposed to both **30** (5-fold excess) and the photoprobe **367**, may provide a better control, presenting the same band pattern as **367** but with the target protein bands being competed out and fainter. The photo-labeling experiment might be attempted by treating the cells with a lower concentration of **367** (for example 5 μM), which may reduce the background, or non-specifically bound proteins, but may also result in a very low amount of target protein being recovered.

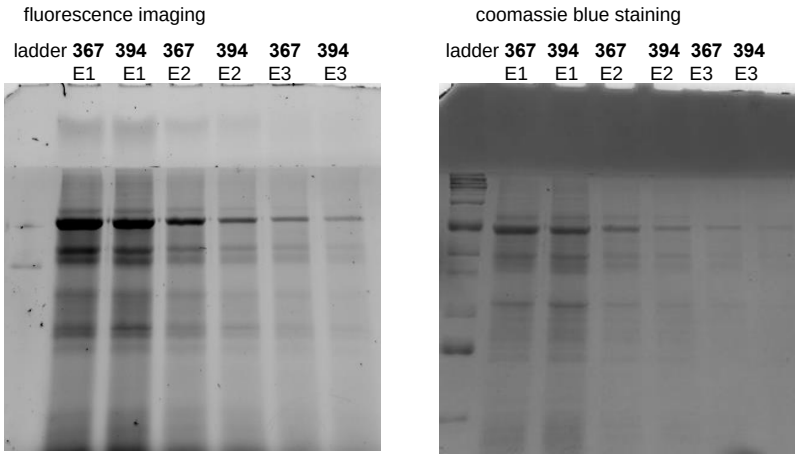

Figure 4.13: Imaging of a 12% SDS-PAGE containing protein samples isolated from Huh7 cells treated with the photoprobe **367** or the negative control **394,** labeled with the fluorescein-azide, and purified with anti-fluorescein antibody-conjugated beads.
Lane 1: ladder, Lane 2: **367** elution #1 (E1), Lane 3: **394** E1, Lane 4: **367** E2, Lane 5: **394** E2, Lane 6: **367** E3, Lane 7: **394** E3. Fluorescence was imaged on a ChemiDoc (left) and the gel was stained with coomassie blue (right).

Unfortunately, all attempts to purify and concentrate the target protein(s) remained unsuccessful. An alternative approach would be to introduce a selective cleavable linker between the target protein and the biotin moiety.[268] That way, the proteins could be isolated by affinity purification using the strong biotin-streptavidin interaction, and eluted using specific mild cleavage conditions, allowing for the release of the target proteins but leaving the non-specific proteins immobilized on the resin. Such tri-functional probes have been designed that contain an azido motif (shown in blue in Figure 4.14), a biotin group, a fluorophore, and a cleavable linker (shown in red in Figure 4.14). Although the fluorophore tag is not necessary, it greatly facilitates the detection of the target proteins on a gel. Unlike the previous biotin-streptavidin affinity purifications, which required harsh conditions, mild and selective elution of the target proteins could be achieved with UV light irradiation (365 nm) for the *o*-nitrobenzyl linker **398**,[268] with sodium periodate for the diol **399**,[268] or with sodium dithionite for the diazobenzene derivative **400**.[269]

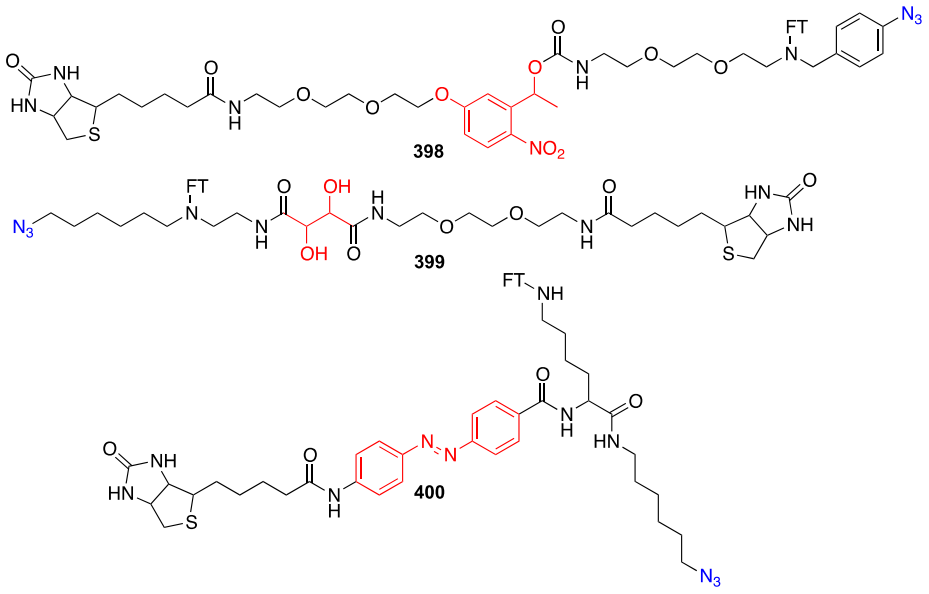

Figure 4.14: Potential tri-functional linkers that would facilitate the isolation of the target proteins following biotin-streptavidin pull-down and specific elution with UV light (**398**), $NaIO_4$ (**399**), or $Na_2S_2O_4$ (**400**). The azide (shown in blue) is required to attach the probe to the protein/small molecule complex using click reaction, the biotin group enables affinity purification with a streptavidin resin, the fluorophore (FT) tags the target proteins and facilitates their detection, and the selective cleavable linker (shown in red) allows for mild non-denaturing elution.

4.3 INVESTIGATION INTO MIR-122 EPIGENETIC REGULATION

As previously mentioned in Chapter 1.3, miRNA promoters share many characteristics with the promoters of protein-coding genes, implying that they are subjected to similar regulatory mechanisms, such as epigenetic modifications. For example, DNA methylation significantly affects gene transcription, either by blocking the binding of important transcriptional proteins to the gene promoter, or by stimulating the interaction between methylated DNA and methyl-CpG-binding domain proteins.[270] These proteins often recruit additional chromatin-modifying enzymes, which promote alteration in chromatin compaction and negatively affect transcription. Since the miR-122 promoter does not contain any CpG

islands,[198] the transcription of miR-122 was not thought to be directly influenced by DNA methylation. However, an increase in miR-122 expression was observed in hESCs (human embryonic stem cells) and HCC cells, following exposure to the DNA methyltransferase inhibitor 5-aza-2′-deoxycytidine (5-Aza-dC).[271] Chromatin immunoprecipitation assays and bisulfite sequencing revealed that miR-122 is repressed in those cell lines due to the hypermethylation of the promoter, which prevents the binding of RNA polymerase II to miR-122 promoter, thus blocking the transcription of miR-122.[271] Similarly, it was recently shown that co-treatment of HCC cells with 5-Aza-dC and the histone deacetylase (HDAC) inhibitor phenylbutyrate (PBA) inhibited the expression of SUV39H1 (an H3K9 methyltransferase), which resulted in a decreased binding between SUV39H1 and the miR-122 promoter and consequently stimulated miR-122 expression.[198] 5-Aza-dC/PBA co-treatment has also been found to induce miR-122 expression in HCC cells through the enhancement of the binding interaction between the transcription factor heterodimer PPARγ/RXRα (peroxisome proliferator-activated receptor-gamma/retinoid X receptor-alpha) and the DNA response elements DR1 and DR2 motifs within the miR-122 promoter.[198] Although some preliminary experiments have been attempted to determine the ability of **30** to interfere with the stimulatory effect of 5-Aza-dC on miR-122 expression, the results have been inconclusive. More work is needed to fully investigate if the miR-122 inhibitor **30** acts via the modulation of this regulatory pathway; for example by co-treating Huh7 cells with 5-Aza-dC and **30** and by measuring the effects on miR-122 expression in the miR-122 luciferase assay and by qRT-PCR.

Gene expression is under the control of a tightly regulated balance, where acetylation of lysine residues in core histones promotes a less compact transcriptionally active chromatin, and conversely deacetylation leads to a strong compaction between the positively charged histones

and the negatively charged DNA, therefore negatively affecting gene transcription. HDAC inhibitors, by disturbing this balance, alter the expression of several genes by inducing either transcriptional activation or repression.[272]

Experiments were carried out to investigate whether **30** may act as an HDAC inhibitor using the HDAC-Glo assay (Promega). The nuclear proteins from Huh7 cells were extracted using the nuclear extraction kit (NE-PER kit, Pierce) and the resulting amount was quantified with a Bradford assay. A titration curve was performed with different amounts of nuclear extract in order to determine the optimal concentration for the assay. The largest dynamic range was obtained with 10 μg/mL of nuclear extract; this concentration was then used in subsequent analysis. The Huh7 nuclear extract was diluted to 10 μg/mL in HDAC-Glo buffer, added to the wells containing increasing concentrations of **30** or TSA (HDAC inhibitor control, trichostatin A), and the plate was incubated at rt for 30 min. The HDAC-Glo reagent was added, the plate was quickly shaken to ensure proper mixing of the reagents, further incubated for 45 min, and the luminescence was measured. Figure 4.15 showed that **30** did not induce any HDAC inhibition even at high concentrations, contrary to the TSA control, which displayed >90% inhibition at 1 μM.

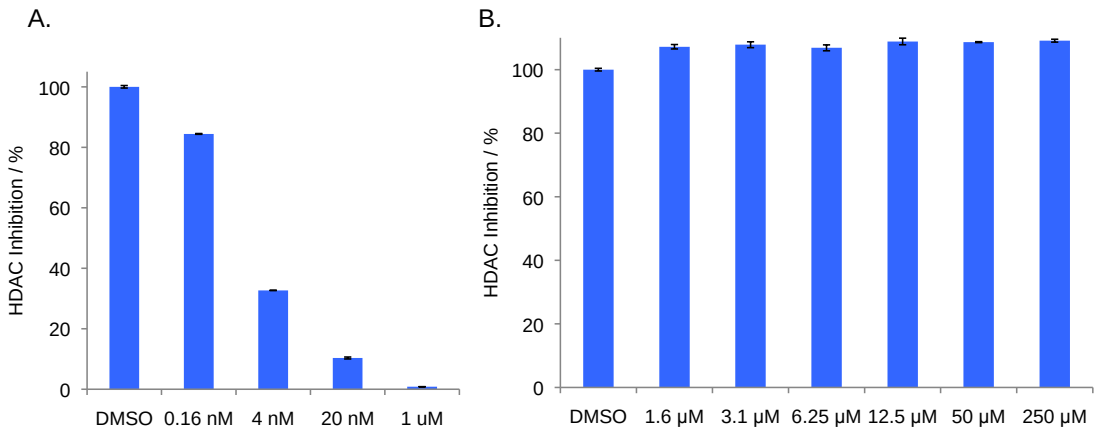

Figure 4.15: Analysis of small molecule **30** interference with HDAC activity**.**
HDAC-Glo assay of Huh7 nuclear extract treated with increasing concentration of **A**. the HDAC inhibitor TSA (positive control), and **B**. the miR-122 inhibitor **30**. Data were normalized to the DMSO control. Experiments were performed in triplicate and the standard deviations of the three independent assays were calculated

4.4 ANALYSIS OF THE SMALL MOLECULE INTERACTION WITH THE MIR-122 PROMOTER

4.4.1 Development of a Reporter Construct to Study miR-122 Promoter Activity

Since the inhibitor **30** does not seem to regulate epigenetic events involved in miR-122 regulation, it was hypothesized that it may target a transcription factor necessary for the expression of the miR-122 gene. To test this theory, a reporter plasmid containing a firefly luciferase gene under the control of the miR-122 promoter was constructed in collaboration with Colleen Connelly.[189] The miR-122 promoter was inserted into the pGL3-basic plasmid (Promega) within the multi-cloning site upstream of the firefly luciferase gene (Figure 4.16). The plasmid was sequentially digested with *KpnI* and *XhoI* at 37 °C for 2 h and gel purified. The promoter region of the miR-122 gene was PCR amplified from Huh7 genomic DNA using

primers containing the restriction sites for *KpnI* (forward primer, Table 4.4; IDT DNA) and *XhoI* (reverse primer, Table 4.4; IDT DNA).[189] The PCR product was gel purified and similarly digested with *KpnI* and *XhoI*. The miR-122 promoter insert was then ligated with the digested pGL3-basic backbone at 4 °C overnight, followed by treatment of the ligation reactions with *NheI* to remove any re-circularized plasmid that did not contain the insert, and were subsequently transformed into Top 10 cells. The resulting colonies were analyzed by PCR screening to detect the presence of the miR-122 promoter insert, and further DNA sequencing validated the construction of the pGL3-basic-miR122promoter.

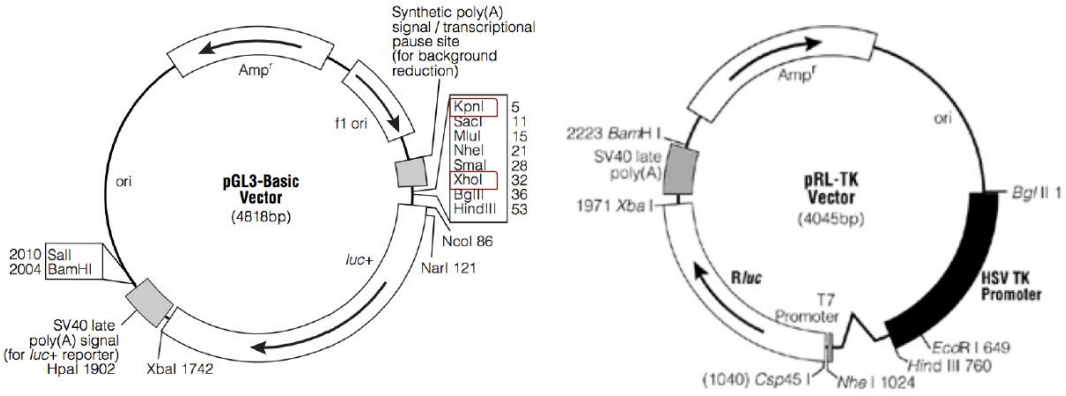

Figure 4.16: Vector map of the pGL3-basic plasmid (left) and the pRL-TK plasmid (right) (Promega).
The miR-122 promoter sequence was inserted in the multi-cloning site upstream of the firefly luciferase gene between the *KpnI* and *XhoI* restriction sites to create the reporter construct pGL3-basic-miR122 promoter.

The pGL3-basic-miR122promoter and the parent construct pGL3-basic were transfected in Huh7 cells in conjunction with the pRL-TK plasmid, which encodes the *Renilla* luciferase and was used as a transfection control; and a Dual Luciferase assay was performed after 48 h incubation. As expected, almost no luminescence was observed for the control pGL3-basic reporter (Figure 4.17A), which does not possess any promoter. In the contrary, high level of luminescence was detected in cells transfected with the pGL3-basic-miR122promoter (Figure 4.17A), which is consistent with the elevated levels of miR-122 in Huh7 cells. Then the ability of

the small molecule **30** to inhibit the activity of the miR-122 promoter was evaluated using the luciferase reporter construct newly established. Huh7 cells were co-transfected with the pRL-TK and the pGL3-basic-miR122promoter plasmids using lipofectamine 2000, following transfection the cells were treated with **30** (10 μM) or DMSO (0.1% final concentration) for 48 h and analyzed with a Dual Luciferase assay (Figure 4.17B). Treatment with **30** resulted in a 60% decrease in firefly luciferase expression, indicating that the mode of action of the inhibitor **30** relies, in part, on its inhibitory effect on the miR-122 promoter. This result is in agreement with the pri-miR-122 quantification (Figure 3.4) and recovery of luciferase silencing through pre-miR-122 transfection (Figure 4.1).

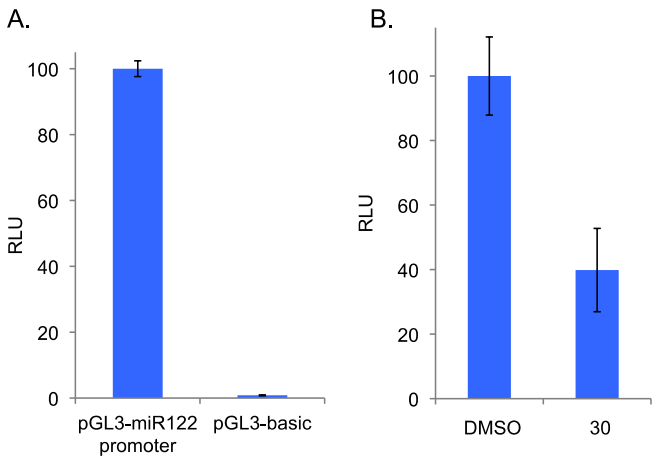

Figure 4.17: Investigation of the miR-122 promoter activity.
A. Dual Luciferase assay of Huh7 cells co-transfected with pRL-TK (transfection control) and pGL3-basic or pGL3basic-miR122-promoter using Lipofectamine 2000. **B**. Dual Luciferase assay of Huh7 cells co-transfected with the pRL-TK and the pGL3basic-miR122-promoter plasmids and treated with DMSO or **30** (10 μM) for 48 h. All experiments were conducted in triplicate. The error bars represent the standard deviation from three independent experiments

4.4.2 Analysis of Potential Interaction between the Inhibitor 30 and known miR-122 Transcription Factors

After confirming that **30** is inhibiting the activity of the miR-122 promoter, a more detailed study was performed to investigate the potential interaction between **30** and one of the miR-122 transcription factors. Five liver-enriched transcription factors, HNF1α, HNF3β, HNF4α, HNF6, and C/EBPα have been reported to regulate miR-122 transcription.[188-190] In addition, it was demonstrated that HNF1α, HNF3β, HNF4α, and HNF6 directly bind to the miR-122 promoter at their corresponding binding sites shown in Figure 4.18. In order to study the effect of **30** on each individual transcription factor, it was first attempted to construct overexpression vectors for the five transcription factors that would be co-transfected with the pGL3-basic-miR122promoter in Huh7 cells. RNA from Huh7 cells was isolated using TRIzol reagent (Life Technologies) and reverse transcribed with the iScript cDNA kit (BioRad). PCR amplification of the transcription factors was performed with the corresponding primers but systematically failed to deliver the expected PCR products. Another strategy was then adopted which consisted in mutating the binding sites for the transcription factors in the miR-122 promoter. New primers were designed in order to introduce specific mutation within the miR-122 promoter sequence using site directed mutagenesis.[273]

The primers (Table 4.5) were designed to introduce the mutation "GC**CTAAG**GTCG" to "GC**TCGGA**GTCG" within the HNF4α binding site, as it was previously reported to significantly decrease the activity of the resulting miR-122 promoter.[188] The primers (Table 4.5) were designed to introduce the following mutation within the HNF6 binding site "**AT**CG**AT**" to "**GA**CG**GG**".[190] Since there is an overlap between the binding sites for the transcription factors

HNF1α and HNF3β, the mutatation was introduced at the three overlapping nucleotides "GTT" to "CAA" as previously reported (primers see Table 4.5).[188]

In addition, the sequence of the miR-122 promoter was analyzed using a publicly available database (http://www.cbrc.jp/research/db/TFSEARCH.html) to identify the putative binding sites for additional transcription factors. Since the AP-1 transcription factor was predicted to bind to the miR-122 promoter (binding site shown in orange in Figure 4.18), a pGL3-basic-miR-122promoter containing a mutated AP-1 binding site was also constructed, using the primers (Table 4.5) to mutate the sequence "GAC" to "TAA". Following PCR amplification of the pGL3-basic-miR-122promoter with the various sets of primers, designed to introduce specific mutations within the promoter, the PCR reactions were treated with *DpnI* to ensure proper removal of any parental DNA. The digested products were then transformed in Top 10 cells, and the presence of the desired mutations was confirmed by sequencing. Although, different conditions were tested (various temperatures) for the amplification of the promoter containing mutations within the HNF6 binding site, the correctly mutated promoter could not be constructed.

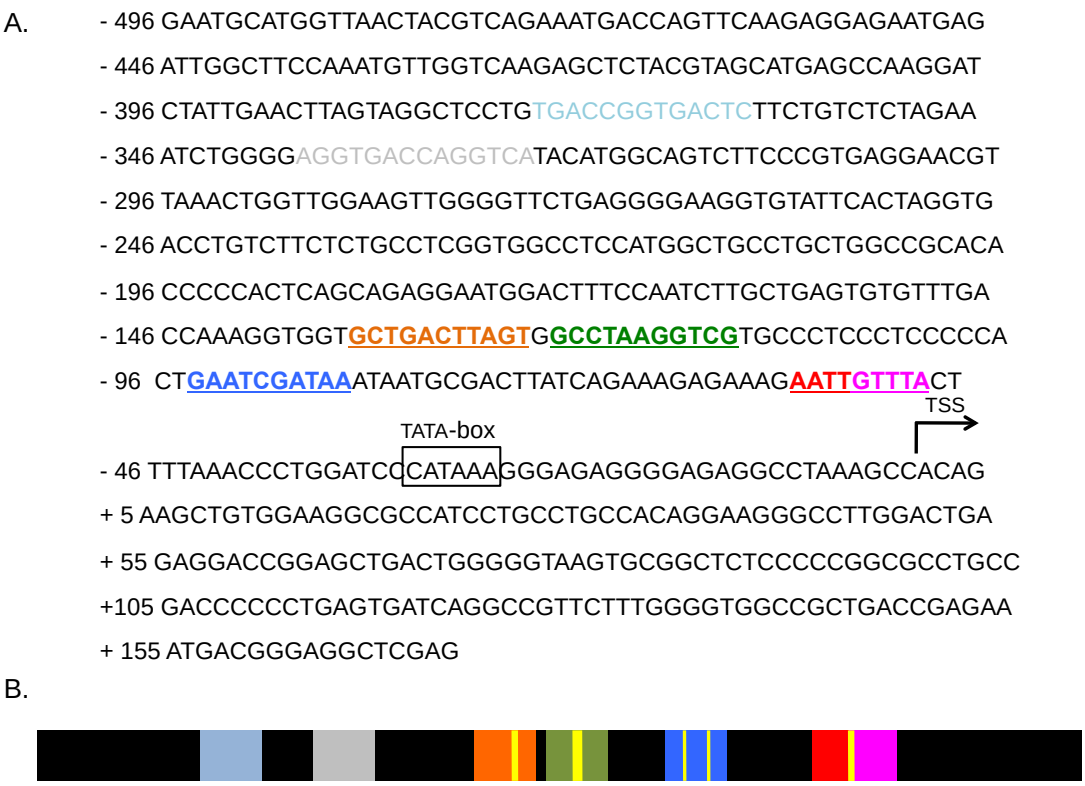

Figure 4.18: Transcription factor analysis.
A. Sequence of the miR-122 promoter. The binding sites for the transcription factors are indicated in color: DR1 is shown in light blue, DR2 is shown in grey, AP-1 is shown in orange, HNF4α is shown in green, HNF6 is shown in blue, HNF3β is shown in red, and HNF1α in magenta. TSS indicates the transcription start site. Figure adapted from *J. Hepatol.*, 52, Li, ZY; et al, Positive regulation of hepatic miR-122 expression by HNF4α, 602. Copyright (2011), with permission from Elsevier. **B**. Representation of the miR-122 promoter, the binding sites for the transcription factors are shown in color, and the locations of the mutation are indicated in yellow.

Once the three mutated miR-122 promoter constructs were established, they were individually co-transfected in Huh7 cells with the control plasmid pRL-TK. All the mutated constructs caused significant reductions in activity compared to the parent reporter pGL3-basic-miR-122promoter (Figure 4.19A), suggesting that the interactions between the transcription factors and their corresponding promoters were efficiently abrogated by the introduction of mutations. It is of note that the inhibitor **30** showed a stronger effect on the pGL3-basic-miR-122promoter activity in Figure 4.17 than in Figure 4.19. Although **30** consistently elicited a reduction in the miR-122 promoter activity, the response was more or less pronounced (40-70%

reduction) and might be explained by day-to-day variations. Then, the ability of **30** to selectively interfere with one of these transcription factors was investigated. Huh7 cells were co-transfected with pRL-TK and either the parent plasmid pGL3-basic-miR122promoter or one of the mutated reporter constructs and treated with the inhibitor **30** (10 μM) or DMSO (0.1% final DMSO concentration) for 48 h. Figure 4.19B shows that **30** was still able to inhibit the activity of the mutated miR-122 promoters, suggesting that the cellular target of **30** may not be the transcription factor AP-1, HNF1α, HNF3β, or HNF4α. The expectation was that if a transcription factor is targeted by **30**, mutation of its corresponding binding site within the miR-122 promoter would relieve the effect of the transcription factor studied and alleviate the inhibitory activity of **30**. Mutations within the binding sites of HNF1α/HNF3β and HNF4α yielded significant reductions in the promoter activity (≥70%), whereas a moderate decrease in activity was observed for the promoter containing a mutated AP-1 binding site (Figure 4.19A). The analysis of the putative binding sites for AP-1 revealed two potential binding sites for AP-1 within the miR-122 promoter. Only the binding site predicted with the highest confidence score (95%) was mutated (shown in orange in Figure 4.18). An additional binding site for AP-1 was predicted, with a lower score (87%), which overlaps with DR1 (shown in light blue in Figure 4.18). A new reporter plasmid would need to be constructed containing mutations within both AP-1 binding sites, to see if that further diminishes the activity of the miR-122 promoter. It would be similarly interesting to combine the mutations within the miR-122 promoter. For example, additional reporters can be constructed that contain either two or multiple mutations within the miR-122 promoter; a reporter encompassing mutations within all the binding sites would provide a control for the background level of promoter activity.

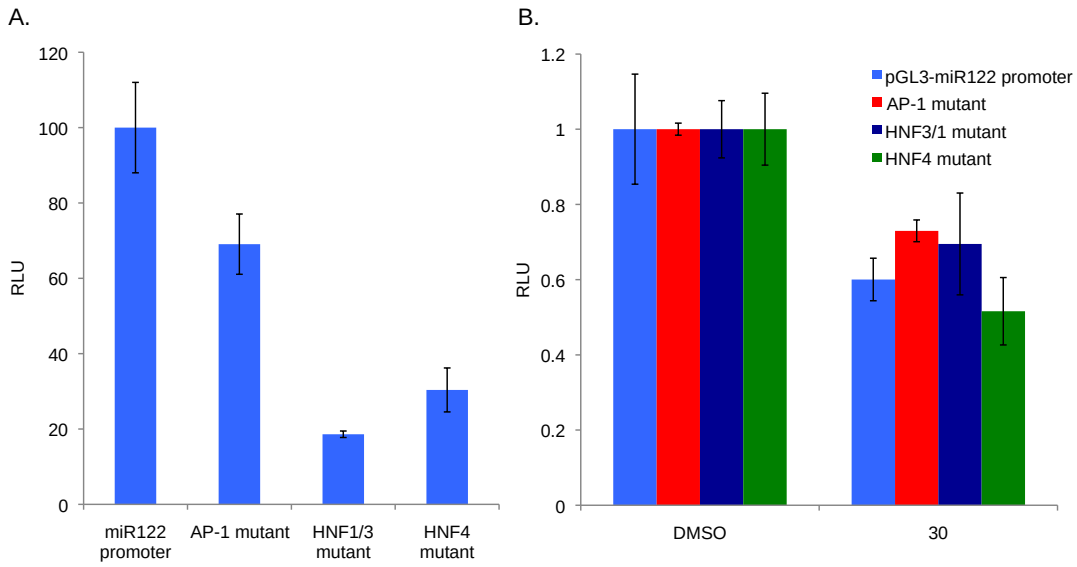

Figure 4.19: Investigation of the potential inhibition of miR-122 transcription factors by **30.**
A. Dual Luciferase assay of Huh7 cells co-transfected with pRL-TK (transfection control) and the miR-122 promoter reporter constructs with mutated binding sites corresponding to the transcription factors AP-1, HNF1α/HNF3B, and HNF4α. **B**. Dual Luciferase assay of Huh7 cells co-transfected with pRL-TK (transfection control) and the three mutated miR-122 promoter reporter constructs and treated with DMSO or the miR-122 inhibitor **30** (10 μM). The data were normalized to the DMSO control. All experiments were conducted in triplicate. The error bars represent the standard deviation from three independent experiments.

Given there is no consensus in the literature regarding the binding site of C/EBPα within the miR-122 promoter, the previous strategy is not applicable to study the ability of **30** to interfere with this transcription factor. Instead, it could be attempted to silence C/EBPα either with an siRNA or an shRNA,[274] and to evaluate the effect of **30** on the miR-122 promoter following C/EBPα knockdown. To determine whether the inhibitor **30** regulates miR-122 expression acts through the regulation of PPARγ/RXRα pathway,[198] additional miR-122 promoter plasmids could be constructed that contain mutations within the DR1 and DR2 binding sites (alone or in combination).

4.5 SUMMARY AND OUTLOOK

Preliminary data indicated that the miR-122 inhibitor **30** acts by blocking the transcription of the miR-122 gene, but its precise mode of action remains to be deciphered. Small molecule miR-122 inhibitors represent potential new antiviral agents for the treatment of HCV, thus the elucidation of the molecular mechanisms of the miR-122 inhibitor **30** could provide new drug targets. The extensive SAR investigation of **30** delivered crucial knowledge about positions in the molecule that could be modified without causing a loss in the miR-122 inhibitory activity. Two photoprobes were synthesized that displayed satisfactory miR-122 inhibition and were substituted with an alkyne motif and either an arylazide (**367**) or a benzophenone (**377**) photoreactive groups. The arylazide analog **394** was designed to provide a negative control, presenting the same functionalities that the active probe **367** but no inhibitory activity. Photoaffinity labeling experiments were performed in Huh7 cells that enabled the detection of two fluorescently-labeled target proteins.

Several strategies were employed to purify the target proteins, such as biotin-streptavidin pull-down, immunopurification with a FITC-probe and an anti-FITC antibody, and using 2-D gel. Following 2-D gel purification, the fluorescently-labeled proteins were isolated and submitted for mass spectrometry analysis. The most probable target protein identified in 3 out 4 submissions was β-tubulin. However, knockdown experiments with a β-tubulin siRNA did not show any effect on miR-122 expression. Unfortunately, despite considerable optimization of each purification method attempted, the efforts to isolate pure target proteins remained unsuccessful. An alternative approach may be attempted in the future which would require the synthesis of a new biotin derivative substituted with a selective cleavable linker, allowing for the release of the target proteins under specific and mild elution conditions.

A luciferase-based reporter construct was established to investigate the effect of **30** on the miR-122 promoter. The compound **30** inhibited the activity of the miR-122 promoter but did not seem to target any of the transcription factors tested AP-1, HNF1α, HNF3β, or HNF4α. Additional reporters will be established in the future, to evaluate the ability of **30** to interfere with the transcription factors C/EBPα, HNF6, and the PPARγ/RXRα pathway. Furthermore, selectivity studies using diverse engineered promoters (i.e. pGL4-basic-miR-21 promoter) should be performed to investigate the selectivity profile of **30** and further assess its effect on transcription.

4.6 EXPERIMENTALS

Cell culture. Experiments were performed using the Huh7 cell line (gift from Dr. Asokan, UNC) cultured in Dulbecco's Modified Eagle Medium (DMEM; Hyclone) supplemented with 10% Fetal Bovine Serum (FBS; Seradigm catalog number 97068-085, lot #093B13) and 2% penicillin/streptomycin (VWR) and maintained at 37 °C in a 5% CO_2 atmosphere. Huh7-psiCHECK-miR122 cells were cultured in Dulbecco's Modified Eagle Medium (DMEM; Hyclone) supplemented with 10% fetal bovine serum (FBS; Seradigm), 500 μg/mL of G418 (Sigma Aldrich), and 2% penicillin/streptomycin (VWR) and maintained at 37 °C in a 5% CO_2 atmosphere.

Target Identification Experiments for the miR-122 Inhibitor 30

Rhodamine labeling and SDS-PAGE analysis. Huh7 cells were passaged into 10 cm plates and were grown to 80% confluency. The media was removed and the cells (in 9.95 mL DMEM

media, antibiotics-free) were treated with either DMSO (50 μL; 0.5% DMSO final concentration), the miR-122 inhibitor **30** (50 μM, 50 μL of a 10 mM DMSO stock), the small molecule probes **367** and **377** (10 μM, 50 μL of a 2 mM DMSO stock), the inactive probe **394** (10 μM, 50 μL of a 2 mM DMSO stock), or a combination of the probe **367** (10 μM) and the miR-122 inhibitor **30** (50 μM). After an overnight incubation at 37 °C, the media was removed, the cells were washed with PBS (1 mL), and irradiated in PBS (5 mL) on a transilluminator (365 nm, 25 W, UVP TFML-20) for 10 min. The PBS was removed, mammalian protein extraction buffer (1 mL, GE Healthcare) was added, the plates were shaken on ice for 10 min, the cells were detached by pipetting them up and down, transferred to a microcentrifuge tube, and pelleted by centrifugation at 12,000 x g for 20 min at 4 °C. The supernatants were collected, the protein concentrations were determined with a Bradford assay (absorbance measured at 595 nm on a Tecan M1000), and an equal amount of proteins (50 μg) for each sample was treated with 16 μL of freshly prepared "click reaction cocktail"[146] (see appendix 6.3.1) containing the rhodamine-azide **396**. The click reaction was performed at room temperature for 2 h. The proteins were subsequently isolated via acetone precipitation, 400 μL of prechilled acetone was added into the click reaction mixtures, which were then incubated for 60 min at −20 °C. The proteins were pelleted by centrifugation (13,000 x g for 10 min at 4 °C), the supernatants were discarded and the pellets were washed twice with prechilled MeOH (200 μL, 4 min centrifugation at 10,000 x g) and finally air dried at rt for 10 min. The pellets were re-suspended in PBS (40 μL), denaturing loading dye (5x) was added (10 μL) and the samples were heated to 95 °C for 5 min. The samples (40 μL) were then analyzed by a 12% SDS-PAGE (4% stacking gel) at 60 V for 30 min followed by 150 V for 90 min. The fluorescence was detected on a ChemiDoc (BioRad, setting: Filter 3: 605/50 nm, light: green epi illumination).

Isolation of the target proteins via biotin-streptavidin affinity purification. Huh7 cells were passaged into 10 cm plates and grown to 80% confluency. The media was removed, and the cells (in 9.95 mL DMEM media, antibiotics-free) were treated with the aryl azide **367** (10 μM, 50 μL of a 2 mM DMSO stock) and incubated overnight. The media was removed, the cells were washed with PBS (1 mL), irradiated in PBS (5 mL) on a transilluminator (365 nm, 25 W, UVP TFML-20) for 10 min. The PBS was removed, trypsin (1 mL) was added, the cells were detached by pipetting them up and down, transferred to a microcentrifuge tube, pelleted by centrifugation (3,000 x g for 10 min), and lysed using mammalian protein extraction buffer (50 μL, GE Healthcare). The cells were quickly vortexed, and incubated on ice for 20 min, vortexing every 5 min. The lysate was centrifuged (12,000 x g for 30 min at 4 °C), the supernatant was collected and the protein extract was quantified by a Bradford assay. The click reaction was then performed using 200 μg of total protein and 66 μL of freshly prepared "click reaction cocktail"[146] (see appendix 6.3.1) containing the rhodamine-azide **396**. Following a 2 h incubation at room temperature, the proteins were isolated via acetone precipitation, as previously described. The proteins were then re-suspended in 50 μL of 0.1% SDS in PBS. The samples were treated with 80, 100, 120, or 160 μL of streptavidin-agarose resin at 4 °C overnight. The samples were centrifuged at 10,000 x g for 5 min, the supernatants were discarded, and the resins were sequentially washed with 0.1% SDS in PBS buffer (100 μL) or PBS buffer (3 x 100 μL, 10,000 x g centrifugation between each wash). The supernatants were discarded and the pellets were re-suspended in 35 μL PBS. SDS-loading dye (5x, 7 μL) was added and the samples were denatured at 95 °C for 15 min. The samples (40 μL) were analyzed on a 12% SDS-PAGE (4% stacking gel) at 60 V for 40 min, followed by 150 V for 70 min. The gel was silver stained using

a Pierce Silver Stain Kit (Thermo Scientific) according to the manufacturer's protocol, and imaged on a ChemiDoc (BioRad, setting: Filter 1: standard, light: white Trans illumination).

2-D gel electrophoresis of rhodamine-labeled target proteins. Huh7 cells were passaged into 10 cm plates and grown to 80% confluency. The media was removed, and the cells (in 9.95 mL DMEM media, antibiotics-free) were treated with the aryl azide probe **367** (10 μM, 50 μL of a 2 mM DMSO stock) and incubated overnight at 37 °C. The media was removed, the cells were washed with PBS (1 mL), and irradiated in PBS (5 mL) on a transilluminator (365 nm, 25 W, UVP TFML-20) for 10 min. The PBS was removed, mammalian protein extraction buffer (1 mL, GE Healthcare) was added, the plates were shaken on ice for 10 min, the cells were detached by pipetting them up and down, transferred to a microcentrifuge tube, and pelleted by centrifugation at 12,000 x g for 20 min at 4 °C. The supernatants were collected, and the protein concentrations were determined with a Bradford assay (absorbance measured at 595 nm on a Tecan M1000). The click reaction was performed using 100 μg of total protein and 33 μL of freshly prepared "click reaction cocktail"[146] containing the rhodamine-azide **396** (see appendix 6.3.1). Following a 2 h incubation at room temperature, the proteins were isolated via acetone precipitation, as previously described. The proteins were then re-suspended in 125 μL of rehydration buffer (ReadyPrep 2-D Starter Kit; BioRad) for analysis by 2-D gel electrophoresis. The samples were loaded onto 7 cm pH 4-7 ReadyStrip IPG strips (BioRad) through passive in-gel rehydration for 24 h at room temperature. The proteins were then separated by IEF on a PROTEAN IEF Cell (BioRad) according to the ReadyPrep 2-D Starter Kit manufacturer protocol (250 V, 20 min, linear ramp; 4,000 V, 2 hr, linear ramp; 4,000 V, 10,000 V/hr, rapid ramp; total run time of 5-6 h). The IPG strips were equilibrated for 10 min in Equilibration Buffers 1 and 2 (ReadyPrep 2-D Starter Kit), and loaded onto a pre-cast 12% SDS-PAGE (pre-cast gel 12% Mini-PROTEAN

TGX Precast Gel, BioRad). The proteins were then analyzed by SDS-PAGE at 200 V for 50 min. The fluorescence was visualized on a ChemiDoc (BioRad, settings: Filter 3: 605/50 nm, light: green epi illumination). The gels were then either fixed (6:3:1 water:ethanol:acetic acid, 20 min), stained with coomassie blue, or silver stained (Pierce Silver Stain Kit; Thermo Scientific) according to the manufacturers' protocols.

Western blot for β-tubulin. Huh7 cells were treated with the photoprobe **367 (**10 μM, 50 μL of a 2 mM DMSO stock), followed by UV irradiation, lysis, click reaction with the rhodamine-azide **396**, and acetone precipitation as described previously. The samples were then analyzed by either a 12% SDS-PAGE (60 V for 40 min, followed by 150 V for 70 min) or a 2-D gel according to the procedure described previously. The fluorescence was imaged on a Typhoon 7000 phosphorimager (laser 580 nm). A Western blot was then performed for each gel. The proteins were transferred to a membrane (80 V for 1.5 h in transfer buffer). The membrane was then washed twice with 20 mL ice-cold TBST. The membrane was incubated with blocking buffer (2.5 g powdered milk in 50 mL TBST) for 1 h at rt. The membrane was washed twice with 20 mL ice-cold TBST. The membrane was separated (with a scalpel) into two parts right under the 46 kDa molecular weight line. The upper part of the membrane (>50 kDa) was incubated with polyclonal anti-β-tubulin antibody (1:1,000 dilution, Santa Cruz Biotechnology), and the lower part of the membrane (<50 kDa) was incubated with anti-GAPDH primary antibody (1:1,000 dilution, Santa Cruz Biotechnology) at 4 °C overnight. The membranes were washed twice with TBST, and incubated with a goat-anti-rabbit-IgG-HRP (1:1,000 dilution, Santa Cruz Biotechnology) secondary antibody at rt for 1 h. The membranes were washed 3 times with TBST (15 mL) and twice with TBS (15 mL). The blots were then developed by HRP colorimetric staining. A solution containing the detection reagent (24 mg of 4-chloro-1-naphthol

(4CN, BioRad) in 8 mL MeOH) was added to a cold peroxide-containing solution (40 mL TBS, 240 μL 3% cold hydrogen peroxide) and quickly added to the membranes. The membranes were incubated with the development reagents for 20 min at rt, and imaged on a Typhoon 7000 phosphorimager (blue laser 473 nm).

Anti-fluorescein antibody purification of FITC-labeled target proteins: with protein A/G resin. Huh7 cells were passaged into 10 cm plates and grown to 80% confluency. The media was removed, and the cells (in 9.95 mL DMEM media, antibiotics-free) were treated with the aryl azide **367** (10 μM, 50 μL of a 2 mM DMSO stock) or the negative control **394** (10 μM, 50 μL of a 2 mM DMSO stock) and incubated overnight at 37 °C. The media was removed, the cells were washed with PBS (1 mL), and irradiated in PBS (5 mL) on a transilluminator (365 nm, 25 W, UVP TFML-20) for 10 min. The PBS was removed, trypsin (1 mL) was added, the cells were detached by pipetting them up and down, transferred to a microcentrifuge tube, pelleted by centrifugation (3,000 x g for 10 min), and lysed using mammalian protein extraction buffer (480 μL, GE Healthcare) supplemented sodium fluoride (NEB, 10 μL of 500 mM stock) and sodium orthovanadate (NEB, 10 μL of 100 mM stock). The cells were quickly vortexed, and incubated on ice for 20 min, vortexing every 5 min. The lysate was centrifuged (12,000 x g for 30 min at 4 °C), the supernatant was collected and the protein extract was quantified by a Bradford assay. The click reaction was then performed using 350 μg of protein (diluted with the corresponding amount of PBS to have a total volume of 350 μL) and 115 μL of freshly prepared "click reaction cocktail"[146] (see appendix protocol 6.3.1) containing the fluorescein-azide **193**. Following a 2 h incubation at room temperature, the proteins were isolated via acetone precipitation as previously described. The pellets were then re-suspended in 420 μL TBS buffer, the anti-fluorescein antibody (Sigma) was added (7 μL), and the samples were slowly agitated overnight at 4 °C. The

resin was quickly washed before being used: an aliquot of 90 μL agarose-proteins A/G beads (Sigma) was transferred to a microcentrifuge tube, pelleted by centrifugation at 1,000 x g for 1 min, the supernatant was removed (77.5 μL), and the same volume of PBS (77.5 μL) was added to re-suspend the beads. Following the overnight incubation, the samples were treated with the protein A/G resin (42 μL) and incubated for 2 h at 4 °C. The mixtures were transferred to spin columns (0.45 μm PVDF microcentrifugal filter, Thermo Scientific) centrifuged for 10 min at 2,000 x g, and the flow-through was discarded. The resins were washed successively with 400 μL buffer A (200 μL of 1 M Tris.HCl pH 7.4, 1.67 mL 3 M NaCl to 10 mL in H_2O) and 400 μL buffer B (200 μL of 1 M Tris.HCl pH 8, 100 μL of $MgCl_2$ to 10 mL in H_2O), followed by centrifugation for 8 min at 3,000 x g. The flow-through was discarded, the columns were placed in a clean tube, 40 μL of PBS and 10 μL of 5x SDS loading buffer were added. The columns were capped, heated to 95 °C for 15 min, and centrifuged for 10 min at 5000 x g. After allowing the elution fractions to cool down to rt, the fractions (40 μL) were analyzed by SDS-PAGE (12%; 60 V for 60 min followed by 150 V for 90 min). The gel was imaged on a Typhoon 7000 phosphorimager (green laser: 532 nm) and coomassie stained.

Immunopurification of the target proteins using the fluorescein azide 193 and anti-FITC antibody. Huh7 cells were passaged into 10 cm plates and grown to 80% confluency. The media was removed and the cells (in 9.95 mL DMEM media, antibiotics-free) were treated with the probes **367** and **394** (10 μM, 50 μL of a 2 mM DMSO stock) and incubated overnight at 37 °C. The media was removed, the cells were washed with PBS (1 mL), and irradiated in PBS (5 mL) on a transilluminator (365 nm, 25 W, UVP TFML-20) for 10 min. The PBS was removed, mammalian protein extraction buffer (1 mL, GE Healthcare) was added, the plates were shaken

on ice for 10 min, the cells were detached by pipetting them up and down, transferred to a microcentrifuge tube, and pelleted by centrifugation at 12,000 x g for 20 min at 4 °C. The supernatants were collected, and the protein concentrations were determined with a Bradford assay (absorbance measured at 595 nm on a Tecan M1000). The click reaction was performed using 500 μg of total protein (diluted with the corresponding amount of PBS to have a total volume of 500 μL), and 165 μL of freshly prepared "click reaction cocktail"[146] (see appendix 6.3.1) containing the fluorescein-azide **191.** Following a 2 h incubation at room temperature, a methanol precipitation was performed. The click reaction mixtures were treated with 4 volumes of MeOH (2.6 ml), 1 volume of chloroform (660 μl), and 3 volumes of H_2O (2 ml). The tubes were quickly vortexed and centrifuged for 1 min at 13,000 x g at rt. The upper phase was removed and discarded, 3 volumes of MeOH (2 ml) were added, the tubes were vortexed, and centrifuged at 13,000 x g for 2 min at rt. The supernatants were removed, the pellets were washed twice with MeOH (200 μL, centrifuged for 1 min at 13,000 x g) and air dried. The pellets were re-suspended in 300 μL IP Lysis buffer (direct IP kit, Pierce) supplemented with 6 μL of each protease inhibitor sodium fluoride and sodium orthovanadate (NEB), transferred to the columns containing the anti-FITC antibody resin, and slowly agitated overnight at 4 °C. The anti-FITC antibody functionalized resin was prepared according to the supplier's protocol. Briefly, 20 μL of AminoLink plus coupling resin (Pierce) was transferred to a spin column (provided in the kit), the column was centrifuged at 1,000 x g for 1 min, the flow-through was discarded, the resin was washed twice with 200 μL of coupling buffer, and centrifuged at 1,000 x g for 1 min. Then the resin was treated with 20 μL of anti-FITC antibody, 3 μL of cyanoborohydride, incubated at rt for 2 h, and thoroughly washed. Following an overnight incubation, the columns containing samples were centrifuged at 1,000 x g for 4 min and washed

according to the supplier's protocol. The samples were washed with 200 µL of IP lysis/wash buffer (4 x), centrifuged at 1,000 x g for 1 min, and once with 100 µL of conditioning buffer. The elution buffer (50 µL) was added, the samples were incubated for 10 min at rt, and the proteins were then eluted by centrifugation at 1,000 x g for 2 min. SDS loading dye (5x, 12 µL) was added to the elution fractions, and the resulting mixtures were heated to 95 °C for 5 min, and analyzed on a 12% SDS-PAGE (60 V for 40 min followed by 150 V for 80 min). The gel was imaged on a ChemiDoc (BioRad, setting: Filter 4: 530/28 nm, light: blue epi illumination) and coomassie stained.

Investigation of β-tubulin as a potential target protein. Huh7-psiCHECK-miR122 cells were seeded at a density of 14,000 cells per well in a white clear-bottom 96-well plate (Greiner), in 200 µL media (DMEM, no-antibiotics) and grown overnight. The media was removed and 170 µL OptiMEM (Life Technologies) was added. The cells were transfected with 50 or 100 pmol of the β-tubulin siRNA (class 4B, Sigma Aldrich, NM_006088) using XtremeGENE (Roche). For the transfection, 3 different transfection mixes were prepared containing (per reaction): mix 1 xtremegene only (control): 0.8 µL XtremeGENE and OptiMEM (the volume was adjusted to obtain a total volume of 30 µL). Mix 2 50 pmol treatment: 0.8 µL XtremeGENE, 1 µL of siRNA (50 µM DEPC water stock), and OptiMEM (the volume was adjusted to obtain a total volume of 30 µL). Mix 3 100 pmol treatment: 0.8 µL XtremeGENE, 2 µL of siRNA (50 µM DEPC water stock), and OptiMEM (the volume was adjusted to obtain a total volume of 30 µL). The siRNA was annealed by heating to 80 °C for 10 min prior to be used in the transfection mix. The mixes were incubated at rt for 20 min, and added to the cells (30 µL/well). The cells were then incubated for 4 h at 37 °C, the media was replaced with DMEM (200 µL, no antibiotics), and the cells were incubated for 48 h, followed by analysis with a Dual Luciferase Reporter Assay Kit

(Promega) using 30 μL passive lysis buffer and 50 μL of each luciferase reagent. The luminescence was measured on a Tecan M1000 platereader with a measurement time of 1 s and a delay time of 2 s. All experiments were performed in triplicates, for each well the *Renilla* readout was normalized to the firefly readout, and the average for each sample was further normalized to the XtremeGENE (no siRNA) control.

HDAC-Glo assay: The nuclear proteins from Huh7 cells were extracted using the NE-PER nuclear and cytoplasmic kit (Pierce), and the concentration was determined with a Bradford assay (absorbance measured at 595 nm on a Tecan M1000). The proteins were diluted to 15 μg/mL in HDAC-Glo buffer (Promega). Serial dilutions of TSA were prepared as follow:

200 μM solution: add 4 μL of a 1 mM DMSO stock to 16 μL HDAC-Glo buffer

2 μM solution: add 1 μL of the 200 μM solution to 99 μL HDAC-Glo buffer

200 nM solution: add 20 μL of the 2 μM solution to 80 μL HDAC-Glo buffer

40 nM solution: add 20 μL of the 200 nM solution to 80 μL HDAC-Glo buffer

8 nM solution: add 20 μL of the 40 nM solution to 80 μL HDAC-Glo buffer

1.6 nM solution: add 20 μL of the 40 nM solution to 80 μL HDAC-Glo buffer

Serial dilutions of **30** were prepared as follow:

500 μM solution: add 5 μL of a 10 mM DMSO stock to 95 μL HDAC-Glo buffer

100 μM solution: add 25 μL of the 500 μM solution to 100 μL HDAC-Glo buffer

50 μM solution: add 50 μL of the 100 μM solution to 50 μL HDAC-Glo buffer

25 μM solution: add 50 μL of the 50 μM solution to 50 μL HDAC-Glo buffer

12.5 μM solution: add 50 μL of the 25 μM solution to 50 μL HDAC-Glo buffer

6.25 μM solution: add 50 μL of the 12.5 μM solution to 50 μL HDAC-Glo buffer

3.13 μM solution: add 50 μL of the 6.25 μM solution to 50 μL HDAC-Glo buffer

The nuclear extract (10 μL) was added to a white 384-well plate, 10 μL of each compound solution was added to the plate (in triplicates), the plate was centrifuged at 1000 x g for 1 min, and incubated for 1 h at rt. The HDAC-Glo reagent (20 μL) was added to each well, the plate was centrifuged at 1000 x g for 1 min, and incubated in the dark for 20 min at rt. The luminescence was measured on a Tecan M1000 platereader with a measurement time of 1 s. All experiments were performed in triplicates, and the average for each sample was further normalized to the DMSO control.

Construction of the pGL3-basic-miR122 promoter reporter. The pGL3-basic plasmid (5 μg; Promega) was sequentially digested with *KpnI* (10 units, 100 μL reaction; New England Biolabs) and *XhoI* (10 units, 50 μL reaction; New England Biolabs) at 37 °C for 2 h. The digestion product was analyzed on a 0.8% agarose gel (90 V, 40 min), the band corresponding to the expected product (4790 bp) was visualized on a transilluminator (365 nm), excised, and gel purified using the E.Z.N.A. Gel Extraction Kit (VWR) according to the manufacturer protocol. The digested plasmid was eluted in 40 μL milliQ water pre-warmed to 65 °C. The promoter region of the miR-122 gene was PCR amplified from Huh7 genomic DNA that was isolated using the Trizol Reagent (Life Technologies) according to the manufacturer's protocol using primers containing *KpnI* (forward primer, Table 4.4) and *XhoI* (reverse primer, Table 4.4) restriction sites. The PCR product was analyzed on a 0.8% agarose gel (90 V, 40 min), the band corresponding to the expected product (665 bp) was visualized on a transilluminator (365 nm), excised, and gel purified using the E.Z.N.A. Gel Extraction Kit (VWR) according to the manufacturer's protocol. The insert was eluted 30 μL milliQ water pre-warmed to 65 °C, and then digested with *KpnI* (5 units, 50 μL reaction) and *XhoI* (10 units) at 37 °C for 2 h, followed by purification with a QIAquick PCR purification kit (Qiagen). The miR-122 promoter insert

was then ligated with T4 DNA ligase (200 units, 10 μL reaction, 1:6 vector/insert ratio; New England Biolabs) into the digested pGL3-basic backbone at 4 °C overnight. The ligation reactions were treated with *NheI* (1 unit; New England Biolabs) at 37 °C for 30 min to remove any re-circularized plasmid that did not contain insert, and the ligation reactions were transformed into Top 10 cells. For the transformation, 1 μL of each ligation reaction was added to Top 10 competent cells, that were incubated on ice for 30 min. The cells were then heat-shocked at 42 °C for 45 s, placed on ice for 2 min, and 500 μL of SOC media was added. The cells were incubated at 37 °C for 1 h, and 250 μL of transformation reaction were plated on LB agar plates treated with ampicillin. Positive colonies were selected by PCR colony screen using the primers described above and construction of the pGL3-basic-miR122 promoter plasmid was confirmed by DNA sequencing.

primers	sequence 5' - 3'
KpnI forward primer	AAGGGGTACCGAATGCATGGTTAACTACGTCAG
XhoI reverse primer	AACCCCTCGAGCCTCCCGTCATTTCTCGGTC
forward sequencing primer	CTAGCAAAATAGGCTGTCCC

Table 4.4: List of primers (IDT) used to construct the miR-122 promoter reporter.

Assessment of the pGL3-basic-miR122 promoter reporter system. Huh7 cells were plated in a 96-well plate at 15,000 cells/well in 200 μL media (DMEM, no antibiotics) and were grown overnight at 37 °C. The cells were co-transfected with pRL-TK (Promega, 5 ng) and pGL3-basic, or pGL3-basic-miR122 promoter (200 ng/well) in triplicate using Lipofectamine 2000 (0.5 μL/well) in 200 μL OptiMEM for 3 h at 37 °C. The media was removed and replaced with DMEM (200 μL) and the cells were incubated at 37 °C for 48 h, before being assayed with a Dual Luciferase assay kit (Promega) using 30 μL passive lysis buffer and 100 μL of each luciferase reagent. The luminescence was measured on a Biotek Synergy 4 plate-reader with a measurement time of 1 s and a delay time of 2 s. All experiments were performed in triplicates,

for each well the firefly readout was normalized to the *Renilla* readout, and the average for each sample was further normalized to the DMSO control.

Site directed mutagenesis. The mutated miR-122 promoter constructs were obtained via PCR amplification of the pGL3-basic-miR-122promoter using the corresponding primers (Table 4.5). A 25 μL PCR reaction was set-up for each transcription factor: 1.74 μL of pGL3-basic-miR-122promoter (5 ng, 2.88 ng/μL stock), 2.5 μL of the forward primer (10 μM stock), 2.5 μL of the reverse primer (10 μM stock), 0.5 μL dNTP (10 μM stock), 5 μL Phusion buffer (5x stock), 4.24 μL H_2O, and 1 μL Phusion DNA polymerase (NEB). The PCR amplifications were performed on a T100 thermocycler (BioRad) using the following settings:

- for HNF4α: 95 °C, 5 min; followed by 12 cycles of 95 °C, 1 min; 58 °C, 1 min; 72 °C, 10 min; 52 °C, 1 min; followed by 72 °C for 30 min.

- for HNF1α/3: 95 °C, 5 min; followed by 12 cycles of 95 °C, 1 min; 44 °C, 1 min; 72 °C, 10 min; 32 °C, 1 min; followed by 72 °C for 30 min.

- for AP-1: 95 °C, 5 min; followed by 12 cycles of 95 °C, 1 min; 44 °C, 1 min; 72 °C, 10 min; 35 °C, 1 min; followed by 72 °C for 30 min.

Following PCR amplification, 2.7 μL of CutSmart buffer (NEB) and 0.3 μL of the *DpnI* restriction enzyme (NEB) were added to the PCR reactions, that were further incubated at 37 °C for 1 h. The *DpnI* digested products (2 μL) were then transformed in Top 10 competent cells, as previously described, and plated on LB agar plates containing ampicillin. The construction of the mutated pGL3-basic-miR122 promoter plasmids was confirmed by DNA sequencing (forward sequencing primer: 5' CTAGCAAAATAGGCTGTCCC 3'; IDT DNA).

gene	sequence 5' - 3'	
HNF4α	forward	AGTGGCTCGGAGTCGTGCCCTCCCTCCCCCACTGAATCG
	reverse	CACGACTCCGAGCCACTAAGTCAGCACCACCTTTGGTCAAACACACT
HNF1α and HNF3β	forward	AAGAATTCAATACTTTTAAACCCTGGATCCCAT
	reverse	AAAAGTATTGAATTCTTTCTCTTTCTGATAAGTCGC
AP-1	forward	GGTGCTTTATTAGTGGCCTAAGGTCGTGC
	reverse	CACTAATAAAGCACCACCTTTGGTCAAACACAC
HNF6	forward	CCACTGAGACGGGAAATAATGCGACTTATCAGAAAGAGAAAGAATTGTTTACTTTTAAACCCTGGAT
	reverse	ATTATTTCCCGTCTCAGTGGGGGAGGGAGGGCACGACC

Table 4.5: sequences of the primers (IDT) used to introduce mutations within the binding sites of the miR-122 transcription factors, the sites of mutation are underlined.

Examination of the potential interaction of the small molecule inhibitor 30 with the miR-122 transcription factors. Huh7 cells were plated in a 96-well plate at 15,000 cells/well in 200 μL media (DMEM, no antibiotics), and were grown overnight at 37 °C. The cells were co-transfected with pRL-TK (Promega, 2 ng) and either the pGL3-basic-miR-122promoter or the mutated promoter reporter construct (200 ng/well) using Lipofectamine 2000 (0.5 μL/well) in 200 μL OptiMEM. After 2 h incubation, the media was removed and replaced with DMEM (198 μL) supplemented with DMSO or the miR-122 inhibitor **30** (10 μM final concentration, 2 μL of a 1 mM 10% DMSO stock) in triplicate. The cells were incubated at 37 °C for 48 h before being assayed using a Dual Luciferase Assay kit (Promega) using 30 μL passive lysis buffer and 50 μL of each luciferase reagent. The luminescence was measured on a Tecan M1000 plate-reader with a measurement time of 1 s and a delay time of 2 s. All experiments were performed in triplicates, for each well the firefly readout was normalized to the *Renilla* readout, and the average for each sample was further normalized to the DMSO control.

Synthetic Protocols

All reactions were performed in flame-dried glassware under a nitrogen atmosphere and stirred magnetically. Reactions were followed by thin layer chromatography (TLC) using glass-backed

silica gel plates (Sorbent technologies, 250 μm thickness). Tetrahydrofuran and DCM were obtained from a dry solvent delivery system. MeCN, EtOH, MeOH and pyridine were distilled from calcium hydride and stored over 4 Å molecular sieves. Other reagents and solvents were obtained from commercial sources (Sigma, VWR, Fisher, Accros), stored under nitrogen and used directly without further purification. Yields refer to pure compounds unless otherwise stated. Flash chromatography was performed on silica gel (60 Å, 40-63 μm (230 × 400 mesh), Sorbtech) as a stationary phase. High resolution mass spectral analysis (HRMS) was performed at the University of Pittsburgh on a Q-Exactive (Thermo Scientific) mass spectrometer. The ^{1}H NMR and ^{13}C NMR spectra were recorded on a 300 MHz or a 400 MHz Varian or Brucker NMR spectrometers. Chemical shifts are given in δ units (ppm) for NMR spectra.

***N*-(4-(*tert*-Butyl)phenyl)-1-(prop-2-yn-1-yl)-1,2,3,4-tetrahydroquinoline-6-sulfonamide (364)**. Propargylbromide (0.022 mL, 0.25 mmol) was added to a stirred solution of **237** (46 mg, 0.14 mmol) and DIPEA (0.036 mL, 0.21 mmol) in DMF (1 mL). The resulting mixture was heated to reflux for 5 h, allowed to cool down to rt, and diluted with Et_2O (5 mL). The mixture was washed with H_2O (3 x 5 mL), brine (4 mL), dried over Na_2SO_4, filtered, and concentrated. The residue was purified by flash chromatography on silica gel, eluting with hexanes/EtOAc (4:1) to give **364** as a yellow solid (12 mg, 38%). ^{1}H NMR (300 MHz, chloroform-d) δ 7.50 (dd, *J* = 8.8, 2.3 Hz, 1H), 7.33 (d, *J* = 2.2 Hz, 1H), 7.24 (d, *J* = 8.6 Hz, 1H), 6.98 (d, *J* = 8.6 Hz, 2H), 6.60 (d, *J* = 9.0 Hz, 2H), 4.01 (d, *J* = 2.4 Hz, 2H), 3.36 (t, *J* = 6.0 Hz, 2H), 2.68 (t, *J* = 6.3 Hz, 2H), 2.18 (t, *J* = 2.4 Hz, 1H), 1.97 - 1.92 (m, 2H), 1.25 (s, 9H). HRMS (ESI^{+}) calcd for $C_{22}H_{26}N_2O_2S$ $(M+H)^{+}$ 383.5270, found 383.1778.

***N*-(4-Acetylphenyl)-1-(prop-2-yn-1-yl)-1,2,3,4-tetrahydroquinoline-6-sulfonamide (365).** Same procedure as **364** using **238** (456 mg, 1.38 mmol) and propargylbromide (0.221 mL, 2.49

mmol) as the starting materials. The residue was purified by flash chromatography on silica gel, eluting with hexanes/EtOAc (2:1) to give **365** as a light brown solid (39 mg, 10%). ^{1}H NMR (300 MHz, Chloroform-d) δ 7.82 (d, *J* = 9.0 Hz, 1H), 7.58 (dd, *J* = 8.8, 2.4 Hz, 1H), 7.44 (dd, *J* = 2.3, 1.2 Hz, 1H), 7.29 (d, *J* = 8.4 Hz, 1H), 7.15 (d, *J* = 8.7 Hz, 2H), 6.63 (d, *J* = 8.8 Hz, 1H), 4.00 (d, *J* = 2.4 Hz, 2H), 3.37 (t, *J* = 6.0 Hz, 2H), 2.71 (t, *J* = 6.4 Hz, 2H), 2.53 (s, 3H), 2.19 (s, 1H), 2.01 - 1.89 (m, 2H).

***N*-(4-Azidophenyl)-1,2,3,4-tetrahydroquinoline-6-sulfonamide (366).** Same procedure as **30** using **385** (606 mg, 1.42 mmol) and K_2CO_3 (3.7 g, 27.1 mmol) as the starting materials. The residue was purified by flash chromatography on silica gel, eluting with hexanes/EtOAc (2:1) to afford **366** as a yellow solid (449 mg, 96%). ^{1}H NMR (300 MHz, acetone-d6) δ 8.65 (s, 1H), 7.32 - 7.19 (m, 4H), 6.96 (d, *J* = 8.8 Hz, 2H), 6.44 (d, *J* = 9.1 Hz, 1H), 5.87 (s, 1H), 3.36 - 3.25 (m, 2H), 2.67 (t, *J* = 6.3 Hz, 2H), 1.87 - 1.76 (m, 2H).

***N*-(4-Azidophenyl)-1-(prop-2-yn-1-yl)-1,2,3,4-tetrahydroquinoline-6-sulfonamide (367).** Same procedure as **364** using **366** (30 mg, 0.09 mmol) and propargyl bromide (0.024 mL, 0.18 mmol) as the starting materials, except the reaction mixture was heated to 50 °C for 2 h. The residue was purified by flash chromatography on silica gel, eluting with hexanes/EtOAc (3:1) to deliver **367** as an orange solid (15 mg, 45%). ^{1}H NMR (300 MHz, acetone-d6) δ 7.25 (d, *J* = 8.9 Hz, 2H), 7.14 - 7.04 (m, 4H), 6.48 (d, *J* = 8.6 Hz, 1H), 6.00 (s, 1H), 4.41 (d, *J* = 2.5 Hz, 2H), 3.39 - 3.30 (m, 2H), 2.76 - 2.66 (m, 2H), 2.05 (m, 1H), 1.89 - 1.84 (m, 2H). HRMS (ESI$^+$) calcd for $C_{18}H_{17}N_5O_2S$ $(M+H)^+$ 368.4328, found 368.1165.

***N*-(Perfluorophenyl)-1,2,3,4-tetrahydroquinoline-6-sulfonamide (368)**. Same procedure as **30** using *N*-(perfluorophenyl)-1-(2,2,2-trifluoroacetyl)-1,2,3,4-tetrahydroquinoline-6-sulfonamide (9

mg, 0.01 mmol) and K_2CO_3 (50 mg, 0.36 mmol) as the starting materials. The residue was purified by flash chromatography on silica gel, eluting with hexanes/EtOAc (2:1) to afford **368** as a white solid (6 mg, 89%). ^{1}H NMR (300 MHz, chloroform-d) δ 7.47 - 7.42 (m, 2H), 6.42 (d, *J* = 9.3 Hz, 1H), 3.39 (t, *J* = 5.7 Hz, 2H), 2.77 (t, *J* = 6.3 Hz, 2H), 1.98 - 1.92 (m, 2H).

***N*-(2-Benzoylphenyl)-1,2,3,4-tetrahydroquinoline-6-sulfonamide (369).** Same procedure as **30** using *N*-(2-benzoylphenyl)-1-(2,2,2-trifluoroacetyl)-1,2,3,4-tetrahydroquinoline-6-sulfonamide (57 mg, 0.11 mmol) and K_2CO_3 (289 mg, 2.09 mmol) as the starting materials. The residue was purified by flash chromatography on silica gel, eluting with hexanes/EtOAc (1:1) to afford **369** as a yellow solid (32 mg, 74%). ^{1}H NMR (300 MHz, chloroform-d) δ 9.89 (s, 1H), 7.78 (d, *J* = 8.4 Hz, 1H), 7.60 - 7.47 (m, 2H), 7.47 - 7.31 (m, 6H), 7.17 - 7.06 (m, 2H), 6.51 (s, 1H), 3.22 (t, *J* = 6.0 Hz, 2H), 2.45 (t, *J* = 6.2 Hz, 2H), 1.77 (t, *J* = 6.4 Hz, 2H). HRMS (ESI$^+$) calcd for $C_{22}H_{20}N_2O_3S$ $(M+H)^+$ 393.4787, found 393.1284.

***N*-(4-Benzoylphenyl)-1,2,3,4-tetrahydroquinoline-6-sulfonamide (371)**. Same procedure as **30** using *N*-(4-benzoylphenyl)-1-(2,2,2-trifluoroacetyl)-1,2,3,4-tetrahydroquinoline-6-sulfonamide (76 mg, 0.15 mmol) and K_2CO_3 (407 mg, 2.9 mmol) as the starting materials. The residue was purified by flash chromatography on silica gel, eluting with hexanes/EtOAc (1:1) to afford **371** as a light pink solid (21 mg, 40%). ^{1}H NMR (300 MHz, chloroform-d) δ 7.72 (dd, *J* = 1.8, 4.8 Hz, 4H), 7.56 (d, *J* = 5.4 Hz, 2H), 7.53 - 7.42 (m, 4H), 7.18 (dd, *J* = 2.1, 6.9 Hz, 1H), 6.37 (d, *J* = 9.0 Hz, 1H), 3.32 (t, *J* = 5.7 Hz, 2H), 2.69 (t, *J* = 5.8 Hz, 2H), 1.90 - 1.86 (m, 2H). HRMS (ESI$^+$) calcd for $C_{22}H_{20}N_2O_3S$ $(M+H)^+$ 393.4787, found 393.1284.

***N*-(2-Benzoylphenyl)-1-(prop-2-yn-1-yl)-1,2,3,4-tetrahydroquinoline-6-sulfonamide (372)**. Same procedure as **364** using **369** (130 mg, 0.33 mmol) and propargyl bromide (0.089 mL, 0.68 mmol) as the starting materials. The residue was purified by flash chromatography on silica gel,

eluting with hexanes/EtOAc (2:1) to afford **372** as a yellow solid (32 mg, 25%). ^{1}H NMR (300 MHz, acetone-d6) δ 7.73 - 7.59 (m, 3H), 7.59 - 7.36 (m, 6H), 7.23 (d, *J* = 8.2 Hz, 1H), 7.12 (s, 1H), 6.63 (d, *J* = 8.8 Hz, 1H), 4.12 (s, 2H), 4.04 (t, *J* = 7.2 Hz, 2H), 3.37 (t, *J* = 5.2 Hz, 2H), 1.97 (s, 1H), 1.94 - 1.81 (m, 2H).

***N*-(4-Benzoylphenyl)-1-(prop-2-yn-1-yl)-1,2,3,4-tetrahydroquinoline-6-sulfonamide (373)**. Same procedure as **364** using 371 (29 mg, 0.07 mmol) and propargyl bromide (0.02 mL, 0.14 mmol) as the starting materials. The residue was purified by flash chromatography on silica gel, eluting with hexanes/EtOAc (3:1) to afford **373** as a yellow solid (32 mg, 48%). ^{1}H NMR (300 MHz, acetone-d6) δ 7.78 (dt, *J* = 1.2, 8.1 Hz, 3H), 7.69 - 7.63 (m, 1H), 7.58 (dt, *J* = 0.6, 6.9 Hz, 2H), 7.47 (d, *J* = 8.8 Hz, 2H), 7.22 - 7.13 (m, 2H), 6.49 (d, *J* = 8.5 Hz, 1H), 6.04 (s, 1H), 4.56 (d, *J* = 2.5 Hz, 2H), 3.34 (t, *J* = 5.9 Hz, 2H), 2.80 (t, *J* = 2.5 Hz, 1H), 2.70 (t, *J* = 6.2 Hz, 2H), 1.84 - 1.82 (m, 2H). HRMS (ESI$^+$) calcd for $C_{25}H_{22}N_2O_3S$ $(M+H)^+$ 431.5267, found 431.1442.

***N*-(4-Benzoylphenyl)indoline-5-sulfonamide (374).** Same procedure as **30** using *N*-(4-benzoylphenyl)-1-(2,2,2-trifluoroacetyl)indoline-5-sulfonamide (65 mg, 0.13 mmol) and K_2CO_3 (360 mg, 2.6 mmol) as the starting materials. The residue was purified by flash chromatography on silica gel, eluting with hexanes/EtOAc (4:1) to afford **374** as a white solid (45 mg, 90%). ^{1}H NMR (300 MHz, chloroform-d) δ 7.75 - 7.68 (m, 4H), 7.60 - 7.54 (m, 3H), 7.50 - 7.44 (m, 2H), 7.16 (d, *J* = 8.4 Hz, 2H), 6.72 - 6.68 (m, 1H), 3.72 (t, *J* = 6.8 Hz, 2H), 3.08 (t, *J* = 7.2 Hz, 2H). HRMS (ESI$^+$) calcd for $C_{21}H_{18}N_2O_3S$ $(M+H)^+$ 379.4522, found 379.1126.

***N*-(4-Benzoylphenyl)-1-(prop-2-yn-1-yl)indoline-5-sulfonamide (375)**. Same procedure as **364** using 374 (41 mg, 0.10 mmol) and propargyl bromide (0.014 mL, 0.16 mmol) as the starting materials. The residue was purified by flash chromatography on silica gel, eluting with

hexanes/EtOAc (1:1) to afford **375** as a light yellow solid (7 mg, 17%). ^{1}H NMR (300 MHz, chloroform-d) δ 7.75 - 7.68 (m, 4H), 7.60 - 7.54 (m, 3H), 7.50 - 7.44 (m, 2H), 7.15 (d, *J* = 8.7 Hz, 2H), 6.45 (d, *J* = 8.7 Hz, 1H), 3.94 (d, *J* = 2.4 Hz, 2H), 3.57 (t, *J* = 8.7 Hz, 2H), 2.99 (t, *J* = 8.4 Hz, 2H), 2.18 (t, *J* = 2.4 Hz, 1H). HRMS (ESI$^+$) calcd for $C_{24}H_{20}N_2O_3S$ $(M+H)^+$ 417.5001, found 417.1285.

2,2,2-Trifluoro-*N*-(4-nitrophenyl)acetamide (382). TFAA (1 mL, 7.24 mmol, in 1.5 mL of Et_2O) was added dropwise to a stirred solution of 4-nitroaniline (500 mg, 3.62 mmol) and TEA (1.5 mL, 10.8 mmol) in Et_2O (1.2 mL) at 0 °C. The resulting mixture was allowed to warm to rt and stirred for 2 h. The mixture was diluted with Et_2O (5 mL), washed with H_2O (3 x 10 mL) and brine (4 mL), dried over Na_2SO_4, filtered, and concentrated. The residue was purified by flash chromatography on silica gel, eluting with hexanes/EtOAc (3:1) to give **382** as a yellow solid (522 mg, 62%). ^{1}H NMR (300 MHz, chloroform-d) δ 8.19 (dd, *J* = 1.8, 9.6 Hz, 2H), 7.85 (dd, *J* = 1.8, 9.3 Hz, 2H), 4.52 (s, 1H). The analytical data is in agreement with literature reports.[275]

***N*-(4-Aminophenyl)-2,2,2-trifluoroacetamide (383).** Same procedure as **274** using **382** (200 mg, 0.85 mmol) and Pd/C (10%, 14 mg) as the starting materials. The residue was purified by flash chromatography on silica gel, eluting with DCM/EtOAc (2:1) to give **383** as a yellow solid (150 mg, 75%). ^{1}H NMR (300 MHz, DMSO-d6) δ 10.85 (s, 1H), 7.28 (dd, *J* = 1.8, 8.8 Hz, 2H), 6.56 (dd, *J* = 2.4, 8.7 Hz, 2H), 5.31 (s, 2H).

***N*-(4-Azidophenyl)-2,2,2-trifluoroacetamide.** $NaNO_2$ (75 mg, 1.1 mmol, in solution in 0.2 mL H_2O) was added to a stirred solution of **383** (150 mg, 0.73 mmol) and HCl (0.36 mL) in H_2O (0.2 mL) at 0 °C. The resulting mixture was stirred at 0 °C for 1 h, then NaN_3 (95 mg, 1.46 mmol, in solution in 0.5 mL H_2O) was added. The reaction mixture was stirred for 30 min at 0 °C and then

at rt for 2 h. The product was isolated by filtration and washed with ice-cold H_2O (3 x 5 mL) to afford a light orange solid (112 mg, 66%). ^{1}H NMR (300 MHz, DMSO-d6) δ 11.34 (s, 1H), 7.75 (d, *J* = 8.8 Hz, 2H), 7.17 (d, *J* = 8.7 Hz, 2H). HRMS (ESI$^-$) calcd for $C_8H_5F_4N_4O$ $(M-H)^-$ 229.1388, found 229.0338.

4-Azidoaniline (384). Same procedure as **30** from *N*-(4-azidophenyl)-2,2,2-trifluoroacetamide (1.3 g, 5.89 mmol) and K_2CO_3 (16.3 g, 118 mmol) as the starting materials. The residue was purified by flash chromatography on silica gel, eluting with hexanes/EtOAc (3:1) to give **384** as a red solid (479 mg, 61%). ^{1}H NMR (300 MHz, acetone-d6) δ 6.80 (dd, *J* = 1.5, 8.4 Hz, 2H), 6.70 (dd, *J* = 1.4, 8.4 Hz, 2H), 4.72 (s, 2H). HRMS (ESI$^+$) calcd for $C_6H_6N_4$ $(M)^+$ 134.0592, found 134.9250. The analytical data is in agreement with literature reports.[276]

***N*-(4-Azidophenyl)-1-(2,2,2-trifluoroacetyl)-1,2,3,4-tetrahydroquinoline-6-sulfonamide (385).** The azide **384** (205 mg, 1.52 mmol) was added to a solution of **196** (500 mg, 1.52 mmol) in pyridine (1.5 mL). The solution was stirred at rt for 2 h and EtOAc (16 mL) was added. The organic layer was washed with 1 M HCl (10 mL), H_2O (2 x 10 mL) and brine (6 mL), dried over Na_2SO_4, filtered, and concentrated. The residue was purified by flash chromatography on silica gel, eluting with hexanes/EtOAc (3:1) to give **385** as a yellow solid (607 mg, 94%). ^{1}H NMR (300 MHz, acetone-d6) δ 9.05 (s, 1H), 7.81 (s, 1H), 7.69 - 7.58 (m, 1H), 7.27 (d, *J* = 8.9 Hz, 2H), 7.01 (d, *J* = 8.9 Hz, 2H), 3.90 (t, *J* = 7.8 Hz, 2H), 2.94 (t, *J* = 6.8 Hz, 2H), 2.85 (t, *J* = 9.7 Hz, 2H).

3-Aminophenyl(phenyl)methanol (386). Sodium borohydride (63 mg, 1.67 mmol) was added to a solution of 3-aminobenzophenone (300 mg, 1.52 mmol) in EtOH (1.5 mL) and the mixture was refluxed overnight. After allowing the mixture to cool down to rt, it was poured into H_2O (8

mL) and extracted with DCM (3 x 8 mL). The combined organic layers were washed with H_2O (10 mL), dried over Na_2SO_4, filtered, and concentrated to give a white solid (267 mg, 88%). ^{1}H NMR (300 MHz, acetone-d6) δ 7.45 - 7.36 (m, 4H), 7.26 (t, *J* = 7.4 Hz, 1H), 7.10 (t, *J* = 7.2 Hz, 1H), 6.77 (d, *J* = 7.7 Hz, 1H), 6.61 (t, *J* = 6.8 Hz, 1H), 5.73 (s, 1H). The analytical data is in agreement with literature reports.[277]

***N*-(3-(Hydroxy(phenyl)methyl)phenyl)-1-(2,2,2-trifluoroacetyl)-1,2,3,4-tetrahydroquinoline-6-sulfonamide (387).** Same procedure as **197** using **386** (160 mg, 0.49 mmol) and **196** (97 mg, 0.49 mmol) as the starting materials. The residue was purified by flash chromatography on silica gel, eluting with hexanes/EtOAc (3:1) to deliver **387** as a white solid (119 mg, 50%). ^{1}H NMR (400 MHz, chloroform-d) δ 7.68 (s, 1H), 7.54 (dd, *J* = 2.2, 1.1 Hz, 1H), 7.30 - 7.24 (m, 7H), 7.20 - 7.05 (m, 3H), 6.98 (dd, *J* = 7.9, 2.3 Hz, 1H), 5.67 (s, 1H), 3.80 (t, *J* = 6.0 Hz, 2H), 2.75 (t, *J* = 6.9 Hz, 2H), 2.03 - 1.97 (m, 3H).

***N*-(3-Benzoylphenyl)-1-(2,2,2-trifluoroacetyl)-1,2,3,4-tetrahydroquinoline-6-sulfonamide (388).** PCC (26 mg, 0.12 mmol) was added to a stirred solution of **387** (40 mg, 0.08 mmol) in DCM (0.2 mL). The reaction mixture was stirred at rt for 4 h. The suspension was filtered through a cotton plug and the filtrate was concentrated in vacuo. The residue was purified by flash chromatography on silica gel, eluting with DCM/EtOAc (6:1) to afford **388** as a yellow oil (36 mg, 90%). ^{1}H NMR (400 MHz, chloroform-d) δ 7.75 (d, *J* = 7.6 Hz, 3H), 7.67 - 7.56 (m, 3H), 7.55 - 7.34 (m, 6H), 3.82 (t, *J* = 5.9 Hz, 2H), 2.84 (t, *J* = 6.9 Hz, 2H), 2.12 - 2.09 (m, 2H).

***N*-(3-Benzoylphenyl)-1,2,3,4-tetrahydroquinoline-6-sulfonamide (370).** Same procedure as **30** from **388** (36 mg, 0.07 mmol) and K_2CO_3 (192 mg, 1.39 mmol) as the starting materials. The residue was purified by flash chromatography on silica gel, eluting with hexanes/EtOAc (6:1) to

afford **370** as a yellow solid (23 mg, 81%). ^{1}H NMR (400 MHz, chloroform-d) δ 7.71 (dd, *J* = 8.3, 1.4 Hz, 2H), 7.62 - 7.54 (m, 1H), 7.54 - 7.30 (m, 8H), 6.34 (d, *J* = 9.1 Hz, 1H), 3.32 (t, *J* = 5.6 Hz, 2H), 2.66 (t, *J* = 6.3 Hz, 2H), 1.87 (t, *J* = 6.2 Hz, 2H). HRMS (ESI$^+$) calcd for $C_{22}H_{20}N_2O_3S$ $(M+H)^+$ 393.1273, found 393.1219.

***N*-(2-Benzoylphenyl)-*N*-methyl-1-(2,2,2-trifluoroacetyl)-1,2,3,4-tetrahydroquinoline-6-sulfonamide (390).** Potassium carbonate (66 mg, 0.60 mmol) and iodomethane (0.01 mL, 0.16 mmol) were slowly added to a stirred solution of *N*-(2-benzoylphenyl)-1-(2,2,2-trifluoroacetyl)-1,2,3,4-tetrahydroquinoline-6-sulfonamide (50 mg, 0.10 mmol) in DMF (0.4 mL). The resulting mixture was stirred at rt for 1 h. The solvent was removed under vacuum and the residue was suspended in Et_2O (4 mL), washed with H_2O (2 x 4 mL) and brine (4 mL), dried over Na_2SO_4, filtered, and concentrated. The residue was purified by flash chromatography on silica gel, eluting with hexanes/EtOAc (1:1) to deliver **390** as a light yellow solid (59 mg, 90%). ^{1}H NMR (300 MHz, chloroform-d) δ 7.75 (d, *J* = 7.2 Hz, 2H), 7.56 - 7.53 (m, 1H), 7.46 - 7.40 (m, 6H), 7.34 (d, *J* = 9.3 Hz, 2H), 7.02 (d, *J* = 8.8 Hz, 1H), 3.79 (t, *J* = 7.2 Hz, 2H), 3.12 (s, 3H), 2.74 (t, *J* = 7.5 Hz, 2H), 2.04 - 2.00 (m, 2H).

***N*-(2-Benzoylphenyl)-*N*-methyl-1,2,3,4-tetrahydroquinoline-6-sulfonamide (376).** Same procedure as **30** using **390** (59 mg, 0.11 mmol) and K_2CO_3 (307 mg, 2.22 mmol) as the starting materials. The residue was purified by flash chromatography on silica gel, eluting with hexanes/EtOAc (1:1) to afford **376** as a light yellow solid (35 mg, 79%). ^{1}H NMR (300 MHz, chloroform-d) δ 7.78 (dd, *J* = 0.9, 8.1 Hz, 2H), 7.58 - 7.51 (m, 1H), 7.46 - 7.40 (m, 5H), 7.11 (dd, *J* = 1.8, 7.8 Hz, 1H), 7.05 - 6.99 (m, 2H), 6.26 (d, *J* = 8.4 Hz, 1H), 3.29 (t, *J* = 5.4 Hz, 2H), 3.00 (s, 3H), 2.56 (t, *J* = 6.0 Hz, 2H), 1.88 - 1.82 (m, 2H).

***N*-(2-Benzoylphenyl)-*N*-methyl-1-(prop-2-yn-1-yl)-1,2,3,4-tetrahydroquinoline-6-sulfonamide (377)**. Same procedure as **364** using **376** (34 mg, 0.08 mmol) and propargyl bromide (0.011 mL, 0.12 mmol) as the starting materials. The residue was purified by flash chromatography on silica gel, eluting with hexanes/EtOAc (2:1) to deliver **377** as a white solid (11 mg, 31%). ^{1}H NMR (300 MHz, chloroform-d) δ 7.80 (dd, *J* = 0.3, 7.5 Hz, 2H), 7.58 - 7.54 (m, 1H), 7.47 - 7.40 (m, 5H), 7.26 - 7.23 (m, 1H), 7.15 (d, *J* = 7.8 Hz, 1H), 7.01 (s, 1H), 6.54 (d, *J* = 9.0 Hz, 1H), 4.00 (d, *J* = 2.1 Hz, 2H), 3.35 (t, *J* = 5.4 Hz, 2H), 3.03 (s, 3H), 2.58 (t, *J* = 6.3 Hz, 2H), 2.21 (t, *J* = 2.0 Hz, 1H), 1.95 - 1.91 (m, 2H). HRMS (ESI$^+$) calcd for $C_{26}H_{24}N_2O_3S$ $(M+H)^+$ 445.5533, found 445.1570.

***N*-(4-Azidophenyl)-*N*-methyl-1,2,3,4-tetrahydroquinoline-6-sulfonamide (378).** Same procedure as **30** using *N*-(4-azidophenyl)-*N*-methyl-1-(2,2,2-trifluoroacetyl)-1,2,3,4-tetrahydroquinoline-6-sulfonamide (21 mg, 0.05 mmol) and K_2CO_3 (127 mg, 0.92 mmol) as the starting materials. The residue was purified by flash chromatography on silica gel, eluting with hexanes/EtOAc (1:1) to deliver **378** as a yellow solid (15 mg, 93%). ^{1}H NMR (300 MHz, chloroform-d) δ 7.15 - 7.10 (m, 4H), 6.94 (d, *J* = 9.3 Hz, 2H), 6.54 (d, *J* = 8.3 Hz, 1H), 3.37 (t, *J* = 5.4 Hz, 2H), 3.11 (s, 3H), 2.73 (t, *J* = 6.2 Hz, 2H), 2.01 - 1.93 (m, 2H). HRMS (ESI$^+$) calcd for $C_{16}H_{17}N_5O_2S$ $(M+H)^+$ 344.4114, found 344.1171.

Methyl quinoline-6-carboxylate. Thionyl chloride (0.629 mL, 8.6 mmol) was slowly added to a solution of 6-quinolinecarboxylic acid (500 mg, 2.88 mmol) in MeOH (3.5 mL). The mixture was stirred at 0 °C for 1 h and then heated to reflux overnight. The solvent was removed under vacuum, the residue was dissolved in EtOAc (12 mL) and washed with $NaHCO_3$ (3 x 10 mL), H_2O (2 x 10 mL) and brine (6 mL), dried over Na_2SO_4, filtered, and concentrated. The residue was purified by flash chromatography on silica gel, eluting with hexanes/EtOAc (1:1) to deliver

a white solid (444 mg, 85%). ^{1}H NMR (300 MHz, chloroform-d) δ 9.01 (dd, *J* = 4.3, 1.8 Hz, 1H), 8.60 (d, *J* = 2.0 Hz, 1H), 8.36 - 8.24 (m, 2H), 8.15 (d, *J* = 8.8 Hz, 1H), 7.48 (dd, *J* = 8.3, 4.2 Hz, 1H), 4.00 (s, 3H). The analytical data is in agreement with literature reports.[278]

Methyl 1,2,3,4-tetrahydroquinoline-6-carboxylate (391). Same procedure as **240** using methyl quinoline-6-carboxylate (430 mg, 2.29 mmol) as the starting material. The residue was purified by flash chromatography on silica gel, eluting with hexanes/EtOAc (2:1) to deliver **391** as a white solid (336 mg, 77%). ^{1}H NMR (300 MHz, chloroform-d) δ 7.68 - 7.61 (m, 2H), 6.42 (d, *J* = 8.9 Hz, 1H), 3.83 (s, 3H), 3.35 (t, *J* = 5.4 Hz, 2H), 2.77 (t, *J* = 6.4 Hz, 2H), 1.99 - 1.87 (m, 2H).

Methyl 1-(prop-2-yn-1-yl)-1,2,3,4-tetrahydroquinoline-6-carboxylate (392). K_2CO_3 (453 mg, 3.28 mmol) and propargyl bromide (87% in toluene, 0.35 mL) were added to a solution of **391** (251 mg, 1.31 mmol) in DMF (1 mL), and the resulting mixture was stirred at 50 °C overnight. Et_2O (6 mL) was added and the organic phase was washed with H_2O (2 x 5 mL), $NaHCO_3$ (2 x 5 mL) and brine (4 mL), dried over Na_2SO_4, filtered, and concentrated. The residue was purified by flash chromatography on silica gel, eluting with hexanes/EtOAc (7:1) to afford **392** as a yellow oil (265 mg, 88%). ^{1}H NMR (300 MHz, chloroform-d) δ 7.78 (dd, *J* = 8.7, 2.2 Hz, 1H), 7.66 - 7.64 (m, 1H), 6.69 (d, *J* = 8.6 Hz, 1H), 4.76 (d, *J* = 2.4 Hz, 1H, rotamer), 4.06 (d, *J* = 2.4 Hz, 2H), 3.84 (s, 3H), 3.39 (t, *J* = 5.7 Hz, 2H), 2.78 (t, *J* = 6.3 Hz, 2H), 2.54 (t, *J* = 2.4 Hz, 0.5H, rotamer), 2.19 (t, *J* = 2.4 Hz, 1H), 2.06 - 1.95 (m, 3H). (free rotation around the amine bond yielded additional peaks for the propargyl group).

1-(Prop-2-yn-1-yl)-1,2,3,4-tetrahydroquinoline-6-carboxylic acid (393). NaOH (363 mg, 9.1 mmol) was added to a solution of **392** (208 mg, 0.91 mmol) in MeOH:H_2O (1.5:1.5 mL). The reaction mixture was heated to 50 °C for 2.5 h. MeOH was removed under vacuum. The residue

was suspended in H_2O (5 mL) and extracted with EtOAc (4 mL). The aqueous layer was acidified with 1 M HCl (pH ~ 3) and extracted with EtOAc (3 x 6 mL). The combined organic layers were dried over Na_2SO_4, filtered and concentrated to give a light yellow solid (168 mg, 86%). ^{1}H NMR (300 MHz, DMSO-d6) δ 12.09 (s, 1H), 7.63 - 7.53 (m, 2H), 6.71 (d, *J* = 9.4 Hz, 2H), 4.13 (s, 2H), 3.11 (s, 1H), 2.69 - 2.71 (m, 2H), 2.54 - 2.45 (m, 2H), 1.94 - 1.81 (m, 2H). HRMS (ESI$^+$) calcd for $C_{13}H_{13}NO_2$ $(M+H)^+$ 216.1025, found 216.0873.

***N*-(4-Azidophenyl)-1-(prop-2-yn-1-yl)-1,2,3,4-tetrahydroquinoline-6-carboxamide (394).** HATU (53 mg, 0.14 mmol) was added to a solution of **393** (20 mg, 0.09 mmol), DIPEA (0.048 mL, 0.28 mmol) and **384** (12.5 mg, 0.09 mmol) in DMF (0.3 mL). The reaction mixture was stirred at rt overnight. The reaction was diluted with Et_2O (4 mL), washed with H_2O (2x 4 mL), $NaHCO_3$ (2x 3 mL) and brine (4 mL), dried over Na_2SO_4, filtered, and concentrated. The residue was purified by flash chromatography on silica gel, eluting with hexanes/EtOAc (3:1) to afford **394** as a yellow solid (10 mg, 46%). ^{1}H NMR (300 MHz, chloroform-d) δ 8.71 (dd, *J* = 4.5, 1.4 Hz, 1H), 8.43 (dd, *J* = 8.4, 1.4 Hz, 1H), 8.03 (dd, *J* = 8.8, 2.3 Hz, 1H), 7.87 (dd, *J* = 2.2, 1.1 Hz, 1H), 7.43 (dd, *J* = 8.4, 4.5 Hz, 1H), 7.26 - 7.23 (m, 1H), 6.77 (d, *J* = 8.8 Hz, 1H), 4.11 (d, *J* = 2.4 Hz, 2H), 3.47 (t, *J* = 5.7 Hz, 2H), 2.82 (t, *J* = 6.4 Hz, 2H), 2.25 (t, *J* = 2.4 Hz, 1H), 2.08 - 1.98 (m, 2H). ^{13}C NMR (100 MHz, chloroform-d) δ 165.5, 147.6, 135.3, 128.4, 126.3, 123.4, 122.3, 121.4, 119.5, 110.9, 78.8, 71.9, 49.3, 40.6, 27.7, 22.3. HRMS (ESI$^+$) calcd for $C_{19}H_{17}N_5O$ $(M+H)^+$ 332.3791, found 332.1501.

1-Azido-6-bromohexane. Sodium azide (142 mg, 2.19 mmol) was added to a solution of 1,6-dibromohexane (0.5 mL, 3.28 mmol) in DMF (1 mL). The reaction mixture was stirred overnight at 60 °C. After allowing the solution to cool down, the solvent was removed under vacuum, the

residue was suspended in Et_2O (3 mL) and washed with 1 M NaOH (3 mL). The aqueous layer was extracted with Et_2O (2 x 3 mL), the organic layers were combined, dried over Na_2SO_4, filtered, and concentrated. The residue was purified by flash chromatography on silica gel, eluting with hexanes/Et_2O (8:1) to give a colorless oil (880 mg, quantitative). ^{1}H NMR (400 MHz, chloroform-d) δ 3.40 (t, *J* = 6.7 Hz, 2H), 3.27 (t, *J* = 6.9 Hz, 2H), 1.66 - 1.56 (m, 2H), 1.53 - 1.36 (m, 6H). The analytical data is in agreement with literature reports.[145]

6-Azido-*N*-methylhexan-1-amine (395). A solution of methylamine (40% aq, 2 mL) in THF (1.7 mL) was added dropwise to a stirred solution of 1-azido-6-bromohexane (240 mg, 1.16 mmol) in THF (0.9 mL). The resulting mixture was stirred at rt for 48 h, and DCM (4 mL) and 1 M NaOH (6 mL) were added. The two layers were separated and the aqueous layer was extracted with DCM (2 x 6 mL), the organic layers were combined, dried over Na_2SO_4, filtered, and concentrated to afford **395** as a light yellow oil (91 mg, 50%). ^{1}H NMR (400 MHz, chloroform-d) δ 3.27 - 3.20 (m, 2H), 2.54 (t, *J* = 6.8 Hz, 2H), 2.41 (s, 3H), 1.61 - 1.55 (m, 2H), 1.49 - 1.43 (m, 2H), 1.41 - 1.30 (m, 4H). The analytical data is in agreement with literature reports.[145]

***N*-(9-(2-((6-Azidohexyl)(methyl)carbamoyl)phenyl)-6-(diethylamino)-3*H*-xanthen-3-ylidene)-*N*-ethylethanaminium (396).** Thionyl chloride (0.038 mL, 0.53 mmol) was added to a solution of rhodamine B (43 mg, 0.09 mmol) in CCl_4 (1.8 mL). The mixture was stirred under reflux for 3 h. The solvent and the excess of thionyl chloride were removed under vacuum. The residue was suspended in DCM (1.8 mL) and **395** (70 mg, 0.45 mmol) and K_2CO_3 (62 mg, 0.45 mmol) were added. The reaction mixture was stirred at rt overnight. The solvent was removed under vacuum, the residue was purified by flash chromatography on silica gel, eluting with 8% MeOH in DCM to deliver **396** as a purple solid (19 mg, 35%). ^{1}H NMR (300 MHz, chloroform-

d) δ 7.69 - 7.62 (m, 2H), 7.56 - 7.51 (m, 1H), 7.38 - 7.29 (m, 3H), 7.09 (dd, *J* = 9.5, 2.4 Hz, 2H), 6.83 - 6.75 (m, 2H), 3.72 - 3.60 (m, 8H), 3.19 (t, *J* = 6.9 Hz, 4H), 2.93 (s, 2H), 2.38 (s, 3H), 1.42 - 1.31 (m, 2H), 1.33 (t, *J* = 7.2 Hz, 12H), 1.28 - 1.10 (m, 4H). HRMS (ESI^+) calcd for $C_{35}H_{45}N_6O_2$ $(M)^+$ 581.3599, found 581.3645.

***N*-(6-Azidohexyl)-5-(2-oxohexahydro-1*H*-thieno[3,4-*d*]imidazol-4-yl)pentanamide (397).** The amine **192** (7.5 mg, 0.05 mmol) and DIPEA (0.011 mL, 0.06 mmol) were added to a solution of biotin-NHS (18 mg, 0.05 mmol) in DMF (0.2 mL). The reaction mixture was stirred overnight at 95 °C, allowed to cool to rt and was slowly poured into Et_2O (5 mL) at 0 °C. The product precipitated out and was isolated by filtration. The solid was washed with ice-cold H_2O (3 mL) and Et_2O (3 x 4 mL) and was dried under vacuum to deliver **397** as a white solid (16 mg, 83%). ^1H NMR (300 MHz, DMSO-d6) δ 7.78 (s, 1H), 6.40 - 6.34 (m, 2H), 4.28 (s, 1H), 4.11 (s, 1H), 3.10 - 3.01 (m, 3H), 2.82 - 2.78 (m, 1H), 2.10 - 2.03 (m, 2H), 1.50 - 1.26 (m, 11H). HRMS (ESI^+) calcd for $C_{16}H_{28}N_6O_2S$ $(M+Na)^+$ 391.1892, found 391.1881. The analytical data are in agreement with literature reports.[279]

5.0 SYNTHESIS OF SMALL MOLECULE PROBES FOR BIOLOGICAL PATHWAYS

5.1 SYNTHESIS OF A FOLIC-ACID DERIVATIVE TO DELIVER ANTISENSE-AGENTS TO CANCER CELLS

5.1.1 Introduction to Antisense Agents

The applicability of traditional medicines, small molecule and antibody drugs, is limited to "druggable" protein targets. The majority of small molecule drugs target well-defined binding-sites within proteins, while antibodies are generally limited to cell-surface receptors and circulating proteins.[280] In contrast, antisense agent oligonucleotides (ASOs) can selectively inhibit any gene of interest, offering tremendous therapeutic opportunities for many diseases whose molecular targets remain inaccessible to other agents.[281] ASOs are synthetic DNA oligonucleotides comprised of 16-21 nucleotides that bind to their complementary RNA targets through sequence-specific Watson-Crick base-pair interactions. There are two main classes of ASOs, 1) single-stranded ASOs whose binding to their mRNA targets either induces mRNA degradation through RNase H, alters its splicing activity, or prevents mRNA translation through steric blocking of the ribosome; and 2) double-stranded RNAs that promote the degradation of their mRNA targets through RNA interference.[281] However as previously discussed in Chapter 1,

the broad application of ASO therapeutics currently faces various challenges, principally their delivery. There are two main approaches to facilitate ASO delivery, the incorporation of ASOs into lipid or polymer nanocarriers, and the conjugation of ASOs to ligands targeting specific cellular receptors.[282]

Cell-penetrating peptides, short basic amino acid-rich peptides, are often conjugated to biomacromolecules, including ASOs, to facilitate their delivery across the plasma membrane, most likely via direct translocation or endocytosis.[283] Cell-targeting peptides have been further developed to improve the cellular uptake as well as to deliver the ASO to specific cell types.[280] For example, a PNA conjugated with a short peptide analog of insulin like growth factor 1 was efficiently and selectively delivered to cells presenting high levels of the insulin like growth factor 1 receptor.[284] As mentioned earlier, the leading ASO conjugate in clinical development is the trivalent-liver targeting-carbohydrate GalNAc (Figure 5.1).[280] Another commonly used modification consists in the introduction of a lipid motif, such as cholesterol or α-tocopherol (Figure 5.1). Cholesterol-siRNA conjugates can form particles with lipoproteins present in the bloodstream, which increases circulation time and enhances the uptake into hepatocytes via lipoprotein receptors.[285] Although, the precise delivery pathway of α-tocopherol-conjugated siRNAs has not been fully elucidated, it was hypothesized that similarly to the cholesterol derivatives, they may be incorporated into serum lipoproteins and enter the hepatocytes via lipoprotein receptors.[286] In addition to carbohydrates and lipids, receptor-specific ligands have been developed which enable targeted delivery. For example, an anisamide-conjugated splice-switching antisense agent was specifically delivered to PC3 cells.[287] Anisamide (Figure 5.1) presents a high affinity for the sigma receptors, which are commonly overexpressed in diverse tumor cells. Similarly, folate- and anandamide-modified ASOs have been developed to promote

selective delivery to cells expressing a high degree of folate or cannabinoid receptors, respectively.[280] The development of these technologies represents clinically valuable approaches for selective delivery of therapeutic ASOs.

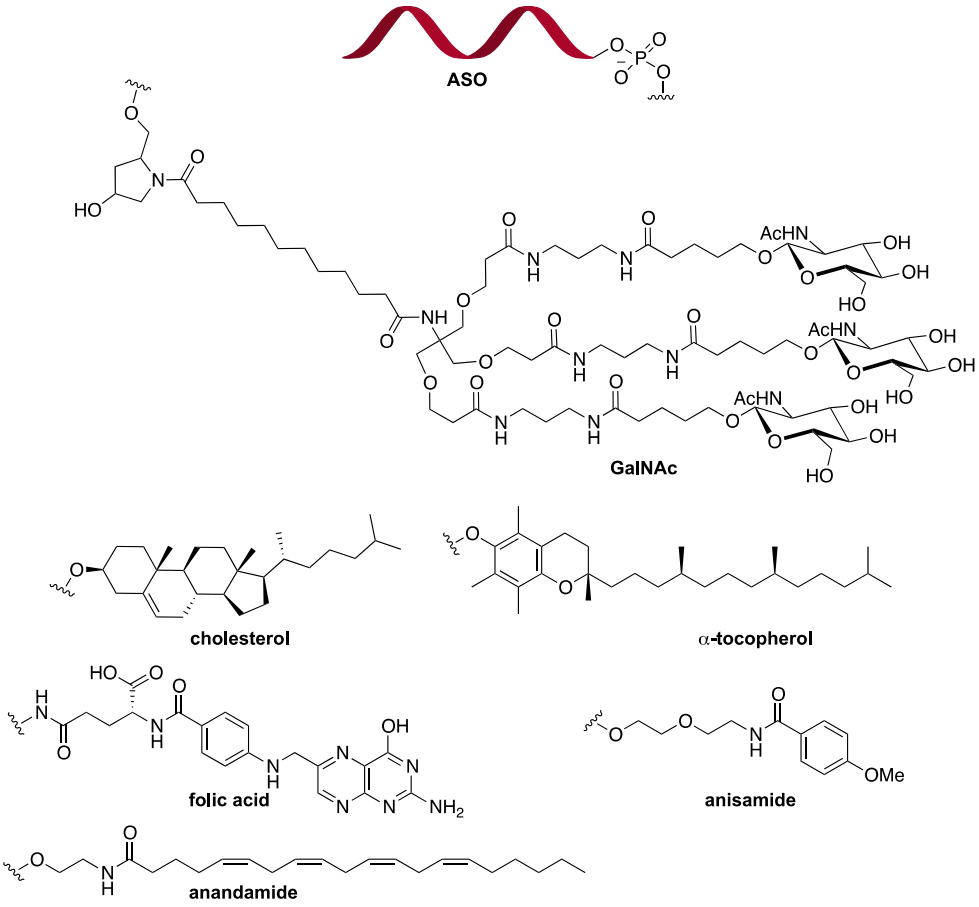

Figure 5.1: Conjugating groups developed to promote targeted delivery of ASO into diseased cells.
.

However, successes of these strategies have been mostly limited to delivery to the liver, and the delivery systems for extrahepatic targets have to be further optimized. Ideally, they must possess cell-targeting ability to enable cell selective delivery, and present an endosomal release functionality.[280] Indeed, the delivery of conjugated ASOs might be limited in some instances, due to endosome trapping. For example, to achieve successful gene inhibition using a folate-conjugated ASO, the agent must be released from the folic acid residue before it can escape the

endosomal compartment.[288] Thus a variety of linkers have been developed to allow direct conjugation of the ligands to the ASOs that are readily cleavable under physiological conditions, such as disulfide- and acylhydrazone-based linkers.[280]

5.1.2 Molecular Caging Technology

Light can also be used as an external trigger to induce selective cleavage of a chemical bond.[289] A classical method to temporally mask the activity of a biomolecule consists in the introduction of a light-removable protecting group, or caging group, on a residue where modifications are known to block the biological activity. Typically, the caging group is introduced through chemical modification, rendering the biomolecule inactive, and upon short UV light irradiation the protecting group is removed and the biological activity is restored (Figure 5.2A).[290] *Ortho*-nitrobenzyl derivatives represent classical caging groups (Figure 5.2B). This technology is most commonly employed as a switch to study biological activity in a spatial and temporal fashion, and is also amenable to the specific release of macromolecules.[291]

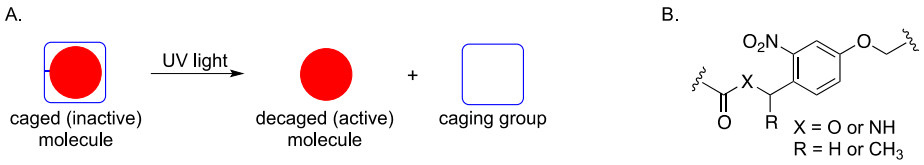

Figure 5.2: A. General decaging mechanism**. B.** Structure of the commonly used ortho-nitrobenzyl caging group. Adapted from *Org. Biomol. Chem*. **2007**, 5, 999, with permission of The Royal Society of Chemistry.

The specific incorporation of the propargyl-6-nitroveratryloxymethyl (PNVOM) caged thymidine phosphoramidite into hairpin protected antisense agents targeting *Renilla* luciferase or the endogenous gene Eg5, allowed the conjugation of the HIV TAT cell-penetrating peptide

(CPP) to the ASOs through a copper-catalyzed $[3+2]$ cycloaddition.[c] Although, the presence of the CPP enabled delivery of the ASOs into mammalian cells without any transfection reagents, the ASOs effectively silenced their target mRNAs only after UV light was applied, removing the caging group and thus releasing the active ASOs (Scheme 5.1).[291]

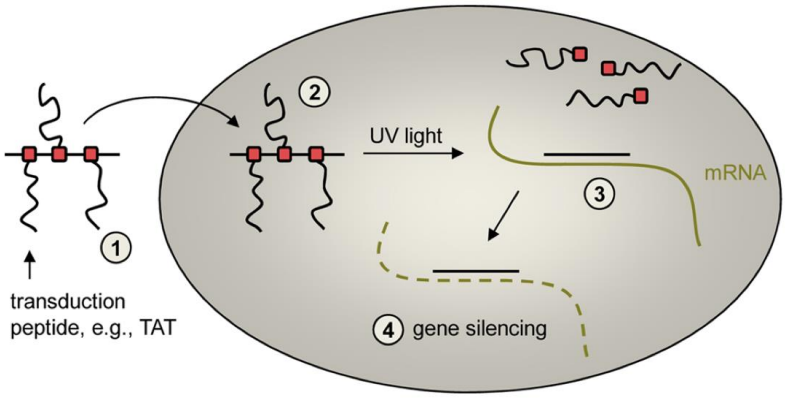

Scheme 5.1: Delivery and light-activation of antisense agents containing caging groups conjugated with cell-penetrating peptides.
PNVOM-caged thymidine nucleotides were site-specifically incorporated into antisense agents and bioconjugated with azido-CPPs. The CPP-caged antisense agent conjugates were **1.** simply added to the cell culture media and **2.** taken up by mammalian cells but remain inactive due to the presence of the caging groups. **3**. UV irradiation triggered decaging, cleaving the CPPs from the antisense agent and induced sequence-specific mRNA binding. This led to **4**. the silencing of gene expression either by blocking the ribosome or by inducing RNase H-mediated mRNA degradation. Adapted from *ACS Chem. Biol.* **2013**, 8, 2272.

The ASOs CNTRL (negative control), Luc-AA (positive control, unmodified ASO), caged CLuc-AA, and caged HIV TAT-conjugated CLuc-AA-TAT were added directly to the cell culture media of human embryonic kidney (HEK) 293T cells, in the absence of any transfection reagent, and incubated overnight. Following brief UV light irradiation (2 min, 365 nm), the cells were co-transfected with the reporter plasmids pGL3 and pRL-TK, encoding the firefly and *Renilla* luciferases, respectively.[291] The same experiment was performed on cells that were kept

[c] Part of this section is reprinted with permission from ACS Chem. Biol., Cellular Delivery and Photochemical Activation of Antisense Agents through a Nucleobase Caging Strategy, Govan JM, Uprety R, Thomas M, Lusic H, Lively MO, Deiters A., 8, 2272. Copyright 2013, American Chemical Society.

in a dark as a control. The pGL3 plasmid was used as a control for normalization purposes and to account for transfection efficiency. The scrambled antisense agent (CNTRL) and a non-caged *Renilla* luciferase antisense agent (Luc-AA) were also transfected as negative and positive controls, respectively. As expected, no inhibition was observed after transfection of the CNTRL antisense agent, while Luc-AA reduced *Renilla* luciferase expression by 85% relative to the CNTRL antisense agent (Figure 5.3). The direct addition of the scrambled ASO, or the caged and non-caged ASOs to the cell media did not affect the *Renilla* luciferase enzyme. In contrast, brief UV irradiation of the cells treated with the CPP conjugate CLuc-AA-TAT elicited a 92% inhibition of *Renilla* luciferase expression (Figure 5.3).[291] These results demonstrated that the CNTRL, Luc-AA, and CLuc-AA ASOs failed to enter the cells without the help of transfection reagents. However, conjugation with the HIV TAT peptide enabled the effective cellular uptake of the ASO, but gene silencing was only achieved after UV irradiation, releasing the sequence of the ASO from the caging group.

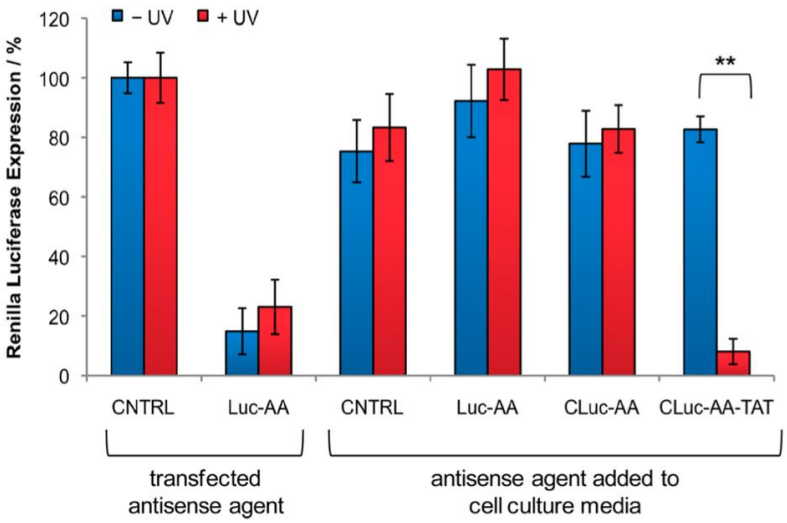

Figure 5.3: Light-activation of antisense agents targeting *Renilla* luciferase**.**
Antisense agents (CNTRL, Luc-AA, CLuc-AA, and CLuc-AA-TAT) were simply added to HEK293T cell culture media or actively transfected (CNTRL and Luc-AA). Cells were either irradiated (365 nm, 2 min, 25 W) or kept in the dark. The cells were expressing firefly and *Renilla* luciferases from pGL3 and pRL-TK plasmids, respectively, and a dual-luciferase assay was performed after 48 h. *Renilla* luciferase expression was normalized to firefly luciferase expression and the negative control antisense agent (CNTRL) was set to 100%. All experiments were performed in triplicate, and error bars represent standard deviations. ** p value <0.005. Experiments were performed by Jeane Govan. Adapted from *ACS Chem. Biol*. **2013**, 8, 2272.

5.1.3 Synthesis of an Azido Folate for Selective Targeting of Cancer Cells

Next, it was hypothesized that replacing the HIV TAT peptide with a folic acid derivative would allow for the selective delivery of the ASO to cancer cells and precise photo-regulation of gene expression.[291] As previously mentioned, folate-modification promotes cellular uptake via natural vitamin endocytosis pathways, specifically to cancer cells that overexpress the folate receptors in comparison with healthy cells, which only express low levels of this receptor.[292] The "folate targeting" strategy has been employed to deliver anticancer drugs, such as doxorubicin or desacetylvinblastine,[293] specifically to cancer cells thereby reducing the toxicity caused to normal cells.[288]

In order to achieve targeted delivery of PNVOM-caged antisense agents, the folic acid azide **401** was synthesized through the coupling of folic acid with the amine **190** in presence of

DCC and pyridine in DMSO, followed by reverse phase HPLC purification (Scheme 5.2).[294] The folate receptor does not recognize the di-substituted derivatives, but retains a strong affinity for the γ-carbonyl modified compounds.[294] Since α-substitutions gave inconclusive results, the γ-azido folate was synthesized for this study. Using the conditions described in Scheme 5.2, the γ-substituted folate was predominantly obtained (≥60% product yield) which was in agreement with previous reports.[294-295] Bioconjugations of **401** and CLuc-AA were conducted via Cu-catalyzed [3 + 2] cycloaddition, the antisense agent containing three PNVOM groups was treated with the azide **401**, copper sulfate, sodium ascorbate, and the tris(3-hydroxypropyl-triazolylmethyl)amine (THPTA) ligand in an aqueous environment.[291] The folate-conjugated ASO was immediately purified using a NAP5 column in order to minimize potential DNA degradation caused by any residual copper catalyst.[296]

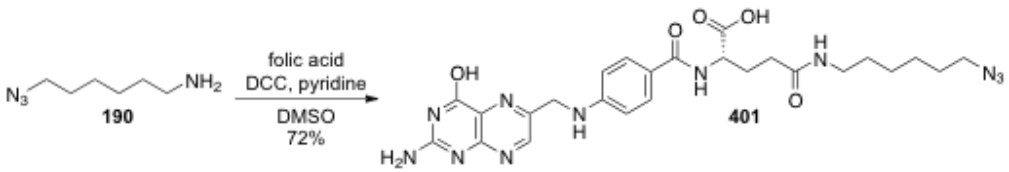

Scheme 5.2: Synthesis of the azido folate **401.**

The cellular delivery of the folic acid-conjugated antisense agent was evaluated in mammalian cell culture using the previously described luciferase assay (see Figure 5.3). The conjugated antisense agent CLuc-AA-FA and the control CLuc-AA were added directly to HeLa cells, which overexpress the folate receptor.[297] Luc-AA was transfected into HeLa cells to provide a positive control, and produced an 80% inhibition in *Renilla* luciferase expression (Figure 5.4A). As expected, no effect on the luminescence signal was detected upon treatment with CLuc-AA, which lacks the cancer cell-targeting agent **401**. In agreement with the previous

assay (Figure 5.3), the addition of the folic acid conjugate CLuc-AA-FA directly to the cell culture media only resulted in a significant inhibition of the *Renilla* luciferase expression after brief exposure to UV light (2 min, 365 nm, Figure 5.4A).[291] To assess the selectivity of the delivery system, the same experiment was then repeated in MCF7 cells that do not express the folate receptor.[298] Under these conditions, CLuc-AA-FA directly added to the cell culture media failed to inhibit *Renilla* luciferase even after UV light irradiation (Figure 5.4B). The lack of gene silencing shown by the folic acid conjugate in MCF7 cells confirmed the ability to selectively deliver light-activated antisense agents into certain cancer cells.[291]

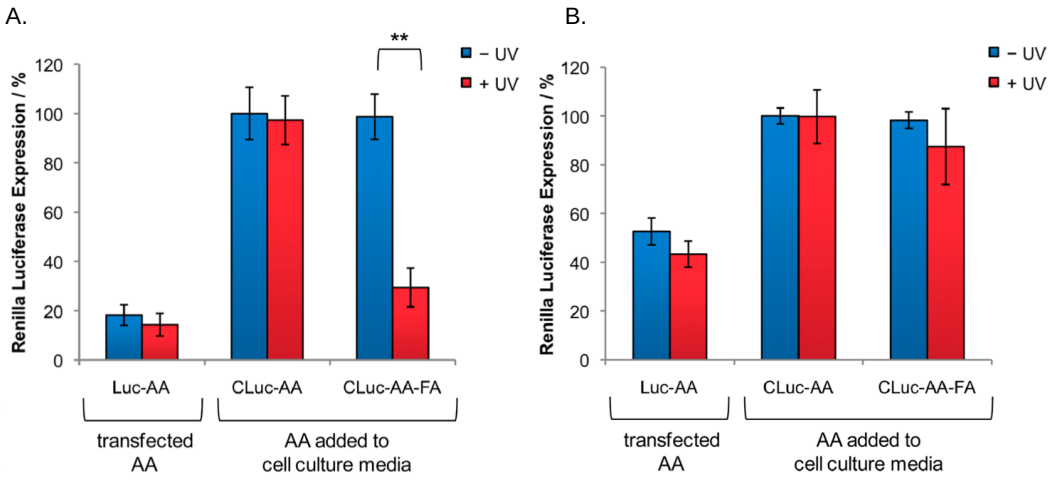

Figure 5.4: Targeted delivery and light-activation of antisense agents.
Antisense agents (CLuc-AA and CLuc-AA-FA) were added directly to cell culture media of **A**. HeLa cells or **B.** MCF7 cells, or alternatively transfected. Cells were either irradiated (2 min, 365 nm, 25 W) or kept in the dark. Firefly and *Renilla* luciferase were expressed from pGL3 and pRL-TK plasmids, respectively, and a dual-luciferase assay was performed after 48 h. *Renilla* luciferase expression was normalized to firefly luciferase expression and the negative control antisense agent (CLuc-AA−UV) was set to 100%. All experiments were performed in triplicate, and error bars represent standard deviations. ** = p value <0.005. These experiments were performed by Jeane Govan. Adapted from *ACS Chem. Biol*. **2013**, 8, 2272.

5.2 SYNTHESIS OF A BIOTINYLATED-HCV INHIBITOR TO FACILITATE MODE OF ACTION STUDIES[A]

As previously discussed in Chapter 3, the development of a new IFN-free regimen has revolutionized HCV therapy. The direct-acting antiviral daclatasvir is a common component of these new combination treatments.[299] It was thought to target the HCV nonstructural protein NS5A, though its precise mechanism of action remained unclear.[300] The NS5A protein plays important roles in the HCV life cycle, particularly in HCV replication and virion assembly (Figure 5.5).[301] One major function of NS5A is to recruit and activate the cellular kinase phosphatidylinositol-4-kinase alpha (PI4KA), which is critical for HCV replication.[302] The NS5A inhibitors block HCV at two different stages of life cycle: HCV replication complex formation and assembly of infectious HCV particles.[303] Since it was noticed that the aggregation of non-structural proteins in the presence of daclatasvir is similar to that observed in cells treated with siRNAs against PI4KA, it was hypothesized that daclatasvir might be altering the NS5A–PI4KA interaction.[301] To enable more detailed mode of action studies a biotinylated analog of daclatasvir was synthesized according to a previous report, which demonstrated that although less potent (EC_{50} value of 33 nM vs 50 pM for daclatasvir) the compound **409** can be used as a probe to facilitate the investigation into the mechanims of daclatasvir.[304]

---

[a] Part of this work was reprinted from *Virology*, 476, Vineela Chukkapalli, Kristi L. Berger, Sean M. Kelly, Meryl Thomas, Alexander Deiters ,Glenn Randall, "Daclatasvir inhibits hepatitis C virus NS5A motility and hyper-accumulation of phosphoinositides", 168. Copyright 2015, with permission from Elsevier.

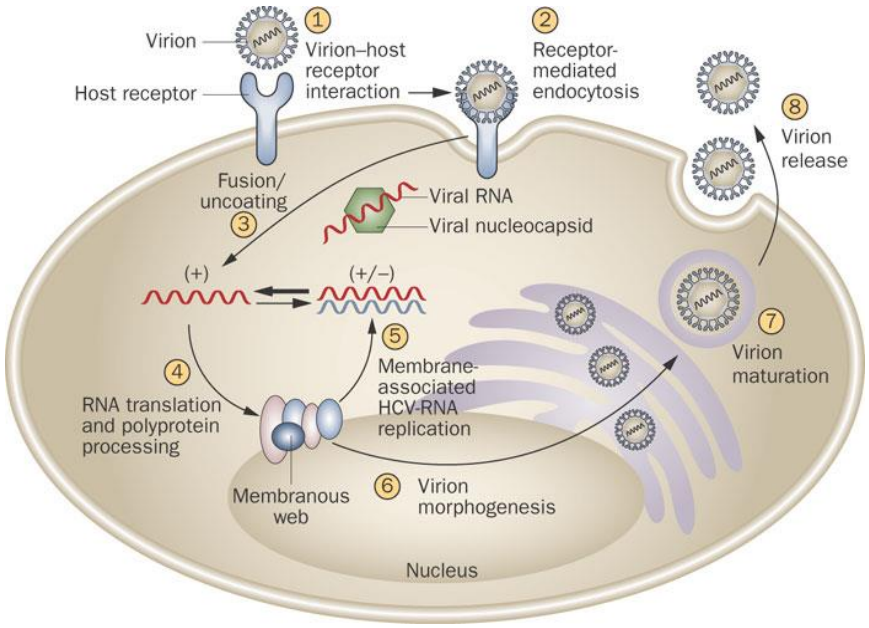

Figure 5.5: Representation of the HCV life cycle.
1. Extracellular HCV virions interact with receptor molecules at the cell surface and **2**. undergo receptor-mediated endocytosis. **3**. Following HCV glycoprotein-mediated membrane fusion, the virion's nucleocapsid is released into the cytoplasm. **4**. The genomic RNA is translated to generate a single large polyprotein that is processed into the 10 mature HCV proteins. The endoplasmic reticulum is modified by viral and cellular factors to form a membranous web, which is the major site of viral RNA amplification. **5**. Six of the mature HCV proteins assist the replication of viral RNA via synthesis of positive strands (+) from a replicative intermediate negative RNA strand (-) template. **6**. A portion of this newly synthesized RNA is packaged into nucleocapsids and associated with the HCV glycoproteins, a process that leads to virion budding into the endoplasmic reticulum, **7**. during processing through the cellular secretory pathway the virions achieve maturation. **8**. Mature virions are released from the cell to complete the life cycle. Reprinted by permission from Macmillan Publishers Ltd: *Nat. Rev. Gastroenterol. Hepatol.*, New and experimental therapies for HCV, Pereira, A.; Jacobson, I., 6, 403. Copyright 2009.[d]

Several synthetic routes were designed to access the biotinylated NS5A inhibitor **409**, it was first attempted to selectively protect one aniline motif with a Boc-protecting group or with a proline derivative (Scheme 5.3). Treatment of 4,4′-diaminostilbene with Boc-proline in the presence of various amide-coupling reagents failed to deliver **403**. Boc-proline was then activated with the succinimide ester, and treated with 4,4′-diaminostilbene under several conditions, varying the solvents, the bases, and the temperature, but **403** still could not be isolated. Similarly the coupling of 4,4′-diaminostilbene and **402** using EDCI, HOBt, and DIPEA

[d] This figure was modified with permission from *J. Virology*, Studying Hepatitis C Virus: Making the Best of a Bad Virus, 81, 8853, Tellinghuisen, L. T.; et al. Copyright 2007, American Society for Microbiology.

did not afford the expected product (Scheme 5.3). Although, the mono Boc-protected intermediate **404** was obtained in decent yield, subsequent coupling with the amine **402** systematically failed to deliver the compound **405** (Scheme 5.3).

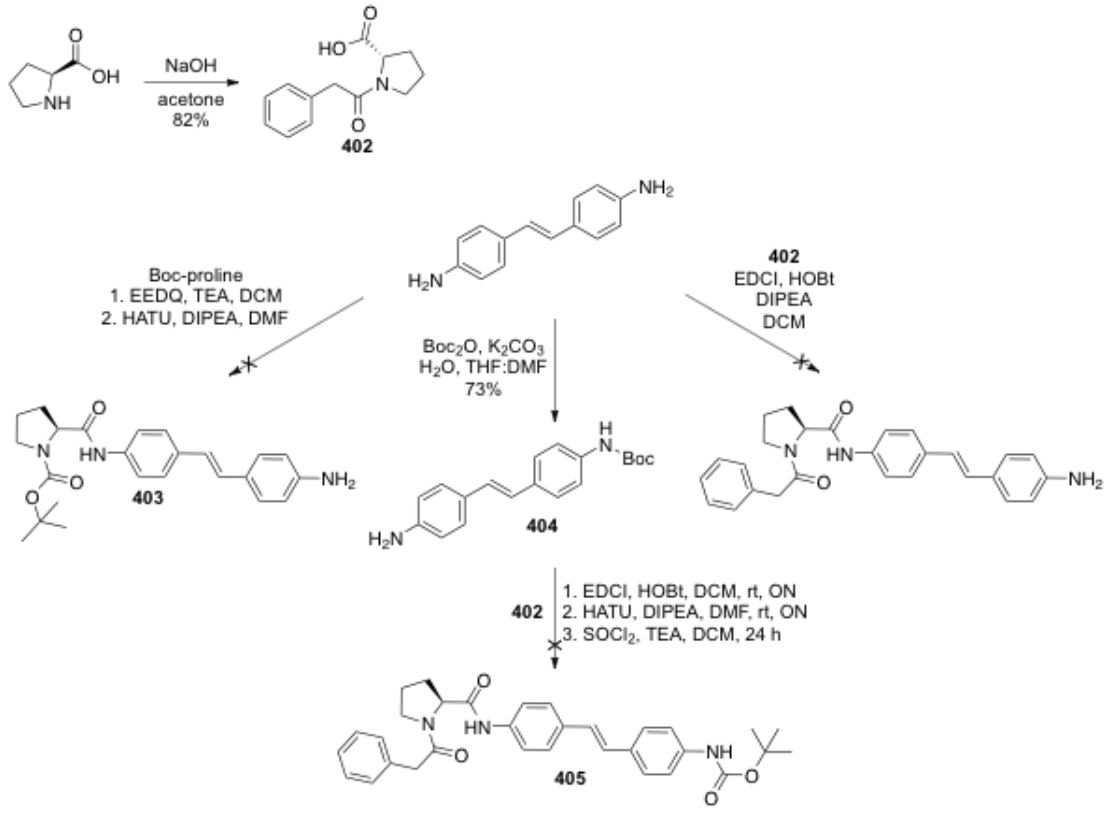

Scheme 5.3: Conditions tested to selectively couple one amine motif.

Finally, it was decided to follow the conditions previously reported to synthesize **409**.[304] Prior to the synthesis, 4,4′-diaminostilbene di-hydrochloride was suspended in H_2O, neutralized through the addition of 2.5 equivalents of K_2CO_3, and extracted with Et_2O to remove the salts. 4,4′-Diaminostilbene was then treated with *N*-Boc proline and EEDQ to obtain the di-Boc substituted intermediate **406**, which was subsequently deprotected with TFA to deliver the diamine **407**. This precursor was treated with phenylacetyl chloride and TEA in DCM to provide

the mono-substituted compound **408**. Finally, treatment of **408** with biotin-NHS and DIPEA afforded the biotinylated probe in the modest yield of 47% (Scheme 5.4).

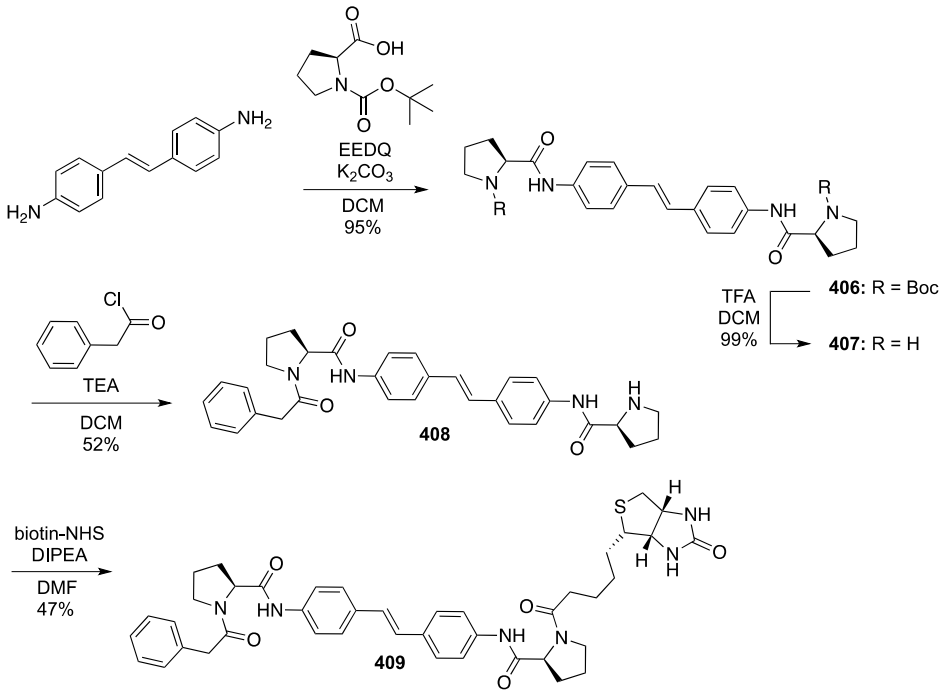

Scheme 5.4: Synthesis of the biotinylated NS5A inhibitor **409**.

The effectiveness against HCV replication of the inhibitor **409** was measured by qRT-PCR in Huh7.5 cells electroporated with HCV RNA (Figure 5.6A).[301] To examine the ability of the drug to bind NS5A expressed from both UHCV (Tet-inducible osteosarcoma cell line that expresses full-length viral proteins independent of replication) and UNS5A (cells expressing NS5A alone) cells, the tool compound **409** was incubated with induced or non-induced cells for 16 h before lysis. The biotinylated drug was then pulled down with streptavidin beads, washed, and the recovery of the NS5A protein was analyzed by western blot. Figure 5.6B shows that the biotinylated drug precipitated NS5A at similar efficiency in both UHCV and UNS5A cells.[301]

In conclusion, a model was suggested wherein daclatasvir inhibits conformational changes in the NS5A protein, or protein complex formations that occur in the context of HCV polyprotein expression. These NS5A conformational changes are likely required to both stimulate PI4P hyper-accumulation and form HCV replication compartment.[301]

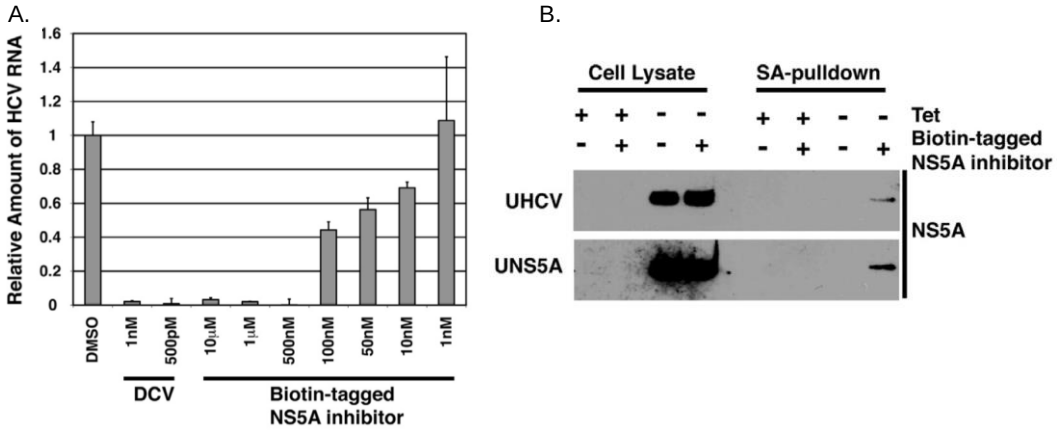

Figure 5.6: Investigation into the mode of action of the biotin-tagged NS5A inhibitor.
A. Huh7.5 cells were electroporated with HCV RNA and treated with either DMSO, daclatasvir (DCV), or the biotin-tagged NS5A inhibitor **409**. The RNA was extracted 72 h post-electroporation and HCV RNA was quantified using real time PCR using the $2^{-\Delta\Delta Ct}$ method. **B**. UHCV cells and UNS5A cells were induced or left non-induced for 72 h and were either treated with DMSO or the biotin-tagged NS5A inhibitor. Cells were lysed, and **409** was precipitated using streptavidin dynabeads. Amount of NS5A that was pulled down with the drug was detected by western blotting. Experiments were conducted by the Randall lab (University of Chicago). Adapted from *Virology*, **2015**, 476, 168.

5.3 SUMMARY AND OUTLOOK

Small organic molecules can be modified with functionalities that enable the precise control of a biomolecule or to facilitate the study of a biological pathway of interest. An azido folate was synthesized and subsequently conjugated, via click reaction, to a PNVOM-caged antisense agent targeting the *Renilla* luciferase. The ASO CLuc-AA-FA was efficiently delivered

to HeLa cells without any transfection reagents, and caused an 80% inhibition in *Renilla* expression only after being briefly exposed to UV light. In comparison, no inhibition in *Renilla* luminescence was observed when CLuc-AA-FA was added to MCF7 cells, which lack the folate receptor. Modification of an ASO with an *o*-nitrobenzyl-caging group derivatized with a folate tumor-targeting motif enabled the specific uptake of the antisense agent into certain cancer cells, in a precise spatial and temporal fashion.[291] The developed technology can be easily adapted to any antisense agent or biomolecule through direct conjugation to a carrier peptide or small molecule ligand for targeted delivery through a cell surface receptor. Additionally, two-photon caging groups, such as 3-nitro-2-ethyldibenzofuran, could be used to allow light-activation of gene control in deeper tissue and with high spatial resolution.[291, 305]

New direct-acting antiviral agents have been developed to provide shorter and broader HCV therapies with limited side-effects. One such agent, the highly potent daclatasvir, targets the HCV nonstructural protein NS5A through a partially unknown mechanism. A biotinylated-analog of daclatasvir was synthesized to provide a tool compound to decipher the mode of action of the inhibitor.[301] Daclatasvir was hypothesized to directly affect the NS5A–PI4KA interaction. However, based on multiple pieces of information complemented with the pull-down experiment using the biotinylated-probe of NS5A at similar efficiency in both UHCV and UNS5A cells, a model was proposed wherein daclatasvir inhibits conformational changes in the NS5A protein or protein complex formations that occur in the context of HCV polyprotein expression.[301] This strategy is applicable to any small molecule drugs, which mechanisms remain to be elucidated, as the modification with a biotin group enable the isolation of a target protein through streptavidin-biotin affinity purification. This method is also amenable to secondary studies to

investigate all of the proteins that show some degree of interaction with the drug of interest, as that may help to better understand or predict potential side-effects.

5.4 EXPERIMENTALS

All reactions were performed in flame-dried glassware under a nitrogen atmosphere and stirred magnetically. Reactions were followed by thin layer chromatography (TLC) using glass-backed silica gel plates (Sorbent technologies, 250 μm thickness). DCM and THF were obtained from a delivery solvent system, DMF and pyridine were distilled from calcium hydride and stored over 4 Å molecular sieves. DMSO was purchased (Accros), stored under nitrogen and used directly without further purification. Yields refer to pure compounds unless otherwise stated. Flash chromatography was performed on silica gel (60 Å, 40-63 μm (230 × 400 mesh), Sorbtech) as a stationary phase. High resolution mass spectral analysis (HRMS) was performed at the University of Pittsburgh on a Q-Exactive (Thermo Scientific) mass spectrometer. The ^{1}H NMR and ^{13}C NMR spectra were recorded on a 300 MHz or a 400 MHz Varian NMR spectrometers. Chemical shifts are given in δ units (ppm) for ^{1}H NMR spectra and ^{13}C NMR spectra.

(S)-2-(4-(((2-Amino-4-hydroxypteridin-6-yl)methyl)amino)-benzamido)-5-((6azidohexyl)amino)-5-oxopentanoic Acid (401). 6-Azidohexan-1-amine (38 mg, 0.26 mmol) and DCC (138 mg, 0.67 mmol) were added to a stirred solution of folic acid (118 mg, 0.26 mmol) and pyridine (0.53 mL) in DMSO (2 mL). The reaction mixture was stirred at rt for 2

days. The mixture was then filtered, and the filtrate was slowly poured into Et_2O (45 mL) at 0 °C. The precipitates were collected by centrifugation (at 5,000 x g for 5 min) and washed 3 times by centrifugation in MeOH:Et_2O (3:30 mL). The solvents were removed, and the precipitate was dried to dryness under vacuum to afford **401** as a yellow solid (106 mg, 72%). The compound was further purified by reverse phase HPLC (Hewlett-Packard 1100, column Agilent Zorbax C18, ACN/H_2O 0.1% TFA). ^{1}H NMR (400 MHz, DMSO-d6) δ 8.63 (s, 1H), 7.94 (d, *J* = 7.9 Hz, 1H), 7.82 (d, *J* = 5.5 Hz, 1H), 7.64 (d, *J* = 8.5 Hz, 2H), 6.61 (d, *J* = 8.5 Hz, 4H), 4.47 (s, 2H), 4.34 - 4.24 (m, 1H), 3.28 - 3.24 (m, 3H), 3.03 - 2.98 (m, 2H), 2.26 - 2.18 (m, 2H), 1.49 - 1.43 (m, 2H), 1.37 - 1.31 (m, 2H), 1.29 - 1.17 (m, 5H). The analytical data matched previous report of azido folate with C4 azido linker.[306] LRMS: m/z calcd for $C_{23}H_{31}N_{11}O_5$ $[M+H]^+$: 566.3 found 566.6.

Synthesis of the biotinylated NS5A inhibitor

(*S*)-1-(2-Phenylacetyl)pyrrolidine-2-carboxylic acid (402). A solution of phenylacetylchloride (268 mg, 1.74 mmol) in acetone (1 ml) was added dropwise to a solution of L-proline (200 mg, 1.74 mmol) in 2 M NaOH (1 ml) and acetone (1 ml) at 0 °C. During the addition the pH was monitored and kept at ~10 via addition of 2 M NaOH. After completion of the addition, the mixture was allowed to warm to rt and stirred for 6 h. The acetone was removed under vacuum, the resulting mixture was acidified to pH ~2 with concentrated HCl. The aqueous layer was saturated with NaCl and extracted with EtOAc (3 x 8 ml). The combined organic layers were dried over Na_2SO_4, filtered, and concentrated to afford **402** as a white solid (334 mg, 82%). ^{1}H NMR (300 MHz, chloroform-d) δ 10.98 (s, 1H), 7.35 - 7.25 (m, 5H), 4.60 - 4.58 (m, 1H), 3.74

(s, 2H), 3.64 - 3.50 (m, 4H), 2.05 - 1.96 (m, 2H). The data is in agreement with literature reports.[307]

(*E*)-*tert*-Butyl (4-(4-aminostyryl)phenyl)carbamate (404). A solution of K_2CO_3 (293 mg, 2.18 mmol) in H_2O (1 ml) was added to a solution of 4,4-diaminostillbene (400 mg, 1.41 mmol) in THF:DMF (1.8 ml:0.6 ml). To this mixture was added di-*tert*-butyl-dicarbonate (154 mg, 0.71 mmol). The reaction mixture was then stirred for 6 h at rt. The solution was poured into ice-cold H_2O (5 ml) and extracted with DCM (3 x 10 ml). The combined organic layers were washed with brine (4 mL), dried over Na_2SO_4, filtered, and concentrated. The residue was purified by flash chromatography on silica gel, eluting with hexanes/EtOAc (2:1) to deliver **404** as a yellow solid (161 mg, 73%). ^{1}H NMR (300 MHz, acetone-d6) δ 8.42 (s, 1H), 7.52 (d, *J* = 8.5 Hz, 2H), 7.42 (d, *J* = 8.7 Hz, 2H), 7.28 (d, *J* = 8.4 Hz, 2H), 7.01 - 6.90 (m, 2H), 6.46 (d, *J* = 8.4 Hz, 2H), 1.48 (s, 9H).

(E)-di-*tert*-Butyl-2,20-(((ethene-1,2-diylbis(4,1-phenylene))bis (azanediyl))bis(carbonyl))bis(pyrrolidine-1-carboxylate) (406). K_2CO_3 (58 mg, 0.42 mmol) was added to a solution of 4,4′-diaminostilbene (60 mg, 0.21 mmol) in DCM (1 ml), and the resulting mixture was stirred at rt for 30 min. Ethyl-2-ethoxyquinoline-1-(2H)-carboxylate (125 mg, 0.50 mmol) and N-Boc proline (104 mg, 0.48 mmol) were added and the reaction mixture was further stirred at rt for 6 h. The solvent was removed under vacuum and the residue was triturated in Et_2O (12 mL). The product was isolated by filtration, washed with H_2O (2 x 5 mL) and Et_2O (2 x 6 mL), and dried under vacuum to afford **406** as a white solid (120 mg, 95%). ^{1}H NMR (300 MHz, DMSO-d6) δ 10.08 (s, 2H), 7.61 - 7.48 (m, 4H), 7.07 (s, 2H), 4.21 - 4.09 (m,

2H), 3.34 - 3.28 (m, 4H), 2.33 - 2.12 (m, 2H), 1.98 - 1.70 (m, 6H), 1.38 (s, 9H), 1.25 (s, 9H). HRMS-ESI (m/z) calcd for $C_{34}H_{45}N_4O_6$ [M-H]+: 605.7443, found: 605.3358.

(E)-N,N′-(Ethene-1,2-diylbis(4,1-phenylene))bis(pyrrolidine-2-carboxamide) (407). TFA (0.15 ml) was slowly added to a solution of **406** (60 mg, 0.01 mmol) in DCM (1.4 ml). The reaction mixture was stirred at rt for 4 h. The solvent was removed under vacuum, the residue was suspended in EtOAc (4 ml), washed with 1 M NaOH (2 ml) and brine (2 ml), dried over Na_2SO_4, filtered, and concentrated to afford **407** as a yellow solid (39 mg, 99%) which was further used without purification. ^{1}H NMR (300 MHz, DMSO-d6): δ 9.97 (s, 2H), 7.62 (d, *J* = 48.7 Hz, 2H), 7.48 (d, *J* = 8.4 Hz, 2H), 7.07 (s, 2H), 3.40 - 3.32 (m, 2H), 2.86 (t, *J* = 6.6 Hz, 4H), 2.10 - 1.99 (m, 2H), 1.98 - 1.62 (m, 6H), HRMS-ESI (m/z) calcd for $C_{24}H_{29}N_4O_2$ $[M-H]^+$: 404.5127, found: 405.2305.

(E)-1-(2-Phenylacetyl)-N-(4-(4-(pyrrolidine-2-carboxamido)styryl)phenyl)pyrrolidine-2-carboxamide (408). A solution of phenylacetylchloride (0.07 ml, 0.05 mmol) in DCM (0.1 ml) was added to a stirred solution of TEA (0.015 ml, 0.09 mmol) and **407** (30 mg, 0.07 mmol) in DCM (0.6 ml) at 0 °C. The reaction mixture was stirred at rt for 4 h, and DCM (5 ml) was added. The organic layer was washed with H_2O (3 ml), $NaHCO_3$ (3 ml) and brine (3 ml), dried over Na_2SO_4, filtered, and concentrated. The residue was purified by flash chromatography on silica gel, eluting with 5% MeOH in DCM to deliver **408** as a white solid (13 mg, 52%). ^{1}H NMR (300 MHz, chloroform-d) δ 7.59 - 7.49 (m, 10 H), 7.31 - 7.28 (m, 3H), 7.06 (d, *J* = 7.2 Hz, 2H), 4.60 - 4.56 (m, 1H), 4.04 - 3.99 (m, 1H), 3.78 (s, 2H), 3.76 - 3.58 (m, 4H), 3.28 - 3.12 (m, 2H), 2.07 - 1.89 (m, 6H), HRMS-ESI (m/z) calcd for $C_{32}H_{35}N_4O_3$ $[M-H]^+$: 523.6453, found: 523.2736.

(*S*)-1-(5-((3a*S*,4*S*,6a*R*)-2-Oxohexahydro-1*H*-thieno[3,4-*d*]imidazol-4-yl)pentanoyl)-*N*-(4-((*E*)-4-((*S*)-1-(2-phenylacetyl)pyrrolidine-2-carboxamido)styryl)phenyl)pyrrolidine-2-carboxamide (409). DIPEA (0.04 ml, 0.21 mmol) and biotin-NHS (14.5 mg, 0.04 mmol) were added to a solution of **408** (22 mg, 0.04 mmol) in DMF (0.3ml). The reaction mixture was stirred overnight at rt, and slowly poured into vigorously stirred Et_2O (6 ml) at 0 °C. The solid was isolated by filtration, purified by trituration in cold Et_2O (2 x 10 ml), and dried under vacuum to afford **409** as a white solid (14 mg, 47%). ^{1}H NMR (300 MHz, DMSO-d6) δ 10.04 (s, 2H), 7.94 (s, 1H), 7.59 - 7.48 (m, 6H), 7.29 - 7.08 (m, 6H), 6.35 (d, *J* = 8.9 Hz, 2H), 4.45 - 4.06 (m, 4H), 3.69 (s, 2H), 3.66 - 4.40 (m, 4H), 3.15 - 2.99 (m, 1H), 2.87 - 2.76 (m, 2H), 2.64 - 1.90 (m, 8H), 1.70 - 1.20 (m, 8H), 1.10 - 1.07 (m, 2H), HRMS-ESI (m/z) calcd for $C_{42}H_{49}N_6O_5S$ $[M-H]^+$: 749.9407, found: 749.3520. The analytical data are in agreement with literature reports.[304]

6.0 APPENDIX

6.1 CELL CULTURE PROTOCOLS

6.1.1 Cell Culture Maintenance

The cells were propagated in 10 cm dishes (Greiner) and passaged when they reached 70-80% confluency. Briefly, the media was removed, the cells were quickly washed with 1 mL PBS (pH 7.4, rt), 1 mL of trypsin (Invitrogen) was added, and the plate was shaken on an orbital shaker for ~2 min ar rt. The cells were detached by pipetting them up and down, 9 mL of fresh media was added, and 1 mL of the cell-containing suspension was transferred to a new 10 cm plate containing 10 mL of fresh media. For all experiments the cells were used at a passage number <25, after which the cells were discarded and a new vial was thawed.

6.1.2 Freezing Cells

The cells were grown in a 15 cm dish (BioExpress) in 25 mL of media until they reached 80% confluency. The media was removed, the cells were quickly washed with 2 mL of PBS (pH 7.4, rt), 3 mL of trypsin (Invitrogen) were added, and the plate was shaken for ~2 min at rt. The cells were detached by pipetting them up and down, and 7 mL of media was added. The cells were counted using the hemacytometer. Cells need to be frozen at a concentration of 5.10^6 to

2.10^7 cells/mL. The cells were transferred to a 15 mL conical tube and pelleted by centrifugation (10 min, rt, 1,600 x g). The supernatant was carefully removed to not disturb the cell pellet, the cells were re-suspended in the appropriate amount of freeze-media, then 1 mL of cells were transferred to each cryo cell storage tubes (Fisher). To prepare the freeze-media, DMSO was filtered through a 0.5 micron filter, and 0.5 mL of DMSO was added to 9.5 mL fresh media (5% final DMSO concentration). The vials were placed at −80 °C for 24 h and then quickly moved to the liquid nitrogen dewar.

6.1.3 Thawing Cells

The frozen vial containing the desired cell line was quickly moved from the liquid nitrogen dewar (the date and initials were properly indicated in the corresponding folder) to a 37 °C water bath. The vial was incubated at 37 °C for ~2 min, or until thawed, thoroughly sprayed with 70% EtOH, and opened inside the cell culture hood. The content was then transferred to a plate containing 10 mL of fresh media, the cells were slowly dispersed throughout the plate when transferring the liquid, the plate was shaken on an orbital shaker for ~2 min at rt, and placed in the CO_2 incubator. After an overnight incubation the media was removed, and replaced with fresh culture media.

6.2 Quantitative Real Time PCR Analysis

Huh7 cells were seeded at a density of 150,000 cells per well in 6-well plates in 2 mL media (DMEM, no antibiotics) and grown overnight. The media was removed, and 1.98 mL fresh DMEM was added. The cells were treated with compounds at a 10 μM (20 μL of a 1 mM DMSO stock) or with DMSO (1% final DMSO concentration). The cells were incubated at 37 °C for 48 h (DMEM, antibiotics-free, 5% CO_2, 2 mL final volume). The media was removed, and the cells were washed with PBS buffer (1 mL, pH 7.4) followed by RNA isolation with the miRNeasy mini kit (Qiagen). Briefly, 700 μL of QiaZOL reagent was added to each well and the plate was shaken for 6 min. The cells were detached by pipetting them up and down, and were transferred to a 1.5 mL microcentrifuge tube. The tubes were vortexed for 1 min, incubated at room temperature for 5 min, and 200 μL of chloroform was added. The tubes were quickly vortexed and incubated at room temperature for 3 min. The tubes were centrifuged at 4 °C, 16,250 x g for 20 min. The aqueous top layer (~200 μL) was transferred to a clean microcentrifuge tube - this step was very delicate as only the top layer containing RNA needed to be collected, if the middle layer was perturbed while transferring the RNA, some DNA will be incorporated into the RNA solution and the purity will be low. Ethanol (525 μL) was added, the solution was mixed by pipetting up and down several times, and then transferred to an RNA wash column (supplied in the miRNeasy kit) and centrifuged at 13,100 x g for 1 min at room temperature. The flow-through was discarded. The column was washed twice with 500 μL RPE buffer (supplied in the miRNeasy kit). The column was dried by centrifugation at 13,100 x g for 4 min at room temperature. The RNA was eluted in 30 μL RNAse-free water (supplied in the miRNeasy kit), quantified using a Nanodrop ND-1000 spectrophotometer, and each sample was diluted to 3 ng/μL in RNAse-free water. The reverse transcription was performed using the

TaqMan microRNA Reverse Transcription Kit (Life Technologies) in conjunction with the RNU19 (control) or the miR-122 TaqMan RT primer. For each assay (RNU19 and miR-122) a mastermix was prepared as follow (per 10 reactions): 1.5 μL dNTP, 15 μL 10x buffer, 41.6 μL H_20 (nuclease free), 1.9 μL RNA inhibitor, and 30 μL primer (5x). Everything was combined (on ice) and then 10 μL reverse transcriptase was added. The mastermix was added to each PCR tube (kept on ice, 10 μL), the RNA (5 μL) was added, the tubes were quickly centrifuged (1 min, 4 °C, 1000 x g), and the reverse transcription was performed on a T100 thermocycler (BioRad, 16 °C, 30 min; 42 °C, 30 min; 85 °C, 5 min). The quantitative real Time PCR was carried out with a TaqMan 2x Universal PCR Master Mix and the appropriate TaqMan miRNA assay (Life Technologies). Similarly, two mastermixes were prepared (on ice): (per 10 reactions) combine 100 μL TaqMan 2x mastermix, 77 μL H_2O (nuclease free), and 10 μL probe (20x). The mastermix (18.7 μL) was added to each well of the PCR plate (BioRad) (kept on ice), the RT-PCR product (1.3 μL) was added (in triplicates), and the plate was quickly centrifuged (1 min, 4 °C, 1000 x g). The PCR amplification was performed on a BioRad CFX96 RT-PCR thermocycler (95 °C, 10 min; followed by 40 cycles of 95 °C, 15 s; 60 °C, 60 s). The triplicate threshold cycles (Ct) obtained for each small molecule treatment were used to determine the relative levels of miR-122 in small molecule treated cells relative to the DMSO control using the $2^{-\Delta\Delta Ct}$ method.[155] This method is commonly and conveniently used to determine the 'fold change' in gene expression between different samples.

fold change = $2^{-\Delta\Delta Ct}$ (1)

One advantage of this method is that it can be used to normalize the experimental data to both an endogenous control (RNU19) and an untreated sample (DMSO). In equation (2), Ct_X corresponds to the Ct value of the gene of interest (miR-21), Ct_{cnt} is the Ct value of the endogenous control (RNU19), *sampleA* corresponds to each inhibitor-treated sample and *sampleB* is the DMSO control sample.[155]

$$2^{-\Delta\Delta Ct} = \left[\left(Ct_X - Ct_{cnt}\right)sampleA - \left(Ct_X - Ct_{cnt}\right)sampleB\right] \quad (2)$$

Tips for qRT-PCR experiments: 1) Before performing an RNA isolation, clean up the hood and bench spaces with ethanol and spray down some RNAse AWAY (Thermo Scientific). Similarly, everything used in the experiments (pipettes, racks, tip boxes, gloves) needs to be sprayed with RNAse AWAY to avoid any contamination of the samples. 2) The RNA needs to be kept on ice at all times to avoid degradation. 3) It is not recommended to freeze/thaw the RNA; for optimal results the RNA needs to be freshly isolated and reverse transcribed the same day. The cDNA can be stored at 4 °C (in PCR tubes properly sealed) for up to 2 weeks. 3) In addition to the RNA concentration, the NanoDrop calculates the ratios A_{260}/A_{280} and A_{260}/A_{230}, which estimate the purity of the RNA. The A_{260}/A_{280} accounts for DNA contamination, and A_{260}/A_{230} accounts for the presence of residual EtOH or phenol contaminants from the RNA isolation. For optimal RNA quality: A_{260}/A_{280} >1.9 and A_{260}/A_{230} ~2. Additional information about qRT-PCR applied to the detection of microRNAs can be found here[308] and here (https://www.genomeweb .com/sites/default/files/pdfs/genomeweb/RTPCRmicroRNATechGuide.pdf).

6.3 RECIPES

6.3.1 Click reaction cocktail

For 200 μL (16 μL of cocktail was used for 50 μg protein)

140 μL PBS

20 μL TCEP (VWR, 50 mM H_2O stock)

20 μL $CuSO_4$ (50 mM H_2O stock)

10 μL TBTA (10 mM DMSO stock)

10 μL rhodamine-azide (10 mM DMSO stock)

6.3.2 Huh7-psiCHECK-miR122 media

For 500 mL, combine:

5.89 g DMEM (Hyclone)

1.63 g sodium bicarbonate

0.145 g L-glutamine

440 mL milliQ water

Mix until everything is dissolved.

Adjust pH to 7.4 with addition of 65% HCl or 2 M NaOH solution.

Then, in the cell culture hood, add 10 mL FBS (Seradigm premium grade, Lot #093B13) + 5 mL Pen/Strep (VWR) + 1.25 mL G418 (VWR, 200 mg/mL H_2O stock filtered through a 0.2 micron filter and stored at −20 °C).

Filter sterilize the media into a plastic 500 mL flask. Store media at 4 °C - for 2 months maximum.

6.3.3 DMEM media

For 500 mL, combine:

5.89 g DMEM (Hyclone)

1.63 g sodium bicarbonate

0.145 g L-glutamine

440 mL milliQ water

Mix until everything is dissolved.

Adjust pH to 7.4 with addition of 65% HCl or 2 M NaOH solution.

Then, in the cell culture hood, add 10 mL FBS (Seradigm premium grade, Lot #093B13) + 5 mL Pen/Strep (VWR).

Filter sterilize the media into a plastic 500 mL flask. Store media at 4 °C - for 2 months maximum.

6.3.4 TBS buffer (10x)

For 1 L, combine:

87.6 g NaCl

12.1 g Tris base (VWR)

1 L milliQ water

Mix until everything is dissolved.

Adjust pH to 7.6 with addition of 60% HCl.

6.3.5 TBST buffer (1X)

For 500 mL, combine:

50 mL TBS buffer (10x)

0.5 g Tween

450 mL milliQ water

Mix until everything is dissolved

6.3.6 SDS running buffer (10x)

For 1 L, combine:

144 g glycine

30.2 g Tris base

10 g SDS

1 L milliQ water

Mix until everything is dissolved.

6.3.7 Staining buffer (coomassie blue)

For 50 mL, combine:

50 mL destaining buffer

15 mg coomassie R250 (brilliant blue)

6.3.8 Destaining buffer

For 1 L, combine:

100 mL glacial acetic acid

200 mL methanol

700 mL milliQ water

6.3.9 Transfer buffer (10x).

For 1 L, combine:

30.3 g Tris

144 g glycine

1 L milliQ water

Mix until everything is dissolved.

6.3.10 Transfer buffer (1x)

For 1 L, combine:

100 mL Transfer buffer (10x)

200 mL methanol

0.25 g SDS

700 mL milliQ water

6.3.11 PBS buffer (10x)

For 500 mL, combine:

40 g NaCl

1 g KCl

7.2 g disodium phosphate

1.2 g monopotassium phosphate

500 mL milliQ water

Mix until everything is dissolved.

Adjust pH to 7.4 with addition of 60% HCl.

Autoclave.

6.3.12 12% SDS-PAGE

For 1 gel, combine:

6.45 mL milliQ water

4.5 mL 40% acrylamide

3.75 mL 1.5 M Tris buffer (pH 8.9)

0.15 mL 10% SDS

0.15 mL 10% APS

0.009 mL TEMED

6.3.13 4% SDS-PAGE stacking gel

For 1 gel, combine:

1.458 mL milliQ water

0.25 mL 40% acrylamide

0.25 mL 1 M Tris buffer (pH 6.8)

0.02 mL 10% SDS

0.02 mL 10% APS

0.002 mL TEMED

LIST OF ABBREVIATIONS

3′-UTR	3′ untranslated region
5-Aza-dC	5-aza-2′-deoxycytidine
μL	micro liter
μM	micromolar
AcOH	acetic acid
ACN	acetonitrile
Ago2	Argonaute 2
AMO	anti-miR oligonucleotide
ASO	antisense agent oligonucleotides
BBr_3	boron tribromide
BIPDeC	Broad Institute's probe development center
Boc	*N-tert*-butoxycarbonyl
BSA	bovine serum albumin
tBuOH	*tert*-butanol
calcd	calculated
CCl_4	carbon tetrachloride
Cs_2CO_3	cesium carbonate
CLL	chronic lymphocitic leukemia

$CuSO_4 \bullet 5H_2O$	copper sulfate pentahydrated
DBU	diazabicycloundecene
DCC	dicyclohexylcarbodiimide
DCM	dichloromethane
DDQ	2,3-dichloro-5,6-dicyanobenzoquinone
DGCR8	DiGeorge syndrome critical region gene 8
DIAD	diisopropyl azodicarboxylate
DIPEA	diisopropylethylamine
DMA	dimethylacetamide
DMAP	4-dimethylaminopyridine
DMF	dimethylformamide
DMSO	dimethyl sulfoxide
DNA	deoxyribonucleic acid
DOS	diversity oriented synthesis
EC_{50}	half maximal effective concentration
EDCI	1-ethyl-3-(3-dimethylaminopropyl) carbodiimide
Et_2O	diethylether
EtOAc	ethylacetate
EtOH	ethanol
g	gram
h	hour
H_2	hydrogen

HATU	2-(1*H*-7-azabenzotriazol-1-yl)-1,1,3,3-tetramethyl uranium hexafluorophosphate)
HBV	hepatitis B virus
HCC	hepatocellular carcinoma
HCl	hydrochloric acid
HCV	hepatitis C virus
HDAC	histone deacetylase
$H_2NOH•HCl$	hydroxylamine hydrochloride
H_2O	water
HOBt	hydroxybenzotriazole
HPLC	high-performance liquid chromatography
HTS	high-throughput screen
HRMS	high resolution mass spectrometry
H_2SO_4	sulfuric acid
Hz	hertz
IP	immunopurification
K_2CO_3	potassium carbonate
KOH	potassium hydroxide
LiOH	lithium hydroxide
LNA	locked nucleic acids
M	molar
Me	methyl
MeOH	methanol

MHz	megahertz
mg	milligram
$MgSO_4$	magnesium sulfate
miRNA	microRNA
mL	milliliter
MLPCN	molecular libraries probe production center network library
mM	millimolar
mmol	millimole
mol	mole
mRNA	messenger RNA
MW	microwave
Na_2CO_3	sodium carbonate
NaH	sodium hydride
NIH	National Institute of Health
NaN_3	sodium azide
$NaNO_2$	sodium nitrite
NaOH	sodium hydroxide
NaOMe	sodium methylate
NMP	*N*-methylmorpholine
NMR	nuclear magnetic resonance
OMe	methoxy
PBA	phenylbutyrate
PBS	phosphate buffered saline

PCC	pyridinium chlorochromate
PCR	polymerase chain reaction
PEG	polyethylene glycol
PNA	peptide nucleic acid
PPh_3	triphenylphosphine
pre-miRNA	precursor miRNA
pri-miRNA	primary miRNA
PS	phosphorothioate
PTSA	*para*-toluenesulfonic acid
qRT-PCR	quantitative real-time PCR
RISC	RNA-induced silencing complex
RNA	ribonucleic acid
rt	room temperature
SAR	structure-activity relationship
$SnCl_2$	tin(II) chloride
$SOCl_2$	thionyl chloride
TBS	tris-buffered saline
TBTA	tris[(1-benzyl-1H-1,2,3-triazol-4-yl)methyl]amine
TCEP	tris(2-carboxyethyl)phosphine
TEA	triethylamine
TFA	trifluoroacetic acid
TFAA	trifluoroacetic anhydride
THF	tetrahydrofuran

TLC	thin layer chromatography
TRBP	TAR RNA binding protein
TSA	trichostatin A
UV	ultraviolet

BIBLIOGRAPHY

1. Wahlestedt, C., Targeting long non-coding RNA to therapeutically upregulate gene expression. *Nat Rev Drug Discov* **2013,** *12* (6), 433-446.

2. Li, Z.; Rana, T. M., Therapeutic targeting of microRNAs: current status and future challenges. *Nat Rev Drug Discov* **2014,** *13* (8), 622-638.

3. Monroig, P. d. C.; Chen, L.; Zhang, S.; Calin, G. A., Small molecule compounds targeting miRNAs for cancer therapy. *Advanced Drug Delivery Reviews* **2015,** *81* (0), 104-116.

4. Lee, R. C.; Feinbaum, R. L.; Ambros, V., The C. elegans heterochronic gene lin-4 encodes small RNAs with antisense complementarity to lin-14. *Cell* **1993,** *75* (5), 843-854.

5. Reinhart, B. J.; Slack, F. J.; Basson, M.; Pasquinelli, A. E.; Bettinger, J. C.; Rougvie, A. E.; Horvitz, H. R.; Ruvkun, G., The 21-nucleotide let-7 RNA regulates developmental timing in Caenorhabditis elegans. *Nature* **2000,** *403* (6772), 901-906.

6. Pasquinelli, A. E.; Reinhart, B. J.; Slack, F.; Martindale, M. Q.; Kuroda, M. I.; Maller, B.; Hayward, D. C.; Ball, E. E.; Degnan, B.; Muller, P.; Spring, J.; Srinivasan, A.; Fishman, M.; Finnerty, J.; Corbo, J.; Levine, M.; Leahy, P.; Davidson, E.; Ruvkun, G., Conservation of the sequence and temporal expression of let-7 heterochronic regulatory RNA. *Nature* **2000,** *408* (6808), 86-89.

7. Bartel, D. P., MicroRNAs: Genomics, Biogenesis, Mechanism, and Function. *Cell* **2004,** *116* (2), 281-297.

8. Iorio, M. V.; Croce, C. M., MicroRNA dysregulation in cancer: diagnostics, monitoring and therapeutics. A comprehensive review. *EMBO Molecular Medicine* **2012,** *4* (3), 143-159.

9. Ha, M.; Kim, V. N., Regulation of microRNA biogenesis. *Nat Rev Mol Cell Biol* **2014,** *15* (8), 509-524.

10. Winter, J.; Jung, S.; Keller, S.; Gregory, R. I.; Diederichs, S., Many roads to maturity: microRNA biogenesis pathways and their regulation. *Nat Cell Biol* **2009,** *11* (3), 228-234.

11. Ling, H.; Fabbri, M.; Calin, G. A., MicroRNAs and other non-coding RNAs as targets for anticancer drug development. *Nat Rev Drug Discov* **2013,** *12* (11), 847-865.

12. Guo, H.; Ingolia, N. T.; Weissman, J. S.; Bartel, D. P., Mammalian microRNAs predominantly act to decrease target mRNA levels. *Nature* **2010,** *466* (7308), 835-840.

13. Pillai, R. S.; Bhattacharyya, S. N.; Artus, C. G.; Zoller, T.; Cougot, N.; Basyuk, E.; Bertrand, E.; Filipowicz, W., Inhibition of Translational Initiation by Let-7 MicroRNA in Human Cells. *Science* **2005,** *309* (5740), 1573-1576.

14. Niwa, R.; Slack, F. J., The evolution of animal microRNA function. *Current Opinion in Genetics & Development* **2007,** *17* (2), 145-150.

15. Peterson, K. J.; Dietrich, M. R.; McPeek, M. A., MicroRNAs and metazoan macroevolution: insights into canalization, complexity, and the Cambrian explosion. *BioEssays* **2009,** *31* (7), 736-747.

16. Garzon, R.; Marcucci, G.; Croce, C. M., Targeting microRNAs in cancer: rationale, strategies and challenges. *Nat Rev Drug Discov* **2010,** *9* (10), 775-789.

17. Hu, J.; Xu, Y.; Hao, J.; Wang, S.; Li, C.; Meng, S., MiR-122 in hepatic function and liver diseases. *Protein Cell* **2012,** *3* (5), 364-371.

18. Calin, G. A.; Dumitru, C. D.; Shimizu, M.; Bichi, R.; Zupo, S.; Noch, E.; Aldler, H.; Rattan, S.; Keating, M.; Rai, K.; Rassenti, L.; Kipps, T.; Negrini, M.; Bullrich, F.; Croce, C. M., Frequent deletions and down-regulation of micro- RNA genes miR15 and miR16 at 13q14 in chronic lymphocytic leukemia. *Proceedings of the National Academy of Sciences of the United States of America* **2002,** *99* (24), 15524-15529.

19. Esquela-Kerscher, A.; Slack, F. J., Oncomirs [mdash] microRNAs with a role in cancer. *Nat Rev Cancer* **2006,** *6* (4), 259-269.

20. Klein, U.; Lia, M.; Crespo, M.; Siegel, R.; Shen, Q.; Mo, T.; Ambesi-Impiombato, A.; Califano, A.; Migliazza, A.; Bhagat, G.; Dalla-Favera, R., The DLEU2/miR-15a/16-1 Cluster Controls B Cell Proliferation and Its Deletion Leads to Chronic Lymphocytic Leukemia. *Cancer Cell* **2010,** *17* (1), 28-40.

21. Calin, G. A.; Sevignani, C.; Dumitru, C. D.; Hyslop, T.; Noch, E.; Yendamuri, S.; Shimizu, M.; Rattan, S.; Bullrich, F.; Negrini, M.; Croce, C. M., Human microRNA genes are frequently located at fragile sites and genomic regions involved in cancers. *Proceedings of the National Academy of Sciences of the United States of America* **2004,** *101* (9), 2999-3004.

22. Bandyopadhyay, S.; Mitra, R.; Maulik, U.; Zhang, M. Q., Development of the human cancer microRNA network. *Silence* **2010,** *1*, 6-6.

23. Volinia, S.; Calin, G. A.; Liu, C.-G.; Ambs, S.; Cimmino, A.; Petrocca, F.; Visone, R.; Iorio, M.; Roldo, C.; Ferracin, M.; Prueitt, R. L.; Yanaihara, N.; Lanza, G.; Scarpa, A.;

Vecchione, A.; Negrini, M.; Harris, C. C.; Croce, C. M., A microRNA expression signature of human solid tumors defines cancer gene targets. *Proceedings of the National Academy of Sciences of the United States of America* **2006,** *103* (7), 2257-2261.

24. Chan, E.; Prado, D. E.; Weidhaas, J. B., Cancer microRNAs: from subtype profiling to predictors of response to therapy. *Trends in molecular medicine* **2011,** *17* (5), 235-243.

25. Wang, K.; Zhang, S.; Marzolf, B.; Troisch, P.; Brightman, A.; Hu, Z.; Hood, L. E.; Galas, D. J., Circulating microRNAs, potential biomarkers for drug-induced liver injury. *Proceedings of the National Academy of Sciences of the United States of America* **2009,** *106* (11), 4402-4407.

26. Zhang, Y.; Jia, Y.; Zheng, R.; Guo, Y.; Wang, Y.; Guo, H.; Fei, M.; Sun, S., Plasma MicroRNA-122 as a Biomarker for Viral-, Alcohol-, and Chemical-Related Hepatic Diseases. *Clinical Chemistry* **2010,** *56* (12), 1830-1838.

27. Witwer, K. W., Circulating MicroRNA Biomarker Studies: Pitfalls and Potential Solutions. *Clinical Chemistry* **2015,** *61* (1), 56-63.

28. Ma, L.; Teruya-Feldstein, J.; Weinberg, R. A., Tumour invasion and metastasis initiated by microRNA-10b in breast cancer. *Nature* **2007,** *449* (7163), 682-688.

29. Zhang, S.; Chen, L.; Jung, E. J.; Calin, G. A., Targeting microRNAs with small molecules: Between Dream and Reality. *Clinical pharmacology and therapeutics* **2010,** *87* (6), 754-758.

30. Tong, A. W.; Nemunaitis, J., Modulation of miRNA activity in human cancer: a new paradigm for cancer gene therapy? *Cancer Gene Ther* **2008,** *15* (6), 341-355.

31. Connelly, C. M.; Deiters, A., Small-Molecule Regulation of MicroRNA Function. In *MicroRNA in Cancer*, Alahari, S., Ed. Springer Netherlands: 2013; pp 119-145.

32. Davis-Dusenbery, B. N.; Hata, A., Mechanisms of control of microRNA biogenesis. *Journal of Biochemistry* **2010,** *148* (4), 381-392.

33. Swierczynski, S.; Klieser, E.; Illig, R.; Alinger-Scharinger, B.; Kiesslich, T.; Neureiter, D., Histone deacetylation meets miRNA: epigenetics and post-transcriptional regulation in cancer and chronic diseases. *Expert Opinion on Biological Therapy 0* (0), 1-14.

34. Sampath, D.; Liu, C.; Vasan, K.; Sulda, M.; Puduvalli, V. K.; Wierda, W. G.; Keating, M. J., Histone deacetylases mediate the silencing of miR-15a, miR-16, and miR-29b in chronic lymphocytic leukemia. *Blood* **2012,** *119* (5), 1162-1172.

35. Han, J.; Pedersen, J. S.; Kwon, S. C.; Belair, C. D.; Kim, Y.-K.; Yeom, K.-H.; Yang, W.-Y.; Haussler, D.; Blelloch, R.; Kim, V. N., Posttranscriptional Crossregulation between Drosha and DGCR8. *Cell* **2009,** *136* (1), 75-84.

36. Tang, X.; Zhang, Y.; Tucker, L.; Ramratnam, B., Phosphorylation of the RNase III enzyme Drosha at Serine300 or Serine302 is required for its nuclear localization. *Nucleic Acids Research* **2010,** *38* (19), 6610-6619.

37. Wada, T.; Kikuchi, J.; Furukawa, Y., Histone deacetylase 1 enhances microRNA processing via deacetylation of DGCR8. *EMBO Reports* **2012,** *13* (2), 142-149.

38. Herbert, K. M.; Pimienta, G.; DeGregorio, S. J.; Alexandrov, A.; Steitz, J. A., Phosphorylation of DGCR8 Increases Its Intracellular Stability and Induces a Progrowth miRNA Profile. *Cell reports* **2013,** *5* (4), 1070-1081.

39. Davis, B. N.; Hilyard, A. C.; Lagna, G.; Hata, A., SMAD proteins control DROSHA-mediated microRNA maturation. *Nature* **2008,** *454* (7200), 56-61.

40. Carthew, R. W.; Sontheimer, E. J., Origins and Mechanisms of miRNAs and siRNAs. *Cell* **2009,** *136* (4), 642-655.

41. Haase, A. D.; Jaskiewicz, L.; Zhang, H.; Lainé, S.; Sack, R.; Gatignol, A.; Filipowicz, W., TRBP, a regulator of cellular PKR and HIV-1 virus expression, interacts with Dicer and functions in RNA silencing. *EMBO Reports* **2005,** *6* (10), 961-967.

42. Tokumaru, S.; Suzuki, M.; Yamada, H.; Nagino, M.; Takahashi, T., let-7 regulates Dicer expression and constitutes a negative feedback loop. *Carcinogenesis* **2008,** *29* (11), 2073-2077.

43. Paroo, Z.; Ye, X.; Chen, S.; Liu, Q., Phosphorylation of the human micro-RNA generating complex mediates MAPK/Erk signaling. *Cell* **2009,** *139* (1), 112-122.

44. Rüdel, S.; Wang, Y.; Lenobel, R.; Körner, R.; Hsiao, H.-H.; Urlaub, H.; Patel, D.; Meister, G., Phosphorylation of human Argonaute proteins affects small RNA binding. *Nucleic Acids Research* **2011,** *39* (6), 2330-2343.

45. Auyeung, V. C.; Ulitsky, I.; McGeary, S. E.; Bartel, D. P., Beyond secondary structure: primary-sequence determinants license pri-miRNA hairpins for processing. *Cell* **2013,** *152* (4), 844-858.

46. Ameres, S. L.; Zamore, P. D., Diversifying microRNA sequence and function. *Nat Rev Mol Cell Biol* **2013,** *14* (8), 475-488.

47. Heo, I.; Joo, C.; Cho, J.; Ha, M.; Han, J.; Kim, V. N., Lin28 Mediates the Terminal Uridylation of let-7 Precursor MicroRNA. *Molecular Cell 32* (2), 276-284.

48. Katoh, T.; Sakaguchi, Y.; Miyauchi, K.; Suzuki, T.; Kashiwabara, S.-i.; Baba, T.; Suzuki, T., Selective stabilization of mammalian microRNAs by 3′ adenylation mediated by the cytoplasmic poly(A) polymerase GLD-2. *Genes & Development* **2009,** *23* (4), 433-438.

49. Xhemalce, B.; Robson, S. C.; Kouzarides, T., Human RNA methyltransferase BCDIN3D regulates microRNA processing. *Cell* **2012,** *151* (2), 278-288.

50. Siomi, H.; Siomi, M. C., Posttranscriptional Regulation of MicroRNA Biogenesis in Animals. *Molecular Cell 38* (3), 323-332.

51. Stenvang, J.; Petri, A.; Lindow, M.; Obad, S.; Kauppinen, S., Inhibition of microRNA function by antimiR oligonucleotides. *Silence* **2012,** *3*, 1-1.

52. Deleavey, Glen F.; Damha, Masad J., Designing Chemically Modified Oligonucleotides for Targeted Gene Silencing. *Chemistry & Biology* **2012,** *19* (8), 937-954.

53. Esau, C. C., Inhibition of microRNA with antisense oligonucleotides. *Methods* **2008,** *44* (1), 55-60.

54. (a) Meister, G.; Landthaler, M.; Dorsett, Y.; Tuschl, T., Sequence-specific inhibition of microRNA- and siRNA-induced RNA silencing. *RNA* **2004,** *10* (3), 544-550; (b) Hutvágner, G.; Simard, M. J.; Mello, C. C.; Zamore, P. D., Sequence-Specific Inhibition of Small RNA Function. *PLoS Biol* **2004,** *2* (4), e98.

55. Davis, S.; Lollo, B.; Freier, S.; Esau, C., Improved targeting of miRNA with antisense oligonucleotides. *Nucleic Acids Research* **2006,** *34* (8), 2294-2304.

56. Lennox, K. A.; Behlke, M. A., Chemical modification and design of anti-miRNA oligonucleotides. *Gene Ther* **2011,** *18* (12), 1111-1120.

57. Krützfeldt, J.; Kuwajima, S.; Braich, R.; Rajeev, K. G.; Pena, J.; Tuschl, T.; Manoharan, M.; Stoffel, M., Specificity, duplex degradation and subcellular localization of antagomirs. *Nucleic Acids Research* **2007,** *35* (9), 2885-2892.

58. Machlin, E. S. S., P.; Sagan, S. M., Combating Hepatitis C Virus by Targeting MicroRNA-122 Using Locked Nucleic Acids. *Current Gene Therapy* **2012,** *12* (4), 301-306.

59. Fabani, M. M.; Gait, M. J., miR-122 targeting with LNA/2′-O-methyl oligonucleotide mixmers, peptide nucleic acids (PNA), and PNA–peptide conjugates. *RNA* **2008,** *14* (2), 336-346.

60. Torres, A. G.; Fabani, M. M.; Vigorito, E.; Gait, M. J., MicroRNA fate upon targeting with anti-miRNA oligonucleotides as revealed by an improved Northern-blot-based method for miRNA detection. *RNA* **2011,** *17* (5), 933-943.

61. Elmén, J.; Lindow, M.; Silahtaroglu, A.; Bak, M.; Christensen, M.; Lind-Thomsen, A.; Hedtjärn, M.; Hansen, J. B.; Hansen, H. F.; Straarup, E. M.; McCullagh, K.; Kearney, P.; Kauppinen, S., Antagonism of microRNA-122 in mice by systemically administered LNA-antimiR leads to up-regulation of a large set of predicted target mRNAs in the liver. *Nucleic Acids Research* **2008,** *36* (4), 1153-1162.

62. Obad, S.; dos Santos, C. O.; Petri, A.; Heidenblad, M.; Broom, O.; Ruse, C.; Fu, C.; Lindow, M.; Stenvang, J.; Straarup, E. M.; Hansen, H. F.; Koch, T.; Pappin, D.; Hannon,

G. J.; Kauppinen, S., Silencing of microRNA families by seed-targeting tiny LNAs. *Nature genetics* **2011,** *43* (4), 371-378.

63. Ebert, M. S.; Neilson, J. R.; Sharp, P. A., MicroRNA sponges: competitive inhibitors of small RNAs in mammalian cells. *Nature methods* **2007,** *4* (9), 10.1038/nmeth1079.

64. Wang, Z., The Principles of MiRNA-Masking Antisense Oligonucleotides Technology. In *MicroRNA and Cancer*, Wu, W., Ed. Humana Press: 2011; Vol. 676, pp 43-49.

65. (a) Liu, Z.; Sall, A.; Yang, D., MicroRNA: an Emerging Therapeutic Target and Intervention Tool. *International Journal of Molecular Sciences* **2008,** *9* (6), 978-999; (b) Kota, J.; Chivukula, R. R.; O'Donnell, K. A.; Wentzel, E. A.; Montgomery, C. L.; Hwang, H.-W.; Chang, T.-C.; Vivekanandan, P.; Torbenson, M.; Clark, K. R.; Mendell, J. R.; Mendell, J. T., Therapeutic microRNA Delivery Suppresses Tumorigenesis in a Murine Liver Cancer Model. *Cell* **2009,** *137* (6), 1005-1017.

66. Trang, P.; Wiggins, J. F.; Daige, C. L.; Cho, C.; Omotola, M.; Brown, D.; Weidhaas, J. B.; Bader, A. G.; Slack, F. J., Systemic Delivery of Tumor Suppressor microRNA Mimics Using a Neutral Lipid Emulsion Inhibits Lung Tumors in Mice. *Molecular Therapy* **2011,** *19* (6), 1116-1122.

67. van Rooij, E.; Purcell, A. L.; Levin, A. A., Developing MicroRNA Therapeutics. *Circulation Research* **2012,** *110* (3), 496-507.

68. Flynt, A. S.; Li, N.; Thatcher, E. J.; Solnica-Krezel, L.; Patton, J. G., Zebrafish miR-214 modulates Hedgehog signaling to specify muscle cell fate. *Nature genetics* **2007,** *39* (2), 259-263.

69. Kloosterman, W. P.; Lagendijk, A. K.; Ketting, R. F.; Moulton, J. D.; Plasterk, R. H. A., Targeted Inhibition of miRNA Maturation with Morpholinos Reveals a Role for miR-375 in Pancreatic Islet Development. *PLoS Biology* **2007,** *5* (8), e203.

70. Jadhav, V. M.; Scaria, V.; Maiti, S., Antagomirzymes: Oligonucleotide Enzymes That Specifically Silence MicroRNA Function. *Angewandte Chemie International Edition* **2009,** *48* (14), 2557-2560.

71. Li, Y.-P.; Gottwein, J. M.; Scheel, T. K.; Jensen, T. B.; Bukh, J., MicroRNA-122 antagonism against hepatitis C virus genotypes 1–6 and reduced efficacy by host RNA insertion or mutations in the HCV 5′ UTR. *Proceedings of the National Academy of Sciences of the United States of America* **2011,** *108* (12), 4991-4996.

72. Lindow, M.; Kauppinen, S., Discovering the first microRNA-targeted drug. *The Journal of Cell Biology* **2012,** *199* (3), 407-412.

73. Nair, J. K.; Willoughby, J. L. S.; Chan, A.; Charisse, K.; Alam, M. R.; Wang, Q.; Hoekstra, M.; Kandasamy, P.; Kel'in, A. V.; Milstein, S.; Taneja, N.; O'Shea, J.; Shaikh, S.; Zhang, L.; van der Sluis, R. J.; Jung, M. E.; Akinc, A.; Hutabarat, R.; Kuchimanchi, S.; Fitzgerald, K.; Zimmermann, T.; van Berkel, T. J. C.; Maier, M. A.; Rajeev, K. G.;

Manoharan, M., Multivalent N-Acetylgalactosamine-Conjugated siRNA Localizes in Hepatocytes and Elicits Robust RNAi-Mediated Gene Silencing. *Journal of the American Chemical Society* **2014,** *136* (49), 16958-16961.

74. Bouchie, A., First microRNA mimic enters clinic. *Nat Biotech* **2013,** *31* (7), 577-577.

75. Spring, D. R., Chemical genetics to chemical genomics: small molecules offer big insights. *Chemical Society Reviews* **2005,** *34* (6), 472-482.

76. Maiti, M.; Nauwelaerts, K.; Herdewijn, P., Pre-microRNA binding aminoglycosides and antitumor drugs as inhibitors of Dicer catalyzed microRNA processing. *Bioorganic & Medicinal Chemistry Letters* **2012,** *22* (4), 1709-1711.

77. Murata, A.; Fukuzumi, T.; Umemoto, S.; Nakatani, K., Xanthone derivatives as potential inhibitors of miRNA processing by human Dicer: Targeting secondary structures of pre-miRNA by small molecules. *Bioorganic & Medicinal Chemistry Letters* **2013,** *23* (1), 252-255.

78. Vo, D. D.; Staedel, C.; Zehnacker, L.; Benhida, R.; Darfeuille, F.; Duca, M., Targeting the Production of Oncogenic MicroRNAs with Multimodal Synthetic Small Molecules. *ACS Chemical Biology* **2014,** *9* (3), 711-721.

79. Shi, Z.; Zhang, J.; Qian, X.; Han, L.; Zhang, K.; Chen, L.; Liu, J.; Ren, Y.; Yang, M.; Zhang, A.; Pu, P.; Kang, C., AC1MMYR2, an Inhibitor of Dicer-Mediated Biogenesis of Oncomir miR-21, Reverses Epithelial–Mesenchymal Transition and Suppresses Tumor Growth and Progression. *Cancer Research* **2013,** *73* (17), 5519-5531.

80. Shan, G.; Li, Y.; Zhang, J.; Li, W.; Szulwach, K. E.; Duan, R.; Faghihi, M. A.; Khalil, A. M.; Lu, L.; Paroo, Z.; Chan, A. W. S.; Shi, Z.; Liu, Q.; Wahlestedt, C.; He, C.; Jin, P., A small molecule enhances RNA interference and promotes microRNA processing. *Nature biotechnology* **2008,** *26* (8), 933-940.

81. Chen, X.; Huang, C.; Zhang, W.; Wu, Y.; Chen, X.; Zhang, C.-y.; Zhang, Y., A universal activator of microRNAs identified from photoreaction products. *Chemical Communications* **2012,** *48* (51), 6432-6434.

82. Meister, G.; Landthaler, M.; Patkaniowska, A.; Dorsett, Y.; Teng, G.; Tuschl, T., Human Argonaute2 Mediates RNA Cleavage Targeted by miRNAs and siRNAs. *Molecular Cell* **2004,** *15* (2), 185-197.

83. Tan, G. S.; Chiu, C.-H.; Garchow, B. G.; Metzler, D.; Diamond, S. L.; Kiriakidou, M., Small Molecule Inhibition of RISC Loading. *ACS Chemical Biology* **2012,** *7* (2), 403-410.

84. Masciarelli, S.; Quaranta, R.; Iosue, I.; Colotti, G.; Padula, F.; Varchi, G.; Fazi, F.; Del Rio, A., A Small-Molecule Targeting the MicroRNA Binding Domain of Argonaute 2 improves the Retinoic Acid Differentiation Response of the Acute Promyelocytic Leukemia Cell Line NB4. *ACS Chemical Biology* **2014,** *9* (8), 1674-1679.

85. Watashi, K.; Yeung, M. L.; Starost, M. F.; Hosmane, R. S.; Jeang, K.-T., Identification of Small Molecules That Suppress MicroRNA Function and Reverse Tumorigenesis. *The Journal of Biological Chemistry* **2010,** *285* (32), 24707-24716.

86. Chiu, Y.-L.; Dinesh, C. U.; Chu, C.-y.; Ali, A.; Brown, K. M.; Cao, H.; Rana, T. M., Dissecting RNA-Interference Pathway with Small Molecules. *Chemistry & Biology* **2005,** *12* (6), 643-648.

87. Rossi, L.; Bonmassar, E.; Faraoni, I., Modification of miR gene expression pattern in human colon cancer cells following exposure to 5-fluorouracil in vitro. *Pharmacological Research* **2007,** *56* (3), 248-253.

88. Zhou, J., Zhou, Y., Yin, B., Hao, W., Zhao, L., Ju, W., Bai, 5-Fluorouracil and oxaliplatin modify the expression profiles of microRNAs in human colon cancer cells in vitro. *Oncology Reports* **2010,** *23*.

89. Tormo, E., Pineda, B., Serna, E., Guijarro, A., Ribas, G., Fores, J., Chirivella, E., Climent, J., Lluch, A. and Eroles, P. , MicroRNA profile in response to doxorubicin treatment in breast cancer. *J. Cell. Biochem* **2015**, Accepted.

90. Phuah, N. H.; Nagoor, N. H., Regulation of MicroRNAs by Natural Agents: New Strategies in Cancer Therapies. *BioMed Research International* **2014,** *2014*, 804510.

91. Song, Y.; Dou, H.; Wang, P.; Zhao, S.; Wang, T.; Gong, W.; Zhao, J.; Li, E.; Tan, R.; Hou, Y., A novel small-molecule compound diaporine A inhibits non-small cell lung cancer growth by regulating miR-99a/mTOR signaling. *Cancer Biology & Therapy* **2014,** *15* (10), 1423-1430.

92. Joven, J.; Espinel, E.; Rull, A.; Aragonès, G.; Rodríguez-Gallego, E.; Camps, J.; Micol, V.; Herranz-López, M.; Menéndez, J. A.; Borrás, I.; Segura-Carretero, A.; Alonso-Villaverde, C.; Beltrán-Debón, R., Plant-derived polyphenols regulate expression of miRNA paralogs miR-103/107 and miR-122 and prevent diet-induced fatty liver disease in hyperlipidemic mice. *Biochimica et Biophysica Acta (BBA) - General Subjects* **2012,** *1820* (7), 894-899.

93. Gumireddy, K.; Young, D. D.; Xiong, X.; Hogenesch, J. B.; Huang, Q.; Deiters, A., Small Molecule Inhibitors of MicroRNA miR-21 Function(). *Angewandte Chemie (International ed. in English)* **2008,** *47* (39), 7482-7484.

94. Diaz, J. P.; Chirayil, R.; Chirayil, S.; Tom, M.; Head, K. J.; Luebke, K. J., Association of a peptoid ligand with the apical loop of pri-miR-21 inhibits cleavage by Drosha. *RNA* **2014,** *20* (4), 528-539.

95. Bose, D.; Jayaraj, G.; Suryawanshi, H.; Agarwala, P.; Pore, S. K.; Banerjee, R.; Maiti, S., The Tuberculosis Drug Streptomycin as a Potential Cancer Therapeutic: Inhibition of miR-21 Function by Directly Targeting Its Precursor. *Angewandte Chemie International Edition* **2012,** *51* (4), 1019-1023.

96. Velagapudi, S. P.; Gallo, S. M.; Disney, M. D., Sequence-based design of bioactive small molecules that target precursor microRNAs. *Nat Chem Biol* **2014,** *10* (4), 291-297.

97. Velagapudi, S. P.; Disney, M. D., Two-dimensional combinatorial screening enables the bottom-up design of a microRNA-10b inhibitor. *Chemical communications (Cambridge, England)* **2014,** *50* (23), 3027-3029.

98. Young, D. D.; Connelly, C. M.; Grohmann, C.; Deiters, A., Small Molecule Modifiers of MicroRNA miR-122 Function for the Treatment of Hepatitis C Virus Infection and Hepatocellular Carcinoma. *Journal of the American Chemical Society* **2010,** *132* (23), 7976-7981.

99. Xiao, Z.; Li, C. H.; Chan, S. L.; Xu, F.; Feng, L.; Wang, Y.; Jiang, J.-D.; Sung, J. J. Y.; Cheng, C. H. K.; Chen, Y., A Small-Molecule Modulator of the Tumor-Suppressor miR34a Inhibits the Growth of Hepatocellular Carcinoma. *Cancer Research* **2014,** *74* (21), 6236-6247.

100. Chandrasekhar, S.; Pushpavalli, S. N. C. V. L.; Chatla, S.; Mukhopadhyay, D.; Ganganna, B.; Vijeender, K.; Srihari, P.; Reddy, C. R.; Janaki Ramaiah, M.; Bhadra, U., aza-Flavanones as potent cross-species microRNA inhibitors that arrest cell cycle. *Bioorganic & Medicinal Chemistry Letters* **2012,** *22* (1), 645-648.

101. Tan, S.-B.; Huang, C.; Chen, X.; Wu, Y.; Zhou, M.; Zhang, C.; Zhang, Y., Small molecular inhibitors of miR-1 identified from photocycloadducts of acetylenes with 2-methoxy-1,4-naphthalenequinone. *Bioorganic & Medicinal Chemistry* **2013,** *21* (20), 6124-6131.

102. Schmidt, M. F.; Korb, O.; Abell, C., MicroRNA-Specific Argonaute 2 Protein Inhibitors. *ACS Chemical Biology* **2013,** *8* (10), 2122-2126.

103. Pan, X.; Wang, Z.-X.; Wang, R., MicroRNA-21: A novel therapeutic target in human cancer. *Cancer Biology & Therapy* **2010,** *10* (12), 1224-1232.

104. Krichevsky, A. M.; Gabriely, G., miR-21: a small multi-faceted RNA. *Journal of Cellular and Molecular Medicine* **2009,** *13* (1), 39-53.

105. (a) Mudduluru, G.; Medved, F.; Grobholz, R.; Jost, C.; Gruber, A.; Leupold, J. H.; Post, S.; Jansen, A.; Colburn, N. H.; Allgayer, H., Loss of programmed cell death 4 expression marks adenoma-carcinoma transition, correlates inversely with phosphorylated protein kinase B, and is an independent prognostic factor in resected colorectal cancer. *Cancer* **2007,** *110* (8), 1697-1707; (b) Chen, Y.; Knösel, T.; Kristiansen, G.; Pietas, A.; Garber, M. E.; Matsuhashi, S.; Ozaki, I.; Petersen, I., Loss of PDCD4 expression in human lung cancer correlates with tumour progression and prognosis. *The Journal of Pathology* **2003,** *200* (5), 640-646.

106. Correa, T. C. S. B., C. A.; Winnischofer, S. M. B.; Cardeal, L. B. d. S.; Sasahara, R. M.; Taboga, S. R.; Sogayar, M. C.; Maria-Engler, S. S, Downregulation of the RECK-tumor

and metastasis suppressor gene in glioma invasiveness. *J. Cell. Biochem* **2006,** (99), 156–167.

107. Sayed, D.; Rane, S.; Lypowy, J.; He, M.; Chen, I.-Y.; Vashistha, H.; Yan, L.; Malhotra, A.; Vatner, D.; Abdellatif, M., MicroRNA-21 Targets Sprouty2 and Promotes Cellular Outgrowths. *Molecular Biology of the Cell* **2008,** *19* (8), 3272-3282.

108. Meng, F.; Henson, R.; Wehbe-Janek, H.; Ghoshal, K.; Jacob, S. T.; Patel, T., MicroRNA-21 Regulates Expression of the PTEN Tumor Suppressor Gene in Human Hepatocellular Cancer. *Gastroenterology* **2007,** *133* (2), 647-658.

109. Shi, G.-h.; Ye, D.-w.; Yao, X.-d.; Zhang, S.-l.; Dai, B.; Zhang, H.-l.; Shen, Y.-j.; Zhu, Y.; Zhu, Y.-p.; Xiao, W.-j.; Ma, C.-g., Involvement of microRNA-21 in mediating chemo-resistance to docetaxel in androgen-independent prostate cancer PC3 cells. *Acta Pharmacologica Sinica* **2010,** *31* (7), 867-873.

110. Medina, P. P.; Nolde, M.; Slack, F. J., OncomiR addiction in an in vivo model of microRNA-21-induced pre-B-cell lymphoma. *Nature* **2010,** *467* (7311), 86-90.

111. Schmittgen, T. D.; Jiang, J.; Liu, Q.; Yang, L., A high-throughput method to monitor the expression of microRNA precursors. *Nucleic Acids Research* **2004,** *32* (4), e43-e43.

112. Jain, A.; Gupta, Y.; Jain, S. K., Azo Chemistry and Its Potential for Colonic Delivery. **2006,** *23* (5), 349-400.

113. Simplício, A.; Clancy, J.; Gilmer, J., Prodrugs for Amines. *Molecules* **2008,** *13* (3), 519-547.

114. Dorman, G.; Prestwich, G. D., Benzophenone Photophores in Biochemistry. *Biochemistry* **1994,** *33* (19), 5661-5673.

115. Mora, F.; Tran, D.-H.; Oudry, N.; Hopfgartner, G.; Jeannerat, D.; Sakai, N.; Matile, S., Interface Engineering of Synthetic Pores: Towards Hypersensitive Biosensors. *Chemistry – A European Journal* **2008,** *14* (6), 1947-1953.

116. Shi, D.-F.; Bradshaw, T. D.; Wrigley, S.; McCall, C. J.; Lelieveld, P.; Fichtner, I.; Stevens, M. F. G., Antitumor Benzothiazoles. 3. Synthesis of 2-(4-Aminophenyl)benzothiazoles and Evaluation of Their Activities against Breast Cancer Cell Lines in Vitro and in Vivo. *Journal of Medicinal Chemistry* **1996,** *39* (17), 3375-3384.

117. Büttner, A.; Seifert, K.; Cottin, T.; Sarli, V.; Tzagkaroulaki, L.; Scholz, S.; Giannis, A., Synthesis and biological evaluation of SANT-2 and analogues as inhibitors of the hedgehog signaling pathway. *Bioorganic & Medicinal Chemistry* **2009,** *17* (14), 4943-4954.

118. Kallashi, F.; Kim, D.; Kowalchick, J.; Park, Y. J.; Hunt, J. A.; Ali, A.; Smith, C. J.; Hammond, M. L.; Pivnichny, J. V.; Tong, X.; Xu, S. S.; Anderson, M. S.; Chen, Y.;

Eveland, S. S.; Guo, Q.; Hyland, S. A.; Milot, D. P.; Cumiskey, A.-M.; Latham, M.; Peterson, L. B.; Rosa, R.; Sparrow, C. P.; Wright, S. D.; Sinclair, P. J., 2-Arylbenzoxazoles as CETP inhibitors: Raising HDL-C in cynoCETP transgenic mice. *Bioorganic & Medicinal Chemistry Letters* **2011,** *21* (1), 558-561.

119. Klingele, Marco H.; Brooker, S., From N-Substituted Thioamides to Symmetrical and Unsymmetrical 3,4,5-Trisubstituted 4H-1,2,4-Triazoles: Synthesis and Characterisation of New Chelating Ligands. *European Journal of Organic Chemistry* **2004,** *2004* (16), 3422-3434.

120. Deepa, K. A., K. Synthesis, characterization, and antifungal studies of transition metal complexes of omega-bromoacetoacetanilide isonicotinylhydrazone, Synthesis, characterization, and antifungal studies of transition metal complexes of omega-bromoacetoacetanilide isonicotinylhydrazone. *Appl. Biochem. Biotechnol.* **2004,** *118*, 283-292.

121. Yogeeswari, P.; Menon, N.; Semwal, A.; Arjun, M.; Sriram, D., Discovery of molecules for the treatment of neuropathic pain: Synthesis, antiallodynic and antihyperalgesic activities of 5-(4-nitrophenyl)furoic-2-acid hydrazones. *European Journal of Medicinal Chemistry* **2011,** *46* (7), 2964-2970.

122. Tai, X. H., M.; Feng, Y, 2 '-Hydroxyacetophenone furan-2-carbohydrazide. *Acta Crystallographica* **2007,** *E63*, o2267-o2268.

123. Sriram, D.; Yogeeswari, P.; Devakaram, R. V., Synthesis, in vitro and in vivo antimycobacterial activities of diclofenac acid hydrazones and amides. *Bioorganic & Medicinal Chemistry* **2006,** *14* (9), 3113-3118.

124. Connelly, C. M.; Thomas, M.; Deiters, A., High-Throughput Luciferase Reporter Assay for Small-Molecule Inhibitors of MicroRNA Function. *Journal of biomolecular screening* **2012,** *17* (6), 822-828.

125. Thorne, N.; Shen, M.; Lea, W. A.; Simeonov, A.; Lovell, S.; Auld, D. S.; Inglese, J., Firefly luciferase in chemical biology: A compendium of inhibitors, mechanistic evaluation of chemotypes, and suggested use as a reporter. *Chemistry & biology* **2012,** *19* (8), 1060-1072.

126. Thorne, N.; Inglese, J.; Auld, D. S., Illuminating insights into firefly luciferase and other bioluminescent reporters used in chemical biology. *Chemistry & biology* **2010,** *17* (6), 646-657.

127. Díez-González, S.; Nolan, S. P., [(NHC)2Cu]X Complexes as Efficient Catalysts for Azide–Alkyne Click Chemistry at Low Catalyst Loadings. *Angewandte Chemie International Edition* **2008,** *47* (46), 8881-8884.

128. Koch, U.; Attenni, B.; Malancona, S.; Colarusso, S.; Conte, I.; Di Filippo, M.; Harper, S.; Pacini, B.; Giomini, C.; Thomas, S.; Incitti, I.; Tomei, L.; De Francesco, R.; Altamura, S.; Matassa, V. G.; Narjes, F., 2-(2-Thienyl)-5,6-dihydroxy-4-carboxypyrimidines as

Inhibitors of the Hepatitis C Virus NS5B Polymerase: Discovery, SAR, Modeling, and Mutagenesis. *Journal of Medicinal Chemistry* **2006,** *49* (5), 1693-1705.

129. Zhuravel, I. O. K., S. M.; Zaremba, O. V.; Detistov, O. S.; Kovalenko, S. S.; Chernykh, V. P., Synthesis

of 5-Hydroxymethyl-8-methyl-3-(3-aryl-[1,2,4]oxadiazol-5-yl)-2H-pyrano[2,3-

c]pyridin-2-ones and Their Esters,. *Synthetic Communications: An International Journal*

for Rapid Communication of Synthetic Organic Chemistry **2008,** *38* (21), 3778-3784.

130. Pokhodylo, N. T. M., V. S.; Obushak, M. D., Synthesis of Triazoles via Regioselective Reactions of Aryl Azides with -Cyanoacetyl Pyrroles and Indoles. *Synthesis* **2009,** *8*, 1297-1300.

131. Pinard, E.; Alanine, A.; Bourson, A.; Büttelmann, B.; Gill, R.; Heitz, M.-P.; Jaeschke, G.; Mutel, V.; Trube, G.; Wyler, R., Discovery of (R)-1-[2-Hydroxy-3-(4-hydroxy-phenyl)-propyl]-4-(4-methyl-benzyl)-piperidin-4-ol: A Novel NR1/2B Subtype Selective NMDA Receptor Antagonist. *Bioorganic & Medicinal Chemistry Letters* **2001,** *11* (16), 2173-2176.

132. Meldal, M.; Tornøe, C. W., Cu-Catalyzed Azide−Alkyne Cycloaddition. *Chemical Reviews* **2008,** *108* (8), 2952-3015.

133. Aizpurua, J. M.; Azcune, I.; Fratila, R. M.; Balentova, E.; Sagartzazu-Aizpurua, M.; Miranda, J. I., "Click" Synthesis of Nonsymmetrical Bis(1,2,3-triazoles). *Organic Letters* **2010,** *12* (7), 1584-1587.

134. Trybulski, E. J.; Benjamin, L.; Vitone, S.; Walser, A.; Fryer, R. I., 2-Benzazepines. [1,2,3]Triazolo[4,5-d][2]benzazepines and dibenzo[c,f][1,2,3]triazolo[3,4-a]azepines. Synthesis and evaluation as central nervous system agents. *Journal of Medicinal Chemistry* **1983,** *26* (3), 367-372.

135. Kumar, A. H., M.; Prasad, A. K.; Singh, I.; Vats, A.; Sharma, N. K.; Sharma, S. K.; Gupta, R. K.; Olsen, C. E.; Bracke, M. E.; Gross, R. A.; Parmar, V. S. , Synthesis of novel heterocyclic compounds: Routes to pyrazolyl 1,2,3-triazoles and their biological activity evaluation. *Indian Journal of Chemistry Section B* **2003,** *42B*.

136. Romagnoli, R.; Baraldi, P. G.; Sarkar, T.; Carrion, M. D.; Cruz-Lopez, O.; Cara, C. L.; Tolomeo, M.; Grimaudo, S.; Di Cristina, A.; Pipitone, M. R.; Balzarini, J.; Gambari, R.; Ilaria, L.; Saletti, R.; Brancale, A.; Hamel, E., Synthesis and biological evaluation of 2-(3′,4′,5′-trimethoxybenzoyl)-3-N,N-dimethylamino benzo[b]furan derivatives as inhibitors of tubulin polymerization. *Bioorganic & medicinal chemistry* **2008,** *16* (18), 8419-8426.

137. Newman, A. H.; Grundt, P.; Cyriac, G.; Deschamps, J. R.; Taylor, M.; Kumar, R.; Ho, D.; Luedtke, R. R., N-(4-(4-(2,3-Dichloro- or 2-methoxyphenyl)piperazin-1-yl)-butyl)-

heterobiarylcarboxamides with Functionalized Linking Chains as High Affinity and Enantioselective D3 Receptor Antagonists. *Journal of medicinal chemistry* **2009,** *52* (8), 2559-2570.

138. Sledz, P.; Silvestre, H. L.; Hung, A. W.; Ciulli, A.; Blundell, T. L.; Abell, C., Optimization of the Interligand Overhauser Effect for Fragment Linking: Application to Inhibitor Discovery against Mycobacterium tuberculosis Pantothenate Synthetase. *Journal of the American Chemical Society* **2010,** *132* (13), 4544-4545.

139. Varnavas, A.; Lassiani, L.; Valenta, V.; Berti, F.; Tontini, A.; Mennuni, L.; Makovec, F., Anthranilic acid based CCK1 antagonists: the 2-indole moiety may represent a "needle" according to the recent homonymous concept. *European Journal of Medicinal Chemistry* **2004,** *39* (1), 85-97.

140. Zhu, J.; Lin, J.-B.; Xu, Y.-X.; Shao, X.-B.; Jiang, X.-K.; Li, Z.-T., Hydrogen-Bonding-Mediated Anthranilamide Homoduplexes. Increasing Stability through Preorganization and Iterative Arrangement of a Simple Amide Binding Site. *Journal of the American Chemical Society* **2006,** *128* (37), 12307-12313.

141. Suzuki, T.; Imai, K.; Nakagawa, H.; Miyata, N., 2-Anilinobenzamides as SIRT Inhibitors. *ChemMedChem* **2006,** *1* (10), 1059-1062.

142. Jopling, C. L.; Yi, M.; Lancaster, A. M.; Lemon, S. M.; Sarnow, P., Modulation of Hepatitis C Virus RNA Abundance by a Liver-Specific MicroRNA. *Science* **2005,** *309* (5740), 1577-1581.

143. Sato, S.-i.; Murata, A.; Shirakawa, T.; Uesugi, M., Biochemical Target Isolation for Novices: Affinity-Based Strategies. *Chemistry & Biology* **2010,** *17* (6), 616-623.

144. Kotzyba-Hibert, F.; Kapfer, I.; Goeldner, M., Recent Trends in Photoaffinity Labeling. *Angewandte Chemie International Edition in English* **1995,** *34* (12), 1296-1312.

145. Romuald, C.; Busseron, E.; Coutrot, F., Very Contracted to Extended co-Conformations with or without Oscillations in Two- and Three-Station [c2]Daisy Chains. *The Journal of Organic Chemistry* **2010,** *75* (19), 6516-6531.

146. Salisbury, C. M.; Cravatt, B. F., Optimization of Activity-Based Probes for Proteomic Profiling of Histone Deacetylase Complexes. *Journal of the American Chemical Society* **2008,** *130* (7), 2184-2194.

147. Zhao, X.; Yang, Z.; Li, G.; Li, D.; Zhao, Y.; Wu, Y.; Robson, S.; He, L.; Xu, Y.; Miao, R.; Zhao, H., The role and clinical implications of microRNAs in hepatocellular carcinoma. *Sci. China Life Sci.* **2012,** *55* (10), 906-919.

148. Connolly, E.; Melegari, M.; Landgraf, P.; Tchaikovskaya, T.; Tennant, B. C.; Slagle, B. L.; Rogler, L. E.; Zavolan, M.; Tuschl, T.; Rogler, C. E., Elevated Expression of the miR-17–92 Polycistron and miR-21 in Hepadnavirus-Associated Hepatocellular Carcinoma

Contributes to the Malignant Phenotype. *The American Journal of Pathology* **2008,** *173* (3), 856-864.

149. Lin, C. J.-F.; Gong, H.-Y.; Tseng, H.-C.; Wang, W.-L.; Wu, J.-L., miR-122 targets an anti-apoptotic gene, Bcl-w, in human hepatocellular carcinoma cell lines. *Biochemical and Biophysical Research Communications* **2008,** *375* (3), 315-320.

150. Qiu, X.; Dong, S.; Qiao, F.; Lu, S.; Song, Y.; Lao, Y.; Li, Y.; Zeng, T.; Hu, J.; Zhang, L.; Zhang, L.; Fan, H., HBx-mediated miR-21 upregulation represses tumor-suppressor function of PDCD4 in hepatocellular carcinoma. *Oncogene* **2013,** *32* (27), 3296-3305.

151. Bao, L.; Yan, Y.; Xu, C.; Ji, W.; Shen, S.; Xu, G.; Zeng, Y.; Sun, B.; Qian, H.; Chen, L.; Wu, M.; Su, C.; Chen, J., MicroRNA-21 suppresses PTEN and hSulf-1 expression and promotes hepatocellular carcinoma progression through AKT/ERK pathways. *Cancer Letters* **2013,** *337* (2), 226-236.

152. Wang, X.; He, H.; Lu, Y.; Ren, W.; Teng, K.-y.; Chiang, C.-l.; Yang, Z.; Yu, B.; Hsu, S.; Jacob, S. T.; Ghoshal, K.; Lee, L. J., Indole-3-carbinol inhibits tumorigenicity of hepatocellular carcinoma cells via suppression of microRNA-21 and upregulation of phosphatase and tensin homolog. *Biochimica et biophysica acta* **2015,** *1853* (1), 244-253.

153. Bai, S.; Nasser, M. W.; Wang, B.; Hsu, S.-H.; Datta, J.; Kutay, H.; Yadav, A.; Nuovo, G.; Kumar, P.; Ghoshal, K., MicroRNA-122 Inhibits Tumorigenic Properties of Hepatocellular Carcinoma Cells and Sensitizes These Cells to Sorafenib. *The Journal of Biological Chemistry* **2009,** *284* (46), 32015-32027.

154. He, X.; Li, J.; Guo, W.; Liu, W.; Yu, J.; Song, W.; Dong, L.; Wang, F.; Yu, S.; Zheng, Y.; Chen, S.; Kong, Y.; Liu, C., Targeting the microRNA-21/AP1 axis by 5-fluorouracil and pirarubicin in human hepatocellular carcinoma. *Oncotarget* **2015,** *6* (4), 2302-2314.

155. Livak, K. J.; Schmittgen, T. D., Analysis of Relative Gene Expression Data Using Real-Time Quantitative PCR and the 2−ΔΔCT Method. *Methods* **2001,** *25* (4), 402-408.

156. Schneider, T. L.; Halloran, K. T.; Hillner, J. A.; Conry, R. R.; Linton, B. R., Application of H/D Exchange to Hydrogen Bonding in Small Molecules. *Chemistry – A European Journal* **2013,** *19* (45), 15101-15104.

157. Wheelhouse, R. T.; Shi, D.-F.; Wilman, D. E. V.; Stevens, M. F. G., Antitumour benzothiazoles. Part 4. An NMR study of the sites of protonation of 2-(4-aminophenyl)benzothiazoles. *Journal of the Chemical Society, Perkin Transactions 2* **1996,** (7), 1271-1274.

158. Elgersma, R. C.; Kroon-Batenburg, L. M. J.; Posthuma, G.; Meeldijk, J. D.; Rijkers, D. T. S.; Liskamp, R. M. J., pH-controlled aggregation polymorphism of amyloidogenic Aβ(16–22): Insights for obtaining peptide tapes and peptide nanotubes, as function of the N-terminal capping moiety. *European Journal of Medicinal Chemistry* **2014,** *88* (0), 55-65.

159. El Aissi, R.; Liu, J.; Besse, S.; Canitrot, D.; Chavignon, O.; Chezal, J.-M.; Miot-Noirault, E.; Moreau, E., Synthesis and Biological Evaluation of New Quinoxaline Derivatives of ICF01012 as Melanoma-Targeting Probes. *ACS Medicinal Chemistry Letters* **2014,** *5* (5), 468-473.

160. Manley, D. W.; McBurney, R. T.; Miller, P.; Walton, J. C.; Mills, A.; O'Rourke, C., Titania-Promoted Carboxylic Acid Alkylations of Alkenes and Cascade Addition–Cyclizations. *The Journal of Organic Chemistry* **2014,** *79* (3), 1386-1398.

161. Jagadeesh Kumar, G.; Sriramkumar Bomma, H. V. S.; Srihari, E.; Shrivastava, S.; Naidu, V. G. M.; Srinivas, K.; Jayathirtha Rao, V., Synthesis and anticancer activity of some new s-triazine derivatives. *Med Chem Res* **2013,** *22* (12), 5973-5981.

162. Kim, M.-S.; Buisson, L. A.; Heathcote, D. A.; Hu, H.; Braddock, D. C.; Barrett, A. G. M.; Ashton-Rickardt, P. G.; Snyder, J. P., Approaches to design non-covalent inhibitors for human granzyme B (hGrB). *Organic & Biomolecular Chemistry* **2014,** *12* (44), 8952-8965.

163. Morjan, R. Y.; Mkadmh, A. M.; Abu-Awwad, F. M.; Helliwell, M.; Awadallah, A. M.; Gardiner, J. M., Synthesis, structural characterization, and computational study of novel (E)-N′-(1-p-tolylethylidene)furan-2-carbohydrazide. *Journal of Molecular Structure* **2013,** *1051* (0), 345-353.

164. Levrand, B.; Fieber, W.; Lehn, J.-M.; Herrmann, A., Controlled Release of Volatile Aldehydes and Ketones from Dynamic Mixtures Generated by Reversible Hydrazone Formation. *Helvetica Chimica Acta* **2007,** *90* (12), 2281-2314.

165. Maurya, M. R.; Agarwal, S.; Abid, M.; Azam, A.; Bader, C.; Ebel, M.; Rehder, D., Synthesis, characterisation, reactivity and in vitro antiamoebic activity of hydrazone based oxovanadium(iv), oxovanadium(v) and [small micro]-bis(oxo)bis{oxovanadium(v)} complexes. *Dalton Transactions* **2006,** (7), 937-947.

166. Andrade, M. M.; Barros, M. T., Fast Synthesis of N-Acylhydrazones Employing a Microwave Assisted Neat Protocol. *Journal of Combinatorial Chemistry* **2010,** *12* (2), 245-247.

167. Ushijima, S.; Moriyama, K.; Togo, H., Facile preparation of aromatic esters from aromatic bromides with ethyl formate or DMF and molecular iodine via aryllithium. *Tetrahedron* **2012,** *68* (24), 4701-4709.

168. Prasad, V.; Kale, R. R.; Mishra, B. B.; Kumar, D.; Tiwari, V. K., Diacetoxyiodobenzene Mediated One-Pot Synthesis of Diverse Carboxamides from Aldehydes. *Organic Letters* **2012,** *14* (12), 2936-2939.

169. Kwok, S. W.; Fotsing, J. R.; Fraser, R. J.; Rodionov, V. O.; Fokin, V. V., Transition-Metal-Free Catalytic Synthesis of 1,5-Diaryl-1,2,3-triazoles. *Organic Letters* **2010,** *12* (19), 4217-4219.

170. Flipo, M.; Desroses, M.; Lecat-Guillet, N.; Dirié, B.; Carette, X.; Leroux, F.; Piveteau, C.; Demirkaya, F.; Lens, Z.; Rucktooa, P.; Villeret, V.; Christophe, T.; Jeon, H. K.; Locht, C.; Brodin, P.; Déprez, B.; Baulard, A. R.; Willand, N., Ethionamide Boosters: Synthesis, Biological Activity, and Structure−Activity Relationships of a Series of 1,2,4-Oxadiazole EthR Inhibitors. *Journal of Medicinal Chemistry* **2011,** *54* (8), 2994-3010.

171. Chun, J.-H.; Pike, V. W., Single-Step Radiosynthesis of "18F-Labeled Click Synthons" from Azide-Functionalized Diaryliodonium Salts. *European Journal of Organic Chemistry* **2012,** *2012* (24), 4541-4547.

172. Kumar, A. S.; Reddy, M. A.; Knorn, M.; Reiser, O.; Sreedhar, B., Magnetically Recoverable CuFe2O4 Nanoparticles: Catalyzed Synthesis of Aryl Azides and 1,4-Diaryl-1,2,3-triazoles from Boronic Acids in Water. *European Journal of Organic Chemistry* **2013,** *2013* (21), 4674-4680.

173. Grimes, K. D.; Gupte, A.; Aldrich, C. C., Copper(II)-Catalyzed Conversion of Aryl/Heteroaryl Boronic Acids, Boronates, and Trifluoroborates into the Corresponding Azides: Substrate Scope and Limitations. *Synthesis* **2010,** *2010* (09), 1441-1448.

174. Boechat, N.; Ferreira, V. F.; Ferreira, S. B.; Ferreira, M. d. L. G.; da Silva, F. d. C.; Bastos, M. M.; Costa, M. d. S.; Lourenço, M. C. S.; Pinto, A. C.; Krettli, A. U.; Aguiar, A. C.; Teixeira, B. M.; da Silva, N. V.; Martins, P. R. C.; Bezerra, F. A. F. M.; Camilo, A. L. S.; da Silva, G. P.; Costa, C. C. P., Novel 1,2,3-Triazole Derivatives for Use against Mycobacterium tuberculosis H37Rv (ATCC 27294) Strain. *Journal of Medicinal Chemistry* **2011,** *54* (17), 5988-5999.

175. Bai, S.; Li, S.; Xu, J.; Peng, X.; Sai, K.; Chu, W.; Tu, Z.; Zeng, C.; Mach, R. H., Synthesis and Structure–Activity Relationship Studies of Conformationally Flexible Tetrahydroisoquinolinyl Triazole Carboxamide and Triazole Substituted Benzamide Analogues as σ2 Receptor Ligands. *Journal of Medicinal Chemistry* **2014,** *57* (10), 4239-4251.

176. Kolarovič, A.; Schnürch, M.; Mihovilovic, M. D., Tandem Catalysis: From Alkynoic Acids and Aryl Iodides to 1,2,3-Triazoles in One Pot. *The Journal of Organic Chemistry* **2011,** *76* (8), 2613-2618.

177. Augustine, J. K.; Akabote, V.; Hegde, S. G.; Alagarsamy, P., PTSA−ZnCl2: An Efficient Catalyst for the Synthesis of 1,2,4-Oxadiazoles from Amidoximes and Organic Nitriles. *The Journal of Organic Chemistry* **2009,** *74* (15), 5640-5643.

178. Yokoyama, M.; Inazawa, H.; Shimizu, T.; Kodera, M.; Imamoto, T., CHEMISTRY OF 1,3-OXAZINE-6-THIONES. RING TRANSFORMATION. *Phosphorus and Sulfur and the Related Elements* **1983,** *16* (1-2), 187-193.

179. Ozcan, S.; Kazi, A.; Marsilio, F.; Fang, B.; Guida, W. C.; Koomen, J.; Lawrence, H. R.; Sebti, S. M., Oxadiazole-isopropylamides as Potent and Noncovalent Proteasome Inhibitors. *Journal of Medicinal Chemistry* **2013,** *56* (10), 3783-3805.

180. Chou, S.-Y.; Chen, S.-S.; Ho, C.-C.; Huang, S.-L.; Huang, T.-M.; Pan, O.-G.; Wang, C.-L.; Chen, Y.; Lu, H.-H.; Liu, S.-H.; Huang, S.-L.; Chiang, R.-S., The Syntheses of Triazole, Sulfur-Containing Diazole and n-Phenylthiatriazole Biphenyltetrazoles as Potential Angiotensin II Receptor Antagonists. *Journal of the Chinese Chemical Society* **1996,** *43* (1), 83-93.

181. Umezawa N, M. N., Iwama S, Kato N, Higuchi T. , Facile synthesis of peptide-porphyrin conjugates: Towards artificial catalase. *Bioorg Med Chem.* **2010,** *18*, 6340 - 6350.

182. Ren L, J. N., PdCl2 catalyzed efficient assembly of organic azides, CO, and alcohols under mild conditions: a direct approach to synthesize carbamates. *Chemical Communications* **2014,** *50*, 3706 - 3709.

183. Stokes, B. J.; Vogel, C. V.; Urnezis, L. K.; Pan, M.; Driver, T. G., Intramolecular Fe(II)-Catalyzed N–O or N–N Bond Formation from Aryl Azides. *Organic letters* **2010,** *12* (12), 2884-2887.

184. Schimler, S. D.; Hall, D. J.; Debbert, S. L., Anticancer (hexacarbonyldicobalt)propargyl aryl ethers: Synthesis, antiproliferative activity, apoptosis induction, and effect on cellular oxidative stress. *Journal of Inorganic Biochemistry* **2013,** *119* (0), 28-37.

185. Jopling, C., Liver-specific microRNA-122: Biogenesis and function. *RNA Biology* **2012,** *9* (2), 137-142.

186. Krutzfeldt, J.; Rajewsky, N.; Braich, R.; Rajeev, K. G.; Tuschl, T.; Manoharan, M.; Stoffel, M., Silencing of microRNAs in vivo with antagomirs. *Nature* **2005,** *438* (7068), 685-689.

187. Esau, C.; Davis, S.; Murray, S. F.; Yu, X. X.; Pandey, S. K.; Pear, M.; Watts, L.; Booten, S. L.; Graham, M.; McKay, R.; Subramaniam, A.; Propp, S.; Lollo, B. A.; Freier, S.; Bennett, C. F.; Bhanot, S.; Monia, B. P., miR-122 regulation of lipid metabolism revealed by in vivo antisense targeting. *Cell Metabolism* **2006,** *3* (2), 87-98.

188. Xu, H.; He, J.-H.; Xiao, Z.-D.; Zhang, Q.-Q.; Chen, Y.-Q.; Zhou, H.; Qu, L.-H., Liver-enriched transcription factors regulate MicroRNA-122 that targets CUTL1 during liver development. *Hepatology* **2010,** *52* (4), 1431-1442.

189. Li, Z.-Y.; Xi, Y.; Zhu, W.-N.; Zeng, C.; Zhang, Z.-Q.; Guo, Z.-C.; Hao, D.-L.; Liu, G.; Feng, L.; Chen, H.-Z.; Chen, F.; Lv, X.; Liu, D.-P.; Liang, C.-C., Positive regulation of hepatic miR-122 expression by HNF4α. *Journal of Hepatology* **2011,** *55* (3), 602-611.

190. Laudadio, I.; Manfroid, I.; Achouri, Y.; Schmidt, D.; Wilson, M. D.; Cordi, S.; Thorrez, L.; Knoops, L.; Jacquemin, P.; Schuit, F.; Pierreux, C. E.; Odom, D. T.; Peers, B.; Lemaigre, F. P., A Feedback Loop Between the Liver-Enriched Transcription Factor Network and Mir-122 Controls Hepatocyte Differentiation. *Gastroenterology* **2012,** *142* (1), 119-129.

191. (a) Hsu, S.-h.; Wang, B.; Kota, J.; Yu, J.; Costinean, S.; Kutay, H.; Yu, L.; Bai, S.; La Perle, K.; Chivukula, R. R.; Mao, H.; Wei, M.; Clark, K. R.; Mendell, J. R.; Caligiuri, M. A.; Jacob, S. T.; Mendell, J. T.; Ghoshal, K., Essential metabolic, anti-inflammatory, and anti-tumorigenic functions of miR-122 in liver. *The Journal of Clinical Investigation* **2012,** *122* (8), 2871-2883; (b) Cheung, O.; Puri, P.; Eicken, C.; Contos, M. J.; Mirshahi, F.; Maher, J. W.; Kellum, J. M.; Min, H.; Luketic, V. A.; Sanyal, A. J., NONALCOHOLIC STEATOHEPATITIS IS ASSOCIATED WITH ALTERED HEPATIC MICRO RNA EXPRESSION. *Hepatology (Baltimore, Md.)* **2008,** *48* (6), 1810-1820.

192. Lanford, R. E.; Hildebrandt-Eriksen, E. S.; Petri, A.; Persson, R.; Lindow, M.; Munk, M. E.; Kauppinen, S.; Ørum, H., Therapeutic silencing of microRNA-122 in primates with chronic hepatitis C virus infection. *Science (New York, N.Y.)* **2010,** *327* (5962), 198-201.

193. Nakao, K.; Miyaaki, H.; Ichikawa, T., Antitumor function of microRNA-122 against hepatocellular carcinoma. *J Gastroenterol* **2014,** *49* (4), 589-593.

194. Tsai, W.-C.; Hsu, S.-D.; Hsu, C.-S.; Lai, T.-C.; Chen, S.-J.; Shen, R.; Huang, Y.; Chen, H.-C.; Lee, C.-H.; Tsai, T.-F.; Hsu, M.-T.; Wu, J.-C.; Huang, H.-D.; Shiao, M.-S.; Hsiao, M.; Tsou, A.-P., MicroRNA-122 plays a critical role in liver homeostasis and hepatocarcinogenesis. *The Journal of Clinical Investigation* **2012,** *122* (8), 2884-2897.

195. El–Serag, H. B.; Rudolph, K. L., Hepatocellular Carcinoma: Epidemiology and Molecular Carcinogenesis. *Gastroenterology* **2007,** *132* (7), 2557-2576.

196. Bandiera, S.; Pfeffer, S.; Baumert, T. F.; Zeisel, M. B., miR-122 – A key factor and therapeutic target in liver disease. *Journal of Hepatology* **2015,** *62* (2), 448-457.

197. Li, C.; Wang, Y.; Wang, S.; Wu, B.; Hao, J.; Fan, H.; Ju, Y.; Ding, Y.; Chen, L.; Chu, X.; Liu, W.; Ye, X.; Meng, S., Hepatitis B Virus mRNA-Mediated miR-122 Inhibition Upregulates PTTG1-Binding Protein, Which Promotes Hepatocellular Carcinoma Tumor Growth and Cell Invasion. *Journal of Virology* **2013,** *87* (4), 2193-2205.

198. Song, K.; Han, C.; Zhang, J.; Lu, D.; Dash, S.; Feitelson, M.; Lim, K.; Wu, T., Epigenetic regulation of MicroRNA-122 by peroxisome proliferator activated receptor-gamma and hepatitis b virus X protein in hepatocellular carcinoma cells. *Hepatology* **2013,** *58* (5), 1681-1692.

199. Peng, F.; Xiao, X.; Jiang, Y.; Luo, K.; Tian, Y.; Peng, M.; Zhang, M.; Xu, Y.; Gong, G., HBx Down-Regulated Gld2 Plays a Critical Role in HBV-Related Dysregulation of miR-122. *PLoS ONE* **2014,** *9* (3), e92998.

200. Kohli, A.; Shaffer, A.; Sherman, A.; Kottilil, S., Treatment of hepatitis c: A systematic review. *JAMA* **2014,** *312* (6), 631-640.

201. Hoofnagle, J. H., Course and outcome of hepatitis C. *Hepatology* **2002,** *36* (5B), s21-s29.

202. Alter, M. J., Epidemiology of hepatitis C virus infection. *World Journal of Gastroenterology : WJG* **2007,** *13* (17), 2436-2441.

203. Nunnari, G. S., M. J., MicroRNA-122: a Therapeutic Target For Hepatitis C Virus (HCV) Infection. *Frontiers in Bioscience* **2011,** *S3*, 1032-1037.

204. Norman, K. L.; Sarnow, P., Hepatitis C virus' Achilles' heel - dependence on liver-specific microRNA miR-122. *Cell Res* **2010,** *20* (3), 247-249.

205. (a) Jesudian, A. B.; Jacobson, I. M., Optimal treatment with telaprevir for chronic HCV infection. *Liver International* **2013,** *33*, 3-13; (b) Bacon, B. R.; Gordon, S. C.; Lawitz, E.; Marcellin, P.; Vierling, J. M.; Zeuzem, S.; Poordad, F.; Goodman, Z. D.; Sings, H. L.; Boparai, N.; Burroughs, M.; Brass, C. A.; Albrecht, J. K.; Esteban, R., Boceprevir for Previously Treated Chronic HCV Genotype 1 Infection. *New England Journal of Medicine* **2011,** *364* (13), 1207-1217.

206. Yau, A. H. L.; Yoshida, E. M., Hepatitis C drugs: The end of the pegylated interferon era and the emergence of all-oral, interferon-free antiviral regimens: A concise review. *Canadian Journal of Gastroenterology & Hepatology* **2014,** *28* (8), 445-451.

207. Colombo, M., Interferon-free therapy for hepatitis C: The hurdles amid a golden era. *Digestive and Liver Disease* **2015,** (0).

208. Jopling, C. L.; Schütz, S.; Sarnow, P., Position-dependent Function for a Tandem MicroRNA miR-122 Binding Site Located in the Hepatitis C Virus RNA Genome. *Cell host & microbe* **2008,** *4* (1), 77-85.

209. (a) Li, Y.; Masaki, T.; Yamane, D.; McGivern, D. R.; Lemon, S. M., Competing and noncompeting activities of miR-122 and the 5′ exonuclease Xrn1 in regulation of hepatitis C virus replication. *Proceedings of the National Academy of Sciences of the United States of America* **2013,** *110* (5), 1881-1886; (b) Shimakami, T.; Yamane, D.; Jangra, R. K.; Kempf, B. J.; Spaniel, C.; Barton, D. J.; Lemon, S. M., Stabilization of hepatitis C virus RNA by an Ago2–miR-122 complex. *Proceedings of the National Academy of Sciences of the United States of America* **2012,** *109* (3), 941-946.

210. Henke, J. I.; Goergen, D.; Zheng, J.; Song, Y.; Schüttler, C. G.; Fehr, C.; Jünemann, C.; Niepmann, M., microRNA-122 stimulates translation of hepatitis C virus RNA. *The EMBO Journal* **2008,** *27* (24), 3300-3310.

211. Masaki, T.; Arend, Kyle C.; Li, Y.; Yamane, D.; McGivern, David R.; Kato, T.; Wakita, T.; Moorman, Nathaniel J.; Lemon, Stanley M., miR-122 Stimulates Hepatitis C Virus RNA Synthesis by Altering the Balance of Viral RNAs Engaged in Replication versus Translation. *Cell Host & Microbe* **2015,** *17* (2), 217-228.

212. (a) Machlin, E. S.; Sarnow, P.; Sagan, S. M., Masking the 5′ terminal nucleotides of the hepatitis C virus genome by an unconventional microRNA-target RNA complex. *Proceedings of the National Academy of Sciences* **2011,** *108* (8), 3193-3198; (b) Roberts, A. P. E.; Lewis, A. P.; Jopling, C. L., miR-122 activates hepatitis C virus translation by a

specialized mechanism requiring particular RNA components. *Nucleic Acids Research* **2011,** *39* (17), 7716-7729.

213. Thibault, P. A.; Huys, A.; Amador-Cañizares, Y.; Gailius, J. E.; Pinel, D. E.; Wilson, J. A., Regulation of hepatitis C virus genome replication by Xrn1, and microRNA-122 binding to individual sites in the 5' UTR. *Journal of Virology* **2015**.

214. Luna, Joseph M.; Scheel, Troels K. H.; Danino, T.; Shaw, Katharina S.; Mele, A.; Fak, John J.; Nishiuchi, E.; Takacs, Constantin N.; Catanese, Maria T.; de Jong, Ype P.; Jacobson, Ira M.; Rice, Charles M.; Darnell, Robert B., Hepatitis C Virus RNA Functionally Sequesters miR-122. *Cell* **2015,** *160* (6), 1099-1110.

215. Jopling, C. L., Targeting microRNA-122 to Treat Hepatitis C Virus Infection. *Viruses* **2010,** *2* (7), 1382-1393.

216. Hildebrandt-Eriksen, E. S.; Aarup, V.; Persson, R.; Hansen, H. F.; Munk, M. E.; Ørum, H., A Locked Nucleic Acid Oligonucleotide Targeting MicroRNA 122 Is Well-Tolerated in Cynomolgus Monkeys. *Nucleic Acid Therapeutics* **2012,** *22* (3), 152-161.

217. Pedersen, I. M.; Cheng, G.; Wieland, S.; Volinia, S.; Croce, C. M.; Chisari, F. V.; David, M., Interferon modulation of cellular microRNAs as an antiviral mechanism. *Nature* **2007,** *449* (7164), 919-922.

218. Sarasin-Filipowicz, M.; Krol, J.; Markiewicz, I.; Heim, M. H.; Filipowicz, W., Decreased levels of microRNA miR-122 in individuals with hepatitis C responding poorly to interferon therapy. *Nat Med* **2009,** *15* (1), 31-33.

219. Bihrer, V.; Friedrich-Rust, M.; Kronenberger, B.; Forestier, N.; Haupenthal, J.; Shi, Y.; Peveling-Oberhag, J.; Radeke, H. H.; Sarrazin, C.; Herrmann, E.; Zeuzem, S.; Waidmann, O.; Piiper, A., Serum miR-122 as a Biomarker of Necroinflammation in Patients With Chronic Hepatitis C Virus Infection. *Am J Gastroenterol* **2011,** *106* (9), 1663-1669.

220. Waidmann, O.; Bihrer, V.; Kronenberger, B.; Zeuzem, S.; Piiper, A.; Forestier, N., Pretreatment serum microRNA-122 is not predictive for treatment response in chronic hepatitis C virus infection. *Dig Liver Dis* **2012,** *44* (5), 438-441.

221. Chang, J.; Nicolas, E.; Marks, D.; Sander, C.; Lerro, A.; Buendia, M. A.; Xu, C.; Mason, W. S.; Moloshok, T.; Bort, R.; Zaret, K. S.; Taylor, J. M., miR-122, a Mammalian Liver-Specific microRNA, is Processed from hcr mRNA and MayDownregulate the High Affinity Cationic Amino Acid Transporter CAT-1. *RNA Biology* **2004,** *1* (2), 106-113.

222. Wulff, J. E.; Siegrist, R.; Myers, A. G., The Natural Product Avrainvillamide Binds to the Oncoprotein Nucleophosmin. *Journal of the American Chemical Society* **2007,** *129* (46), 14444-14451.

223. Greig, I. R.; Idris, A. I.; Ralston, S. H.; van't Hof, R. J., Development and Characterization of Biphenylsulfonamides as Novel Inhibitors of Bone Resorption. *Journal of Medicinal Chemistry* **2006,** *49* (25), 7487-7492.

224. Zhang, C.; Westaway, S. M.; Speake, J. D.; Bishop, M. J.; Goetz, A. S.; Carballo, L. H.; Hu, M.; Epperly, A. H., Tetrahydroquinoline derivatives as opioid receptor antagonists. *Bioorganic & Medicinal Chemistry Letters* **2011,** *21* (2), 670-676.

225. Skupinska, K. A.; McEachern, E. J.; Skerlj, R. T.; Bridger, G. J., Concise Preparation of Amino-5,6,7,8-tetrahydroquinolines and Amino-5,6,7,8-tetrahydroisoquinolines via Catalytic Hydrogenation of Acetamidoquinolines and Acetamidoisoquinolines. *The Journal of Organic Chemistry* **2002,** *67* (22), 7890-7893.

226. Upadhyay, S. K.; Pingali, S. R. K.; Jursic, B. S., Comparison of microwave-assisted and conventional preparations of cyclic imides. *Tetrahedron Letters* **2010,** *51* (17), 2215-2217.

227. Jenkins, T. J.; Guan, B.; Dai, M.; Li, G.; Lightburn, T. E.; Huang, S.; Freeze, B. S.; Burdi, D. F.; Jacutin-Porte, S.; Bennett, R.; Chen, W.; Minor, C.; Ghosh, S.; Blackburn, C.; Gigstad, K. M.; Jones, M.; Kolbeck, R.; Yin, W.; Smith, S.; Cardillo, D.; Ocain, T. D.; Harriman, G. C., Design, Synthesis, and Evaluation of Naphthalene-Sulfonamide Antagonists of Human CCR8. *Journal of Medicinal Chemistry* **2007,** *50* (3), 566-584.

228. Shaffer, C. L.; Morton, M. D.; Hanzlik, R. P., N-Dealkylation of an N-Cyclopropylamine by Horseradish Peroxidase. Fate of the Cyclopropyl Group. *Journal of the American Chemical Society* **2001,** *123* (35), 8502-8508.

229. Kolmakov, K.; Belov, V. N.; Wurm, C. A.; Harke, B.; Leutenegger, M.; Eggeling, C.; Hell, S. W., A Versatile Route to Red-Emitting Carbopyronine Dyes for Optical Microscopy and Nanoscopy. *European Journal of Organic Chemistry* **2010,** *2010* (19), 3593-3610.

230. Bassin, J. P.; Cremlyn, R. J.; Swinbourne, F. J., CHLOROSULFONATION OF SOME POLYNUCLEAR HETEROCYCLIC COMPOUNDS. *Phosphorus, Sulfur, and Silicon and the Related Elements* **1992,** *72* (1-4), 157-170.

231. Huang, H.; Yan, X.; Zhu, W.; Liu, H.; Jiang, H.; Chen, K., Efficient Copper-Promoted N-Arylations of Aryl Halides with Amines. *Journal of Combinatorial Chemistry* **2008,** *10* (5), 617-619.

232. Kumar, R. A.; Maheswari, C. U.; Ghantasala, S.; Jyothi, C.; Reddy, K. R., Synthesis of 3H-Quinazolin-4-ones and 4H-3,1-Benzoxazin-4-ones via Benzylic Oxidation and Oxidative Dehydrogenation using Potassium Iodide-tert-Butyl Hydroperoxide. *Advanced Synthesis & Catalysis* **2011,** *353* (2-3), 401-410.

233. Tominaga, M. T., H.; Nakagawa, K.; Takada, K.; Hoshino, Y.; Watanabe, K., Syntheses and beta-adrenergic blocking activities of carbostyril derivatives. *Chem Pharm Bull* **1981,** *29* (8), 2166-81.

234. Baell, J. B.; Holloway, G. A., New Substructure Filters for Removal of Pan Assay Interference Compounds (PAINS) from Screening Libraries and for Their Exclusion in Bioassays. *Journal of Medicinal Chemistry* **2010,** *53* (7), 2719-2740.

235. Auld, D. S.; Thorne, N.; Maguire, W. F.; Inglese, J., Mechanism of PTC124 activity in cell-based luciferase assays of nonsense codon suppression. *Proceedings of the National Academy of Sciences of the United States of America* **2009,** *106* (9), 3585-3590.

236. Cao, H.; Alper, H., Palladium-Catalyzed Double Carbonylation Reactions of o-Dihaloarenes with Amines in Phosphonium Salt Ionic Liquids. *Organic Letters* **2010,** *12* (18), 4126-4129.

237. Lima, L. d. M.; Castro, P.; Machado, A. L.; Fraga, C. A. M.; Lugnier, C.; de Moraes, V. L. G.; Barreiro, E. J., Synthesis and anti-inflammatory activity of phthalimide derivatives, designed as new thalidomide analogues. *Bioorganic & Medicinal Chemistry* **2002,** *10* (9), 3067-3073.

238. Wang, Z.; Wan, W.; Jiang, H.; Hao, J., One-Pot Cyclization of 2-Aminophenethyl Alcohols: A Novel and Direct Approach to the Synthesis of N-Acyl Indolines. *The Journal of Organic Chemistry* **2007,** *72* (24), 9364-9367.

239. DeBergh, J. R.; Niljianskul, N.; Buchwald, S. L., Synthesis of Aryl Sulfonamides via Palladium-Catalyzed Chlorosulfonylation of Arylboronic Acids. *Journal of the American Chemical Society* **2013,** *135* (29), 10638-10641.

240. Shen, Q.; Zhang, L.; Zhou, Y.-R.; Li, J.-X., Oxidant-dependent Cu-catalyzed alkynylation and aminomethylation: C–H versus C–C cleavage in TMEDA. *Tetrahedron Letters* **2013,** *54* (49), 6725-6728.

241. Liwosz, T. W.; Chemler, S. R., Copper-Catalyzed Oxidative Amination and Allylic Amination of Alkenes. *Chemistry – A European Journal* **2013,** *19* (38), 12771-12777.

242. Zhichkin, P. E.; Peterson, L. H.; Beer, C. M.; Rennells, W. M., The Use of Formamidine Protection for the Derivatization of Aminobenzoic Acids. *The Journal of Organic Chemistry* **2008,** *73* (22), 8954-8959.

243. Sharma, S.; Kumar, M.; Kumar, V.; Kumar, N., Metal-Free Transfer Hydrogenation of Nitroarenes in Water with Vasicine: Revelation of Organocatalytic Facet of an Abundant Alkaloid. *The Journal of Organic Chemistry* **2014,** *79* (19), 9433-9439.

244. Vasuki, G.; Perumal, S.; Vijayabaskar, V.; Selvaraj, S.; Ramalingam, M.; Venuvanalingam, P., A proton and carbon NMR spectroscopic study of 5-substituted acenaphthenes. *Magnetic Resonance in Chemistry* **1998,** *36* (12), 943-946.

245. Quintana-Espinoza, P.; García-Luis, J.; Amesty, Á.; Martín-Rodríguez, P.; Lorenzo-Castrillejo, I.; Ravelo, A. G.; Fernández-Pérez, L.; Machín, F.; Estévez-Braun, A., Synthesis and study of antiproliferative, antitopoisomerase II, DNA-intercalating and

DNA-damaging activities of arylnaphthalimides. *Bioorganic & Medicinal Chemistry* **2013,** *21* (21), 6484-6495.

246. Balsells, J.; Walsh, P. J., The Use of Achiral Ligands to Convey Asymmetry: Chiral Environment Amplification. *Journal of the American Chemical Society* **2000,** *122* (8), 1802-1803.

247. Fan, X.; Fu, L.-A.; Li, N.; Lv, H.; Cui, X.-M.; Qi, Y., Iron-catalyzed N-alkylation using [small pi]-activated ethers as electrophiles. *Organic & Biomolecular Chemistry* **2013,** *11* (13), 2147-2153.

248. (a) Dormán, G.; Prestwich, G. D., Using photolabile ligands in drug discovery and development. *Trends in Biotechnology* **2000,** *18* (2), 64-77; (b) Lomenick, B.; Olsen, R. W.; Huang, J., Identification of Direct Protein Targets of Small Molecules. *ACS Chemical Biology* **2011,** *6* (1), 34-46; (c) Disney, M. D.; Yildirim, I.; Childs-Disney, J. L., Methods to enable the design of bioactive small molecules targeting RNA. *Organic & Biomolecular Chemistry* **2014,** *12* (7), 1029-1039.

249. Dubinsky, L.; Krom, B. P.; Meijler, M. M., Diazirine based photoaffinity labeling. *Bioorganic & Medicinal Chemistry* **2012,** *20* (2), 554-570.

250. Schnapp, K. A.; Poe, R.; Leyva, E.; Soundararajan, N.; Platz, M. S., Exploratory photochemistry of fluorinated aryl azides. Implications for the design of photoaffinity labeling reagents. *Bioconjugate Chemistry* **1993,** *4* (2), 172-177.

251. Gansäuer, A.; Behlendorf, M.; von Laufenberg, D.; Fleckhaus, A.; Kube, C.; Sadasivam, D. V.; Flowers, R. A., Catalytic, Atom-Economical Radical Arylation of Epoxides. *Angewandte Chemie International Edition* **2012,** *51* (19), 4739-4742.

252. Su, B.; Tian, R.; Darby, M. V.; Brueggemeier, R. W., Novel Sulfonanilide Analogs Decrease Aromatase Activity in Breast Cancer Cells: Synthesis, Biological Evaluation, and Ligand-Based Pharmacophore Identification. *Journal of Medicinal Chemistry* **2008,** *51* (5), 1126-1135.

253. González-Gómez, Á.; Domínguez, G.; Pérez-Castells, J., Synthesis of Benzazepines by Gold-Catalysed Reactions of N-Allenylamides. *European Journal of Organic Chemistry* **2009,** *2009* (29), 5057-5062.

254. Meshram, G. A.; Patil, V. D., A simple and efficient method for sulfonylation of amines, alcohols and phenols with cupric oxide under mild conditions. *Tetrahedron Letters* **2009,** *50* (10), 1117-1121.

255. Chun, J.; Yin, Y. I.; Yang, G.; Tarassishin, L.; Li, Y.-M., Stereoselective Synthesis of Photoreactive Peptidomimetic γ-Secretase Inhibitors. *The Journal of Organic Chemistry* **2004,** *69* (21), 7344-7347.

256. Tomioka, H.; Watanabe, T.; Hattori, M.; Nomura, N.; Hirai, K., Generation, Reactions, and Kinetics of Sterically Congested Triplet Diphenylcarbenes. Effects of Bromine Groups. *Journal of the American Chemical Society* **2002,** *124* (3), 474-482.

257. Beihoffer, L.; Craven, R.; Knight, K.; Sisson, C.; Waddell, T., Pyridinium chlorochromate (PCC) oxidation of bishomoallylic tertiary alcohols. A structure–reactivity study. *Transition Met Chem* **2005,** *30* (5), 582-585.

258. Park, K. K.; Lee, J. J.; Ryu, J., Photo-Fries rearrangement of N-arylsulfonamides to aminoaryl sulfone derivatives. *Tetrahedron* **2003,** *59* (39), 7651-7659.

259. Srinivasan, R.; Tan, L. P.; Wu, H.; Yang, P.-Y.; Kalesh, K. A.; Yao, S. Q., High-throughput synthesis of azide libraries suitable for direct "click" chemistry and in situ screening. *Organic & Biomolecular Chemistry* **2009,** *7* (9), 1821-1828.

260. Shi, H.; Zhang, C.-J.; Chen, G. Y. J.; Yao, S. Q., Cell-Based Proteome Profiling of Potential Dasatinib Targets by Use of Affinity-Based Probes. *Journal of the American Chemical Society* **2012,** *134* (6), 3001-3014.

261. Yan, R.; El-Emir, E.; Rajkumar, V.; Robson, M.; Jathoul, A. P.; Pedley, R. B.; Årstad, E., One-Pot Synthesis of an 125I-Labeled Trifunctional Reagent for Multiscale Imaging with Optical and Nuclear Techniques. *Angewandte Chemie International Edition* **2011,** *50* (30), 6793-6795.

262. Nguyen, T.; Francis, M. B., Practical Synthetic Route to Functionalized Rhodamine Dyes. *Organic Letters* **2003,** *5* (18), 3245-3248.

263. Pinney, K. G.; Carlson, K. E.; Katzenellenbogen, B. S.; Katzenellenbogen, J. A., Efficient and selective photoaffinity labeling of the estrogen receptor using two nonsteroidal ligands that embody aryl azide or tetrafluoroaryl azide photoreactive functions. *Biochemistry* **1991,** *30* (9), 2421-2431.

264. Kato, K.; Kiyonaka, S.; Sawaguchi, Y.; Tohnishi, M.; Masaki, T.; Yasokawa, N.; Mizuno, Y.; Mori, E.; Inoue, K.; Hamachi, I.; Takeshima, H.; Mori, Y., Molecular Characterization of Flubendiamide Sensitivity in the Lepidopterous Ryanodine Receptor Ca2+ Release Channel. *Biochemistry* **2009,** *48* (43), 10342-10352.

265. Friedman, D. B.; Hoving, S.; Westermeier, R., Chapter 30 Isoelectric Focusing and Two-Dimensional Gel Electrophoresis. In *Methods in Enzymology*, Richard, R. B.; Murray, P. D., Eds. Academic Press: 2009; Vol. Volume 463, pp 515-540.

266. Molnár E, F. G., Klem J, Darula Z, Hunyadi-Gulyás E, Medgyesi A, Medzihradszky KF, Puskás LG., Removal of nonspecific binding proteins from cell and tissue extracts using 2-aminobenzimidazole-tethered affinity resin. *Pharmazie* **2011,** *66* (9).

267. Tamura, T.; Terada, T.; Tanaka, A., A Quantitative Analysis and Chemical Approach for the Reduction of Nonspecific Binding Proteins on Affinity Resins. *Bioconjugate Chemistry* **2003,** *14* (6), 1222-1230.

268. Leriche, G.; Chisholm, L.; Wagner, A., Cleavable linkers in chemical biology. *Bioorganic & Medicinal Chemistry* **2012,** *20* (2), 571-582.

269. Landi, F.; Johansson, C. M.; Campopiano, D. J.; Hulme, A. N., Synthesis and application of a new cleavable linker for "click"-based affinity chromatography. *Organic & Biomolecular Chemistry* **2010,** *8* (1), 56-59.

270. Choy, M.-K.; Movassagh, M.; Goh, H.-G.; Bennett, M. R.; Down, T. A.; Foo, R. S. Y., Genome-wide conserved consensus transcription factor binding motifs are hyper-methylated. *BMC Genomics* **2010,** *11*, 519-519.

271. Jung, C. J.; Iyengar, S.; Blahnik, K. R.; Ajuha, T. P.; Jiang, J. X.; Farnham, P. J.; Zern, M., Epigenetic Modulation of miR-122 Facilitates Human Embryonic Stem Cell Self-Renewal and Hepatocellular Carcinoma Proliferation. *PLoS ONE* **2011,** *6* (11), e27740.

272. Kim, Y. J.; Greer, C. B.; Cecchini, K. R.; Harris, L. N.; Tuck, D. P.; Kim, T. H., HDAC inhibitors induce transcriptional repression of high copy number genes in breast cancer through elongation blockade. *Oncogene* **2013,** *32* (23), 2828-2835.

273. Liu, H.; Naismith, J. H., An efficient one-step site-directed deletion, insertion, single and multiple-site plasmid mutagenesis protocol. *BMC Biotechnology* **2008,** *8*, 91-91.

274. Zeng, C.; Wang, R.; Li, D.; Lin, X.-J.; Wei, Q.-K.; Yuan, Y.; Wang, Q.; Chen, W.; Zhuang, S.-M., A novel GSK-3 beta–C/EBP alpha–miR-122–insulin-like growth factor 1 receptor regulatory circuitry in human hepatocellular carcinoma. *Hepatology* **2010,** *52* (5), 1702-1712.

275. Tao, C.-Z.; Li, J.; Fu, Y.; Liu, L.; Guo, Q.-X., Copper-catalyzed synthesis of primary arylamines from aryl halides and 2,2,2-trifluoroacetamide. *Tetrahedron Letters* **2008,** *49* (1), 70-75.

276. Stacy, D. M.; Le Quement, S. T.; Hansen, C. L.; Clausen, J. W.; Tolker-Nielsen, T.; Brummond, J. W.; Givskov, M.; Nielsen, T. E.; Blackwell, H. E., Synthesis and biological evaluation of triazole-containing N-acyl homoserine lactones as quorum sensing modulators. *Organic & Biomolecular Chemistry* **2013,** *11* (6), 938-954.

277. Mannam, S.; Sekar, G., An enantiopure galactose oxidase model: synthesis of chiral amino alcohols through oxidative kinetic resolution catalyzed by a chiral copper complex. *Tetrahedron: Asymmetry* **2009,** *20* (4), 497-502.

278. Patel, R. V.; Park, S. W., Access to a new class of biologically active quinoline based 1,2,4-triazoles. *European Journal of Medicinal Chemistry* **2014,** *71* (0), 24-30.

279. Zill, A.; Rutz, A. L.; Kohman, R. E.; Alkilany, A. M.; Murphy, C. J.; Kong, H.; Zimmerman, S. C., Clickable polyglycerol hyperbranched polymers and their application to gold nanoparticles and acid-labile nanocarriers. *Chemical Communications* **2011,** *47* (4), 1279-1281.

280. Ming, X.; Laing, B., Bioconjugates for targeted delivery of therapeutic oligonucleotides. *Advanced Drug Delivery Reviews* **2015,** (0).

281. Geary, R. S.; Norris, D.; Yu, R.; Bennett, C. F., Pharmacokinetics, biodistribution and cell uptake of antisense oligonucleotides. *Advanced Drug Delivery Reviews* **2015,** (0).

282. Juliano, R. L.; Ming, X.; Nakagawa, O., The Chemistry and Biology of Oligonucleotide Conjugates. *Accounts of Chemical Research* **2012,** *45* (7), 1067-1076.

283. Madani, F.; Lindberg, S.; Langel, Ü.; Futaki, S.; Gräslund, A., Mechanisms of Cellular Uptake of Cell-Penetrating Peptides. *Journal of Biophysics* **2011,** *2011*, 414729.

284. Basu, S.; Wickstrom, E., Synthesis and Characterization of a Peptide Nucleic Acid Conjugated to a d-Peptide Analog of Insulin-like Growth Factor 1 for Increased Cellular Uptake. *Bioconjugate Chemistry* **1997,** *8* (4), 481-488.

285. Wolfrum, C.; Shi, S.; Jayaprakash, K. N.; Jayaraman, M.; Wang, G.; Pandey, R. K.; Rajeev, K. G.; Nakayama, T.; Charrise, K.; Ndungo, E. M.; Zimmermann, T.; Koteliansky, V.; Manoharan, M.; Stoffel, M., Mechanisms and optimization of in vivo delivery of lipophilic siRNAs. *Nat Biotech* **2007,** *25* (10), 1149-1157.

286. Nishina, K.; Unno, T.; Uno, Y.; Kubodera, T.; Kanouchi, T.; Mizusawa, H.; Yokota, T., Efficient In Vivo Delivery of siRNA to the Liver by Conjugation of [alpha]-Tocopherol. *Mol Ther* **2008,** *16* (4), 734-740.

287. Nakagawa, O.; Ming, X.; Huang, L.; Juliano, R. L., Targeted Intracellular Delivery of Antisense Oligonucleotides via Conjugation with Small-Molecule Ligands. *Journal of the American Chemical Society* **2010,** *132* (26), 8848-8849.

288. Vlahov, I. R.; Leamon, C. P., Engineering Folate–Drug Conjugates to Target Cancer: From Chemistry to Clinic. *Bioconjugate Chemistry* **2012,** *23* (7), 1357-1369.

289. Hansen, M. J.; Velema, W. A.; Lerch, M. M.; Szymanski, W.; Feringa, B. L., Wavelength-selective cleavage of photoprotecting groups: strategies and applications in dynamic systems. *Chemical Society Reviews* **2015,** *44* (11), 3358-3377.

290. Deiters, A., Light Activation as a Method of Regulating and Studying Gene Expression. *Current opinion in chemical biology* **2009,** *13* (5-6), 678-686.

291. Govan, J. M.; Uprety, R.; Thomas, M.; Lusic, H.; Lively, M. O.; Deiters, A., Cellular Delivery and Photochemical Activation of Antisense Agents through a Nucleobase Caging Strategy. *ACS Chemical Biology* **2013,** *8* (10), 2272-2282.

292. Leamon, C. P., Folate-targeted drug strategies for the treatment of cancer. *Curr Opin Investig Drugs* **2008,** *9* (12), 1277-1286.

293. Du, C.; Deng, D.; Shan, L.; Wan, S.; Cao, J.; Tian, J.; Achilefu, S.; Gu, Y., A pH-sensitive doxorubicin prodrug based on folate-conjugated BSA for tumor-targeted drug delivery. *Biomaterials* **2013,** *34* (12), 3087-3097.

294. Schneider, R.; Schmitt, F.; Frochot, C.; Fort, Y.; Lourette, N.; Guillemin, F.; Müller, J.-F.; Barberi-Heyob, M., Design, synthesis, and biological evaluation of folic acid targeted tetraphenylporphyrin as novel photosensitizers for selective photodynamic therapy. *Bioorganic & Medicinal Chemistry* **2005,** *13* (8), 2799-2808.

295. Gabizon, A.; Horowitz, A. T.; Goren, D.; Tzemach, D.; Mandelbaum-Shavit, F.; Qazen, M. M.; Zalipsky, S., Targeting Folate Receptor with Folate Linked to Extremities of Poly(ethylene glycol)-Grafted Liposomes: In Vitro Studies. *Bioconjugate Chemistry* **1999,** *10* (2), 289-298.

296. Hong, V.; Presolski, S. I.; Ma, C.; Finn, M. G., Analysis and Optimization of Copper-Catalyzed Azide–Alkyne Cycloaddition for Bioconjugation. *Angewandte Chemie International Edition* **2009,** *48* (52), 9879-9883.

297. Shakeri-Zadeh, A.; Ghasemifard, M.; Ali Mansoori, G., Structural and optical characterization of folate-conjugated gold-nanoparticles. *Physica E: Low-dimensional Systems and Nanostructures* **2010,** *42* (5), 1272-1280.

298. Lee, S.-M.; Chen, H.; O'Halloran, T. V.; Nguyen, S. T., "Clickable" Polymer-Caged Nanobins as a Modular Drug Delivery Platform. *Journal of the American Chemical Society* **2009,** *131* (26), 9311-9320.

299. Au, J. S.; Pockros, P. J., Novel Therapeutic Approaches for Hepatitis C. *Clinical Pharmacology & Therapeutics* **2014,** *95* (1), 78-88.

300. Aagaard, L.; Rossi, J. J., RNAi Therapeutics: Principles, Prospects and Challenges. *Advanced drug delivery reviews* **2007,** *59* (2-3), 75-86.

301. Chukkapalli, V.; Berger, K. L.; Kelly, S. M.; Thomas, M.; Deiters, A.; Randall, G., Daclatasvir inhibits hepatitis C virus NS5A motility and hyper-accumulation of phosphoinositides. *Virology* **2015,** *476* (0), 168-179.

302. Berger, K. L.; Kelly, S. M.; Jordan, T. X.; Tartell, M. A.; Randall, G., Hepatitis C Virus Stimulates the Phosphatidylinositol 4-Kinase III Alpha-Dependent Phosphatidylinositol 4-Phosphate Production That Is Essential for Its Replication. *Journal of Virology* **2011,** *85* (17), 8870-8883.

303. McGivern, D. R.; Masaki, T.; Williford, S.; Ingravallo, P.; Feng, Z.; Lahser, F.; Asante-Appiah, E.; Neddermann, P.; De Francesco, R.; Howe, A. Y.; Lemon, S. M., Kinetic Analyses Reveal Potent and Early Blockade of Hepatitis C Virus Assembly by NS5A Inhibitors. *Gastroenterology* **2014,** *147* (2), 453-462.e7.

304. Gao, M.; Nettles, R. E.; Belema, M.; Snyder, L. B.; Nguyen, V. N.; Fridell, R. A.; Serrano-Wu, M. H.; Langley, D. R.; Sun, J.-H.; O'Boyle Ii, D. R.; Lemm, J. A.; Wang,

C.; Knipe, J. O.; Chien, C.; Colonno, R. J.; Grasela, D. M.; Meanwell, N. A.; Hamann, L. G., Chemical genetics strategy identifies an HCV NS5A inhibitor with a potent clinical effect. *Nature* **2010,** *465* (7294), 96-100.

305. Lusic, H.; Uprety, R.; Deiters, A., Improved Synthesis of the Two-Photon Caging Group 3-Nitro-2-Ethyldibenzofuran and Its Application to a Caged Thymidine Phosphoramidite. *Organic Letters* **2010,** *12* (5), 916-919.

306. Mindt, T. L.; Müller, C.; Melis, M.; de Jong, M.; Schibli, R., "Click-to-Chelate": In Vitro and In Vivo Comparison of a 99mTc(CO)3-Labeled N(τ)-Histidine Folate Derivative with Its Isostructural, Clicked 1,2,3-Triazole Analogue. *Bioconjugate Chemistry* **2008,** *19* (8), 1689-1695.

307. Abraham, D. J.; Gazze, D. M.; Kennedy, P. E.; Mokotoff, M., Design, synthesis, and testing of potential antisickling agents. 5. Disubstituted benzoic acids designed for the donor site and proline salicylates designed for the acceptor site. *Journal of Medicinal Chemistry* **1984,** *27* (12), 1549-1559.

308. Redshaw N, W. T., Whale A, Cowen S, Huggett J, Foy CA, A comparison of miRNA isolation and RT-qPCR technologies and their effects on quantification accuracy and repeatability. *Biotechniques* **2013,** *54*.